

ÄSPÖ HRL - Geoscientific evaluation 1997/4

**Results from pre-investigations and detailed site
characterization**

Comparison of predictions and observations

**Hydrogeology, groundwater chemistry and transport
of solutes**

Ingvar Rhén¹, Gunnar Gustafson², Peter Wikberg³

1 VBB Viak, Göteborg

2 VBB Viak/CTH, Göteborg

3 SKB, Stockholm

June 1997

SVENSK KÄRNBRÄNSLEHANTERING AB

SWEDISH NUCLEAR FUEL AND WASTE MANAGEMENT CO

P.O.BOX 5864 S-102 40 STOCKHOLM SWEDEN

PHONE +46 8 459 84 00

FAX +46 8 661 57 19

ÄSPÖ HRL - GEOSCIENTIFIC EVALUATION 1997/4

**RESULTS FROM PRE-INVESTIGATIONS AND
DETAILED SITE CHARACTERIZATION**

**COMPARISON OF PREDICTIONS AND
OBSERVATIONS**

**HYDROGEOLOGY, GROUNDWATER CHEMISTRY
AND TRANSPORT OF SOLUTES**

Ingvar Rhén¹, Gunnar Gustafson², Peter Wikberg³

- 1 VBB Viak, Göteborg**
- 2 VBB Viak/CTH, Göteborg**
- 3 SKB, Stockholm**

June 1997

Information on SKB technical reports from 1977-1978 (TR 121), 1979 (TR 79-28), 1980 (TR 80-26), 1981 (TR 81-17), 1982 (TR 82-28), 1983 (TR 83-77), 1984 (TR 85-01), 1985 (TR 85-20), 1986 (TR 86-31), 1987 (TR 87-33), 1988 (TR 88-32), 1989 (TR 89-40), 1990 (TR 90-46), 1991 (TR 91-64), 1992 (TR 92-46), 1993 (TR 93-34), 1994 (TR 94-33), 1995 (TR 95-37) and 1996 (TR 96-25) is available through SKB.

ÄSPÖ HRL

GEOSCIENTIFIC EVALUATION 1997/4

**RESULTS FROM PRE-INVESTIGATIONS
AND DETAILED SITE CHARACTERIZATION**

**COMPARISON OF PREDICTIONS AND
OBSERVATIONS**

**HYDROGEOLOGY, GROUNDWATER
CHEMISTRY AND TRANSPORT OF
SOLUTES**

**Ingvar Rhén, VBB Viak, Göteborg
Gunnar Gustafson, VBB Viak/CTH, Göteborg
Peter Wikberg, SKB, Stockholm**

June 1997

Keywords: site characterization, Äspö hydrogeology, groundwater, chemistry, transport of solutes, tunnel documentation, predictions and observations, borehole investigations.

FOREWORD

The booklet *Äspö Hard Rock Laboratory - 10 years of research*, available from SKB, provides the reader with a popular review of the achievements. This report is No 4 of six Technical Reports summarizing the pre-investigation and construction phase of the Äspö Hard Rock Laboratory.

The reports are:

- 1 Stanfors R, Erlström M, Markström I.
Äspö HRL - Geoscientific evaluation 1997/1.
Overview of site characterization 1986-1995
SKB TR 97-02.
- 2 Rhén I (ed), Bäckblom (ed), Gustafson G, Stanfors R, Wikberg P.
Äspö HRL - Geoscientific evaluation 1997/2.
Results from pre-investigations and detailed site characterization.
Summary report.
SKB TR 97-03.
- 3 Stanfors R, Olsson P, Stille H .
Äspö HRL - Geoscientific evaluation 1997/3.
Results from pre-investigations and detailed site characterization.
Comparison of predictions and observations.
Geology and Mechanical stability.
SKB TR 97-04.
- 4 Rhén I, Gustafson G, Wikberg P.
Äspö HRL - Geoscientific evaluation 1997/4.
Results from pre-investigations and detailed site characterization.
Comparison of predictions and observations.
Hydrogeology, Groundwater chemistry and Transport of solutes.
SKB TR 97-05.
- 5 Rhén I (ed), Gustafson G, Stanfors R, Wikberg P.
Äspö HRL - Geoscientific evaluation 1997/5.
Models based on site characterization 1986-1995.
SKB TR 97-06.
- 6 Almén K-E (ed), Olsson P, Rhén I, Stanfors R, Wikberg P
Äspö Hard Rock Laboratory
Feasibility and usefulness of site investigation methods.
Experiences from pre-investigation phase.
SKB TR 94-24.

The background and objectives of the project are presented in a background report to SKB R&D Programme 1989 (Hard Rock Laboratory), which contains a detailed description of the HRL project.

The purpose of this report, *No. 4*, is to present the evaluation of hydrogeology, groundwater chemistry and transport of solutes of the pre-investigation for the Äspö HRL. An overview of all the investigations performed is summarized in *Report 1*. The evaluation of the pre-investigation is presented in *Reports 2-4*. *Report 5* presents the 1996 models of the Äspö HRL, the concepts and some comments on how the models have developed, based on data from the pre-investigation and construction phases of the Äspö HRL. Finally, *Report 6* outlines the usefulness and feasibility of pre-investigation methods.

June 1997

Ingvar Rhén

Gunnar Gustafson

Peter Wikberg

ABSTRACT

The pre-investigations for the Äspö Hard Rock Laboratory were started in 1986 and involved extensive field measurements, aimed at characterizing the rock formations with regard to geology, hydrogeology, hydrochemistry and rock mechanics.

Prior to excavation of the laboratory which was started in the autumn of 1990 predictions for the excavation phase were made. The predictions concern five key issues: geology, groundwater flow, groundwater chemistry, transport of solutes and mechanical stability.

Comparisons between these predictions and observations were made during excavation in order to verify the reliability of the pre-investigations. This report presents a comparison between the groundwater flow, groundwater chemistry and transport of solutes predictions and observations and an evaluation of data and investigation methods used for the 700 - 2874 m section of the tunnel.

The main conclusions from the comparisons presented in this report are:

- To construct a reliable model it is important to perform hydraulic tests on different scales systematically in the boreholes, both for scale relationships but also to gain flexibility in the interpretation of how to divide the rock mass into subdomains.
- It is probable that there is some spatial correlation of hydraulic conductivity within the hydraulic rock mass domains due to some large and more transmissive features not accounted for in the present concept used. Efforts should be made to develop a more realistic spatial correlation model for the hydraulic conductivity.
- The multivariate groundwater mixing and mass balance modelling concept M3 seems to be one of the tools that can be useful for the interpretation of the flow paths and transport times.
- Tracer tests are useful for checking the connectivity within and between hydraulic conductor domains (water bearing fracture zones). At a relatively small scale, about 50-100 m, it seems possible to get rough estimates of the flow porosity and dispersivity within a hydraulic conductor domain. At larger scales it is difficult to evaluate the transport properties but the tests can be useful for defining hydraulic connectivity.
- The influence of the microbial processes on the hydrochemistry was unknown from pre-investigations but has now been found to determine the groundwater chemistry under certain conditions.

ABSTRACT (in Swedish)

Förundersökningarna för Äspölaboratoriet startade 1986 med syfte att karakterisera berget geologiskt, hydrogeologiskt, grundvattenkemiskt och bergmekaniskt.

Innan byggandet av Äspölaboratoriet startade hösten 1990 gjordes prediktioner för byggfasen av laboratoriet avseende fem huvudfrågor: geologi, grundvattenflöde, grundvattenkemi, transport av lösta ämnen och mekanisk stabilitet.

Jämförelser mellan prediktioner och observationer har gjorts under byggfasen med syfte att verifiera förundersökningarnas tillförlitlighet. Denna rapport redovisar resultat av den jämförelse som gjorts mellan prediktioner och utfall av grundvattenflöde, grundvattenkemi, transport av lösta ämnen för delsträckan 700 - 2874 m av tunneln.

Följande huvudslutsatser i rapporten kan framhållas:

- För att kunna skapa en pålitlig modell är det viktigt att hydrauliska tester utförs i flera testskalor och systematiskt i borrhålen för att dels erhålla skalfunktioner för hydraulisk konduktivitet och dels erhålla en flexibilitet i tolkningen av hur bergmassan bör delas upp i olika hydrauliska enheter.
- Sannolikt har den hydrauliska konduktiviteten en rumslig korrelation, som beror av ett antal stora och permeabla sprickor, som den nuvarande modellen ej beskriver. En bättre modell för rumslig korrelation av hydraulisk konduktivitet bör utvecklas.
- Multivariata grundvattenblandnings- och massbalansberäkningar med konceptet M3 förefaller vara användbart för tolkning av flödesvägar och transporttider.
- Spårförsök är användbara för att kontrollera de hydrauliska förbindelserna mellan hydrauliskt konduktiva sprickzoner. Vid relativt liten skala, ca 50-100 m, förefaller det vara möjligt att erhålla ungefärliga värden på flödesporositet och dispersivitet inom en sprickzon. Vid större testskalor är det svårt att utvärdera transportegenskaper, men testerna kan dock vara användbara för att kontrollera hydrauliska förbindelser.
- Mikrobiella processer har visat sig vara av stor betydelse för vattenkemin under vissa förhållanden. Förundersökningarna indikerade ej att dessa processer var viktiga.

CONTENTS

	FOREWORD	i
	ABSTRACT	iii
	ABSTRACT (in Swedish)	iv
	CONTENTS	v
	EXECUTIVE SUMMARY	vii
1	INTRODUCTION	1
1.1	ÄSPÖ HARD ROCK LABORATORY (Äspö HRL)	1
1.2	OVERALL GOALS OF THE ÄSPÖ PROJECT	4
1.3	AIM OF THIS REPORT	5
1.4	COORDINATE SYSTEM	5
1.5	CHAINAGE DIFFERENCES DUE TO MODIFIED LAYOUT OF THE TUNNEL	6
	ACKNOWLEDGEMENT	9
	 PART 1 - GROUNDWATER FLOW	
1	SUBJECT: WATER-BEARING ZONES - SITE SCALE	1
1.1	SCOPE AND CONCEPTS	1
1.2	METHODOLOGY FOR TESTS OF CONCEPTS AND MODELS	1
1.2.1	Prediction methodology	1
1.2.2	Methodology for determining outcome	10
1.3	COMPARISON OF PREDICTED AND MEASURED ENTITIES	15
1.3.1	Position and extent of water-bearing zones	15
1.3.2	Properties of water-bearing zones	22
1.4	SCRUTINY AND EVALUATION	26
2	SUBJECT: HYDRAULIC CONDUCTIVITY - SITE SCALE	35
2.1	SCOPE AND CONCEPTS	35
2.2	METHODOLOGY FOR TESTS OF CONCEPTS AND MODELS	36
2.2.1	Prediction methodology	36
2.2.2	Methodology for determining outcome	36
2.3	COMPARISON OF PREDICTED AND MEASURED ENTITIES	37
2.4	SCRUTINY AND EVALUATION	40
3	SUBJECT: INFLOW TO TUNNEL - SITE SCALE	75
3.1	SCOPE AND CONCEPTS	75
3.2	METHODOLOGY FOR TESTS OF CONCEPTS AND MODELS	75

3.2.1	Prediction methodology	75
3.2.2	Methodology for determining outcome	76
3.3	COMPARISON OF PREDICTED AND MEASURED ENTITIES	81
3.4	SCRUTINY AND EVALUATION	88
4	SUBJECT: BOUNDARY CONDITIONS AND PRESSURES - SITE SCALE	91
4.1	SCOPE AND CONCEPTS	91
4.2	METHODOLOGY FOR TESTS OF CONCEPTS AND MODELS ...	91
4.2.1	Prediction methodology	91
4.2.2	Methodology for determining outcome	92
4.3	COMPARISON OF PREDICTED AND MEASURED ENTITIES	95
4.4	SCRUTINY AND EVALUATION	118
5	SUBJECT: FLUX DISTRIBUTION - SITE SCALE	121
5.1	SCOPE AND CONCEPTS	121
5.2	METHODOLOGY FOR TESTS OF CONCEPTS AND MODELS ...	129
5.2.1	Prediction methodology	129
5.2.2	Methodology for determining outcome	130
5.3	COMPARISON OF PREDICTED AND MEASURED ENTITIES ...	130
5.4	SCRUTINY AND EVALUATION	144
6	SUBJECT: HYDRAULIC CONDUCTIVITY - BLOCK SCALE ..	149
6.1	SCOPE AND CONCEPTS	149
6.2	METHODOLOGY FOR TESTS OF CONCEPTS AND MODELS ...	149
6.2.1	Prediction methodology	149
6.2.2	Methodology for determining outcome	150
6.3	COMPARISON OF PREDICTED AND MEASURED ENTITIES ...	150
6.4	SCRUTINY AND EVALUATION	152
7	SUBJECT: CONDUCTIVE STRUCTURES - BLOCK SCALE ...	155
7.1	SCOPE AND CONCEPTS	155
7.2	METHODOLOGY FOR TESTS OF CONCEPTS AND MODELS ...	155
7.2.1	Prediction methodology	155
7.2.2	Methodology for determining outcome	156
7.3	COMPARISON OF PREDICTED AND MEASURED ENTITIES ...	157
7.4	SCRUTINY AND EVALUATION	160
8	SUBJECT: FLOW IN CONDUCTIVE STRUCTURE - BLOCK SCALE	163
8.1	SCOPE AND CONCEPTS	163
8.2	METHODOLOGY FOR TESTS OF CONCEPTS AND MODELS ...	163
8.2.1	Prediction methodology	163
8.2.2	Methodology for determining outcome	164
8.3	COMPARISON OF PREDICTED AND MEASURED ENTITIES ...	164
8.4	SCRUTINY AND EVALUATION	167
9	SUBJECT: AXIAL FLOW IN DISTURBED ZONE - BLOCK SCALE	169
9.1	SCOPE AND CONCEPTS	169

9.2	METHODOLOGY FOR TESTS OF CONCEPTS AND MODELS	169
9.2.1	Prediction methodology	169
9.2.2	Methodology for determining outcome	169
9.3	COMPARISON OF PREDICTED AND MEASURED ENTITIES	170
9.4	SCRUTINY AND EVALUATION	173
10	SUBJECT: HYDRAULIC CONDUCTIVITY - DETAILED SCALE	175
10.1	SCOPE AND CONCEPTS	175
10.2	METHODOLOGY FOR TESTS OF CONCEPTS AND MODELS	175
10.2.1	Prediction methodology	175
10.2.2	Methodology for determining outcome	176
10.3	COMPARISON OF PREDICTED AND MEASURED ENTITIES	176
10.4	SCRUTINY AND EVALUATION	179
11	SUBJECT: POINT LEAKAGE - DETAILED SCALE	181
11.1	SCOPE AND CONCEPTS	181
11.2	METHODOLOGY FOR TESTS OF CONCEPTS AND MODELS	181
11.2.1	Prediction methodology	181
11.2.2	Methodology for determining outcome	181
11.3	COMPARISON OF PREDICTED AND MEASURED ENTITIES	182
11.4	SCRUTINY AND EVALUATION	186
12	SUBJECT: DISTURBED ZONE - DETAILED SCALE	189
12.1	SCOPE AND CONCEPTS	189
12.2	METHODOLOGY FOR TESTS OF CONCEPTS AND MODELS	189
12.2.1	Prediction methodology	189
12.2.2	Methodology for determining outcome	190
12.3	COMPARISON OF PREDICTED AND MEASURED ENTITIES	195
12.4	SCRUTINY AND EVALUATION	196
PART 1 - APPENDIX 1 - OVERVIEW OF SECTIONS HYDRAULICALLY TESTED IN COREHOLES KAS02-08 AND KLX01		
PART 2 - GROUNDWATER CHEMISTRY		
1	SUBJECT: GROUNDWATER CHEMISTRY IN FRACTURE ZONES, SITE SCALE	1
1.1	SCOPE AND CONCEPTS	1
1.2	METHODOLOGY FOR TESTS OF CONCEPTS AND MODELS	3
1.2.1	Data collection	3
1.2.2	Evaluation and prediction	5
1.2.3	Methodology for determining the outcome	8
1.3	COMPARISON OF PREDICTED AND MEASURED ENTITIES	9
1.4	SCRUTINY AND EVALUATION	24
1.4.1	Major fracture zones	25
1.4.2	Test of different spatial assignment methods	28
1.4.3	Chemical and biological processes	46

1.4.4	Conclusions	50
1.5	BRIEF ANALYSIS OF ACCURACY AND CONFIDENCE	51
2	SUBJECT: QUALITY CHANGES (BLOCK SCALE REDOX EXPERIMENT)	53
3	SUBJECT: REDOX CONDITIONS AND WEATHERING, DETAILED SCALE	59
4	CONCLUSIONS	61
	PART 2 - APPENDIX 1 GROUNDWATER CHEMISTRY IN FRACTURE ZONES	
	PART 3 - TRANSPORT OF SOLUTES	
1	SUBJECT: SALINITY- SITE SCALE	1
1.1	SCOPE AND CONCEPTS	1
1.2	METHODOLOGY FOR TESTS OF CONCEPTS AND MODELS	1
1.2.1	Prediction methodology	1
1.2.2	Methodology for determining outcome	2
1.3	COMPARISON OF PREDICTED AND MEASURED ENTITIES	3
1.3.1	Salinity of the water flowing into the tunnel	3
1.3.2	Salinity in borehole sections	5
1.3.3	Salinity field	20
1.4	SCRUTINY AND EVALUATION	28
2	SUBJECT: NATURAL TRACERS, FLOW PATHS AND ARRIVAL TIME- SITE SCALE	31
2.1	SCOPE AND CONCEPTS	31
2.2	METHODOLOGY FOR TESTS OF CONCEPTS AND MODELS	32
2.2.1	Prediction methodology	32
2.2.2	Methodology for determining outcome	35
2.3	COMPARISON BETWEEN PREDICTION AND MEASURED ENTITY	39
2.3.1	Introduction	39
2.3.2	Results: Fracture zone NE-1	41
2.3.3	Results: Fracture zone NE-2	45
2.3.4	Results: Fracture zone NNW-4	47
2.3.5	Hydraulic connectivity	52
2.4	SCRUTINY AND EVALUATION	52

PART 4 - REFERENCES

EXECUTIVE SUMMARY

The report presents the comparison between groundwater flow, groundwater chemistry and transport of solutes, predictions and observations in the 700 - 2874 m section of the Äspö tunnel.

GROUNDWATER FLOW

Scope and concepts

The model comprises the following geometrical concepts:

- hydraulic conductor domains,
- hydraulic rock mass domains.

Hydraulic conductor domains are large two-dimensional features with hydraulic properties different from the surrounding rock. They are generally defined geologically as major discontinuities but in some cases they may mainly be defined by interpretation of results from hydraulic interference testing.

Hydraulic rock mass domains are geometrically defined volumes in space with properties different from surrounding domains (rock mass and conductors). They may either be defined by lithological domains or purely by interpretation of results from hydraulic tests.

The hydraulic properties of the hydraulic conductor domains and the hydraulic rock mass domains were characterized by means of a number of different hydraulic tests:

- airlift pumping of percussion drilled boreholes and 100 m sections of core drilled boreholes,
- pump testing and cleaning of borehole (performed directly after drilling),
- flow-meter logging,
- injection tests (packer spacing 3 or 30 m),
- interference tests,
- dilution tests,
- monitoring of water pressure in the rock-mass.

Long-term monitoring was also performed during the pre-investigation phase.

The hydraulic data collected during the construction were mainly:

- pressure build-up tests (single-hole test),
- interference test (tunnel boreholes used as sinks),

- dilution test (surface boreholes),
- monitoring of water pressure in the rock-mass,
- flow-meter logging or logging by inflow observation during drilling,
- observation of pressure responses in monitored boreholes during drilling of core holes,
- mapping of water-conducting and grouted fractures in the tunnel,
- measuring the water flow into the tunnel.

Hydraulic conductor domains (Major water-bearing zones)

The types of method and number of hydraulic tests used were mostly sufficient to define the hydraulic conductor domains near the Äspö HRL (*Figure 1*). However, the hydraulic tests in the coreholes were less extensive in the uppermost 100 m of the boreholes and due to this the interpretation became more difficult and uncertain. Standardized investigations should be performed in a consistent way in the entire borehole using a few methods. Specially designed tests may then be performed in parts of the borehole where a hydraulic conductor domain is interpreted as intersecting the borehole.

It is also valuable to have a good three-dimensional CAD system in which results from the investigations, the geological and hydrogeological model can be visualized during the investigations. An effective tool was not available during the pre-investigation and construction phases of the tunnel.

Hydraulic rock mass domains (Rock between the hydraulic conductor domains)

The statistical properties of the hydraulic conductivity of the hydraulic rock mass domains were estimated approximately correctly for southern Äspö with the methods used. It is judged that the effective values of the hydraulic conductivity of the rock mass domains between the major conductor domains or for lithological domains can be predicted if several boreholes penetrate the volume to be predicted. Extrapolation of results to rock volumes outside the investigated volume should be made with caution if the geological characteristics can be expected to be different from the investigated volume.

There are, however, a few problems concerning the evaluation of the properties of the hydraulic rock mass domains. It will be a cumbersome task to estimate properties if the rock mass is heterogenous on a large scale. Anisotropic conditions will also make it more difficult to perform relevant tests and evaluate the properties. There is a scale dependency that has been handled using data from a number of boreholes, with tests performed over different lengths in them, to formulate an empirical relationship. Efforts should be made to continue performing tests in a systematic way so that at least two test scales, besides tests in which the entire borehole is pumped, are used as long as no reliable method for scaling is available. More efforts should also be made to

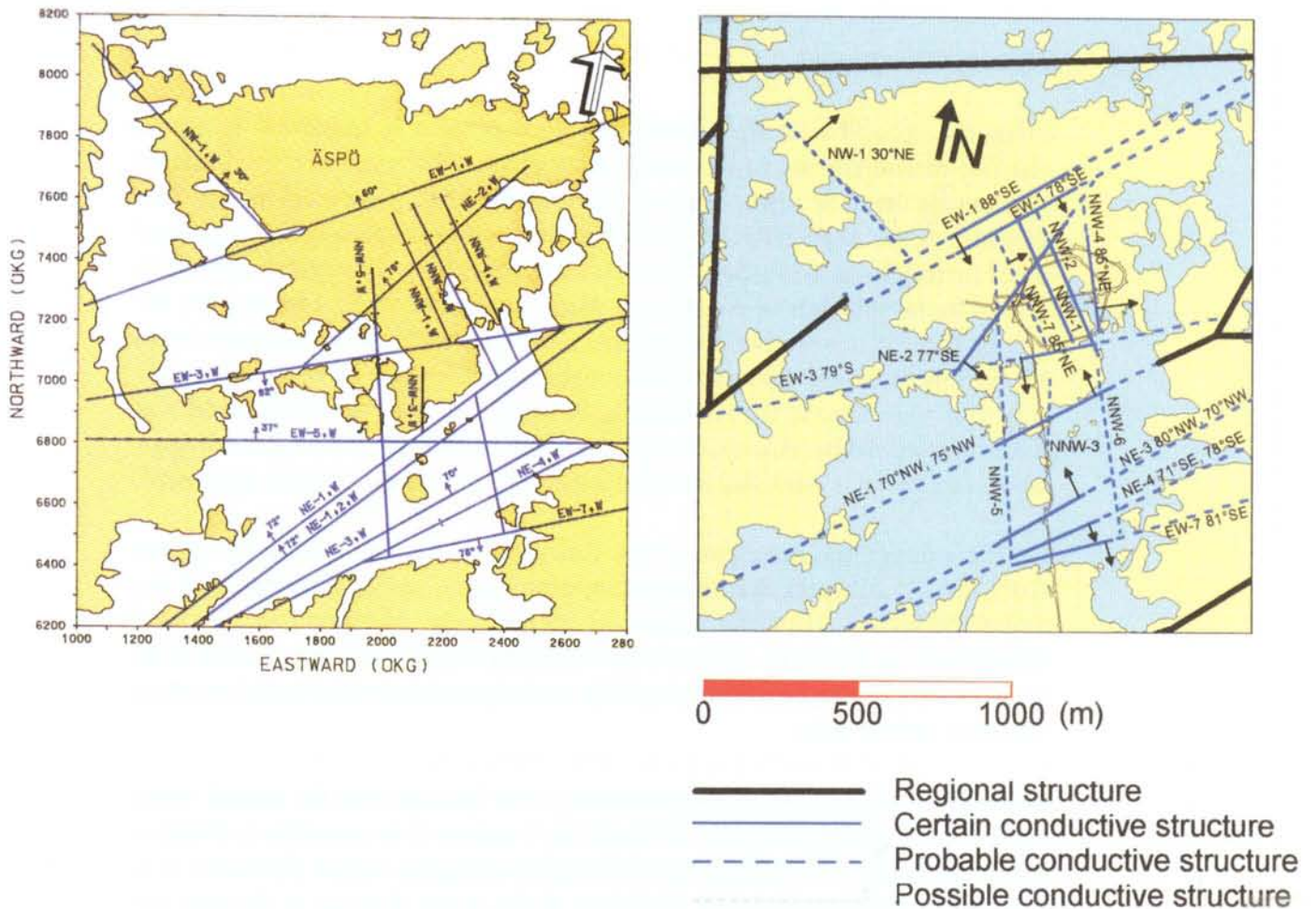


Figure 1. Left: Model 1990 of hydraulic conductors from the pre-investigation phase - site scale /Gustafson et al 1991/. Right: 1996 model of hydraulic conductors - site scale /Rhén et al, 1997b/.

develop a somewhat more realistic spatial correlation model for the hydraulic conductivity.

Methods

Hydraulic conductor domains and hydraulic rock mass domains

It is important to perform tests at different scales systematically in the boreholes, for scale relationships as mentioned previously, but also for the flexibility in the interpretation of how to divide the rock mass into hydraulic conductor domains and hydraulic rock mass domains. It is also important to perform larger scale interference tests both for defining hydraulic conductor domains and for calibrating and obtaining test cases for numerical groundwater models.

Flow into the tunnel

From the groundwater flow modelling view point it is important to obtain reliable measurements in time and space of the flow rates if more detailed simulations are to be made to test or calibrate the hydrogeological model. One problem at the Äspö HRL was the delay in the construction of the dams and other facilities for measuring flow rates from the dams. For practical reasons it was found difficult to construct a dam closer than about 150 m from the tunnel face, if it were not to interfere too much with the excavation work. Measurements of the flow into the tunnel can, and should be made in a better way than was done at the Äspö HRL, but it should also be remembered that more detailed measurements in space and time would also have a great impact on the contractor's work and also that a dam of good quality is quite expensive.

On the average the main part of the flow into the tunnel is from the tunnel floor, which indicates that the hydraulic properties are different around the tunnel periphery. However, there are rather large variations in the flow distribution on the floor, walls and roof along the tunnel, and there seems to be a more even flow distribution around the tunnel periphery along tunnel sections with low inflow rates.

The quantification and characterization of the leakage into the tunnel when mapping the walls and roof is difficult but it seems to be possible to obtain a rough estimate of the quantity and distribution along the tunnel. However, it is difficult to make quantitative estimates of the water flowing in through the tunnel walls and, frequently, also identifying leaking fractures and locating leaks along fractures.

If the flow into the tunnel is quantified by just mapping flowing features, neglecting dripping features and moisture on the rock surface, this seems to give around 80% of the total flow from the walls and roof. The mapping and quantifying of flowing features only in the tunnel can be done rather quickly and gives then approximately the right flow rate through walls and roof.

Water pressure around the tunnel

The pressure measurements clearly show the heterogeneity of the rock mass. They indicate that there is a sparsely connected fracture network in the rock mass, otherwise the pressure distribution would have been much more regular. The measurements also show that high water pressures occur rather frequently just a few metres from the tunnel wall. The variability of the pressure affects the possibility of grouting the fracture system close to the tunnel.

Another evident conclusion is that large samples are needed to obtain a reliable estimate of the pressure distribution near the tunnel. In order to obtain better resolution of the pressure increase outside the tunnel wall several measurement sections in each borehole would also have been preferred. This would have provided a more certain definition of a representative point for the pressure

measurements. But this would also have been more expensive as it would have been necessary to use a more complicated packer system.

The pressures were higher in the rock that had been reinforced compared with the non-reinforced rock. This clearly indicates that there is a difference in the hydraulic resistance (skin factor) around the tunnel, and that a large part of the resistance must be within a few metres (5-9 m) from the tunnel wall, considering the representative point for the pressure measurements.

Skin factor for the tunnel

It is very difficult to estimate the skin factor around a tunnel. The heterogenous nature of the rock mass makes it difficult to establish a pressure profile around the tunnel that is useful for the calculations. Shorter measurement sections at several distances from the tunnel wall would have been preferred, but as the variability of the pressure is large due to the heterogeneity there must also be a large number of measurement sections to obtain a reliable estimate of the pressure distribution.

There are also some difficulties, besides the problems with the pressure measurements, with data needed for the calculations of the skin factor. One approach assumes homogenous conditions and a simple boundary condition. They may be neither homogenous conditions nor a simple boundary condition. The other approach assumes that it is possible to estimate a representative value of the hydraulic conductivity (or transmissivity, if it is a hydraulic conductor domain) for the undisturbed rock mass around the tunnel for a specified tunnel section and also that the flow into the tunnel is measured for the same tunnel section.

Despite the difficulties outlined above it seems that for prediction purposes, before any flow rates into the tunnel are known, it is reasonable to choose a skin factor between about 0 and 10 for the rock mass outside the hydraulic conductor domains for a sensitivity study. The skin factor for the hydraulic conductor domains must be calibrated on the basis of an inflow assumption.

Models

The stochastic continuum approach chosen in 1990 involved state-of-the-art modelling approaches used at that time. The model approach used in 1990 was both useful and feasible. It has been shown to be a model that is rather easy to develop and, in that respect, a good choice. The international co-operation within the Task Force on Modelling of Groundwater flow and Transport of Solutes has, however, also shown that several approaches can be used to obtain results that reproduce the pressure observations fairly well.

For the future, new developments are needed so that correlation models can be estimated from the field data, and also implemented in the numerical models, in order to generate the hydraulic conductivity field in a more realistic way. The

hydraulic conductivity field in the models should also be conditioned against available field data, which also demands developments of the numerical models.

New knowledge from the tunnel

During the construction work anisotropic conditions of the rock mass were established. These were based on the systematic hydraulic testing along the tunnel ramp, and, as the tunnel was made in a spiral on southern Äspö, the possibility of testing the anisotropy of the rock mass became quite good.

The mapping of grouted fractures also gave good indications of fracture sets that were hydraulically active on a local scale.

The probe holes used for systematic hydraulic testing along the tunnel were also used for pressure measurements. These measurements give a good picture of the heterogeneous nature of the crystalline rock, shown as a large variability of the pressures close to the tunnel.

The investigation along the tunnel also increased the level of detail in the model. The new data resulted in more precise dips of zones intersecting the tunnel and more data on the transmissivities for the zones.

Summary of prediction and outcome results

A summarized evaluation, based on data from a comparison between prediction and outcome is presented in *Table 1* and *Table 2*. The (+) sign represents the most common parameter result. Our ability to predict a certain subject (parameter) at Äspö is shown by the number of outcome results inside the predicted range. Results outside the predicted results are discussed with respect to the reason for the deviation,

The hydrogeological concepts have mostly been found to be relevant. The usefulness of individual subjects, however, can be questioned.

Table 1. Comparison between prediction and outcome. The '+' sign represents the most common parameter result.

Subject	Site scale		Block scale		Detailed scale		Comments
	Within predicted range	Outside predicted range	Within predicted range	Outside predicted range	Within predicted range	Outside predicted range	
Major water-bearing zones							
<i>Geometry</i>							
Position in or close to tunnel	+						Interpretation based mainly on geology but interference tests were important for defining the NNW structures. The important zones were approximately at the predicted positions and a few corrections of others were made.
<i>Properties</i>							
Transmissivity	+						The most transmissive zones were within the predicted range.
Hydraulic rock mass domains							
<i>Geometry</i>							
Depth dependance	+						No depth dependance was predicted down to 500 m depth.
<i>Properties</i>							
Hydraulic conductivity	++		+*		+*		Site scale: Outside range below the Baltic Sea south of Äspö. Close to the predicted range for depth level 200-400 m. Block scale: Two of six predictions within range. Detailed scale: Outcome both within and just outside predicted ranges. The outcome of the difference between the lithological units was as predicted.
Boundary conditions and pressures							
	++						Pressures were predicted using a groundwater flow model.

* Uncertainties mainly due to anisotropic and heterogenic conditions.

** No strict ranges were given in the predictions. However, the results from simulations with two different skin factors for the tunnel are here used as prediction ranges and a judgement was made if the results were relatively close to the predicted range(=within predicted range) or not (outside range). The predictions generally comprise both point estimates and a confidence interval at a certain confidence level. These point estimates and confidence intervals are obtained from sample properties. Predicted ranges are the results of expert judgements. The confidence level was 95% for the confidence limits of the point estimate. 'Range' in the table above may be the confidence limits or the ranges based on expert judgements.

Table 2. Comparison between predictions and outcomes. The ‘+’ sign represents the most common parameter result.

Subject	Site scale		Block scale		Detailed scale		Comments
	Within predicted range	Outside predicted range	Within predicted range	Outside predicted range	Within predicted range	Outside predicted range	
Flow into the tunnel	(+)						Fairly close to predictions. The flow rate is more dependent on the grouting in the tunnel than on the hydraulic properties of the rock mass and zones.
Flux distribution		+					The directions of the predicted changes of flux rates in the borehole sections are generally as the measured ones. Predicted rates are generally much larger than those observed. Long borehole sections for measurements are probably one of the reasons.
Conductive structures			+	*			The distance between hydraulic conductors along boreholes with a transmissivity greater than a specified value was predicted.
Flow in conductive structures			+	**			Flow distribution around the tunnel periphery was predicted.
Pressure around the tunnel			+			+	The variability in the measured pressure is large.
Point leakage							
<i>Wet tunnel area</i>						+	Wet tunnel area by rock type
<i>Inflow characteristics</i>						+	Characteristics: Flows, drips or moisture to sporadic drips.
<i>Inflow types</i>						+	Types: Bolthole, node, extensive, point or diffusive.

* Uncertainties mainly due to anisotropic and heterogenic conditions.

** No strict ranges were given in the predictions. However, the results from simulations with two different skin factors for the tunnel are here used as prediction ranges and a judgement is made if the results are relatively close to the predicted range(=within predicted range) or not (outside range). The predictions generally comprise both point estimates and a confidence interval at a certain confidence level. These point estimates and confidence intervals are obtained from sample properties. Predicted ranges are expert judgement. The confidence level was 95% for the confidence limits of the point estimate. ‘Range’ in the table above may be the confidence limits or the ranges based on expert judgements.

Conclusions

- The hydraulic test methods used can in general be said to be adequate for the models made. Minor problems are that the results are to some extent dependent on the equipment used and thus method developments during a project can possibly affect the results to some extent. It is also difficult to get reliable results from low conductivity sections of a borehole because of the elasticity of the equipment and also because of pressure oscillations.
- To construct a reliable model it is important to perform tests on different scales systematically in the boreholes, both for scale relationships but also to gain flexibility in the interpretation of how to divide the rock mass into hydraulic conductor domains and hydraulic rock mass domains. It is also important to perform large-scale interference tests for modelling purposes.
- For the interpretation of the hydraulic conductor domains it is important to work in close co-operation with the geologists. It is also important to have a good three-dimensional CAD system in which results from the investigations, the geological and the hydrogeological model can be visualized during the investigations.
- A site that is heterogenous on a large scale and anisotropic makes the investigations and evaluation work more extensive and difficult. However, this character may only be established after quite extensive investigations.
- It is probable that there is some spatial correlation within the hydraulic rock mass domains due to some large and more transmissive features not accounted for in the present concept used. Efforts should be made to develop a more realistic spatial correlation model for the hydraulic conductivity.
- The groundwater flow models used work satisfactorily in several aspects but developments are still needed. For example, new developments are needed so that spatial correlation models set up can be used to generate the hydraulic conductivity field in a more realistic way and also to condition the hydraulic conductivity field against field data. Developments are needed to achieve more efficient handling of input data and calibrations and also to obtain better visualization of the results.
- Interference tests can be rather time-consuming in planning, execution, processing of data and evaluation of data. It is very important to plan interference tests and other activities, which may cause pressure responses (for example drilling) so that they do not interfere with each other. If other tests or activities causes pressure responses, they may ruin the interference test.

- Measurements and evaluation methodologies of dilution rates should be further studied to obtain more confidence in how to calculate more reliable flow rates in the rock mass from the dilution rates.
- The measurement intensity of the monitoring of the water pressures in space and time is judged to be mainly sufficient. However, it would have been preferable to have had somewhat more reliable measurements of the natural conditions. To some extent the natural conditions were disturbed by performance of the investigations, mainly the hydraulic tests.
- More reliable measurements of the absolute pressures along the boreholes at natural (undisturbed) conditions should also be made to provide better possibilities for interpretation of the water chemical sampling, especially in open boreholes.

GROUNDWATER CHEMISTRY

Scope and concepts

The hydro-geochemical properties of the Äspö site were characterized by samples from different points in the rock mass and fracture zones. The hydraulic properties of the water conducting fractures vary over several orders of magnitude. This in combination with the prevailing hydraulic gradient has a large influence on the chemistry of the groundwater in the different zones.

Predictions of conditions to be observed during the construction phase were made along two different lines. The main line - the one presented here - considers a static situation in which the conditions described in the model of the undisturbed Äspö site are also the conditions to be found in the tunnel phase. The other line is to base the conditions to be found in the tunnel on scoping calculations of what changes the inflow to the tunnel will have on the groundwater composition. This transient prediction is reported in *Transport of solutes*.

The spatial assignment was based on a combination of expert judgement and principal component analyses. Later, during the construction phase, several other spatial assignment methods were tested.

As a basis for the groundwater chemistry predictions it was assumed that the first sample collected at the tunnel front would represent the undisturbed conditions, which would be similar to those that prevailed during pre-investigations. The predicted conditions should therefore be compared with the very first data collected at the tunnel front.

Data collection

During pre-investigations groundwater samples were collected at several occasions. Samples were collected during interruption of the drilling, during hydraulic interference pumping tests and during separate groundwater sampling campaigns. The data obtained in the different sampling campaigns were analysed for main constituents, trace elements, isotopes, pH and Eh. The sampling procedures are quite different from each other and so the quality of the data varies. Thus, the usefulness of the data for modelling purposes varies. The analytical protocols for groundwater sampling during the pre-investigations and the construction phases are listed in *Table 3*.

Figure 2 presents the different sequences in the pre-investigation phase, used to evaluate the hydrochemistry.

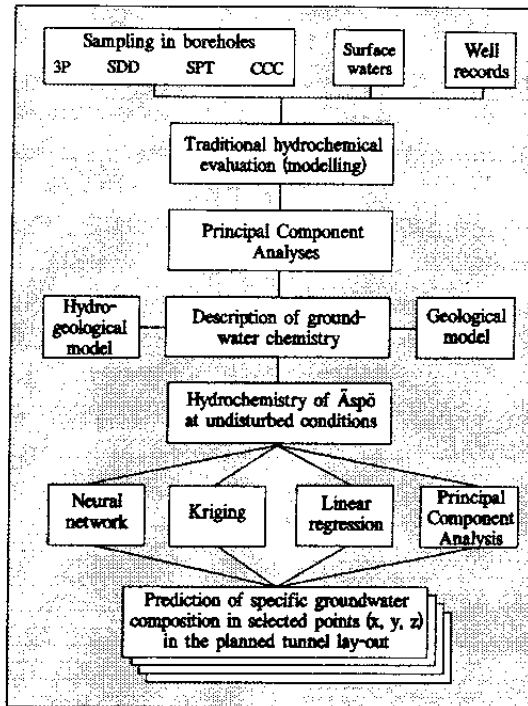


Figure 2. A schematic presentation of the methods used for the hydrochemical investigations. '3P', 'SDD', 'SPT', 'CCC' and 'Surface Waters' complemented by well records comprise the sample collection and chemical analysis made by the Äspö HRL project, see *Table 3*.

Table 3. Chemical analyses of samples collected on different occasions at Äspö.

Constituents	3P	SDD	SPT	CCC	Tunnel 1	Tunnel 2
pH	3	-	1	1	0	0
Eh	-	-	-	1	-	4
Sodium	2	3	1	1	-	0
Potassium	2	3	1	1	-	0
Calcium	2	3	1	1	-	0
Magnesium	2	3	1	1	-	0
Chloride	2	3	1	1	0	0
Bicarbonate	2	3	1	1	0	0
Sulphate	2	3	1	1	-	0
Silica	-	3	1	1	-	0
Iron (total)	-	-	1	1	-	0
Iron(II)	-	-	-	1	-	0
Manganese	-	-	1	1	-	0
Strontium	-	-	2	2	-	0
Lithium	-	-	3	3	-	0
Sulphide	-	-	1	1	-	4
Bromide	-	-	3	3	-	4
DOC	-	-	2	2	-	4
Colloids	-	-	-	4	-	-
Uranium	-	-	3	3	-	4
Uranium isotopes	-	-	3	3	-	4
Oxygen-18	3	-	2	2	5	0
Deuterium	3	-	2	2	5	0
Carbon-14	-	-	3	3	-	-
Carbon-13	-	-	-	-	-	4
Strontium-87 -	-	-	-	-	4	-
Sulphur-34	-	-	3	3	-	4
Dissolved gas	-	-	-	3	-	4

3P	=	sampling of shallow percussion drilled holes, pumping for 12 hours
SDD	=	sampling during drilling of deep, cored holes, pumping for a minimum of 1 hour
SPT	=	sampling during pumping tests, pumping for three days
CCC	=	complete chemical characterization in separate campaigns, pumping for ten days
Tunnel 1	=	sampling at the end of the probe hole drilling in the tunnel
Tunnel 2	=	repeated sampling in the selected probe holes = the constituent has not been analysed
0	=	analyses are made each time a sample is collected
1	=	analyses are made daily during a pumping campaign lasting for at least three days
2	=	samples are collected for analyses on a few occasions during a pumping period
3	=	samples are collected at the end of a pumping period
4	=	samples are analysed only when some specific questions arise
5	=	stored samples are analysed afterwards if specific needs arise

Prediction methodology

Initially (before tunnel construction was started) the predictions were made by a combination of principal component analysis and expert judgement. The predicted values were fairly easy to calculate, but the variability had to be estimated. At an early stage of the tunnel construction phase, it was evident that there were many disagreements between predictions and observations. It was not clear why there were large discrepancies, because sometimes, in the case of NE-1, for example, there was agreement between predictions and observat-

ions. However, one explanation could be that an unsuitable method had been used for the predictions. Therefore, tests of different interpolation methods were made to see which could be used to perform spatial assignment of groundwater chemistry properties. The tested tools were:

- Linear regression analysis
- Principal component analysis
- Kriging
- Neural networks

The multiple *Linear regression* model is based on the least-square method. The linear regression analysis minimizes the squared difference between the observations and a straight line as a function of the position (x,y,z). The basic requirements of the model are that the observations are independent, normally distributed and have the same variance. In order to give a good correlation all observations need to be linearly dependent on the position (x,y,z).

Multivariate (principal component) analysis is a mathematical way of treating the different parameters all together. The values to be predicted could be considered as missing data in a matrix. The principal components are computed directly from the known data values as a linear function of all the underlying parameters. The principal components are independent and extrapolated to the position (x,y,z).

Kriging is an interpolation method based on a non-linear correlation function. The basic assumption is that the modelled properties are continuous and that positions physically close to each other also have properties numerically close to each other. Thus, an observation physically close to a position to be predicted has a larger weight than an observation which is physically further away from the position to be predicted.

Neural networks contain artificial neurones organized in layers and connected to each other in a way simulating the human brain. The neural network is non-linear, highly interconnected and is therefore able of capturing complex relationships between input and output. Thus, neural networks possess an ability to treat complicated non-linear problems, generalize, analyse large amounts of data, interpolate and optimize data.

Methodology for determining the outcome

The groundwater chemical predictions were compared with the samples collected from probing holes along the tunnel. Samples have been taken from all boreholes with an inflow above 1 l/min. Analysis were performed according to *Table 3*. Mainly data collected close to the tunnel face was used in the comparison.

Predictions compared with measurements

Prediction tools

The careful testing of the different tools shows that there are differences in the results which could be related to a systematic difference in the way the models are constructed. Some general conclusions are:

- Neural networks and kriging reflect surprisingly well the variations in the concentrations and are therefore also closer to the observations. Kriging is generally closer than the neural network but the differences are small.
- The principal component analyses and linear regression analyses give a larger difference between predicted and observed concentrations than the other two methods. This is probably due to the fact that these methods only include linear combinations, in this case the predicted value as a linear function of the data from coordinates (x,y,z).

Figure 3 illustrates the predicted and observed chloride concentration along the tunnel for all the tested methods.

Chemical and biological processes

The groundwater composition was changed by the **grouting materials** which were used to seal off and reduce the water inflow to the tunnel. The effect of the grouting is very distinct, a large increase in the pH-value and the potassium concentration in the groundwater. However, only a few of the grouting occasions have given an observable effect on the water composition in the boreholes.

Biological processes were not considered to influence the chemistry. All predictions were based on chemical reactions and the mixing of water with a different composition. In the results of the sampling made during tunnel construction phase, it is predominantly the bacterial processes which yielded a groundwater chemistry different from the expected one.

Summary of prediction and outcome results

The predictions made for the deterministic fracture zones were based on a static approach, which was considered to be applicable to the purpose. We considered the situation from the pre-investigations to be valid at least until the time when the tunnel excavation reached the point of sampling. We now have strong reasons to believe that the tunnel construction affected the groundwater situation ahead of the tunnel front. Therefore the characterization of a rock volume must be done from surface boreholes before the excavation starts.

The water inflow to the tunnel during the construction phase changes significantly even when the salinity does not change a lot. The reason for this

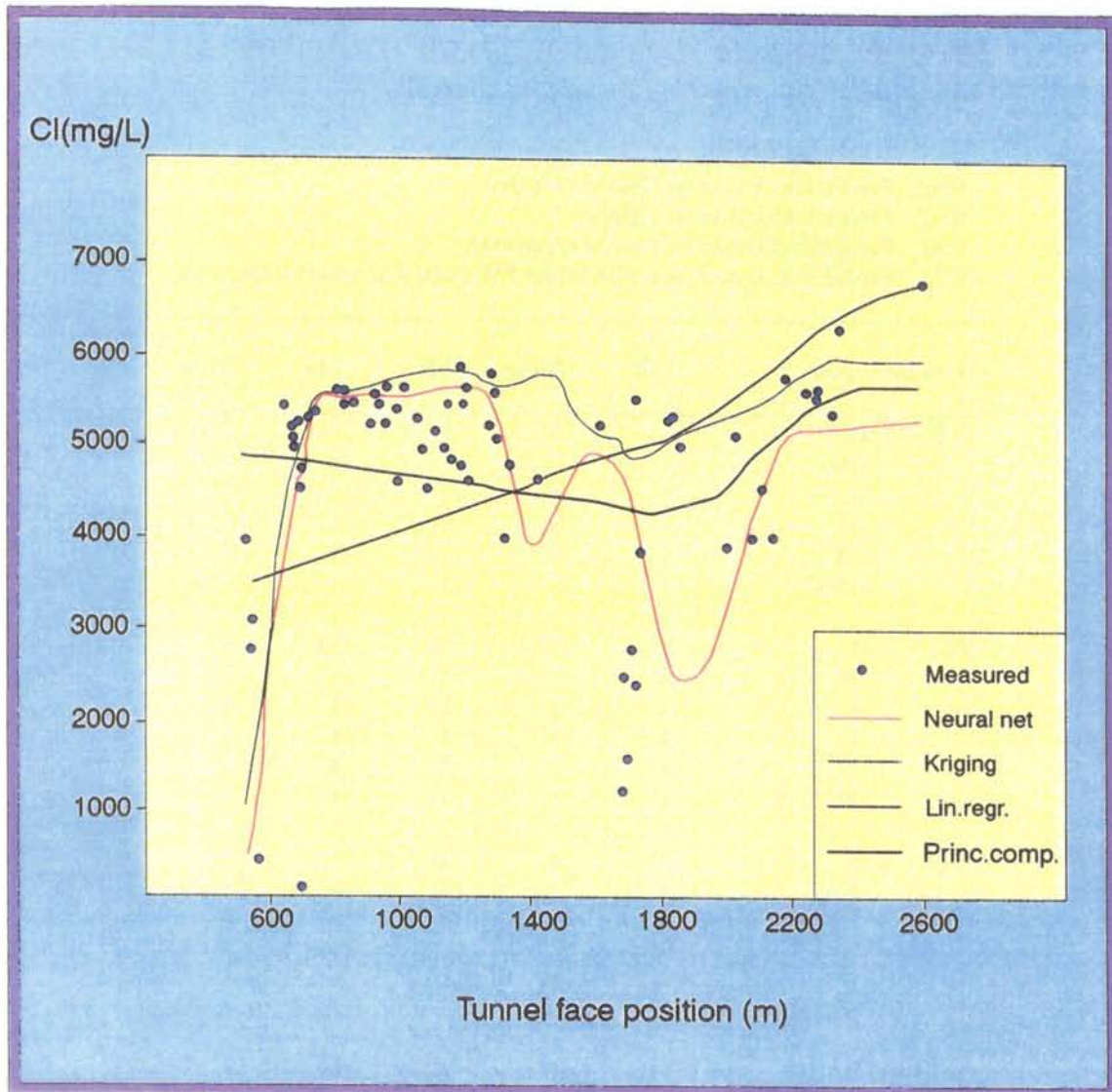


Figure 3. Predicted and observed concentrations of chloride calculated by different mathematical methods, but with exactly the same input data.

is that there are several end-members involved in the mixing process. There are deep saline, Baltic Sea water and altered marine water which all contain considerable amounts of chloride. Therefore a shift in the proportions of e.g. deep saline and Baltic Sea water is not seen in the salinity.

The concept of static conditions for predicting the groundwater chemistry during construction phase has several weaknesses. The justification of using the concept is nevertheless that it is the only way we could utilize the data and knowledge of the pre-investigations to assess the usefulness as a tool to test the pre-investigation methodology.

Table 4 summarizes the scores where the prediction closest to observation gets one point, the second two points etc. At the end all the scores are added and the prediction method having the lowest scores is considered to be the most suited.

Table 4. Results of scores summing for the different fracture zones. Bold figures indicate the lowest score, i.e. best fit.

Init: Initial predictions

Neur: Predictions based on Neural network

Kri: Predictions based on Kriging

Lin: Predictions based on Linear regression

PCA: Predictions based on multivariate Principal Component Analysis

Fracture zone	Init	Neur	Kri	Lin	PCA
NE-1 Sum:	10	11	9	16	22
Na	1	1	1	5	4
Ca	3	4	1	1	5
Cl	1	1	4	5	3
SO ₄	4	1	2	2	5
HCO ₃ 1	4	1	3	5	
NE-2 Sum	21	12	9	20	10
Na	5	2	3	4	1
Ca	4	2	1	5	2
Cl	5	3	1	4	2
SO ₄	5	2	3	3	1
HCO ₃ 2	3	1	4	4	
NE-3 Sum	17	7	6	12	17
Na	3	1	1	4	5
Ca	5	3	2	1	4
Cl	5	1	2	4	3
SO ₄	4	2	1	3	5
HCO ₃ --	--	--	--	--	
NE-4 Sum	19	13	11	15	14
Na	1	4	2	2	4
Ca	5	4	2	3	1
Cl	5	1	1	3	3
SO ₄	4	3	1	2	5
HCO ₃ 4	1	5	3	1	
EW-7 Sum	18	18	12	6	18
Na	3	3	1	1	5
Ca	5	4	3	2	1
Cl	5	4	3	1	2
SO ₄	3	3	2	1	5
HCO ₃ 2	4	3	1	5	
NNW-4 Sum	16	11	11	10	8
Na	5	2	2	4	1
Ca	5	1	4	1	3
Cl	5	3	1	3	2
SO ₄	1	5	4	2	2
HCO ₃ --	--	--	--	--	
Sum of all const.	101	72	58	79	89
Sum of chloride	26	13	12	22	15

Conclusions

There are simple ways of checking the predictive ability of a model. The simplest is to compare the prediction and the outcome to see if they agree. In practice this was the intention when the predictions of construction phase groundwater chemistry were made on the basis of the pre-investigation models. Some general comments on this approach are:

- The initial predictions were based on a combination of expert judgements and principal component analyses. However, the range was only estimated by expert judgements. It seems now that the estimated ranges were too narrow, because the estimate did not include the natural variability, only the inaccuracy in the data.
- When different mathematical methods were tested, the range of variation was calculated on the basis of the variation in input data. The same variation was expected for the observations. The result is that most of the observations fall within the predicted ranges. In some cases the range of variations is so wide that it could be questioned whether the prediction is meaningful or not.

The approaches to consider the hydrochemistry as a static system reflecting the conditions of the pre-investigations are of course dubious. However, by selecting a suitable predictive tool, kriging or neural networks, the observations all fall within the predicted ranges. It is therefore possible to predict a repository rock volume on the basis of pre-investigation data. Observations must then be made in a way to be comparable to predictions, perhaps through long probing holes in the tunnel front.

The approach of predicting the groundwater composition to be observed during construction might not be worthwhile for a real repository anyway. The reason is that too many conditions which will affect the outcome cannot be foreseen. Also the need for predictions is not urgent, since the chemical conditions during construction are expected to be different from the conditions prevailing after closure of the repository. These conditions are important and probably more close to the initial undisturbed conditions. Therefore, it is important to obtain a good description of the chemical conditions during the pre-investigations when the groundwater system has not been mixed up by drawdown into excavated tunnels. A carefully planned and performed site investigation programme can fulfill such requirements.

Quantitative predictions of groundwater composition are sometimes useful for planning construction work. The salinity of the groundwater has a severe impact on the corrosion of steel constructions in the tunnel. Such predictions could however, be made as quantitative estimates of the salinity, for instance.

If hydrochemical predictions were to be made at Äspö, or elsewhere, they would be based on the concept of mixing and include the mixing proportions of the identified and selected end-members and reference waters. These predictions would have two different purposes. One to assess the long-term

performance issues and the second to assess the groundwater flow model with the mixing caused by the tunnel draw-down.

TRANSPORT OF SOLUTES

Scope

Studies of the transport of solutes have focussed on two large experiments, that give relevant insights into this subject - the long-term pumping and tracer test LPT-2 conducted in 1990-1991 and the study of the flow of saline water during the tunnel excavation.

A few attempts were made during the pre-investigation and construction phases to estimate the flow porosity of the rock mass. For example, prior to construction a combined long-term pumping and tracer test (LPT-2) was conducted to test the hydraulic connectivity of hydraulic conductors and to derive estimates on flow porosity. During the construction period some efforts were directed to the use of other types of natural tracers as well as to derive transport parameters for non-sorbing transport. However, more tests need to be performed to obtain data on the flow porosity and other transport parameters.

Prior to construction, scoping calculations were made to assess the change of salinity in the groundwater as a consequence of the drawdown caused by construction of the facility. When the flow paths in some major zones (from the surface, the sea and deep down in the rock) are compared with the water chemical composition of the water flowing into the tunnel and the water found in the Baltic Sea, the calculated results are in fair agreement with the measured values.

Predictions compared with measurement

Salinity

Based on the pre-construction *Model 90* and assessing the impact of excavation response on the flow field, changes in salinities were modelled. Under undisturbed, natural, conditions the maximum depth of the freshwater layer was predicted to some 200 m and the measurements indicate a maximum depth of about 250 m (see *Figure 4*). Observations in boreholes from the surface show that water with a salinity of 17000 mg/l under undisturbed, natural, conditions was found at a depth of about 700-800 m. A salinity of 8000-10000 mg/l under undisturbed, natural, conditions was found at a depth of 400-500 m.

After excavation of the tunnel, water in short boreholes drilled from the tunnel at a depth of about 360 m showed a salinity of about 17000 mg/l. Minor changes in the salinity were observed in boreholes at some distance from the tunnel. The predictions made using the numerical model also indicated an up-coning of saline water (see *Figure 5*). The sections in *Figures 4 and 5* showing the measured values are based on interpolation of the measured values from

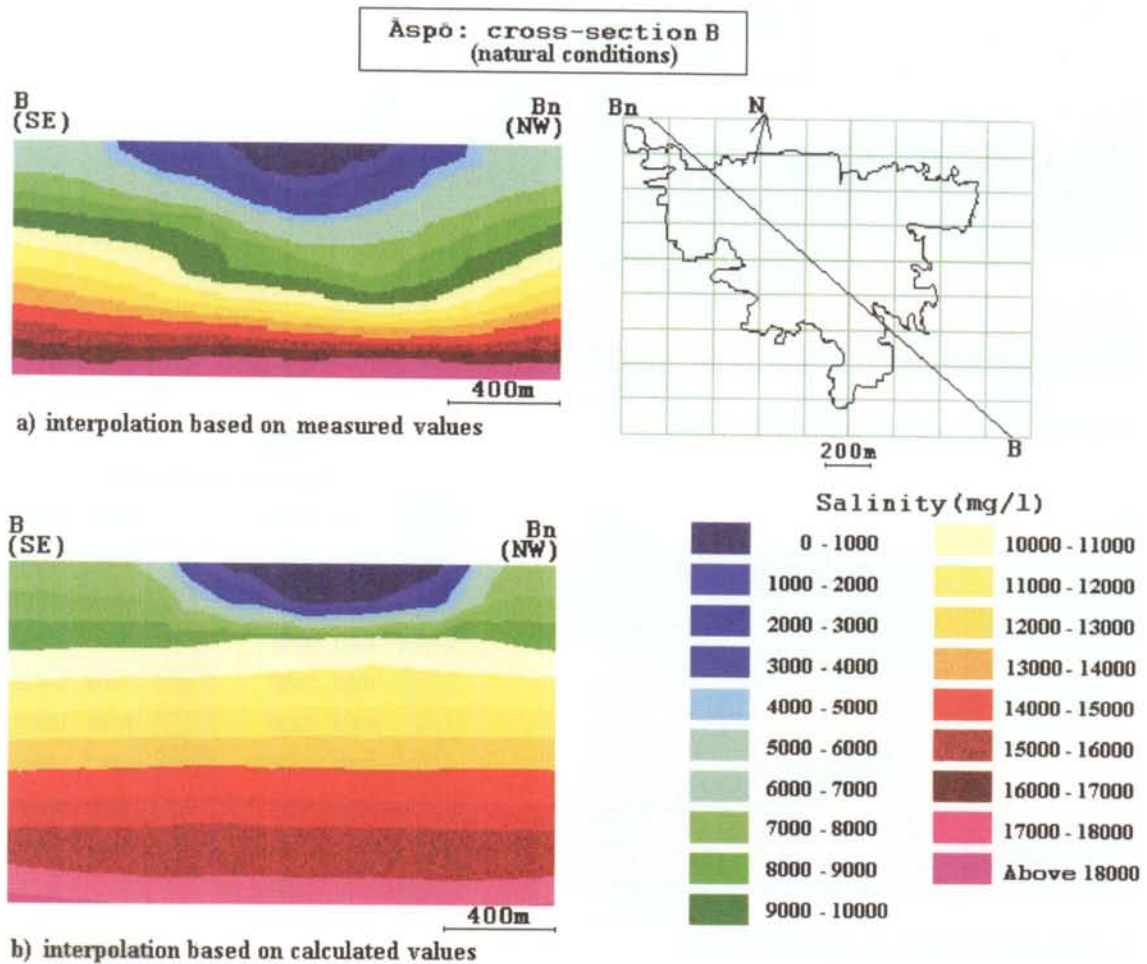


Figure 4. Salinity shown for a vertical section through Äspö from NW to SE. Ambient conditions. Numerical simulations (bottom) shown down to a depth of 1250 m. Measured values (top) based on interpolation, shown down to a depth of 850 m = the deepest measurement point. Salinity in mg/l.

Baltic Sea water, meteoric water (on land), 29 borehole observations during the pre-investigations and 37 borehole observations during construction. The measured values are concentrated in the central part of the figures and mainly above 600 m depth. Outside this region the interpolated values should be considered uncertain. The numerical model, *Model 90*, was a stationary simulation.

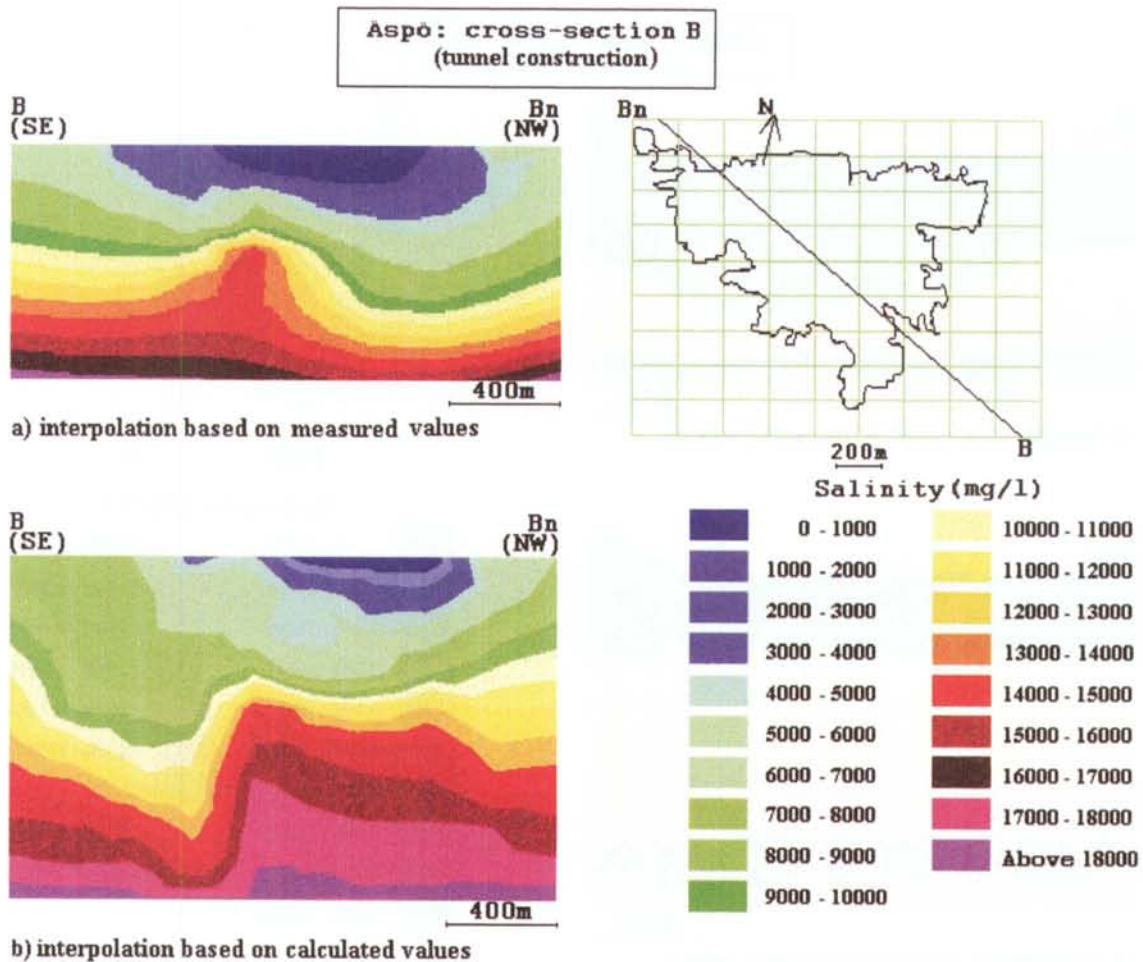


Figure 5. Salinity shown for a vertical section through Äspö from NW to SE. After construction. Numerical simulations (bottom) shown down to a depth of 1250 m. Measured values (top) based on interpolation, shown down to a depth of 850 m = the deepest measurement point. Salinity in mg/l.

Natural tracers

The proportions of different water types, (reference waters, such as glacial, deep saline, Baltic Sea and meteoric) were evaluated from samples collected in the main hydraulic conductors on several occasions during construction. The results can be used to assess the hydraulic connectivity and flow direction in the zones as the proportions of the reference waters change with time in the zones. The conclusions from the data are that fracture zones NE-4, NE-3, NE-1 and NNW-4 are connected to the Baltic Sea. Fracture zone NE-2 has good contact with the deep saline water. Gradually there is a complete mixing situation in the fracture zones, and it is quite clear that the flow directions are changing during the construction phase.

In future site investigations, more emphasis should be given to the natural tracers as a means of understanding the hydraulic connectivity. The technique developed for evaluating the groundwater types and proportions can be utilized.

Methods

It is important to have a sampling strategy that gives a reasonable number of points in space where time series are established for natural conditions and for the construction phase of the important chemical constituents. This forms the basis for evaluation and simulation of flow paths and flow times on a large scale. It is also important to measure the flow rates into the tunnel sections during construction and the chemical composition of the water flowing into the tunnel sections.

Large-scale tracer tests are to some extent difficult to perform and interpret but are useful to obtain information on large-scale connectivity. Test methods and methodology for evaluation have to be better developed to obtain relevant transport parameters. Work of this kind has already started at the Äspö HRL.

A few deep boreholes for sampling of groundwater and hydraulic tests are also needed to support the modelling of transport of solutes, and also groundwater flow and groundwater chemistry.

Summary of prediction and outcome results

A summarized evaluation, based on data from comparisons between calculations and outcomes is presented in *Table 5*. The '+' sign represent the most common parameter result. The results are discussed briefly below.

Salinity

It was possible to reproduce approximately the salinity field by numerical simulations with the groundwater flow model and the material properties assumed for the transport of solutes. As regards the transport of salt the simple approach used seems to work satisfactorily. However, more realistic descriptions of material properties and boundary conditions should be tested in the future.

Transport parameters and hydraulic connectivity

The LPT2 test was performed on a large test scale, several 100 m, and several hydraulic conductor domains were tested. As a connectivity test it was useful but the evaluation of the transport properties was more difficult.

Flow paths and arrival times

The combined effect of sparsely made predictions (with only a few points in tunnel and surface boreholes with complete time series of chemical, head and flow data) together with changed tunnel lay-out, revised fracture zones and changed chemical end-members, makes evaluation of prediction reliability cumbersome. However, the overall conclusion is that the predictions made during the pre-investigation as a whole are in accordance with the outcome, although the tunnel breach of zone NE-1 changed the transport of solutes and chemical composition in zones NE-2 and NNW-4 to a larger extent than was predicted. The surface type of waters also penetrated the fracture zones to a lesser extent than expected from the predictions.

Flow paths and arrival times were not specifically assessed, mainly because these subjects were not particularly important at this stage. However, it may be concluded that the models for calculation of flow paths and arrival times must be further developed.

Table 5. Comparisons between predictions and outcomes. The ‘+’ sign represent the most common parameter result. (+): Results only based on scoping calculations.

Subject	Site scale		Comments
	Within range	Outside range	
Salinity			
<i>In boreholes</i>	+ **		
<i>Saline interface</i>	+ **		
Flow paths	(+)		The flow paths in the groundwater flow model do not contradict the groundwater chemical measurements in the tunnel boreholes, surface boreholes or Baltic Sea.
Arrival time	(+)		A few results based on the groundwater chemical measurements in the tunnel boreholes indicate transport times in the same range as estimated using the groundwater flow model.
Natural tracers	-	-	A systematic scrutiny of the separate measurement points could not be made (see text).

** No strict ranges were given in the calculations. However, the results from simulations with two different tunnel skins are here used as prediction ranges and a judgement is made as to whether the results are relatively close to the predicted range (=within predicted range) or not (outside range).

Conclusions

- The multivariate groundwater mixing and mass balance modelling concept M3 seems to be one of the tools that can be useful for the interpretation of the flow paths and transport times. Another tool is of course a groundwater flow model for calculations of flow paths in the rock mass that can be compared to the multivariate groundwater mixing and mass balance modelling. However, there is still much work to be done to improve the integration between the groundwater flow, groundwater chemistry and transport of solutes models. Work is on-going.
- Tracer tests are useful for checking the connectivity within and between hydraulic conductor domains. At a relatively small scale, about 50-100 m, it seems possible to get rough estimates of the flow porosity and dispersivity within a hydraulic conductor domain. At larger scales it is difficult to evaluate the transport properties but the tests can be useful for defining hydraulic connectivity.
- The tests on larger scales may also demand a fairly long test time, involve a large number of observation points for pressure and points for tracer injection. Because of this the large-scale tests also become quite expensive to perform.
- It should be pointed out that few attempts have been made to estimate the transport properties of the rock mass at Äspö HRL so far. In the next phase of the Äspö HRL a much greater effort will be made on finding useful concepts and parameters for calculations of transport of solutes.

1 INTRODUCTION

1.1 ÄSPÖ HARD ROCK LABORATORY (Äspö HRL)

The Äspö Hard Rock Laboratory (HRL) constitutes an important part of the work of developing a deep repository and developing and testing methods for investigating and licensing a suitable site. The plan to build an underground rock laboratory was presented in *R&D Programme 86 /1986/* and was received very positively by the reviewing bodies. In the autumn of 1986, SKB initiated the field work for the siting of the underground laboratory in the Simpevarp area of the municipality of Oskarshamn. At the end of 1988, SKB arrived at a decision in principle to site the laboratory on southern Äspö, about 2 km north of the Oskarshamn Nuclear Power Station (see *Figure 1-1*). After regulatory review and approval, construction work on the facility was commenced in the autumn of 1990.

The Äspö HRL has been designed to meet the projected needs of the planned research, development and demonstration activities. The underground part takes the form of a tunnel from the Simpevarp peninsula to the southern part of the island of Äspö (see *Figure 1-2*). Below Äspö, the tunnel runs in two turns down to a depth of 450 m (see *Figure 1-3*). The total length of the tunnel is 3600 m. The first part of the tunnel was excavated using the drill-and-blast technique. The last 400 metres were excavated by a tunnel boring machine (TBM) with a diameter of 5 metres. The underground excavations are connected to the surface facilities by a hoist shaft and two ventilation shafts. The Äspö Research Village with offices, stores and hoist and ventilation building is located at the surface, (see *Figure 1-4*).

The work at the Äspö HRL was divided into three phases: the pre-investigation phase, the construction phase and the operating phase. The **pre-investigation phase**, 1986–1990, involved siting the Äspö HRL. The natural conditions in the bedrock were described and predictions made with respect to the geohydrological and other conditions that would be observed during the construction phase /*Gustafson et al, 1991/*. Planning for the construction and operating phases was also carried out.

During the **construction phase**, 1990–1995, extensive investigations, tests and experiments were carried out in parallel with the civil engineering activities, mainly to check the reliability of the pre-investigations. The tunnel was excavated to a depth of 450 m and construction of the Äspö Research Village was completed. The Äspö Research Village was taken into service during the summer of 1994. The underground civil engineering works were mostly completed in the summer of 1995.

The **operating phase** began in 1995. A programme for these studies is presented in *RD&D Programme 95 /1995/*.

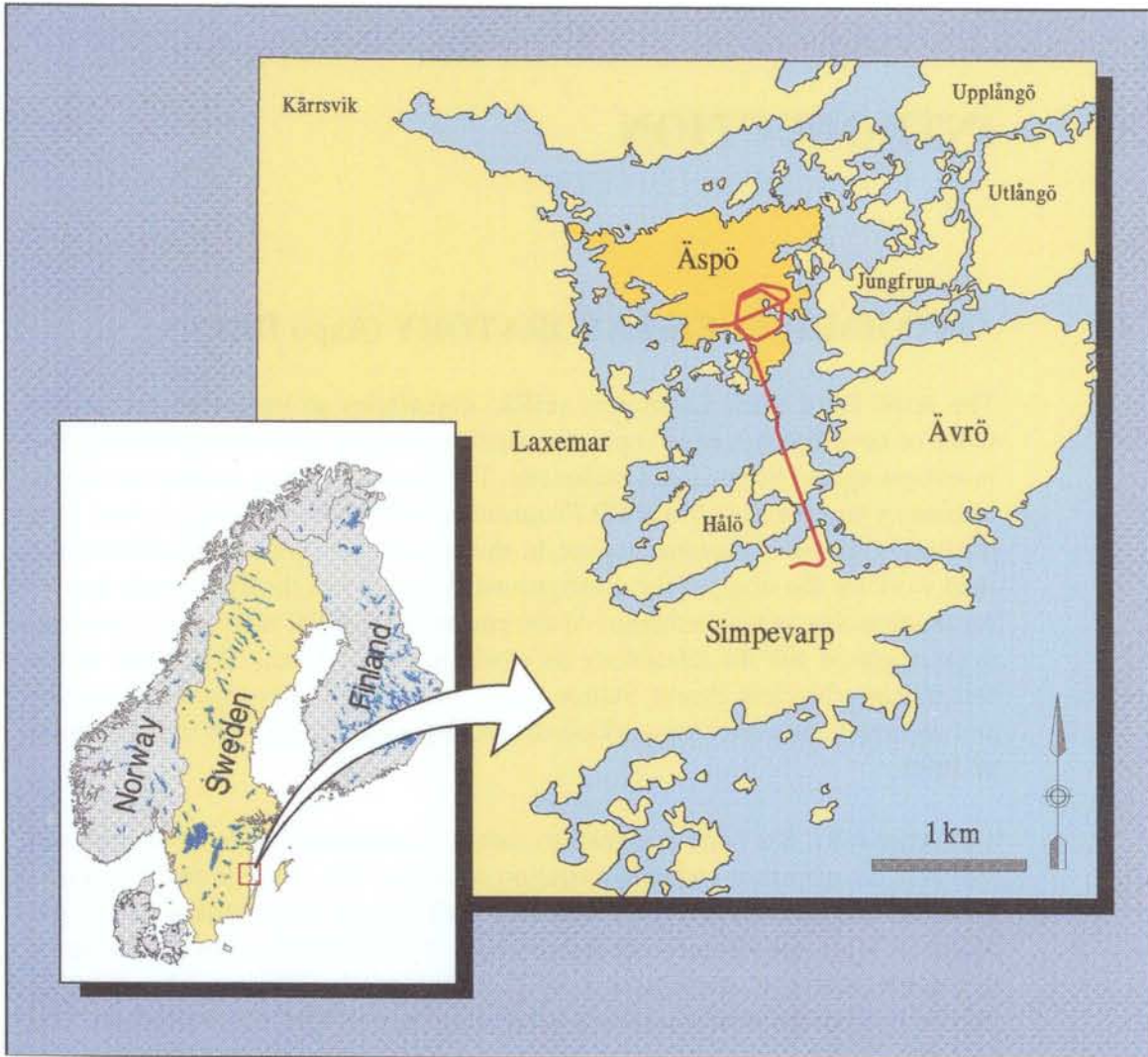


Figure 1-1. Location of the Äspö Hard Rock Laboratory.



Figure 1-2. Overview of the area around the Äspö HRL.

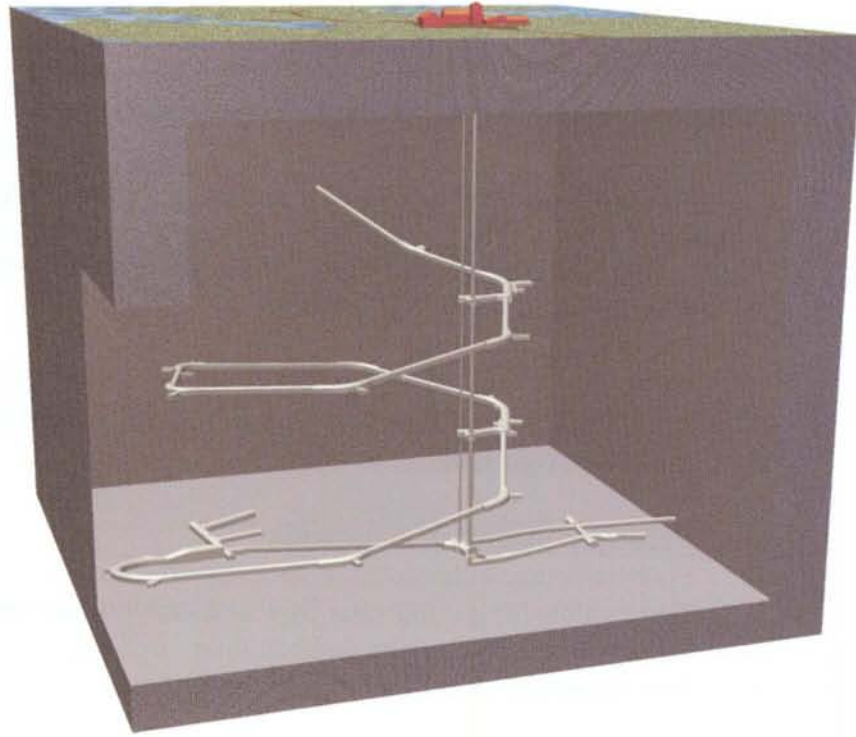


Figure 1-3. General layout of the Äspö HRL. The total length of the tunnel is 3600 m. The first part of the tunnel was excavated using the drill-and-blast technique. The last 400 metres were excavated by a Tunnel Boring Machine (TBM) with a diameter of 5 metres. The underground excavations are connected to the Äspö Research Village, containing offices, stores, hoist and ventilation building, by a hoist shaft and two ventilation shafts.



Figure 1-4. Bird's-eye view of the Äspö Research Village.

1.2 OVERALL GOALS OF THE ÄSPÖ PROJECT

One of the basic motives for SKB's decision to build the Äspö HRL was to provide an opportunity for research, development and demonstration in a realistic and undisturbed rock environment down to the depth planned for a future deep repository.

To meet the overall schedule for SKB's RD&D work, the following (here abbreviated) stage goals were set up in *R&D-Programme 89 /1989/* for the activities at the Äspö HRL.

- 1 Verify pre-investigation methods.
- 2 Finalize detailed characterization methodology.
- 3 Test models for groundwater flow and radionuclide migration.
- 4 Demonstrate construction and handling methods.
- 5 Test important parts of the repository system.

In the planning and design of activities to be performed at the Äspö HRL during the operating phase, priority is being given to projects which aim to:

- increase scientific understanding of the deep repository's safety margins,
- develop and test technology which reduces costs and simplifies the repository concept without sacrificing high quality and safety, and
- demonstrate technology that will be used for the deposition of spent nuclear fuel and other long-lived waste.

The start of the operating phase has motivated a revision and focusing of the goals of the Äspö HRL, based on the experience gained to date. For the operating phase, the stage goals have been worded as follows, */R&D-Programme 95 /1995/*:

- 1 Verify pre-investigation methods**
Demonstrate that investigations at the ground surface and in boreholes provide sufficient data on essential safety-related properties of the rock at repository level.
- 2 Finalize detailed characterization methodology**
Refine and verify the methods and the technology needed for characterization of the rock in the detailed characterization of a site.
- 3 Test models for description of the barrier function of the rock**
Refine and at repository depth test methods and models for describing groundwater flow, radionuclide migration and chemical conditions during the repository's operating period and after closure.
- 4 Demonstrate the technology for and function of important parts of the repository system**
Test, investigate and demonstrate on a full scale different components of importance for the long-term safety of a deep repository system and show

that high quality can be achieved in the design, construction and operation of system components.

The four reports mentioned in the foreword mainly address the first and, to some extent, the second of the above stage goals.

The Äspö HRL comprises an important part of the work being pursued within SKB's RD&D-Programme.

1.3 AIM OF THIS REPORT

The purpose of this report, No. 4, is to present the evaluation of groundwater flow, groundwater chemistry and transport of solutes predictions made during the pre-investigation phase.

Part 1 presents the evaluation of groundwater flow.

Part 2 presents evaluation of groundwater chemistry.

Part 3 presents evaluation of transport of solutes.

1.4 COORDINATE SYSTEM

For various reasons a number of coordinate systems have been used during the pre-investigation and construction phases.

At Äspö four different coordinate systems are used. The systems are rotated relative to one another and have different North directions. Within the Äspö Project all geological information on the orientation of structures is given relative to magnetic North. This reference direction is generally used in this report. Geographic North is also used occasionally as a reference direction, but for practical purposes this is the same as magnetic North, considering the accuracy in orientation that can be obtained for geological features.

Location of drifts and boreholes are always given in the local Äspö coordinate system.

The relative orientation between the four coordinate systems are:

- RAK-38 North is 11.819 degrees East of Äspö local North map system.
- Geographic North is 11.119 degrees East of Äspö local North.
- Magnetic North is approximately 12 degrees East of Äspö local North (1985-1990).

The coordinate transformation between the RAK-38 and local Äspö systems is according to the equations below:

$$X_{\text{RAK-38}} = 6367978.295 + 0.978799 (X_{\text{Äspö}} - 7484.309) + 0.204822 (Y_{\text{Äspö}} - 1956.68)$$

$$Y_{\text{RAK-38}} = 1551210.173 - 0.204822 (X_{\text{Äspö}} - 7484.309) + 0.978799 (Y_{\text{Äspö}} - 1956.68)$$

$$(6360251.890, 1550827.928)_{\text{RAK-38}} = (0,0)_{\text{Äspö}}$$

The length correction between the systems is as follows:

$$L_{\text{RAK-38}} = 0.999999852 \cdot L_{\text{Äspö}}$$

1.5 CHAINAGE DIFFERENCES DUE TO MODIFIED LAYOUT OF THE TUNNEL

There are chainage differences in the tunnel between the planned layout and the actual excavated layout. The reason is that the layout was modified during construction.

In September 1991 the layout of the tunnel was changed because core borehole KBH02 was hit by the tunnel. It was decided to move the tunnel about 35 m to the east and then go back to the original position of the tunnel close to the position of the shafts at about chainage 1 650 m (see *Figure 1-5*).

During excavation of the tunnel SKB decided to test full-face boring using a Tunnel Boring Machine (TBM). Because of this the tunnel layout was changed from about tunnel section 2600 m, As a result of this it was decided that the comparison of predictions and measured entities should only be made up to tunnel section 2875 m (excavated length) as from there the difference between planned an excavated layout was considered to be too large for a relevant comparison (see *Figure 1-6*).

The layout modification during construction affected the evaluation of the concepts and models to a minor degree. Where this is considered relevant for the evaluation it is discussed in the report.

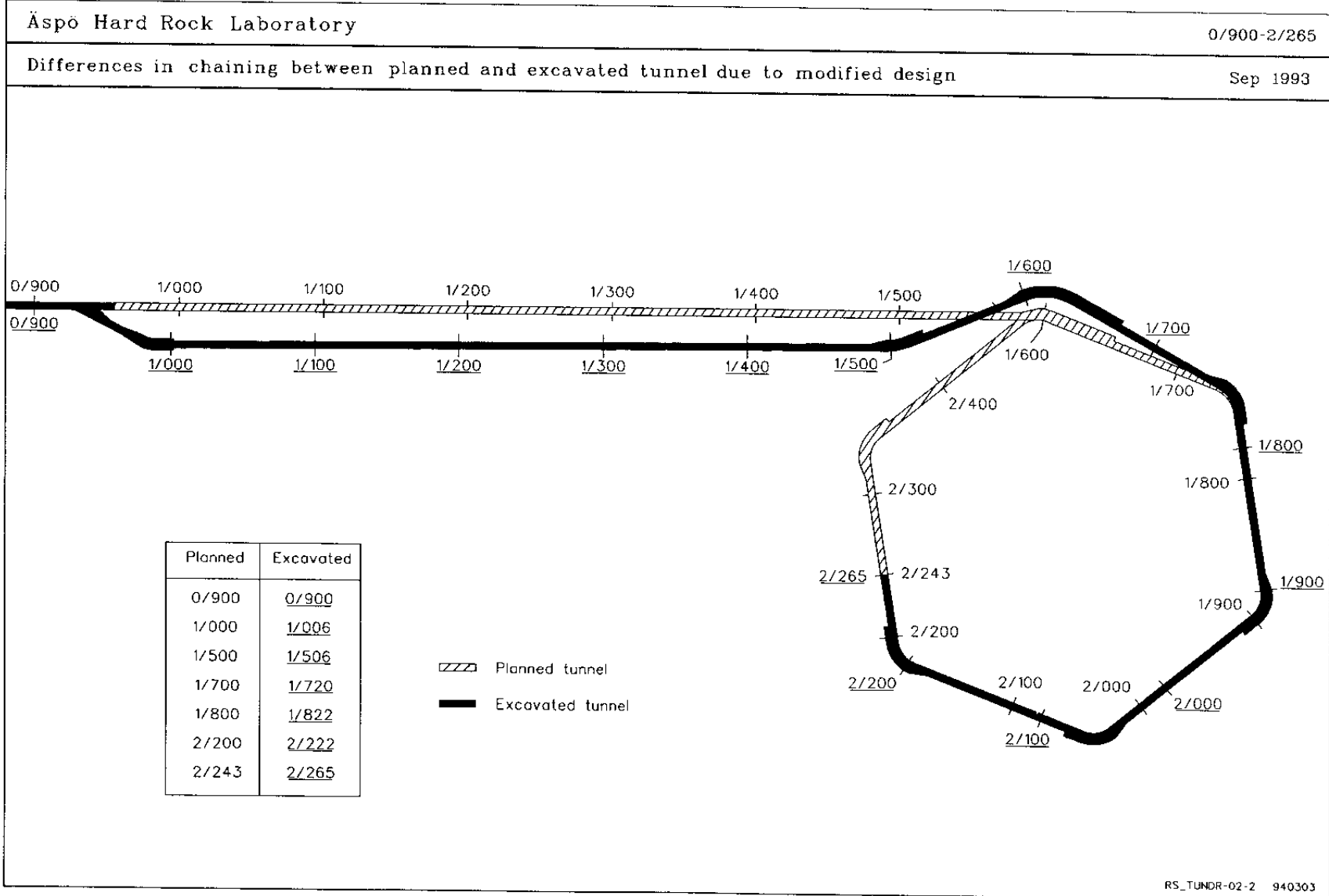


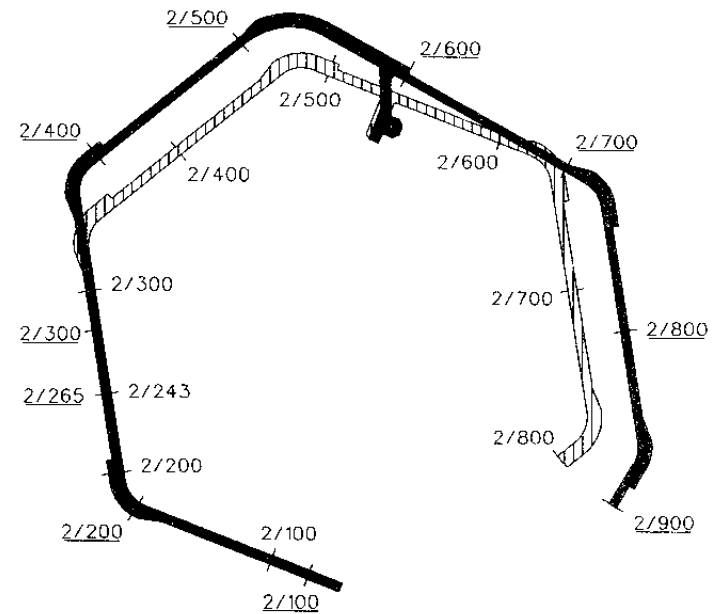


Figure I-5. The planned and excavated tunnel layouts.

Figure I-6. The planned and excavated tunnel layouts.

Planned	Excavated
2/100	<u>2/122</u>
2/200	<u>2/222</u>
2/243	<u>2/265</u>
2/300	<u>2/322</u>
2/400	<u>2/436</u>
2/500	<u>2/560</u>
2/600	<u>2/661</u>
2/700	<u>2/774</u>
2/793	<u>2/900</u>
2/800	<u>2/907</u>

 Planned tunnel
 Excavated tunnel



ACKNOWLEDGEMENT

The listed reports in the foreword summarize the investigation and evaluation work carried out by a large number of skilled and enthusiastic people. A few of these have been involved throughout the entire project and made important contributions to the realization of the reports. Especially we wish to mention:

Karl-Axel Kornfält and Hugo Wikman, Geological Survey of Sweden. (Bedrock investigations and petrographic analyses).

Håkan Stille, KTH, Stockholm, Pär Olsson, Skanska, Stockholm, Bengt Leijon, SKB, Stockholm and Bengt Stillborg, LTH, Luleå. (Rock stress measurement and Rock mechanics modelling).

Raymond Munier, Scandiaconsult, Stockholm and Jan Hermansson, Golder Associates, Stockholm. (Geological-structural field investigations and structural modelling).

Seje Carlsten and Per Askling, Geosigma, Uppsala. (Borehole radar investigations and CAD-illustrations).

Mikaël Erlström, Sedrock, Lund, and Ingemar Markström, Sydkraft Konsult, Malmö. (XRD analyses and CAD-illustrations).

Peter Danielsson, Torbjörn Forsmark, Lars Nilsson, VBB Viak, - Gothenburg. (Evaluation of hydraulic tests and data compilation for groundwater flow modelling).

Magnus Liedholm, VBB Viak, Gothenburg. (Analyses of geohydrological data, accuracy and confidence of geological estimates).

Leif Stenberg, Kristian Annertz, Mats Olsson, Katinka Klingberg, SKB Äspö HRL, Robert Gass, Per Nilsson, VBB Viak, Bengt Gentzschein, Geosigma. (Tunnel data documentation).

Urban Svensson, CFE. (Numerical groundwater flow modelling).

Karl-Göran Nederfeldt, ÅF-IPK, Agne Bern, John Olausson, Kent Hansson, Lennart Ekman, Göran Nyberg, Stig Jönsson, Geosigma. (Field work, field support and groundwater monitoring).

Eva-Lena Tullborg, Terralogica. (Fracture mineralogy).

Marcus Laaksoharju, Intera KB, John Smellie, Conterra. (Hydrochemical modelling).

Bill Wallin, Geokema. (Isotope chemistry).

Ann-Chatrin Nilsson, KTH. (Hydro-chemical data quality control).

We are also grateful for the review comments on this report provided by our colleagues at SKB.

PART 1

GROUNDWATER FLOW

1 **SUBJECT: WATER-BEARING ZONES - SITE SCALE**

1.1 **SCOPE AND CONCEPTS**

The concept is hydraulic conductor domains – or water-bearing zones – which are planar features with hydraulic properties different from the surrounding rock and identified as to position, extent and properties. Generally, they are defined geologically as major fracture zones but in some cases they may mainly be defined by interpretation of results from hydraulic interference testing.

The material properties chosen for the hydraulic conductor domains are:

- Transmissivity (T)
- Storage coefficient (S)

Transmissivities (T) for the hydraulic conductor domains are assigned deterministically as a constant value. T is based on evaluation of transient hydraulic tests in most cases but is sometimes based on geological classification combined with the evaluated transmissivities for the hydraulic conductor domains at Äspö, when no hydraulic tests have been performed in the features.

Storage coefficients (S) for the hydraulic conductor domains were not predicted and are therefore not discussed in the text below.

1.2 **METHODOLOGY FOR TESTS OF CONCEPTS AND MODELS**

A number of different methods have been used to estimate the position, extent and properties of water-bearing zones. These are outlined briefly below and summarized in *Figure 1-1*.

1.2.1 **Prediction methodology**

Geological model and geophysical investigations

The geological model and geophysical investigations are important for defining the location and extent of the water-bearing zones (see *Stanfors et al /1997b/* for more details concerning these methods).

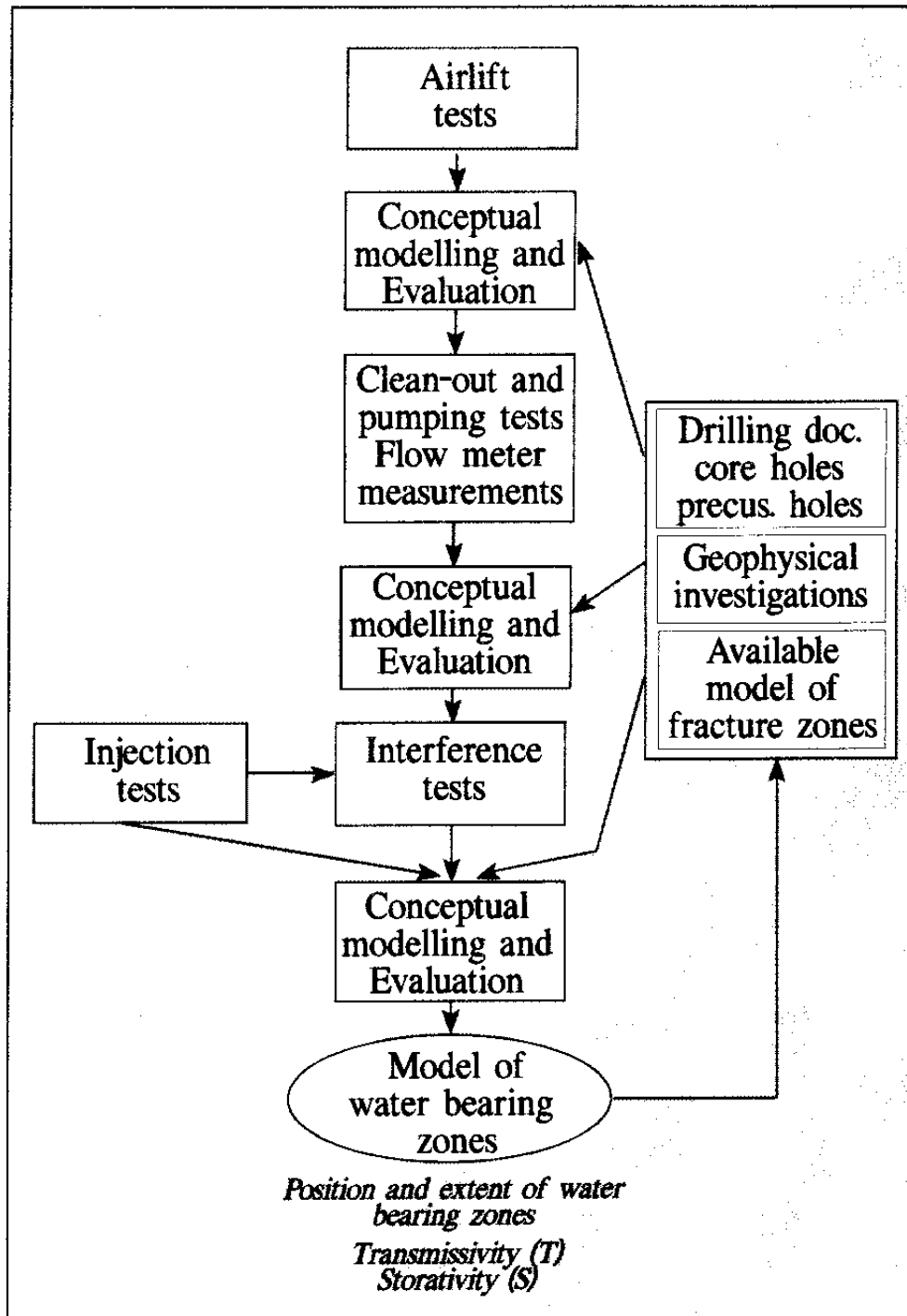


Figure 1-1. Hydraulic conductor domains - or water-bearing zones - site scale. Flow chart (After Almén et al /1994/).

Drilling documentation – percussion holes and cored holes

Inflow rates and increased fracturing were assessed during drilling. The rock type was also assessed from drill-cuttings when drilling the percussion holes. From these investigations it was possible to identify an **intersection** between the borehole and a possible hydraulic conductor domain. The boreholes are shown in *Figures 1-2 and 1-3*.

Air-lift tests or short time pumping tests

The air lift tests (air lift pumping) were generally performed for 100-m sections of cored boreholes (*Figure 1-4*). Percussion holes, generally with a drill depth of 100-200 m, were also air-lift tested. Draw-down and recovery periods were normally approximately 1 h + 1 h. If pressures were observed in surrounding boreholes, **directions and positions of water-bearing zones** could in some cases be indicated. The **transmissivity** of the tested section of the borehole was evaluated /*Almén and Zellman, 1991, Almén et al, 1994*/. Radial flow was assumed in the evaluation of the pressure-time curve /*Cooper and Jacob, 1946*/ and an Agarwal time correction for recovery curve was used /*Earlougher, 1977*/. About 100 tests were performed with a test section of 100 m or longer. Some of these tests were performed using a submersible pump.

Clean-out and pumping test of borehole

In order to clean-out cored holes they were pumped for approximately one day. By measuring the draw-down and recovery in the pumped borehole it was possible to get a **first estimate of the transmissivity as seen from the borehole** and the skin factor for the borehole. If pressures were observed in surrounding boreholes, **directions and positions of water-bearing zones** could be indicated in some cases. /*Almén and Zellman, 1991, Almén et al, 1994*/.

The flow regime was evaluated from the pressure response in the borehole and was generally found to be radial. Radial flow was assumed in the evaluation of the pressure-time curve /*Cooper and Jacob, 1946*/ and an Agarwal time correction for the recovery curve was used /*Earlougher, 1977*/.

Flow-meter measurement in boreholes

During the clean-out pumping the borehole was flow-meter logged. (*Figures 1-5 and 1-6*). These measurements indicate the inflow distribution along the borehole and provide both an estimate of the **location of the intersection** between a possible **water-bearing zones** and the borehole and also an **estimate of the transmissivity** of the fracture zone. If T is evaluated for the entire borehole (T_{tot}) and flow logging has been done, the approximate T distribution

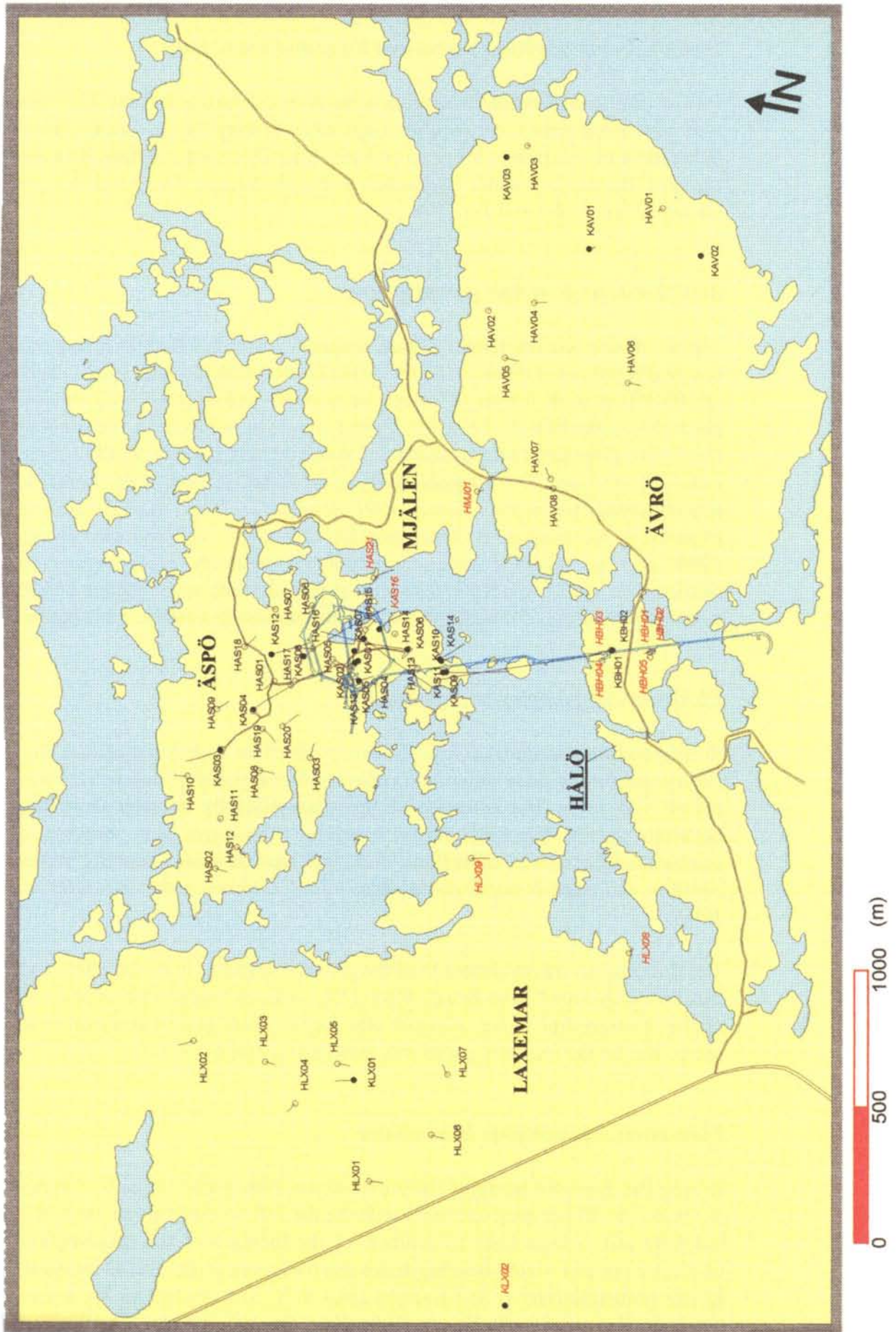


Figure 1-2. Plan of the boreholes (black label) included in the predictions of the piezometric levels reported in Rhén et al /1991a/. Boreholes with a red label were drilled during the construction of the Äspö HRL. Filled circle: Cored boreholes. Un-filled circles: Percussion boreholes.

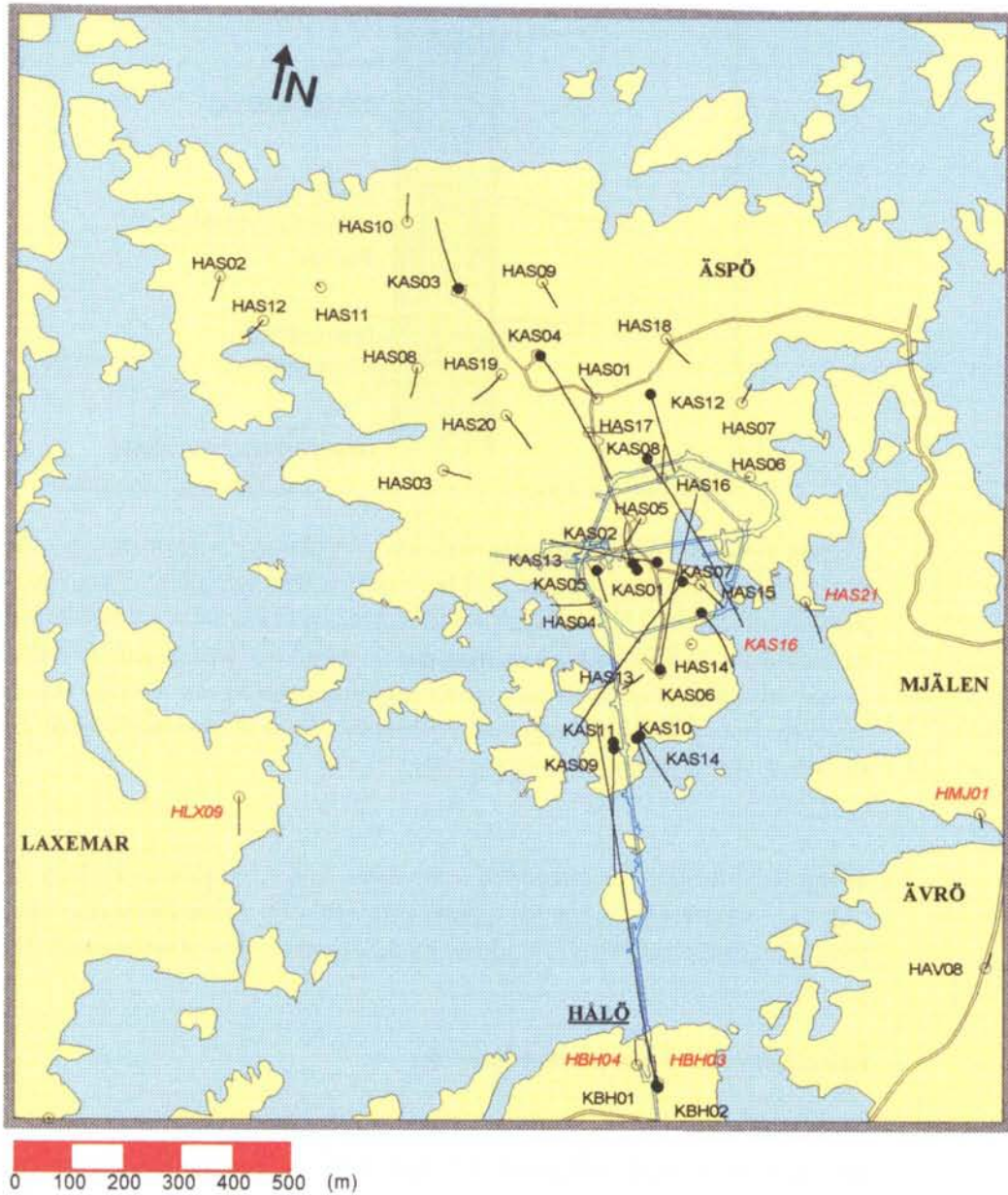


Figure I-3. Plan of the boreholes (black label) included in the predictions of the piezometric levels reported in Rhén et al /1991a/. Boreholes with a red label were drilled during the construction of the Äspö HRL. Filled circle: Cored boreholes. Un-filled circles: Percussion boreholes.

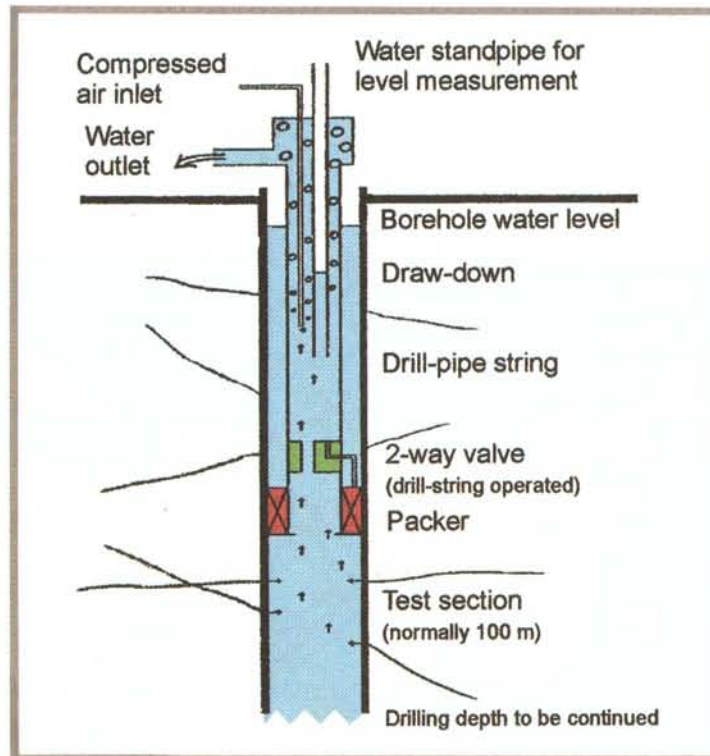


Figure 1-4. Air lift test during drilling. The drilling was normally interrupted every 100 m in order to do airlift tests and water sampling. This was done by pulling up the drill bit and then lowering a test string with an inflatable packer at the lower end. Then air was injected to pump the water out. The drawdown in the tested section was measured during pumping as well as the recovery after the pump had been stopped. Normally, the test time was about 1+1 hour for draw-down and recovery periods.

along the borehole is estimated according to Earlougher /1977/ as $T_i = T_{tot} \cdot dQ_i/Q_{tot}$, where Q_{tot} is the total flow rate and dQ_i is the flow rate change per length i . /Earlougher 1977, Almén and Zellman 1991, Almén et al, 1994/.

Injection tests – 3 m packer spacing

Injections tests with injection and recovery periods of approximately 10 + 10 minutes were used. (Figures 1-5 and 1-6). A constant pressure, normally 200 kPa above static pressure, was used during the injection period. The tests were evaluated assuming stationary conditions or transient conditions. The latter are considered to give better estimates of the transmissivities. The evaluation for stationary conditions was based on the injection period and theory according to Moye /1967/. The flow regime and the flow properties are evaluated from transient tests. The evaluation for transient conditions was based on the recovery period, assuming radial flow and using an Agarwal time correction /Earlougher, 1977/. **Transmissivity** was evaluated for the 3-m section. Dividing the transmissivity by the section length 3 m gives an effective

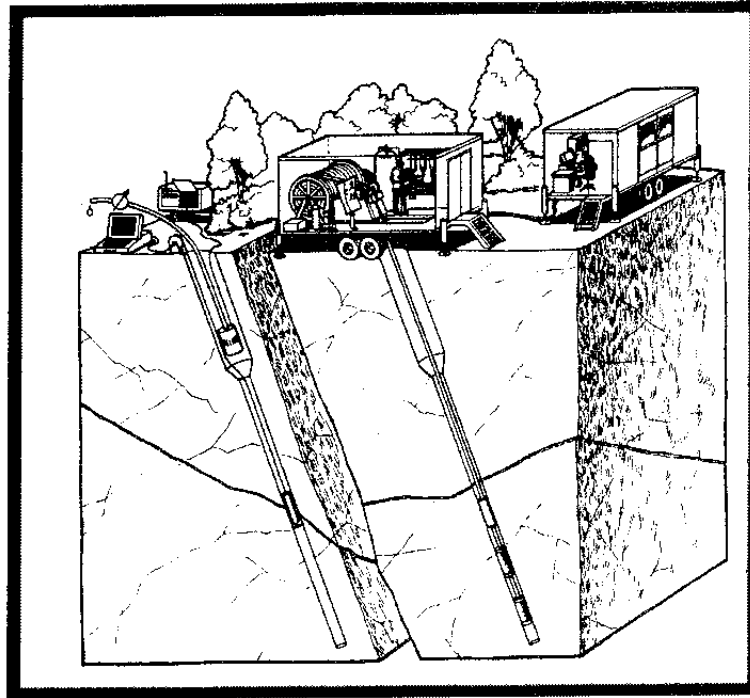


Figure 1-5. Flowmeter logging (left) is a method where the flow velocity change along the borehole is measured. Using flowmeter logging it is possible to exactly define the most conductive parts of the borehole. These data, together with core logging, are useful for deciding packer positions for interference tests and long-time monitoring of the groundwater pressure.

During an injection test (right) water is injected into the rock mass between two packers. The pressure in the test section and the flow rate is measured continuously during the test. Generally, a constant pressure of a few bars is used during the injection phase of the test and the measured flow rate slowly decreases. When the injection stops the pressure recovery in the test section is measured for a period approximately as long as the injection period.

value of the hydraulic conductivity. 1302 tests were performed during the pre-investigations in 7 cored holes on Äspö (KAS02-KAS08) and in one cored hole on Laxemar (KLX01).

Injection tests – 30 m packer spacing

The injection and recovery periods were approximately 2 h + 2 h and the section length 30 m. The **transmissivity** of the test section was evaluated. For more details concerning the evaluation see injection test – 3 m packer spacing. 65 tests were performed during the pre-investigations in three cored holes on Äspö (KAS02 and 03) and Laxemar (KLX01).

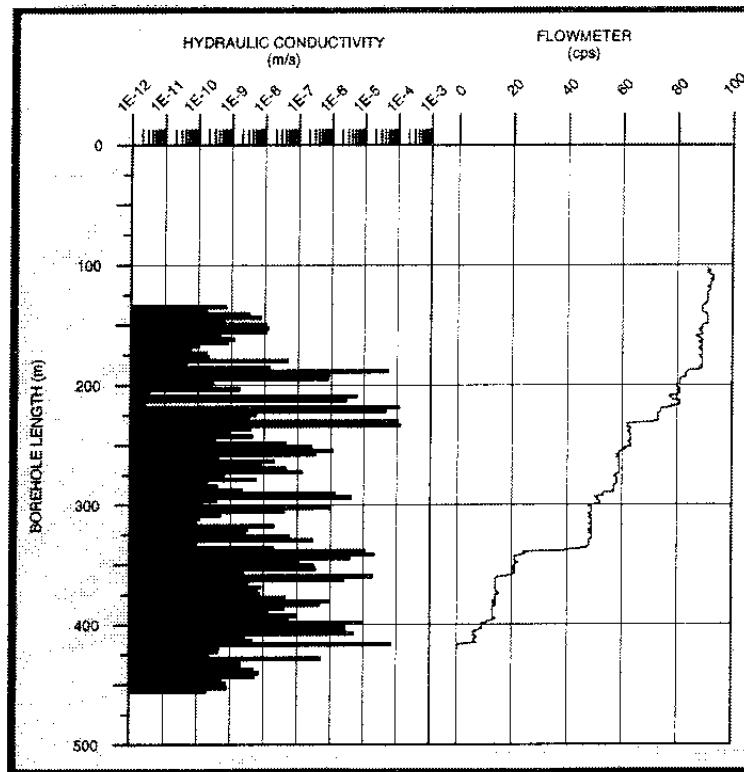


Figure 1-6. Evaluated hydraulic conductivity from injection tests and flowmeter curve in borehole KAS04. CPS (counts per second) is proportional to the water velocity.

Interference test – test section between two packers - short-term pumping

The interference tests were performed as constant rate tests. If the pumped section in a borehole is surrounded by packers it is possible to test an individual fracture zone. (Figure 1-7). This procedure offers good opportunities for evaluating the flow regime for early, middle and late times and thus provides a generally good estimate of the flow properties of the fracture zone close to the borehole. The draw-down and recovery periods were generally 3 days + 2 days.

The flow regime was generally found to indicate radial flow during some period and a **transmissivity** was generally evaluated from the pressure-time curve assuming radial flow /Cooper and Jacob, 1946/. An Agarwal time correction for the recovery curve was used /Earlougher, 1977/.

Draw-down and recovery were not only measured in the pumped borehole but also in observation sections (surrounded by packers) in other boreholes. If these sections intersect the same water-bearing zone as the pumped one, it is possible to estimate the **storage coefficient** of the water-bearing zone if no other intersecting zones affect the draw-down for the evaluation period considered.

The responses in the observation sections also provide **indications of water-bearing zones, positions and extents**. Sometimes the indications of these water-bearing zones may only be seen in the interference test but generally

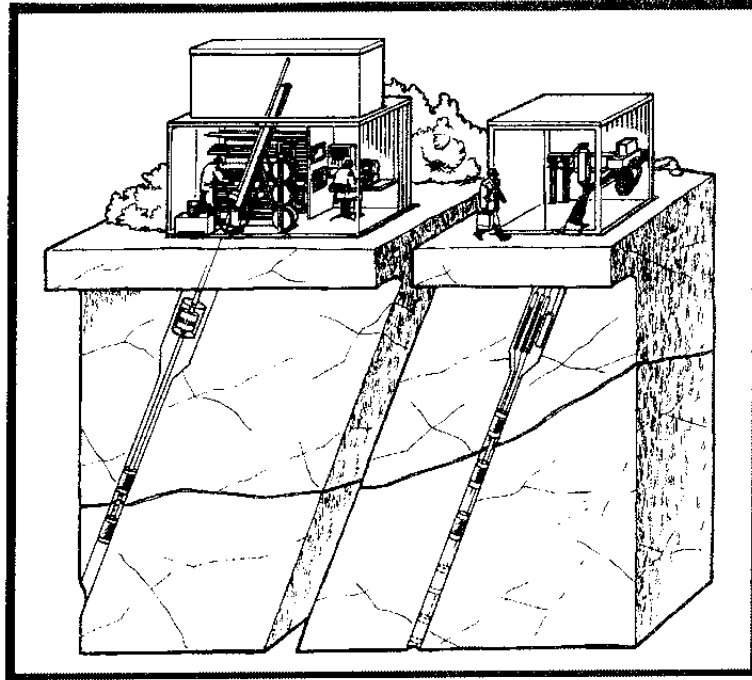


Figure 1-7. During an interference test water is pumped from a borehole, or a section of it, and the drawdown is measured in the pumped borehole (left) as well as in a number of other boreholes, called observation boreholes (right). These boreholes are generally equipped with several packers making it possible to monitor the drawdown at different packers making it possible to monitor the drawdown at different sections along a borehole. Generally pumping has to be undertaken for a few days in order to observe the pressure responses in observation boreholes several hundred metres away from the pumped borehole.

geological and geophysical data have to be used to support the discussion of the location and extent of the water-bearing zones. In all 13 tests were performed.

Interference test – open borehole – short-term pumping

In some of the interference tests the pumped borehole was not packed off. In these cases the **transmissivity of the entire borehole** was evaluated, as for the clean-out pumping test. Depending on whether one or several fracture zones intersected the pumped borehole and the way in which the observation sections were situated it was possible or not possible to evaluate the storage coefficient of a zone. Compared with interference tests, where a fracture zone has been packed off, it was also generally more difficult to draw conclusions from the **location and extent of water-bearing zones**. The draw-down and recovery period was generally 3 days + 2 days. In all 8 tests were performed but one test in KAS11 had to be excluded due to disturbances from drilling and tests in HAS18 and 19 and also drilling and water chemistry sampling in KAS12 and 13.

Interference test - open borehole - long-term pumping

Two interference tests were performed as Long-term Pumping Tests (LPT), with draw-down and recovery periods of 53 + 33 days and 92 + 31 days. The pumped boreholes were KAS07 and 06. The **purpose was the same as for the other interference tests** and also to obtain better information on the **boundary conditions** and **a larger influence radius** (draw-down within a larger rock volume).

All interference tests were valuable as **calibration cases** for the numerical groundwater flow model, but these long-term pumping test were considered most valuable.

Overview of test sections and test scales

Appendix 1 shows an overview of tests in cored holes. "Test scale" in these figures corresponds to the length of the tested section and "Depth" is the vertical depth for the test section.

1.2.2 Methodology for determining outcome

Probing and pressure build-up tests

Approximately every fourth round two 20-m long probe holes were drilled about 4 m from the tunnel face, one in the left wall and one in the right wall. The main purpose of the probe holes was to estimate the hydraulic properties of the rock. Generally the borehole direction was 20° from the tunnel line in the horizontal plane and with a plunge of approximately 10° (see *Figure 1-8* and *1-9*). During drilling the inflow of water (flow rate and position in the borehole) and the rock composition were documented.

After drilling, a pressure build-up test was performed. Generally the packer was installed 5 m into the borehole. In order to minimize the risk of obtaining a pressure response in the observation borehole from the other flowing borehole, of a such a magnitude that it would affect the evaluation possibilities the following test procedure was adopted. Both boreholes were left flowing for about 30 minutes and then one borehole was closed to start the pressure build-up. About 30 minutes later the other borehole was closed to start the pressure build-up. The flow and pressure build-up periods were at least about 30 + 30 min. The **transmissivity** of the tested section was evaluated from the pressure build-up test. The type of rock in the tested section was estimated from the documentation of the probing and mapping of the tunnel wall.

The transmissivities (T) evaluated from the probe holes that penetrated the most intensive parts of the mapped fracture zones were used for estimating the fracture zone transmissivities. Radial flow was assumed in the evaluation of the pressure-time curve /Cooper and Jacob, 1946/ and an Agarwal time correction for recovery curve was used /Earlougher, 1977/. If it was only possible to

estimate the specific capacity (Q/s) of the probe holes the linear relation between $\text{Log}_{10}(T)$ and $\text{Log}_{10}(Q/s)$ for probeholes in the tunnel was used to estimate T (see *Rhén (ed) et al /1997/*).

The method of using probe holes close to the tunnel face and pressure build-up tests was chosen for the following reasons:

- 1 To estimate the hydraulic properties of the undisturbed rock. The properties are more undisturbed behind the tunnel face than in front of it, at least if short boreholes are tested.
- 2 The pressure build-up test is a simple and reliable method.
- 3 The probe holes drilled ahead of the tunnel face provide the builder and contractor with information about the rock properties and of water problems.

The number of drilled probe holes along the entire tunnel was 316. Hydraulic tests were performed in most of the probeholes */Stanfors et al, 1997a/*.

Supplementary drilling

Supplementary investigations were performed along the tunnel in order to define positions of expected water-bearing zones behind the tunnel face. Investigations were also performed to characterize in more detail fracture zones or the EDZ (Excavation Disturbed Zone), see *Stanfors et al /1997a/*. It was drilled 139 percussion boreholes with borehole lengths up to about 40 m. The number of core-drilled boreholes was 48 (excluding those performed for the projects SELECT and ZEDEX, see *Stanfors et al /1997a/*) with borehole lengths up to 340 m. Most of the coreholes were short.

Hydraulic tests of some kind were performed in most of the boreholes.

Water inflow measurements during drilling

During drilling of boreholes from the tunnel the water flow into the borehole was measured or estimated as a function of borehole depth.

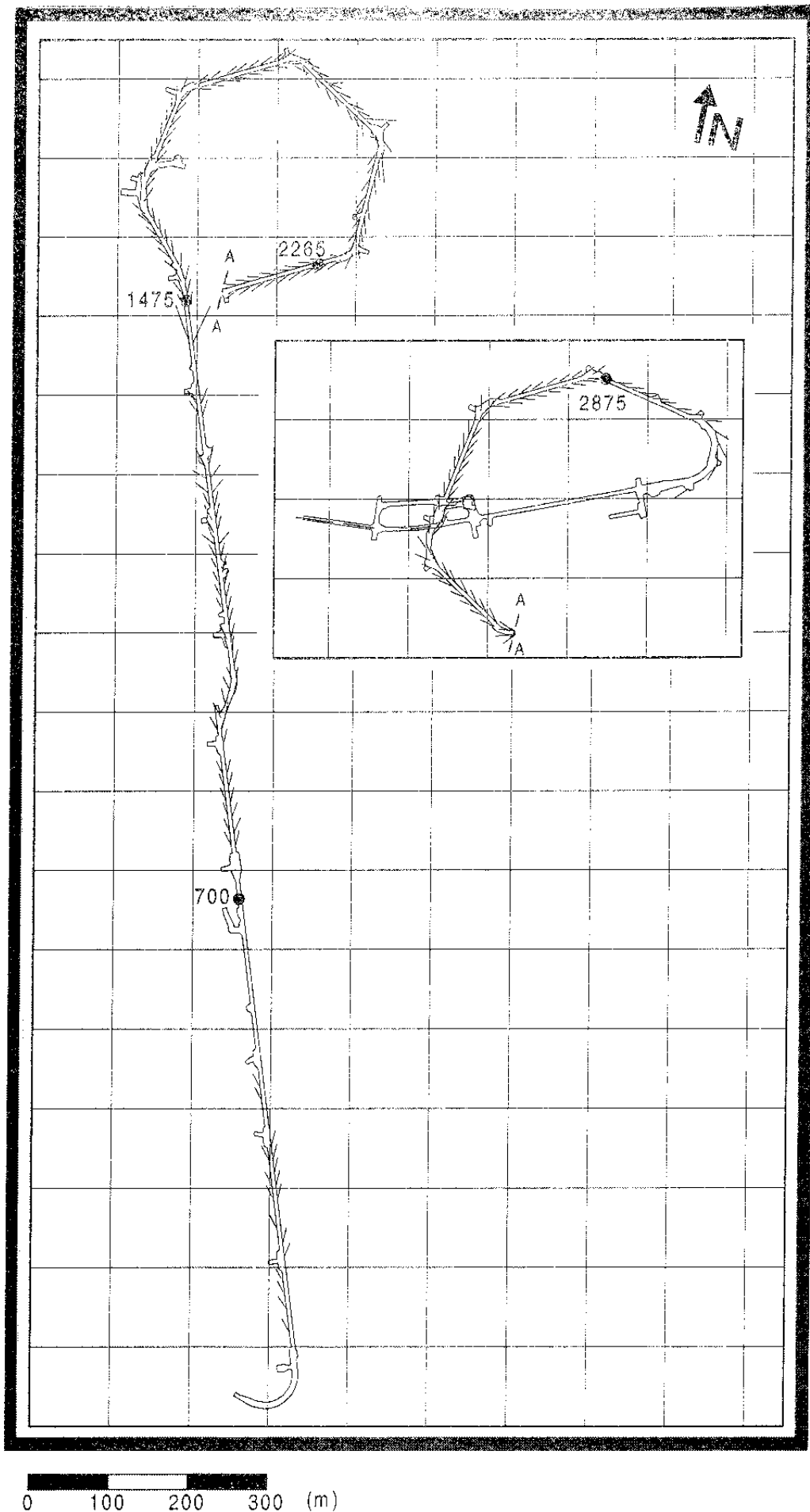


Figure I-8. Location of probe holes along the tunnel. The lines indicate the Äspö coordinate system. N = Magnetic North.



Figure 1-9. Probing and pressure build-up tests.

Top: During construction of the tunnel, 20 m long boreholes were drilled on both sides of the tunnel near the tunnel face for every fourth round (about every 16 m of tunnel advance). During drilling the drill rate, colour of water and water inflow were recorded. Directly after drilling a mechanical packer was installed about 5 m down the hole and pressure build-up tests were performed in the two boreholes.

Bottom: During a pressure build-up test the valve on the pipe coming out of the borehole is opened and water flows out of the borehole for a period. The valve is then closed and the pressure increase in the borehole is measured. The pressure in the boreholes was also measured approximately twice a year in order to see if there would be any pressure changes by time.

Pressure registration during drilling

During drilling of boreholes pressure was in several cases monitored in a number of observation boreholes. Based on the drill record (the borehole depth as a function of time and water inflow as a function of borehole depth) and the measured pressure (as a function of time) in the observation boreholes and, also the draw-down pattern, a conclusion was drawn on the connectivity between water-bearing zones.

Flow-meter measurement in boreholes

After drilling or during periods when the drilling was interrupted flow-meter logging was generally performed in cored holes using an MLS spinner probe or UCM acoustic probe /*Almén and Zellman, 1991*/.

Pressure build-up tests in cored holes

Pressure build-up tests were performed for the entire length of most cored holes. A few times double packers were used to be able to test smaller sections of the cored borehole. In a few cases the drilling was interrupted and single-packers were used to test the last part of the borehole drilled. Draw-down and recovery periods were generally about 30 + 30 minutes. Radial flow was assumed in the evaluation of the pressure-time curve /*Cooper and Jacob, 1946*/ and an Agarwal time correction for recovery curve was used /*Earlougher, 1977*/.

Interference test

A few interference tests were performed by allowing boreholes to flow from the tunnel and monitoring pressures in surrounding boreholes. Draw-down and recovery periods were generally from one up to about 40 hours. Radial flow was assumed in the evaluation of the pressure-time curve /*Cooper and Jacob, 1946*/ and an Agarwal time correction for recovery curve was used /*Earlougher, 1977*/.

Drilling into features with high transmissivity from the tunnel

During the initial construction phase there was compromise made on limitations to grout that could satisfy both the contractor and SKB. On a few occasions the excavation of the tunnel was quite problematic, because of large water inflow. This happened below the sea where several very transmissive structures were intersected. In order to manage the high water pressures and the high flow rates during drilling a new methodology was developed for the investigations. When a very conductive fracture zone was expected to be drilled into, casing was placed a few metres into the borehole before the drilling was continued. A valve was mounted at the top of the casing, outside the borehole,

so that it would be easy to stop the outflow of water. In *Figure 1-10* the outer part of the casing is shown.

Other methods

The identification of the positions of zones in the tunnel was mainly based on the geological identification (see *Stanfors et al /1997b/*).



Figure 1-10. When the valve on the casing was opened about 1600 litres per minute flowed out of a borehole (with a diameter 57 mm) drilled into the structure NE-1 (below the Baltic sea).

1.3 COMPARISON OF PREDICTED AND MEASURED ENTITIES

1.3.1 Position and extent of water-bearing zones

The geometry of the water-bearing zones is mainly defined by the major fracture zones in *Stanfors et al /1997b/*. However, a few of the water-bearing zones predicted in 1990 and included in the *Model 96 /Rhén et al, 1997/* are only defined in the geohydrological model. The reason is that measured responses during some interference tests indicated the presence of one or more possible water-bearing zones, but geologically it has been difficult to define the zone(s). In these cases the position and extent of the zone are chosen in a way that can explain the hydraulic responses. Except for NNW-8 and NW-1 the water-bearing zones (or hydraulic conductor domains) are also defined as zones in the geological model (see *Stanfors et al /1997b/*).

A simplified hydraulic discontinuity domain model was made in *Model 90 /Gustafson et al, 1991/* and also used in Model 96 by fitting a plane to the observations at the surface and in the boreholes. These models are shown in *Figure 1-11*.

NNW-8

One deterministic water-bearing zone, NNW-8, is not shown in *Figure 1-12*. The reason is that it is assumed that this structure never reaches the surface. Three interference tests in KAS03 at depths between 350 and 620 m indicated good hydraulic communication with the northern part of EW-1 */Rhén, 1988/*, but as the geologically defined EW-1 does not intersect KAS03 there may be a subvertical feature of limited extent close to the borehole. All three tests indicated about the same transmissivity, similar flow regimes and similar responses in observation boreholes. A vertical feature with the same strike as, for example, NNW-1, here called NNW-8, close to borehole KAS03 and in hydraulic contact with EW-1 can explain the responses.

In the *Model 90* the hydraulic responses mentioned above were explained by the feature EW-1w. In order to better comply with the geological model the data were re-evaluated and the new suggestion is given above.

NW-1

The hydraulic conductor domain NW-1 was indicated by responses when two interference tests were performed in KAS03 at depths between 200 and 250 m */Rhén, 1988/*. At the surface there are geological indications of a feature with the same strike as in *Figure 1-11* but with a dip 65-70° to the east. This dip indicates that the feature cannot intersect KAS03 at a depth between 200 and 250 m. However, it is here assumed that hydraulic conductor domain NW-1 can be used as an approximation of the conductor system in the upper part of the bedrock.

NNW-NW conductors

Some of the hydraulic conductor domains have a clear increase of fracture density but some are rather diffuse and are in *Stanfors et al /1997b/* called fracture swarms. However, in a number of interference tests, made in boreholes from from surface, the hydraulic responses indicated subvertical hydraulic conductor domains with a strike of NNW to NW */Rhén, 1988 and 1990a/*. During 1993 several cored holes and percussion boreholes were drilled from the tunnel with the main purpose of investigating fracture zones around the tunnel. Cored hole KA2162B was drilled to obtain a better definition of NNW features */Rhén et al, 1993c and Forsmark and Stenberg, 1993/*.

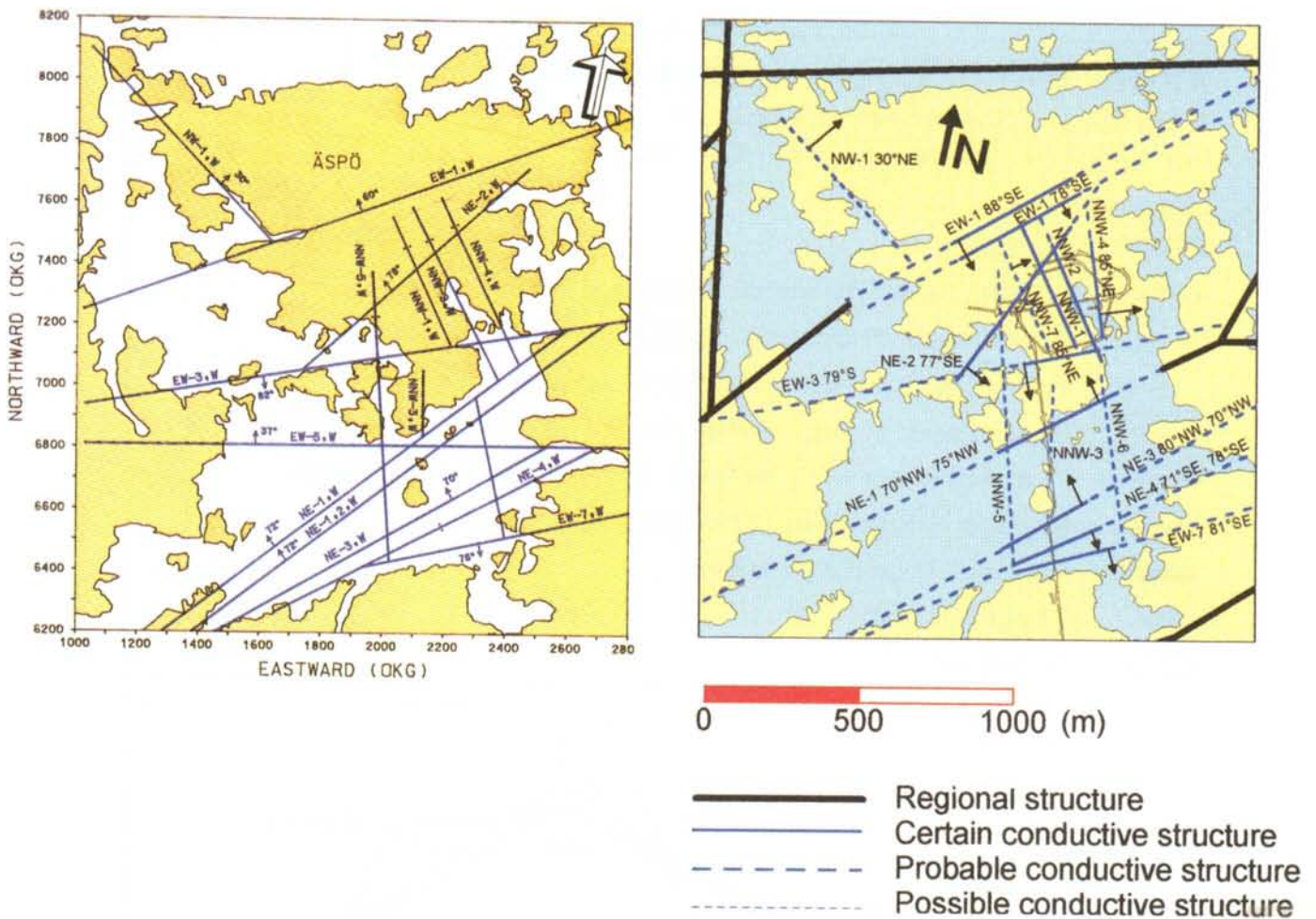


Figure 1-11. Left: Model 90 of hydraulic conductors from the pre-investigation phase - site scale. /Gustafson et al, 1991/.

Right: Model 96 of hydraulic conductors - site scale. (Åspö coordinate system, approximately the same as the OKG co-ordinate system).

During the drilling of KA2162B water pressures were monitored in some boreholes in the tunnel and boreholes from ground level. On a few occasions the borehole were drilled into a very conductive rock mass and large inflows were recorded. For these events the draw-down was studied. The draw-down cone, with its main axis trending approximately NW to NNW, in Figures 1-12 and 1-13 is based on the maximum draw-down in boreholes drilled from the tunnel spiral and in measurement sections in surface boreholes. The draw-down cone was constructed assuming a draw-down for the inflow point in the borehole and then using logarithmic interpolation between the flow point and the section where the draw-down was measured. Several of the observed draw-downs were considered uncertain (for different reasons) but still the elliptical form of the draw-down was considered to be correct.

Among the predicted NNW features only NNW-4 was clearly found in the tunnel by geological mapping. By combining the results from tests in different boreholes and data from supplementary investigations /Rhén and Stanfors, 1995 and Rhén et al, 1995a/ it was indicated that a few subvertical features

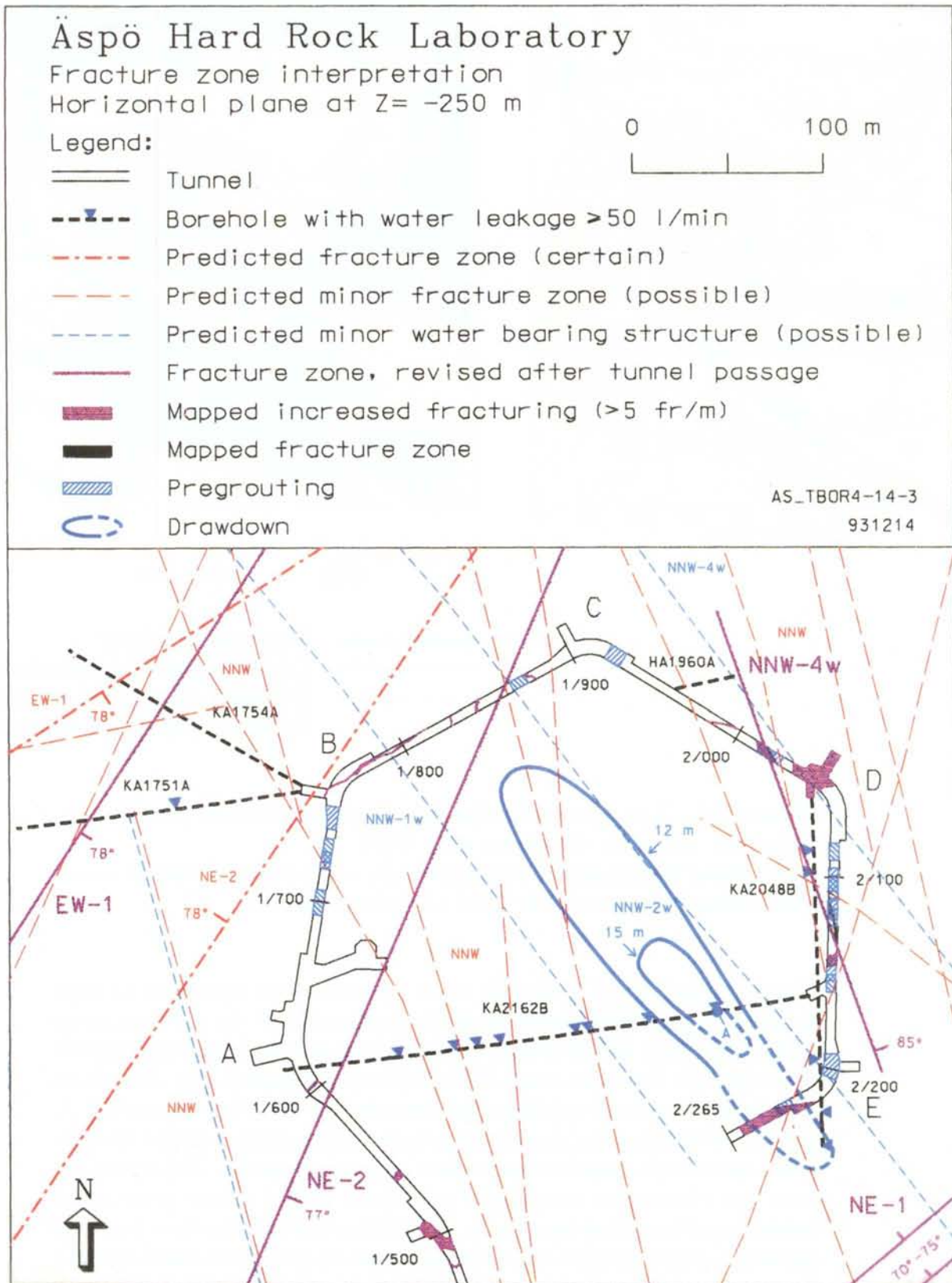


Figure 1-12. Draw-down ellipse during drilling through a water conductor at drill depth 49-53 m. (Although not seen in the figure, a fracture zone was mapped where NNW-4w intersects the tunnel.) /Rhén et al, 1994a/.

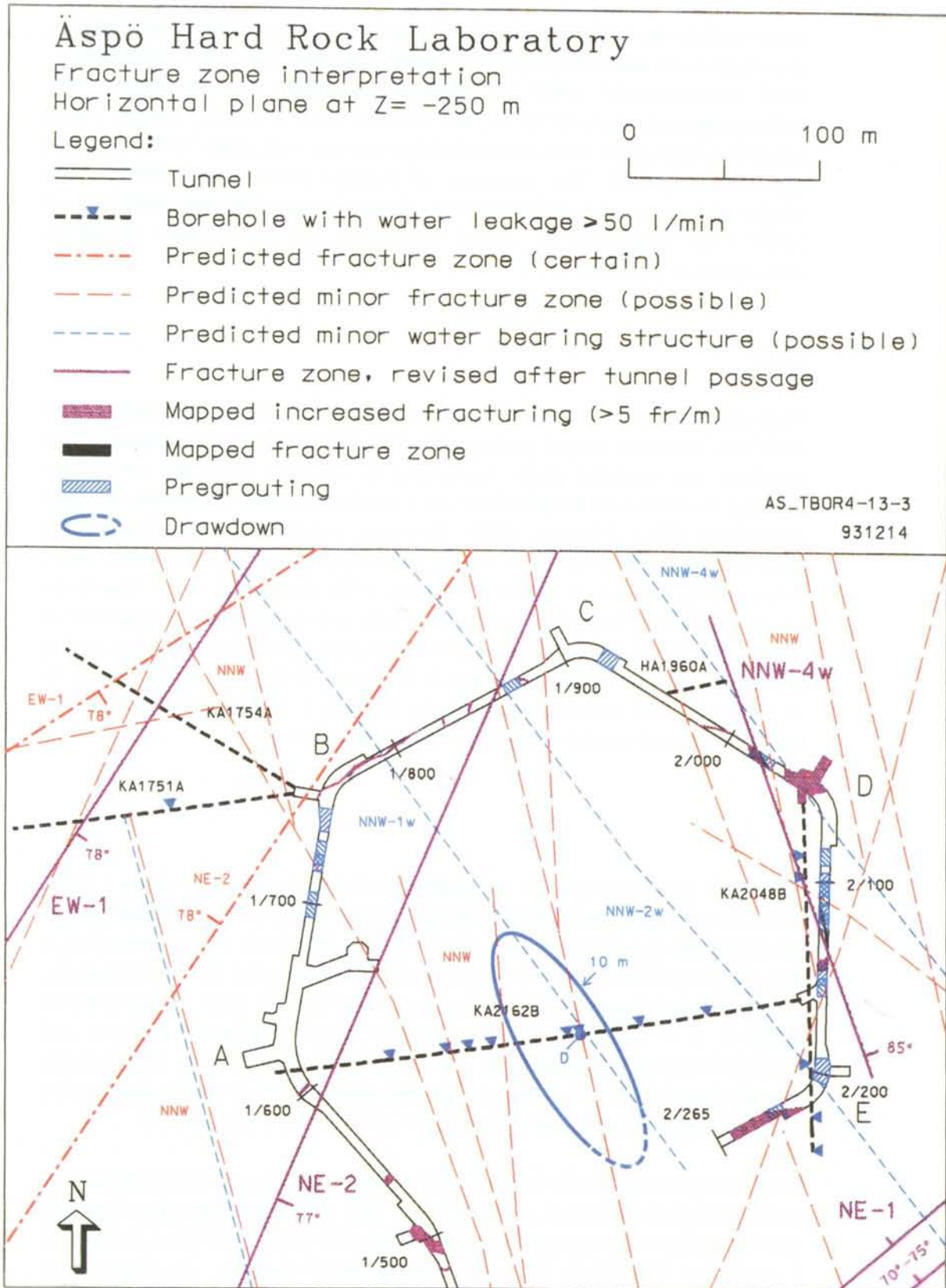


Figure 1-13. Draw-down ellipse during drilling through a water conductor at drill depth 121 m. (Although not seen in the figure a fracture zone was mapped where NNW-4w intersects the tunnel.) /Rhén et al, 1994a/.

could explain the responses seen in the interference tests. Other investigations also support the idea behind fracture swarms trending NW to N-S */Hermanson, 1995, and Kickmaier, 1993/*. The hydraulic conductor domains called NNW, striking approximately N 35°W, are believed to be a fracture swarm which consists mainly of the main subvertical fracture sets with strike WNW-NW and approximately N-S. The existence of features NNW-1 and NNW-2 are supported by a number of indications. The existence of features NNW-5 and NNW-7 are supported by a few indications and the features should be considered as possible.

EW-1

Hydraulic conductor domain EW-1 is a complex structure (see *Stanfors et al /1997b/*), which is judged geologically to be more intensely fractured in its northern and southern parts. According to injection tests and flow-meter logging in cored hole KAS04 there are a number of rather conductive sections throughout EW-1 */Nilsson, 1989/*. However, a number of interference test showed that the core of EW-1 acts as a semi-permeable barrier */Rhén, 1988, Rhén, 1990a, Rhén et al, 1991b, Forsmark, 1992, Rhén et al, 1992/*. Due to the evaluated results from the interference tests and the geological character of EW-1 it is judged that the core of EW-1 has parts of low-conductivity, giving a average hydraulic conductivity that is less in the N-S direction than in the E-W direction. The transmissivities given in *Table 1-1* and *Figure 1-16* are for the northern and southern parts of fracture zone EW-1.

EW-3

Hydraulic tests indicate that hydraulic conductor domain EW-3 has a transmissivity which is approximately the geometric mean of the transmissivities of the deterministic structures (see *Figure 1-16*). However, the interpretation is that the core of EW-3 on the average is of low conductivity, for several reasons. The geological character is that the core of the fracture zone is clay rich (see *Stanfors et al /1997b/*). The mapping of water conducting features and documentation of pre-grouting in the tunnel */Rhén and Stanfors, 1995/* shows that the tunnel is fairly wet and pre-grouted south of EW-3 but dry and with no pre-grouting some hundred metres north of EW-3, see *Figure 1-14*.

On a few occasions there were large flows of water into the tunnel during the construction of the tunnel south of Äspö. The measured hydraulic responses show good hydraulic communication through EW-3 where NNW-4 and NNW-2 intersects EW-3 but not west of these NNW features, see *Figure 1-15 /Stanfors et al, 1992, Rhén and Stanfors, 1993/*. The interpretation is therefore that the conductivity of the core of EW-3 is fairly low but the outer part of EW-3 is rather conductive and the evaluated transmissivity probably represents the outer part of EW-3.

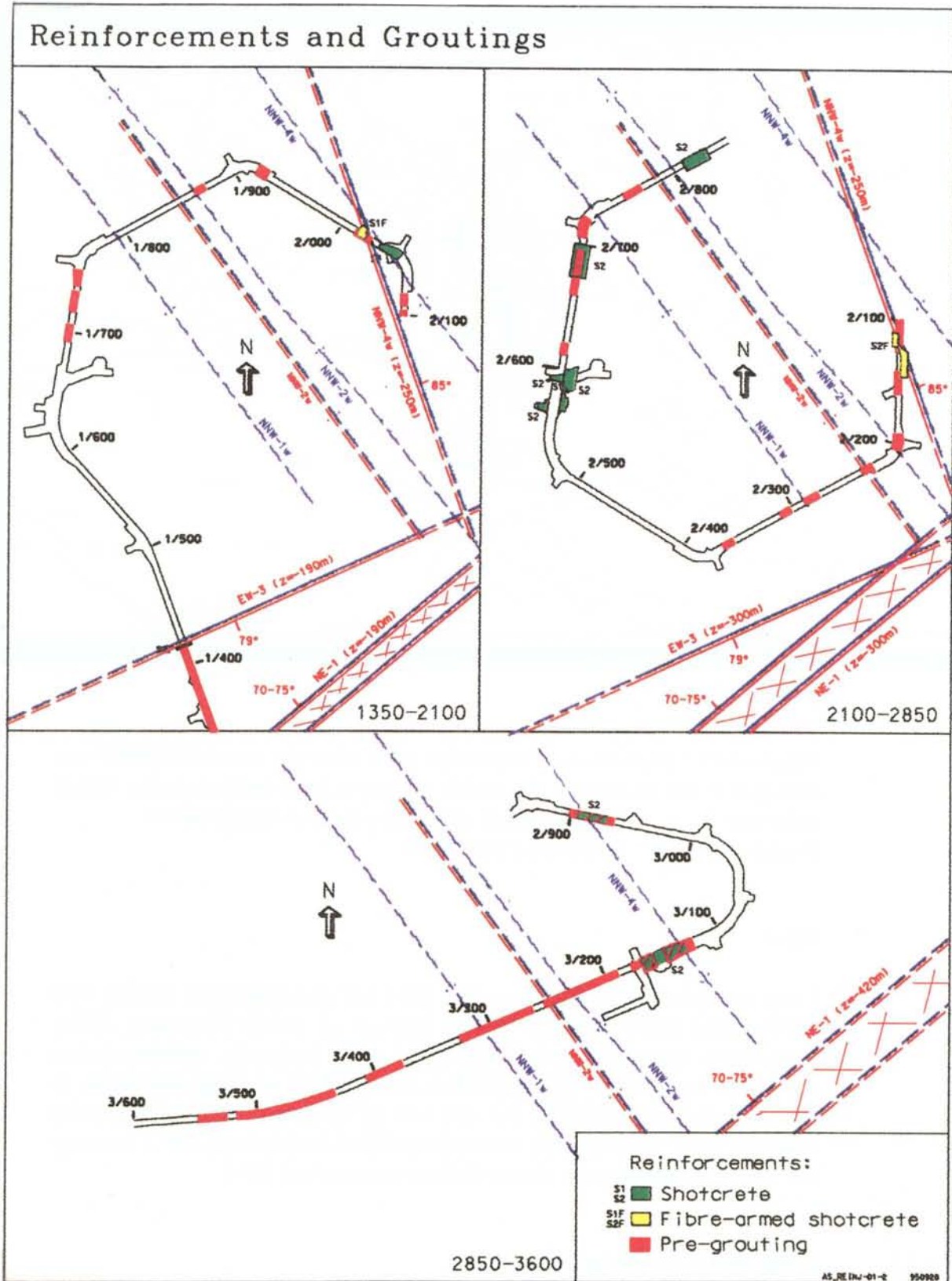


Figure 1-14. Overview of reinforcements. Pre-grouting was the main reinforcement method employed in order to limit the water flow into the tunnel. At a few places it was necessary to use shotcrete for rock stability reasons. The predicted position of the NNW features is shown as single broken line. NNW-1w has the same position in Model 96 as in Model 90. /Rhén and Stanfors. 1995/.

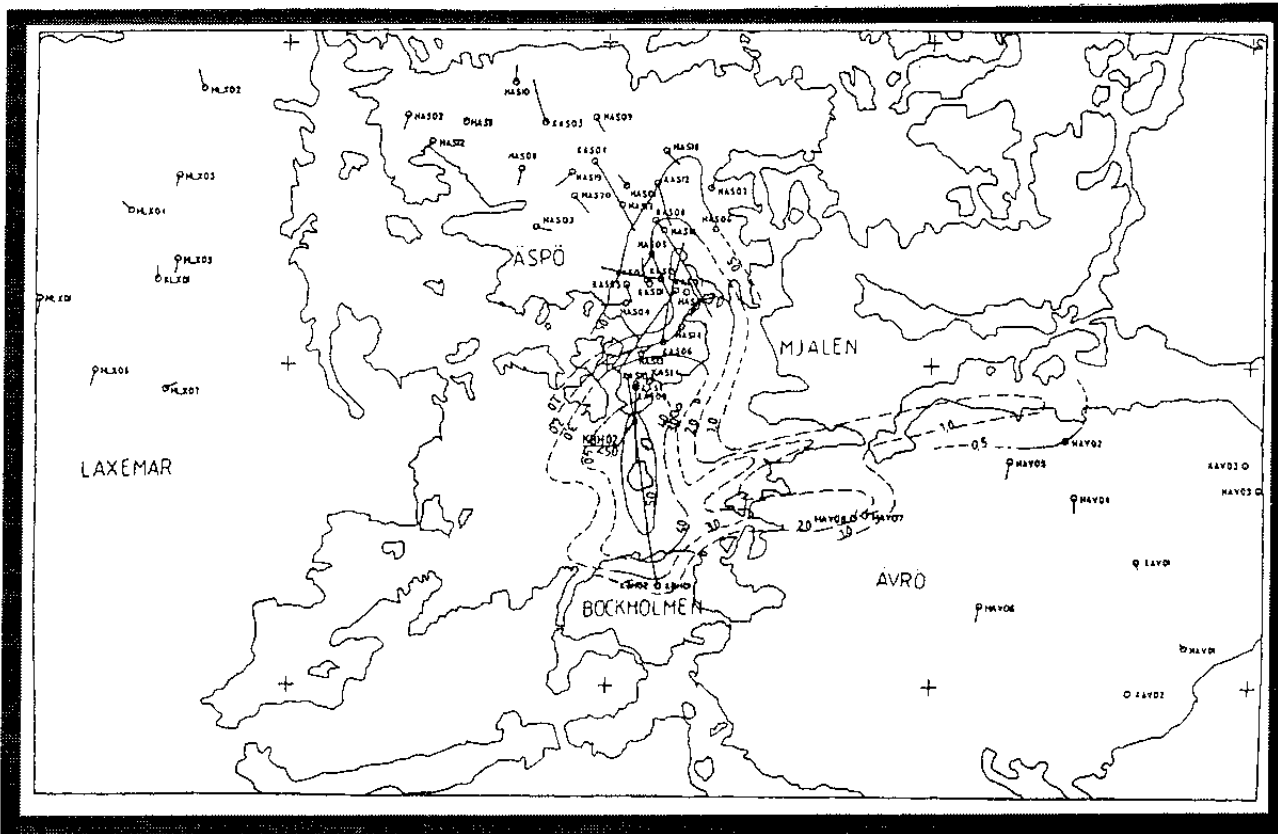


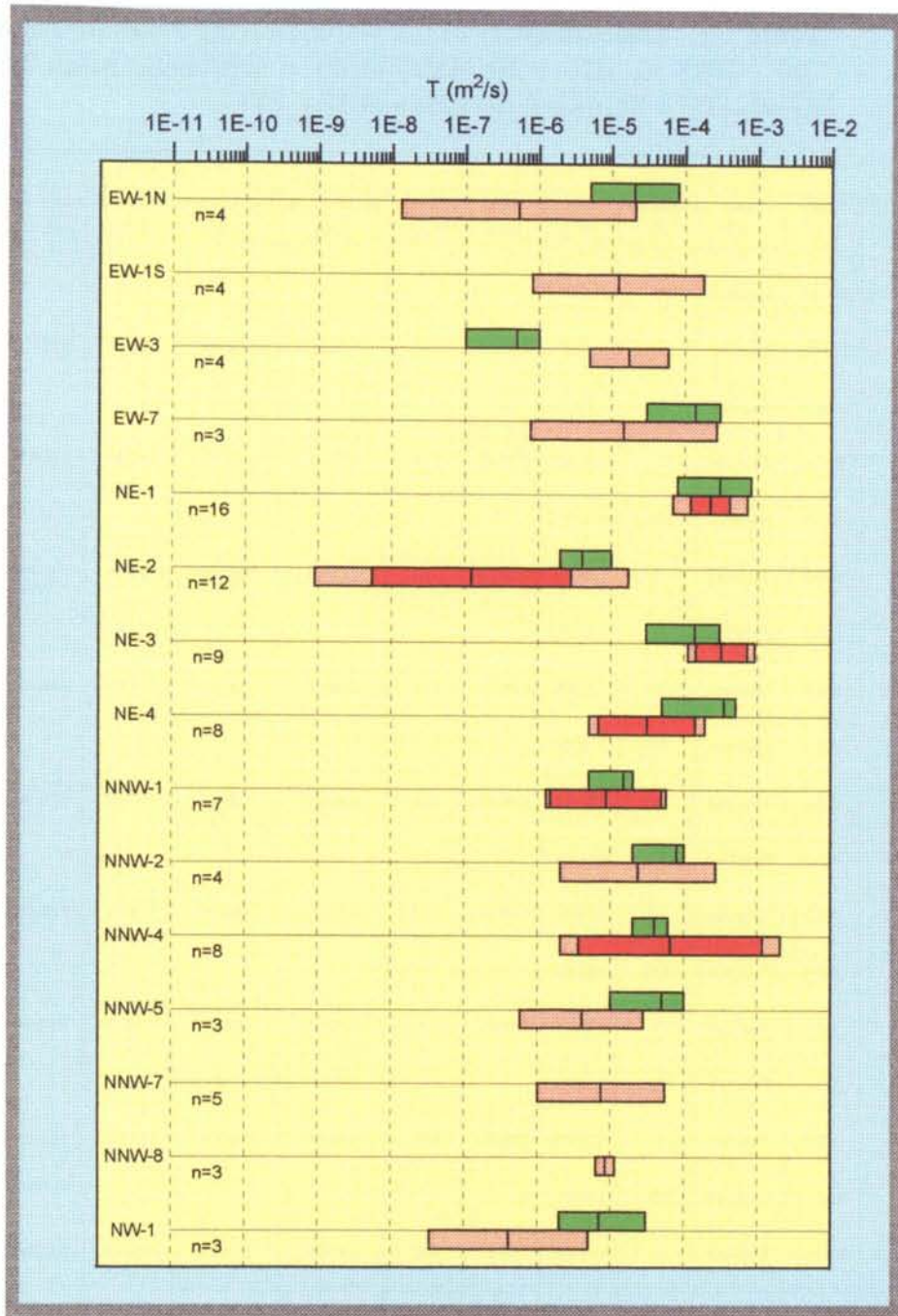
Figure 1-15. Drawdown 19 September 1991 when the corehole KBH02 was damaged by the blasting in the tunnel, causing a large inflow into the tunnel.
 Solid line: Measurements supporting the shown drawdown.
 Broken line: Interpreted drawdown.

NE-1

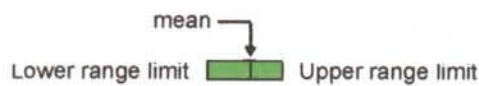
There are several tests that show that NE-1 has good hydraulic contact with NNW-2 and NNW-4 /Rhén, 1990a, Rhén et al, 1991b, Forsmark, 1992/. Draw-down responses clearly indicated good hydraulic communication northward from NE-1 where NNW-4 and NNW-2 are supposed to be in hydraulic contact with NE-1 but not west of these two features /Rhén and Stanfors, 1993/. It is therefore assumed that NE-1 cuts through EW-3 in a way that does not significantly reduce the transmissivity of NE-1.

1.3.2 Properties of water-bearing zones

The predictions and outcomes of the transmissivities of the water-bearing zones are shown in Figure 1-16 and Table 1-1. The range of the outcome is between the maximum and minimum values of the transmissivities. The uncertainty range for the predictions was expert judgement.



PREDICTION



OUTCOME

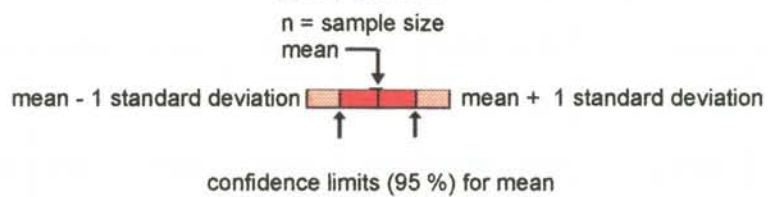


Figure 1-16. Transmissivity of water-bearing zones for tunnel section 700 - 2875 m. Site scale.(mean = arithmetic mean of $\text{Log}_{10}(T)$, standard deviation = Standard deviation of $\text{Log}_{10}(T)$, n = sample size). EW-1S, NNW-7, 8 are new water-bearing zones and NW-1 was re-evaluated.

Table 1-1. Transmissivity (T) of water-bearing zones for tunnel section 700 - 2875 m. (ET = No data, mean = arithmetic mean of $\text{Log}_{10}(T)$, $s(\text{Log}_{10}(T))$ = Standard deviation of $\text{Log}_{10}(T)$).

Zone (-)	Status (-)	Sample size (-)	Mean (m ² /s)	Median (m ² /s)	s (Log ₁₀ T) (-)	Conf. lim. (97.5 %) (m ² /s)	Conf. lim. (2.5 %) (m ² /s)	Mean + st.dev (m ² /s)	Mean - st.dev (m ² /s)	Upper range (m ² /s)	Lower range (m ² /s)
EW-1N	Prediction	ET	2.0E-05							8.0E-05	5.0E-06
EW-1N	Outcome	4	5.2E-07	1.5E-06	1.60	1.8E-04	1.5E-09	2.1E-05	1.3E-08		
EW-1S	Prediction	ET	ET							ET	ET
EW-1S	Outcome	4	1.2E-05	2.2E-05	1.17	8.8E-04	1.7E-07	1.8E-04	8.1E-07		
EW-3	Prediction	ET	5.0E-07							1.0E-06	1.0E-07
EW-3	Outcome	4	1.7E-05	2.4E-05	0.54	1.2E-04	2.4E-06	5.9E-05	5.0E-06		
EW-7	Prediction	ET	1.4E-04							3.0E-04	3.0E-05
EW-7	Outcome	3	1.5E-05	6.8E-05	1.27	2.1E-02	1.0E-08	2.7E-04	7.8E-07		
NE-1	Prediction	ET	3.0E-04							8.0E-04	8.0E-05
NE-1	Outcome	16	2.2E-04	3.0E-04	0.51	4.2E-04	1.2E-04	7.2E-04	6.9E-05		
NE-2	Prediction	ET	4.0E-06							1.0E-05	2.0E-06
NE-2	Outcome	12	1.2E-07	4.1E-07	2.14	2.8E-06	5.3E-09	1.7E-05	8.8E-10		
NE-3	Prediction	ET	1.4E-04							3.0E-04	3.0E-05
NE-3	Outcome	9	3.2E-04	2.9E-04	0.46	7.2E-04	1.4E-04	9.2E-04	1.1E-04		
NE-4	Prediction	ET	3.5E-04							5.0E-04	5.0E-05
NE-4	Outcome	8	3.1E-05	3.0E-05	0.79	1.4E-04	6.8E-06	1.9E-04	5.0E-06		
NNW-1	Prediction	ET	1.5E-05							2.0E-05	5.0E-06
NNW-1	Outcome	7	8.6E-06	1.1E-05	0.82	4.9E-05	1.5E-06	5.6E-05	1.3E-06		
NNW-2	Prediction	ET	8.0E-05							1.0E-04	2.0E-05
NNW-2	Outcome	4	2.4E-05	5.6E-05	1.06	4.4E-03	1.3E-07	2.7E-04	2.1E-06		
NNW-4	Prediction	ET	4.0E-05							6.0E-05	2.0E-05
NNW-4	Outcome	8	6.5E-05	1.5E-04	1.50	1.2E-03	3.6E-06	2.1E-03	2.1E-06		
NNW-5	Prediction	ET	5.0E-05							1.0E-04	1.0E-05
NNW-5	Outcome	3	4.0E-06	2.0E-06	0.84	4.9E-04	3.3E-08	2.8E-05	5.9E-07		
NNW-7	Prediction	ET	ET							ET	ET
NNW-7	Outcome	5	7.5E-06	4.8E-06	0.87	8.9E-05	6.3E-07	5.5E-05	1.0E-06		
NNW-8	Prediction	ET	ET							ET	ET
NNW-8	Outcome	3	8.4E-06	1.0E-05	0.13	1.8E-05	4.1E-06	1.1E-05	6.3E-06		
NW-1	Prediction	ET	7.0E-06							3.0E-05	2.0E-06
NW-1	Outcome	3	4.1E-07	1.7E-07	1.08	2.0E-04	8.4E-10	5.0E-06	3.4E-08		

In *Figure 1-17* and *Table 1-2* the outcome is described in relation to the depth of the measured values. The base for the outcome is the evaluated transmissivities for borehole sections which are interpreted to be intersected by a water-bearing zone, as defined by the evaluation and the fitting of a plane to the observations on surface and in boreholes.

Table 1-2. Statistics of the outcome of transmissivity of hydraulic conductor domains shown in *Table 1-1*. Zonation. Äspö area. (ET = No data, mean = arithmetic mean of $\text{Log}_{10}(T)$, $s(\text{Log}_{10}(T))$ = Standard deviation of $\text{Log}_{10}(T)$).

Upper level	Lower level	Sample size	Mean	Median	$s(\text{Log}_{10} T)$	Conf.lim.(97.5 %)	Conf.lim.(2.5 %)	Mean + st.dev	Mean - st.dev
0	-100	18	4.9E-06	1.1E-05	1.36	2.3E-05	1.0E-06	1.1E-04	2.1E-07
-100	-200	28	9.9E-05	1.8E-04	0.93	2.3E-04	4.3E-05	8.4E-04	1.2E-05
-200	-300	19	1.3E-05	1.1E-05	1.26	5.4E-05	3.3E-06	2.4E-04	7.4E-07
-300	-400	16	1.8E-06	1.0E-05	2.36	3.3E-05	9.9E-08	4.2E-04	7.8E-09
-400	-500	10	1.0E-05	1.8E-05	1.20	7.2E-05	1.4E-06	1.6E-04	6.4E-07
-500	-600	ET	ET	ET	ET	ET	ET	ET	ET
-600	-700	ET	ET	ET	ET	ET	ET	ET	ET
-700	-800	ET	ET	ET	ET	ET	ET	ET	ET
0	-500	91	1.4E-05	3.1E-05	1.55	2.9E-05	6.5E-06	4.9E-04	3.9E-07

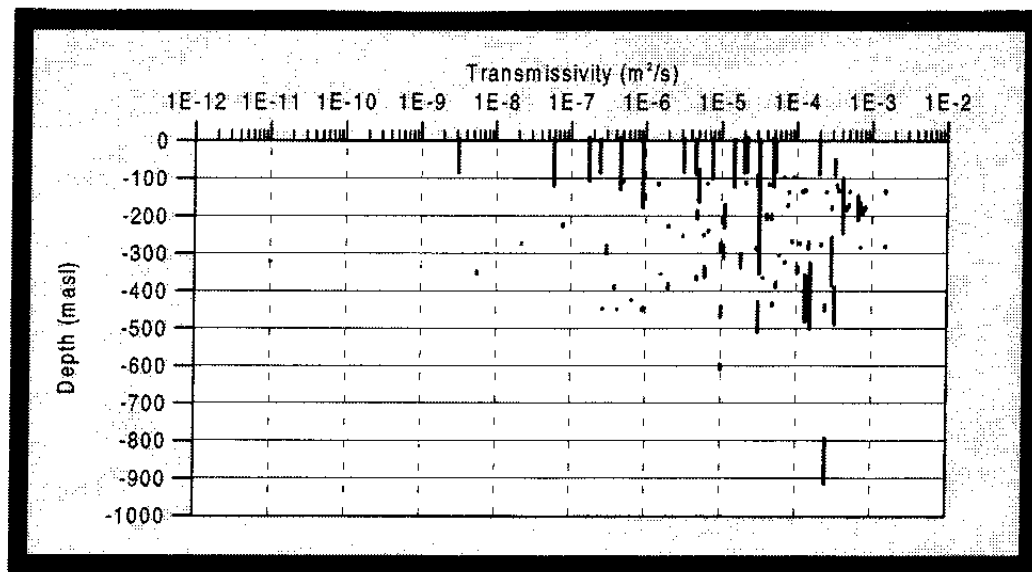


Figure 1-17. Distribution of transmissivities of hydraulic conductors shown in *Table 1-2*. Äspö area.

1.4 SCRUTINY AND EVALUATION

Water-bearing zones EW-7, NE-4, NE-3, NE-1 and EW-3

The prediction of the transmissivity of EW-7 was based on an air-lift test in KBH01. The predictions for NE-4 and NE-3 were based on two of the air-lift tests in KBH02 and the prediction in NE-1 was based on several tests in NE-1. The value of the transmissivity of EW-3 was based solely on one air-lift test in the uppermost part of KAS06. The outcome for NE-1, NE-3 and NE-4 correspond well to the predictions but the outcome for EW-3 and EW-7 does not correspond well to the predictions.

Considering EW-7, it was the geological model of EW-7 which showed the intersection between the zone and KBH01 giving reasons to believe that the evaluated transmissivity was that of EW-7. However, during the '*Passage of fracture zones*' project EW-7 turned out to be somewhat different from the prediction concerning the position and character. It was possibly N-S features which were tested in KBH01 */Stanfors et al, 1992/*.

The hydraulic tests in KBH02 showed the existence and local properties of water-bearing zones NE-4, NE-3 and NE-1 and tests in the tunnel confirmed the results. The very limited investigations gave no major indications of the geometry of the features to support the geological interpretation. The hydraulic test conditions were difficult as KBH02 was rather sharply curved after approximately 100 m. Better test conditions would have given better description of the hydraulic conditions along the borehole and probably more reliable properties but probably not much more considering the geometry.

Considering EW-3, the air-lift test may have been of poor quality. During the LPT2 test the transmissivity of EW-3 was estimated at $2.1 \cdot 10^{-5} \text{ m}^2/\text{s}$ */Rhén et al, 1992/*. However, not only the air-lift test indicated a low transmissivity, the injection tests in the part of the borehole where EW-3 was assumed to intersect also indicated low transmissivity. The geological characterization also indicated low transmissivity (see *Wikberg et al, /1991/*).

Geological investigations in the tunnel confirmed the existence and geometry of EW-3. Supplementary hydraulic tests from the tunnel supported the estimated transmissivity in *Rhén et al /1992/*. No investigations were performed to confirm the lower values of the transmissivity at deeper levels.

The errors in the position and properties of EW-7 are of minor importance for the groundwater flow calculations near the tunnel spiral of the Äspö HRL because NE-4, NE-3 and NE-1 dominate the conductivity field south of Äspö. The error in the properties of EW-3 are of some importance for the groundwater flow calculations.

Water-bearing zones EW-5 and NE-2

The prediction of EW-5 was based on pumping test No 2 in KAS06 /*Rhén, 1990*/ and the geological interpretation of the possible fracture zone EW-5 /*Wikberg et al, 1991*/. The outcome for EW-5 is not shown in *Figure 1-11*. The reason is that EW-5 was not confirmed underground. At a depth of about 300-350 m a larger volume of fine-grained granite seems to be present /*Rosén and Gustafson, 1995*/. As fine-grained granite has a higher hydraulic conductivity than the other main rock types at Äspö the responses may be explained by the presence of this body.

NE-2 was geologically well defined at some points /*Stanfors et al, 1993 and Wikberg et al, 1991*/ and was judged to be moderately hydraulically conductive. Only one hydraulic test was judged to give a representative transmissivity of NE-2, an air-lift test in the upper part of KAS08 /*Nilsson, 1990*/. The reason was that the NNW features seemed to dominate the responses in the pumping tests in borehole sections which were considered to intersect NE-2.

Water-bearing zones NNW-1, 2, 4, 5 and 7

The prediction of NNW-1 was based on pumping test No. 2 in KAS02 /*Rhén, 1988*/ and tests 1 and 3 in KAS06 /*Rhén, 1990*/>.

The prediction of NNW-2 was based on pumping test No. 4 in KAS06 /*Rhén, 1990*/. However, several pumping tests in fracture zone NE-1 and inflows into the tunnel south of Äspö caused draw-downs which could be explained by NNW-2 /*Rhén et al, 1990a, Rhén et al, 1991b, Rhén and Stanfors, 1993*/>.

The test in cored hole 2162B confirms the existence and approximately the position of two of the predicted NNW-features; NNW-1 and NNW-2.

The conductive part in cored borehole KA3191F, drilled along the TBM tunnel /*Rhén et al 1995*/, and in KC0045F /*Olsson et al, 1994*/ complies rather well with the predicted NNW-2. Based on results from the supplementary investigations /*Rhén and Stanfors 1995*/ NNW-2 was moved to the west (see *Figure 1-15*). Where NNW-1 was supposed to intersect the tunnel and the boreholes conductive features were found in some cases and in some cases not /*Rhén and Stanfors, 1995*/>.

The prediction of NNW-4 has been confirmed in several tunnel sections (see *Stanfors et al /1997b*). The character is more a fracture zone (defined in *Stanfors et al /1997b*/) than a fracture swarm.

A few boreholes were drilled from the tunnel towards the west. These boreholes intersect conductive features at about the position where NNW-5 was expected. It was interpreted that the feature could possibly be NNW-5. However, the interpretation should be considered uncertain /*Olsson et al, 1994*/>.

NNW-7 was not predicted. The flow-meter logging in KAS13 /*Rhén et al, 1991b*/ indicated a conductive feature where NNW-7 now is, but as the draw-down observed did not give any indication of the direction of the feature and nor did the geological investigations provide any conclusive information, so the feature was not put into the model. Later when the draw-down due to the inflow into the tunnel was modelled with the measured flow into the tunnel it was noted that it was impossible to reproduce the draw-down around the shaft without a new feature at approximately the same position as NNW-7/ *Svensson, 1994, and Rhén et al, 1994a*/.

Water-bearing zones NW-1 , and NNW-8

The outcome was for these zones based on re-evaluation of data from the pre-investigations.

Conclusions

By making a comparison between the prediction based on the pre-investigation data and the tunnel documentation it is possible to make a judgement of the reliability of the methodology and methods used are for predicting rock-mass properties of interest. This is summarized below.

Geometrical framework

Identification of a water-bearing zone (hydraulic conductor domain) with respect to its existence, position and extent must generally be based on geological and geophysical investigations. However, interference tests may be a very useful compliment to the geological and geophysical interpretations of the position and extent of a certain zone. Hydraulic tests must be performed to estimate the hydraulic connectivity within the zone and the connectivity to other zones. Low transmissivity of a zone and/or long distances between the observation points for the pressure responses, however, give less chance to confirm by means of interference tests a zone suggested from the geological and geophysical investigations.

In some cases, as for what are here called fracture swarms, it is difficult to define the water-bearing zones by means of geological and geophysical investigations, but the position can be indicated from the interpretation of interference tests. However, the possibility of making an identification is very dependent on the number of observation boreholes and the way in which they are equipped (number of packed of sections) and their positions in relation to the pumped borehole.

Even though it has not been shown at the Äspö HRL there should be good possibilities of identifying by means of an interference test a subhorizontal conductive feature in the case where several boreholes penetrate the feature

within a distance of a few hundred metres and with the boreholes packed off in a proper manner.

The concept of deterministic hydraulic conductor domains is found useful and feasible. The hydraulic conductor domains of importance were found in approximately the predicted intersections of the tunnel or at positions close to the tunnel spiral. The numerical groundwater flow modelling shows that the measured hydraulic potential can be fairly well described using the hydraulic conductor domains and their transmissivities given in the descriptive geohydrological model /Wikberg *et al*, 1991, Svensson, 1991, 1994, 1995, Gustafson and Ström, 1995/. Based on the results from the groundwater flow modelling and re-evaluation of available data a few minor changes in the hydraulic conductor domains were made in 1996. However, the fracture swarms given deterministic positions and extents can possibly be modelled as stochastic features in space or by assigning anisotropic material properties to the rock mass where these features were defined.

The extension of the hydraulic conductor domains outside southern Äspö and deeper than some 1000 m should be considered uncertain due to the limited investigations. The reason for the limited investigations is that the pre-investigations were focused on the actual site for the Äspö HRL. Somewhat more investigations should probably have been performed to provide a better opportunity of defining the geometry of the hydraulic conductor domains somewhat outside the rock volume for the facility. Therefore, at some distance from a facility in the rock mass it will be of less importance to know the exact geometries and properties of the hydraulic conductor domains for calculations of the flow field in the rock volume for the facility. At some distance from the facility less intensive investigations than in the site area for the facility should be sufficient for the regional description of the hydraulic conductor domains.

In the cases where the predictions were less good, a number of uncertainties were announced in the predictions but still the features were judged to be deterministic because several indications pointed in the same direction. If a number of uncertainties concerning a domain are announced a thorough re-evaluation and possibly some new investigations can reduce the uncertainties. If no new investigations are possible at the time there will probably remain uncertainties and these must of course be expressed in the model.

Material properties

If there are a few boreholes through an identified hydraulic conductor domain where reliable hydraulic tests have been performed the transmissivity of the feature can be predicted fairly well. Estimation of the storativity, which was not a predicted property, of the feature is more difficult as it is necessary to have observation boreholes in the same feature rather near the pumped borehole, which is not always the case.

It is important for the borehole section intersecting the hydraulic conductor domain to be at some distance from hydraulic conductor domains with higher

transmissivities than the tested zone, otherwise it is likely that the evaluation of the test will not give the correct transmissivity for the domain. The test can, however, be useful for the interpretation of the connectivity between domains.

If the hydraulic conductor domains are well defined, the air-lift tests seem generally to give reasonable transmissivities of the hydraulic conductor domains. However, flow rates and draw-down/recovery are generally much better controlled during a pumping test and permit more reliable estimates.

The results show that the variability of the transmissivity within a geologically well defined hydraulic conductor domain is rather large (standard deviation of $\text{Log}_{10}(\text{transmissivity})$ is about 0.5 to 1) but the predicted ranges for the mean transmissivity (arithmetic mean of $\text{Log}_{10}(\text{transmissivity})$) are generally within confidence limits for the mean for the outcome. The variability of the transmissivity within a hydraulic conductor domain geologically defined as a fracture swarm or complex zone (EW-1) is rather large (standard deviation of $\text{Log}_{10}(\text{transmissivity})$ is about 1 to 1.5). The standard deviation for the low transmissive feature NE-2 is, however, high (the standard deviation of $\text{Log}_{10}(\text{transmissivity})$ is about 2).

Spatial assignment method

The assignment of the transmissivity as a constant value for each hydraulic conductor domain seems useful if solely the hydraulic potential within the model is considered. The numerical groundwater flow modelling shows that the measured hydraulic potential can be described fairly well using the hydraulic conductor domains and their transmissivities given in the descriptive hydrogeological model /Wikberg *et al*, 1991, Svensson 1991, 1994, 1995b, Gustafson and Ström, 1995/. A stochastically distributed transmissivity within a hydraulic conductor domain would be more realistic but has only been tested so far on the site scale /Svensson, 1994/ and on the detailed scale for a fracture /Kuylenstierna and Svensson, 1994/. The evaluated properties indicate that the standard deviation for the $\text{Log}_{10}(\text{transmissivity})$ is about 0.5 to 1. The number of samples per domain is so small (see *Figure 1-16*), that it is difficult to judge if lognormal distribution (or any other distribution) of the transmissivity values for a domain is justified in general, but the more transmissive domains with sample size larger than 4 data points seem to be of approximately lognormal distribution. The sample sizes were also so small that it was not justifiable to estimate a correlation model within a domain. It is a difficult task to decide the design of tests and the number of tests needed to find estimate of the correlation models within the hydraulic conductor domains. Probably one needs many and well-controlled tests. A specific problem is for example how to evaluate the support scale (or influence radius) for an effective parameter that is evaluated.

There does not seem to be any significant change in the transmissivity with depth. *Table 1-2* seems to indicate a decrease with depth but is here considered to be a false interpretation because the depth interval -100 to -200 m mainly represents data from the domains below the Baltic Sea, which have high

transmissivities, and the other depth intervals represents mainly southern Äspö.

In order to better estimate the spatial distribution of transmissivity within hydraulic conductor domains at least a few more hydraulic tests should be performed in some of the major domains than was done during the investigations.

Methods

The types of methods and number of hydraulic tests used seem to have been sufficient to define the hydraulic conductor domains near the Äspö HRL correctly. However, the hydraulic tests in the cored holes were less extensive in the uppermost 100 m in the boreholes. Due to this the interpretation became more difficult and uncertain. The standardized investigations should be performed in a consistent way in the entire borehole using a few methods. Specially designed tests may then be conducted in, for example, parts of the borehole where a hydraulic conductor domain is assumed to intersect the borehole.

Flow rates and drawdown/recovery are generally much better controlled during a pumping test and permit more reliable estimates compared with an air-lift test. However, in cases where both pumping tests and air-lift tests were performed the air-lift tests seem generally to give relatively reliable transmissivities of the hydraulic conductor domains.

Transient testing methods are preferred because they provide an opportunity to evaluate the flow regime and give some rationale for the choice of evaluation method. The hydraulic resistance around the borehole ('skin') that is always more or less present may also be separated from the properties of surrounding rock, which cannot be done using stationary evaluation methods. Transient tests are also useful for calibration of numerical models.

Interference tests can be rather time-consuming in planning, execution, processing of data and evaluation of data. It is very important to plan interference tests and other activities, which may cause pressure responses (for example drilling) so that they do not interfere with each other. If other tests or activities causes pressure responses, they may ruin the interference test.

During interference tests the drawdown and recovery period was generally 3+2 days. This was a good choice in terms of the influence on a large volume of rock, which is good for calibration purposes, and to reduce the negative influence earth tides may have on the evaluation of the hydraulic properties. Far away from the pumped borehole the responses are generally small and earth tides generally disturb the responses. If the measurement period is several days, the approximate trends caused by the pumping can still be seen, but if the pumping period is 0.5 - 1 day it may be impossible to judge if the response seen is caused by pumping or earth tides. *Figures 1-18 and 1-19* illustrates the problem with earth tides.

Minor problems are that the results are to some extent dependent on the equipment used and thus method developments during a project can possibly affect the results to some extent. It is also difficult to get reliable results from low conductivity sections of a borehole because of the elasticity of the equipment and also because of pressure oscillations.

A large number of the tests with 3 m packer spacing and the tests in the probeholes, with test length about 15 m, were low conductive giving a typical well-bore storage response for the entire test time. In the re-evaluation of the data the specific capacity was used to estimate the transmissivity of these low conductive test sections, see *Rhén (ed) et al /1997/*.

Flow-meter logging is a fast, useful and feasible method for finding hydraulic features in a borehole and obtaining a rough estimate of their transmissivities. However, in boreholes in which there is a high transmissivity in the upper part of the borehole and water with high salinity at depth in the borehole, flow-meter logging may give false results in the lower part of the borehole. The reason is that the dense, saline, water rises in the borehole up to a level where it balances the drawdown in the borehole, and the result is stagnant water in the lower part of the borehole. The results from KAS09 have indicated this problem. To obtain estimates of the hydraulic properties along the entire borehole it is therefore important to perform systematic injection or pumping tests or pumping tests within limited sections of a borehole with a double-packer system. These tests can also be performed step by step during drilling by testing the last section drilled with a single-packer system.

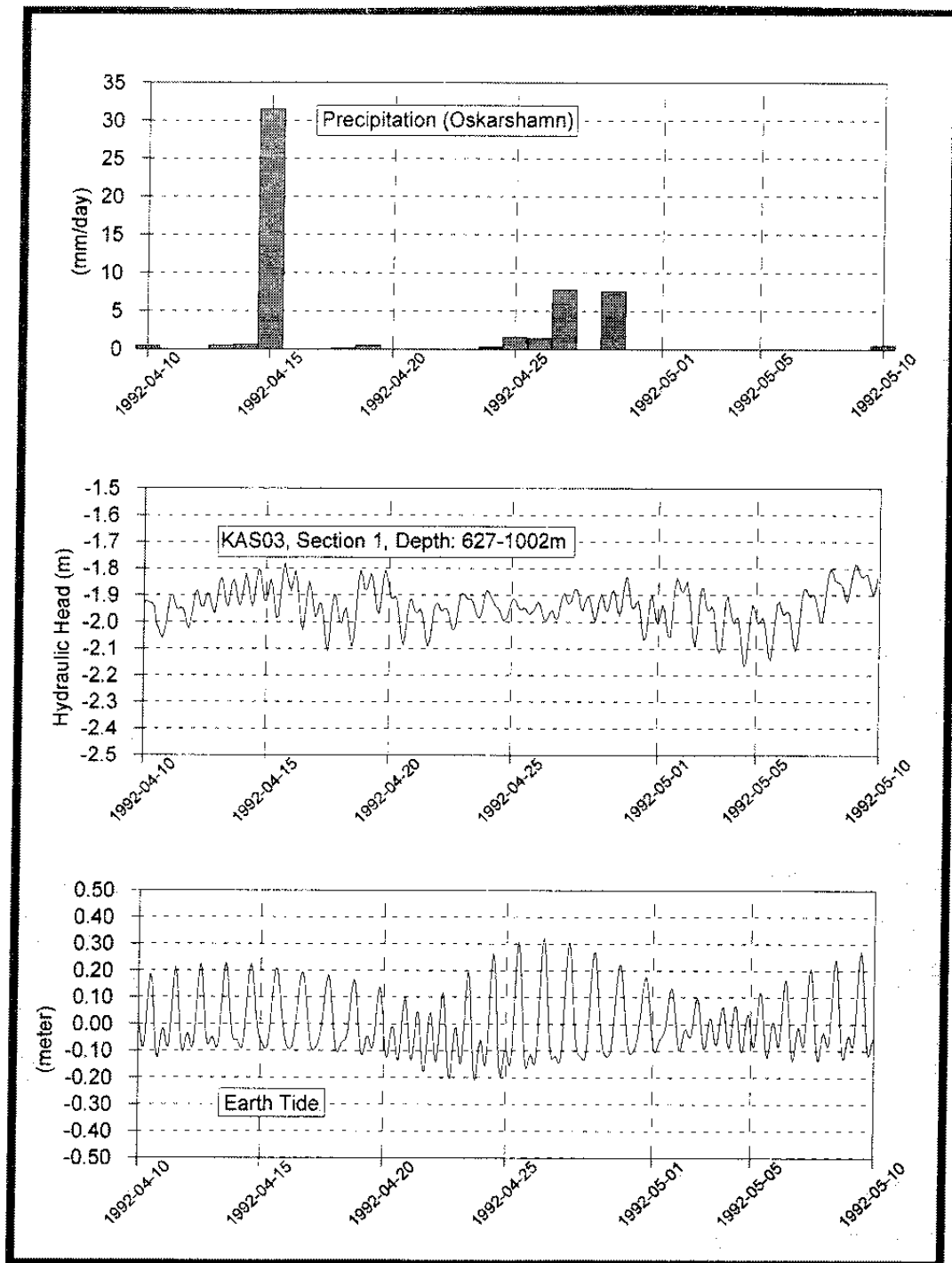


Figure 1-18. Calculated earth tides, measured precipitation and hydraulic head. The figure illustrates the influence of earth tides on hydraulic head measurements. Close to surface the influence on hydraulic head is generally small.

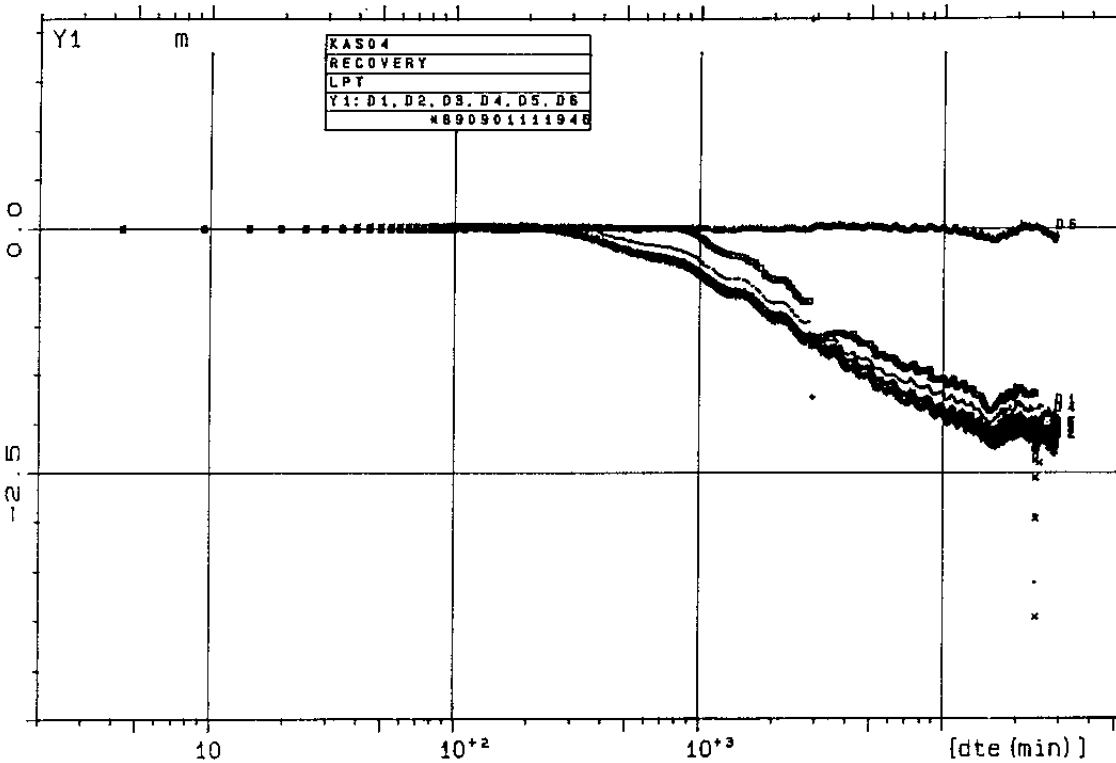
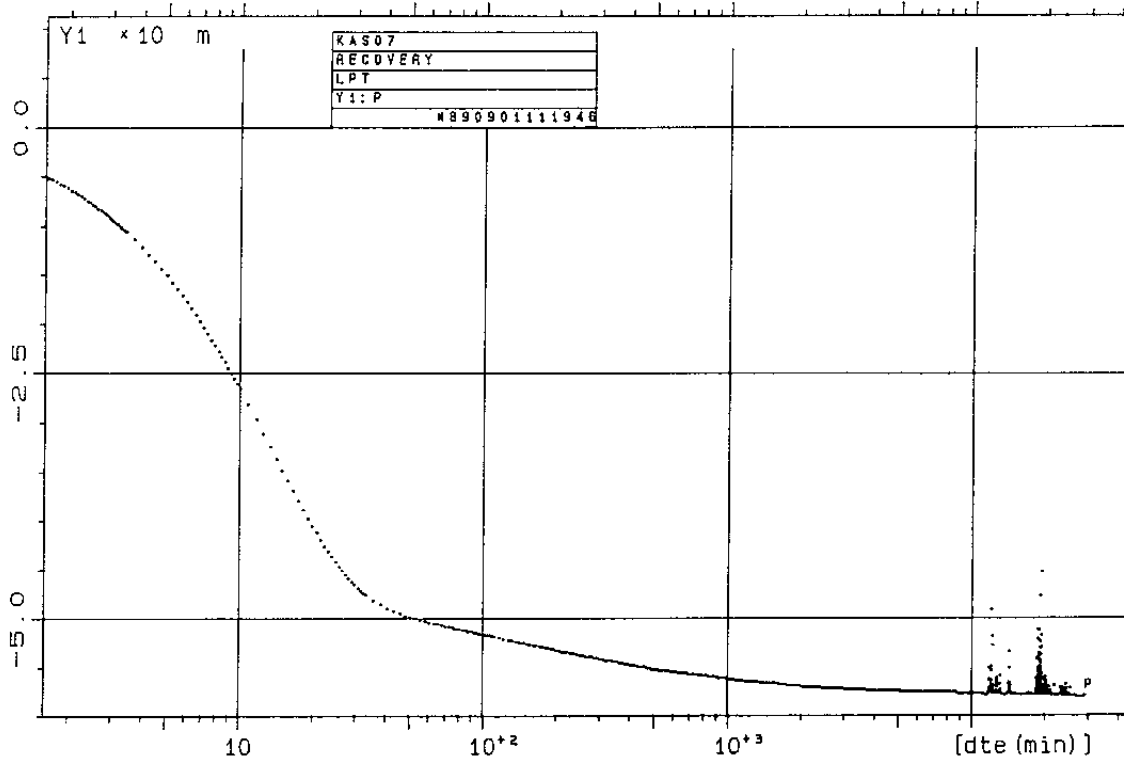


Figure 1-19. The LPT1 test.

Top: Recovery phase for the pumped borehole KAS07.

Bottom: Recovery phase in borehole KAS04. If the drawdown is just a few dm the effects of the earth tide can cause difficulties in the evaluation of the response.

2 SUBJECT: HYDRAULIC CONDUCTIVITY - SITE SCALE

2.1 SCOPE AND CONCEPTS

Hydraulic rock mass domains are geometrically defined volumes in space with properties differing from surrounding domains (rock mass domains and hydraulic conductor domains). They may either be defined by lithological domains or purely by interpretation of results from hydraulic tests. Within a domain there is a defined distribution of the properties.

The material properties chosen for the hydraulic rock mass domains are:

- Hydraulic conductivity ($K(x,y,z)$)
- Specific storage ($S_s(x,y,z)$).

K is based on evaluation of transient hydraulic tests. The properties within a domain may be given as a mean effective value for the entire domain, a trend within the domain, a statistical distribution within the domain with or without spatial correlation or any other function describing the distribution within the domain. The description of the properties assumes that the domains can be described as a continuum considering the processes. For the groundwater flow model at the Äspö HRL the following spatial assignment methods were used.

The properties of a hydraulic rock mass domain are given as a stochastic distribution for the domain. The distribution of K is assumed to be lognormal with characteristic values K_g (geometric mean) and $s_{\text{LOG}_{10}K}$ (standard deviation of $\text{Log}_{10}(K)$). K_g and $s_{\text{LOG}_{10}K}$ are scaled according to the cell size in the numerical model (see *Wikberg et al /1991/* for scale function used in the predictions). No spatial correlation is assumed between the cells used in the flow model.

Hydraulic conductivity was predicted for 100 m thick plates (vertical zonation). The zonation was not based on difference of the properties with depth but a decision that the properties along the tunnel were to be predicted for sub- volumes limited by horizontal layers 100 m apart.

The specific storage values (S_s) for the hydraulic rock mass domains were not predicted and are therefore not discussed in the text below.

2.2 METHODOLOGY FOR TESTS OF CONCEPTS AND MODELS

2.2.1 Prediction methodology

The predictions made for depth interval 200-500 m the were based on the injection tests with 3 m packer spacing (see *Chapter 1*). The hydraulic conductivity (K) was evaluated as T/L, where L = test section length and T the evaluated transmissivity for the test section.

As no injection tests were performed south of Äspö and a very limited number of hydraulic tests were performed in that area different methods were tried to estimate the properties of tunnel section 700-1475 m. These methods were outlined in Rhén *et al /1993a/*.

As the injection test scale was 3 m and the expected test scale for the probe holes was 20 m it was necessary to scale the estimated mean and standard deviation of $\text{Log}_{10}(\text{K})$ according to what was found in *Liedholm /1991b/* and also presented in *Wikberg et al /1991/*. The scaling of the standard deviation in *Gustafson et al /1991/* was based on *Liedholm /1991b (TN 19, Fig. App. 2:2)/*.

As the predictions in *Gustafson et al /1991/* were made for 20 m test sections (based on the tests with 3 m packer spacing) and the actual test sections (see *Section 2.2.2*) were about 14 m the predictions shown in the rest of the report have been scaled to 14 m as below:

- The predicted geometric mean (or median) values in *Gustafson et al /1991/* for test scale 20 m sections were multiplied by 0.7.
- The predicted standard deviation in *Gustafson et al /1991/* for the test scale of 20 m was multiplied by 1.5.

The scaling of the standard deviation in *Gustafson et al /1991/* is based on *Liedholm /1991b (TN 19, Fig. App. 2:2)/*. The relationship in *Liedholm /1991b (TN 19, Fig App. 2:1)/* was considered to possibly give a better estimate of the standard deviation and, thus, when scaling from 20 m to 14 m, *Fig. App. 2:2* was used for scale 20 m and *Fig. App. 2:1* was used for scale 14 m to obtain the value of 1.5 above.

2.2.2 Methodology for determining outcome

The hydraulic conductivity (K) was evaluated as T/L, where L = test section length (distance between bottom of borehole and packer) and T the evaluated transmissivity for the test section. The test section length was approximately 14 m. For other details see *Chapter 1*.

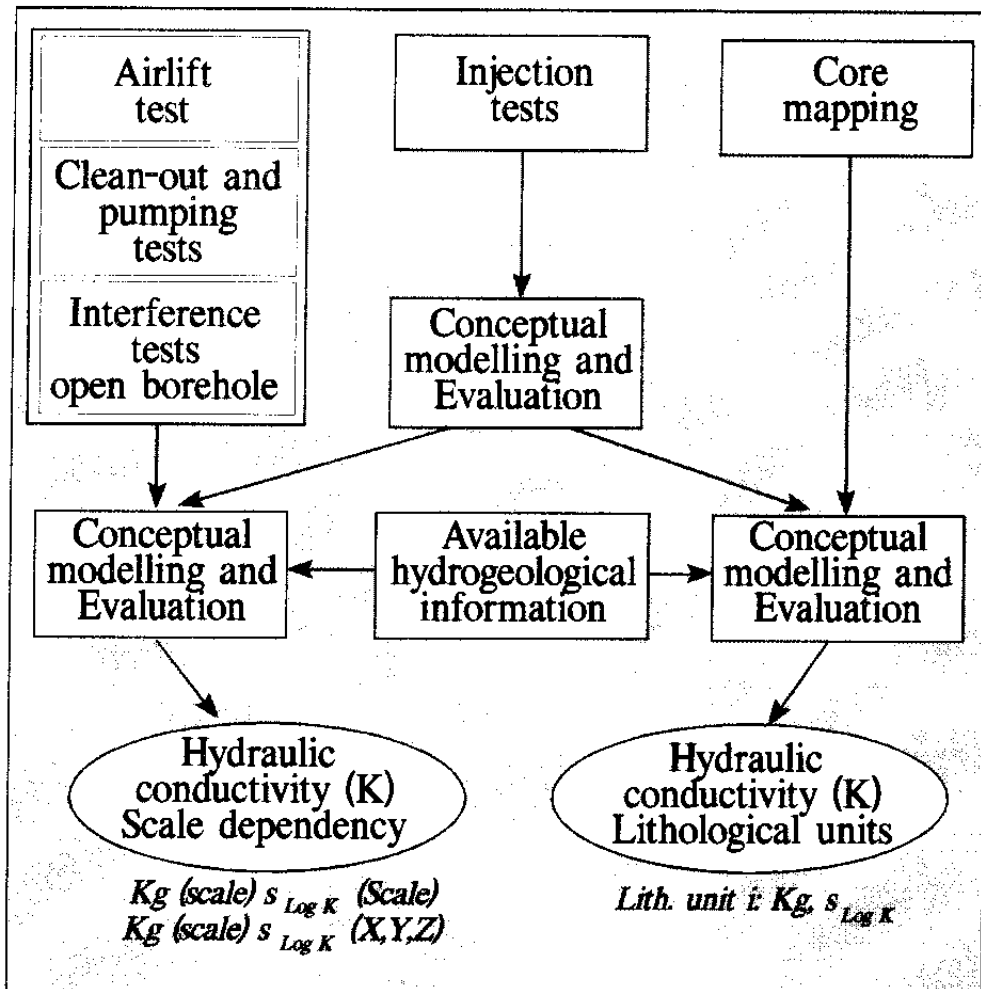


Figure 2-1. Hydraulic conductivity (K) - site scale and detailed scale. Flow chart (After Almén et al /1994/). ($K_g = 10^{\text{mean}}$, mean = arithmetic mean of $\text{Log}_{10}(K)$, $s_{\text{Log } K}$ = standard deviation of $\text{Log}_{10}(K)$, (x,y,z) = coordinates).

2.3 COMPARISON OF PREDICTED AND MEASURED ENTITIES

The predictions were based on 3-m injection tests performed in KAS02, KA05-08 for the depth intervals $Z = 200\text{-}500$ m /Liedholm, 1991a, TN 14, and Liedholm 1991b, TN 19/. These depth intervals corresponded to tunnel sections 1475 -2265, 2265 -3064 and 3064-3854 m in the predicted layout.

The prediction for tunnel section 700-1475 m was based on relation between rock composition and hydraulic conductivity Liedholm /1991a (TN No. 16)/ and the predicted lithology. Further details about the prediction are found in Rhén et al /1993a/.

Table 2-1. Hydraulic conductivity (K) from site scale test. Scale = 14 m.

Prediction = P Outcome = O	Tunnel section (m)	Geometric mean (GM) (m/s)	Lower Conf. limit 2.5% (GM) (m/s)	Upper Conf. limit 97.5% (GM) (m/s)	Standard dev. s(Log ₁₀ (K))	Sample size	Depth for sample (m)
P	0700-1475	9.8E-10	6.2E-11	1.6E-08	(1.65)	-	100-200
	1475-2265	1.1E-09	7.4E-10	1.6E-09	1.2	185	200-300
	2265-2875	1.4E-09	9.4E-10	2.1E-09	1.2	182	300-400
O	0700-1475	6.46E-07	2.6E-07	1.6E-06	1.55	62	100-200
	1475-2265	7.24E-09	2.8E-09	1.9E-08	2.03	93	200-300
	2265-2875	6.76E-10	2.1E-10	2.1E-09	2.16	74	300-400

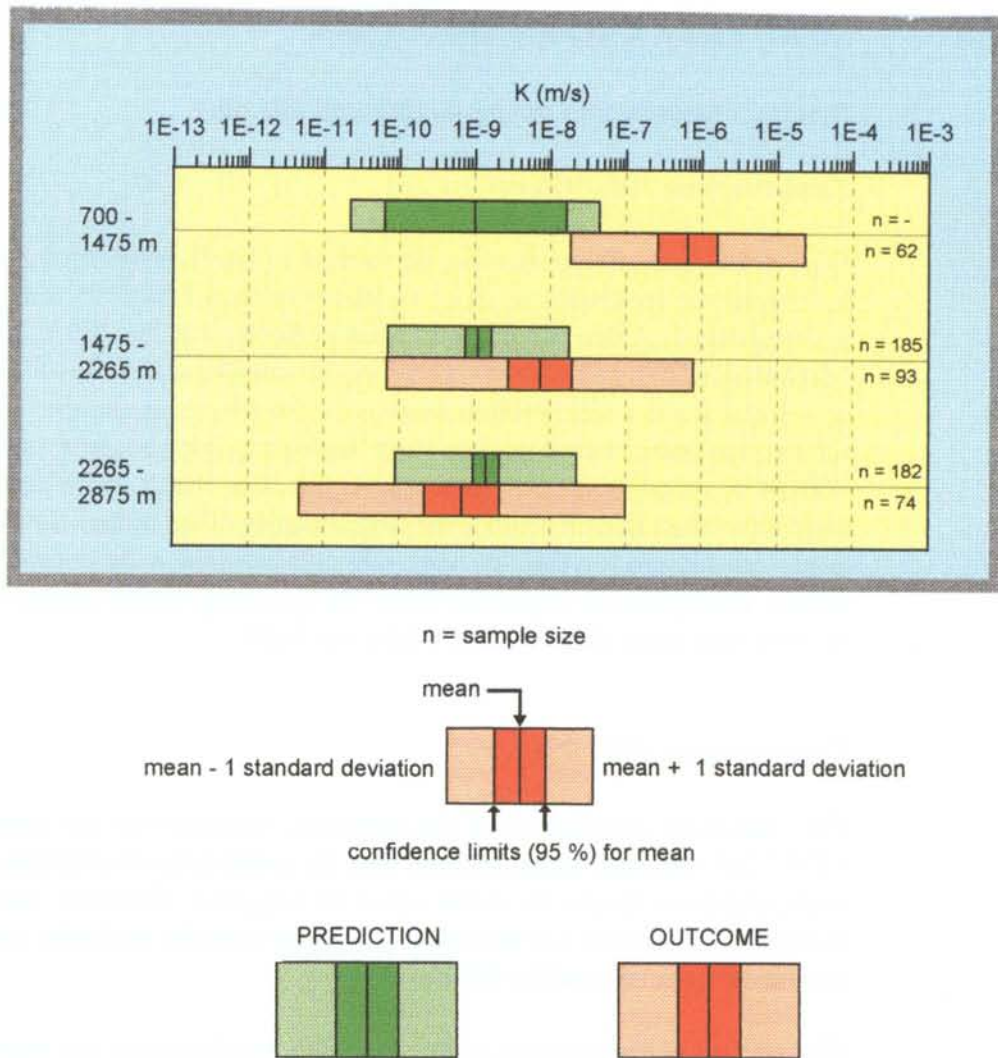


Figure 2-2. Hydraulic conductivity in tunnel section 700 - 2875 m. Site scale. Test scale 14 m (mean = arithmetic mean of $\text{Log}_{10}(K)$, standard deviation = Standard deviation of $\text{Log}_{10}(K)$, n = sample size). Evaluated data comprises both hydraulic rock mass domains and hydraulic conductor domains, but as the number of samples belonging to the latter, the statistics for the rock mass domains are almost identical to the total sample shown here, as shown in Rhén et al /1997/. It should also be observed that the predicted values were scaled from the 3 m test scale to the 14 m test scale according to the relations suggested in Wikberg et al /1991/. Scaling of test results is discussed in the text below.

Tunnel section 700 - 1475 m: depth interval 100-200 m.

Tunnel section 1475 - 2265 m: depth interval 200-300 m.

Tunnel section 2265 - 2875 m: depth interval 300-400 m.

2.4 SCRUTINY AND EVALUATION

General comments on the prediction and outcome

Tunnel section 700-1475 m

Only a few hydraulic tests were performed in boreholes drilled from ground level into the rock volume close to tunnel section 700-1475 during the pre-investigations. A few air-lift tests were performed at the 100 m test scale in borehole KBH02, no tests were performed at smaller scales. Results from Äspö at 3 m test scale were therefore used as a base for extrapolation. The result of the extrapolation (based on data from Äspö) was poor because tunnel section 700-1475 m penetrated a rock mass that was much more fractured and conductive than that on Äspö, over long stretches of the tunnel. Several fracture zones are intersected that are very transmissive and wide in that part of the tunnel. The hydraulic properties below the sea along tunnel section 700 - 1475 m were thus quite different from those on Äspö.

Tunnel section 1475-2875 m

The statistical distribution of the hydraulic conductivity for tunnel section 1475-2265 m agrees approximately with the predictions considering the ranges and confidence limits for mean value of $\text{Log}_{10}(K)$. However, the estimated hydraulic conductivity in the tunnel is greater than the hydraulic conductivity estimated from the surface holes.

The statistical distribution of the hydraulic conductivity for tunnel section 2265-2875 m agrees with the predictions considering the ranges and confidence limits for mean value of $\text{Log}_{10}(K)$. The estimated hydraulic conductivity in the tunnel is somewhat less than the hydraulic conductivity estimated from the surface holes.

Geometrical framework

The data based on the injection tests with 3 m spacing does not indicate any change in the hydraulic conductivity with depth according to *Figure 2-2* but the result based on the probe holes indicates that the hydraulic conductivity decreases from depth interval 200-300 m to 300-400 m. (Data based on probe holes and the depth interval 100-200 m should not be included in the comparison as the geology is quite different from the volume where the tunnel spiral is located.)

Several investigations in Sweden and Finland indicate that the rock becomes less permeable with depth /*Ahlbom et al, 1991a, 1991b, 1992a, 1992b, Rhén and Gustafson, 1990 and Öhberg et al, 1994*/. Rock down to a depth of 100 or 200 m has an effective hydraulic conductivity (K) 100-1000 times greater than the effective K for the depth 500-1500 m according to the regression lines in the reports.

At the four SKB study sites there are hardly any low-conductivity borehole sections down to 100-200 m depth, but below this depth a large number were recorded as being at the lower measurement limit /*Ahlbom et al, 1991a, 1991b, 1992a, 1992b*/, see examples in *Figure 2-3*. The hydraulic conductivity is definitely lower below 100 to 200 m compared with above, but the suggested decrease based on a power function can be discussed. From an examination of the plots it is not obvious that there is a clear decrease below 100-200 m. A similar conclusion is drawn in *Winberg /1989/*. In that report it is concluded that there is mainly a variation with depth around a constant mean value for the hydraulic conductivity below 200 m depth at the sites Gideå, Fjällveden and Kamlunge.

For three of the sites (Gideå, Fjällveden and Kamlunge) the fracture frequency is 4-5.5/m down to 100 to 200 m and 2-2.5/m below 200 m at two sites and below 500 m at one site (Gideå). The fracture frequency is fairly constant below the depths mentioned above. The rock types at these three sites are mainly sedimentary gneiss (Fjällveden and Gideå) or a mixture of sedimentary gneiss and granite (Kamlunge). The fourth site is dominated by Småland granite (Klipperås) .

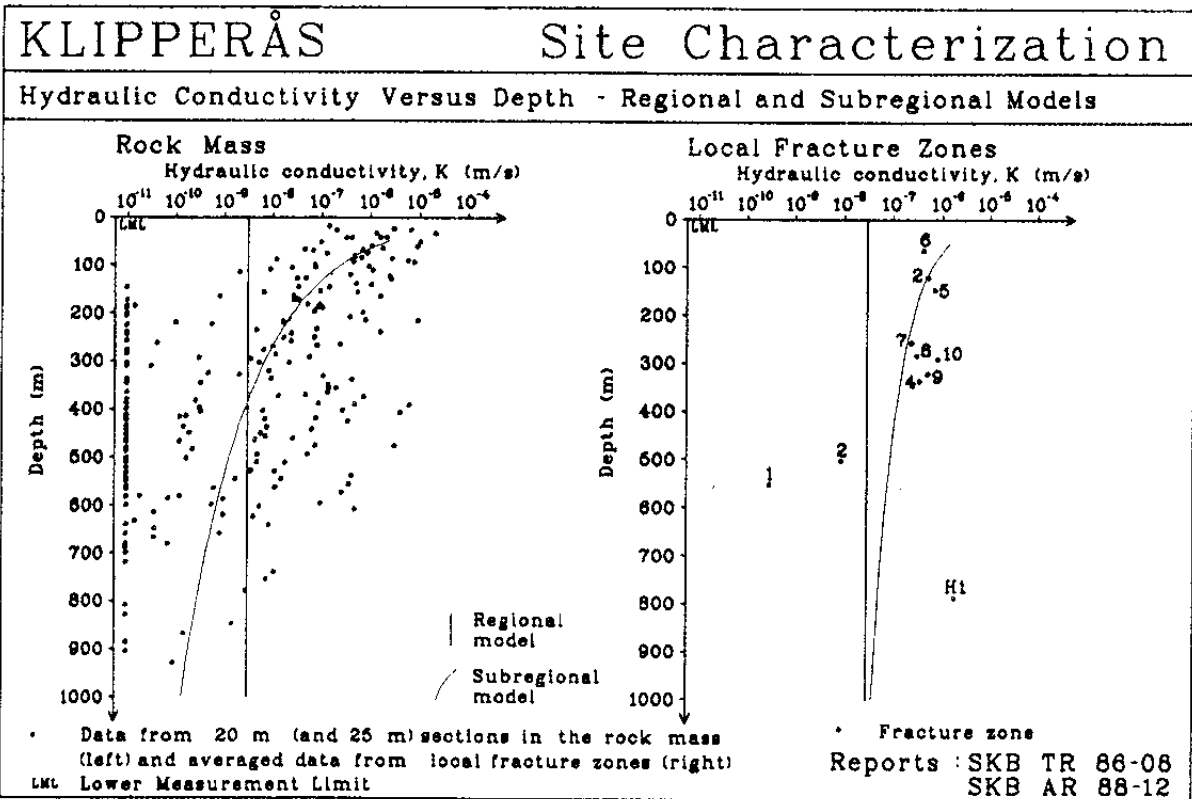
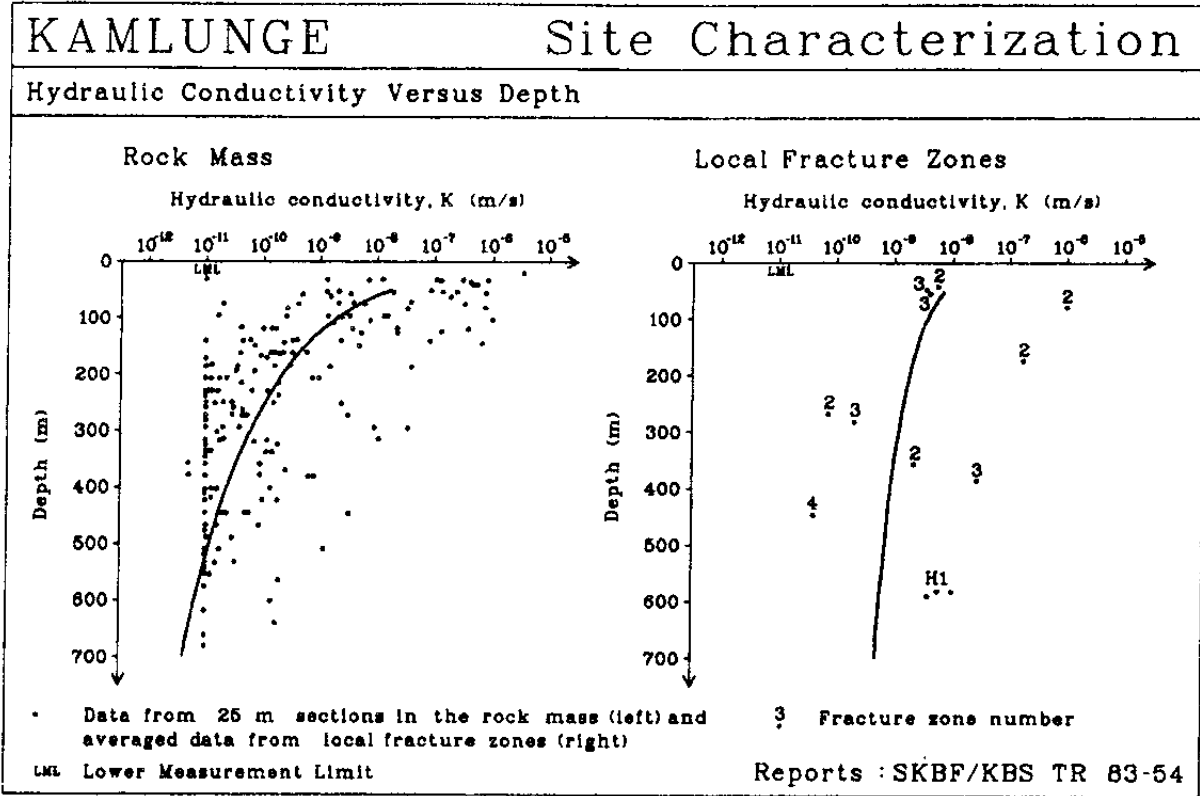


Figure 2-3. Hydraulic conductivities evaluated Kamlunge (test scale 25 m) and Klipperås (test scales 20 and 25 m) /Ahlbom et al, 1992a, 1992b/.

The statistics for the injection tests with 3 m spacing in 1996 were re-evaluated /*Rhén et al, 1997*/. The data was divided into two parts:

- 'zones' - parts of the borehole where it is judged that the deterministically defined hydraulic conductors domains intersect the borehole.
- 'rock' - parts of the borehole where it is judged that no deterministically defined hydraulic conductors domains intersect the borehole.

On the southern part of Äspö the sample size for each zonation range is quite large except for the depth range 0-100 m and below 500 m. The measurements in depth range 0-100 m are from several boreholes but the depth is just somewhat less than 100 m. The estimate is probably rather relevant. The measurements below 500 m are from more or less one single borehole, KAS02, which is a subvertical borehole. The evaluation shows that the hydraulic conductivity of 'rock' is somewhat higher in the interval 0-100m than in the interval 200-500 m, where the hydraulic conductivity is more or less constant. Below 500 m there is decrease in hydraulic conductivity, but it should be considered uncertain as it is based on only one vertical borehole. Statistics for injection tests with 30 m packer spacing were also compiled. These tests do not indicate any clear decrease in hydraulic conductivity with depth either, but data are only available from three boreholes (KAS02, KAS03 and KLX01). Nor do the tests located at Äspö island with the approximate test scale of 100 m indicate any decrease in hydraulic conductivity with depth.

One can conclude that at the Äspö HRL the decrease in K with depth is not so clear (see *Figures 2-4--2-6*). On Äspö K is fairly constant down to 600 m, and below that, data were only obtained from only one subvertical corehole (KAS02). Below 600 m there are relatively few measurements but the tests indicate that the effective K is around 20% of the effective K within the depth range of 0-600 m. (All boreholes within the Äspö and in surrounding areas with test scales of approximately 100 m are included, see *Rhén et al, 1997*.) Taking into account the fact that the test scale below 600 m is around 300 m and above about 100 m and also the relations between K and different test scales shown in *Rhén et al/ 1997*/, the effective K value below 600 m should rather be 10% of the effective K within depth range 0-600 m for test scale 100 m. The base for the conclusion that K does not decrease down to a depth of 600 m is the injection tests with 3 m packer spacing and the hydraulic tests at the 100 m test scale performed at Äspö (see *Figure 2-6*) /*Rhén et al, 1997*/.

The mean fracture frequency on southern Äspö is about 3.4/m for 50 m depth intervals down to 400 m depth /*Liedholm, 1991a*/. The fracture frequency for the uppermost 100 m is about 4.2/m. At the deepest part of cored boreholes KAS07 and KAS08 (depth about 450-500 m) the fracture frequency increases due to fracture zone NE-1. Below about 700 m the fracture frequency increases in KAS02, possibly because NE-1 is close to the borehole. Thus, there is no clear decrease in fracture frequency with depth at Äspö.

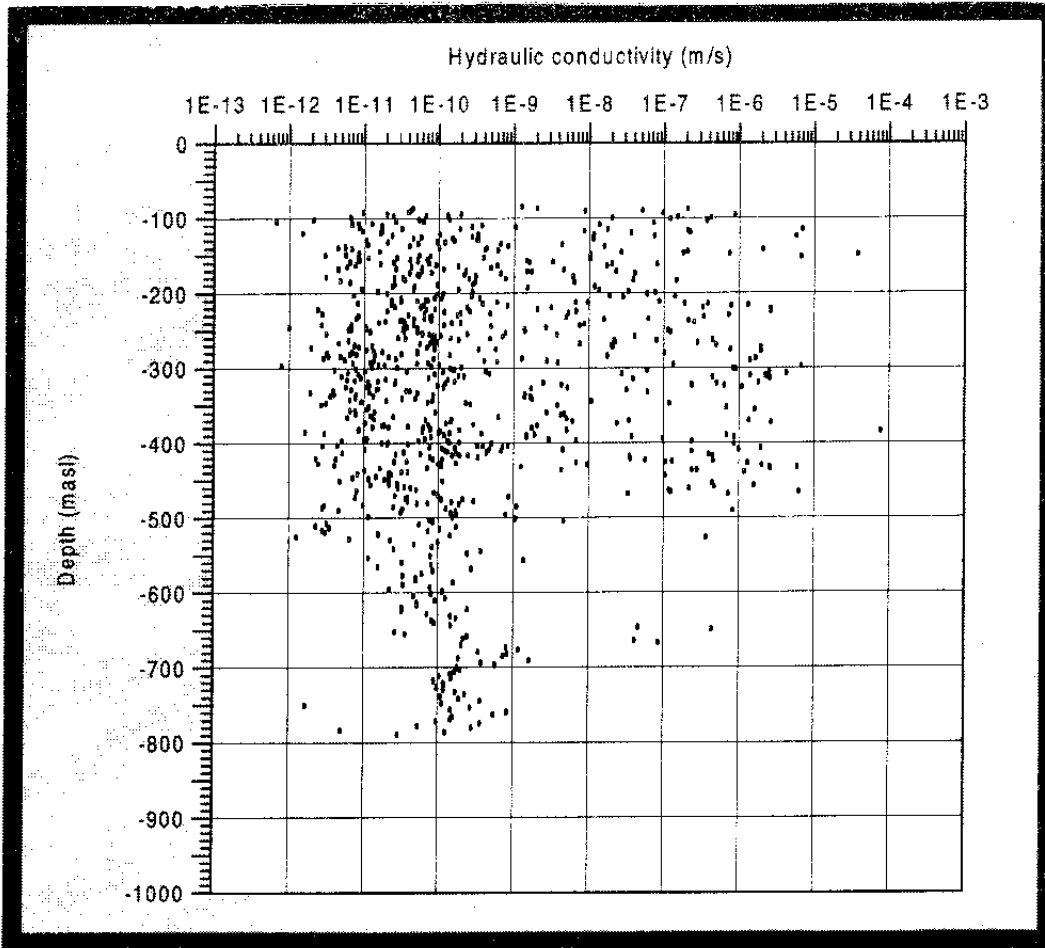


Figure 2-4. Hydraulic conductivities evaluated for southern Äspö (test scale 3 m) based on data from coreholes KAS02, 05-08. Data for borehole sections which are intersected by the hydraulic conductor domains in Model 96 are excluded in the figure. Data below depth about 525 m is only from one borehole, KAS02.

According to *Rhén et al /1997/* there is a difference in the hydraulic conductivity of the lithological units on Äspö, but that does not seem to be the reason for the differences. According to *Rhén et al /1997/* the amount of different lithological units along the tunnel is about the same for the depth intervals 200-300 m and 300-400 m. The amount of different lithological units in KAS02, 05-08 is also about the same as in the tunnel */Stanfors et al, 1997a/*.

In summary, the hydraulic conductivity is fairly constant down to a depth of 500 m at Äspö and below that level there is possibly a decrease according to the pre-investigations. (Exclusion of borehole sections interpreted to be intersected by the deterministic hydraulic conductor domains in the 3 m test scale does not change the conclusion, see *Figure 2-4* and *2-5*). Based on the additional data from the construction phase this conclusion still holds.

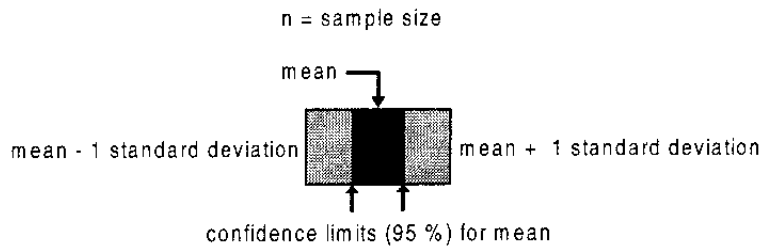
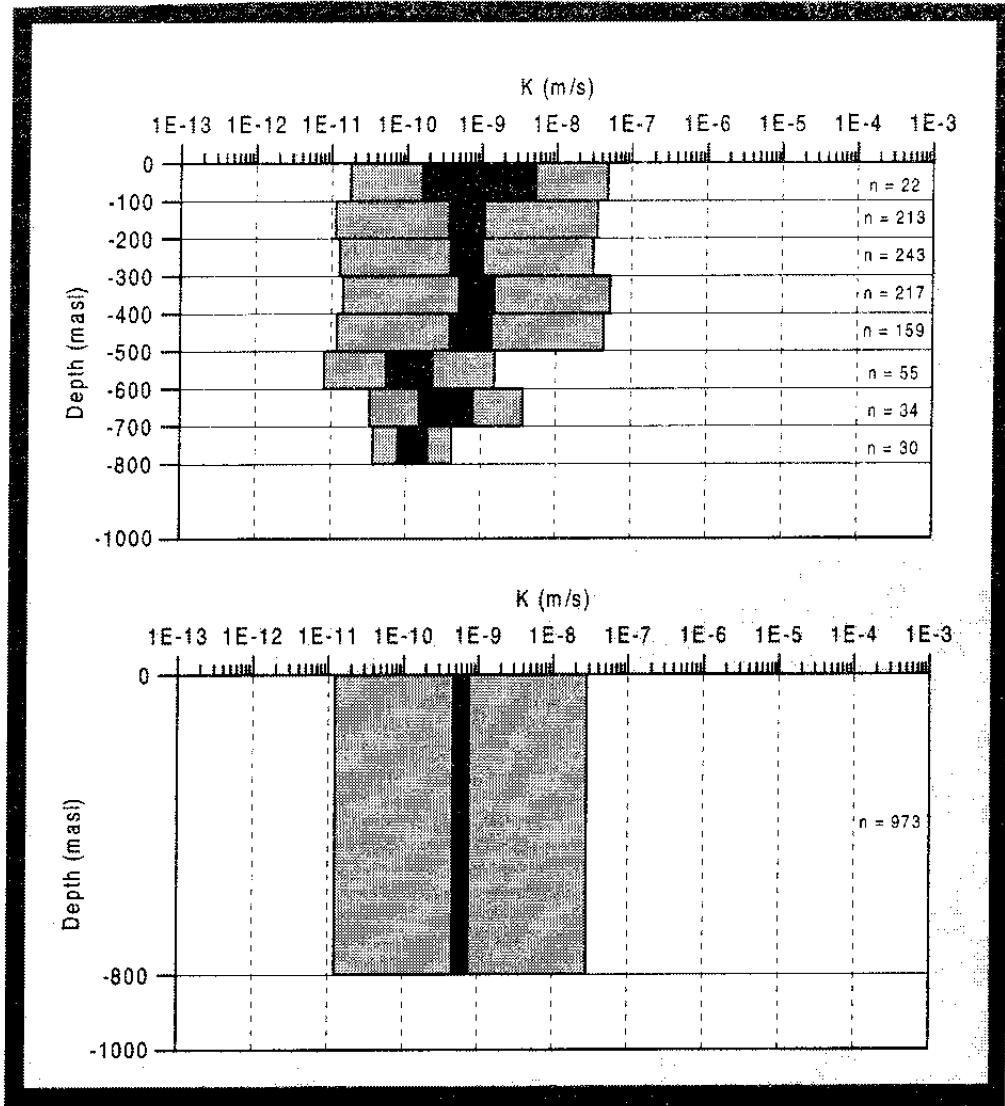


Figure 2-5. Hydraulic conductivity (K) distribution on the site scale. (mean= arithmetic mean of $\text{Log}_{10}(K)$, standard deviation=Standard deviation of $\text{Log}_{10}(K)$, n =sample size). Test scale 3 m. Data from cored boreholes KAS02,05-08 on Äspö. Sample statistics based on the data presented in Figure 2-4.

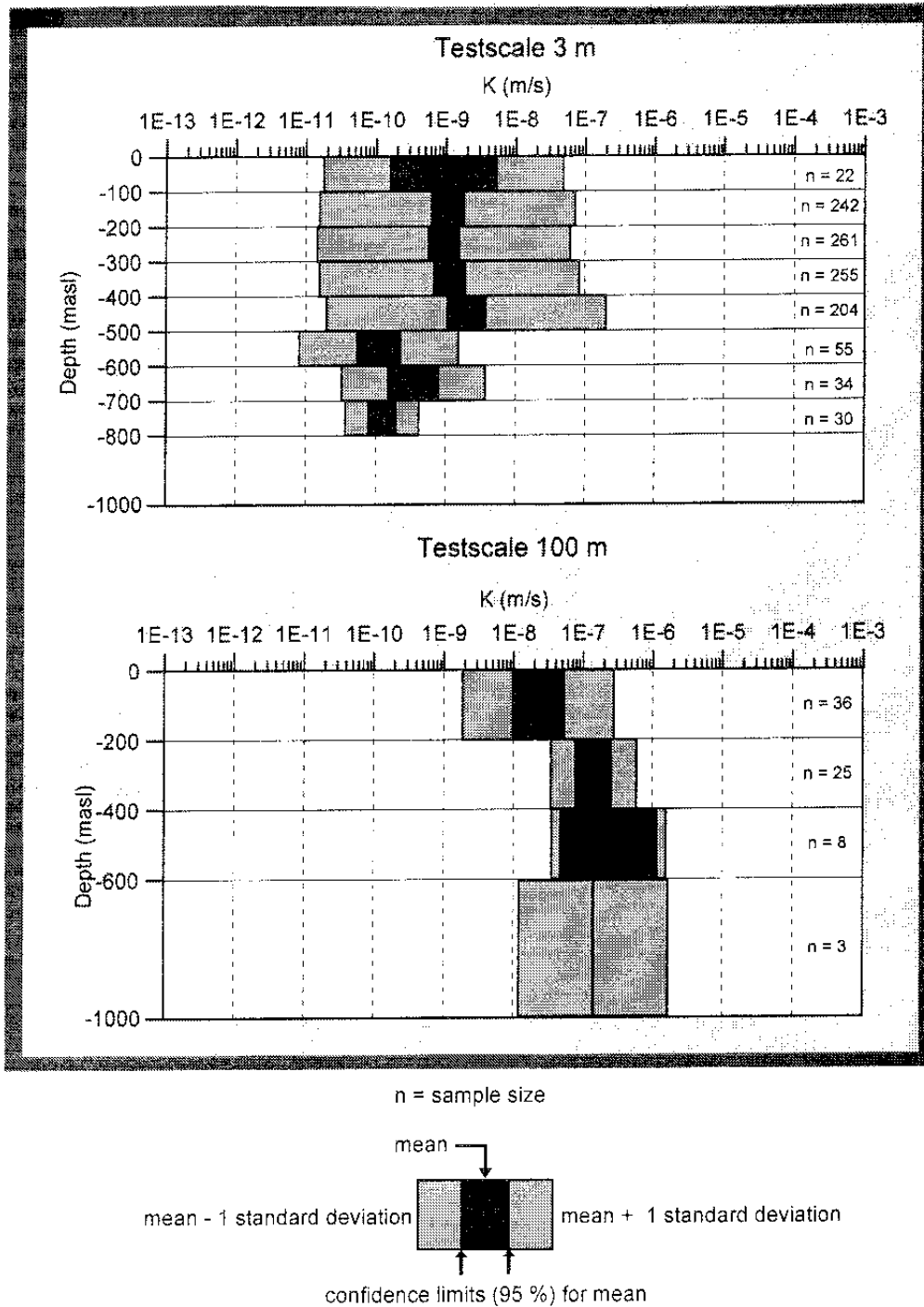


Figure 2-6. Hydraulic conductivity (K) distribution on the site scale. (mean= arithmetic mean of $\text{Log}_{10}(K)$, standard deviation=Standard deviation of $\text{Log}_{10}(K)$, n =sample size). Data for both test scales include all test sections, thus sections interpreted to be hydraulic conductor domains and hydraulic rock mass domains.

Top: Test scale 3 m. Sample statistics based on cored boreholes KAS02-08 on Äspö.

Bottom: Test scale 100 m. Sample statistics based on tests in cored and percussion-drilled boreholes on Äspö.

Material properties

General view

The predictions of the geometric mean hydraulic conductivity were close to the predicted range for depths of 200-400 m (see *Figure 2-2*). The predictions were outside the range below the Baltic south of Äspö, tunnel section 700-1475 m. The predicted standard deviation was somewhat less than the outcome.

The measurements in tunnel section 1475-2875 m seem to indicate a decreasing hydraulic conductivity with depth. However, this is probably due to the large-scale heterogeneity and the anisotropic conditions. Tunnel section 1475-2265 m covers an entire spiral turn but tunnel section 2265-2875 only cover covers two-thirds of a tunnel spiral turn, and thus the anisotropic conditions found must affect the result. It is also clear that large-scale heterogeneity can have caused the difference between the two depth intervals, if the individual boreholes on southern Äspö are considered. Below the results are discussed in more detail.

Concept for population characteristics

The hydraulic conductivity is assumed to be lognormally distributed. This is somewhat questionable for the 3 m test scale but seems to be a rather good approximation for the larger scales (see *Figure 2-7*).

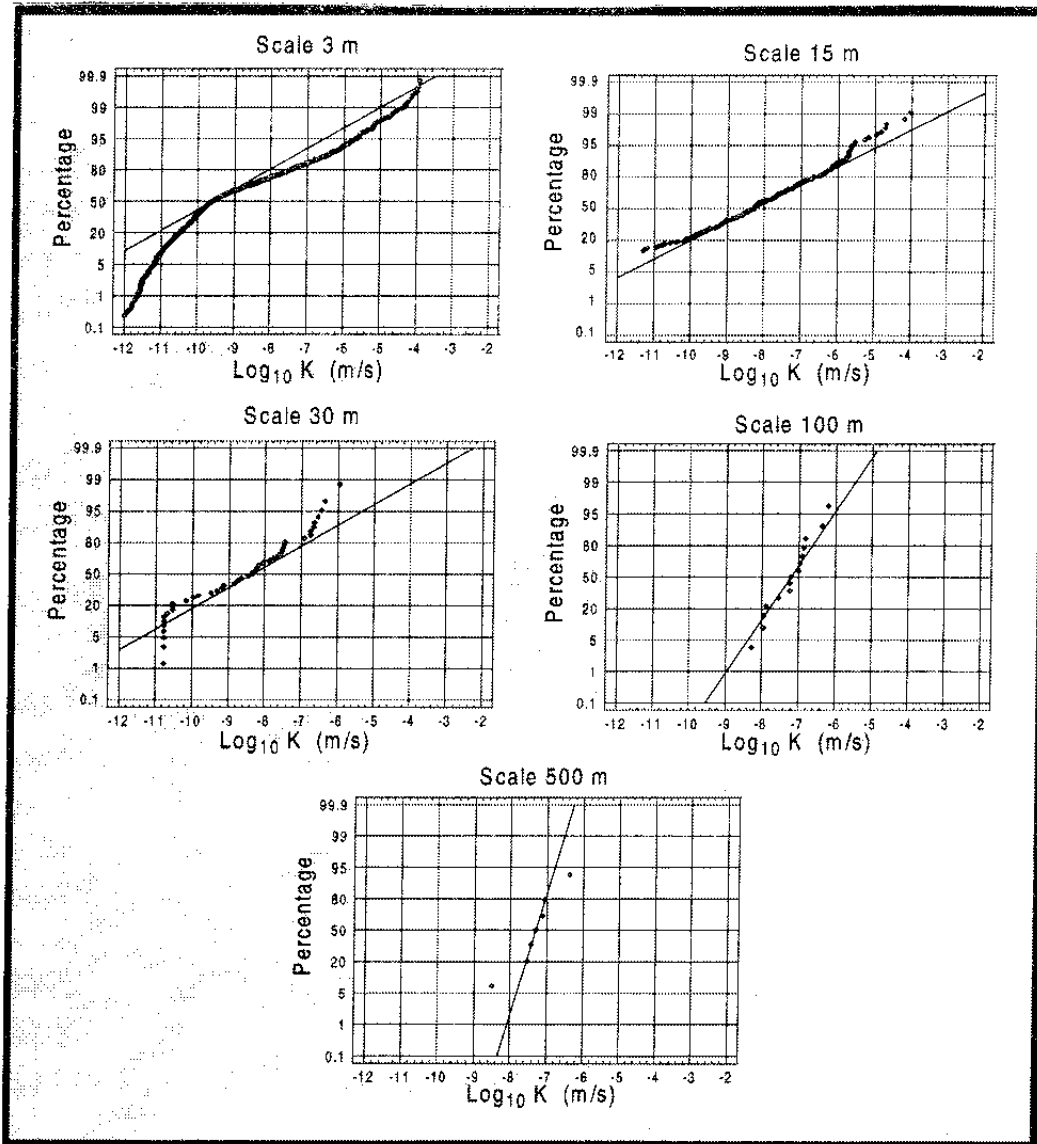


Figure 2-7. Normal probability plot of $\text{Log}_{10}(K)$, where K = effective hydraulic conductivity in m/s, for different test scales. Data for 3, 30, 100 and 500 m scales are from the pre-investigation phase. The 3 m scale is based on KAS02-08, the 30 m scale is based on KAS02-03 and the 100 and 500 m scales are based on KAS02-08,12,13. (KAS09-11,14 were excluded as they mainly represent the hydraulic conductor domain NE-1.) The tests at 15 m scales are the tests in probe holes in tunnel section 1400 - 3600 m. Black line: Line through median value with slope according to the standard deviation.

Laboratory tests of the permeability (k) of rock cores and also hydraulic tests in boreholes at the 5 cm scale indicate that more or less unfractured rock at Äspö has a k value of about $10^{-20} - 10^{-19} \text{ m}^2$ /*Olsson et al, 1996*/. (Re-evaluation 1997 indicated that the permeability may be about 10 times larger than suggested in *Olsson et al /1996*/). Equation 2-1 expresses the relationship between the hydraulic conductivity (m/s) and permeability (m^2) :

$$K = \frac{k \cdot \rho \cdot g}{\mu} \quad (2-1)$$

μ = Dynamic viscosity
 ρ = Density
 g = Gravitational force

ρ and μ are dependent on the temperature, and an example of the dependency is given below in *Table 2-2*. The temperature at a depth of 500 m is $14.6 \pm 0.3^\circ\text{C}$ and the temperature gradient is $15.0 \pm 0.3^\circ\text{C}/\text{km}$ at Äspö /*Sundberg, 1991*/ and approximately the same at Laxemar /*Ahlbom et al, 1995*/. The salinity has even less influence on the viscosity, at least down to a depth of 1000 m at Äspö, as the salinity is less than 2% down to that depth /*Rhén et al, 1997, Earllougher, 1977*/. Considering the values in *Table 2-2* a lower limit of the hydraulic conductivity at small scales – a metre or so – should be around $K = 10^{-12} \text{ m/s}$.

Table 2-2. Example of the way in which temperature affects the relationship between the hydraulic conductivity (K) and permeability (k).

T (°C)	$\frac{\rho \cdot g}{\mu}$ (1/(ms))
10	$0.75 \cdot 10^7$
20	$0.98 \cdot 10^7$
30	$1.22 \cdot 10^7$
40	$1.49 \cdot 10^7$

In the evaluation of the hydraulic properties the effect of temperature on the dynamic viscosity and density was neglected. However, as can be seen in *Table 2-2* the temperature effect is of minor importance for the hydraulic properties at least to 1000 m, considering the temperature gradient. If zonation with 100-200 m plates is adopted the error will become very small, if it can be assumed that temperature will be the same as when the hydraulic tests were performed. For future hydraulic tests the temperature for the formation should be reported in the database so that it will be easy to make corrections if needed.

Parameter estimation from sample characteristics

The hydraulic rock mass domain properties were based on the entire sample of the injection tests at the 3 m scale. *Figure 2-8* shows the re-evaluated data for KAS02, 05-08. As can be seen in *Figure 2-8* the distribution for 'rock' and 'rock + zone' are almost identical. The reason is that the deterministically defined hydraulic conductor domains are relatively few and intersect a limited part of the total borehole length. If the deterministically defined hydraulic conductor domains are as sparsely distributed within the site and are thin relative to the distances between the domains, as defined for the Äspö site, the hydraulic rock mass domain properties can be estimated fairly well from the entire sample. However, the test lengths must be so short that the number of test sections belonging to 'zone' are much less than the total sample. When the hydraulic conductor domains are defined the data should of course be separated into 'rock' and 'zone' and be re-analysed.

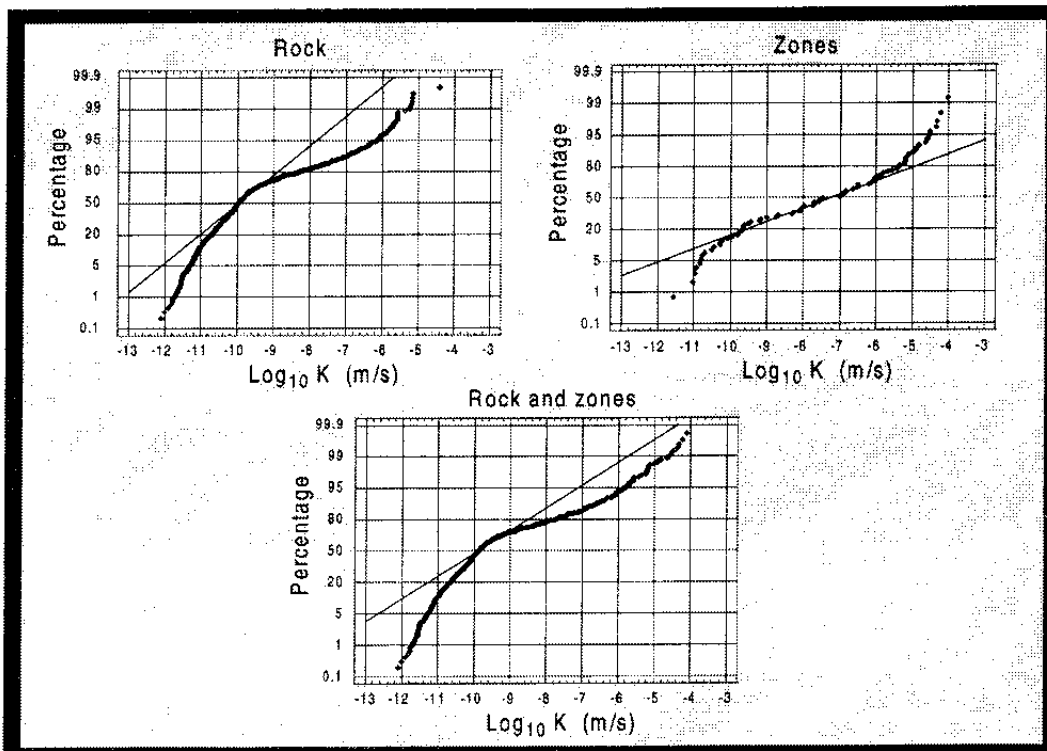


Figure 2-8. Hydraulic conductivity (K) distribution at the site scale. Test scale 3 m. Statistics for 'rock', 'zone' and 'rock + zone' on southern Äspö. Based on results from boreholes KAS02, 05-08.

Heterogeneity

The large-scale heterogeneity within a site strongly affects the chances of making reliable estimates of the hydraulic properties using a few boreholes. One reason for the deviations from the Äspö site predictions is the heterogeneity within the site, illustrated by *Figure 2-9* and *2-10*.

Figure 2-9 shows the statistical distributions for all injection tests with 3 m packer spacing. KAS02 and KAS05 are close to the western part of the spiral, and the median hydraulic conductivities are about 10^{-11} - 10^{-10} m/s. KAS07 is close to the south-western part of the spiral, and the median hydraulic conductivity is slightly higher than 10^{-10} m/s. KAS06 and KAS08 are close to the eastern and southern parts of the spiral, and the median hydraulic conductivities are between 10^{-10} and 10^{-9} m/s. Considering this and the way the probe holes are distributed around the tunnel probe holes for depth level 300-400 m could possibly have been expected to have lower hydraulic conductivities than probe holes for depth level 200-300 m.

If a population has a normal distribution it is easy to estimate new sample characteristics if the standard deviation and mean for the sub-samples are known. This is called pooling. To illustrate the uncertainty of the estimated sample statistics in a heterogeneous site like Äspö, the sample statistics for each borehole on Äspö (KAS02-08) were used to estimate sample statistics for the Äspö site. Each borehole constitutes a sub-sample with mean = arithmetic mean of $\text{Log}_{10}(K)$ and standard deviation = standard deviation of $\text{Log}_{10}(K)$ (K = hydraulic conductivity). The variation of the sample statistics can be shown by calculating the sample characteristics for all combinations of 1, 2, 3, 4, 5, 6, and 7 boreholes (see *Figure 2-10*).

As pointed out above, the distribution of $\text{Log}_{10}(K)$ for the 3 m scale is not so well described by a normal distribution. In a statistical analysis of the sample based on the original data of the sub-samples the statistics would probably become somewhat different compared with pooling, but a variation of similar magnitude would very probably be seen.

Based on *Figure 2-10* it is concluded that even if the confidence limits for the mean value are narrow for the sample from one or a few boreholes, these limits may be irrelevant if the site is heterogeneous on a large scale. It is concluded that on a site that is heterogeneous on a large scale it is necessary to have more than just a few boreholes to estimate sample characteristics for the entire site. It should, however, be pointed out that the geological model is important both for the investigation strategy and the evaluation of the tests. Understanding of the geological heterogeneity can of course give insight into how to interpret the data and how to assign properties to different domains.

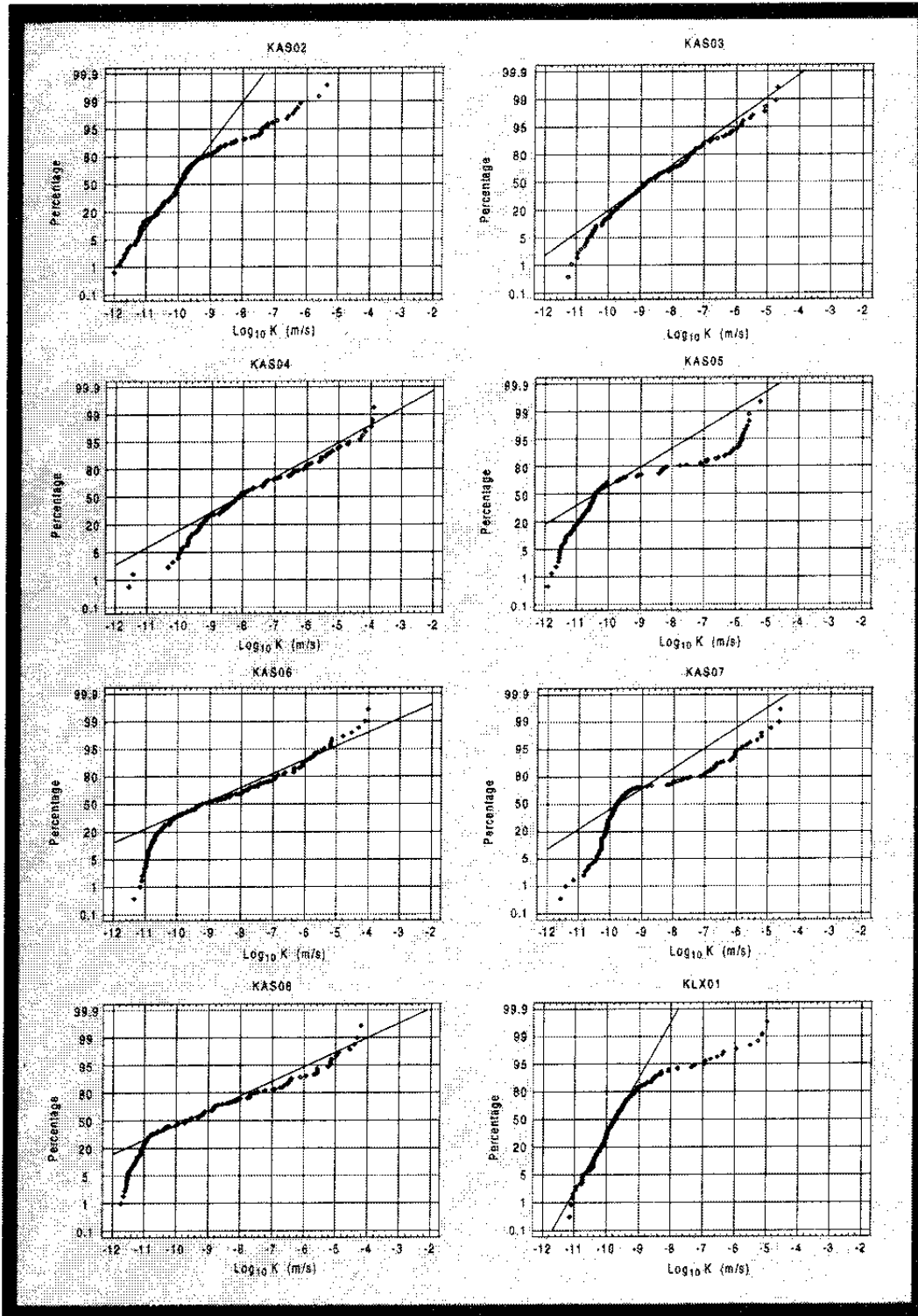
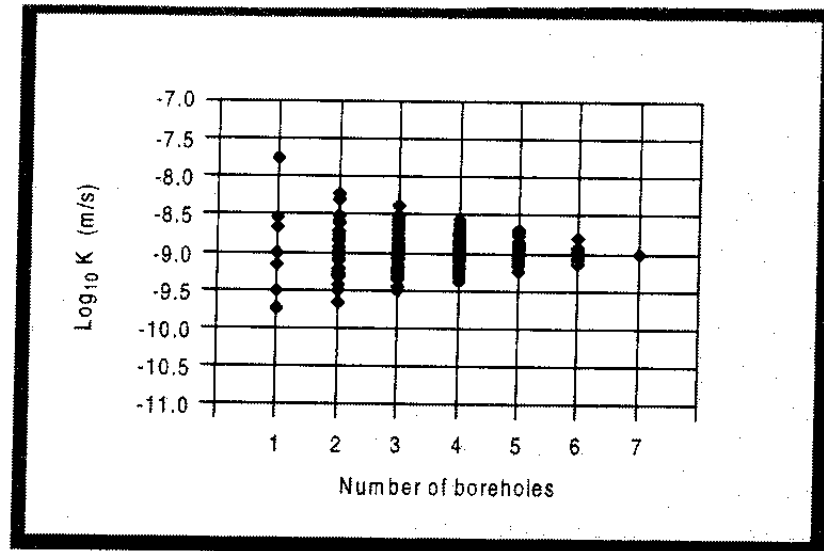
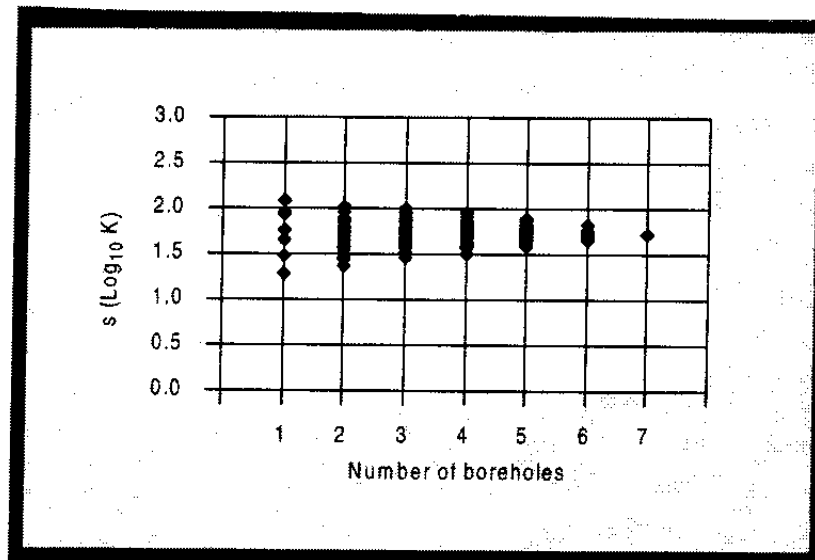


Figure 2-9. Normal probability plot of $\text{Log}_{10}(K)$, where K = effective hydraulic conductivity in m/s, for 3 m test scale. Data are from the pre-investigation phase. Black line: Line through median value with slope according to the standard deviation. (The values that were reported as measurement limit values in Nilsson /1989 and 1990/ were recalculated using the calculated specific capacity (Q/s) and the function shown in Rhén et al /1997/ for estimating the transmissivity for the test section. This is the reason for the difference between these figures and those in Nilsson /1989 and 1990/).



◆ Mean (Log₁₀ K)



◆ Standard deviation for (Log₁₀ K)

Figure 2-10. Estimated effective hydraulic conductivity (K) for Äspö, based on the means and standard deviations evaluated for the individual boreholes by pooling under the assumption that $\text{Log}_{10}(K)$ on the 3 m test scale has a normal distribution (mean = arithmetic mean of $\text{Log}_{10}(K)$, standard deviation = Standard deviation of $\text{Log}_{10}(K)$). Each point in the figures above represents estimates of properties based on pooling of data from the number of boreholes shown on the horizontal axis. All possible combinations of boreholes KAS02-08 are shown. (The high value for one borehole and $\text{Log}_{10}(K)$ is borehole KAS04.)

Top: Mean of $\text{Log}_{10}(K)$.

Bottom: Standard deviations of $\text{Log}_{10}(K)$.

Anisotropy

Special consideration in estimating the hydraulic properties of the rock mass domains should be taken in the design of a field programme if anisotropic conditions exist, as illustrated in *Figure 2-11*. The results indicate that at the Äspö site the hydraulic conductivity may be around 100 times greater in the most conductive direction than in the least conductive direction (see *Figure 2-12*). The figure is based on data for tunnel section 1400-3600 m, thus also including the fracture swarms, or as they are also called in this chapter: NNW hydraulic conductor domains. This is essentially a result due to the fact that the main hydraulic conductors on a local scale in the rock mass are fractures trending WNW with high frequency. But as can be seen in *Figure 2-12* the fractures trending N-S are also transmissive.

In order to see if there were any different results for a subhorizontal plane the data from the cored boreholes in the tunnel spiral area were analysed. Data from KAS02, 05-08 depth interval -200 to -500 m were used. Most of the cored boreholes on southern Äspö slope down at an angle of 60° and the average slope of KAS02 and 05 is about 85°. However, the injection tests available were performed with a packer spacing of 3 m. In order to permit comparison with the measurements in the probe holes the transmissivities (T) were estimated as the sum of T values for 3 m sections. The sum was then slightly reduced (multiplied with 0.7) depending on the way in which the arithmetic mean value of the hydraulic conductivity is expected to decrease (see *Rhén et al, 1997*).

The results indicate that the hydraulic properties in the 10-20 m scale are anisotropic. The results are summarized in *Table 2-3*. It should be remembered that the data in *Figure 2-11* and *Table 2-3* are based on all data, including fracture zones. The results should also be regarded as an approximate relation as the testing methods were different.

The results above can provide a reasonable explanation for the differences between prediction and outcome. In *Figure 1-8* it can be seen that the probe holes for depth level 300-400 m only cover 2/3 of a tunnel spiral turn and for depth level 200-300 m they cover almost a complete tunnel spiral turn. Due to this, probe holes for depth level 300-400 m are somewhat over represented by boreholes striking about SW-W (Äspö co-ordinate system), which means that the average hydraulic conductivity should become underestimated because of the anisotropy shown in *Figure 2-11*.

In conclusion there is a need to have boreholes in directions that are not subparallel to find if anisotropic conditions exist. The evaluation methodology of the hydraulic tests may have to be improved for the evaluation of anisotropic conditions.

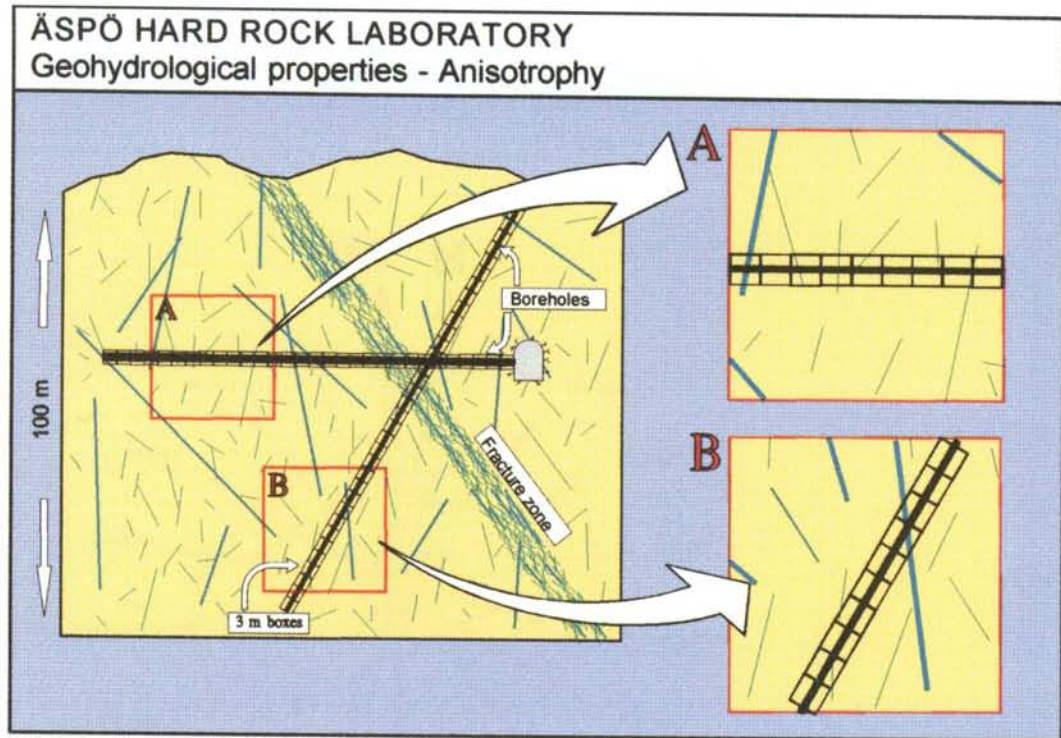


Figure 2-11. The evaluated hydraulic properties are dependent on the borehole direction if there are anisotropic conditions.

Table 2-3. Estimates of transmissivities in different directions within the tunnel spiral at the Äspö HRL.

Probe holes		
Strike of plane perpendicular to the probe hole directions (°) (Äspö co-ordinate system)	Scale (m)	T (m ² /s)
120-140	15	$8 \cdot 10^{-7}$
20 - 80	15	$4.5 \cdot 10^{-9}$
Cored boreholes		
Direction of plane perpendicular to the probe hole directions	Scale (m)	T (m ² /s)
≈Horizontal	15	$5 \cdot 10^{-8}$

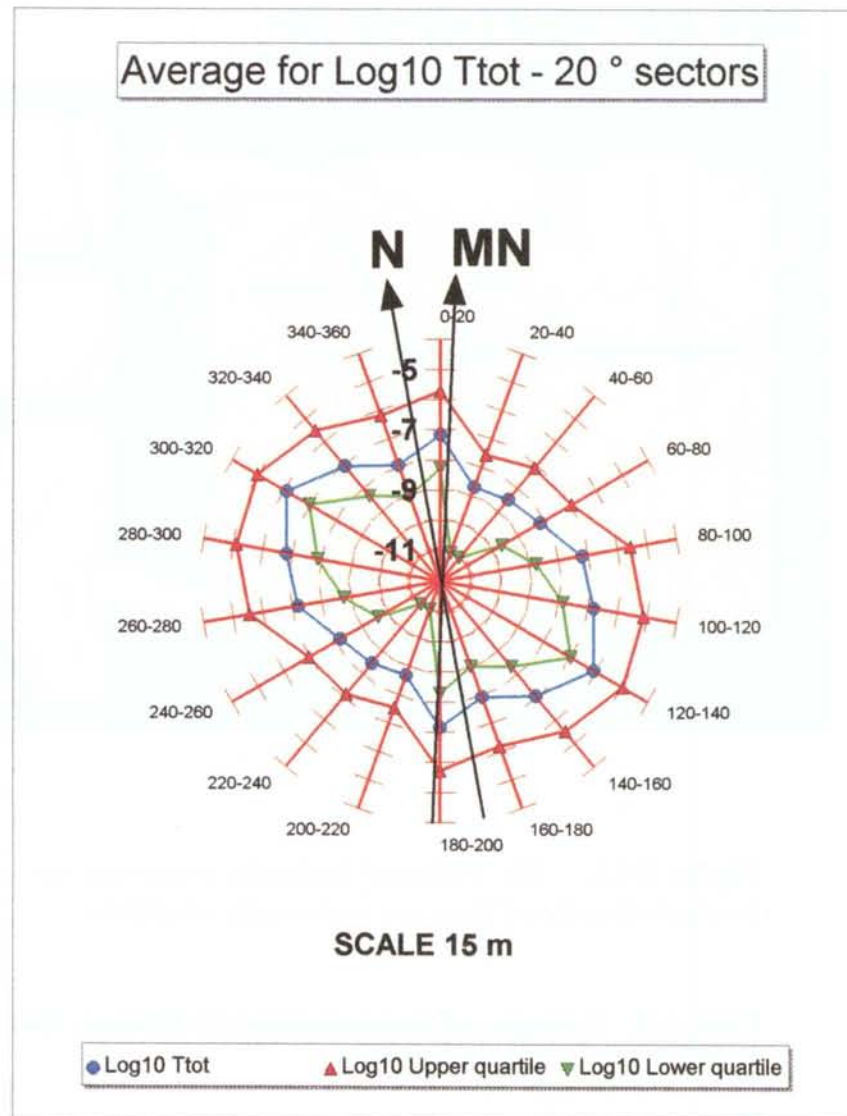
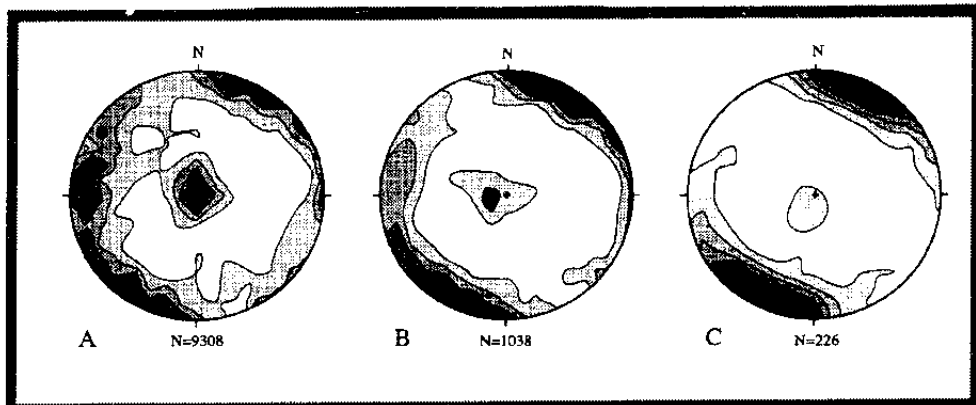


Figure 2-12. Estimated transmissivities (T) for different directions according to the Äspö co-ordinate system in the spiral of the Äspö HRL. The direction is given as the strike of a plane perpendicular to the borehole. Data : probe holes in tunnel section 1400-3600 m. The points in the figure represents arithmetic mean, upper quartile and lower quartile of $\text{Log}_{10}(T)$ for planes within a 20° sector in the horizontal plane. The points are in the middle of the sector and the directions of the sector is given for the Äspö coordinate system. N = North for the Äspö coordinate system. MN = Magnetic North. Scale 15 m = Length of test section is 15 m.

An investigation of the structural geology of water-bearing fractures was made in the tunnel /Hermanson, 1995/. It was found that the entire fracture system can be grouped into five main sets. The mapped water-bearing fractures and the fractures filled with grout (from the pre-grouting ahead of the tunnel face) are dominated by a subvertical fracture set striking WNW-NW. The N-S and NNW-SSW subvertical sets are also present but these subvertical sets are less

pronounced compared with the entire fracture set (see *Figure 2-13*). The relevance of the orientation of the mapped water-bearing fractures can be questioned as the zone closest to the tunnel wall was damaged to some extent by the excavation, giving increased fracturing and possibly a change in the hydraulic properties. Due to this the flow paths near the tunnel wall may be different than those of the undisturbed rock mass. However, the mapped grout-filled fractures should be a good indicator of the water conducting fractures, as the grouting was performed generally 5-15 m ahead of the tunnel face where the rock mass should be fairly undisturbed.



- A : All fractures
 B : Waterbearing fractures
 C : Fractures filled with grout

Figure 2-13. Schmidt nets with lower hemisphere projection of Kamb contoured poles to fracture planes. Contour interval 2.0 sigma. N= sample size. /Hermanson, 1995/.

- A: All fractures from 705 m to the end of the TBM tunnel, 3600 m. The plot shows five concentrations of fracture orientations, one sub-horizontal set, four steep sets striking N-S, NNW, WNW-NW and a comparatively less pronounced NE set.
- B: Water-bearing fractures from the same part of the tunnel as A. The steep set striking WNW-NW is more pronounced compared with the same set in plot A. The other sets are less evident.
- C: Fractures with grout from the same part of the tunnel as A. The plot is dominated by steep fractures striking WNW-NW. All other sets mentioned earlier are still visible, though not as pronounced as the WNW-NW set.

A mapping campaign of major larger (intersecting more or less the entire tunnel) water-bearing fractures in the spiral showed that all mapped fractures either had a substantial water inflow and/or grout and often gouge, brecciation or ductile precursors /Hermanson, 1995/. They were not in any case classified as zones and their widths ranged from millimetres to centimetres. *Figure 2-14* shows the mapped fractures. The fractures shown were mainly subvertical. According to *Hermanson /1995/* the fault system trending NW and NNW generally appears as sub-planar fractures with a central water-bearing fault plane that often contains fault breccia and/or fault gouge as well as mineral assemblage.

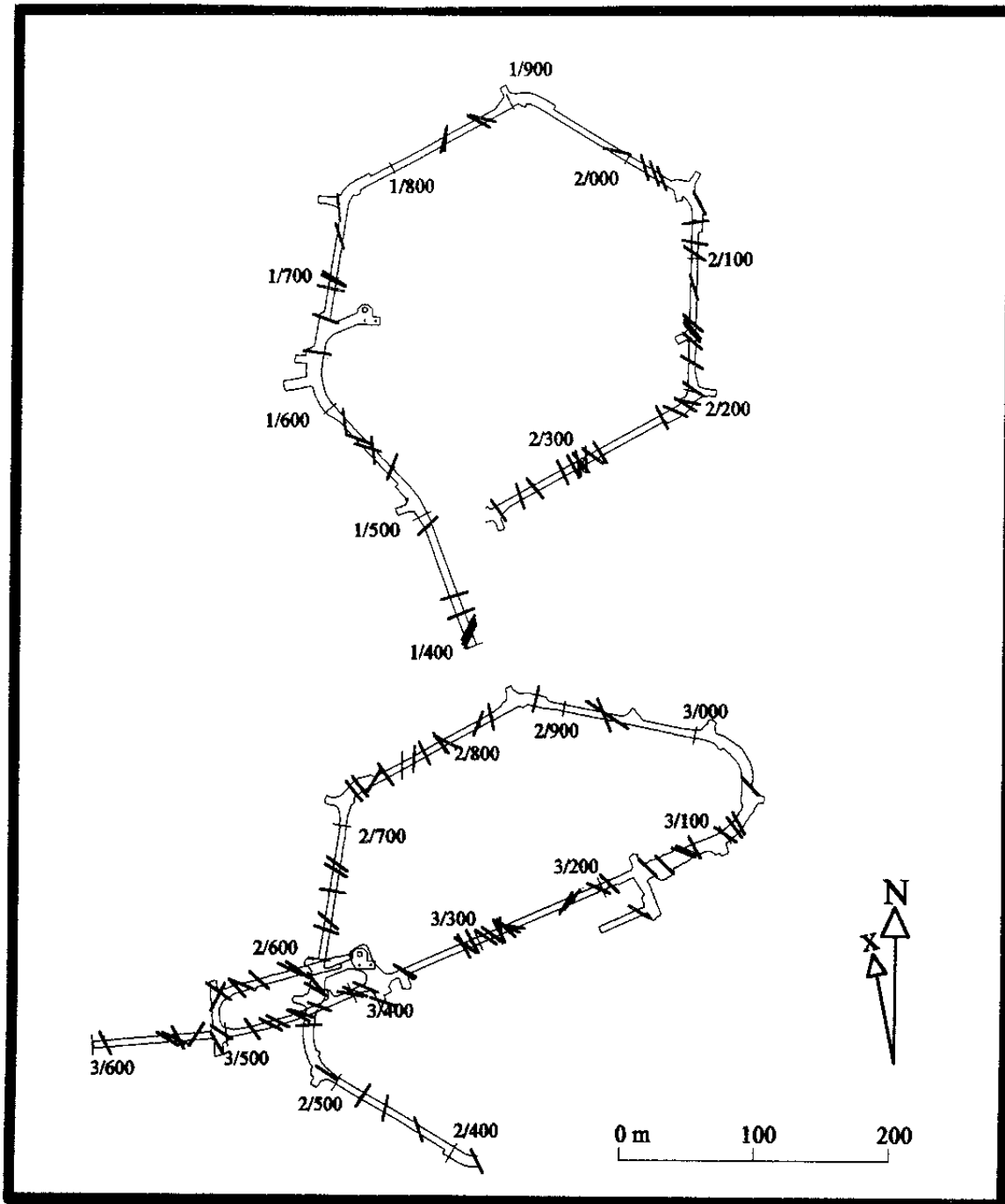


Figure 2-14. Mapped large, single, open, water-bearing fractures in the tunnel. The fractures are mainly subvertical. N = Magnetic north, x = North in the Äspö coordinate system.

Spatial assignment method

Scale dependant properties

The hydraulic conductivities based on measurements has a more or less lognormal distribution (see *Figure 2-15*). The figure shows normal probability plots and a frequency plot of $\text{Log}_{10}(\text{K})$. The diagrams are based on tests at different test scales (3, 30, 100 m and 'entire hole' ≈ 500 m) performed in boreholes KLX01, KAS02-08. The tests at the 30 and 100 m scales were not performed systematically in all boreholes, giving some uncertainty in the interpretation that follows here. From *Figure 2-15* it can be seen that it is convenient to evaluate the mean and standard deviation for $\text{Log}_{10}(\text{K})$ and describe the population characteristics using these values as the distributions are more or less lognormal. The assumption that the population can be described by a lognormal distribution makes it easy to generate the hydraulic conductivity field in a stochastic continuum model - where effective values of hydraulic conductivity have to be used. However, the way of using the values in a numerical model is not obvious. The mean of $\text{Log}_{10}(\text{K})$ is equal to the geometric mean of K, and, as can be seen in *Figure 2-15*, both the geometric mean of K and the standard deviation of $\text{Log}_{10}(\text{K})$ change with the test scale. In the cases shown the test times also increase from about 10 minutes to 3 days. The evaluated arithmetic mean of K, geometric mean of K and standard deviation of $\text{Log}_{10}(\text{K})$ are shown in *Figure 2-17*. It can be argued that the great change in geometric mean in *Figure 2-17* is due to the way in which the characteristic values for the distribution of the hydraulic conductivity is calculated. This is partly true since sections with higher transmissivities will always dominate the statistics increasingly with increasing test scale.

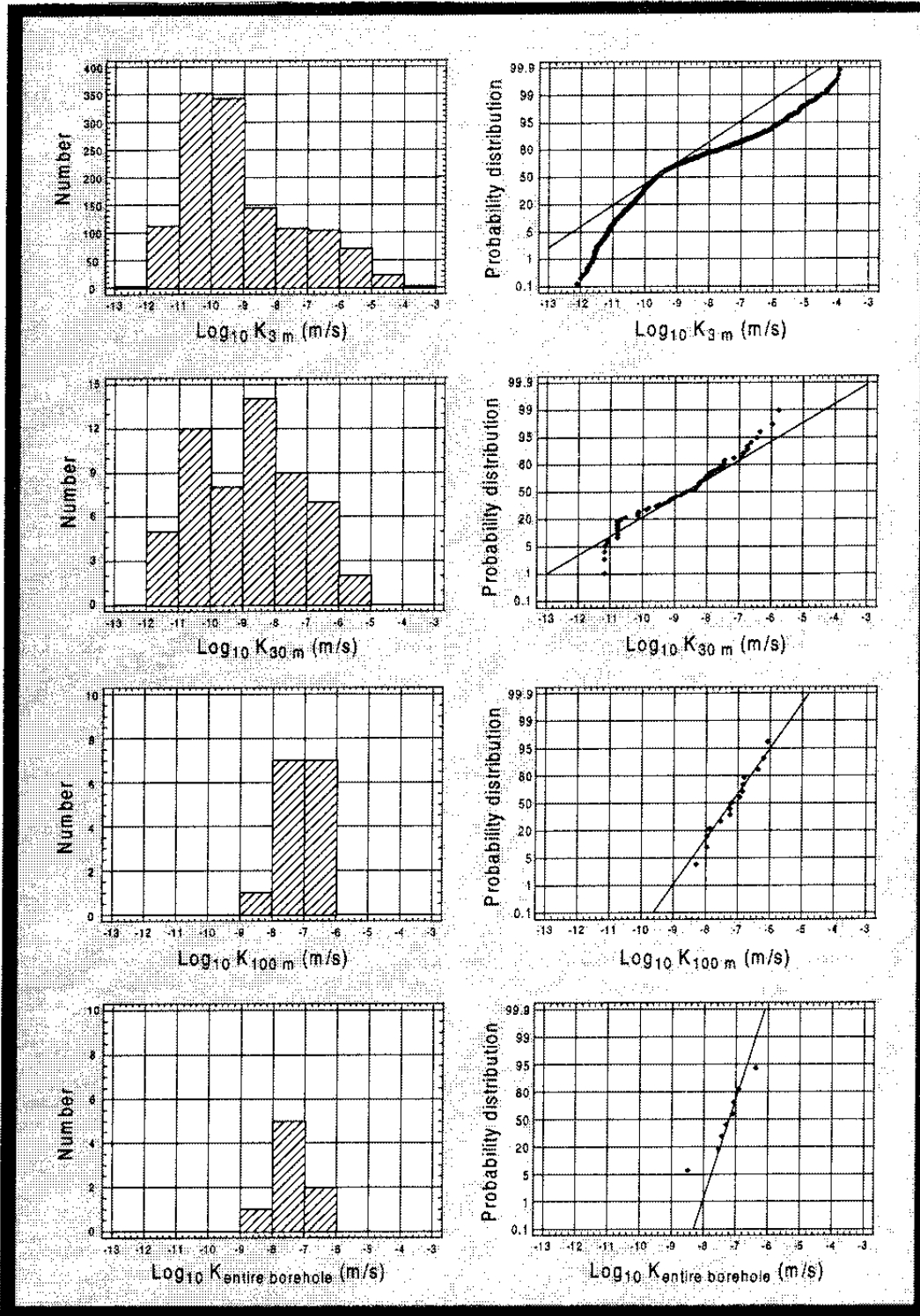


Figure 2-15. Normal probability plots and frequency plots of $\text{Log}_{10}(K)$, where K = effective hydraulic conductivity in m/s, for different test scales. (In the figure, for example, the 3 m test scale is shown as K_{3m}). Data are from the pre-investigation phase, including boreholes KLX01, KAS02-08.

Figure 2-16 shows the results of a synthetic data set for test scales 30 m, 90 m and 'entire boreholes' (chosen as an even number of 90 m sections) calculated from the 3 m injection tests. The transmissivities were calculated for the section (30, 90 m or 'entire borehole') as the sum of the 3 m transmissivities and then divided by the section length (30, 90 m or 'entire borehole'). As 'entire borehole' was not exactly the same section as in *Figure 2-15*, two cases with synthetic data were calculated starting from the bottom or top borehole sections for the boreholes in *Figure 2-15*. Only one of these cases is shown in *Figure 2-16* as the other is almost identical. The evaluated arithmetic mean of K and geometric mean of K and standard deviation of $\text{Log}_{10}(K)$ are shown in *Figure 2-17* for the real and synthetic cases. As can be seen the geometric mean behaves in a similar way for the synthetic case and the data based on different test sections, which is not strange at all. More interesting is the arithmetic mean, which decreases with increasing test scale and test time for the real case but is constant for the synthetic data. This is interpreted as good evidence that the connectivity between the fractures is limited (see illustrations in *Figure 2-18*). True scale effects exist! *Figure 2-17* illustrates well the problem of defining an effective hydraulic conductivity as a single value for a homogeneous case or a statistical distribution appropriate for a stochastic simulation. How this problem has been handled so far and the probable reasons behind the behaviour of the statistics is discussed below.

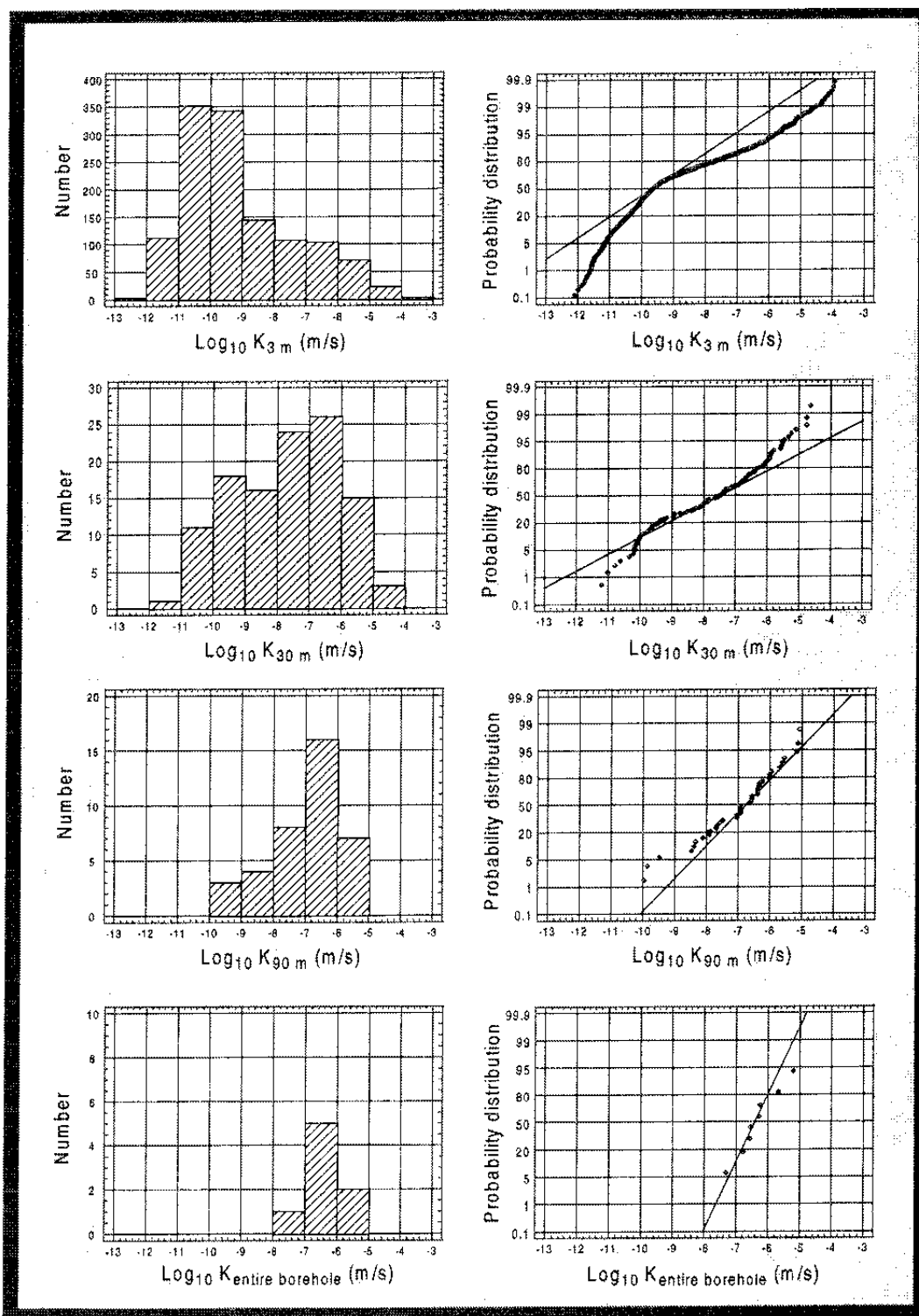


Figure 2-16. Normal probability plots and frequency plots for $\text{Log}_{10}(K)$. K = effective hydraulic conductivity in m/s. The base for the presented data is the injection tests with packer spacing 3 m in boreholes KLX01, KAS02-08. The diagrams for 30, 90 and 'entire borehole' are based on the tests on the 3 m scale by calculating the transmissivity for the section 30, 90 m 'entire hole' divided by the length 30, 90 m or 'entire hole' for more or less the same part of each borehole as was used in Figure 2-15 (see text for comments). (In the figure, for example, the 3 m test scale is shown as K_{3m} .)

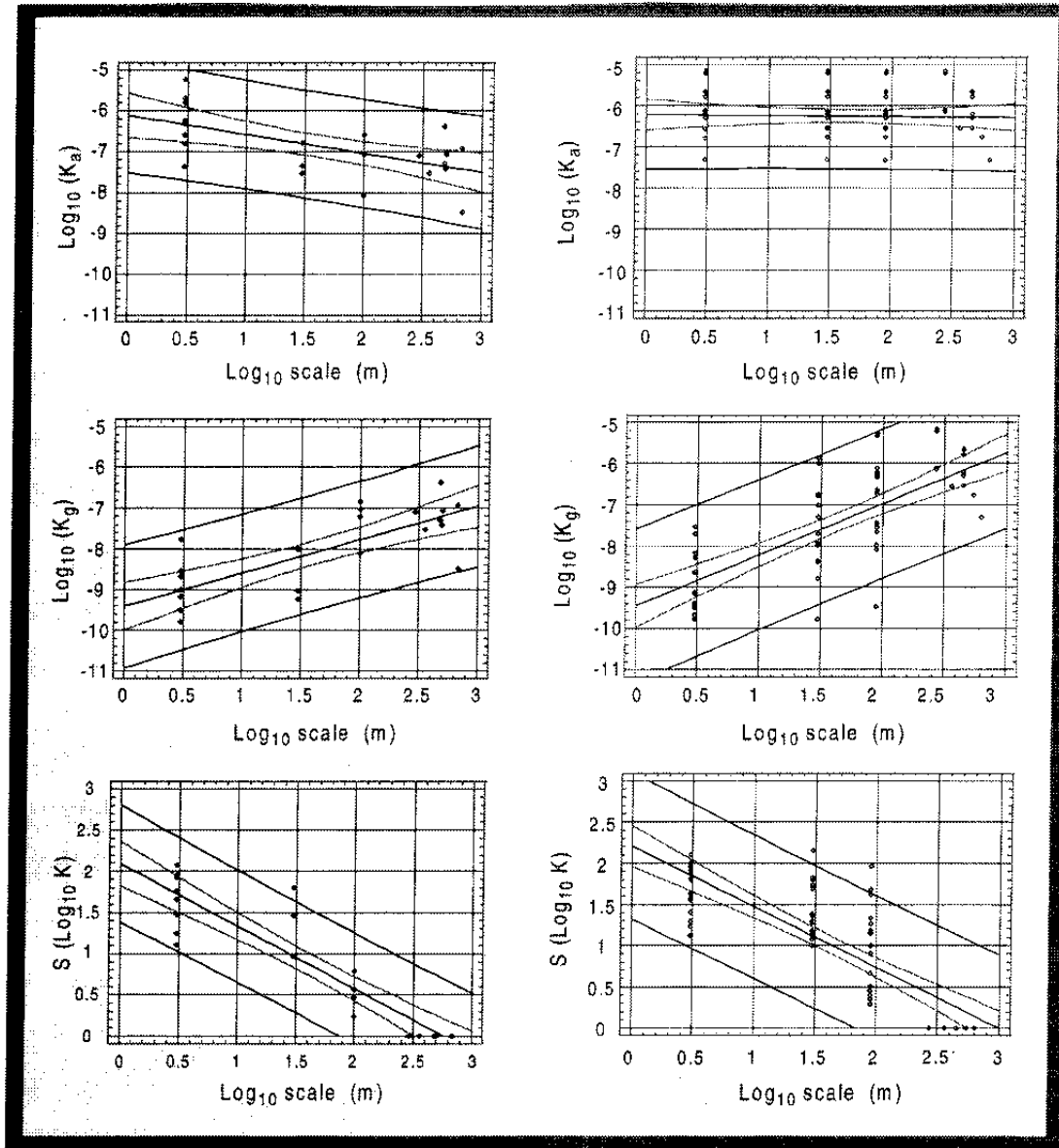


Figure 2-17. Regression of Y versus $\text{Log}_{10}(\text{scale})$. $Y = \text{Log}_{10}(K_a)$, $\text{Log}_{10}(K_g)$ or $s(\text{Log}_{10}(K))$. K = hydraulic conductivity, K_a = arithmetic mean of K , K_g = geometric mean of K . Scale = length of test section in the borehole. The values of K_g and K_a for $\text{Log}_{10} \text{ scale} \approx 2.5-3$ are identical as they are the effective hydraulic conductivity for the entire borehole. Data are from the pre-investigation phase, including boreholes KLX01, KAS02-08. (Standard deviation was set to zero for the 'entire borehole' value as there is only one value for K_a and K_g)

Middle black line: Mean of Y .

Inner grey lines: 95 % confidence band on mean of Y .

Outer-most black

lines: 95 % prediction band on Y as a function of $\text{Log}_{10}(\text{scale})$.

Left figure: Data from the pre-investigation phase where tests were made on different test scales (see Figure 2-15).

Right figure: Synthetic data based on the 3 m injection tests (see Figure 2-16).

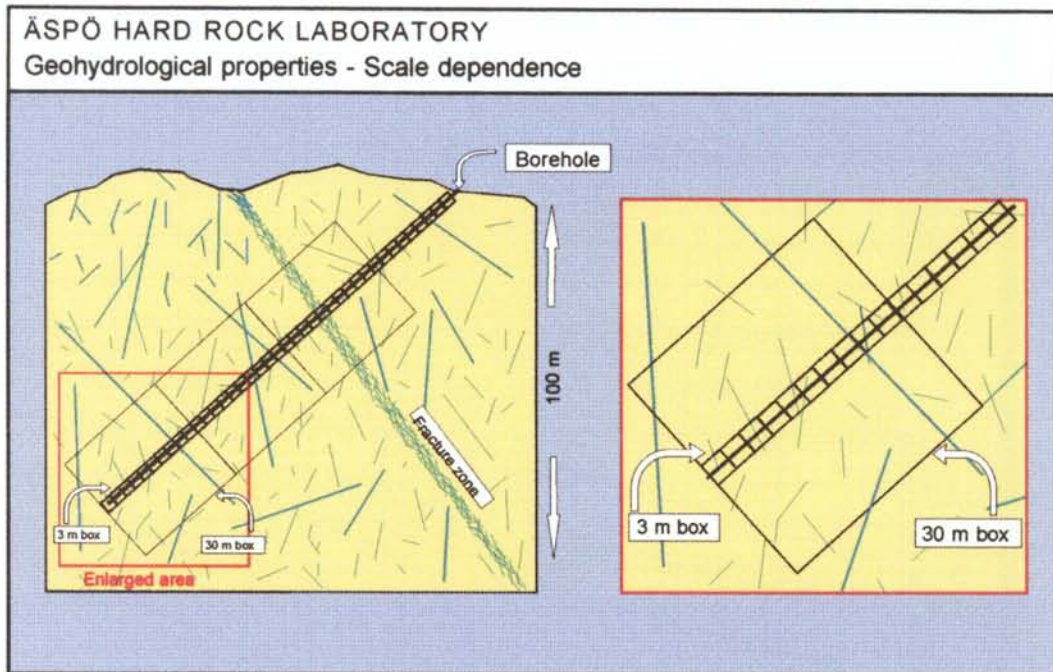


Figure 2-18. The evaluated hydraulic properties are dependent on the test scale (length of the tested section) and test time. Larger test scales and longer test time result in fewer fractures being hydraulically active for the duration of the test. Some of the minor features intersecting the boreholes have no or poor connection with other conductive features.

The relations for the geometric mean and standard deviation shown in *Figure 2-19* were used to scale the hydraulic conductivities used in the numerical groundwater flow models in *Model 96 /Rhén et al, 1997/*. A similar relationship was used for *Model 90 /Wikberg et al, 1991/*. *Table 2-4* shows the base for the scale transformation for the predictions shown in *Wikberg et al/1991/*, and the revised base for the scale transformation shown in the new model */Rhén et al, 1997/*. The predictions were made for the 20 m scale in *Gustafson et al /1991/*, but as the actual test length was 14 m, so all predictions were rescaled to 14 m. From *Table 2-4* it can be calculated that the geometric mean hydraulic conductivity for the 3 m scale should be multiplied by 5 according to the model used for the predictions and by 3.5 according to the new model in order to obtain the geometric mean hydraulic conductivity for the 14 m scale. The standard deviation for $\text{Log}_{10} (K)$ for the 3 m scale should be multiplied by 0.7 according both models. In *Table 2-1* it was shown that the outcome of the geometric mean hydraulic conductivity was 6.6 times greater than the predicted value (1475-2265 m) or about 0.5 of the predicted value (2265-2875). It was also shown that the standard deviation of $\text{Log}_{10} (K)$ was 1.7 times greater than the predicted value. If the revised model is used the difference in the geometric mean hydraulic conductivity becomes greater (about 9 times) for tunnel section 1475-2265 m but about as predicted for tunnel section 2265-2875 m. It remains the same for the standard deviation.

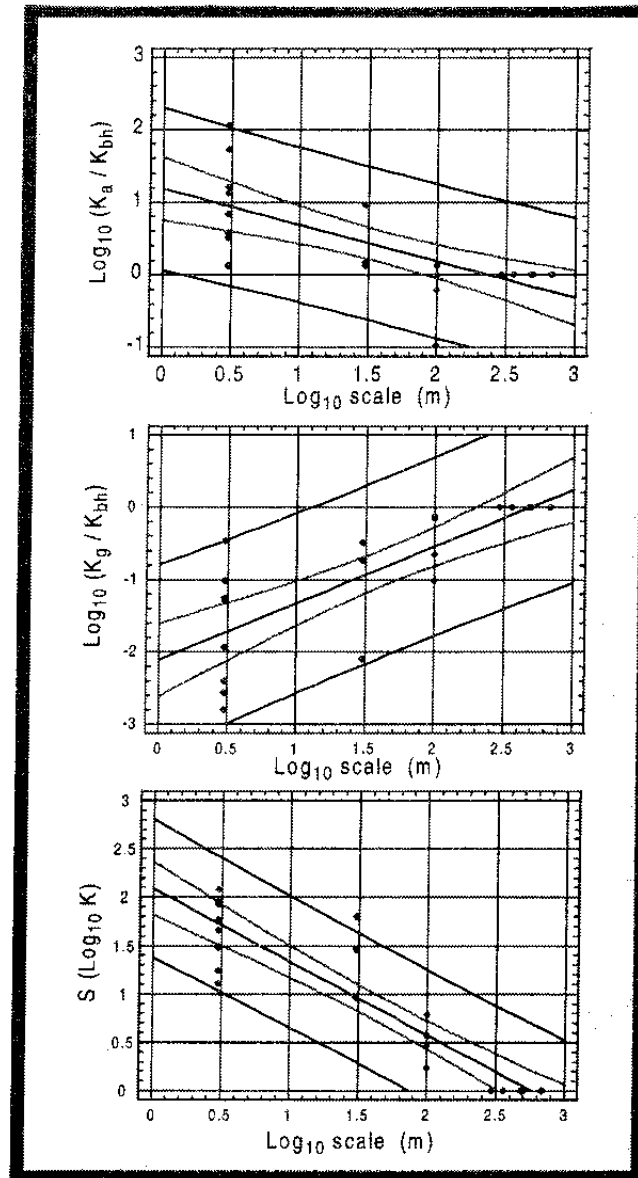


Figure 2-19. Regression of Y versus $\text{Log}_{10}(\text{scale})$. $Y = \text{Log}_{10}(K_a/K_{bh})$, $\text{Log}_{10}(K_g/K_{bh})$ or $s(\text{Log}_{10}(K))$. K = hydraulic conductivity, K_a = arithmetic mean K , K_g = geometric mean K . K_{bh} = mean K when entire borehole was tested, corrected according to test sections outside the range for other test scales. Scale = test section length in the borehole. The values of K_g and K_a for $\text{Log}_{10} \text{ scale} \approx 2.5-3$ are identical as they are the effective hydraulic conductivity for the entire borehole. The linear relation should not be used for test scales larger than $\text{log}_{10} \text{ scale} \sim 2.3 \approx 200 \text{ m}$. Data are from the pre-investigation phase, including boreholes KLX01, KAS02-08. (Standard deviation was set to zero for the 'entire borehole' value as there is only one value for K_a and K_g).

Middle black line: Mean of Y .

Inner grey lines: 95 % confidence band on mean of Y .

Outer-most black

lines: 95 % prediction band on Y as a function of $\text{Log}_{10}(\text{scale})$.

Table 2-4. The scale transformation of the statistics for the hydraulic conductivity made in the predictions /Gustafson et al , 1991, Wikberg et al /1991/ and according to the new model /Rhén et al /1997/. K = hydraulic conductivity, K_g = geometric mean, K_{bh} = effective hydraulic conductivity for the entire borehole , $s(\text{Log}_{10}(K))$ = standard deviation of $\text{Log}_{10}(K)$, Entire borehole length \approx 500 m.

Model	Test scale (m)	$\text{Log}_{10}(K_g / K_{bh})$	$s(\text{Log}_{10}(K))$
Prediction ¹	3	-2.1	2.3
	14	-1.4	1.7
	20	-1.2	1.5
New model ²	3	-1.7	1.7
	14	-1.2	1.2
	20	-1.1	1.1

¹ Wikberg et al /1991/

² Rhén et al /1997/

The use of a linear relationship as suggested in *Figure 2-19* can be discussed. It was used because it was not considered justified to use a more complicated relationship. The linear relationship cannot be used for test scales larger than log_{10} scale $\sim 2.7 \approx 500$ m, which is the maximum length of test section used in the individual boreholes. Possibly it should not be used for scales larger than about 200 m. As can be seen in the figures there is a spread of K_a and K_g values for test scale ≈ 500 m indicating a standard deviation that probably should be taken into account considering scaling of values for a site and not just a borehole. However, several other functions give about the same correlation coefficients as the linear fit and the functions can be made to converge asymptotically to the estimated values for the entire borehole. The difference will be larger correction for smaller test scale, (less than about 3 m) and smaller corrections for larger test scales (>3 m).

In order to see if it was possible to estimate effective values of the hydraulic conductivity of a rock block measuring 50 m simulations using a Discrete Fracture Network (DFN) model were made /*Axelsson et al, 1990, La Point et al, 1995*/. The first attempt was not successful as it turned out that the results depended very much on the boundary conditions. The simulations performed in *La Point et al /1995/* suggest that the conductive network was sparsely connected and that the block permeability decreases when the block size exceed the scale of well-connected fracture networks. The results showed that the block permeability was sensitive to the mean fracture size and fracture intensity, not surprisingly. They also noted that anisotropic conditions may exist with the permeability (k) in the north-south direction, followed by the k in the vertical direction and with the k in the east-west direction that was evaluated to be the least. The results also showed a need for improved data collection and better methodology for using the well test data in the numerical models. A good representation in 3-D of mapped fracture intersections in boreholes and fracture traces on rock surfaces is needed to improve the description of the orientation- and size distributions of the fractures, and also fracture intensity. A difficulty in the mapping and testing in boreholes is to distinguish water-conducting fractures and non-water-conducting fractures, which also affects the modelling.

The reasons for the scale dependency seen in the evaluated statistical properties are:

- The hydraulically active fractures are sparsely distributed and not very well interconnected hydraulically.
- Longer test time result in fewer fractures being hydraulically active. Some of the minor features intersecting the boreholes have no or poor connection with other conductive features and with increasing test time the flow will decrease in these features. The larger and more transmissive features will control the flow towards the borehole.
- Part of the scale dependency observed, is due to the way in which the statistical properties are calculated. Features with large transmissivities will dominate the statistics for larger test sections.

Spatial correlation model

A few spatial correlation studies have been made: Variogram models in 1-D and 3-D, based on the injection tests from the surface with a 3 m packer spacing, indicate that the hydraulic conductivity is dominated by a random component /*Liedholm et al, 1991a, Niemi, 1995, La Pointe, 1994*/. In all studies all data were used, thus including both hydraulic rock mass domains and hydraulic conductor domains.

Liedholm /1991a/ evaluated the auto- correlation structure of the injection data in KAS02-08, based on tests with 3 m packer spacing. He concluded that the significant ranges at which the data were correlated along the boreholes were

less than 6 m in boreholes KAS03-06 and 18 m to 30 m in KAS02, 07 and 08. Trend corrections did not usually have any effect.

Niemi /1995/ analysed the same data from the pre-investigation phase as in *Liedholm /1991a/*. She fitted variogram models to find the correlation structure along the boreholes. The results are shown in *Table 2-5*. As can be seen in *Table 2-5* the range is greater than was found by *Liedholm /1991a/*. The difference is, however, an artifact as *Liedholm /1991a/* defined the range where there was a statistically significant correlation, while *Niemi /1995/* defined the range as that used in the variograms.

The spatial correlation was evaluated in *La Point /1994/*. The conclusion from the evaluation of injection tests with a 3 m packer spacing was that the sample could be described as a single population and that no very significant trends were present. The spatial correlation in three dimensions indicated a nugget effect of about 60% of the observed variance. The model considered to perform most accurately was a model with Nugget + Spherical model (short range) + Exponential model (long range), data according to *Table 2-6*. The difference, however, was considered to be small between the different models. *La Point /1994/* made directional variograms and mentioned that it was difficult to make any reliable variograms due to the spacing between the boreholes. He concluded that the conditions were possibly isotropic.

Table 2-5. Models and model parameters for variograms of $\text{Log}_{10}(\mathbf{K})$, (\mathbf{K} : (m/s)). /Niemi, 1995/.

Borehole	Model	Nugget C_0	Sill C_1	Range a_1 (m)
KAS02	Gaussian ¹	1.9	3.0	50
KAS03	Exponential ²	2.0	3.2	20
KAS04	Exponential ²	4.0	5.6	20
KAS05	Exponential ²	1.8	2.9	17
KAS06	Exponential ²	2.7	4.7	14
KAS07	Gaussian ¹	1.7	2.6	56
KAS08	Gaussian ¹	1.5	2.6	65
KLX01	Exponential ²	1.2	1.9	20

$$^1 \gamma(h) = C_0 + C_1 \cdot (1 - \exp(-(h/a)))$$

$$^2 \gamma(h) = C_0 + C_1 \cdot (1 - \exp(-(h/a)^2))$$

$$\text{Gaussian model: } a^1 = a \cdot (3)^{0.5}$$

$$\text{Exponential model: } a^1 = a \cdot 3$$

h = length of lag vector \mathbf{h}

Table 2-6. Models and model parameters for variograms of $\text{Log}_{10}(\text{K})$, (K : (m/s)). Data below the measurement limits defined in the evaluation shown in the original report was excluded in the analysis, thus reducing the total variance compared to the total sample /La Point, 1994/.

Borehole	Model 1	Nugget C_0	Sill C_1	Range a_1 (m)	Model 2	Sill C_2	Range a_2 (m)
KAS02-08	Spher. ¹	1.251	0.683	50	Spher. ¹	0.211	200
KAS02-08	Spher. ¹	1.252	0.680	50	Expon. ²	0.298	200
KAS02-08	Spher. ¹	1.445	0.765	70			
KAS02-08	Expon. ²	1.487	0.951	200			

¹ Spherical model

² Exponential model

The evaluated correlation ranges are around 20 to 70 m and the modellers assumed that isotropic conditions prevailed. However, the hydraulic conditions at the Äspö HRL are anisotropic and the correlation ranges may be different in different directions. The correlation range is fairly short compared with the cell size in the numerical model and, what is more important, the nuggets in the variogram models are large (generally about 60% of the total variance). The assumption of no correlation between the 20 • 20 • 20 m cells on the site scale numerical models seems justified, based on the correlation models mentioned above.

However, there is most likely too little correlation in the stochastic model without any correlation structure for features with higher transmissivities when cell sizes in the numerical model are tens of metres or less with the modelling approach used so far. The radius of influence for a specific test depends on the hydraulic properties around the borehole. So far, the radius of influence has just been estimated roughly using the test section length as an indication of mean influence radius. Using the suggested relationships between hydraulic conductivity and specific storativity shown in *Rhén et al /1997/* the arithmetic mean influence radius is about 6, 22, 17 and 62 m for test scales 3, 15, 30 and 100 m respectively, using the simple approach of radial flow (see *Figure 2-20*). (Total test time was used if no upper time for the evaluation period was given.) The values above and in *Figure 2-20* should be seen as indications of influence region and not absolute values. The radius of influence linked to the evaluated hydraulic property can possibly be evaluated and incorporated into the model description, thus improving the base for a spatial correlation model.

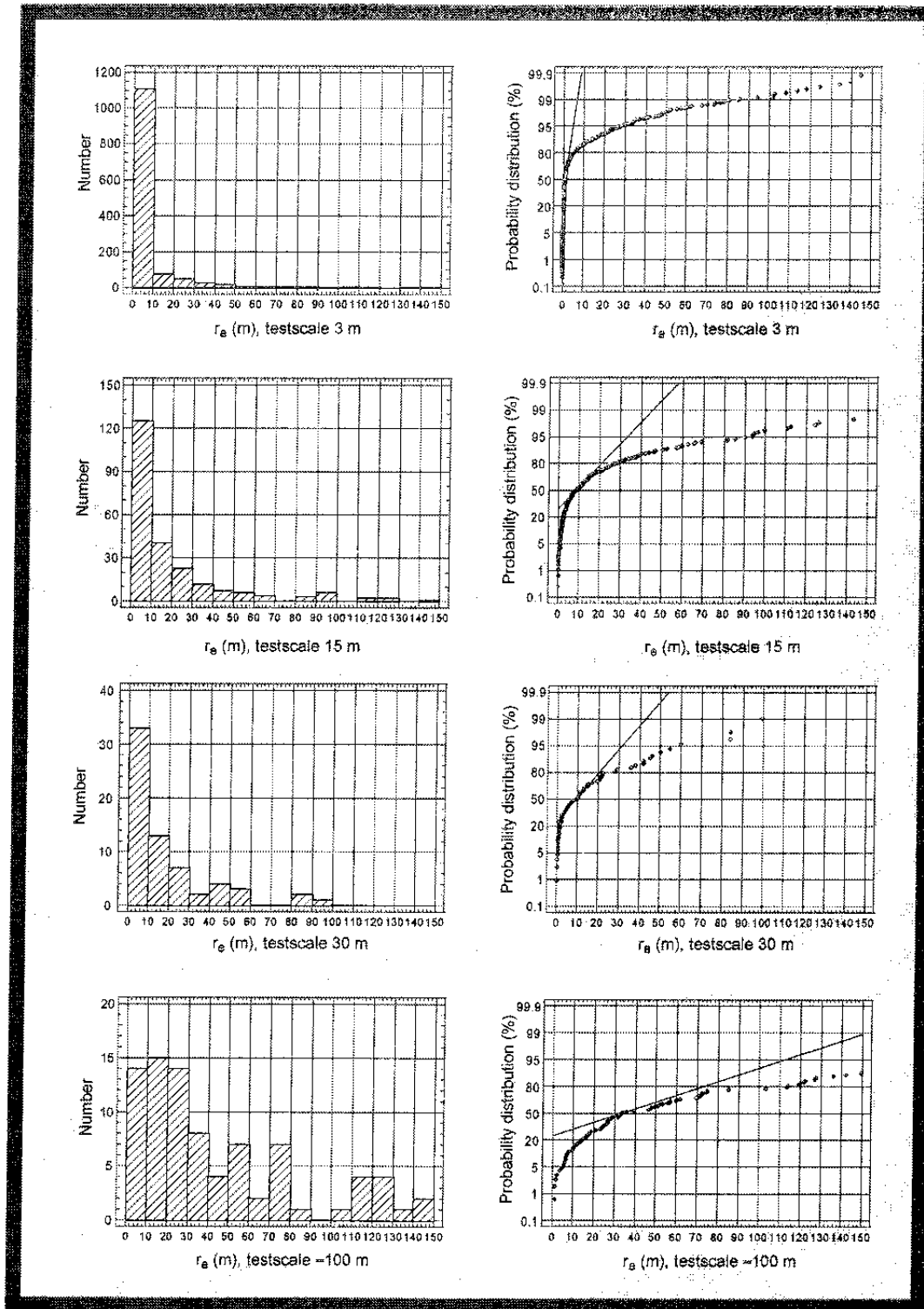


Figure 2-20. Indication of radius of influence assuming a power law relationship between specific storativity and hydraulic conductivity according to Rhén et al /1997/ and radial flow. Data from the pre-investigation and construction phase at Äspö HRL. Total test time was used if no upper time for the evaluation period was given.

Evaluation methodology and testing methods

Evaluation methodology

Transient tests are preferred because they provide an opportunity to judge the flow regime and then obtain some rationale for the evaluation. It also makes it possible to separate the local hydraulic resistance around the borehole (= skin factor) from the formation properties. The stationary methods do not permit this separation.

Based on the flow regime a decision was taken as to whether it was possible to use a transient evaluation method or if it was only possible to calculate the specific capacity. If it was not possible to use a transient evaluation method the reason was generally that the Well Bore Storage (WBS) was disturbing the entire pressure response. This effect was often seen in low-conductivity sections. If it was only possible to estimate the specific capacity (Q/s), the linear relationship between $\text{Log}_{10}(T)$ and $\text{Log}_{10}(Q/s)$ for sections where the transmissivity (T) was evaluated was used to estimate T (see *Rhén (ed) et al /1997/*). As can be seen in *Rhén (ed) et al /1997/* the 95% confidence band on mean $\text{Log}_{10}(T)$ is quite narrow but the 95% prediction band on $\text{Log}_{10}(T)$ as a function of $\text{Log}_{10}(Q/s)$ is about ± 1 mean $\text{Log}_{10}(T)$. If the radial flow concept is assumed to be relevant for most cases, on average the estimated T will thus be a good estimate and of value for the statistics. But an individual estimate is somewhat uncertain according to the text above.

If the flow regime indicated a period with no WBS effects a transient evaluation method was used to estimate the hydraulic properties. Radial flow assumption was used. The rationale for this was that in most cases a radial flow regime after WBS was identified.

To make it easier to test different concepts in the future using new data the following should be reported in the data base beside the hydraulic properties: Test section length, specific capacity (Q/s), starting time for the evaluation period, stopping time for the evaluation period.

Testing methods

It may be said that there were a few problems with the first injection tests using the 3 m packer spacing and flow-meter tests in KAS02 and KAS03. These are therefore of somewhat lesser quality than the tests that followed. Some other tests also failed, resulting in less information on the rock mass than expected. The hydraulic test methodology in the field has improved and the quality of data from the field tests will very probably be better in the future compared with the those from the pre-investigations for the Äspö HRL. However, some tests should always be expected to fail and the planning of tests must take this into consideration.

It is also difficult to get reliable results from low conductivity sections of a borehole because of the elasticity of the equipment and also because of pressure oscillations.

Conclusions

General

Effective values of the hydraulic conductivity of the rock mass domains between the major conductor domains or for lithological domains can be predicted approximately if several boreholes penetrate the volume to be predicted. Extrapolation of results to rock volumes outside the investigated volume should be made with caution if the geological characteristics can be expected to be different from the investigated volume. There are, however, a few problems concerning the evaluation of the properties of the hydraulic rock mass domains. These are outlined below.

Geometrical framework

At several sites it has been shown that the hydraulic conductivity decreases with depth. At Äspö the pre-investigations indicated that the hydraulic conductivity is fairly constant down to 500 m and below 500 m there is possibly a decrease. It is not possible to draw any other conclusions based on the data from the construction phase.

Material properties

The hydraulic conductivity follows approximately a lognormal distribution for test scales longer than about 15 m. With a test scale of 3 m the distribution deviates somewhat from the lognormal distribution. The lowest values from the injection tests with a packer spacing of 3 m was estimated at about 10^{-12} m/s, which compares well with the results from a test at the 5 cm scale that was performed in the Äspö HRL tunnel.

Temperature and salinity have only a minor influence on the evaluated hydraulic properties if the natural temperature gradient and depth down to around 1000 m are considered.

The large scale heterogeneity within a site strongly affects the possibilities of making reliable estimates of the hydraulic properties using few boreholes.

The anisotropic conditions make it much more difficult to sample data that are useful for the analysis intended to provide a quantitative description of the anisotropic conditions. If the rock mass is anisotropic the evaluated properties will be dependent to some extent on the borehole direction. Indications of anisotropy at an early stage of an investigation programme are therefore

important for the planning of the main part of the investigations and also for the evaluation of data.

Transient testing methods are preferred because they make it possible to judge the flow regime and give some rationale for the choice of evaluation method. The hydraulic resistance around the borehole ('skin factor') that is more or less always present may also be separated from the formation properties, which is not possible with stationary evaluation methods.

Spatial assignment method

The results, based on the injection tests from the surface with a 3 m packer spacing, indicate that the hydraulic conductivity is dominated by a random component. The evaluated correlation ranges are around 20 to 70 m and the modellers assumed that isotropic conditions prevailed. However, the hydraulic conditions at the Äspö HRL are anisotropic and the correlation ranges may be different in different directions. The anisotropy also makes it difficult to sample data useful for estimating a correlation structure in three dimensions.

The influence radius for a specific test is very dependent on the hydraulic properties around the borehole. So far the influence radius has been just roughly estimated with the rest section length. It remains to be seen if a more realistic description of the influence radius linked to the evaluated hydraulic property and the test time can be incorporated into the model description.

3 SUBJECT: INFLOW TO TUNNEL - SITE SCALE

3.1 SCOPE AND CONCEPTS

The geometrical concepts for the groundwater flow model consists of:

- hydraulic conductor domains and
- hydraulic rock mass domains.

When the tunnel is introduced into the groundwater flow model the tunnel geometry and the tunnel cross-section define the internal boundaries. A concept for applying atmospheric pressure in the tunnel and a hydraulic resistance (e.g. due to grouting) around the tunnel has to be made.

One purpose of the groundwater flow modelling was to test the ability to make predictions of the total water inflow to the tunnel and inflow to defined parts of the laboratory tunnel based on the predicted geohydrological model.

3.2 METHODOLOGY FOR TESTS OF CONCEPTS AND MODELS

3.2.1 Prediction methodology

Numerical tool

The data in the model presented in *Wikberg et al /1991/* were used to make a three-dimensional groundwater flow model that was calibrated using a number of the interference tests as well as the natural level of the water table. The code used was PHOENICS */Spalding, 1981/*.

Data for the groundwater flow model

At the outset of the project it was decided that a more or less tight tunnel was not needed and due to hydrochemical reasons the grouting should be limited and controlled. From the geohydrological point of view it was also of interest to obtain sufficiently large inflows to get clear responses in the observation boreholes around the excavated tunnel. At the outset of the planning for the groundwater flow simulations it was decided to take into account the working environment and probable grouting in a realistic way. Accordingly, the flow into the tunnel from the deterministically defined water-bearing zones was limited to a maximum of approximately 3 l/s. Fracture zones which ungrouted would give higher flow rates than this were expected to be grouted. In the numerical model each zone intersecting the tunnel was given, if necessary, a

hydraulic resistance, here called a 'skin factor', in order to maximize the flow rate to approximately 3 l/s. The skin factor of the rock between the zones was 0 as a first simulation case and 10 for a second one. These two different values were used to test how it would affect the flow rate into the tunnel and the pressure outside the tunnel. The way the tunnel cross-sections and skin factors were modelled is described in *Svensson /1991/*, *Rhén /1991b/*, and *Liedholm /1991b/*.

The salinity of the water was assumed to be 0.7‰ at sea level and increase linearly at the vertical boundaries to 1.8‰ at 1300 m below sea level. The precipitation was assumed to have 0 ‰ salinity. At the vertical side boundaries hydrostatic pressure, based on the salinity distribution, was used as boundary condition. The sea and the peatlands on Äspö were set to a constant head. The lower boundary was a no-flow boundary. The boundary conditions in the tunnel was atmospheric pressure.

The infiltration rate was estimated to be 3 mm/year by calibration of the model with the natural (undisturbed) water table. The infiltration rate is considered to be an estimate of the deep infiltration as the 3 mm/year is much less than the calculated run-off from near-by areas, which is 150-200 mm/year.

The data for the hydraulic conductor domains and hydraulic rock mass domains are shown in *Svensson /1991/*.

Numerical simulations

The way in which the density-dependent groundwater flow was modelled in the numerical code is shown in *Svensson /1991/* and *Rhén et al /1997/*.

The predictions were made for a number of tunnel face positions as steady-state simulations. The total flow into the tunnel (from tunnel section 700 m to the tunnel face), the flow into the tunnel from each water-bearing zone intersecting the tunnel and the flow into defined tunnel sections (in the predictions called 'legs') were predicted. The positions of the legs are shown in *Figure 3-1*. The predictions in this report are shown for the tunnel section 700 to 2875 m, where the last leg is No. 16. The reason for not comparing the predictions with the outcome after tunnel section 2875 m was because of that the new tunnel layout was considered to deviate too much from the predicted position of the tunnel, see *Introduction* in this report.

A summary of the calibrated model was presented in *Wikberg et al /1991/*. The detailed predictions were presented in *Rhén et al /1991a/* and *Svensson /1991/* and the main predictions in *Gustafson et al /1991/*.

3.2.2 Methodology for determining outcome

At tunnel chainage 700 m the total inflow and outflow of water were measured. At tunnel section 682 m a dam and weir were constructed for measuring the

flow (Q_{wl}) of water into the tunnel section 0 - 682 m. The total amount of water pumped out of the tunnel (Q_{po}) was measured using a flow meter at tunnel chainage 687 m. The total amount of water fed down into the tunnel (Q_{pi}) (mainly for drilling purposes) was measured at tunnel chainage 690 m (see *Figure 3-4*). The air-velocity, humidity and temperature were also measured for the air flowing in and out at tunnel chainage 710 m. The flows of vapour in (Q_{ai}) and out (Q_{ao}) of the tunnel were estimated from these values (see *Rhén et al /1994a/*). The net inflow to the tunnel beyond tunnel chainage 700 m was calculated at:

$$Q_T = Q_{po} - Q_{pi} - Q_{wl} + (Q_{ao} - Q_{ai}) \quad (3.1)$$

Approximately every 150 m along the tunnel a concrete dam was built in the tunnel floor, and the dam was connected to a weir downstream (see *Figure 3-2* and *3-3*). In this way the flow (Q_{wi}) into a number of tunnel sections could be measured more or less continuously.

In most cases there were several mapped fracture zones between two dams. In such cases the inflow from each zone could only be estimated very approximately. The flows into the 6 first legs were also estimated approximately as the dams did not correspond to the legs (see *Rhén et al /1994a/*). The distribution along the tunnel of the mapped flow into the tunnel formed the basis for distributing the measured flow rate at the weirs onto fracture zones and legs.

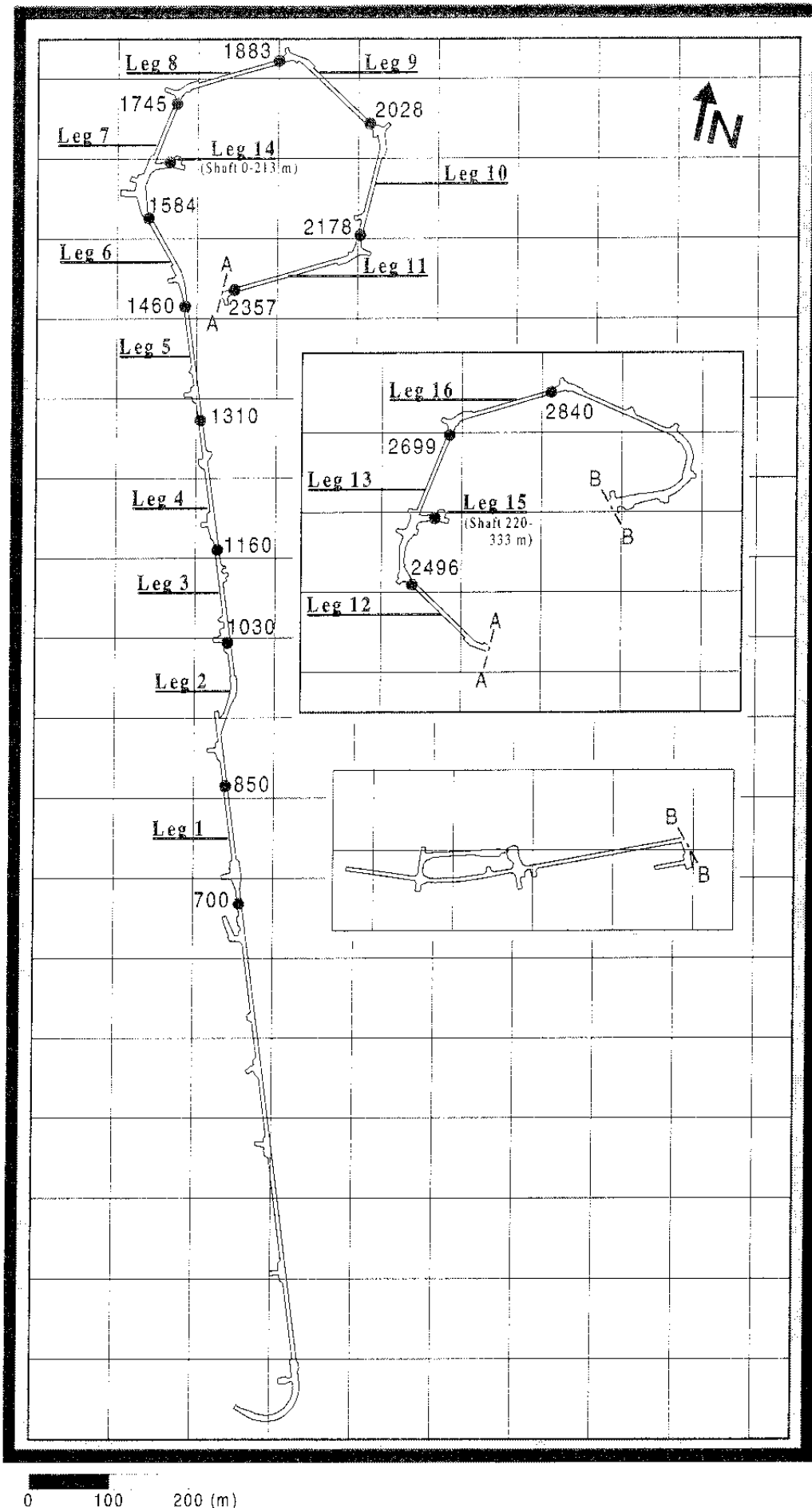


Figure 3-1. Plan of tunnel sections, called 'legs' in the prediction, which were used for predictions of the flow into the tunnel. N = Magnetic North.

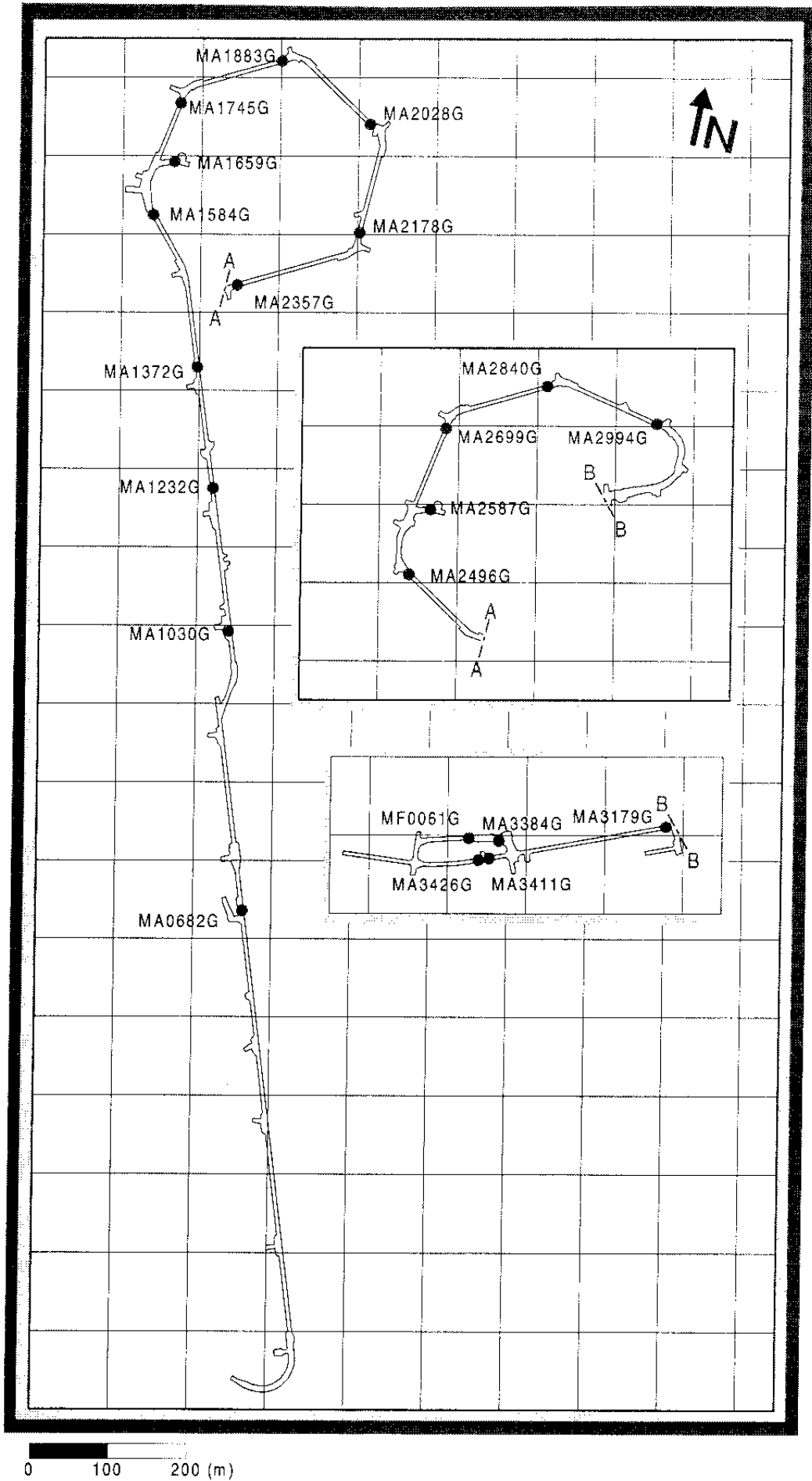


Figure 3-2. Plan of weirs along the tunnel. N = Magnetic North.

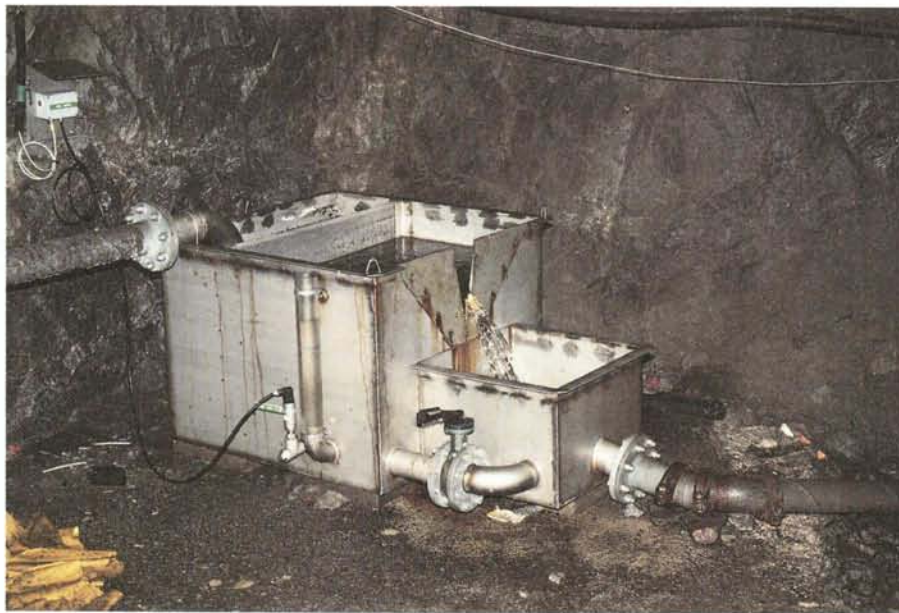
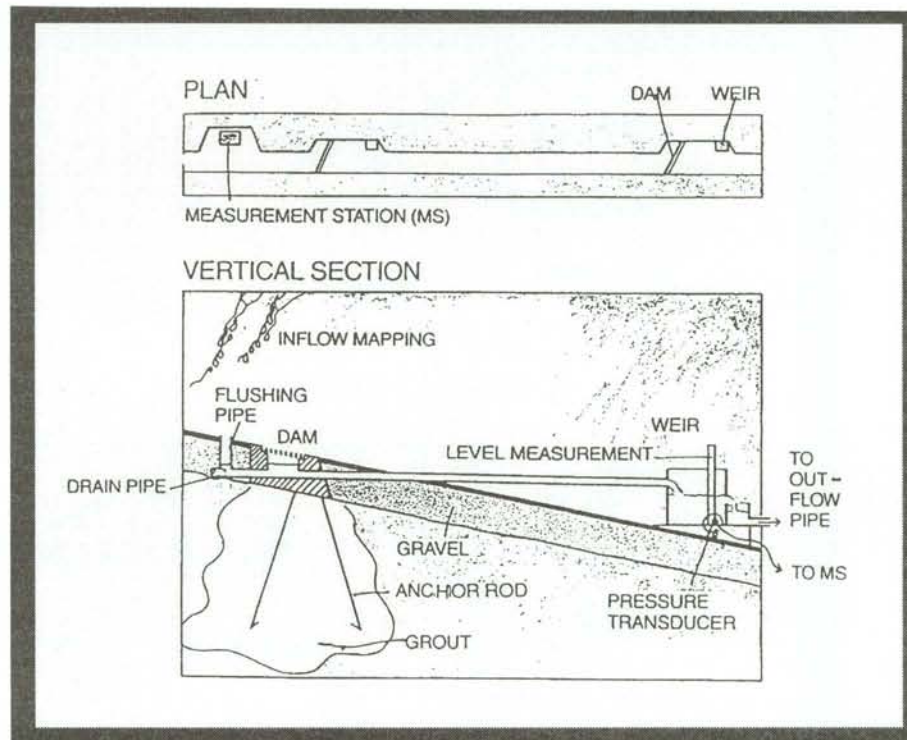


Figure 3-3. Flow measurements with dam and weir. The total flow into and out from the tunnel were measured as well as flow into a number of tunnel sections. Approximately every 150 m along the tunnel a concrete dam was built in the tunnel floor and the dam was connected, by pipework, to a weir downstream. In this way the flow into a number of tunnel sections could be measured continuously. The Measurement Station (MS) is a part of The Hydro Monitoring System (HMS). Normally the level is monitored every 10th second but stored only every 30th minute unless the change since last stored value exceeds in predefined change of value, normally 1 mm. (Nyberg et al, 1996/.

Top: Basic layout of the flow measurement.
 Bottom: Weir.

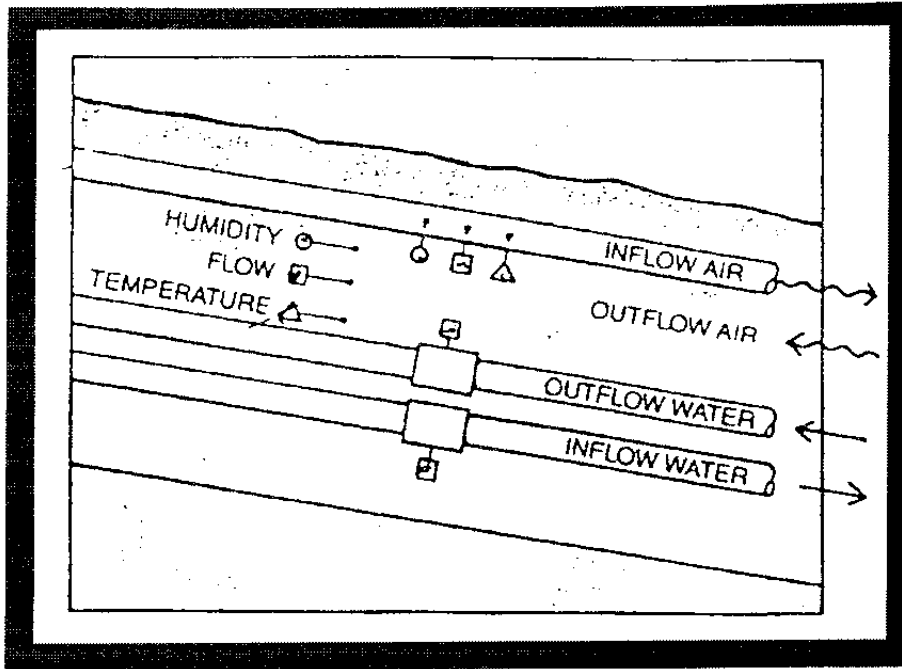


Figure 3-4. Flow measurements at chainage 700 m. Measurements of the water transport by the ventilation air were made at section 700 m up to 1995.

3.3 COMPARISON OF PREDICTED AND MEASURED ENTITIES

Cumulative flow into tunnel

The total net flow into the tunnel is shown in *Figure 3-5*. The prediction and outcome of the flow into tunnel section 700 - 2875 m are presented in *Figure 3-6* and *Table 3-1*. As can be seen the outcome is 84 - 93% of the prediction. The decrease in flow rate during the spring of 1995 shown in *Figure 3-5* is probably due to the permanent reinforcement of the tunnels performed from January to late May 1995.

The net inflow of water at the air was approximately $0 - 0.035 \cdot 10^{-3} \text{ m}^3/\text{s}$ in May to August and the net outflow of water in the air was approximately $0 - 0.06 \cdot 10^{-3} \text{ m}^3/\text{s}$ from September to April, which are small flow rates compared with the flow rates at the weirs.

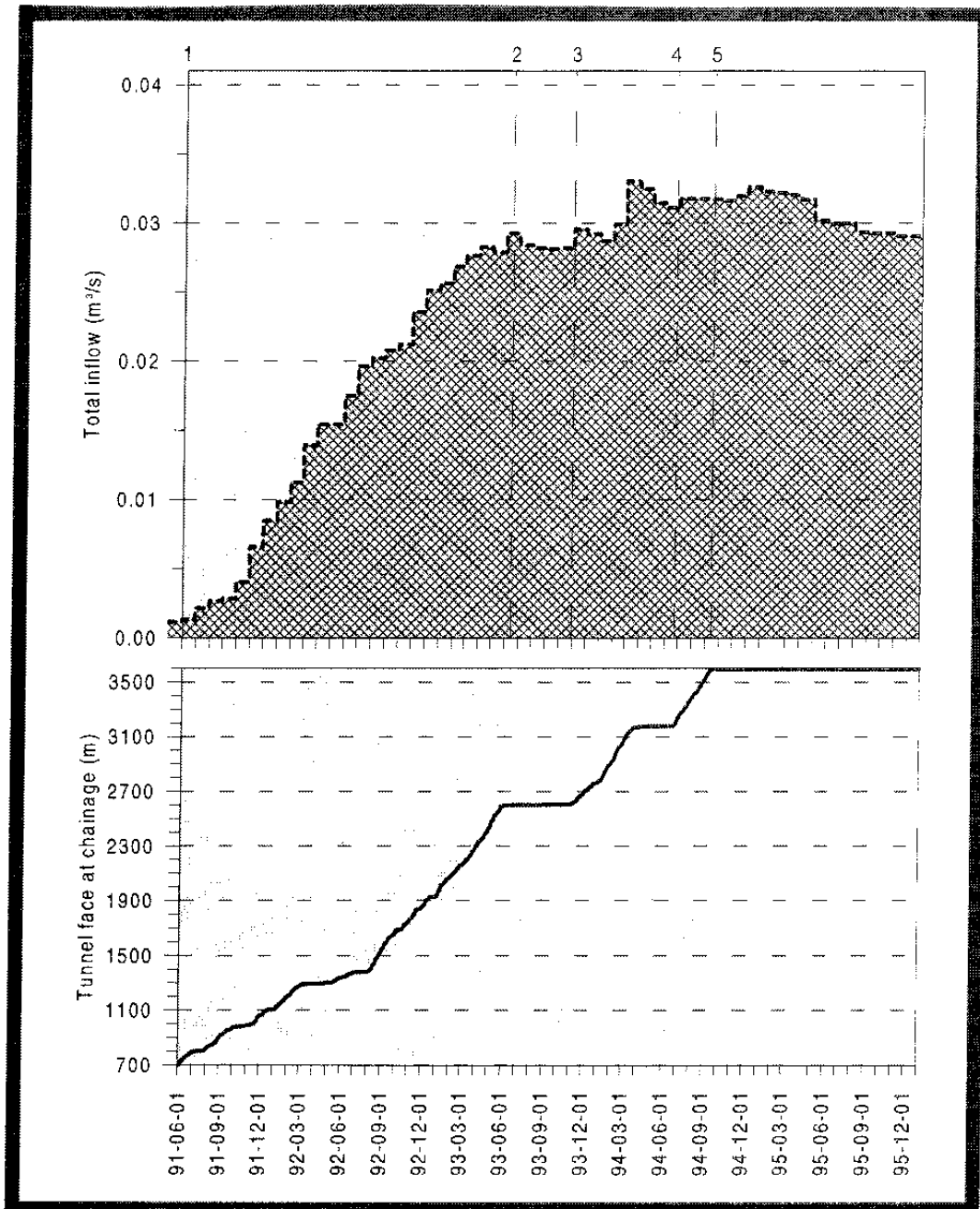
Table 3-1. Water flow into tunnel section 700 - 2875 m, when the tunnel face was at 2875 m. (Skin factor = SK).

Tunnel section (m)	Outcome (m ³ /s) · 10 ⁻³	Prediction		Depth for sample (m)
		SK = 0 (m ³ /s) · 10 ⁻³	SK = 10 (m ³ /s) · 10 ⁻³	
700-1475	20.2*	15	14	100-200
700 - 2265	27.6**	27.5	24.5	100-300
700-2875	28.7	34***	31***	100-400

* August 1992

** March 1993

*** Tunnel section 700 - 2790 m according to predictions /*Rhén et al, 1991a*/, which corresponds approximately to the actual tunnel section 700-2875 m (see *Chapter 1* in the introduction to the report).



- 1 Passage of tunnel section 700 m
- 2 Stop of excavation at 2600 m
- 3 Start of excavation at 2600 m
- 4 Start of TBM drilling
- 5 End of TBM drilling

Figure 3-5. Flow into tunnel section 0 - 3600 m. The monthly inflow to the tunnel is the sum of the estimated monthly mean inflows measured at each weir.

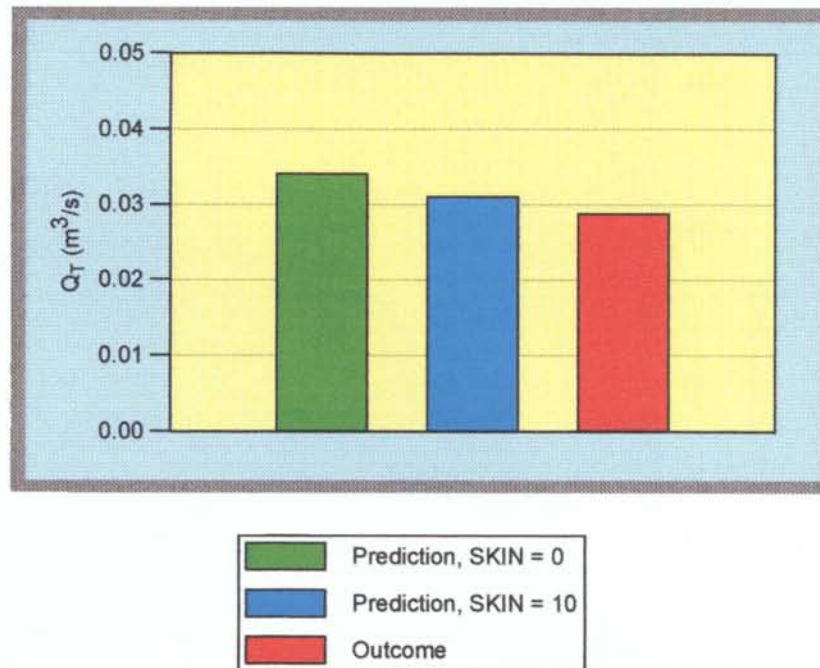


Figure 3-6. Water flow into tunnel section 700 - 2875 m, when the tunnel face was at 2875 m. Predictions were for section 700 - 2790 m according to /Rhén et al, 1991a/, which approximately corresponds to the actual tunnel section 700-2875 m (see Chapter 1 in the introduction to the report).

Flow from zones into tunnel

The outcome and predictions are shown in *Figure 3-7* and *Table 3-2*. Fracture zones are shown in *Figure 1-11*.

It has not been possible to identify NNW-1, NNW-2 and EW-5 in the tunnel, so no inflow estimates are given for these zones. NE-2 was predicted to be just outside the spiral - so there are no predicted values. NNW-4 was predicted to intersect corner D in the spiral - so there is only one predicted value.

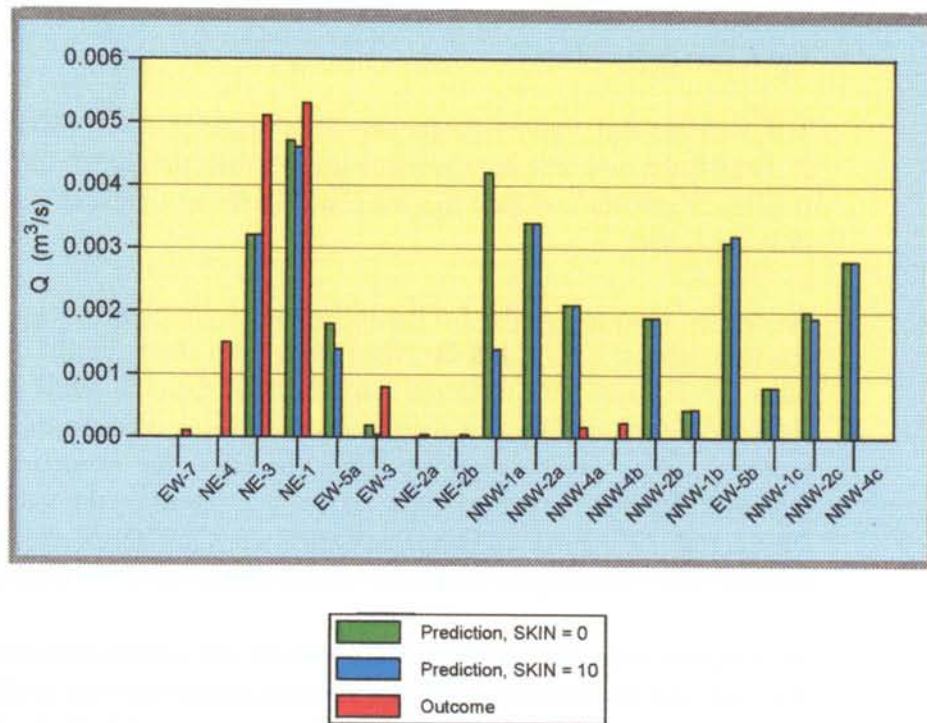


Figure 3-7. Water flows out of fracture zones along tunnel section 700 - 2875 m. Measurement based on data from Rhén et al /1994a/.

Table 3-2. Water flows out of fracture zones along tunnel section 700 - 2875 m. Measurement based on data from Rhén et al /1994a/. (Skin factor = SK).

Fracture zone	Outcome (m³/s) · 10 ⁻³	Prediction	
		SK = 0 (m³/s) · 10 ⁻³	SK = 10 (m³/s) · 10 ⁻³
EW-7	0.1	- ⁽¹⁾	- ⁽¹⁾
NE-4	1.2	- ⁽²⁾	- ⁽²⁾
NE-3	3.9	3.2 ⁽²⁾	3.2 ⁽²⁾
NE-1	5.0	4.7	4.6
EW-5a	- ⁽³⁾	1.8	1.4
EW-3	0.8	0.19	0.05
NE-2a	0.003 ⁽⁶⁾	- ⁽¹⁾	- ⁽¹⁾
NE-2b	0.003 ⁽⁶⁾	- ⁽¹⁾	- ⁽¹⁾
NNW-1a	- ⁽⁴⁾	4.2	1.4
NNW-2a	- ⁽⁴⁾	3.4	3.4
NNW-4a	0.06	- ⁽⁵⁾	- ⁽⁵⁾
NNW-4b	0.12	2.1 ⁽⁵⁾	2.1 ⁽⁵⁾
NNW-2b	- ⁽⁴⁾	1.9	1.9
NNW-1b	- ⁽⁴⁾	0.44	0.45
EW-5b	- ⁽³⁾	3.1	3.2
NNW-1c	- ⁽⁴⁾	0.8	0.8
NNW-2c	- ⁽⁴⁾	2.0	1.9
NNW-4c	- ⁽⁴⁾	2.8	2.8

⁽¹⁾ Not predicted

⁽²⁾ NE-3 + NE-4 treated as one conductive zone in the numerical model

⁽³⁾ EW-5 not confirmed in the tunnel

⁽⁴⁾ Intersection of tunnel not identified

⁽⁵⁾ NNW-4a and b treated as one zone

⁽⁶⁾ Uncertain

Flow into tunnel legs

The outcome and predictions are shown in *Figure 3-8* and *Table 3-3*. For Legs 2, 3 and 6 the outcome is somewhat greater than predicted, for Legs 3 and 14 it is much greater and for Legs 8-12 and 16 the outcome is less or much less than predicted.

As can be seen in *Figure 3-8* the inflow rates are high in legs intersected by fracture zones EW-7, NE-3, NE-4 and NE-1 both in the prediction and outcome. For Leg 3 the outcome is much larger than the predicted values. The reason for this may be that there are some mapped fracture zones in tunnel section 1100 - 1200 which are not included in the numerical model. The hydraulic conductivity used in the model was based on the values from *Äspö /Rhén et al, 1993a/* and as these predicted values are below the measured ones for this tunnel section the predicted values should be lower than the measured.

No fracture zone was predicted to intersect the uppermost part of the shaft (Leg 14) and the outcome is therefore much greater than the predictions. In the new model there is a fracture zone that intersects the shaft (NNW-7) (see *Chapter 1*).

The main reason that the outcome is less than predicted for Legs 8-12 and 16 is that the conductive features NNW-1 and NNW-2 did not provide the predicted inflows and there was no fracture zone predicted to intersect the uppermost part of the shaft (Leg 14). It was not possible to identify these conductive features by mapping in the tunnel, but interference tests and grouting indicated that they possibly intersected the tunnel at approximately the predicted position (see *Chapter 1* for more details). These features were also found to be easily grouted, which may explain the fact that no high flow rates were observed on the tunnel wall.

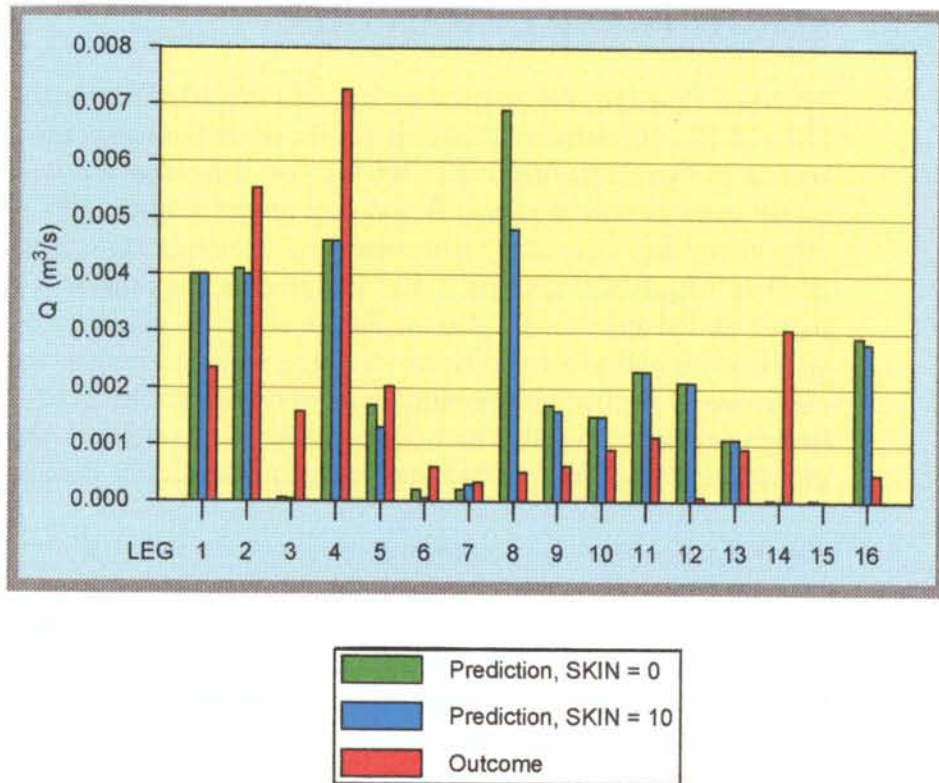


Figure 3-8. Water flows into tunnel legs along tunnel section 700 - 2875 m. Measurement based on data from Rhén et al /1994a/.

Table 3-3. Water flows into tunnel legs along tunnel section 700 - 2840 m. Measurements based on data from November 1993. (Skin factor = SK).

Leg. (No)	Tunnel section (m)	Outcome (m³/s) · 10 ⁻³	Prediction	
			SK = 0 (m³/s) · 10 ⁻³	SK = 10 (m³/s) · 10 ⁻³
1	700 - 850	2.36	4.0	4.0
2	850 - 1030	5.52	4.1	4.0
3	1030 - 1160	1.58	0.06	0.03
4	1160 - 1310	7.26	4.6	4.5
5	1310 - 1460	2.03	1.7	1.3
6	1460 - 1584	0.61	0.2	0.06
7	1584 - 1745	0.34	0.2	0.3
8	1745 - 1883	0.52	6.5	4.6
9	1883 - 2028	0.63	1.6	1.6
10	2028 - 2178	0.92	1.5	1.4
11	2178 - 2357	1.15	2.3	2.2
12	2357 - 2496	0.07	1.9	1.9
13	2496 - 2699	0.93	1.0	1.0
14	-z (0 - 222)	3.05	0.02	0.01
15	-z(222 - 333)	0	0.02	0.007
16	2699 - 2840	0.48	2.7	2.7

3.4 SCRUTINY AND EVALUATION

The total flow into the tunnel was less than predicted for tunnel section 700-2875 m. The difference in flow rates for the predictions and outcome for tunnel section 1475-2265 m (depth 200-300 m) were somewhat less than for the other tunnel sections. The predicted flow rate to tunnel section 1475-2265 m (depth 200-300 m) was somewhat higher than the outcome and to tunnel section 2265-2875 m (depth 300-400 m) it was higher than the outcome. An important reason for the difference is that the inflow is greatly governed by the grouting which is difficult to predict. However, some of the difference may possibly be explained by the hydraulic conductivity of tunnel section 2265-2875 m being lower than that of the other sections (see *Chapter 2*) although the effect of the grouting is judged to have had the greatest impact on the results.

The difference between the prediction and outcome is small for the total flow into the tunnel but when separated into individual fracture zones and tunnel sections some of the individual differences in flow rates for the zones or legs become very large. The reason is that the inflow predictions must be considered uncertain due to the fact that the hydraulic resistance around the tunnel because of grouting and disturbed zone effects could not be predicted on the basis of a sound theory. As pointed out in *Section 3.2.1* it was necessary to estimate reasonable skin factors for the conductive zones to reduce the inflow to what was considered an acceptable level. Another problem is of course the way the flow rates for individual zones and some legs were estimated. Using the mapped flow from the tunnel roof and walls for the distribution of the measured flow at the weir must of course be uncertain as the most of the flow into the tunnel enters via the tunnel floor (see *Chapter 8*).

Conclusions

The prediction of the total flow into the tunnel was successful, but it should also be said that the flow rate into a tunnel is difficult to predict as the amount and effect of the grouting is not known beforehand. The flow rate is more or less governed by the effect of the grouting as grouting is only performed when the tunnel intersects conductive parts of the rock mass.

It can also be added that the total flow into the tunnel after the excavation was somewhat less than the total pumping capacity of the drainage system. As a drainage system may be expensive and difficult to change it is of course interesting to make reliable predictions of the flow rate before construction is started.

From the groundwater flow modelling view point it is also important to get reliable measurements in time and space of the flow rates if more detailed simulations are to be made to test or calibrate the geohydrological model. Dams should be constructed upstream and downstream of a hydraulic conductor's domain, where high inflow rates are expected. One problem at the Äspö HRL was the delay in the construction of the dams and other facilities for measuring flow rates from the dams. For practical reasons it was found difficult to

construct a dam closer than about 150 m from the tunnel face, if it were not to interfere too much with the excavation work. However, a number of dams were constructed far beyond the tunnel face, which of course made the estimation of the flow (as a function of time) into the tunnel uncertain and cumbersome. Measurements of the flow into the tunnel can, and should, certainly be made in a better way than was done at the Äspö HRL, but it should also be remembered that more detailed measurements in space and time would also have a great impact on the contractor's work and also that a dam of good quality is quite expensive.

4 SUBJECT: BOUNDARY CONDITIONS AND PRESSURES - SITE SCALE

4.1 SCOPE AND CONCEPTS

The geometrical concepts for the groundwater flow model consists of:

- hydraulic conductor domains and
- hydraulic rock mass domains.

When the tunnel is introduced into the groundwater flow model the tunnel geometry and the tunnel cross-section define the internal boundaries. A concept for applying atmospheric pressure in the tunnel and a hydraulic resistance (e.g. due to grouting) around the tunnel has to be made, (see *Chapter 3* for more details). In the groundwater flow model the pressure is calculated for all cells defining the domains.

One purpose of the groundwater flow modelling was to test the ability to make predictions of the water pressure within the rock mass surrounding the laboratory based on the predicted geohydrological model.

The excavation itself can be seen as a very long-term hydraulic test which can be used to obtain a general understanding of the flow around the facility by observing where and when draw-downs occur and also how great they are. The other reason for making the measurements is that measured values can as a first step be used for a systematic comparison with the predicted values for a detailed evaluation of the groundwater flow model. The second step is to use the data for calibrating the updated groundwater flow model.

4.2 METHODOLOGY FOR TESTS OF CONCEPTS AND MODELS

4.2.1 Prediction methodology

A groundwater flow model was used to make the predictions (see *Section 3.2.1* for an overview of the model). The predictions were made for all borehole sections that were expected to be monitored on Äspö and also for one borehole on Bockholmen (KBH02) (see *Figure 1-3*).

A summary of the calibrated model was presented in *Wikberg et al /1991/*. The detailed predictions were presented in *Rhén et al /1991a/* and *Svensson /1991/* and the main predictions in *Gustafson et al /1991/*.

4.2.2 Methodology for determining outcome

Monitoring of pressures

The piezometric levels of the groundwater in the Äspö, Ävrö and Laxemar areas were measured in a large number of boreholes drilled from ground level (see *Figures 1-2 and 1-3*). The percussion boreholes, generally 100-200 m deep, contained 1-3 measurement sections. The cored holes, which are up to 1 000 m deep, had up to 6 measurement sections, see *Figures 4-2 and 4-3*. Some of the boreholes drilled from the tunnel were also equipped with packers and connected to the monitoring system in the tunnel.

The monitoring system is described in more detail in *Almén and Zellman /1991/, Almén and Johansson /1992/ and Nyberg et al/1996/*.

The pressures in the probe holes not connected to the automatic monitoring system were measured approximately twice a year manually.

The monitoring of the water pressures in the rock mass was used for:

- interpreting interference tests,
- interpreting hydraulic responses during the excavation of the Äspö tunnel,
- interpreting hydraulic responses during drilling from the tunnel,
- measuring the natural water pressures (undisturbed by the tunnel) and
- measuring the drawdown during excavation.

The measured data are very important for the numerical groundwater simulations. The data were used for calibrating the groundwater flow models and to test how well the models reproduce the measured pressures. The boundary conditions used in the numerical groundwater flow simulations are presented in *Section 3.2.1*.

The absolute pressure along parts of the coreholes was also estimated from the transient injection tests with a packer spacing of 3 m. These estimates were considered uncertain as the pressure-transducers used and calibration procedures were not aimed at getting a good resolution of the absolute pressures. The pressure distribution along the boreholes is useful to know so the flow directions in the borehole before packer installation can be estimated and used for interpretation of the water chemical sampling.

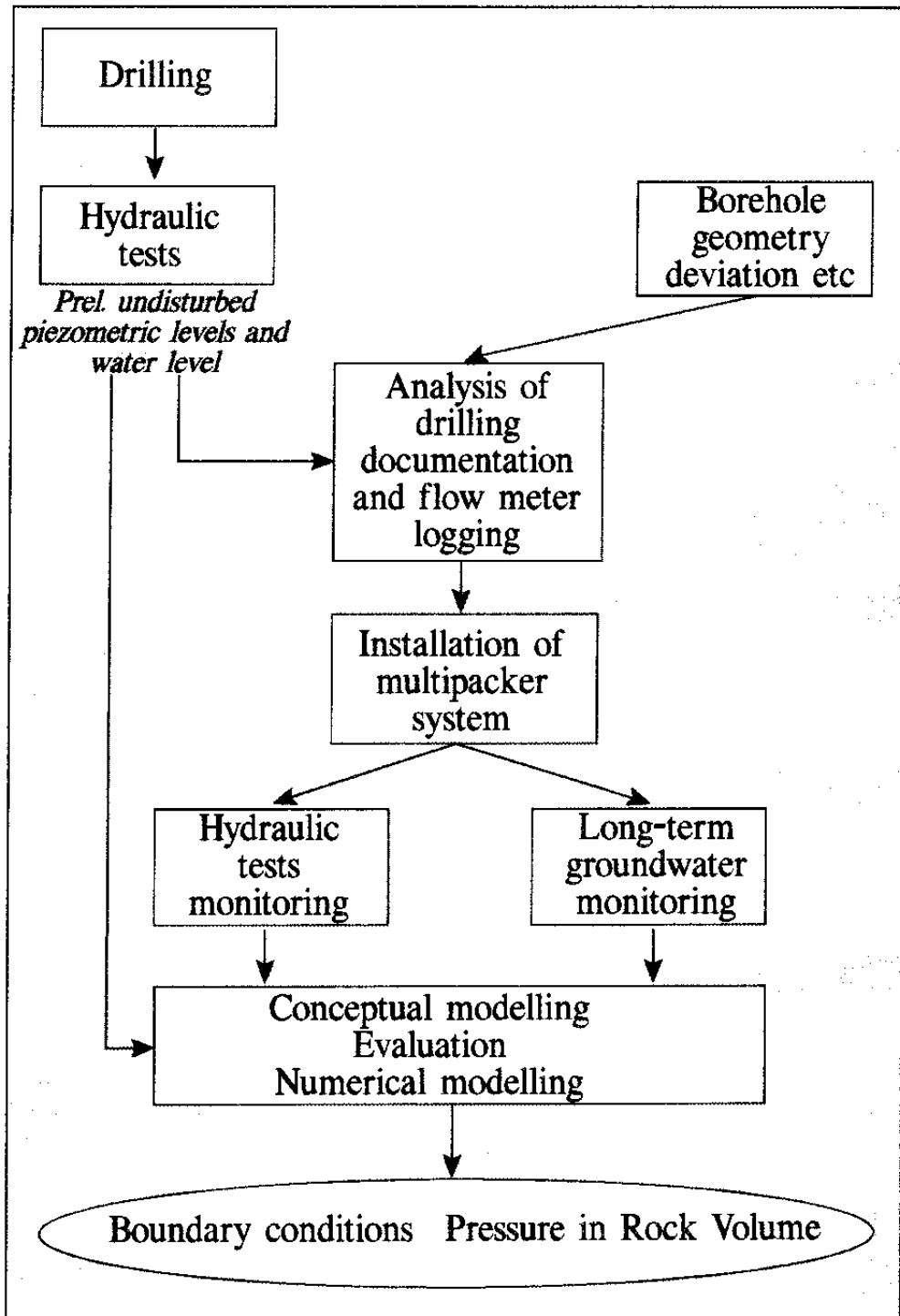


Figure 4-1. Boundary conditions and pressures, in the rock mass. Pressure measurements are the base for assessing suitable initial and boundary conditions in groundwater flow models. (After Almén et al /1994/).

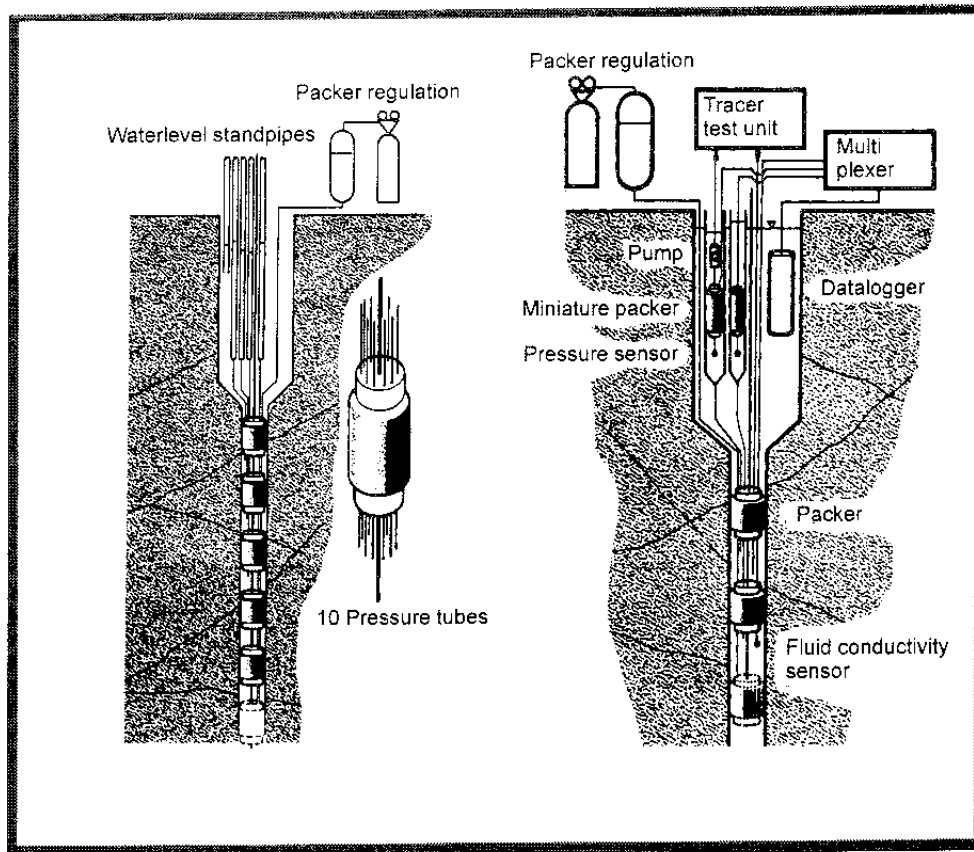


Figure 4-2. Groundwater monitoring.

Left: Multi packer system in a telescope shaped borehole.

Right: Schematic set-up of monitoring system with a data logger. The figure also shows water circulation equipment for one section, the tracer test unit and the fluid conductivity sensor.



Figure 4-3. Top of monitoring borehole, showing bundles of pressure tubing, signal cables etc. Calibration of pressure recording is made by means of dipping a water level sensor in the stand-pipes.

4.3 COMPARISON OF PREDICTED AND MEASURED ENTITIES

The draw-downs are presented in this section. A detailed description of piezometric levels for individual boreholes is given in *Rhén et al /1993b, d, 1994b/*.

Groundwater flow modelling

Predictions of the drawdown due to the construction of the Äspö HRL were made in 1990 and presented in *Gustafson et al /1991/*, *Rhén et al /1991/* and *Svensson /1991/* (here called *Model 90*). The boundary condition in the tunnel was atmospheric pressure. In 1995 the drawdown was once again calculated using the same model as in 1990 but in that case with the measured flow of water into the tunnel up to tunnel section 2874 m (here called *Recalc 90*) */Svensson, 1995b/*. Another modelling case in 1995 was a modified model of the hydraulic conductor domains (here called *Model 95*) and a third modelling case was with one hydraulic conductor domain (EW-5) excluded (here called *Model 95 without EW-5*). Only a few tests with different realizations of the

hydraulic conductivity field within the hydraulic conductor domain, sometimes called Monte Carlo simulations, were performed with *Model 90*. It was found that the influence on the drawdown was limited and thus the predictions were based on one realization of the hydraulic conductivity field. *Recalc 90* was performed as Monte Carlo simulations with 10 realizations of the hydraulic conductivity field between the hydraulic conductor domains. The transmissivities of the hydraulic conductor domains were the same in all realisations.

Measured and predicted values

Figures 4-4 to 4-6 show the 1990 prediction (*Model 90*) of the water table. *Figure 4-7* shows the water table for the *Recalc 90* and finally in *Figure 4-8* the mean value of the predicted water tables for the *Model 95* and *Model 95 without EW-5* are shown. *Figures 4-9 to 4-18* show the draw-down as a function of time for five boreholes representing northern Äspö (KAS03), the Äspö shear zone (KAS04) and southern Äspö (KAS02, KAS05 and KAS06). The mean values of the draw-downs are shown for *Recalc 90*, and *Model 95*. An example of the variability of the predicted draw-downs for *Recalc 90*, *Model 95* and *Model 95 without EW-5* is shown in *Figure 4-19*. Detailed presentation of the variability in the predictions is shown in */Svensson, 1995/*. Time-draw-down curves for other boreholes and the draw-downs in a few horizontal sections are presented in *Rhén et al /1993b, d, 1994b/* and in *Rhén et al /1993a, c, 1994a/*. (The piezometric levels are given as metres above sea level.)

Discussion on the measured and predicted water tables. Figures 4-4 to 4-8

Water table - tunnel face at 1475 m. Model 90

As can be seen in *Figure 4-4* there is reasonable correspondence between the prediction and outcome. On the southernmost part of Äspö the predicted level is higher than the outcome. This may be due, at least in part, to the measured inflow rate being larger than predicted.

There is also a difference in the northeastern part of Äspö. This is most probably because there are no boreholes in this part of the island to be included in kriging of the water table. The estimation of the water table by kriging in that region must thus be considered very uncertain. The water table level is probably up to +3 m in this area considering the topography and the relation between the water table and topography show in *Rhén et al /1997/*.

Water table - tunnel face at 2195 m. Model 90

As can be seen in *Figure 4-5* there is correspondence between the prediction and outcome. However, the predicted level is lower than the outcome just south of EW-1 and higher than the outcome near the shafts. This is due, at least in

part, to the measured inflow rate being lower than predicted for the spiral but higher for the shafts. The minimum measured water level was about -90 m, close to the shaft.

The predicted water level north of EW-1 corresponds fairly well to the measured one, which is about -0 m.

Water table - tunnel face at 2875 m. Model 90

As can be seen in *Figure 4-6* there is a relatively good correspondence between the prediction and outcome, somewhat better than that shown in *Figures 4-4* and *4-5*. However, the predicted level is lower than the outcome just south of EW-1 and higher than the outcome near the shafts. This is due, at least partly, to the measured inflow rate being lower than predicted for the spiral but higher for the shafts.

North of EW-1 the predicted levels are somewhat lower than the measured levels.

Water table - tunnel face at 2875 m. Recalc 90

Ten realisations of the conductivity field between the hydraulic conductor domains were made and the mean value of the level of the water table is shown in *Figure 4-7*. As can be seen in *Figure 4-7* there is correspondence between the prediction and outcome. However, the predicted level is lower than the outcome near the shafts. This is due, at least partly, to the lack of a conductive structure near the shafts. In the *Model 95* the subvertical hydraulic conductor domain NNW-7, intersecting the shafts, was added to the model.

North of EW-1 the predicted levels are somewhat lower than the measured levels.

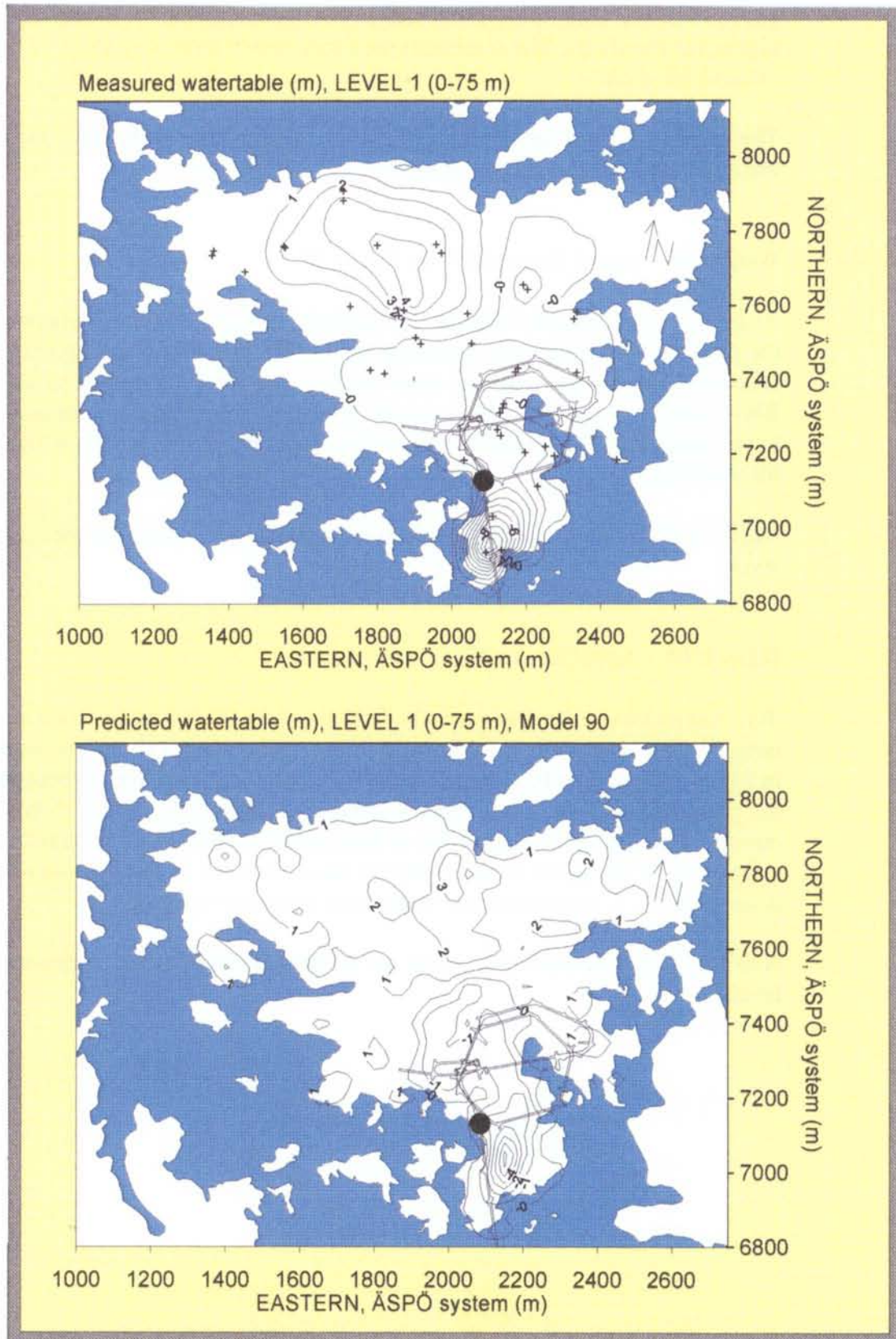


Figure 4-4. Water table with the tunnel face at chainage 1475 m. Outcome above and prediction below. Prediction made in 1990 (Model 90). '+' shows the position of the borehole sections for the measured water level and the black dot the tunnel face position.

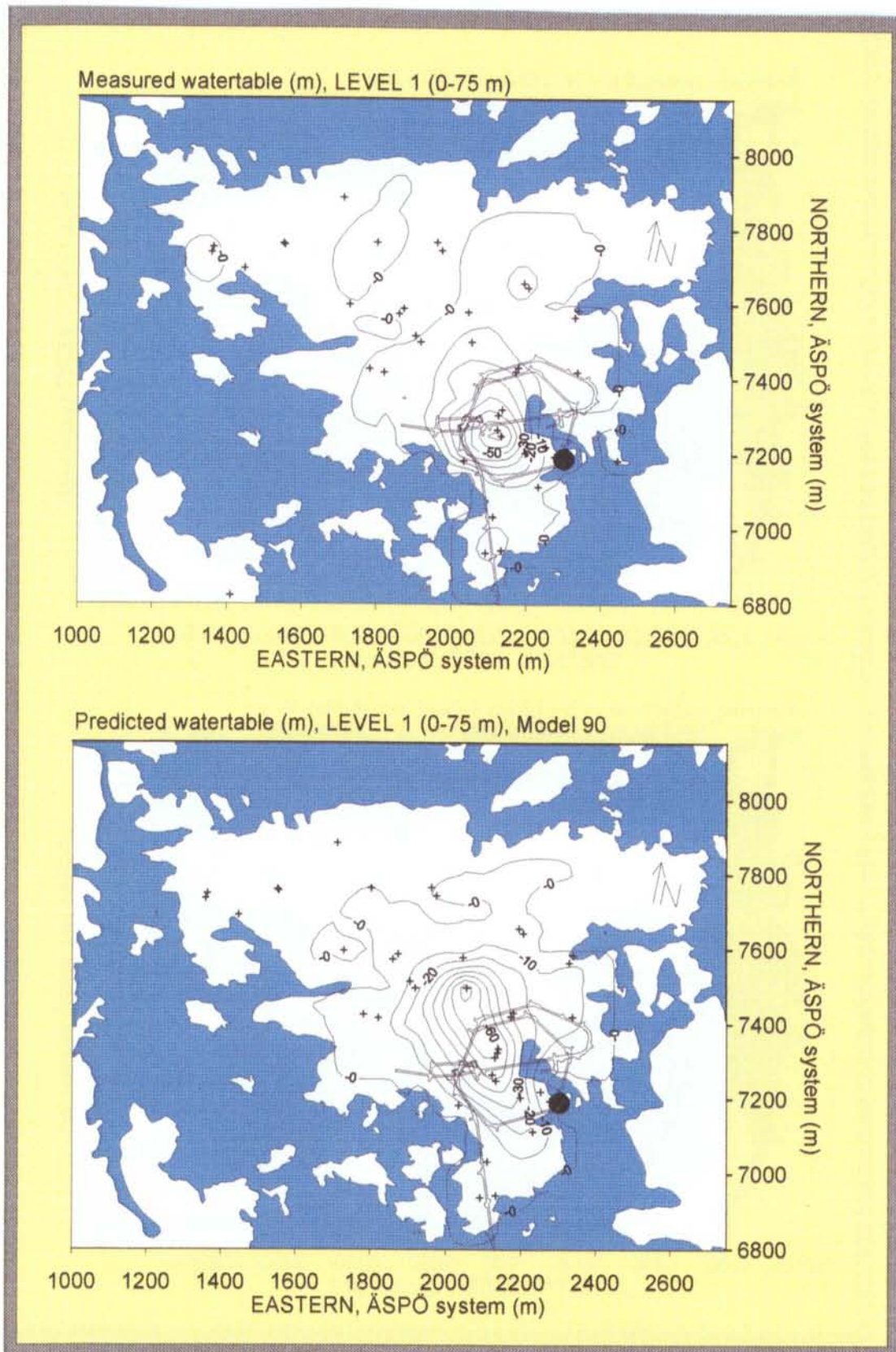


Figure 4-5. Water table with the tunnel face at chainage 2195 m. Outcome above and prediction below. Prediction made in 1990 (Model 90). '+' shows the position of the borehole sections for the measured water level and the black dot the tunnel face position.

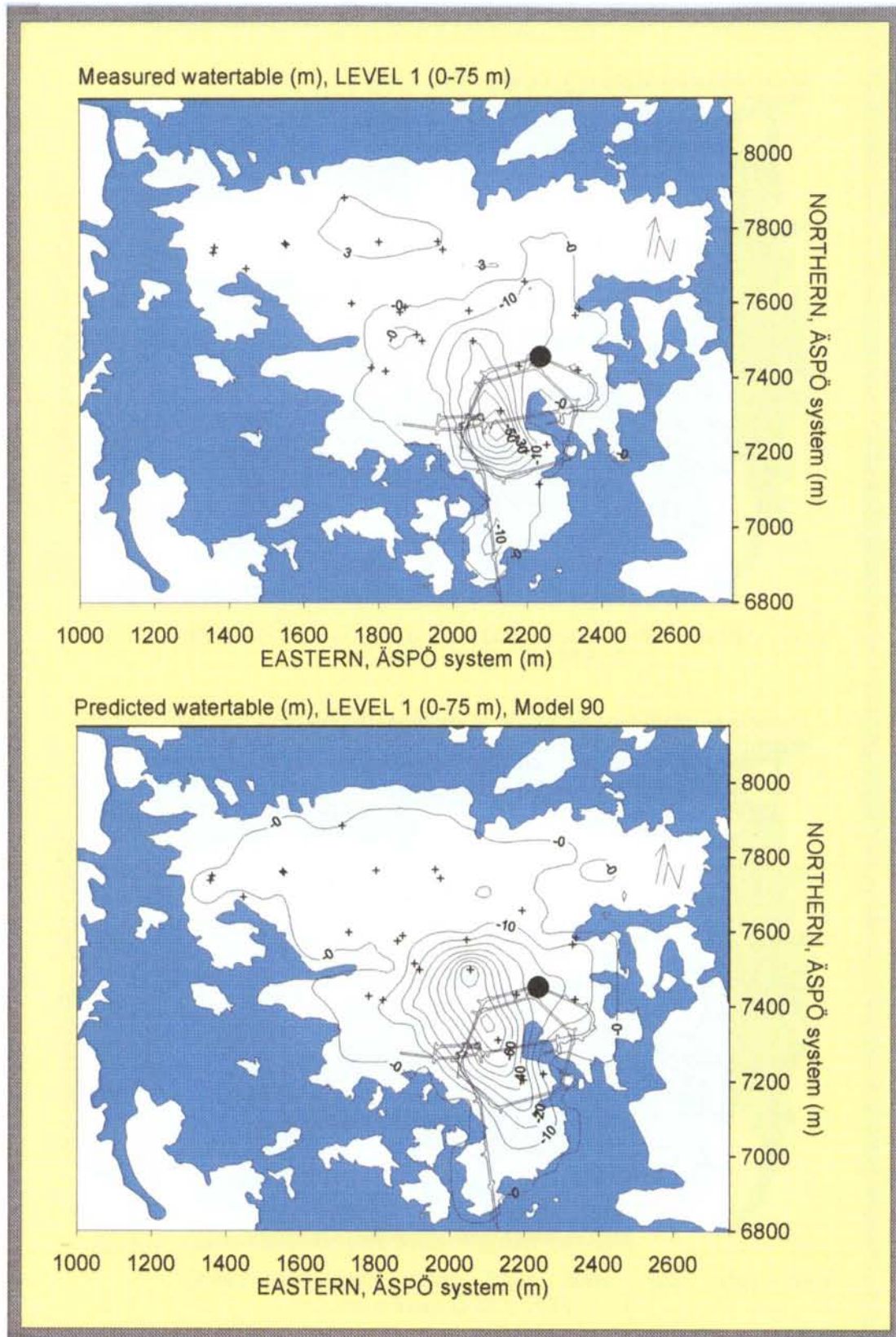


Figure 4-6. Water table with the tunnel face at chainage 2875 m. Outcome above and prediction below. Prediction made in 1990 (Model 90). '+' shows the position of the borehole sections for the measured water level and the black dot the tunnel face position.

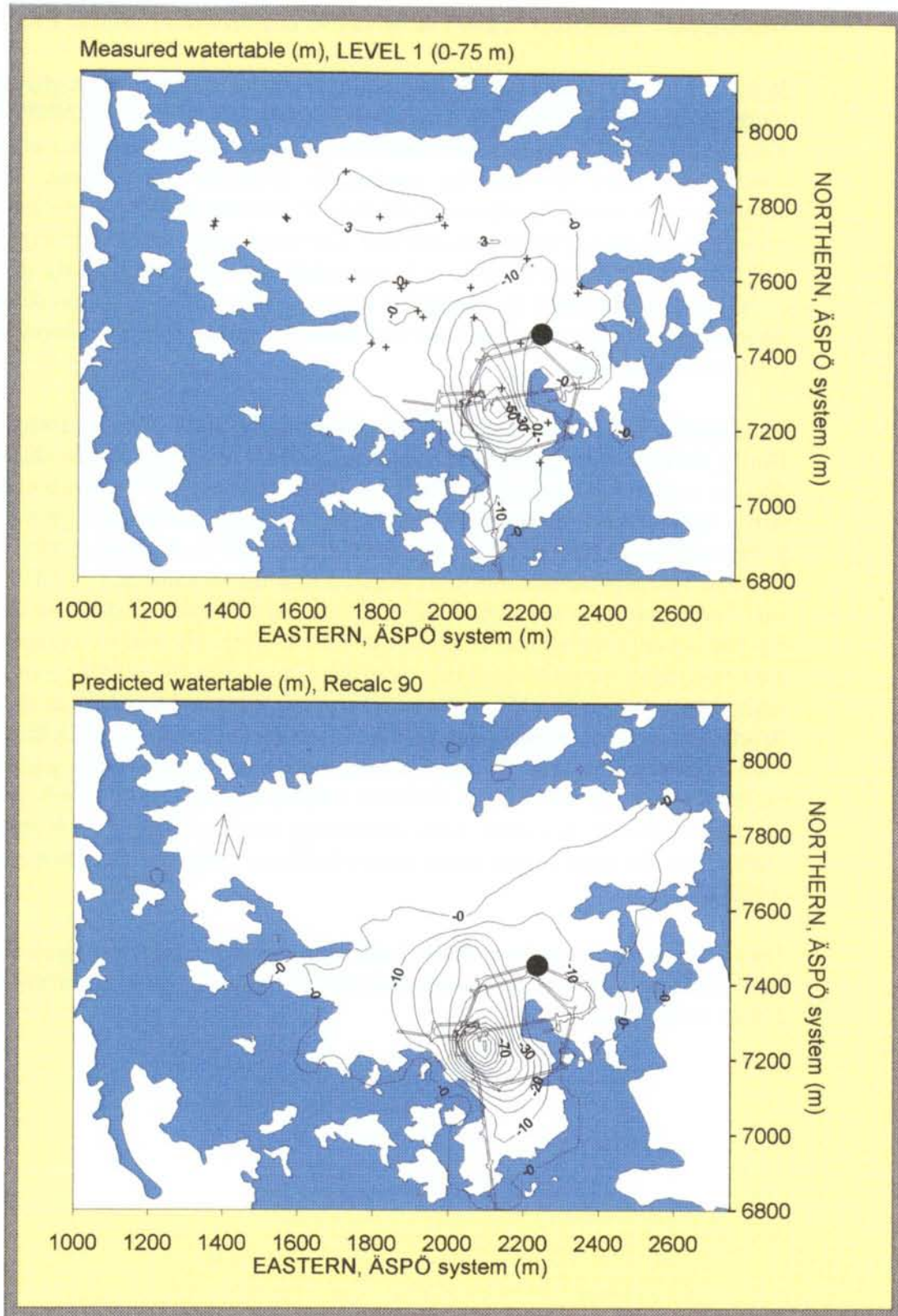


Figure 4-7. Water table with the tunnel face at chainage 2875 m. Outcome above and prediction below. Prediction made in 1995 (Recalc 90). '+' shows the position of the borehole sections for the measured water level and the black dot the tunnel face position.

Water table - tunnel face at 2875 m. Model 95 and Model 95 without EW-5

In *Model 95* the position of the hydraulic conductor domains were slightly modified according to *Stanfors et al /1994/*. A new structure, called NNW-7, intersecting the shafts was also included in the model. Ten realisations of the conductivity field between the conductive structures were made. One simulation was also done where the conductive structure EW-5 was excluded in order to see the impact of this structure. The results are presented in *Figure 4-8*. As can be seen in *Figures 4-7* (outcome) and *4-8* there is fairly good correspondence between the prediction and outcome. However, the predicted level is higher than the outcome near the shafts. Excluding EW-5 improves the prediction somewhat.

The rationale for the introduction of the new structure NNW-7 was as follows. During the pre-investigations there were suggestions of a hydraulic conductor domain somewhere around the shaft but there was no clear evidence of its strike, dip or extent. The spinner log indicated a conductive feature in KAS13 at borehole depth (length along the borehole) 195-215 m */Rhén et al, 1991b/*. The rock type and the fractures were mapped near the elevator and ventilation shaft before the Äspö research village was constructed and the shafts were later mapped between the ground level and the -230 m level. The surface mapping, after excavating the pit showed that there were steep (dip 70° to 85°E) joint or fault planes striking N ±15° in the western part of the pit. The extent of these structures was large. Several steep fractures similar to the ones seen in the pit were intersected between 150 and 200 m in the elevator shaft. Mapping in the tunnel showed that sub-vertical fractures striking approximately WNW-NW and approximately N-S were water conducting and they were present along more or less the entire tunnel below Äspö island (see *Chapter 1* and *Rhén et al /1997/*).

Thus, during the excavation of the Äspö HRL several results indicated that there probably is a NW-NNW conductive feature similar to NNW-1 and NNW-2 close to the shafts.

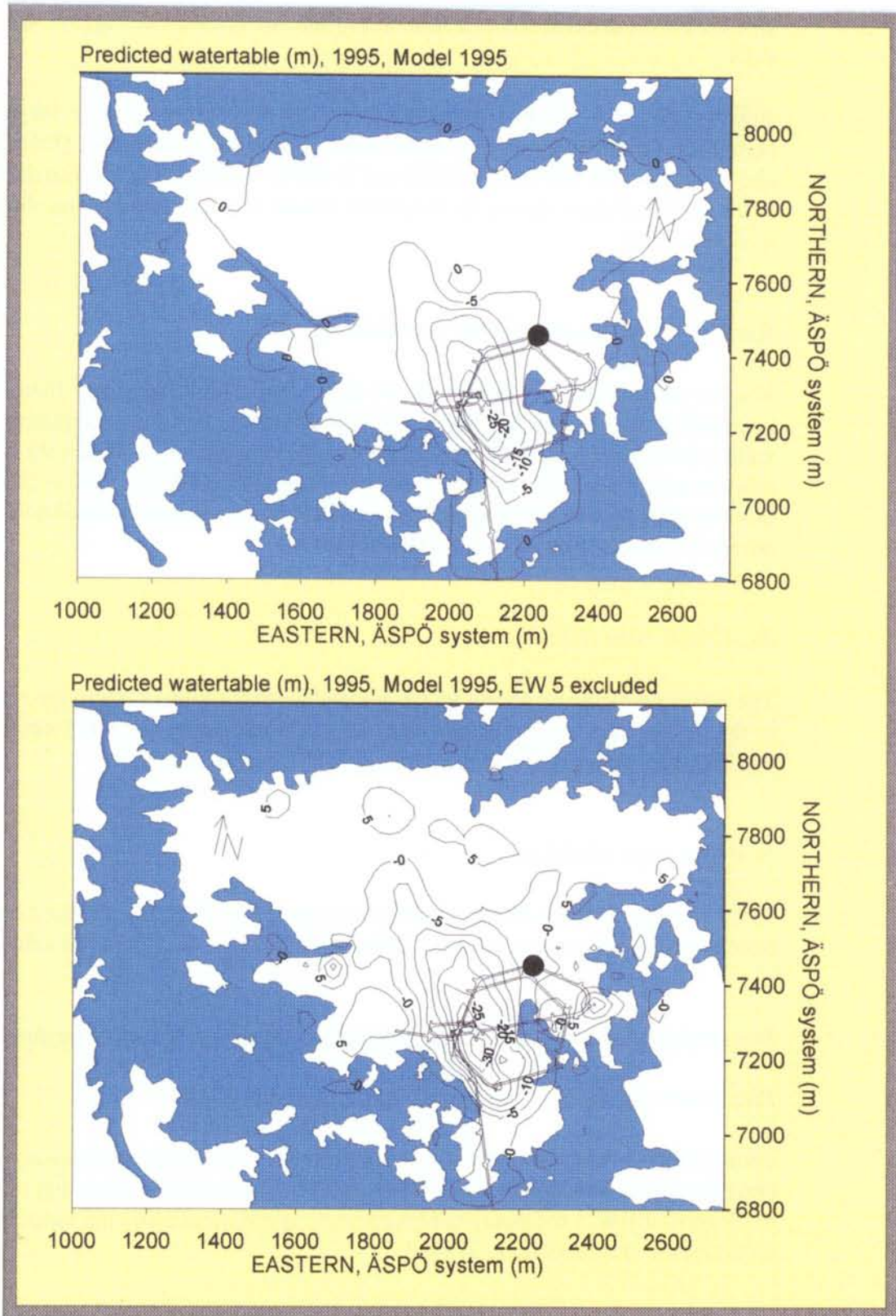


Figure 4-8. Water table with the tunnel face at chainage 2875 m. Prediction made in 1995 with Model 95 (above) and Model 95 without EW-5 (below).

Discussion on draw-down as a function of time in KAS02-06. Figures 4-9 to 4-18

Figures 4-9 to 4-18 show the draw-down as a function of time for five boreholes representing northern Äspö (KAS03), the Äspö shear zone (KAS04) and southern Äspö (KAS02, KAS05 and KAS06). Examples of the variability of the predicted draw-downs for Model 90, Recalc 90, and Model 95 are shown in Figure 4-19.

Southern Äspö (KAS02, KAS05 and KAS06)

The levels predicted by *Model 95* are generally somewhat higher than the measured levels. As can be seen in *Figure 4-19* the variability in the predicted values for KAS02 was reduced with *Model 95* compared with *Model 90*. The main reason is the new hydraulic conductor domain NNW-7, which is rather close to KAS02. The variability of the predicted values decreases for almost all borehole sections (see *Svensson /1995/*).

Äspö shear zone (KAS04)

The levels predicted by *Model 95* are somewhat higher than or about the same as the measured ones, if it is assumed that the measured levels in the summer of 1993 were approximately the same as in the winter 1993/94.

Northern Äspö (KAS03)

The levels predicted by *Model 95* are somewhat higher than the measured ones except for the uppermost section which corresponds to the measured value.

Discussion on the measured and predicted values for horizontal sections

Piezometric levels for $-75 < z \leq -200$ m. Prediction in 1990

South of EW-1 the predicted levels were somewhat higher than those measured until the tunnel face had reached section 1475 m and thereafter lower (up to 50 m). North of EW-1 the predicted levels were approximately as the measured levels */Rhén et al, 1993a, c, 1994a/*.

Piezometric level for $-200 < z \leq -400$ m. Prediction 1990

South of EW-1 the predicted levels were somewhat higher than those measured until the tunnel face had reached section 1475 m and thereafter lower (up to 60 m). North of EW-1 the predicted levels were approximately as those measured */Rhén et al, 1993a, c, 1994a/*.

Piezometric level for $-400 < z \leq -600$ m. Prediction 1990

South of EW-1 the predicted levels were higher than those measured until the tunnel face had reached section 1475 m and thereafter lower (approximately 20 m). North of EW-1 the predicted levels were higher (1-2 m) than those measured /*Rhén et al, 1993a, c, 1994a/*.

Piezometric levels for z below -600 m

South of EW-1 the predicted levels were higher until the tunnel face had reached section 1475 m and lower (approximately 10 m) thereafter lower than those measured. North of EW-1 the predicted levels were higher (0-3 m) than those measured /*Rhén et al, 1993a, c, 1994a/*.

Hålö area

The piezometric levels near the tunnel at Hålö had decreased down to - 7 m (below sea level) when the tunnel face was at 1475 m. The piezometric levels had decreased approximately one more metre when the tunnel face was at 2265 m, and thereafter the levels remained steady /*Rhén et al, 1993b, d, 1994b/*.

Ävrö area and Mjälén area

The piezometric levels at the northern and central parts of Ävrö had declined up to 2 m when the tunnel face was at 1475 m. On southern Ävrö no drawdown has been seen, only annual variations. The boreholes on southern part of Mjälén and borehole HAV08 show a decline of 3-4 m. The piezometric levels were steady after the tunnel face passed section 1475 m /*Rhén et al, 1993b, d, 1994b/*.

Laxemar area

The piezometric levels at Laxemar were steady during the construction of the Äspö HRL, except for annual variations and draw-downs because of pumping in KLX02 /*Rhén et al, 1993b, d, 1994b/*.

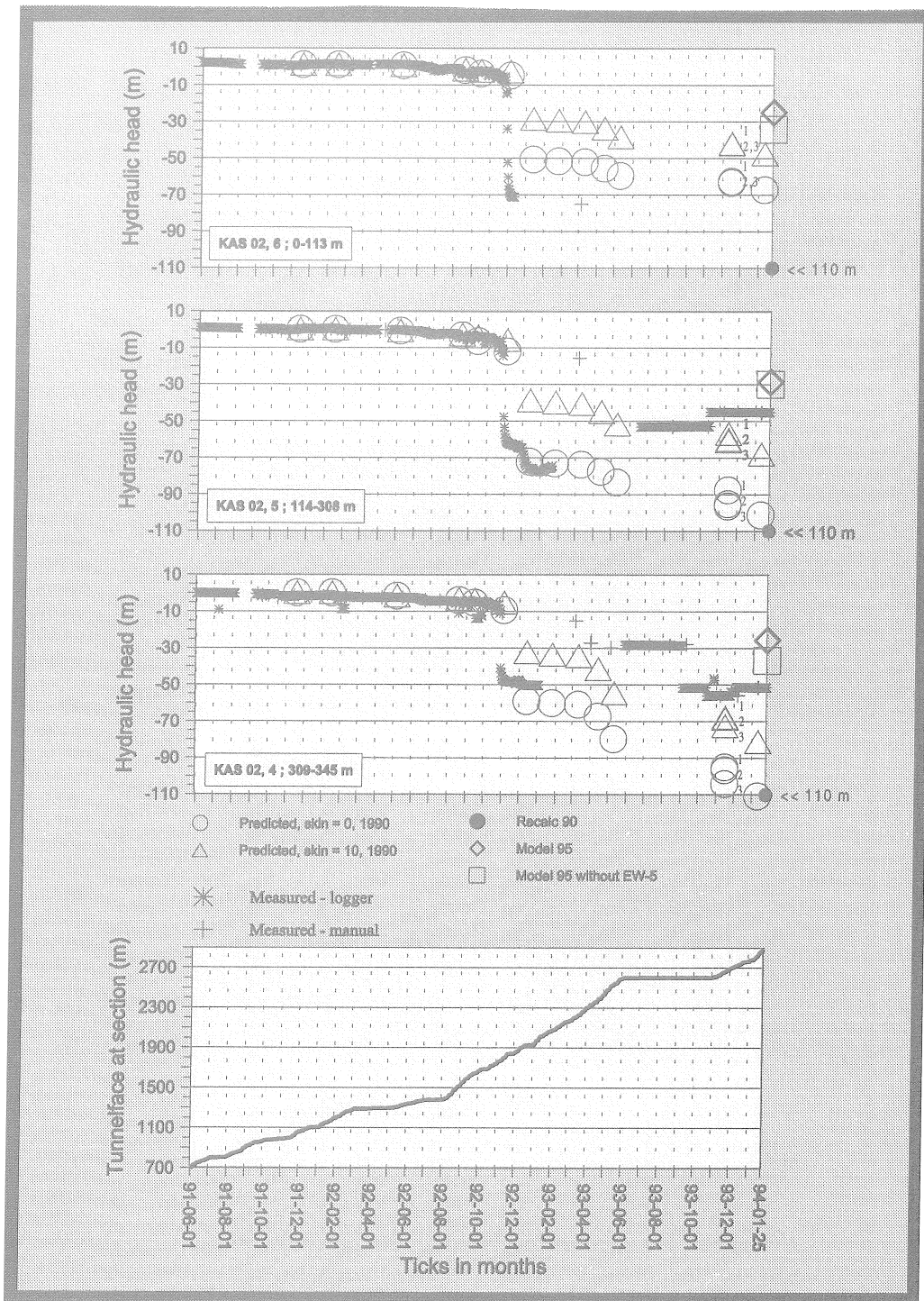


Figure 4-9. Measured and predicted piezometric levels in KAS02, borehole sections 4-6.

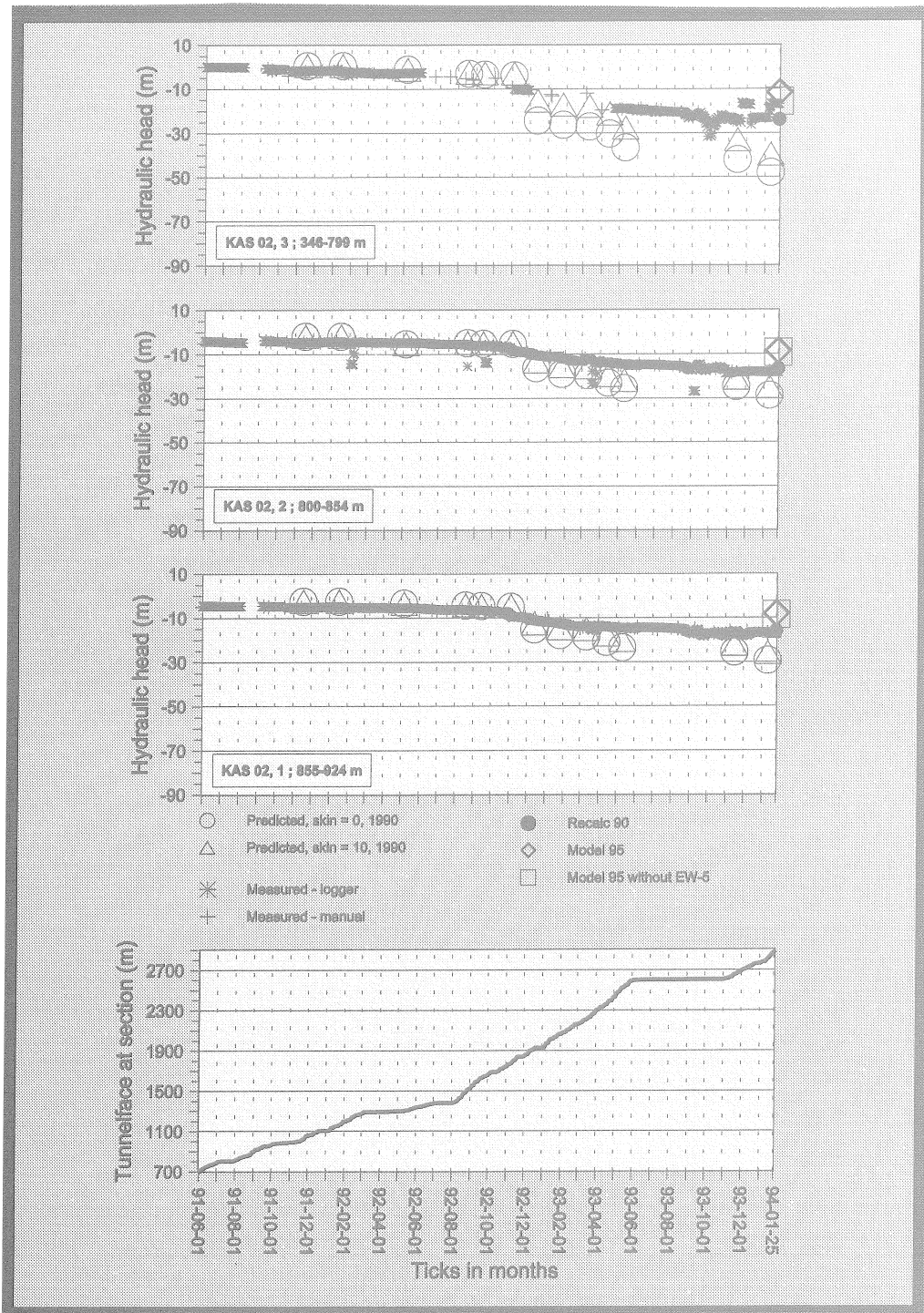


Figure 4-10. Measured and predicted piezometric levels in KAS02, borehole sections 1-3.

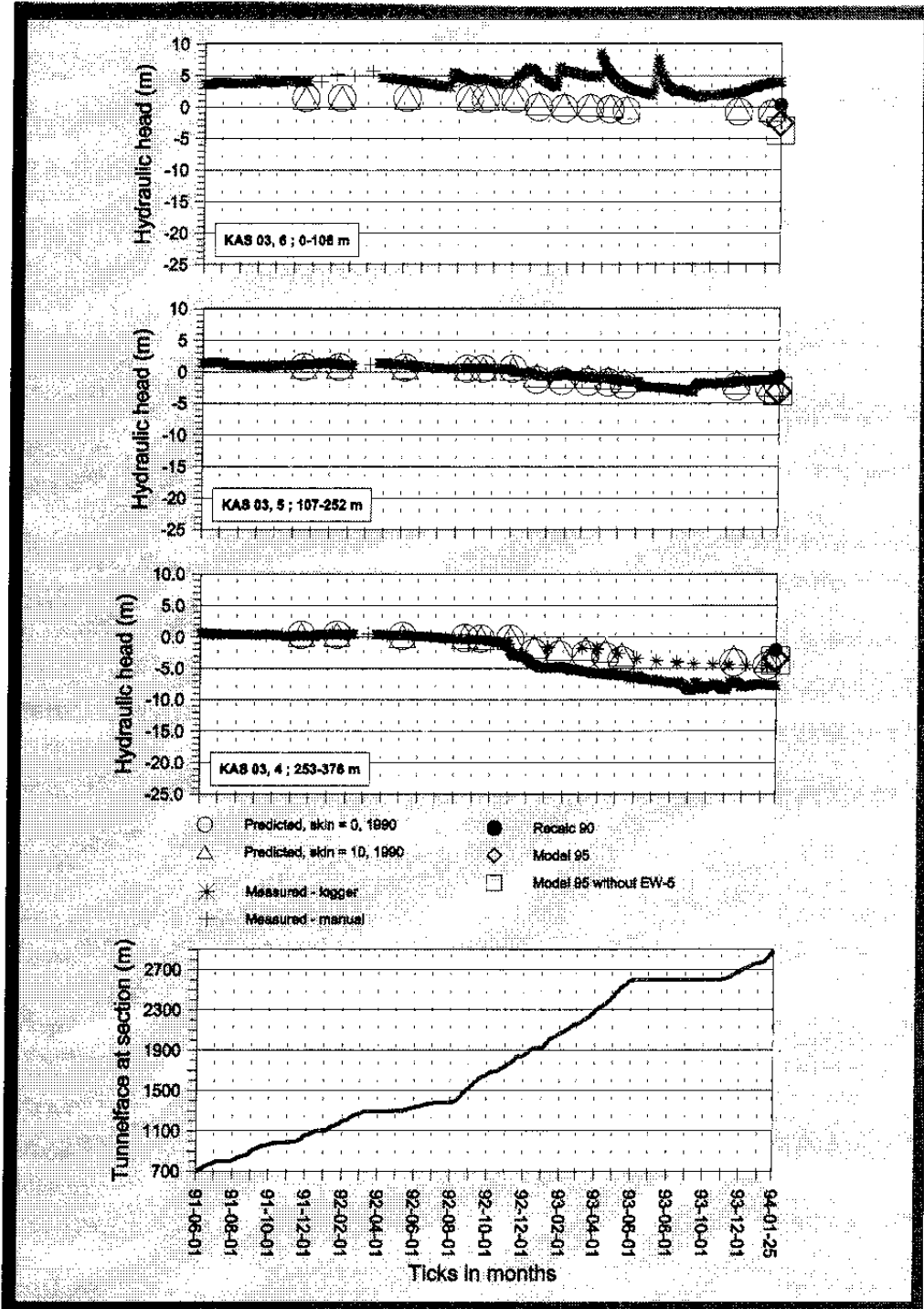


Figure 4-11. Measured and predicted piezometric levels in KAS03, borehole sections 4-6.

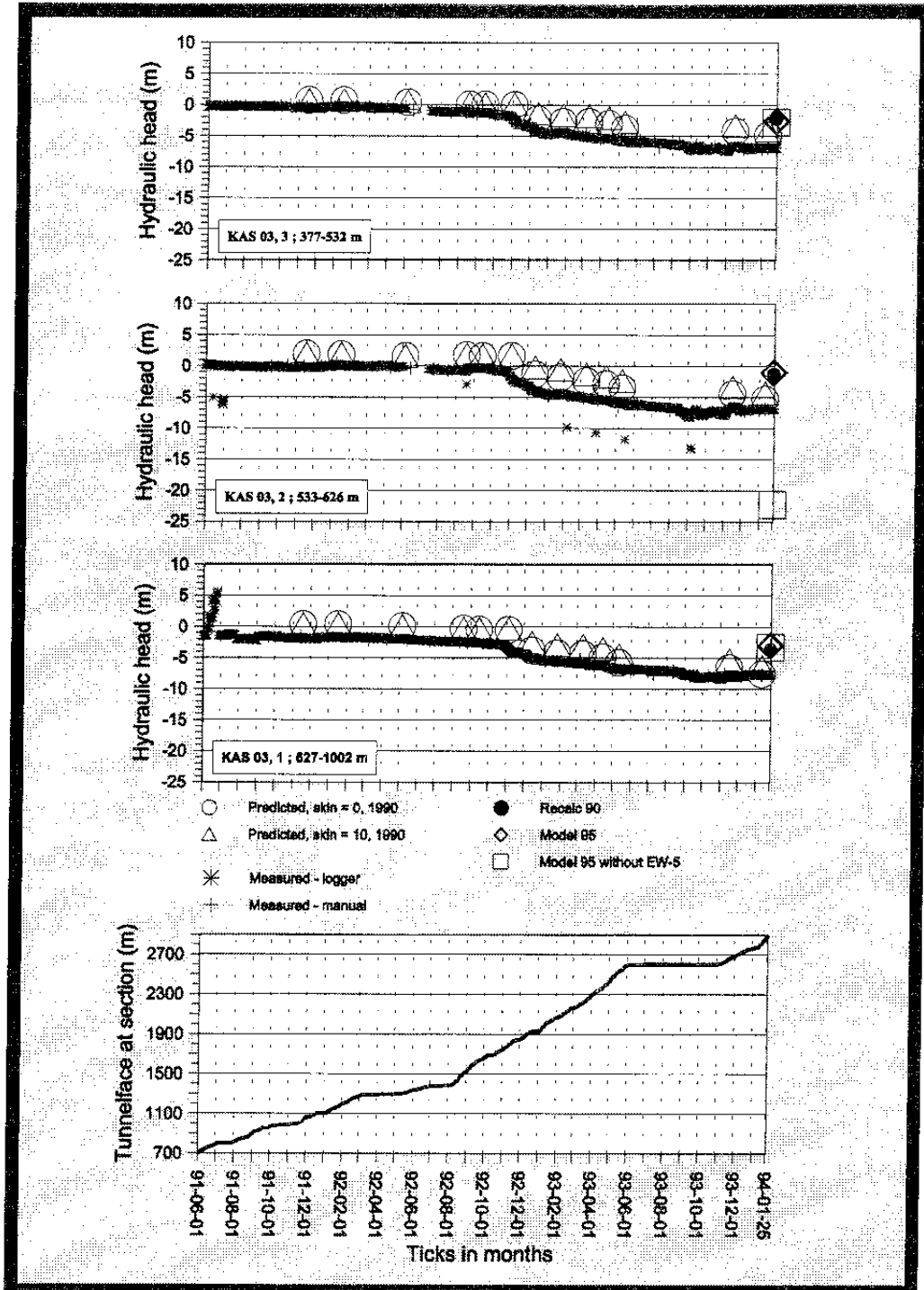


Figure 4-12. Measured and predicted piezometric levels in KAS03, borehole sections 1-3.

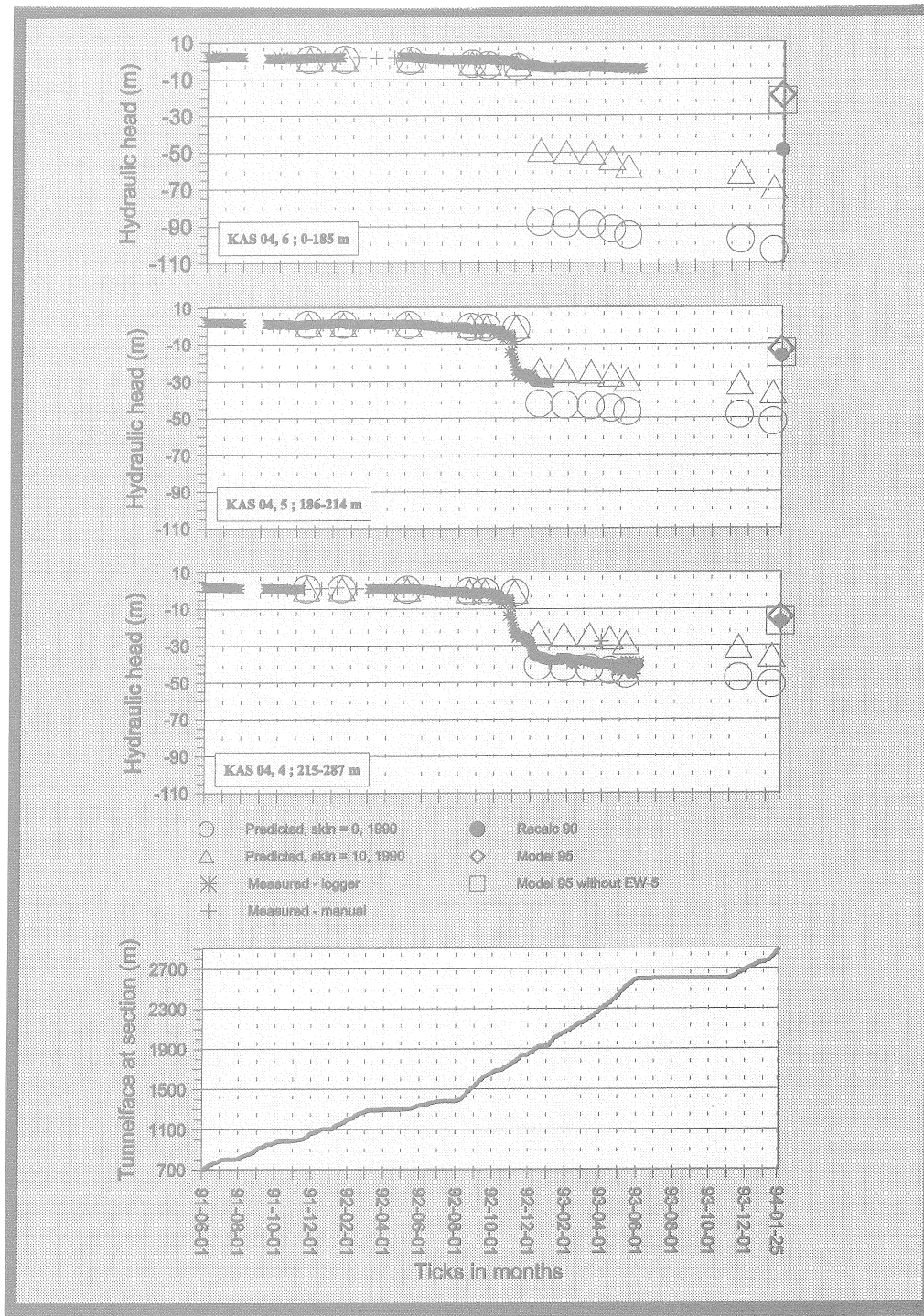


Figure 4-13. Measured and predicted piezometric levels in KAS04, borehole sections 4-6.

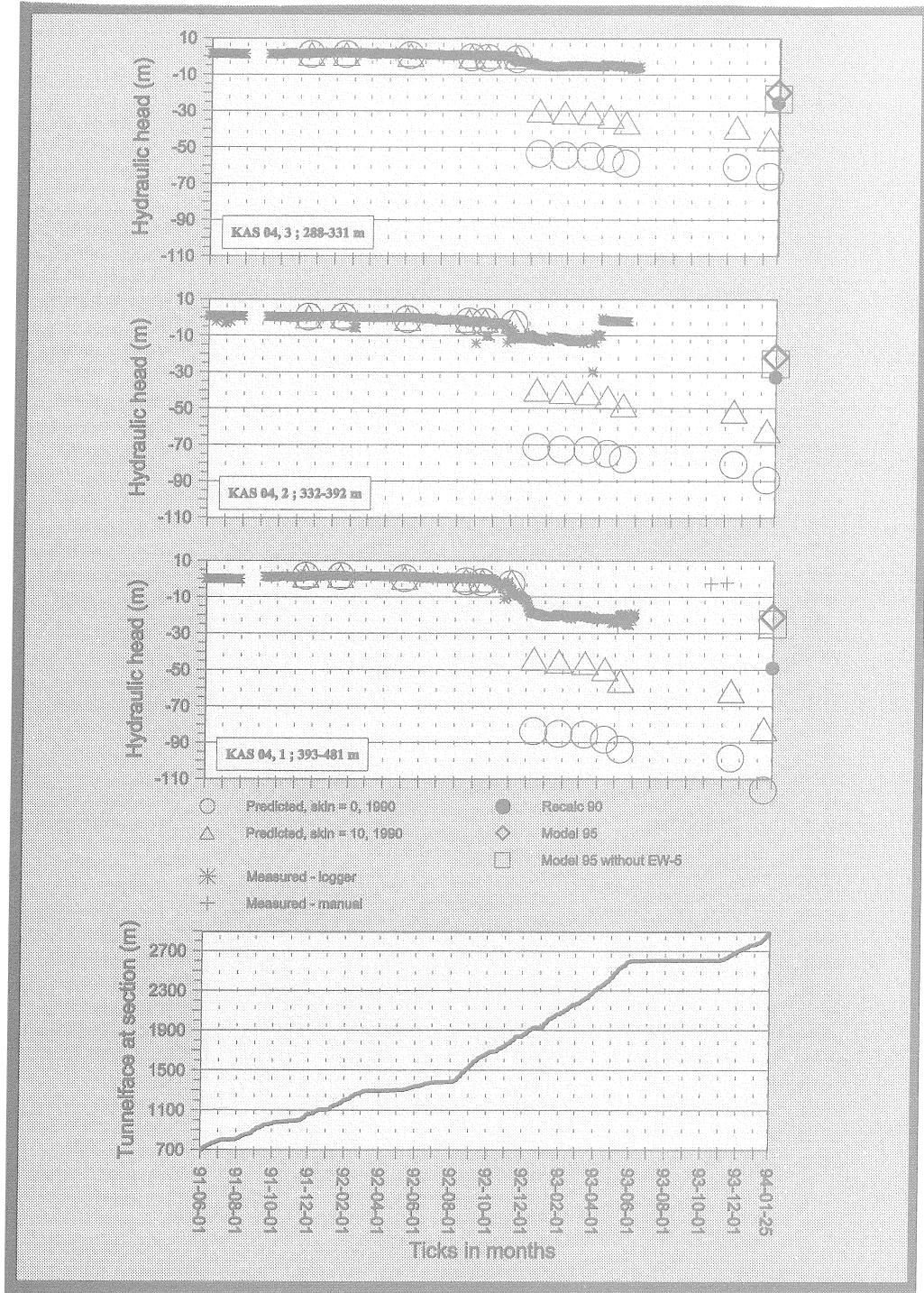


Figure 4-14. Measured and predicted piezometric levels in KAS04, borehole sections 1-3.

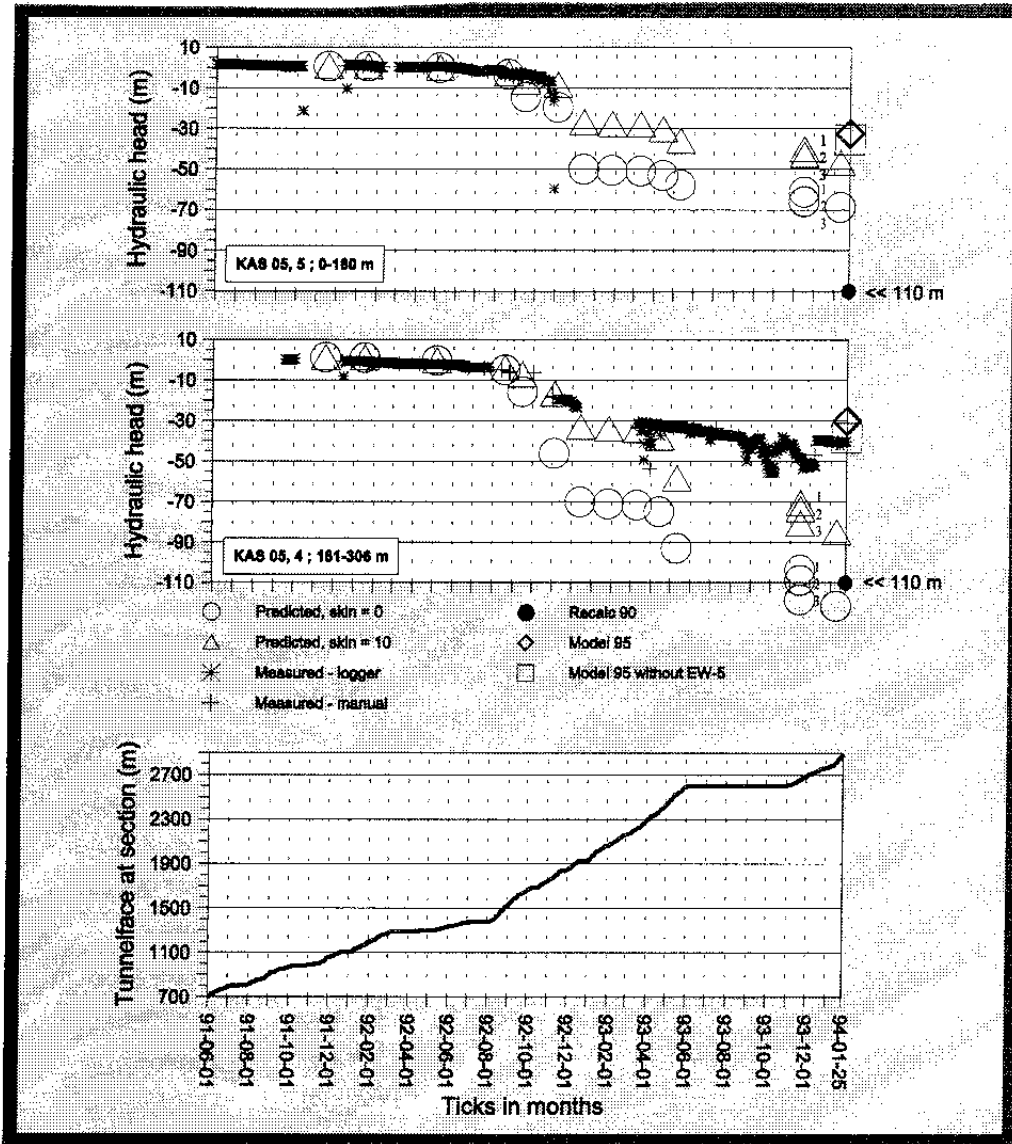


Figure 4-15. Measured and predicted piezometric levels in KAS05, borehole sections 4-6.

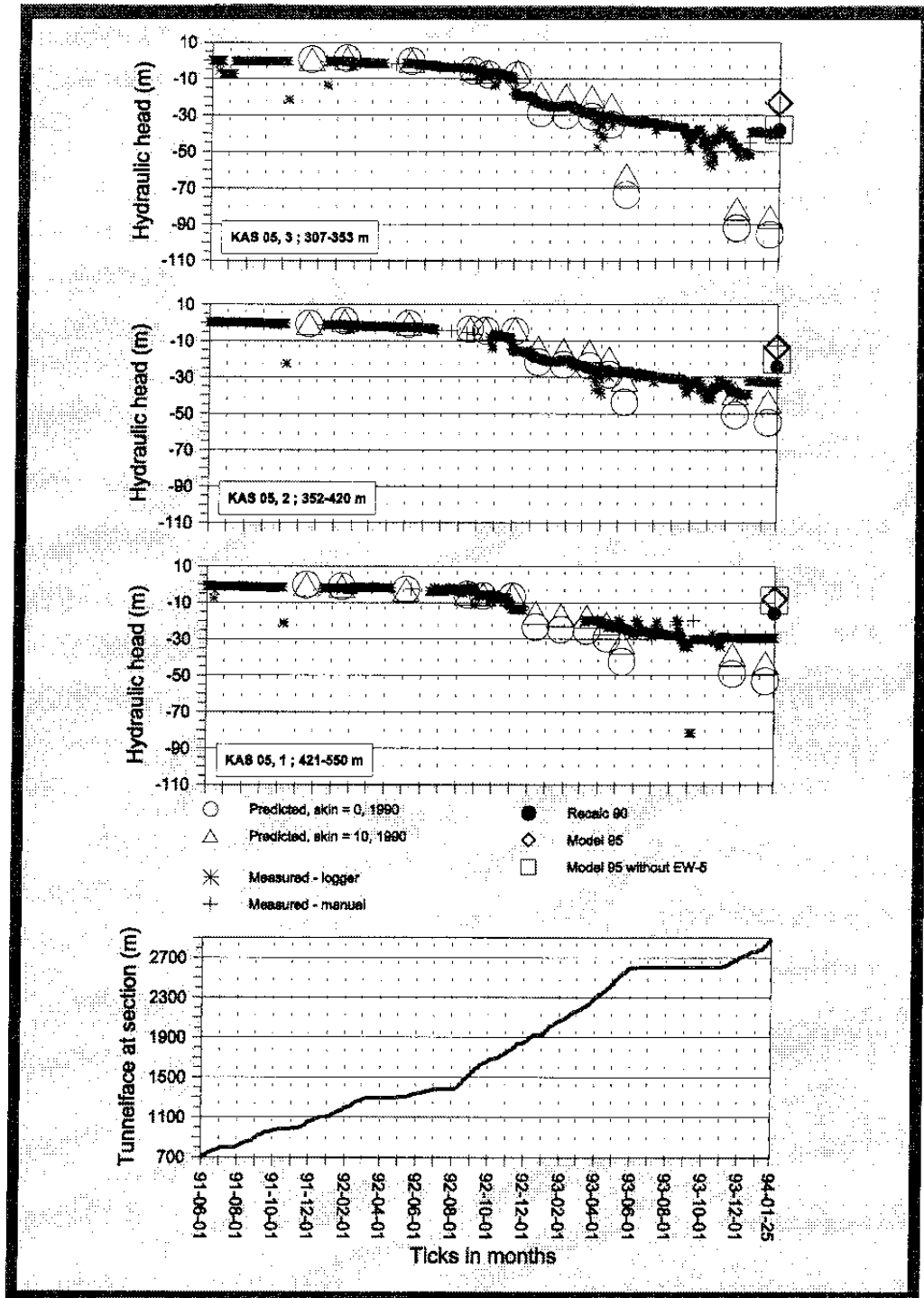


Figure 4-16. Measured and predicted piezometric levels in KAS05, borehole sections 1-3.

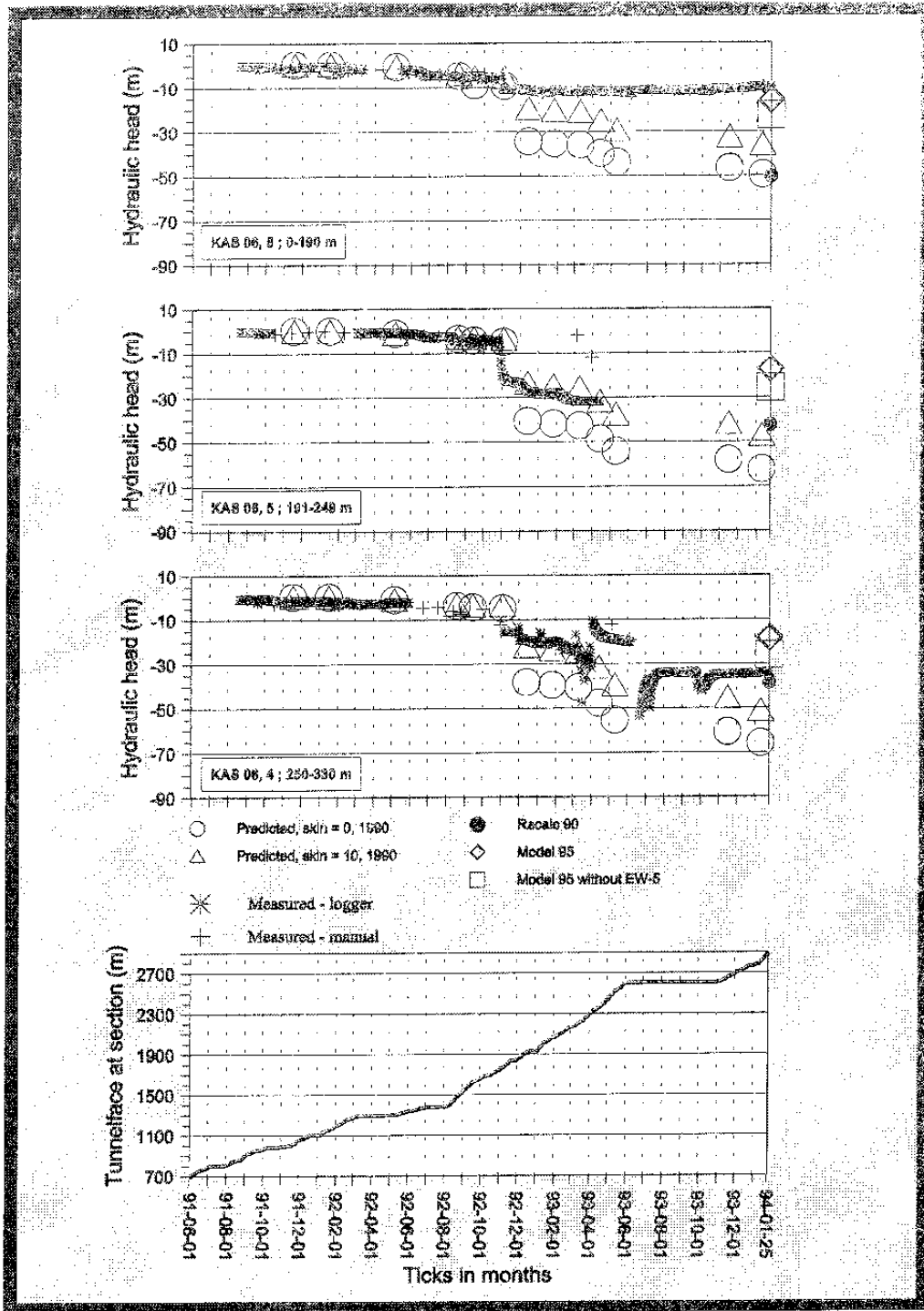


Figure 4-17. Measured and predicted piezometric levels in KAS06, borehole sections 4-6.

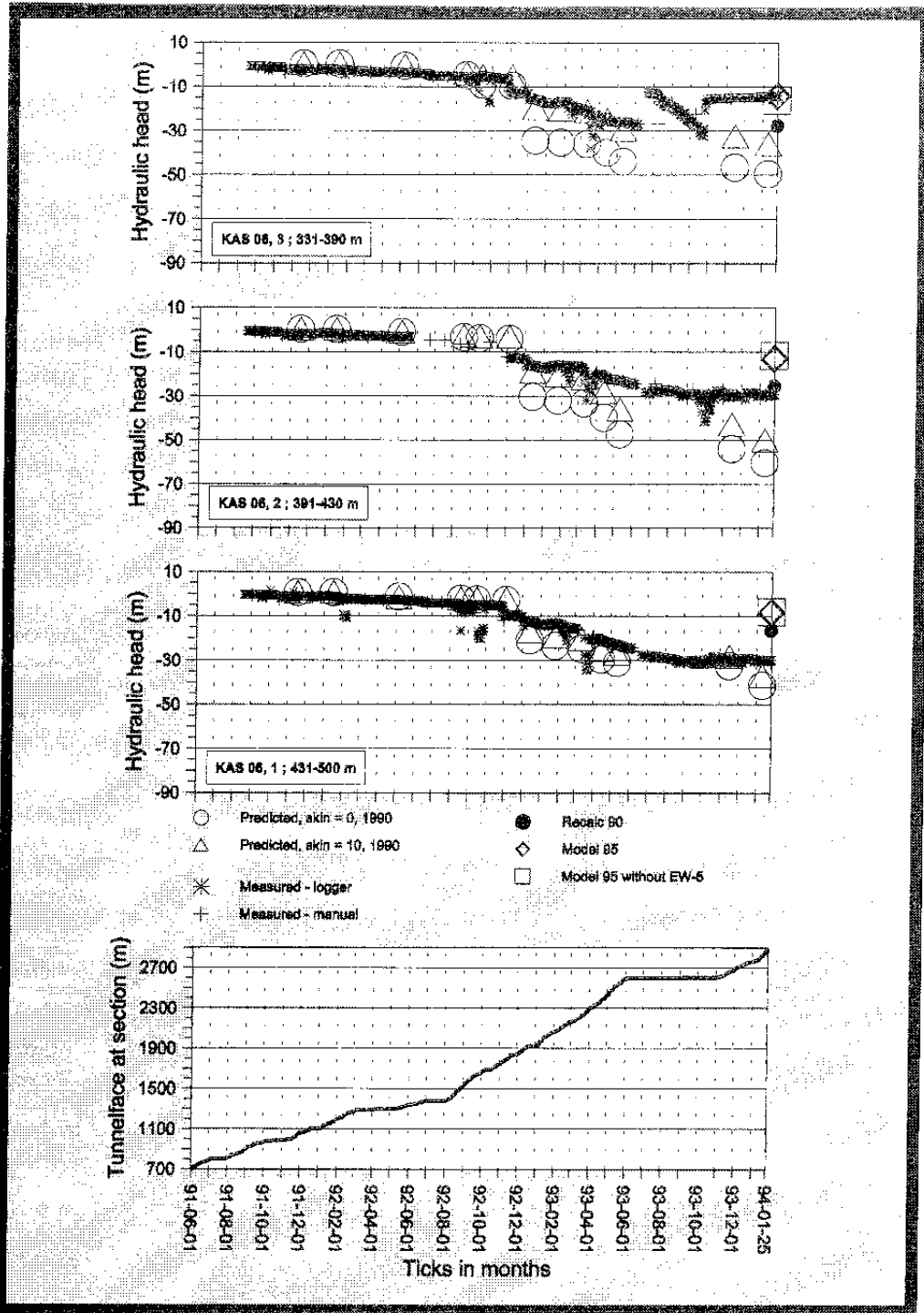


Figure 4-18. Measured and predicted piezometric levels in KAS06, borehole sections 1-3.

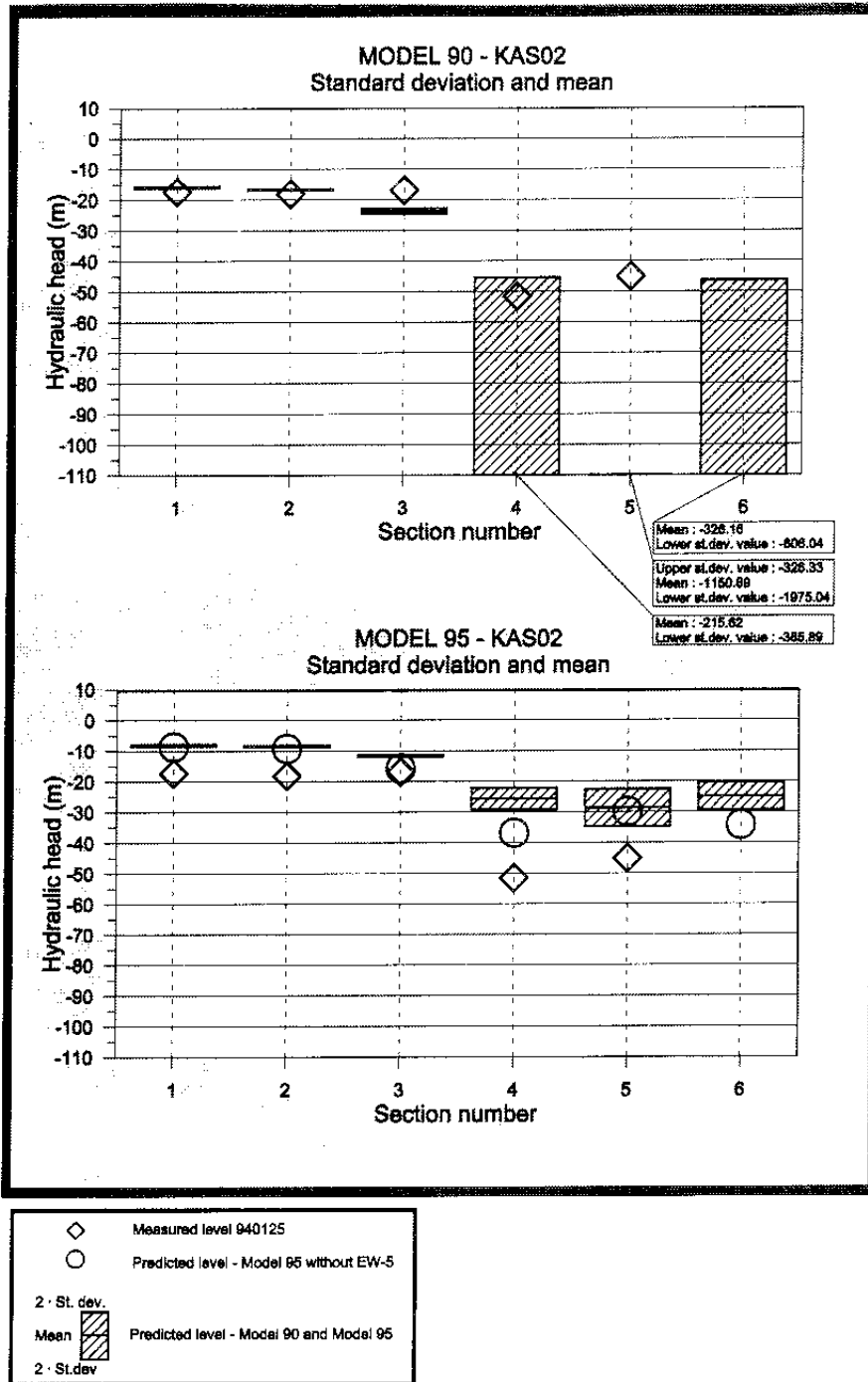


Figure 4-19. Measured and predicted piezometric levels in KAS02. Tunnel face at section 2875 m.

Summary of predictions and outcome

For comparison between different predictions the mean error and accuracy were estimated as below. The results are shown in *Table 4-1*. The mean error and accuracy are less for *Model 95* than for *Recalc 90*. The model was also improved, in terms of decreasing lower values for dh , $dh(abs)$ and Dh , to some extent when the subhorizontal conductor domain EW-5 was excluded.

MEAN ERROR

$$dh = \frac{\sum_{i=1}^n (h_i^m - h_i^c)}{n} \quad (m)$$

$$dh(abs) = \frac{\sum_{i=1}^n |h_i^m - h_i^c|}{n} \quad (m)$$

ACCURACY

$$Dh = \sqrt{\frac{\sum_{i=1}^n (h_i^m - h_i^c - dh)^2}{n - 1}} \quad (m)$$

n: Number of points with measured data used to compare with calculated points.

h: Piezometric level (freshwater head) in metres above sea level (masl).

index m: Measured value.

index c: Calculated value.

Table 4-1. Mean error and accuracy of predictions. SK= skin for tunnel.

Tunnel face position (m)	Model. year	Model	dh	dh	abs(dh)	abs(dh)	Dh	Dh
			SK=0 (m)	SK=10 (m)	SK=0 (m)	SK=10 (m)	SK=0 (m)	SK=10 (m)
1475	1990	Model90	0.34	-0.89	3.44	2.73	10.24	4.85
2265	1990	Model90	6.62	-0.78	13.45	10.64	20.48	16.73
2875	1990	Model90	12.87	5.48	16.84	10.93	22.21	14.22
2875	1995	Recalc90 ¹	19.93		26.13		120.41	
2875	1995	Model95 ² -	9.03		11.02		11.23	
2875	1995	Model95 ³ -	8.04		9.78		10.25	

¹ Measured flow rates into the tunnel used.

² Measured flow rates into the tunnel and updated model of the hydraulic conductor domains used

³ Measured flow rates into the tunnel and updated model of the hydraulic conductor domains used. Hydraulic conductor domain EW-5 excluded.

4.4 SCRUTINY AND EVALUATION

The draw-downs on Äspö are in rough agreement with the predictions (*Model 90*), if the measured inflow rate is taken into consideration. The measured flow rates into the tunnel and the new model of the hydraulic conductor domains indicate that the southern part of Äspö may be somewhat too conductive because the predicted draw-down is less than the outcome. This is also the case for northern Äspö, indicating that there should be somewhat better hydraulic communication between northern and southern Äspö.

There are, however, some differences. The predicted draw-downs are more elliptical for the three uppermost layers. The reason may be that in the prediction no fracture zone intersected the shafts and thus the inflow and draw-down were limited around the shafts. Recalculation with the measured flow rates into the tunnel and including a NW-NNW striking conductive feature close to the shafts improves the predictions. There were several results from investigations during the construction of the Äspö HRL which indicated that there possibly should be a NW-NNW striking conductive feature close to the shaft. The pre-investigations indicated the possibility of a conductive feature in this area but it was not possible to define the strike, dip and extent and was therefore not included in the model.

Another reason for the differences is that the measured inflow in parts of the tunnel where structures NNW-1 and NNW-2 are assumed to intersect the tunnel are very low but in the prediction the inflow was rather large. The differences in inflow from NNW-1 and NNW-2 may also explain the large

differences between the prediction and outcome for the draw-down in KAS04 at least for measurement sections below the uppermost one.

Interference tests indicated good hydraulic communication between some of the borehole sections, mostly explained by a hydraulic conductor domain intersecting the borehole sections. In some cases neither a deterministic hydraulic conductor domain intersected the borehole sections nor was a hydraulic conductor domain added to the model to better reproduce the hydraulic responses, as it was difficult to define the domain in space. There are two good examples. First, some of the interference tests showed good hydraulic communication between the upper part of KAS05 and the upper part of KAS02, which indicated that one or several conductive features exist in the upper part of the bedrock between these two boreholes. Secondly, pumping test LPT2 in KAS06 showed that there were good hydraulic communication between the two uppermost borehole sections in KAS07 and KAS06 that could not be reproduced by the groundwater flow model /Gustafson and Ström, 1995/. On a heterogenous site like Äspö it is probably necessary to accept that there will be a number of features with fairly high transmissivities that will cause good local hydraulic communication between borehole sections that are not easily reproduced.

Conclusions

Predictions of drawdown

The recalculations of the drawdowns with the measured flow rate into the tunnel indicate that the drawdowns could approximately be predicted with *Model 90*. However, close to the shaft and north of the spiral the differences were rather large, mainly due to the absence, in the model, of a hydraulic conductor domain intersecting the shaft. In the *Model 90* the transmissivities of 5 conductive domains were slightly modified based on calibration of the model /Wikberg et al, 1991/. In the *Model 95* these transmissivities were used, and according to *Table 4-1* the overall conductivity of the model seems to be a bit too high as the measured drawdown is greater than the predicted.

The hydraulic conductor domains control the drawdowns to a large extent in the modelling approach used. If the properties of the hydraulic conductor domains are changed (by calibration) the average error of the drawdown can be reduced. There will, however, remain greater or lesser individual errors. To obtain better agreement between the model and the observations there should probably be some correlation of the hydraulic conductivity within the hydraulic rock mass domains. The 'correlation length' in the simulations was about 20 m, as that was the cell size and no correlation model was used when the hydraulic conductivities was assigned to the model. There are very probably a number of conductive features larger than the cell size that are not modelled deterministically. If a reasonably good model for the correlation within the model could be defined for the spatial assignment of the hydraulic conductivity, the errors within the hydraulic rock mass domains would probably be reduced to some extent.

Monitoring

The measurement intensity of the monitoring of the water pressures in space and time is judged to be mainly sufficient. However, it would have been preferable to have had somewhat more reliable measurements of the natural conditions. To some extent the natural conditions were disturbed by performance of the investigations, mainly the hydraulic tests. It also turned out that the equipment for monitoring the pressure in the boreholes was not designed for the large drawdowns close to the tunnel spiral. At the end of the excavation period several of the borehole sections close to the tunnel spiral stopped functioning. It is, however, judged that these two problems did not have a major detrimental impact on the possibilities of evaluating the hydraulic properties and testing the groundwater flow models.

Effects of earth-tide, precipitation, barometric pressure and sea level changes on the water pressures can be seen with the measurement intensity chosen (surface holes connected to the HMS (Hydro Monitoring System): measurements every 8th minute and the value is not stored unless the change is more than 0.2 m from the latest stored value. However, a value is always stored every second hour). See *Chapter 1* for an example.

The undisturbed pressure distribution along the deep cored boreholes were estimated from the transient injection tests. These absolute pressure estimates were considered uncertain but were useful for the interpretation of the chemical sampling. However, more reliable measurements or the absolute pressure during natural conditions should be made in the future.

During interference tests individual sampling rates were chosen for those borehole sections that were judged to show responses to the test. The measurement in the pumped or flowing (in the tunnel) borehole was generally made with an interval of one or a few seconds the first minutes and then with a stepwise increasing time step. The initial time step for observation sections was generally 5 minutes or less, depending on the distance to the pumped or flowing borehole. If about 20 measurements were performed for each log-cycle it is judged that it gives good possibilities for evaluation of the test.

5 SUBJECT: FLUX DISTRIBUTION - SITE SCALE

5.1 SCOPE AND CONCEPTS

The geometrical concepts for the groundwater flow model consists of:

- hydraulic conductor domains and
- hydraulic rock mass domains.

When the tunnel is introduced into the groundwater flow model the tunnel geometry and the tunnel cross-section define the internal boundaries. A concept for applying atmospheric pressure in the tunnel and a hydraulic resistance (e.g. due to grouting) around the tunnel has to be made, (see *Chapter 3* for more details). In the groundwater flow model the groundwater flux is calculated for all cells defining the domains.

One purpose of the groundwater flow modelling was to test the ability to make predictions of the groundwater fluxes within the rock mass surrounding the laboratory based on the predicted geohydrological model. As the borehole itself is much more conductive than the rock mass, a model was also made to describe the relationship between the flux in the rock mass and in the borehole, based on a porous media assumption /*Liedholm, 1991b*/. This relationship was used to transform the fluxes in the numerical groundwater model to flows in the borehole sections. The borehole sections used were the ones that were used for dilution measurements and the assumption was that the transformed fluxes would better correspond to the actual measured flows, based on the dilution method, in the borehole sections. The transformation concept is outlined below.

It is well known that a borehole will disturb the natural flow close to the borehole and that this has implications for the interpretation of dilution tests. The corrections applied usually assume that the direction of the natural groundwater flow is perpendicular to the borehole centre line /*Halevy et al, 1967, Drost et al, 1968, Landberg J, 1982*/. These corrections are based on the borehole radius (r_w), the hydraulic conductivity just outside the borehole (K_1) within radius r_w to r_1 and the hydraulic conductivity of the formation (K) (see *Figure 5-1*). Solutions are also available for two different hydraulic conductivities (K_1 and K_2) around the borehole (within $r_w - r_1$ and $r_1 - r_2$). The flow rate through the borehole (Q_{bh}) is related to the specific discharge (or filtration velocity or Darcy velocity, q) in the rock mass by a correction coefficient (α) and the cross-sectional area of the borehole section open for dilution ($A_{bh} = 2 \cdot r_w \cdot L_{bh}$):

$$Q_{bh} = \alpha \cdot A_{bh} \cdot q \quad (5-1)$$

If K_1 is small compared to K α becomes small. If K_1 is large compared to K α becomes about 4 and if $K_1 = K$ α will become 2.

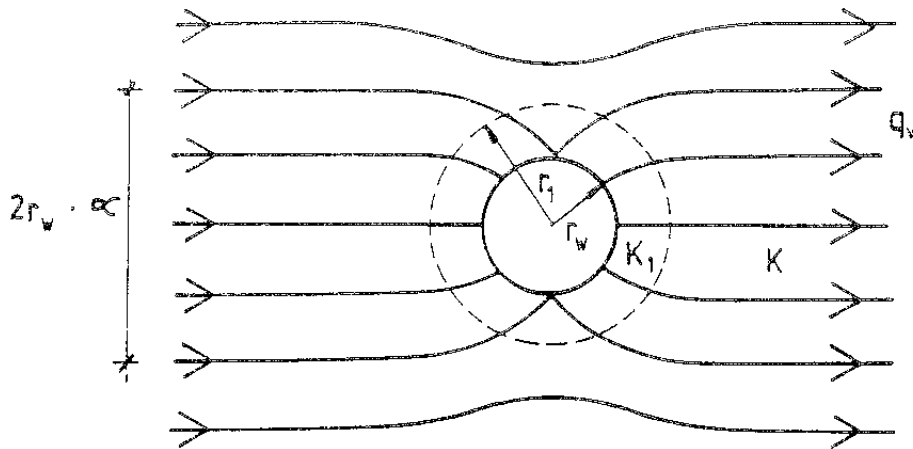


Figure 5-1. Flow lines around a borehole with the flow perpendicular to the borehole ($\beta = 0^\circ$) /In Liedholm, 1991b/.

If the undisturbed flow direction is not perpendicular to the direction of the borehole the calculation of Q_{bh} will not be correct using the relations found in *Halevy et al /1967/*, *Drost et al /1968/*. An approximate relationship for α , depending on the angle between the undisturbed flow and the borehole length axis (β), borehole radius (r_w) and section length in the borehole open to flow ($2 \cdot L = L_{bh}$, see *Figure 5-2*) was made in *Liedholm /1991b/*.

The flow into and along the borehole was solved by assuming that the hydraulic conductivity of the borehole itself is infinite compared with that of the rock mass, which means that the potential difference along the borehole will be zero, and that outside the borehole there was a porous medium. The undisturbed potential difference (h) as function of position (d) along the borehole centre line is described by *Equation 5-2*.

$$h(d) = i \cdot d \cdot \cos(\beta) \quad (5-2)$$

By applying point sources with different strengths along the borehole it is possible to calculate the flow distribution along the borehole that gives a potential field as in *Equation 5-2* but with the opposite sign, thus giving a zero potential difference along the borehole. It was solved approximately by assuming that the flow distribution could be approximated by a polynomial. Examples of the dimensionless flow distribution into or out of the borehole (q_D) as function of the position along the borehole axis (λ_D , dimensionless) with and borehole radius (r_D , dimensionless) is shown in *Figure 5-3*. q_D is described by a polynomial with coefficients a_{Dj} (see *Equation 5-6*). The function $h_D(d_D)$ is shown for the different r_D values in *Figure 5-4*. In *Figure 5-5* an example of $h(d)$ and $q(\lambda)$ for $r_w = 0.25$ and 0.0025 m, $L = 25$ m, $\beta = 0$, $i = 0.1$ and $K = 10^{-7}$ m/s, is shown.

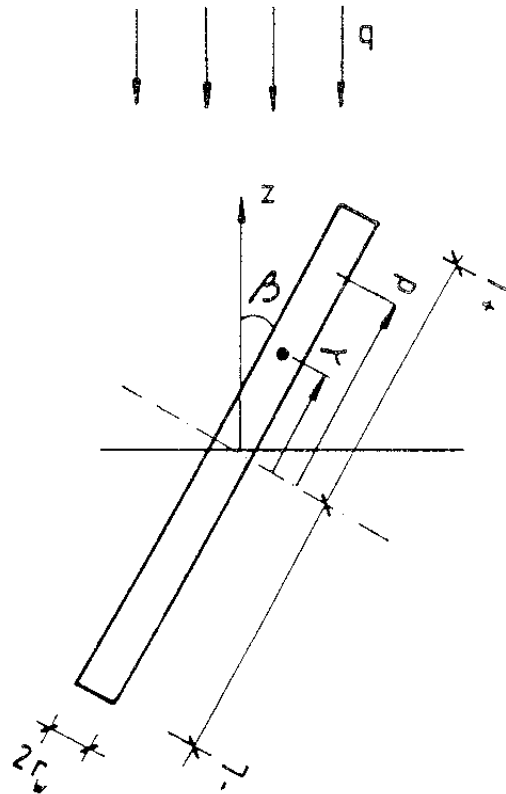


Figure 5-2. Definition of variables. β = the angle between the undisturbed flow (q) and the borehole length axis, r_w = borehole radius, $2 \cdot L$ = section length in the borehole open for flow along the borehole, λ = position for point source, d = position for calculated potential [In Liedholm, 1991b].

$$\lambda_D = \frac{\lambda}{L} \quad d\lambda_D = \frac{d\lambda}{L} \quad (5-3)$$

$$d_D = \frac{d}{L} \quad (5-4)$$

$$r_D = \frac{r_w}{L} \quad (5-5)$$

$$q_D(\lambda_D) = \sum_{j=1}^N (a_{Dj} \lambda_D^{j^2-1}) = \frac{q(\lambda)}{4\pi K \cdot i(\cos\beta) \cdot L} \quad (5-6)$$

The polynomial estimated was:

$$q_D(\lambda_D) = a_{D1} \cdot \lambda_D + a_{D2} \lambda_D^3 + a_{D3} \lambda_D^5 \quad (5-7)$$

Table 5-1 shows the coefficients a_{D_i} , for some values of r_D .

Table 5-1. Coefficients a_{D_i} in Equation 5-7 /in Liedholm, 1991b/.

r_D	a_{D1}	a_{D2}	a_{D3}
$1 \cdot 10^{-1}$	0.228534	-0.560533	1.25262
$6 \cdot 10^{-2}$	0.181855	-0.274389	0.716291
$3 \cdot 10^{-2}$	0.145338	-0.125069	0.388355
$1 \cdot 10^{-2}$	0.111374	-0.043831	0.172195
$6 \cdot 10^{-3}$	0.100513	-0.022178	0.107604
$3 \cdot 10^{-3}$	0.088650	-0.015653	0.080212
$1 \cdot 10^{-3}$	0.074533	-0.007195	0.046461
$6 \cdot 10^{-4}$	0.069356	-0.005262	0.037568
$3 \cdot 10^{-4}$	0.055699	-0.002088	0.020510

The diameter of the cored holes at Äspö is 0.058 m and the packed off sections are generally in the range 5-100 m and in some cases up to 400 m. Thus, r_D is generally in the range 10^{-2} - $5 \cdot 10^{-4}$ and in some cases down to $1 \cdot 10^{-4}$.

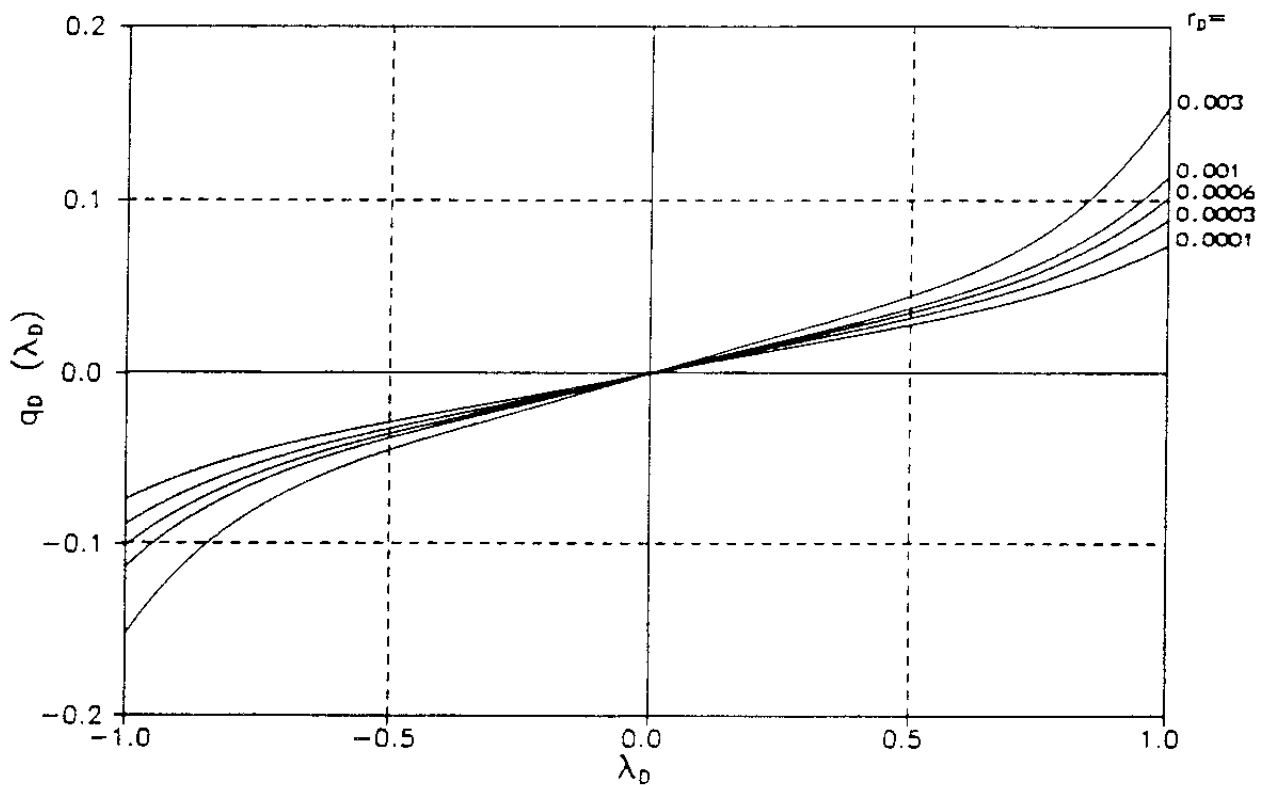
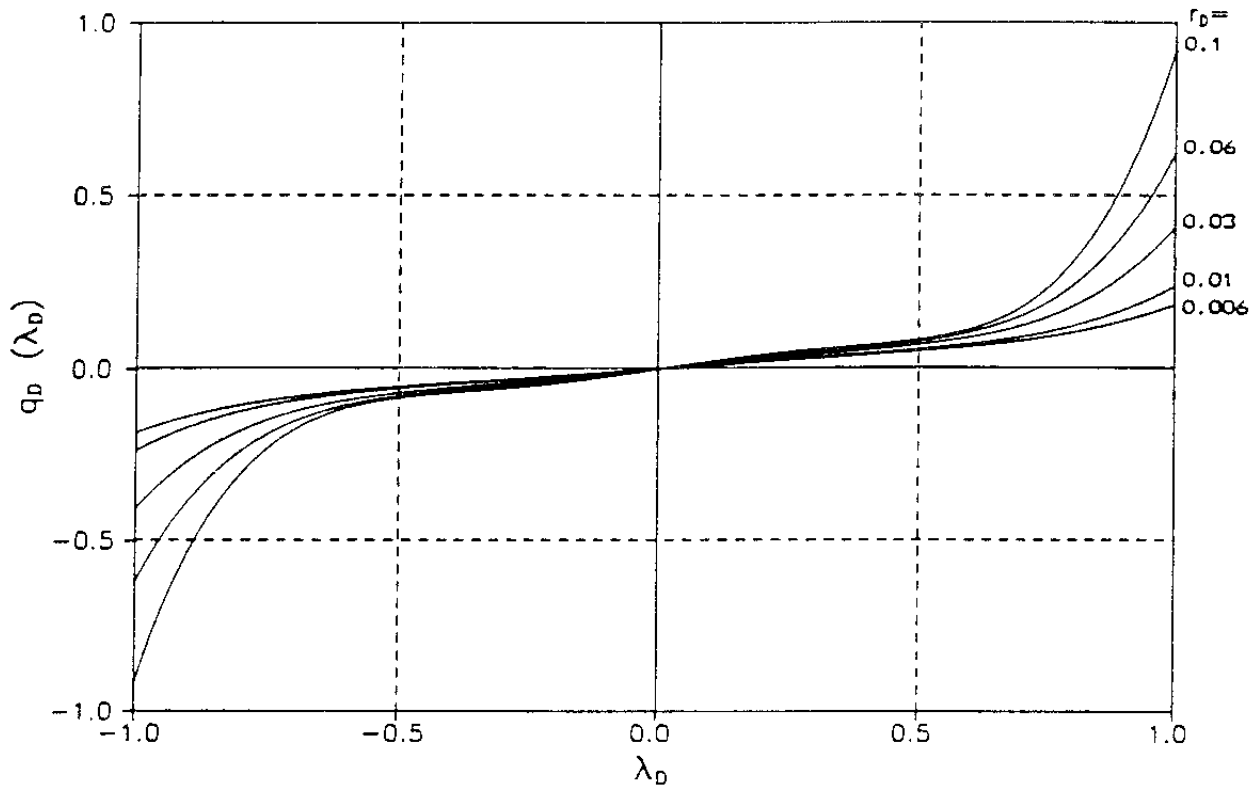


Figure 5-3. Dimensionless flow distribution into or out of the borehole (q_D) as a function of the position along the borehole axis (λ_D , dimensionless) and borehole radius (r_D , dimensionless), /in Liedholm, 1991b/.

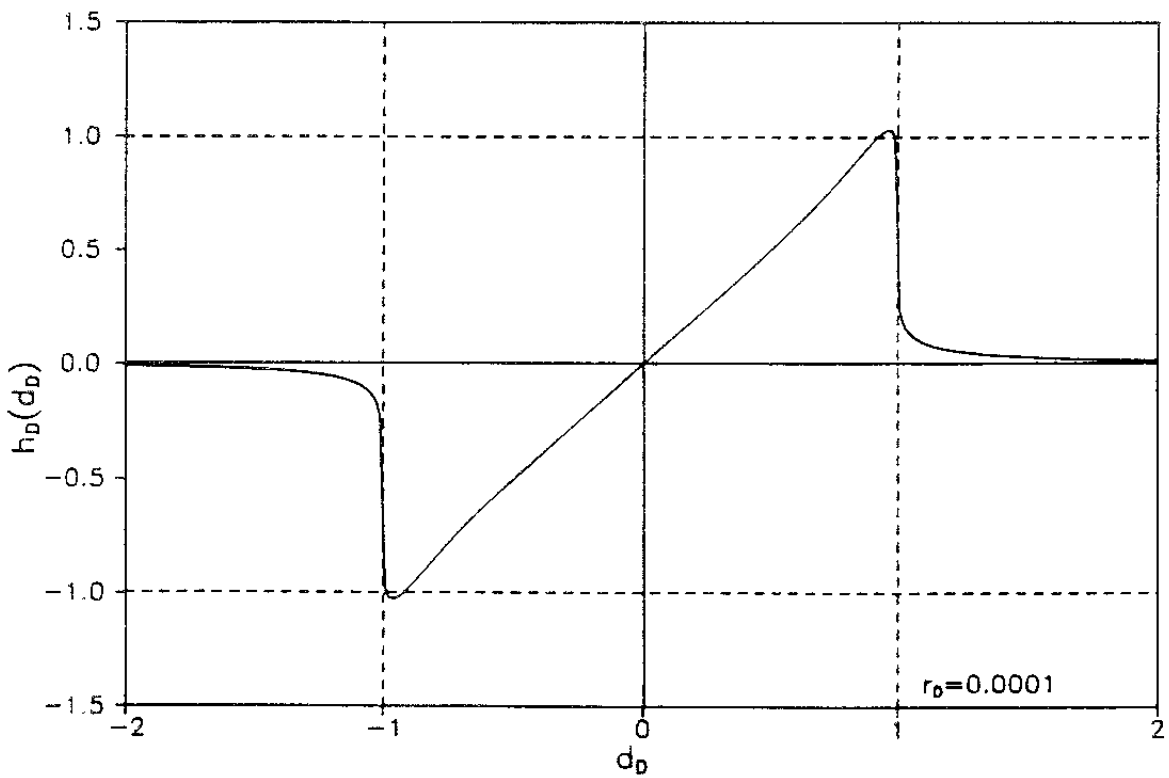
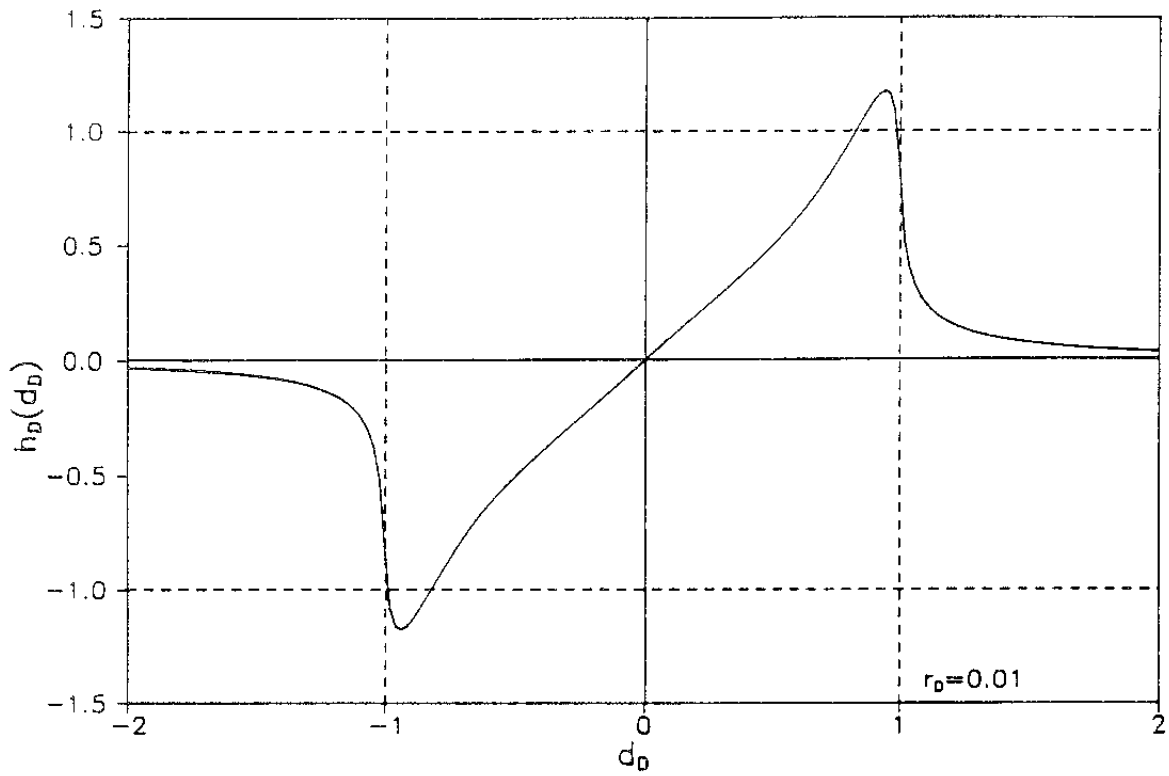


Figure 5-4. $h_D(d_D)$ for some r_D values, $\beta = 0$, /in Liedholm, 1991b/.

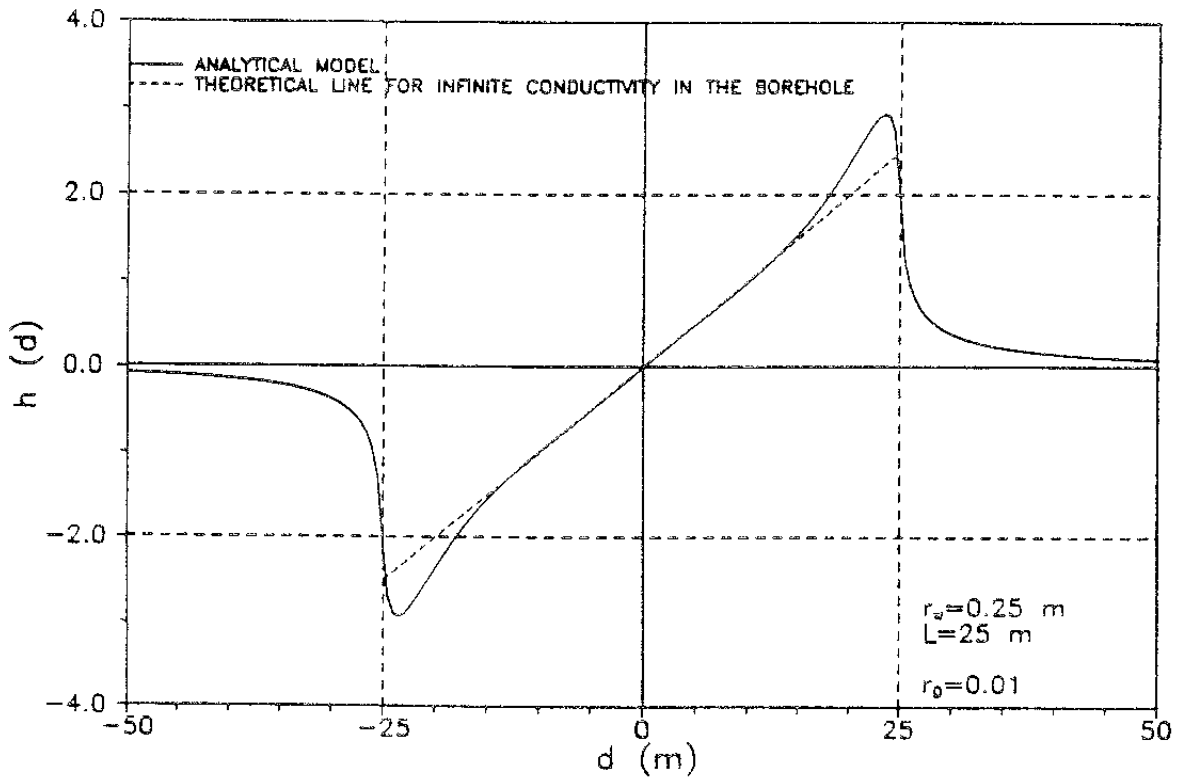
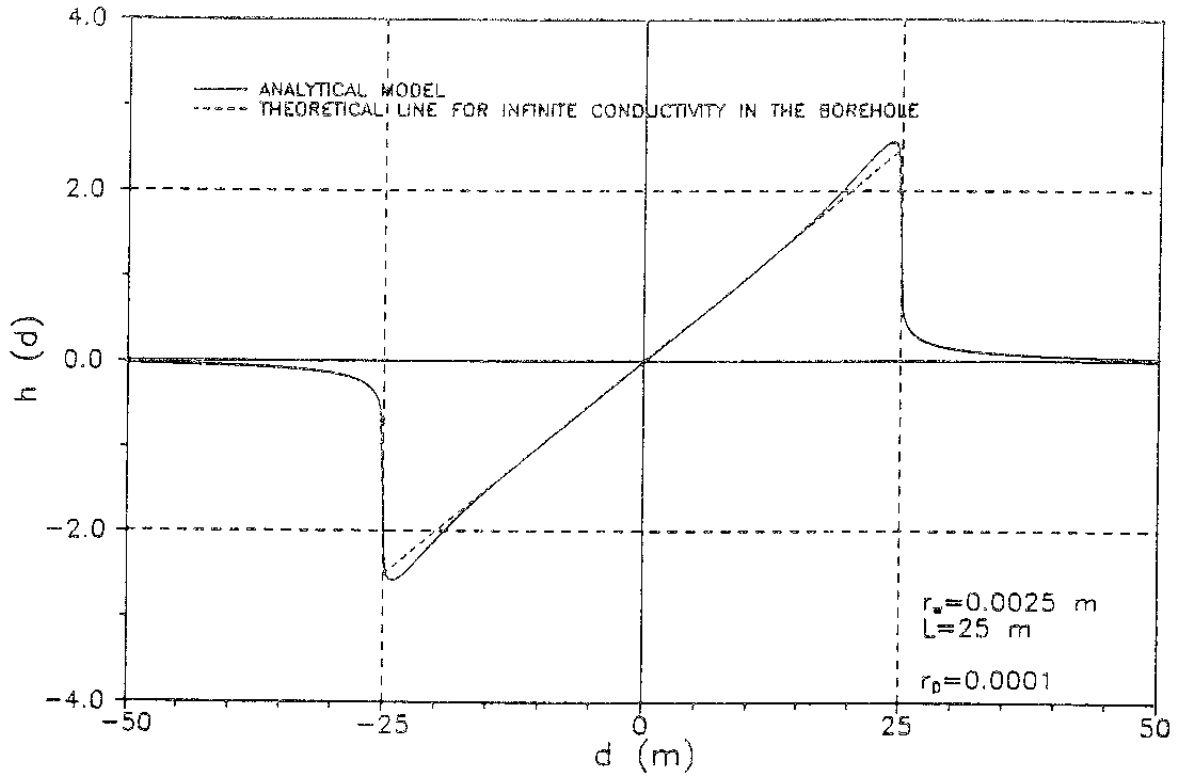


Figure 5-5. $h(\lambda)$ for $r_w = 0.25$ and 0.025 m , $L = 25 \text{ m}$, $\beta = 0$, $i = 0.1$ and $K = 10^7 \text{ m/s}$, /in Liedholm, 1991b/.

By integrating the flow into the borehole from $\lambda_D = 0$ to 1.0 the maximum flow rate along the borehole, passing the point where $\lambda_D = 0$, can be calculated. This is the total flow that will dilute a tracer well mixed in the water volume in the borehole. However, when β increases the flow into the borehole will decrease more than it should, due to the formulation of the boundary conditions on the borehole wall (see *Liedholm /1991b/*). As an approximation it was therefore suggested to total the flow calculated as above with the flow calculated according to *Halevy et al /1967/* or *Drost et al /1968/*:

$$Q_{bh}(\lambda=0) = q \cdot L_{bh}^2 \cdot (2r_D \cdot \alpha \cdot \sin\beta + \pi \cdot \cos\beta \cdot \delta(r_D)) \quad (5-8)$$

$$\delta(r_D) = \left(\frac{a_{D1}}{2} + \frac{a_{D2}}{4} + \frac{a_{D3}}{6} \right) \quad (5-9)$$

In *Figure 5-6* $\delta(r_D)$ is shown.

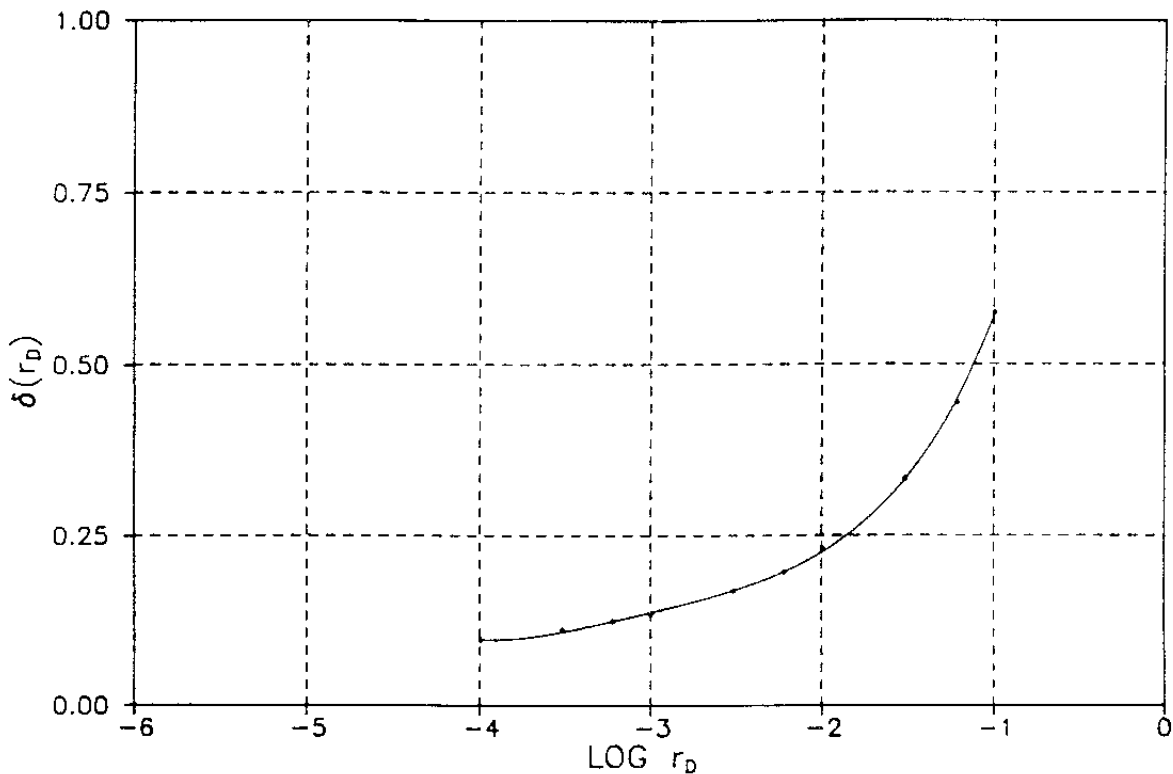


Figure 5-6. The function $\delta(r_D)$, /in *Liedholm, 1991b/*.

Table 5-2. The function $\delta(r_D)$ tabulated, /in Liedholm, 1991b/.

r_D	$\delta(r_D)$
$1 \cdot 10^{-1}$	0.575
$6 \cdot 10^{-2}$	0.445
$3 \cdot 10^{-2}$	0.333
$1 \cdot 10^{-2}$	0.231
$6 \cdot 10^{-3}$	0.197
$3 \cdot 10^{-3}$	0.169
$1 \cdot 10^{-3}$	0.136
$6 \cdot 10^{-4}$	0.124
$3 \cdot 10^{-4}$	0.111
$1 \cdot 10^{-4}$	0.0966

The curve in *Figure 5-6* is at least square-fit of a polynom and the polynom can be expressed as *Equation 5-10*. *Equation 5-8* was used for calculating the dilution rates from the filtration velocities.

$$\delta(r_D) = 1.750 + 1.878 \cdot (\log r_D) + 0.8728 \cdot (\log r_D)^2 + 0.1879 \cdot \log r_D)^3 + 0.01531 \cdot (\log r_D)^4 \quad (5-10)$$

5.2 METHODOLOGY FOR TESTS OF CONCEPTS AND MODELS

5.2.1 Prediction methodology

The prediction was made in two steps. First a groundwater flow model was used to make the predictions of the groundwater fluxes (specific discharge or filtration velocity (see *Rhén et al /1997/*)) in the rock mass (see *Section 3.2.1* for an overview of the model). Two cases were modelled, with a skin factor for the tunnel that was 0 or 10. The predictions were made for positions in the model for the borehole sections where dilution measurements could be performed.

The second step was to transform the calculated fluxes in the rock mass near a borehole section into a flow rate in the borehole section according to *Section 5-1* and *Liedholm /1991b, (TN 30)/*.

A summary of the calibrated model was presented in *Wikberg et al /1991/*. The detailed predictions of the filtration velocities and the transformed flow rates were presented in *Rhén et al /1991a/*. It should be observed that the tunnel position in the predictions after tunnel section 2900 m deviates from the actual tunnel position (see *Chapter 1* in the introduction to the report). The comparison between predictions and outcome naturally become more uncertain after the tunnel face passed tunnel section 2900 m.

5.2.2 Methodology for determining outcome

Dilution measurements were made in some of the cored hole sections (see *Figures 4-2* and *5-7*). The measurements were made before the start of tunnel excavation and were repeated for some of the borehole sections during the construction phase. The dilution measurements were not used for calibration of the numerical groundwater flow model. The dilution measurement technique is described in *Almén and Zellman /1991/* and *Almén et al /1994/*. The results are summarized in *Ittner and Gustafsson /1995/* and reported in detail in *Ittner et al /1991/*, *Ittner /1992, 1994/*, *Andersson et al /1992/* and *Stanfors et al /1992 (PR 25-92-18C)/*. The values in this text referred to as 'measured' are the ones evaluated from a dilution curve. The concentration of a tracer (C) circulating down to, through and up from the measurement section to the surface is measured as a function of time (t). It is assumed that the dilution only takes place in the measurement section and that the circulation is sufficient to achieve homogenous distribution of the tracer in the measurement section. The calculated flow rate is proportional to the slope of the natural logarithm of C/C_0 as a function of t, where C_0 is a reference concentration. The flow through the borehole (Q_{bh}) with the total water volume in the section equal to V will be coupled to C/C_0 and t according to the equation below */Halevy et al /1967/*, *Drost et al /1968/*:

$$Q_{bh} = (V/t) \cdot \ln(C/C_0) \quad (5-11)$$

5.3 COMPARISON OF PREDICTED AND MEASURED ENTITIES

The prediction and outcome are shown in *Figures 5-8* to *5-19*. A few of the measurements shown in the figures are plotted as if they were measured on 1 January 1990. They were actually measured in September 1989.

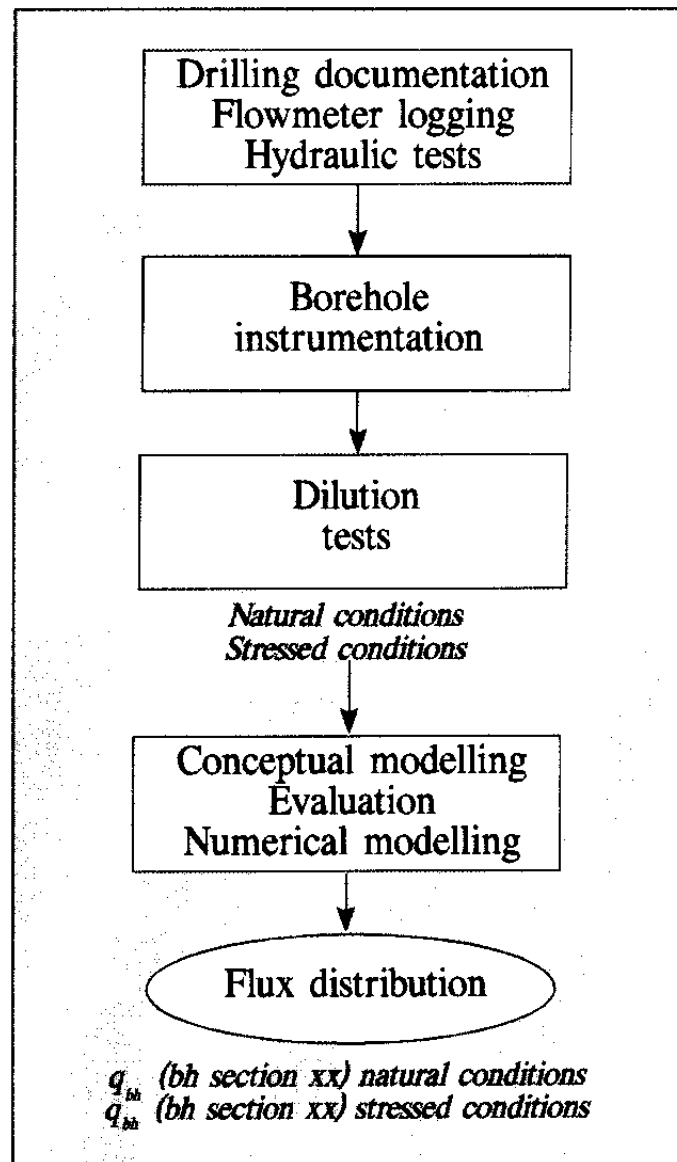


Figure 5-7. Flux distribution in the rock mass. The dilution test gives the flow rate through the borehole section. /After Almén et al, 1994/.

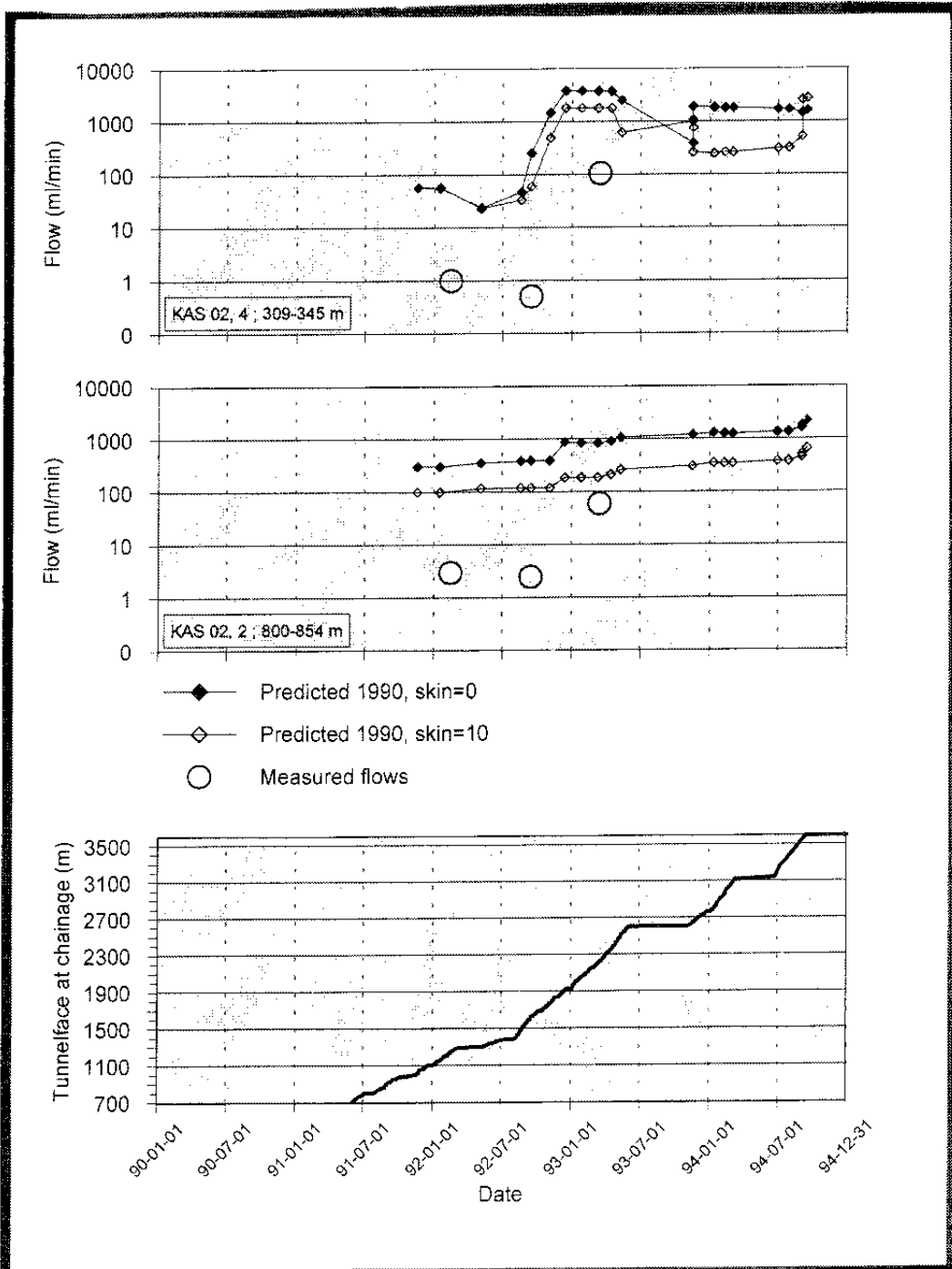


Figure 5-8. Measured and predicted flow through the borehole sections given in the figure above.

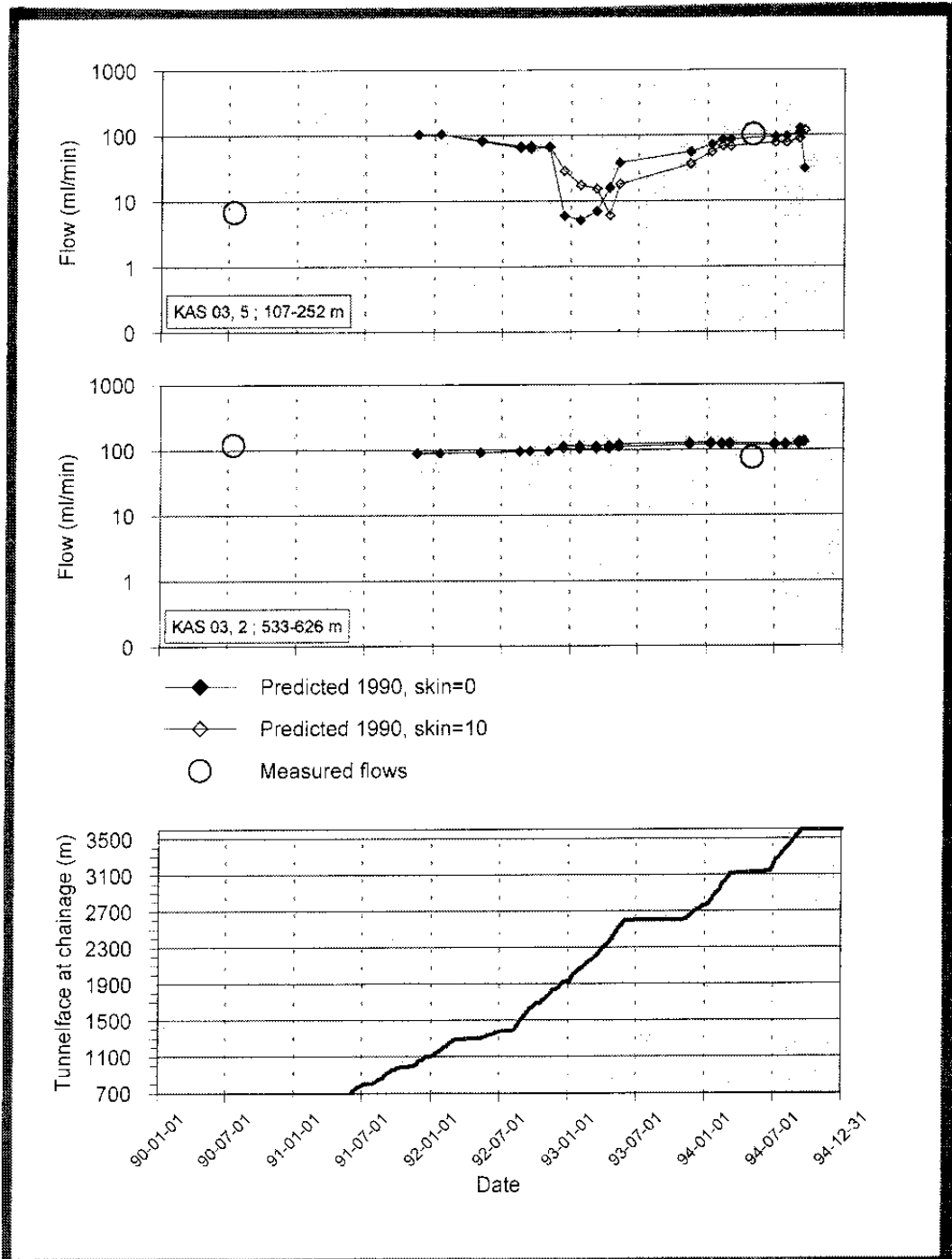


Figure 5-9. Measured and predicted flow through the borehole sections given in the figure above.

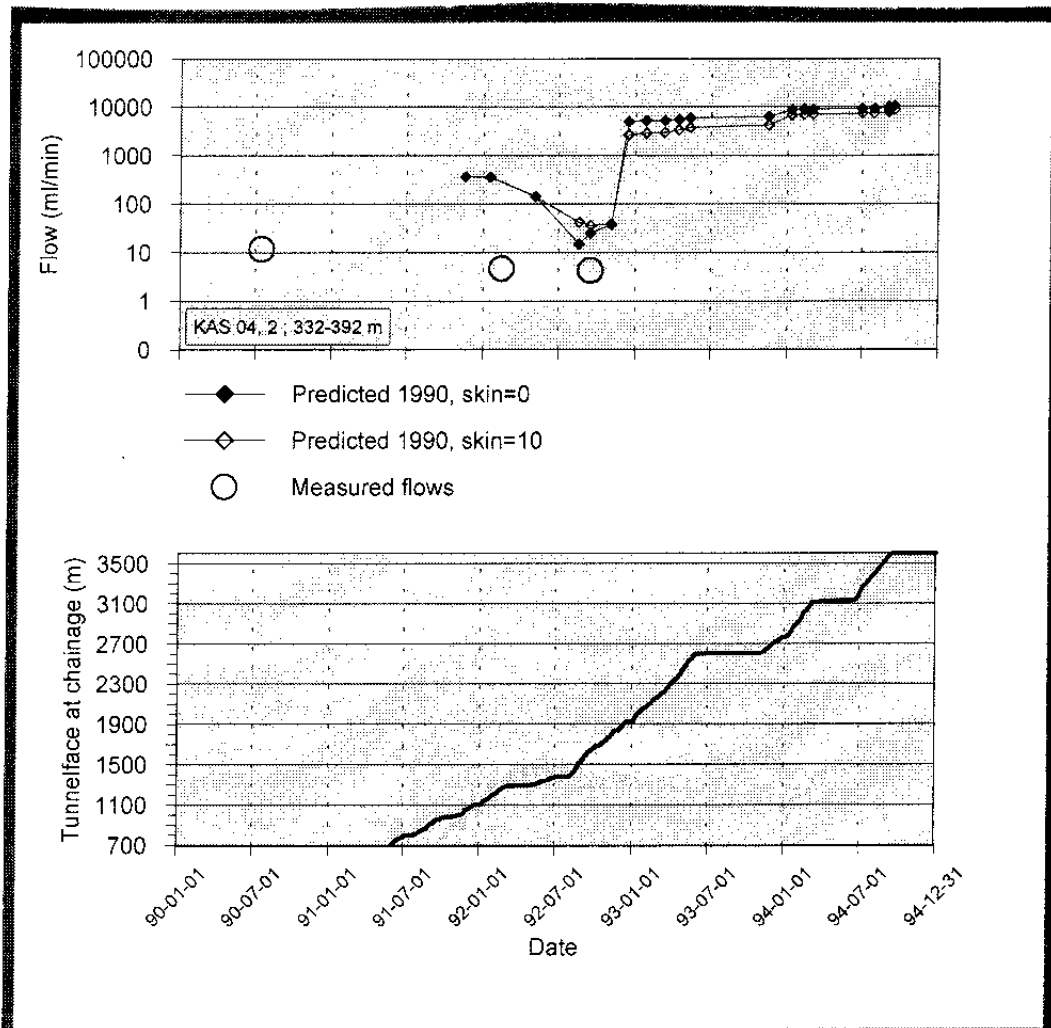


Figure 5-10. Measured and predicted flow through the borehole sections given in the figure above.

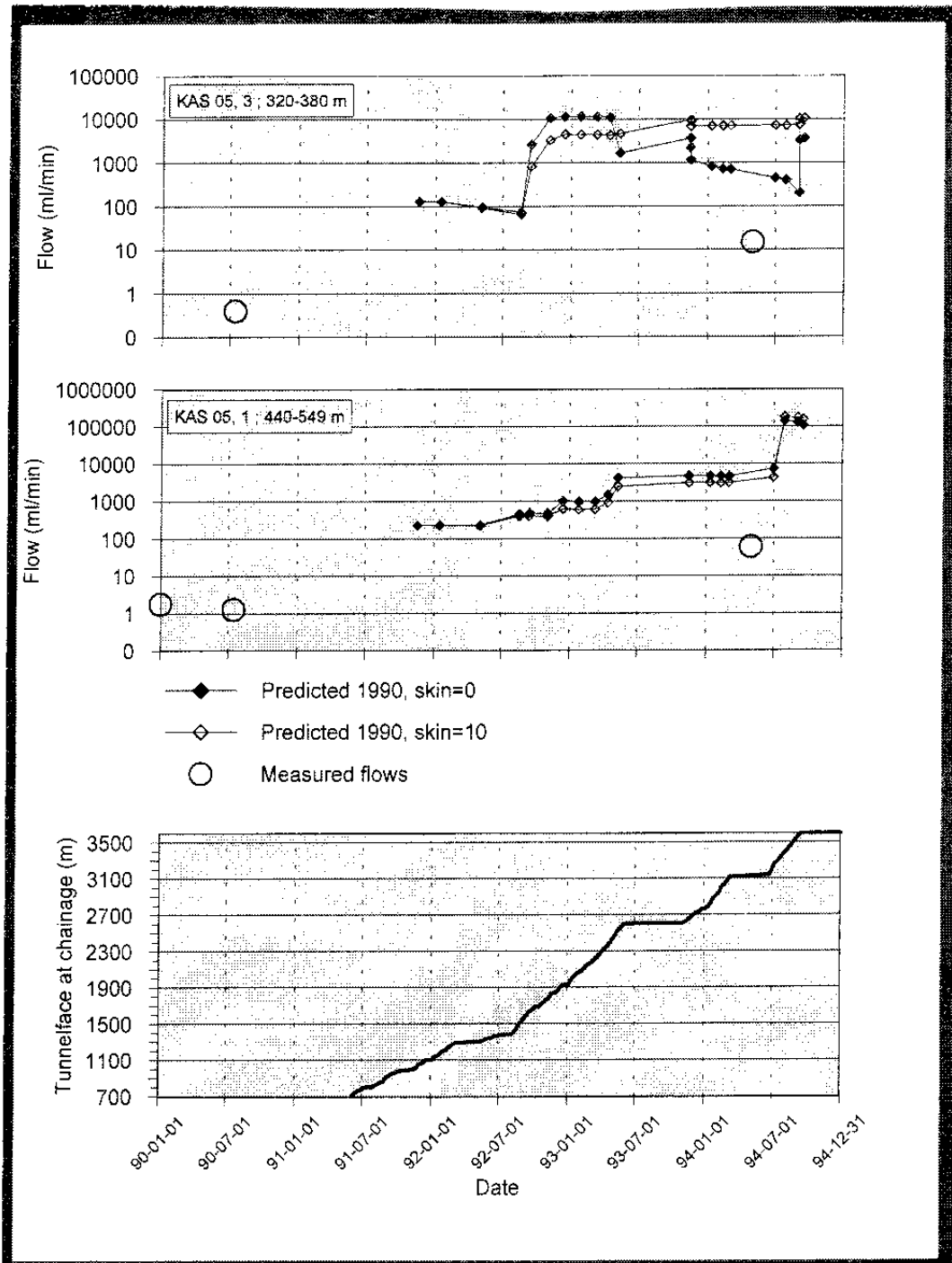


Figure 5-11. Measured and predicted flow through borehole sections.

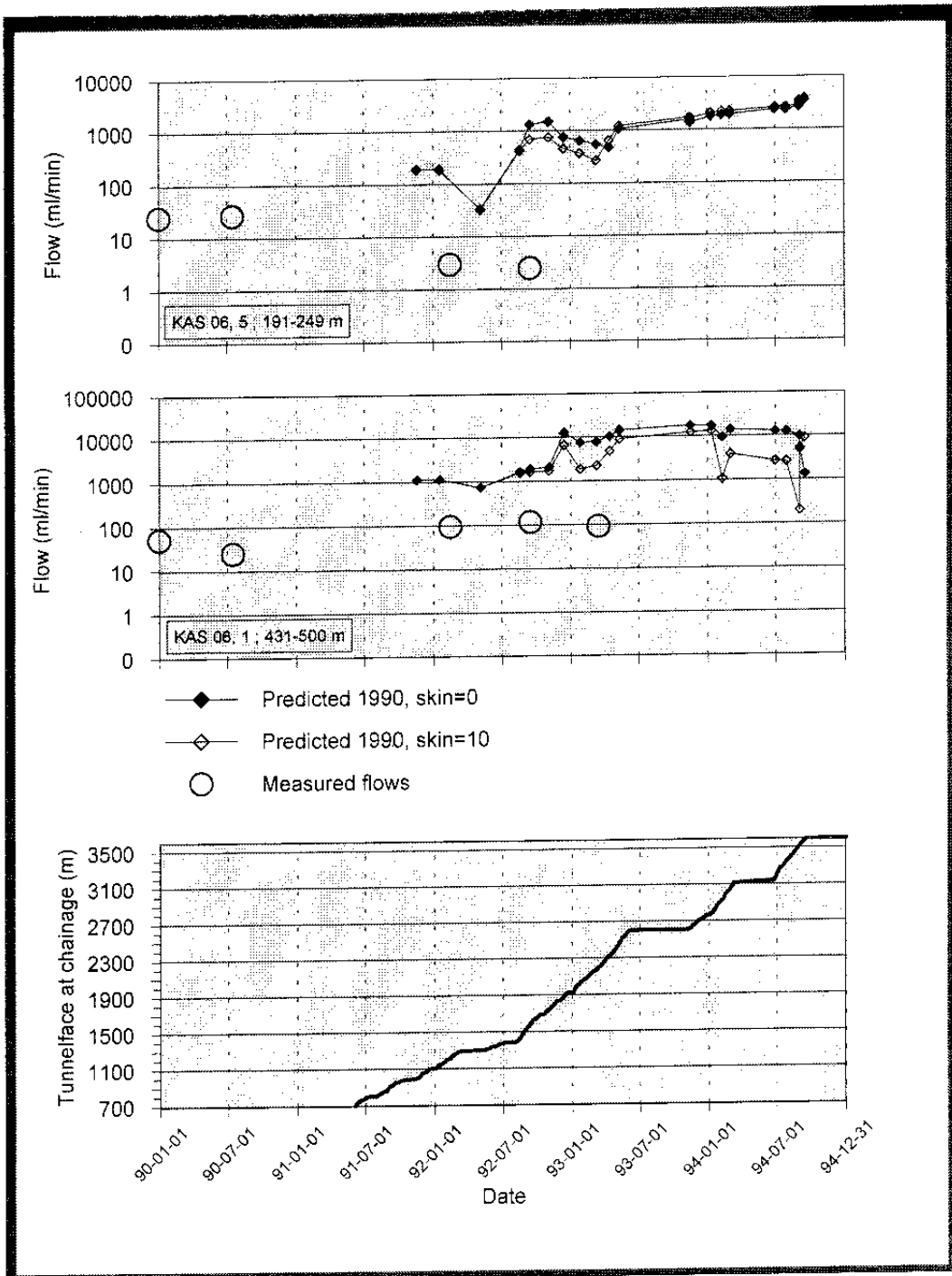


Figure 5-12. Measured and predicted flow through the borehole sections given in the figure above.

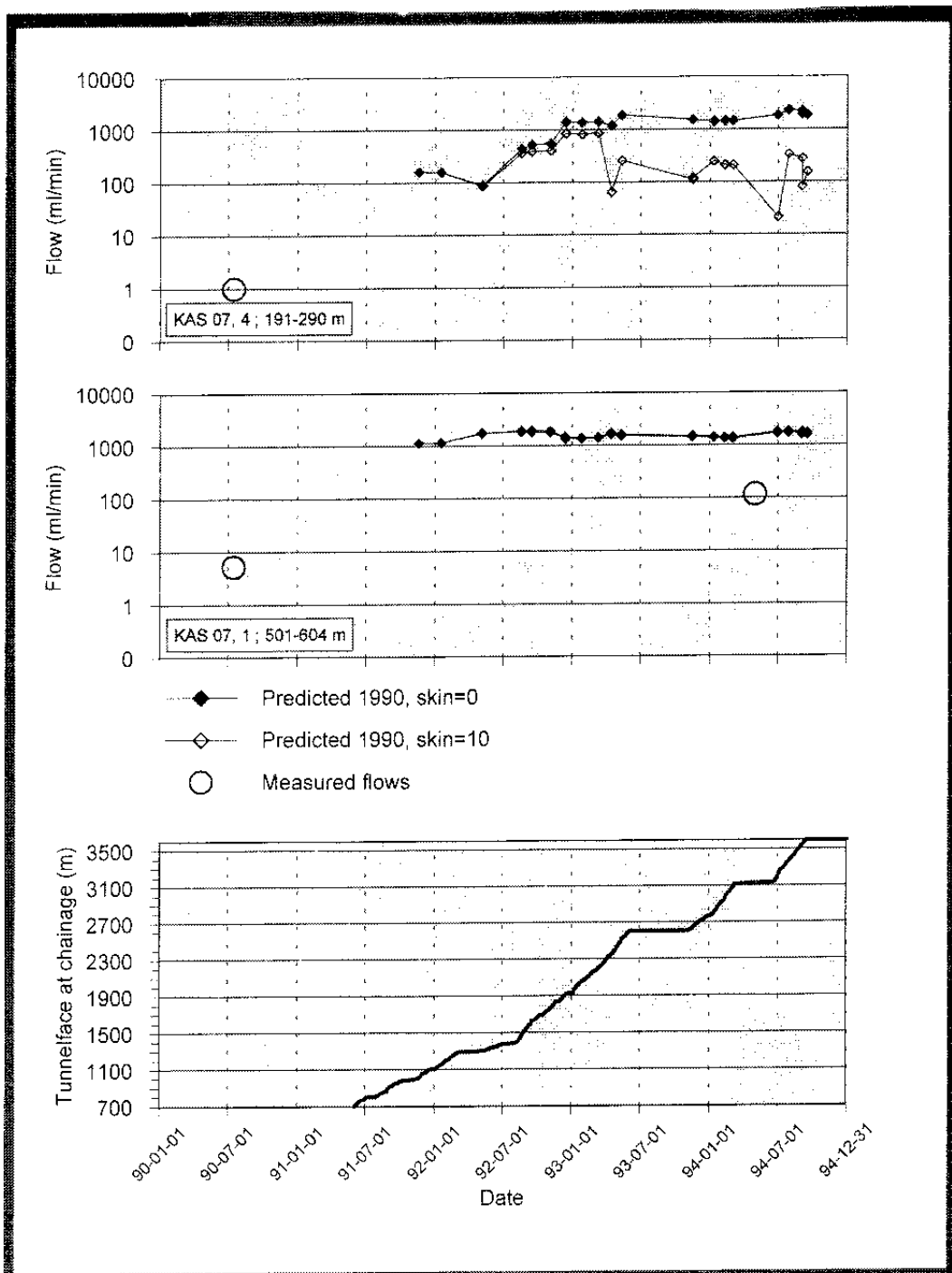


Figure 5-13. Measured and predicted flow through the borehole sections given in the figure above.

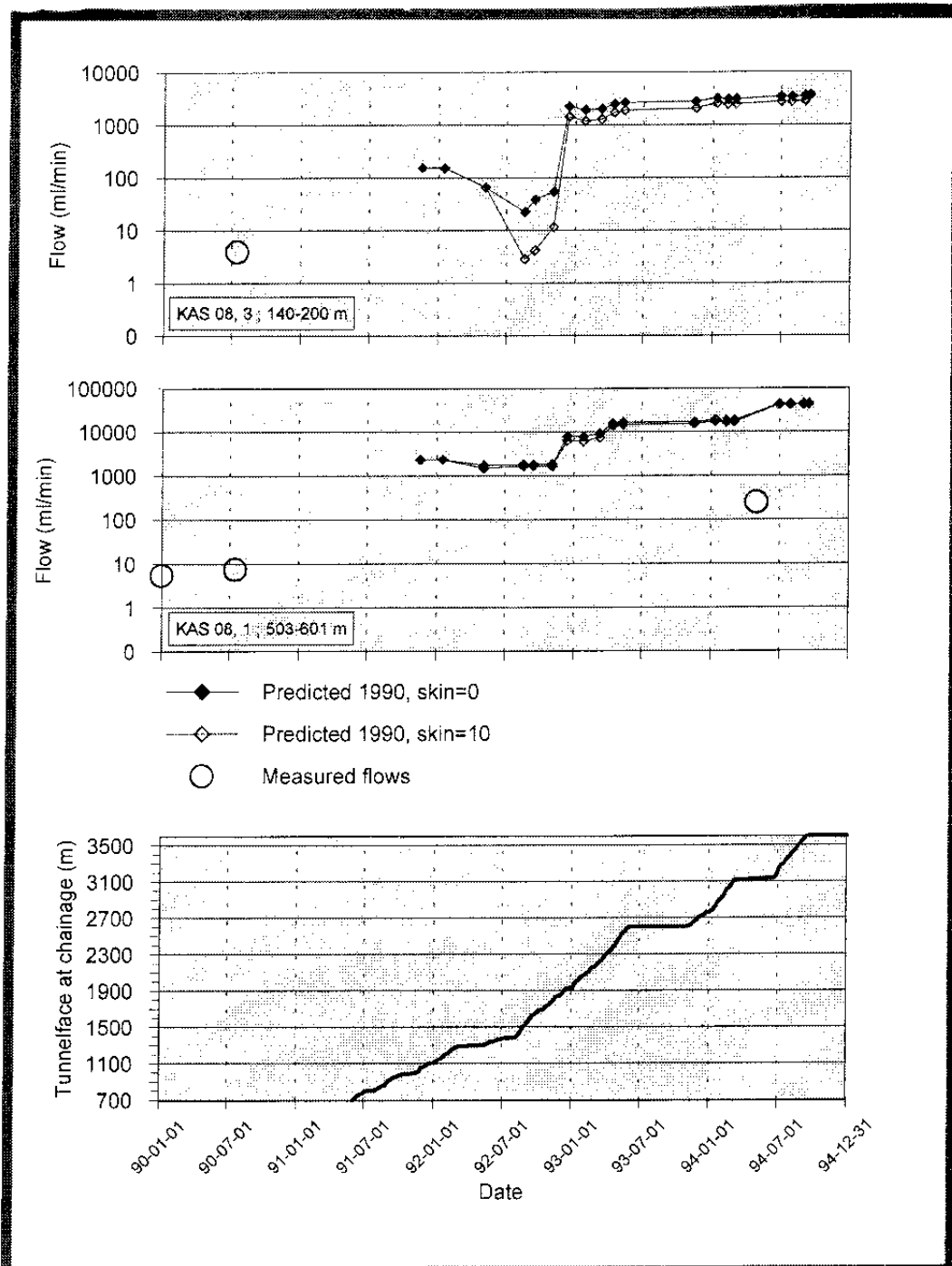


Figure 5-14. Measured and predicted flow through the borehole sections given in the figure above.

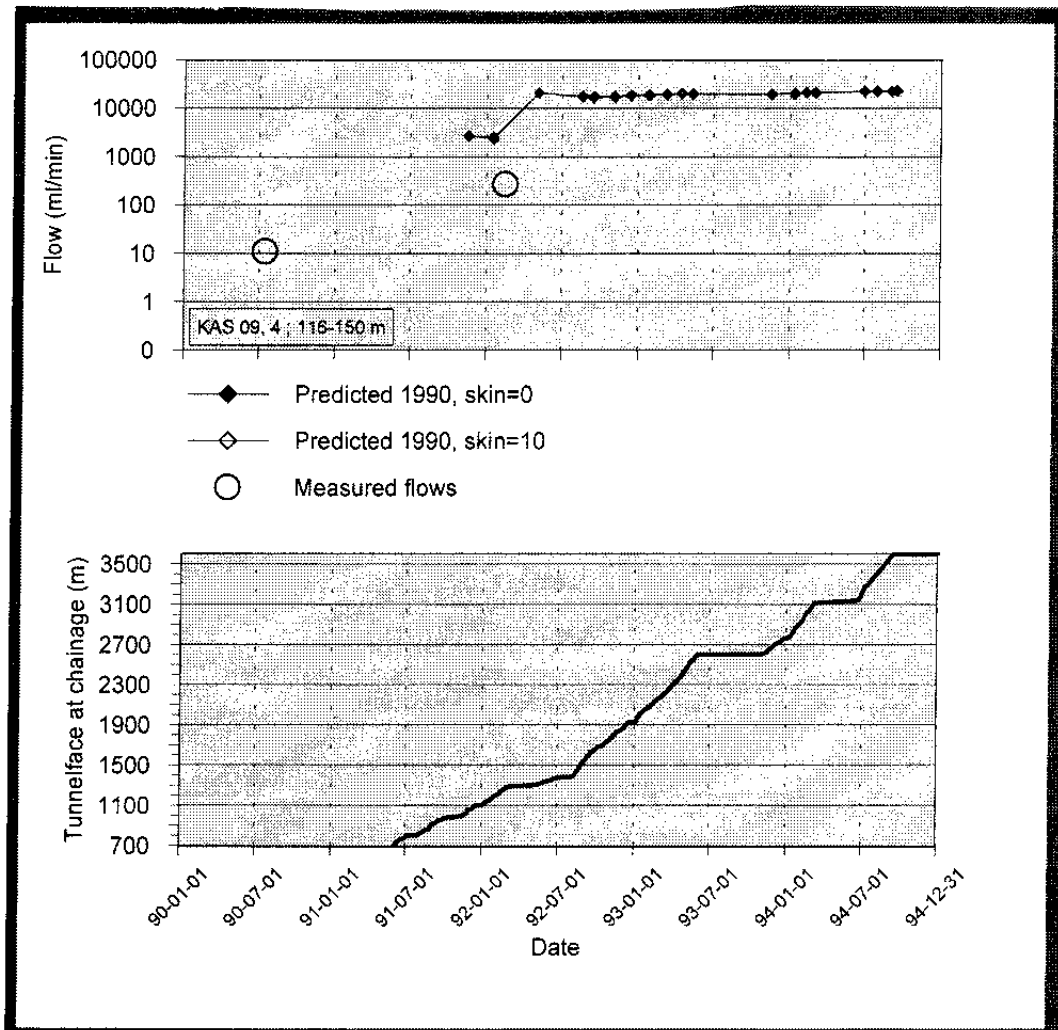


Figure 5-15. Measured and predicted flow through the borehole sections given in the figure above.

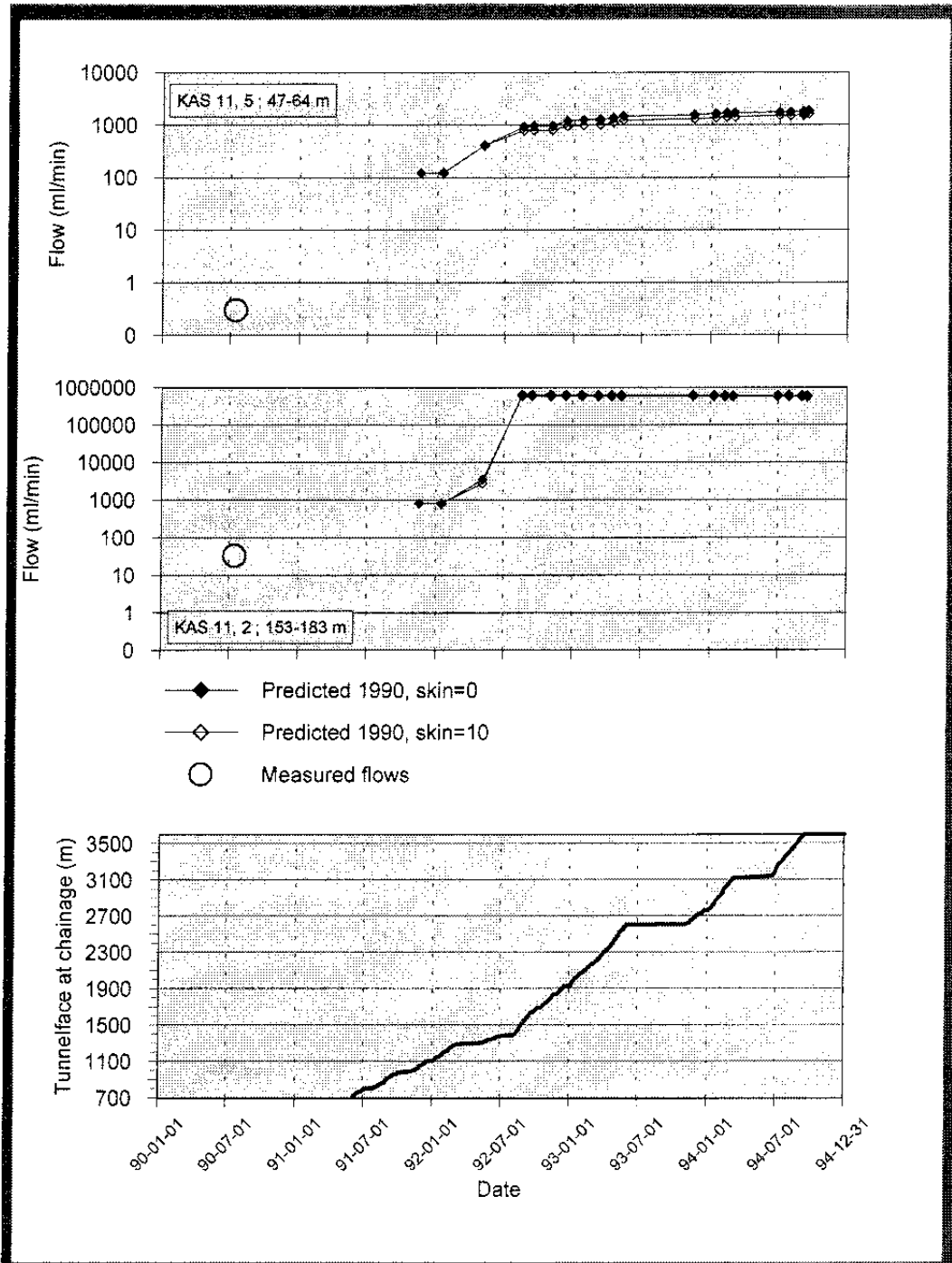


Figure 5-16. Measured and predicted flow through the borehole sections given in the figure above.

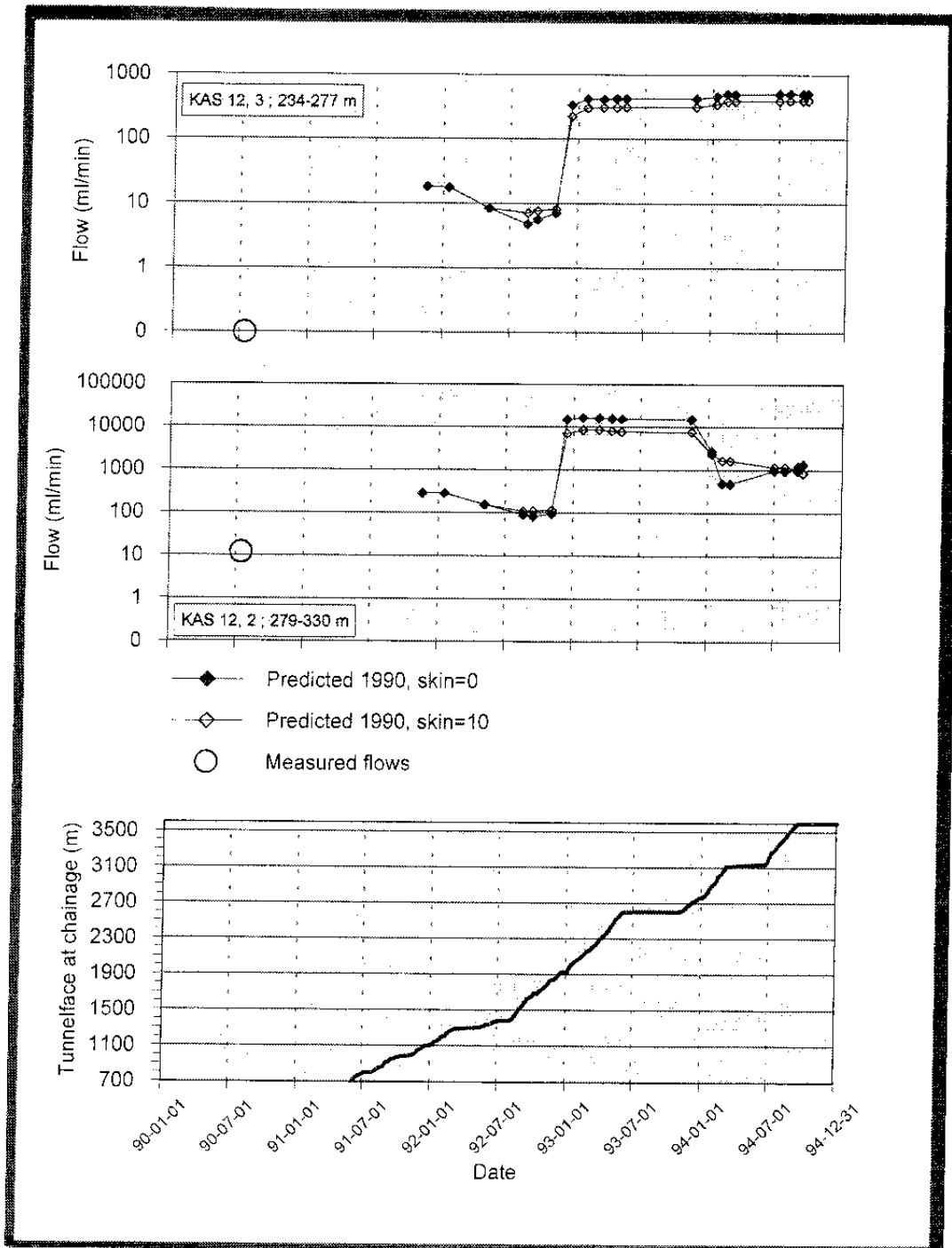


Figure 5-17. Measured and predicted flow through the borehole sections given in the figure above.

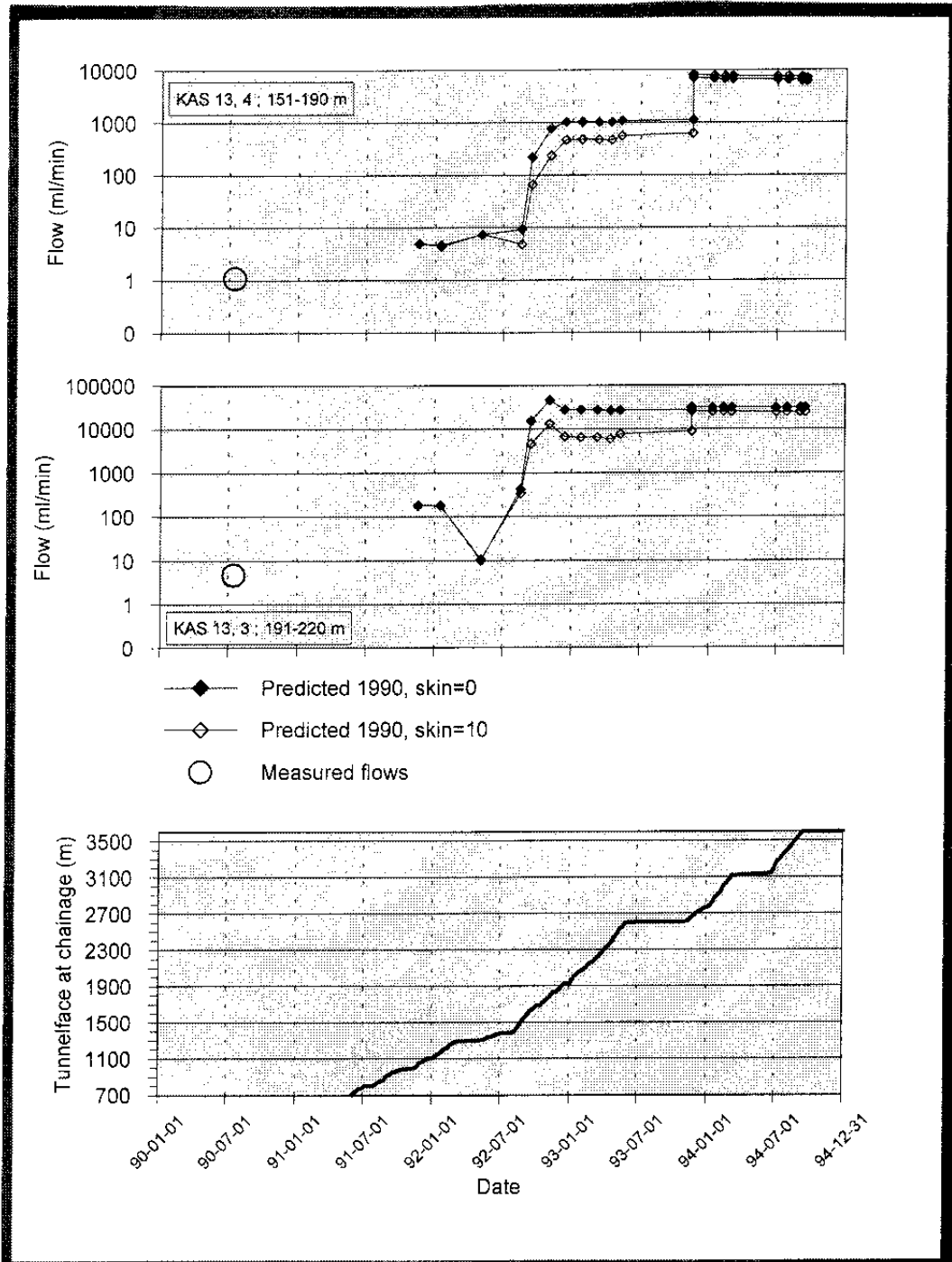


Figure 5-18. Measured and predicted flow through the borehole sections given in the figure above.

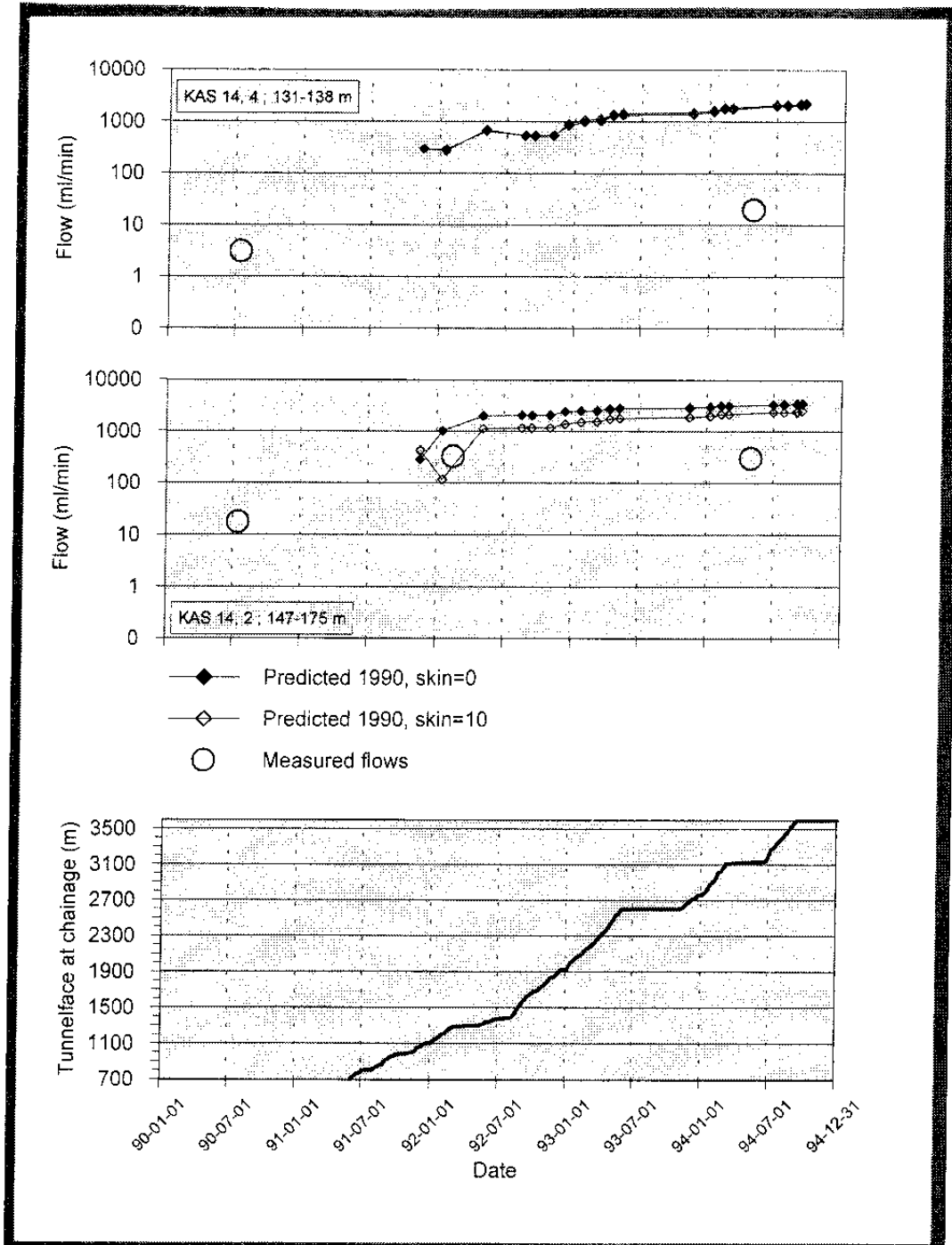


Figure 5-19. Measured and predicted flow through the borehole sections given in the figure above.

5.4 SCRUTINY AND EVALUATION

Discussion

The calculated filtration velocities on southern Äspö are around 10^{-10} to 10^{-9} m/s under undisturbed conditions and around 10^{-8} to 10^{-7} m/s during the final part of the excavation of the tunnel /*Rhén et al, /1991a/*. On northern Äspö (only two points shown in the report) the calculated filtration velocities are around 10^{-10} m/s under undisturbed conditions and around 10^{-10} to 10^{-9} m/s during the final part of the excavation of the tunnel. These filtration velocities were then transformed according to *Section 5.1* to the flow rates in the boreholes shown in *Figures 5-8 to 5-19*. According to these figures the calculated flow rates in the specified borehole sections on southern Äspö were around 100 ml/min (excluding boreholes through the very transmissive hydraulic conductor domain NE-1) under undisturbed conditions and generally around 100 to 10000 ml/min during the final part of the excavation of the tunnel. The measured flow rates in the specified borehole sections on southern Äspö were generally around 1 to 10 ml/min, a few up to 100 ml/min and a few below 1 ml/min under undisturbed conditions. The measured flow rates were generally around 10 to 100 ml/min during the final part of the excavation of the tunnel.

As can be seen in *Figures 5-8 to 5-19* the predicted flow rates are generally 10 to 100 times greater than measured except for borehole KAS03 on northern Äspö, where predicted values were approximately as measured. There are few measurements, but in several cases it is possible to see that the magnitude of the increase in the flows, from undisturbed conditions to conditions during construction, is about the same in the predictions as for the measured values.

If a simplified approach is used assuming that the calculated filtration velocity flows perpendicularly to the borehole centre line a correction factor can be estimated from the measured flows. The measured flow rate is divided by the calculated filtration velocity multiplied by the borehole diameter and the section length gives the correction factor. The correction factor will in this case be between about from 0.1 to 200, depending on borehole section.

There are three main difficulties in predicting and measuring the flow through a borehole section:

Modelling uncertainties

First, there may be large errors in the predicted filtration velocity in the rock mass close to the borehole section as the hydraulic conductivity field along the borehole was not conditioned to the measured values. If the measured hydraulic conductivity along the borehole section is greater than the hydraulic conductivities assigned to the cells close to the borehole section, and with the same average gradient in the rock volume near the borehole section, there certainly will be a difference in the flow rates due to imperfection in the model.

Moreover, the modeller had some difficulties defining representative fluxes in the model for each borehole section.

Uncertainties in the transformation of fluxes

The second problem is the transformation of the filtration velocity to a flow rate in the borehole. The transformation from the filtration velocity assumes that it is a porous medium and that the undisturbed (by the influence of the borehole) direction of the filtration velocity is known. If these assumptions are valid and no borehole skin factor (local hydraulic resistance around the borehole) is assumed, the flow through a borehole section is twice the filtration velocity if the flow is perpendicular to the borehole, as was mentioned in *Section 5.1*. If the skin factor is negative (increased hydraulic conductivity around the borehole compared with the surrounding rock) the flow through a borehole section will increase up to twice the value for a skin factor of 0. If the skin factor is positive the flow through a borehole section will decrease.

If the filtration velocity of the flow is parallel to the borehole with diameter of 56 mm and the test section length is 50-100 m the flow through the middle part of the borehole section is 100-300 times larger than if the flow rate were perpendicular to the borehole, with $\alpha=2$, according to *Section 5.1*. If the flow is parallel to the borehole with diameter 56 mm and test section length 50-100 m the filtration velocity (m/s) should be multiplied by something like 700-3000 to obtain the flow through the middle part of the borehole section (Q_{bh} , m³/s) according to *Section 5.1*.

In the transformations made the entire borehole section between the packers was set equal to $2L$. As the packers were positioned in fairly unfractured and low-conductivity rock, there were parts of the boreholes near the packers whose conductivity was low and which should not be included in the estimate of $2L$. A reduction of $2L$ would decrease the predicted flow rate in the borehole. Another problem is whether the concept for transformation based on a porous medium can be used to obtain approximate correction factors in a fractured medium. For some cases it certainly can be questioned. Consider a case where there is one hydraulic conductor domain whose width is much less than the distance between the packers straddling the domain and that most of the flow is through the domain, and not in the rock mass outside it. The direction of the filtration velocity in the hydraulic conductor domain is used for the calculation of the correction factor. In this case the correction factor will be greatly overestimated as $2L$ is approximated by the packer distance but should be the length of the borehole through the hydraulic conductor domain. If there are several hydraulic conductor domains intersecting the borehole section and they have the same hydraulic potential $2L$ should be the sum of the borehole lengths through the hydraulic conductor domains. However, if there is a hydraulic potential difference between the hydraulic conductor domains there will be a flow along the borehole from one domain to the other. The flow in the borehole section straddling both domains will be higher than the sum of the flows in the borehole sections straddling each domain separately, in line with the suggested transformation.

Uncertainties in the dilution measurements

Thirdly, the dilution measurements are in some cases performed in long test sections and there may be a problem of achieving good mixing and circulation along the entire borehole section. Most sections were 30 to 60 m long and in one case 145 m long. In the evaluation of the dilution measurements it is assumed that there is perfect mixing, giving a homogenous distribution of the tracer within the borehole section during the entire test. This may not always be true. Some tests also show that there are no nice linear relationships between $\ln(C/C_0)$ plotted as a function of time, which causes problems for the evaluation /Ittner *et al*, 1991, Ittner, 1992, 1994, Andersson *et al*, 1992 and Stanfors *et al*, 1992 (PR 25-92-18C) /.

Conclusions

If it is assumed that the measured values are reliable estimates of the flow rate through the borehole section it is found in general that the transformation factor from filtration velocity to flow rate through the borehole section is generally 10-100 times too high. In most cases the transformation factor was around 100 to 1000, which then indicates that some correction of the filtration velocity is needed if it is to be compared with measured flow rates in a borehole. It is, however, interesting to note that the transformation factor is around 1000 for sections in KAS03, where there is a good match between the predicted and measured values!

Even though it is evident for a number of reasons that there are difficulties in estimating the proper fluxes in the rock mass from dilution measurements, the dilution measurements are useful and a feasible way of finding out whether or not there are hydraulic communication interims of flows and not just pressure responses.

Dilution measurements

More reliable predictions and measurements can most probably be achieved if shorter test sections for dilution measurements are used. The test section should also preferably just straddle the hydraulic conductor domain or just be in what is considered to be a hydraulic rock mass domain. This may stand in conflict with the way in which the entire borehole is instrumented as only a limited number of test sections can be installed.

Modelling

If a hydraulic conductor domain intersects a borehole section and it dominates the flow field in that section, the flux rate and the direction in the hydraulic conductor domain must be the ones that are used together with the width of the domain to calculate the correction factor. In many other cases it is probably difficult to define representative flux rates and flux directions in the model that

are useful for estimating the flow rate in the borehole. To some extent the flux rates and flux directions in the model would be more representative if the hydraulic conductivity field around the boreholes were conditioned to the measured ones. However, it is not evident how the measured hydraulic conductivities along the borehole are best applied, considering correlation ranges and the way in which the representative flux rates and directions in the model should be evaluated.

Generic studies were also tested to simulate a sub-model the borehole section itself surrounded by the measured hydraulic conductivities and taking the boundary conditions from the site scale model /Svensson, 1992/. In this way it could be expected to be more reasonable to compare the actual measurements with the simulated flows in the borehole. This approach should be tested. In such a case no transformation is needed as it is possible to calculate the flow in the borehole section directly.

Transformation

If the impact of the borehole flow field itself and the flow in the borehole are not modelled, some correction of the filtration velocity has to be made if the filtration velocity in the numerical model is to be compared with dilution measurements. The transformation should be based on the evaluated geometrical framework and the local material properties around each borehole section but also on a thorough evaluation of the flow field around the borehole section in the groundwater flow model in order to obtain relevant parameters for the transformation. It is then likely that the transformation can be improved compared with what was achieved in the predictions, and possibly that at least the right magnitude of the flow rate can be predicted.

However, the heterogeneity will most probably cause problems in the evaluation of relevant parameters in the groundwater flow model and also in correctly describing the way in which the borehole is hydraulically connected to the formation, especially when there is a positive skin factor around the borehole. The fracture itself is very heterogenous and the measured dilution rate will depend on where the borehole intersects the fracture plane.

6 SUBJECT: HYDRAULIC CONDUCTIVITY - BLOCK SCALE

6.1 SCOPE AND CONCEPTS

Hydraulic rock mass domains are geometrically defined volumes in space with properties differing from those of surrounding domains (rock mass domains and hydraulic conductor domains). They may either be defined by lithological domains or purely by interpretation of results from hydraulic tests. Within a domain there is a defined distribution of the properties.

The material properties chosen for the hydraulic rock mass domains are:

- Hydraulic conductivity ($K(x,y,z)$)
- Specific storage ($S_s(x,y,z)$).

K is based on evaluation of transient hydraulic tests. The properties within a domain may be given as a mean effective value for the entire domain, a trend within the domain, a statistical distribution within the domain with or without spatial correlation or any other function describing the distribution within the domain.

The specific storage values (S_s) for the hydraulic rock mass domains were not predicted and are therefore not discussed in the text below.

The purpose of the predictions was to test the ability to predict the hydraulic properties of 50 m blocks deterministically localized along the planned tunnel, thus, a more detailed prediction in space than that shown in *Chapter 2*.

6.2 METHODOLOGY FOR TESTS OF CONCEPTS AND MODELS

6.2.1 Prediction methodology

Based on the positions of the blocks along the planned tunnel and the predicted geological conditions for each block, different kinds of prediction methods were used. The predicted hydraulic conductivity of each block was primarily estimated using several methods presented in *Liedholm /1991 a, b/ (TN 16: Predicted lithology of each block, TN 14: K for depth interval of 50 m data from KAS02, 05-08, TN 20: Level 100 - 150 m in KAS05-07 Småland-granite, TN 21: Based on correlation between fracture frequency and hydraulic conductivity)*. Details of the way in which each block was predicted are presented in *Rhén et al /1993a, c, 1994a/*.

6.2.2 Methodology for determining outcome

The data for the geological outcome for a 50 m block is based on the geological documentation along the part of the tunnel where the 50 m block was predicted to be, ± 25 m, thus, along 100 m of the tunnel. The evaluated hydraulic conductivity from tests performed in the probe holes which penetrated this rock mass along the tunnel were used to estimate the hydraulic conductivity of each block. The hydraulic conductivity was calculated as the transmissivity of each probe hole divided by the test section length (distance from the bottom of the borehole to the packer). For more details of the pressure build-up tests and scaling of the hydraulic conductivity, see *Chapter 2*.

6.3 COMPARISON OF PREDICTED AND MEASURED ENTITIES

The prediction and outcome are shown in *Figure 6-1* and *Table 6-1*. The positions of the blocks P50-01 to P50-06 are shown in *Stanfors et al /1997b/*.

It should be observed that the tunnel position in the predictions after tunnel section 2900 m deviates from the actual tunnel position (see *Chapter 1* in the introduction to the report). Comparisons between predictions and outcome for blocks P50-7 to P50-10 shown in *Gustafson et al /1991/* have therefore not been included in the comparison.

Table 6-1. Hydraulic conductivity (K) block scale. Test scale = 14 m,

Prediction = P Outcome = O	Tunnel section (m)	Block	Geometric mean (GM) (m/s)	Standard dev. s(Log ₁₀ (K))	No. of samples
P	0700-1475	P50-01	1.4E-09	2	(130)
	0700-1475	P50-02	1.4E-09	2	(130)
	0700-1475	P50-03	1.4E-09	2	(130)
	1475-2265	P50-04	2.8E-09	1.9	(130)
	2265-2875	P50-05	4.9E-09	1.9	(130)
	2265-2875	P50-06	2.1E-09	1.7	(130)
O	0700-1475	P50-01	2.09E-06	2.07	3
	0700-1475	P50-02	1.02E-07	1.57	6
	0700-1475	P50-03	4.57E-07	1.21	12
	1475-2265	P50-04	1.62E-09	2.12	14
	2265-2875	P50-05	3.56E-11	1.49	12
	2265-2875	P50-06	7.39E-11	1.95	12

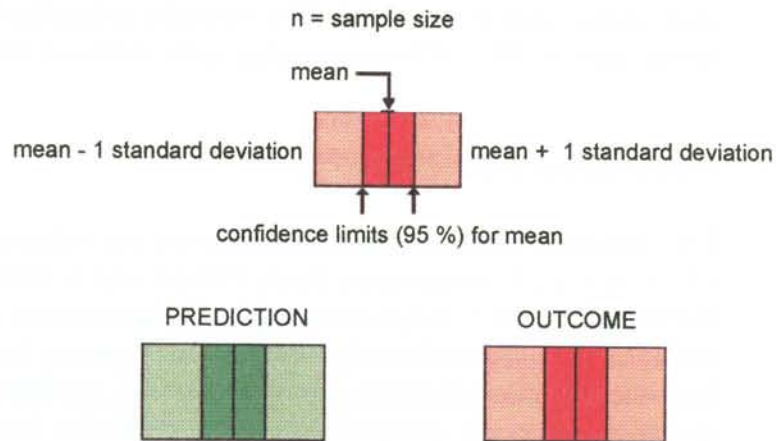
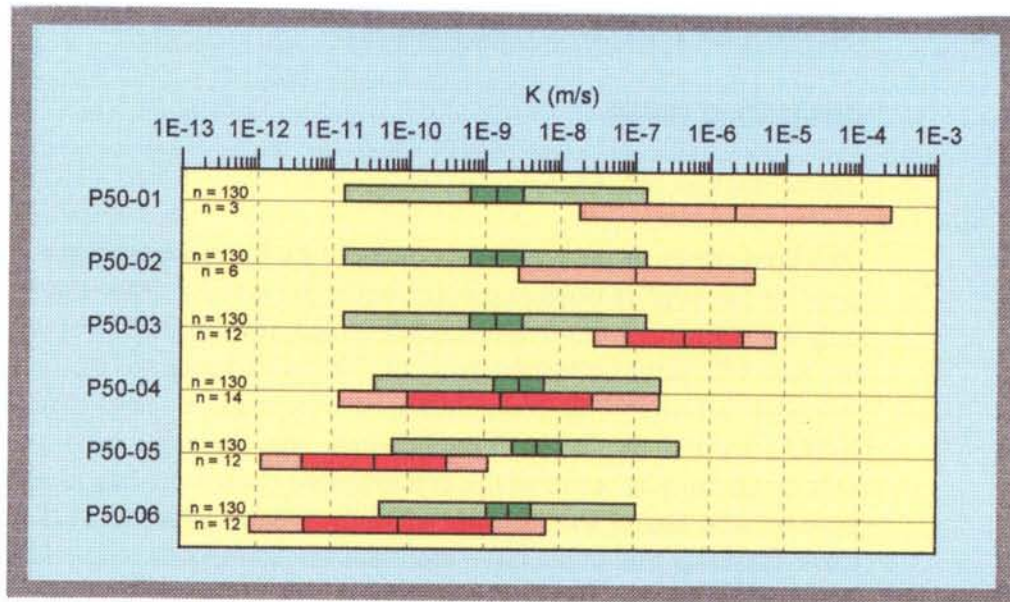


Figure 6-1. The outcomes and predictions of the hydraulic conductivity of 50 m blocks for defined positions of the blocks along the Äspö HRL tunnel, in tunnel section 700 - 2875 m. Block scale. Test scale 14 m. (mean= arithmetic mean of $\text{Log}_{10}(K)$, standard deviation = Standard deviation of $\text{Log}_{10}(K)$, n = sample size).

6.4 SCRUTINY AND EVALUATION

Summary of results

Tunnel section 700-1475 m

The predictions of the hydraulic conductivity for this part of the tunnel were poor for the same reasons as pointed out in *Section 2.4*. The reasons were that only a few hydraulic tests in boreholes drilled from ground level were made in the rock volume close to tunnel section 700-1475 during the pre-investigations. A few air-lift tests at the 100 m test scale were made, no tests at smaller scales. Results from Äspö at the 3 m test scale was therefore used as a base for extrapolation. The result of the extrapolation (based on data from Äspö) was poor because tunnel section 700-1475 m penetrated a rock mass that was much more fractured and conductive than that on Äspö, over long stretches of the tunnel. Several fracture zones are intersected that are very transmissive and wide in that part of the tunnel. The hydraulic properties below the sea along tunnel section 700 - 1475 m were thus quite different from those on Äspö.

Tunnel section 1475- 2265 m

The prediction of the hydraulic conductivity was rather good. Tunnel section 1570-1620 ± 25 m represents block P50-04, and is rather close to boreholes KAS05 and KAS13. The predicted hydraulic conductivity based on correlations between hydraulic conductivity and fracture frequency for KAS05 and fracture frequency data from KAS05, section 210-230 m, and KAS13, section 240-260 m was closer to the outcome than to the prediction based on the geometric mean hydraulic conductivity for a 50 m depth interval relevant for the block, with data taken from boreholes KAS02, 05-08.

Tunnel section 2265- 2875 m

The predictions of the hydraulic conductivity were higher than the outcome. Tunnel section 2422-2472 ± 25 m represents block P50-05, and is rather close to boreholes KAS05 and KAS13. Tunnel section 2752-2802 ± 25 m represents block P50-06, and is rather close to borehole KAS04. Among the methods used the geometric mean hydraulic conductivity for a 50 m depth interval relevant for the blocks, with data taken from boreholes KAS02, 05-08 gave somewhat better results than the other methods.

Discussion

The predictions were based on a number of correlations between hydraulic conductivity and fracture frequency, lithology or just depth. The predicted geological properties of each block were the base when the correlations between hydraulic conductivity and fracture frequency or lithology were used. In general, there turned out to be large differences between the methods for a

specific block. The predicted mean hydraulic conductivity for a block was calculated as the geometric mean value of the predicted geometric mean hydraulic conductivities by the different methods chosen. An important reason for the large differences between the methods and also between prediction and outcome is the large scale heterogeneity within the site and also the anisotropic conditions present at Äspö (see *Chapter 2*).

Conclusions

The predicted values exhibited great variation depending on the approach selected, and it is difficult to judge if any one method was better than another. Use of the lithology would have given the best result for the first three blocks, but a result still far from the outcome. For block P50-4 the fracture frequency approach would have given the best result and, finally, for the last two blocks the injection tests with 3 m spacing (K for a depth interval of 50 m, data from KAS02, 05-08 and the test in KAS02 section 307-357 m) would have given somewhat better results.

Based on the results from Äspö it seems more or less impossible to predict the hydraulic conductivity accurately for a 50 m block in a site as heterogenous and anisotropic as Äspö, at least if no cored hole intersects the block, or runs close to it.

A sufficient number of hydraulic tests is also needed in the region of the block if reliable estimates of the mean properties are to be obtained, with a fairly narrow confidence interval around the mean due to the high variability of the hydraulic conductivity.

7 SUBJECT: CONDUCTIVE STRUCTURES - BLOCK SCALE

7.1 SCOPE AND CONCEPTS

Hydraulic rock mass domains are geometrically defined volumes in space with properties that differ from those in surrounding domains (rock mass domains and hydraulic conductor domains). They may either be defined by lithological domains or purely by interpretation of results from hydraulic tests. Within a domain there is a defined distribution of the properties.

The material properties chosen for the hydraulic rock mass domains are:

- Hydraulic conductivity ($K(x,y,z)$)
- Specific storage ($S_s(x,y,z)$).

An alternative to the material properties chosen above can be a spatial description of the fracture distribution and fracture properties, as for example the transmissivity of the domains. This was not predicted, but the frequency of conductive features with a transmissivity higher than a specified value was predicted. It is a useful measure for estimating the probable size of blocks not intersected by features more transmissive than a specified value.

The purpose of the predictions was to test the ability to predict for each block the frequency of conductive features with a transmissivity higher than a specified limit for 50 m blocks deterministically localized along the planned tunnel.

7.2 METHODOLOGY FOR TESTS OF CONCEPTS AND MODELS

7.2.1 Prediction methodology

The prediction on Äspö was based on the injection tests with 3 m packer spacing in boreholes KAS02 and KAS04-08. The predictions were based on the transmissivities obtained at the 3-m scale, see *Figure 7-1*.

As there were no core holes with injection tests close to blocks P50-01, P50-02 and P50-03 the estimates of the distances were the same as for the prediction for tunnel section 700 - 3854 m. These predictions were based on the entire data set available from KAS02 and KAS04-08 /Liedholm, 1991 b, TN 18/. The 95% confidence interval was chosen as the maximum interval for blocks P50-04 to P50-10.

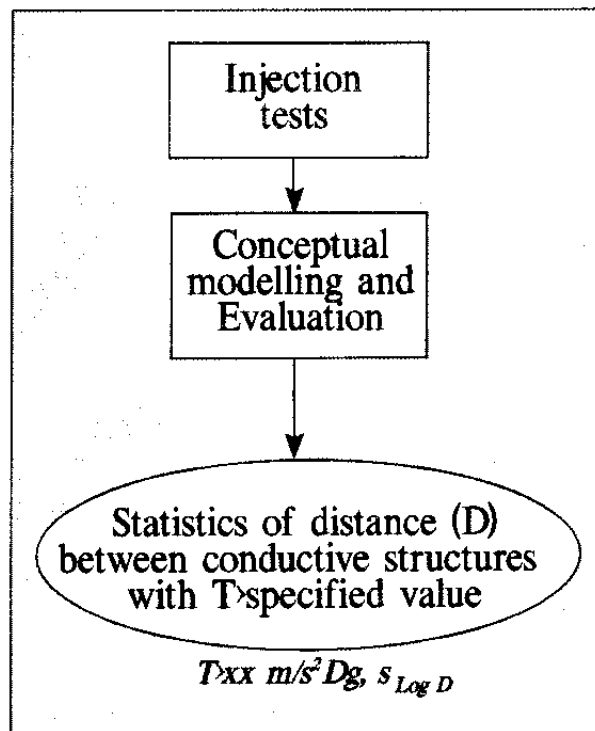


Figure 7-1. Pre-investigation methodology. Block scale. Statistics of distance between conductive features. The 1-D approach is used by studying the distance (D) between conductive features, with a transmissivity (T) greater than a specified value along boreholes. The characteristic values evaluated for the distribution is the geometric mean distance (Dg) and the standard deviation of $\text{Log}_{10} D$ ($s_{\text{Log}D}$).

The predictions for block P50-04 were based on data from KAS02 section 199 m (secup) to 250 (seclow). The predictions for block P50-05 were based on data from KAS05 section 307 m to 357 m and the predictions for P50-07 were based on data from KAS08, 462-530 m. And, finally, the predictions for block P50-06 were based on the arithmetic mean of the distances found for P50-05 and P50-07.

7.2.2 Methodology for determining outcome

The data for the geological outcome for a 50 m block are based on the geological documentation along the part of the tunnel where the 50 m block was predicted to be, ± 25 m, thus along 100 m of the tunnel. The probe holes which penetrated these 100 m rock mass along the tunnel was too few to form a base for the statistics. Tunnel sections according to *Table 7-1* were therefore used.

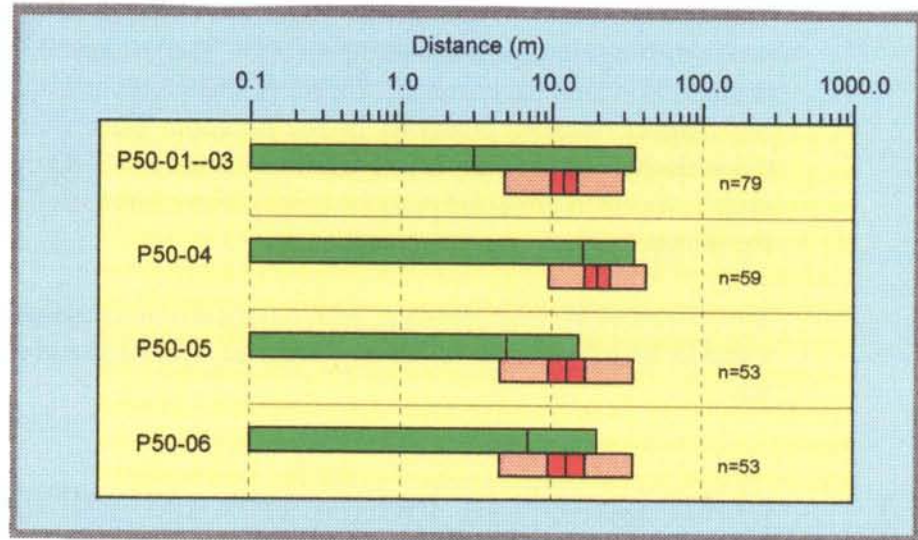
The distance between conductive features was based on the results from the probe drillings and pressure build-up tests. The evaluated transmissivity (T), the total flow into the borehole (Q) and estimated, or measured, inflow (Q_i) for the mapped leaking positions in the borehole were used to calculate the transmissivity of the conductive features using: $T_i = T \cdot Q_i / Q$. The position of each T_i was then projected onto the tunnel centre line to define a position along the tunnel for each transmissive feature.

The distances between features with a transmissivity greater than a specified value ($3 \cdot 10^{-5}$, $3 \cdot 10^{-7}$ or $3 \cdot 10^{-9}$ m²/s) were then calculated and evaluated statistically.

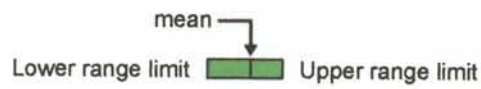
7.3 COMPARISON OF PREDICTED AND MEASURED ENTITIES

The prediction and outcome are shown in *Figures 7-2 and 7-3* and in *Table 7-1*. The positions of the blocks P50-01 to P50-06 are shown in *Stanfors et al /1997b/*.

It should be observed that the tunnel position in the predictions after tunnel section 2900 m deviates from the actual tunnel position (see *Chapter 1* in the introduction to the report). The comparison between predictions and outcome for blocks P50-7 to P50-10 shown in *Gustafson et al /1991/* has therefore not been included in the comparison.



PREDICTION



OUTCOME

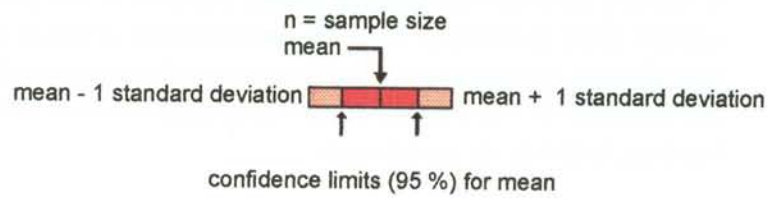
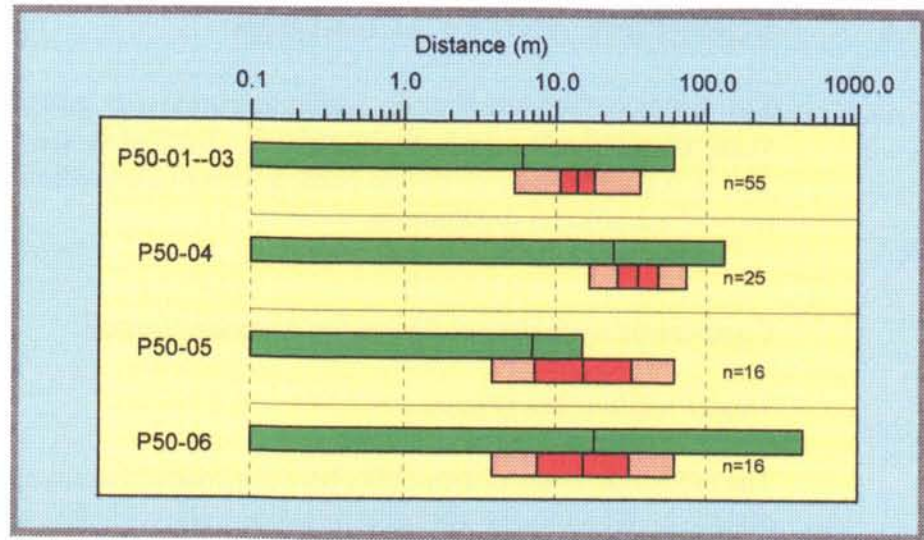
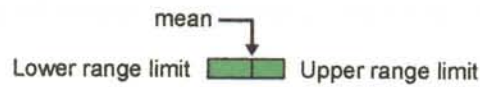


Figure 7-2. The outcomes and predictions of the geometric mean distance between transmissivities above $3 \cdot 10^9 \text{ m}^2/\text{s}$.



PREDICTION



OUTCOME

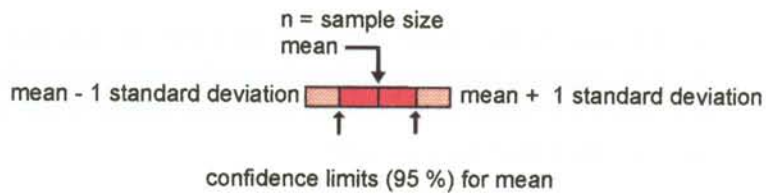


Figure 7-3. The outcomes and predictions of the geometric mean distance between transmissivities above $3 \cdot 10^{-7} \text{ m}^2/\text{s}$.

Table 7-1. Geometric mean distance (D_g). Block scale.

Outcome (O) based on tunnel section: (m)	Prediction (P) given for:	$T > 3 \cdot 10^{-9} \text{ m}^2/\text{s}$		$T > 3 \cdot 10^{-7} \text{ m}^2/\text{s}$		$T > 3 \cdot 10^{-5} \text{ m}^2/\text{s}$	
		O	P	O	P	O	P
		(m)	(m)	(m)	(m)	(m)	(m)
700-1475	Entire tunnel	12	3	15	6	43	55
1475-2265	Entire tunnel	20	3	35	6	-	55
2265-2875	Entire tunnel	13	3	15	6	-	55
700-1475,P50-01	P50-01	12	3	15	6	-	-
700-1475,P50-02	P50-02	12	3	15	6	-	-
700-1475,P50-03	P50-03	12	3	15	6	-	-
1475-2265,P50-04	P50-04	20	16	35	24	-	-
2265-2874,P50-05	P50-05	13	5	15	7	-	-
2265-2874,P50-06	P50-06	13	7	15	18	-	-

7.4 SCRUTINY AND EVALUATION

The distances between features with a transmissivity greater than a specified value are more or less perfectly lognormally distributed (see *Rhén et al /1997/*). This is a good quality as it then becomes easy to describe the samples in the form of a statistical distribution.

Comparison with the prediction for the entire tunnel

Tunnel section 700-1475 m

The prediction of the distance (D_g) between conductive structures was approximately as the outcome for transmissivities above $3 \cdot 10^{-5} \text{ m}^2/\text{s}$ but for transmissivities above $3 \cdot 10^{-7} \text{ m}^2/\text{s}$ and above $3 \cdot 10^{-9} \text{ m}^2/\text{s}$ the predicted D_g were smaller than the outcome. However, the comparison must be considered very uncertain due to the reasons mentioned in *Sections 6.4 and 2.4*.

Tunnel sections 1475- 2265 m and 2265- 2875 m

As the data points were clustered and few, it was not possible to obtain a reliable distance estimate in the tunnel for transmissivities above $3 \cdot 10^{-5} \text{ m}^2/\text{s}$. For transmissivities above $3 \cdot 10^{-7} \text{ m}^2/\text{s}$ and above $3 \cdot 10^{-9} \text{ m}^2/\text{s}$ the predicted D_g were smaller than the outcome.

Comparison with the prediction for blocks P50-04 to 06

As the data points were clustered and few, it was not possible to obtain a reliable distance estimate in the tunnel for transmissivities above $3 \cdot 10^{-5} \text{ m}^2/\text{s}$. For transmissivities above $3 \cdot 10^{-7} \text{ m}^2/\text{s}$ and above $3 \cdot 10^{-9} \text{ m}^2/\text{s}$ the predicted D_g were smaller than the outcome, except for P50-06 with $T > 3 \cdot 10^{-7} \text{ m}^2/\text{s}$. Considering the confidence limits for D_g in the outcome, the outcome nearly straddles the predicted point estimate of D_g .

Discussion

There may be at least two reasons for the outcome of D_g being larger than the prediction. First, the method used (identifying transmissive structures in the probe holes during drilling) leads to underestimation of low-conductivity features, because they are masked by higher flow rates. Secondly, it was not possible to drill every fourth round giving some 'long' distances (probably false) and this probably affects the statistics of $T > 3 \cdot 10^{-7} \text{ m}^2/\text{s}$ and $T > 3 \cdot 10^{-9} \text{ m}^2/\text{s}$ more than those of $T > 3 \cdot 10^{-5} \text{ m}^2/\text{s}$. However, this second problem is probably of minor importance (see *Figure 1-8*, showing the probe holes).

As discussed in *Chapters 2* there are anisotropic conditions at Äspö. As the predictions were based on subvertical boreholes and the outcome on

subhorizontal boreholes the comparison must be considered uncertain. Another problem is the scale dependency mentioned in *Chapter 2*. The test scale in the subhorizontal boreholes was about 14 m and in the subvertical 3 m.

Conclusions

The method for estimating statistics of the distance between low-conductivity structures in the tunnel was unsatisfactory but probably reasonable adequate for relatively high conductivities. The estimates of the distance between highly conductive structures in the tunnel was also unsatisfactory, but the reason for this is the scale. As the distance between these features is long and the tunnel covers a relatively small area compared with the distance between the features it is not possible to obtain a sufficiently large sample for adequate statistics. The way in which sampling should be done in space for the features with high transmissivities can also be discussed.

Another problem is the number of sampling points needed. The sample for a block that should be used for the outcome should have been data from only the tunnel section where the block was positioned, but the sample size then became too small for reliable statistics. Based on the data presented it is difficult to judge the possibility of predicting the distance between conductive structures for a 50 m block, as the method of estimating the outcome probably underestimates the number of low-conductivity fractures and the problems of anisotropic conditions at Äspö.

8 SUBJECT: FLOW IN CONDUCTIVE STRUCTURE - BLOCK SCALE

8.1 SCOPE AND CONCEPTS

The geometrical concepts for the groundwater flow model consists of:

- hydraulic conductor domains and
- hydraulic rock mass domains.

When the tunnel is introduced into the model the concepts added to the groundwater flow model are the tunnel geometry and the boundary conditions with atmospheric pressure in the tunnel, the planned tunnel cross-section and a hydraulic resistance around the tunnel (see *Chapter 3* for more details). The hydraulic properties of the domains around the tunnel periphery may be different from those of the undisturbed rock mass for a number of reasons. One reason is that the excavation of the tunnel will create a zone around the tunnel, often named EDZ (Excavation Disturbed Zone), with properties that differ from those of the undisturbed rock mass. The disturbed zone may provide a preferential pathway for radio nuclide transport and is therefore of interest in conjunction with performance assessments. Mechanical damage to the rock due to the excavation method, stress changes due to the excavated rock volume, chemical precipitation in the fractures after the excavation and gas intrusion into fractures may be reasons for changes in the hydraulic properties in the EDZ. At the Äspö HRL some studies of the EDZ were made and reported in *Olsson /1996/*. An other reason for a change in the hydraulic properties is the reinforcing work done in the tunnel, such as shotcreting and grouting. Grouting has a large impact on the hydraulic resistance around the tunnel periphery. A concept of how to model the hydraulic resistance on a site scale groundwater flow model was outlined in *Section 3.2.1*.

This chapter presents the attempts to describe the hydraulic resistance around the tunnel periphery in somewhat more detail than was used in the site scale groundwater flow model. The purpose of the predictions was to test the ability to predict the flow distribution around the tunnel periphery.

8.2 METHODOLOGY FOR TESTS OF CONCEPTS AND MODELS

8.2.1 Prediction methodology

The predictions of the inflow distribution around the tunnel periphery were based on numerical groundwater simulations */Liedholm, 1991b (TN 26)/*. However, some modifications were made on the basis of expert judgement,

because the numerical groundwater simulations were generic. Predictions were made for the inflow through the roof, walls and floor.

8.2.2 Methodology for determining outcome

The inflow distributions were estimated from the mapped inflow rates on the tunnel walls and roof and the total flow into the tunnel. It was only possible to separate the flow into the floor and walls + roof. It was not possible to measure the inflow rates for individual hydraulic conductor domains as no dams were constructed surrounding individual domains (see *Chapter 3* for more details concerning the measurement made using the dams in the tunnel). The mapping procedure of the inflow is described in more detail in *Rhén et al /1994a/*, where the re-mapping of the inflow in 1994 is also presented. Details of the outcome for each tunnel section in the predictions are shown in *Rhén et al /1993a, c, 1994a/*.

8.3 COMPARISON OF PREDICTED AND MEASURED ENTITIES

Flow mapping close to tunnel face during construction

Tunnel section 700-1475 m

The mapped inflow rate through the walls and roof were approximately 470 l/min and the total inflow rate approximately 1300 l/min. About 65% of the inflow of water is estimated to leak through the floor. The prediction was 30% from the floor, 25 + 25% from the walls and 20% from the roof.

Tunnel section 1475- 2265 m

The mapped inflow rates through the walls and roof were approximately 125 l/min and the total inflow rates approximately 209 l/min, shafts excluded. About 40% of the inflow of water is estimated to leak through the floor. The prediction was 30% from the floor, 25 + 25% from the walls and 20% from the roof.

Tunnel section 2265- 2875 m

The mapped inflow rates through the walls and roof were approximately 35 l/min and the total inflow rates approximately 139 l/min, shafts excluded. According to the ordinary mapping approximately 75% of the inflow of water is estimated to leak through the floor. The prediction was 30% from the floor, 25 + 25% from the walls and 20% from the roof .

Supplementary flow mapping 1994

The flow into tunnel section 1584 - 2496 m was mapped in July 1994 to obtain a better estimate of flow distribution around the tunnel periphery. The result is shown in *Figure 8-1*. Although the floor is just about 25% of the tunnel circumference, 43% of the flow into the tunnel occurs through the floor. This is an indication of a local change in the hydraulic conductivity around the tunnel due to the excavation. Since the difference in hydraulic potential is approximately constant between the water table and points around the tunnel circumference, with the tunnel deep down under the water table, the flow distribution around the tunnel periphery would be evenly distributed if the hydraulic conductivity were the same near the tunnel as in the undisturbed rock mass /Liedholm, 1991b (TN 26) /. In *Figure 8-2* the flow rate is divided among tunnel sections between measuring dams in the tunnel. The general picture of the flow rate distribution around the tunnel circumference is rather different for the different sections, although the flow through the floor dominates in most cases (flow/m²). It can also be seen in *Figure 8-2* that the measured/estimated flow rates during the first mapping are larger 4 times out of 6, compared with the measurements made in July 1994. The reasons for this may be reinforcement and clogging of fractures. The reason for the flow rate increase may be that the pre-grouted rock has begun to leak more than when the tunnel face passed the section.

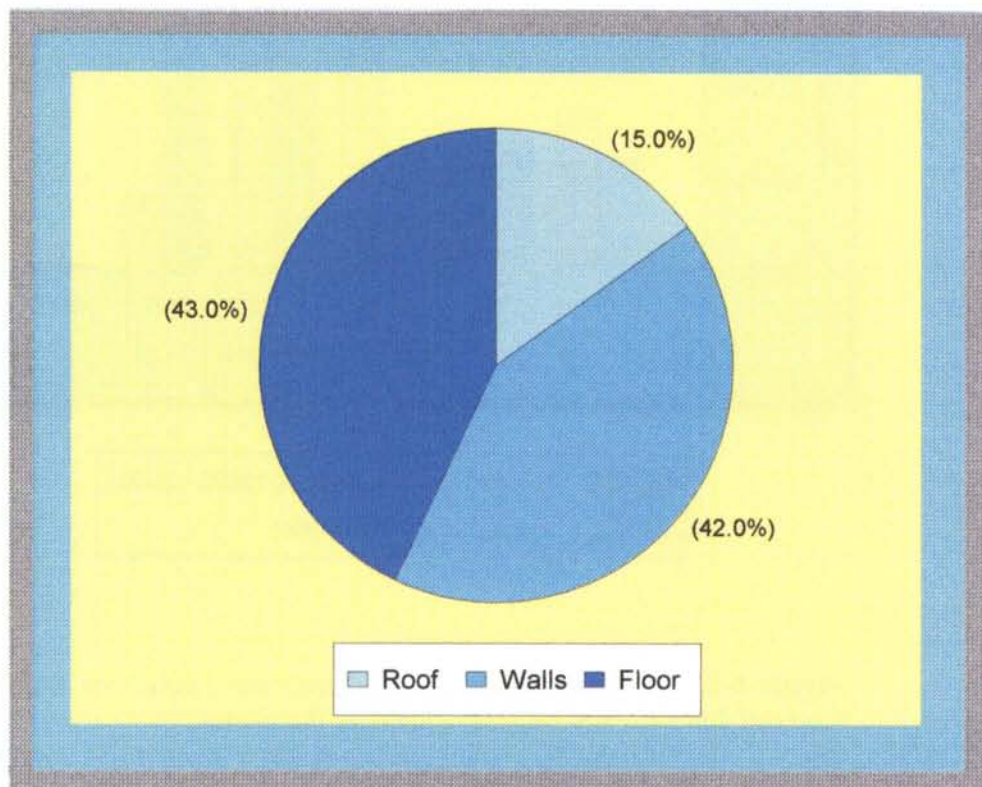


Figure 8-1. *Distribution of flow rates through the roof, walls and floor for tunnel section 1584 - 2496. Measurement, July 1994.*

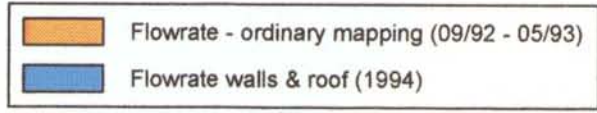
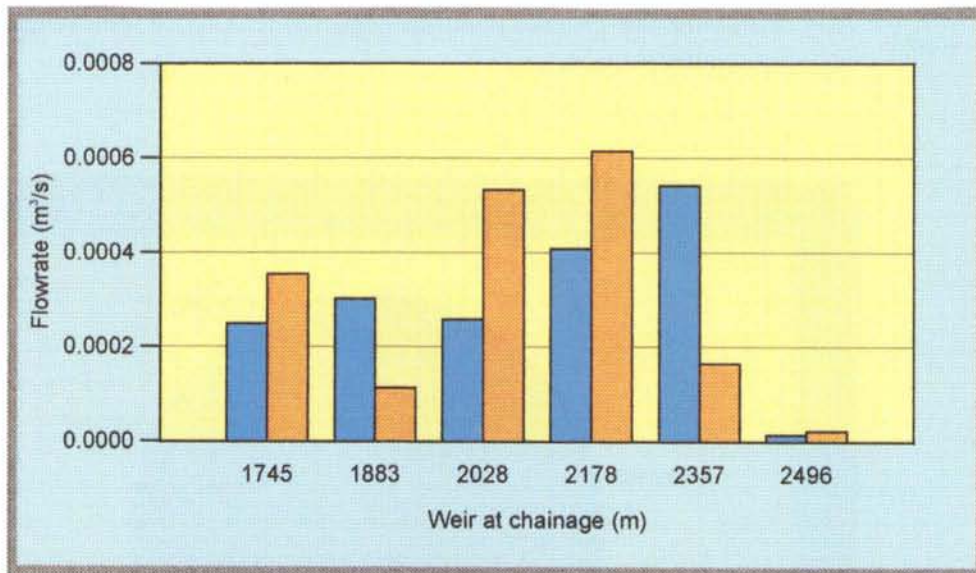
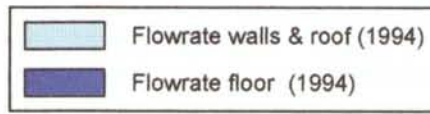
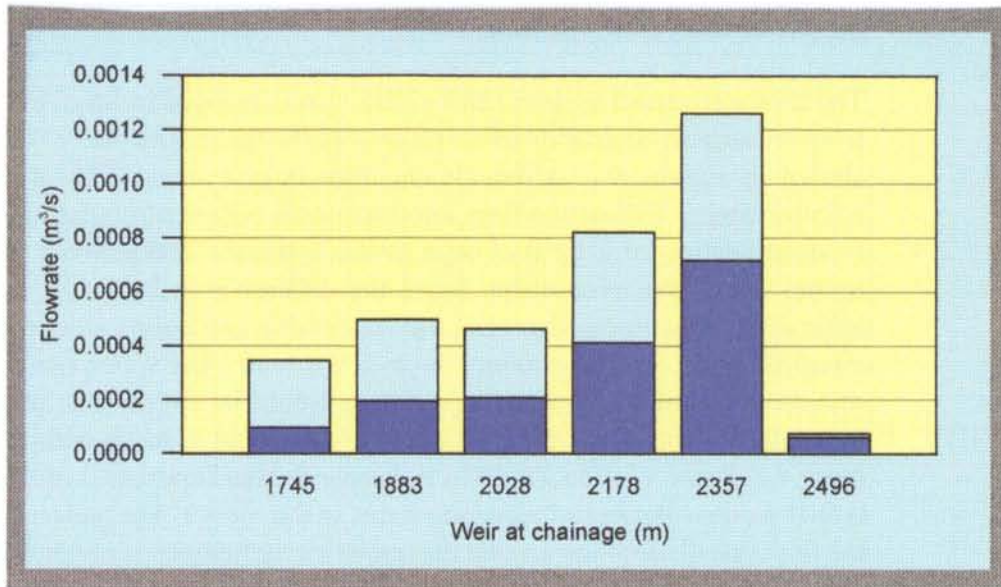


Figure 8-2. Distribution of flow into the tunnel for tunnel sections between dams for flow measurements in the tunnel.

Top : Measurements from July 1994. Flow rate through the walls and roof (Q_{w+r}) based on estimated or measured flows from fractures. The flow rate through the floor (Q_F) was calculated as the total flow into the tunnel section measured at a weir (Q_{TOT}) minus Q_{w+r} . The total height of the bars are thus $Q_{TOT}/\rho h$ et al, 1994a/.

Bottom: Flow rate through the roof and walls (Q_{w+r}) from July 1994 and during ordinary mapping February 1992 to May 1993 /Rhén et al, 1994a/.

8.4 SCRUTINY AND EVALUATION

The main part of the flow into the tunnel is from the floor, according to both the predictions and outcome, but the proportion of the flow rate coming through the floor is greater than predicted. One reason for this is of course that the tunnel floor is more damaged than the walls and roof due to blasting and also that the effect of the grouting may be different in the floor than in the walls and roof, thereby permitting a large inflow through the floor. The blasting design, with larger charges in the lifter holes, also indicates that the damage should be greater in the floor than in the walls and roof. The different extents of the damaged zone in the floor compared with the walls has been confirmed in the a project called ZEDEX /*Olsson et al, 1996*/. As was shown in *Liedholm /1991b (TN 26)*/ there will also be an increased flow rate through the floor if there is an general increase in the hydraulic conductivity all-around the tunnel periphery, compared with the hydraulic conductivity of undisturbed rock mass, due to gravity effects.

One other possible reason for the above may be that the observed flow rate through the walls has been underestimated. It is difficult to estimate the inflow seen on walls. However, in 1994 great efforts were made to try to measure the flow rates from the walls and roof accurately, and it is felt that the differences between the floor and walls + roof shown in *Figures 8-1 and 8-2* are approximately correct. It should, however, also be noted that there are rather large differences in the flow distribution in different tunnel sections (see *Figure 8-2, Top figure*). (It should be mentioned here that in the site scale groundwater model the tunnel was not simulated with any differences in the hydraulic conductivity around the tunnel periphery. Predictions shown in this chapter were made as scoping calculations for a tunnel with a cross section like the one planned for the Äspö tunnel.)

The estimates of the flow distribution around the tunnel periphery made in 1994 are more reliable than those based on the ordinary mapping during construction. The reason is that the leakage measured (or estimated) during construction was mapped close to the tunnel face and the total inflow into the tunnel for each tunnel section was measured later when this became possible. As the measurements were not made at the same time, the leakage in from the walls and roof may have been reduced by the use of shotcrete and supplementary grouting. There are differences between the mapped flow rates for the same tunnel sections for the two different occasions (see *Figure 8-2, Bottom figure*). However, it is judged that the inflow proportions between the floor and walls + roof are probably fairly correct even for the construction phase.

Conclusions

On the average the main part of the flow into the tunnel is from the tunnel floor, which indicates that the hydraulic properties are different around the tunnel periphery. However, there are rather large variations in the flow distribution on the floor, walls and roof along the tunnel, and there seems to be a more even flow distribution around the tunnel periphery along tunnel sections with low inflow rates.

9 SUBJECT: AXIAL FLOW IN DISTURBED ZONE - BLOCK SCALE

9.1 SCOPE AND CONCEPTS

Section 8.1 contains an outline of the concepts behind the EDZ (Excavation Disturbed Zone). As was mentioned there the disturbed zone may provide a preferential pathway for radio nuclide transport, and is therefore of interest in performance assessments.

The purpose of the predictions was to test the ability to predict the pressure distribution around the tunnel and the axial flow along the tunnel near to the tunnel.

9.2 METHODOLOGY FOR TESTS OF CONCEPTS AND MODELS

9.2.1 Prediction methodology

The pressures around tunnel were calculated for the grouted and non-grouted rock mass. Prediction of the pressure distribution around the tunnel was based on numerical groundwater flow simulations and the pressure was calculated for a point 10 m from the tunnel centre line.

Axial flows in the disturbed zone were obtained from scoping calculations according to *Gustafson et al /1991/*.

9.2.2 Methodology for determining outcome

Pressures around the tunnel were derived from pressure measurements in the probe holes. The distribution of probe holes along the tunnel is shown in *Chapter 1*. All probe holes were divided into three rock categories based on the geological mapping of the tunnel:

- 1 rock (normal rock)
- 2 increased fracturing (areas with increased fracturing)
- 3 fracture zone (tectonic zone)

For definitions of 'fracture zone' and 'increased fracturing' see *Stanfors et al /1997b/*. If the probe hole did not penetrate a 'fracture zone' or rock mass was mapped as 'increased fracturing' the results from the probe hole were assumed to represent 'normal' rock, here called 'rock'.

All probe holes were also divided into grouting and reinforcement categories:

- 1 No grouting or reinforcement
- 2 Pre-grouting
- 3 Shotcrete and/or supplementary grouting
- 4 Pre-grouting and shotcrete and/or supplementary grouting

In the plots in *Section 9.3* 'reinforced' means that the probe holes belong to one of the categories 2-4.

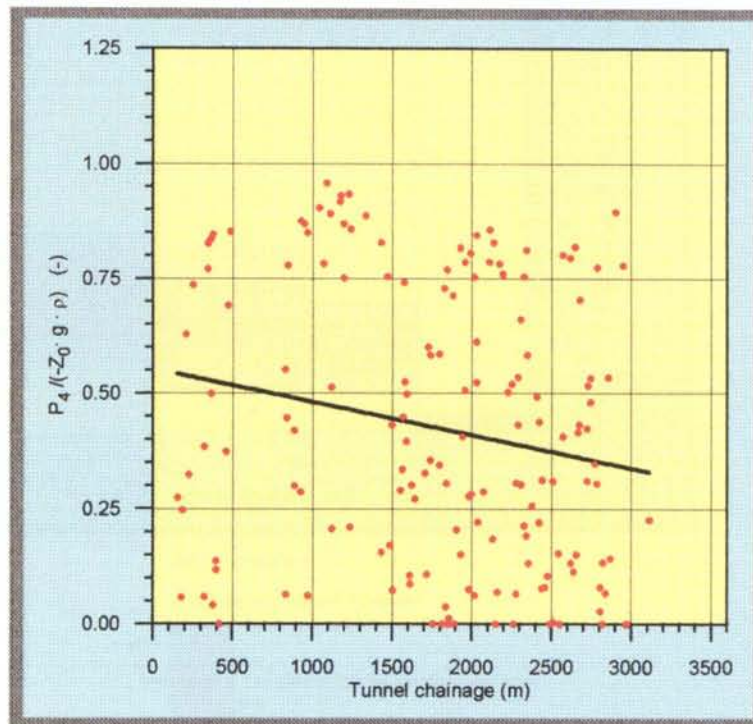
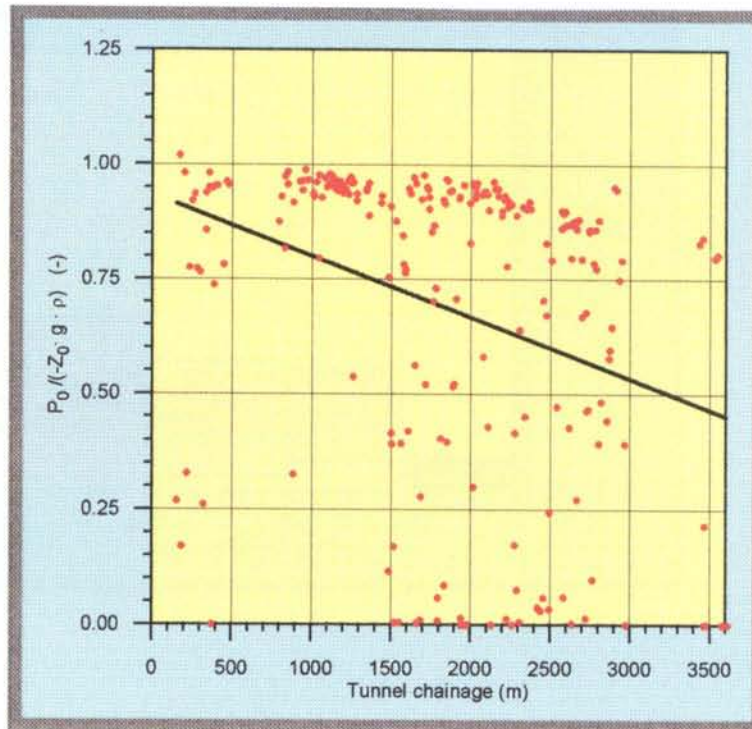
The packer was generally installed about 5 m into the borehole and the borehole depth was generally about 20 m. In order to estimate the pressure distribution around the tunnel it was necessary to estimate a representative point along the borehole for the measured pressure. The flow rate distribution along the borehole and the borehole direction relative to the tunnel centre line were used to estimate the point of application (see *Rhén et al /1994a/* for details). The flow field towards the tunnel was assumed to be approximately radial, and because of this assumption a linear fit between pressure and Log_{10} (radial distance from tunnel centre) line was used to estimate the pressures outside the tunnel.

No attempts were made to measure the axial flow during the construction period.

9.3 COMPARISON OF PREDICTED AND MEASURED ENTITIES

The parts of the tunnel which have been pre-grouted, subjected to supplementary grouting, sealed with shotcrete or reinforced are shown in detail in *Stanfors et al /1993a, b, 1994/* and overview is shown in *Figure 1-14*.

The water pressures in the probe holes were measured approximately twice a year, and the measurements show that on the average the pressure is slowly decreasing with time (see *Rhén et al /1994a/*). The measurements also show that the variability of the pressure is high, from zero pressure up to nearly hydrostatic, due to the heterogeneity of the rock-mass (see *Figure 9-1*). The statistics for pressures in probe holes classified as representing 'Non-reinforced rock' and 'Reinforced rock' are shown in *Figure 9-2*. The representative point for the pressures was generally estimated to be between 8 and 12 m from the tunnel centre line (5-9 m outside the tunnel wall). Detailed presentation of the results is found in *Rhén et al /1994a/*. *Table 9-1* shows the prediction and outcome.



● Pressure divided by hydrostatic pressure

— Linear regression of relative pressures

Figure 9-1. Relative water pressure outside the tunnel wall. The line in the figure is a linear regression of the relative pressures as a function of tunnel chainage. z_0 = the level of the borehole below sea level, $\rho = 1000 \text{ kg/m}^3$. Data from tunnel section 0-3600 m. Pressure measured in February 1995.

Top: Pressure ahead of tunnel face (2-16 m) measured during excavation.

Bottom: Pressure measured in February 1995.

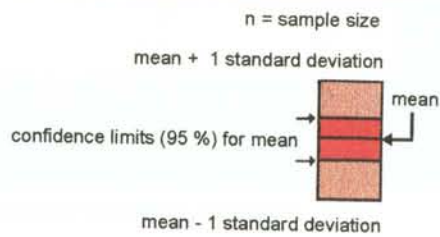
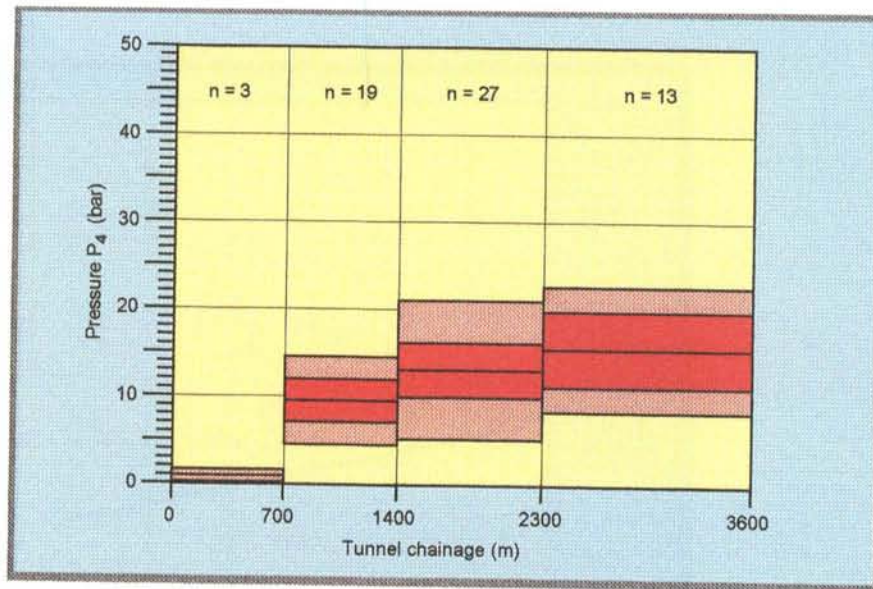
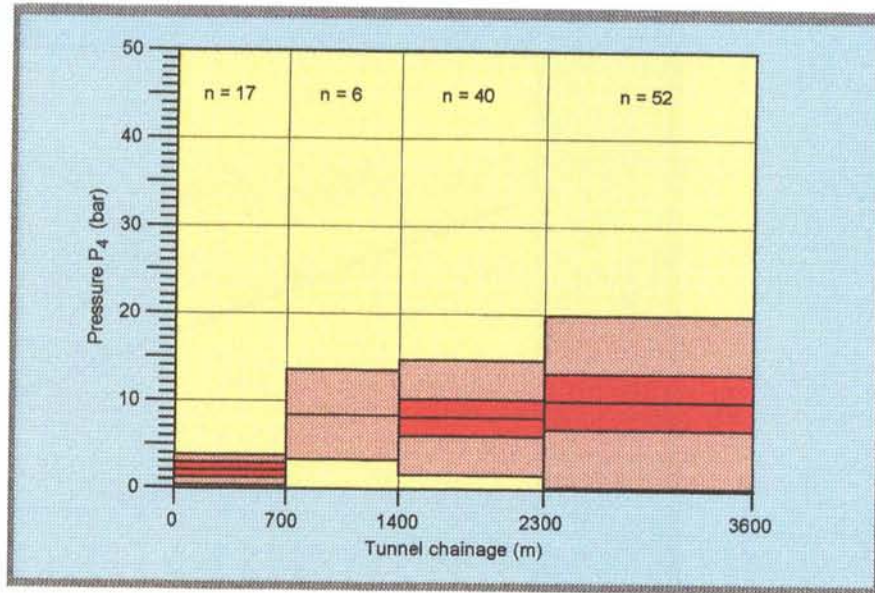


Figure 9-2. Water pressure outside the tunnel wall. Data: tunnel chainage 0-3600 m. Pressure measured in February 1995.

Top: Pressure - Non-reinforced rock. Standard deviation and confidence limits for mean.

Bottom: Pressure - Reinforced rock. Standard deviation and confidence limits for mean.

Table 9-1. Outcome and prediction of pressures around the tunnel. Data from tunnel section 700 - 2875 m. The pressure is estimated for a point $r = 10$ m from the tunnel centre line. /Rhén *et al*, 1993a, c, 1994a/.

Rock mass- grouted	Pressure (P)	
	Prediction Range (kPa)	Outcome Point estimate* (kPa)
No	50 - 500	700
Yes	500 - 2000	1200

* estimated from a least-square fitted line passing through $r = 3$ m $P = 0$ kPa in a $\ln(P)$ - $\log(r)$ diagram.

9.4 SCRUTINY AND EVALUATION

The pressure in conductive structures intersecting the tunnel was approximately as predicted for the grouted and shotcrete-covered rock mass, but higher than predicted for rock mass which was not grouted and not covered with shotcrete.

Conclusion

The pressure measurements clearly show the heterogeneity of the rock mass. They indicate that there is a sparsely connected fracture network in the rock mass, otherwise the pressure distribution would have been much more regular. The measurements also show that high water pressures occur rather frequently just a few metres from the tunnel wall. Close to the tunnel face during excavation the variability of the pressures is about the same as for outside the excavated tunnel, see *Figure 9-1*, but the absolute pressure is higher /Rhén *et al*, 1997/. This variability of the pressure affects the possibility of grouting the fracture system close to the tunnel.

Another evident conclusion is that large samples are needed to obtain a reliable estimate of the pressure distribution near the tunnel. In order to obtain better resolution of the pressure increase outside the tunnel wall several measurement sections in each borehole would also have been preferred. This would have provided a more certain definition of a representative point for the pressure measurements. But this would also have been more expensive as it would have been necessary to use a more complicated packer system.

The pressures were higher in the rock that had been reinforced compared with the non-reinforced rock. This clearly indicates that there is a difference in the hydraulic resistance around the tunnel (called skin factor or skin effect in some of the chapters), and that a large part of the resistance must be within a few metres (5-9 m) of the tunnel, considering the representative point for the pressure measurements.

10 SUBJECT: HYDRAULIC CONDUCTIVITY - DETAILED SCALE

10.1 SCOPE AND CONCEPTS

As was noted in *Chapter 2* the hydraulic rock mass domains are geometrically defined volumes in space with properties that differ from those of surrounding domains (rock mass domains and hydraulic conductor domains) and they may either be defined by lithological domains or purely by interpretation of results from hydraulic tests.

The material properties chosen for the hydraulic rock mass domains are:

- Hydraulic conductivity ($K(x,y,z)$)
- Specific storage ($S_s(x,y,z)$).

K is based on evaluation of transient hydraulic tests. Based on the geological documentation, each hydraulic test is classified to find which tests that can be considered representative of each of the lithological units defined in the geological model. The evaluated hydraulic properties for each unit and the geological model form basis for deciding whether or not lithological units should be used as a base for the division of the rock mass into hydraulic rock mass domains.

The properties of a hydraulic rock mass domain are given as a stochastic distribution for the domain. The distribution of K is assumed to be lognormal with characteristic values K_g (geometric mean) and $s_{\text{LOG}_{10}K}$ (standard deviation of $\text{Log}_{10}(K)$). K_g and $s_{\text{LOG}_{10}K}$ are scaled according to the cell size in the numerical model (see *Wikberg et al/1991/* for scale function used in the predictions). No spatial correlation is assumed.

The specific storage values (S_s) for the hydraulic rock mass domains were not predicted and are therefore not discussed in the text below.

The purpose of the predictions was to test the ability to predict the hydraulic properties of the lithological units.

10.2 METHODOLOGY FOR TESTS OF CONCEPTS AND MODELS

10.2.1 Prediction methodology

The prediction of the point estimate, the confidence interval of the point estimate and the standard deviation of the hydraulic conductivity were based on data from KAS02-08 /*Liedholm /1991b /TN 29/*. The point estimates were chosen as the median values which were the same as the geometric mean

values for Småland granite and fine-grained granite but somewhat less than the geometric mean for Äspö diorite and greenstone. (All distributions used for the predictions are truncated due to measurement limits, but the truncation does not cause any problem when fitting a lognormal distribution for fine-grained granite and Småland granite. Estimation of the characteristic lognormal parameters for the other rock types is more difficult because of truncation and a partly non-lognormal shape.)

10.2.2 Methodology for determining outcome

The hydraulic conductivities of the four lithological units, Småland granite (P5-01), Äspö diorite (P5-02), greenstone (P5-03) and fine-grained granite (P5-04) were estimated from tests in probe holes and core holes drilled along tunnel section 700 - 2875 m. Tests where more than 80% (Q_2) of the total documented flow (Q_{TOT}) into the borehole was situated in one lithological unit were used as a representative test for the lithological unit. The test section length (L_2) was estimated as the mapped length along the borehole of the lithological unit with $Q_2 \geq 80\% \cdot Q_{TOT}$. The hydraulic conductivity was estimated at:

$$K_2 = \frac{T}{L_2}$$

where T is the evaluated transmissivity of the entire test section. For details of the pressure build-up test and scaling of the hydraulic conductivity, see *Chapter 2*.

10.3 COMPARISON OF PREDICTED AND MEASURED ENTITIES

Prediction and outcome are shown in *Figure 10-1* and *Table 10-1*. All data from the probe holes that met the conditions mentioned in *Section 10.2.2* were used for the calculation of the outcome. As the predictions were based on the entire data set available from the cored boreholes and not related to any specified depth interval, the entire data set from tunnel section 1475-2875 m was also used for the outcome. (In the case of greenstone, tunnel section 700-2875 m was used to provide a few more samples, see *Table 10-1*). This is probably rather acceptable as most of the tests in the cored boreholes are from a depth of 100 to 500 m, and the corresponding depth interval in the tunnel for samples taken between tunnel sections 1475 and 2875 m is 200 m to 400 m. As can be seen in *Table 10-1* the prediction is quite different from the outcome for tunnel section 700-1475 m. The reasons for this have already been discussed in *Chapter 2*. The comparison in *Figure 10-1* is therefore based on data from tunnel section 1475-2875 m for three of the lithological units.

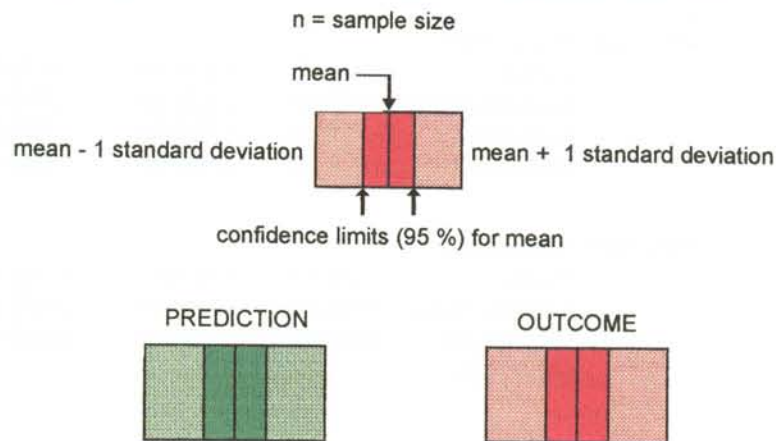
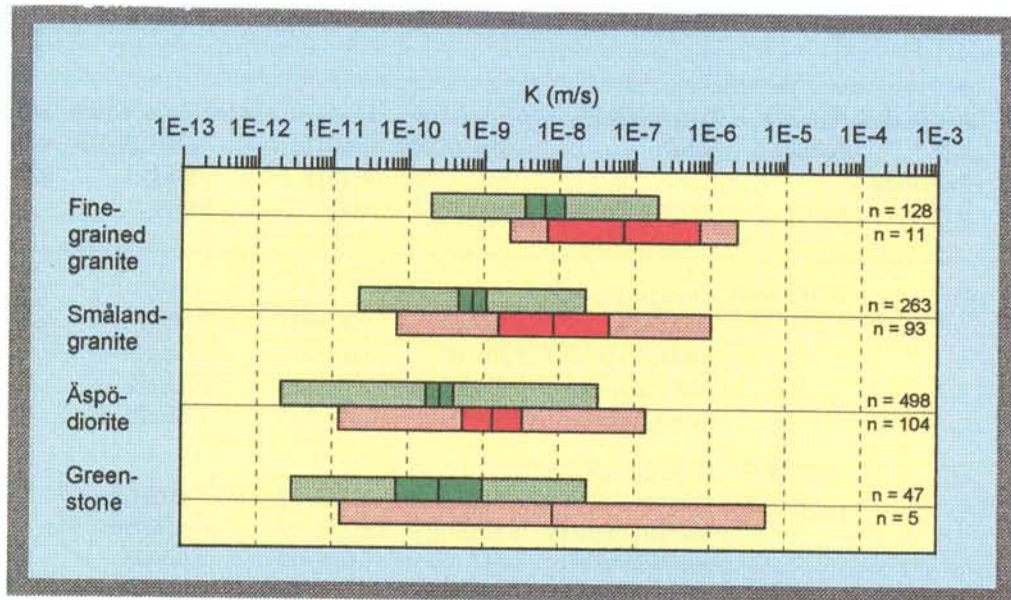


Figure 10-1. Hydraulic conductivity for different rock types along the tunnel. Detailed scale. Test scale 14 m. The outcome shown is for tunnel section 1475-2875 m except for greenstone which is for tunnel section 700-2875 m (mean = arithmetic mean of $\text{Log}_{10}(K)$, standard deviation = Standard deviation of $\text{Log}_{10}(K)$, n = sample size).

Table 10-1 Hydraulic conductivity (K) at detailed scale. Test scale = 14 m.

Prediction = P Outcome = O	Tunnel section (m)	Lithological unit	Geometric mean (GM) (m/s)	Lower Conf. limit 2.5% (GM) (m/s)	Upper Conf. limit 97.5% (GM) (m/s)	Standard dev. s(Log ₁₀ (K))	Sample size
P	0700-3854	Fine-grained granite	6.3E-09	1.5E-09	2.6E-08	1.5	128
		Småland granite	7.0E-10	4.6E-10	1.1E-09	1.5	263
		Åspö Diorite	2.6E-10	1.1E-10	6.1E-10	2.1	498
		Greenstone	2.6E-10	1.8E-11	3.7E-09	1.95	47
O	700-1475	Fine-grained granite	7.59E-06	7.98E-07	7.36E-05	1.63	13
		Småland granite	1.86E-06	5.37E-07	6.45E-06	1.37	27
		Åspö Diorite	4.68E-07	1.09E-07	2.0E-06	1.6	27
		Greenstone	1.15E-05	9.6E-09	1.4E-02	1.14	2
O	1475-2265	Fine-grained granite	4.37E-08	5.24E-10	3.63E-06	1.83	6
		Småland granite	2.86E-08	2.82E-09	2.95E-07	2.1	19
		Åspö Diorite	5.89E-09	1.71E-09	2.02E-08	1.94	53
		Greenstone	8.39E-09	2.69E-12	2.66E-05	2.82	5
O	2265-2875	Fine-grained granite	1.22E-07	8.4E-09	1.76E-06	0.934	5
		Småland granite	1.59E-09	1.04E-10	2.45E-08	2.06	14
		Åspö Diorite	2.59E-10	6.59E-11	1.02E-09	2.12	51
		Greenstone					0
O*	700-2875	Fine-grained granite	8.8E-07			1.58	24
		Småland granite	9.5E-08			1.79	60
		Åspö Diorite	4.3E-09			1.95	131
		Greenstone	6.6E-08			2.57	7
O*	1475-2875	Fine-grained granite	7.0E-08			1.50	11
		Småland granite	8.4E-09			2.08	33
		Åspö Diorite	1.3E-09			2.03	104
		Greenstone	8.39E-09			2.82	5

* Pooled estimates of \bar{x} and s where \bar{x} and s are based on Log₁₀(K):

$$\bar{x} = \frac{\sum_{i=1}^N \bar{x}_i \cdot n_i}{\sum_{i=1}^N n_i}$$

$$s^2 = \frac{\sum_{i=1}^N ((n_i - 1) \cdot s_i^2)}{\sum_{i=1}^N (n_i) - i}$$

\bar{x}_i mean value for sample i
 s_i standard deviation for sample i
 n_i Sample size within sample i
 N Sample size

10.4 SCRUTINY AND EVALUATION

Discussion

Tunnel section 700-1475

The predictions of the hydraulic conductivity for each lithological unit were poor, for the reasons pointed out in *Section 2.4*. The rock mass along tunnel section 700-1475 was much more fractured and conductive than the rock mass below Äspö island, and the predictions were based on Äspö data from Äspö island.

Tunnel section 1475-2875 m

The predictions of the hydraulic conductivity for each lithological unit were somewhat less good than the predictions of the hydraulic conductivities along the tunnel presented in *Chapter 2*. However, the relative relationship between the lithological units is almost the same in the prediction and outcome (see *Figure 10-1*).

Conclusions

The relative relationship between the lithological units is almost the same in the prediction and outcome, in spite of the uncertainties coupled to the anisotropic conditions and different test scales for the hydraulic tests! The predicted hydraulic conductivities were somewhat smaller than the outcome, most probably due to the anisotropic conditions at Äspö. The influence of anisotropy makes it difficult to compare the predictions with the outcome, and it can be concluded that it is important to take anisotropy into account in the future investigations (see *Chapter 2* for further comments).

There is a need for large samples if the statistical properties are to be estimated for a variable with large variance. On the detailed scale all tests have been divided among four main lithological units, which decreases the number per lithological unit. Some of the lithological units are also less frequent along the tunnel, which makes the samples even smaller for them (fine-grained granite and greenstone). Another problem is of course that some of the tested borehole sections contain several lithological units and the leakage into the borehole comes from more than one of them, and thus, the evaluated transmissivity cannot be connected to one particular lithological unit alone. This reduces the sample size that can be included in the statistics. This problem is greater for the probe holes and coreholes (test scale approximately 10-20 m) along the tunnel compared with the injection tests at the 3-m scale.

Another problem is the length that should be used to estimate the average hydraulic conductivity. The approach used gives a somewhat higher average hydraulic conductivity for the lithological unit sampled compared with the hydraulic conductivity estimated for tunnel section 2265 - 2875 m, where the total test length was used. However this only introduce a small bias.

A third problem is the transformation of the hydraulic conductivity from one test scale to another. The transformation may give some bias, and therefore not entirely comparable prediction and outcome values (see *Chapter 2* for further comments).

11 SUBJECT: POINT LEAKAGE - DETAILED SCALE

11.1 SCOPE AND CONCEPTS

The geological model at detailed scale comprises the lithological units and their characteristics in the form of mineral composition, density, matrix porosity, fracture frequency, fracture orientations, fracture lengths, fracture spacing and fracture infillings. The geohydrological model at detailed scale comprises the geohydrological characteristics of the lithological units, where hydraulic conductivity was presented in *Chapter 10*. Other geohydrological characteristics that can be described are the hydraulic properties of the fractures. Although the EDZ (Excavation Disturbed Zone) can be expected to control the flow pattern closest to the tunnel, an attempt was made to describe the expected flow patterns and rates that could be expected to be observed on the tunnel walls and roof for the different lithological units, based on the geological description and expert judgement. The flow pattern and rates were expected to be linked to the fracture pattern and the expected flow properties of the fractures for each lithological unit.

Thus, the predictions were made to test the ability to describe the general flow characteristics at the detailed scale, as seen on the tunnel walls and roof, of rock types identified.

11.2 METHODOLOGY FOR TESTS OF CONCEPTS AND MODELS

11.2.1 Prediction methodology

Predictions of the wet tunnel area and inflow characteristics were made for the lithological units Småland granite, Äspö diorite, greenstone and fine-grained granite. The predictions were mainly based on expert judgement /*Gustafson et al, 1991*/, but in *Axelsson et al /1990/* some indications of the flow distribution on the tunnel periphery were also given.

11.2.2 Methodology for determining outcome

The lithological units, rock boundaries, fracture properties and water-bearing structures were mapped for every blasting round. For each water-bearing object the flow rate was estimated or measured. Each object was also classified into one of three characters (1: patch of moisture, sporadic drips, 2: drips, 3: flows) and five types (1: diffuse, 2: point, 3: node, 4: extensive, 5: bolt hole). An object was mapped as 'diffuse' when it was not possible to identify where the water came from or, if it was a fracture, the part of the fracture that was leaking. In these cases the wet area was documented. When the object was

mapped as 'node' there was a point leakage in the intersection between two fractures. If the inflow was mapped as 'extensive' the inflow was spread over a part of the fracture length. This length was documented. If there were several observations documented as 'point', 'node' or 'extensive' inflows along a fracture, they were documented as separate objects.

Details of the outcome are presented in *Rhén et al /1993a, c, 1994a/ and Rhén and Stanfors /1995/*.

11.3 COMPARISON OF PREDICTED AND MEASURED ENTITIES

The outcomes and predictions are shown in *Figures 11-1 to 11-3*.

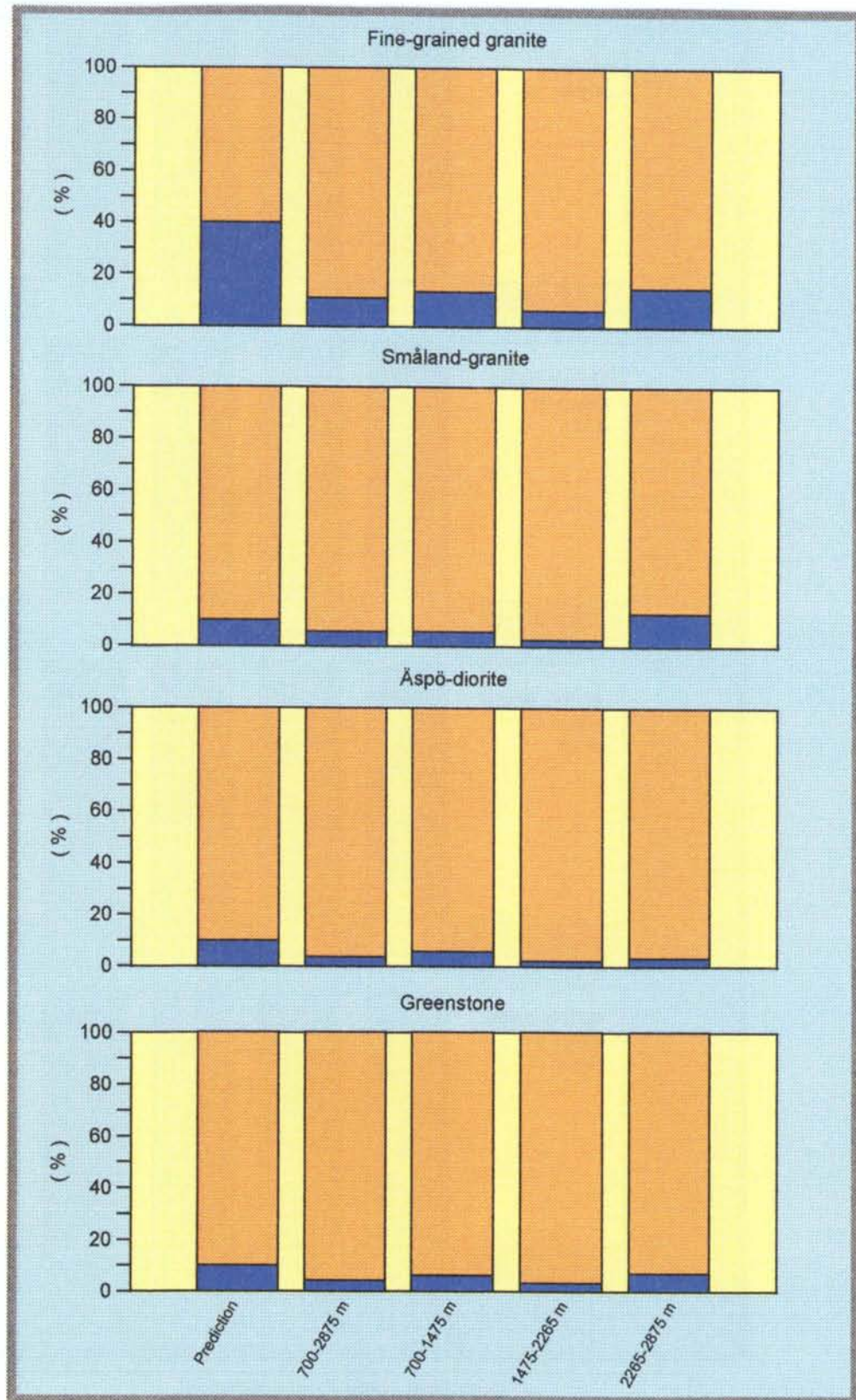


Figure 11-1. The outcome and prediction of wet tunnel area for different rock types. Data from tunnel section 700 - 2875 m. The prediction was given for the entire tunnel. In the figure above the outcome for tunnel section 700-2875 m should be compared with the prediction. The outcome is also shown for tunnel sections 700-1475 m, 1475-2265 m and 2265-2875 m.

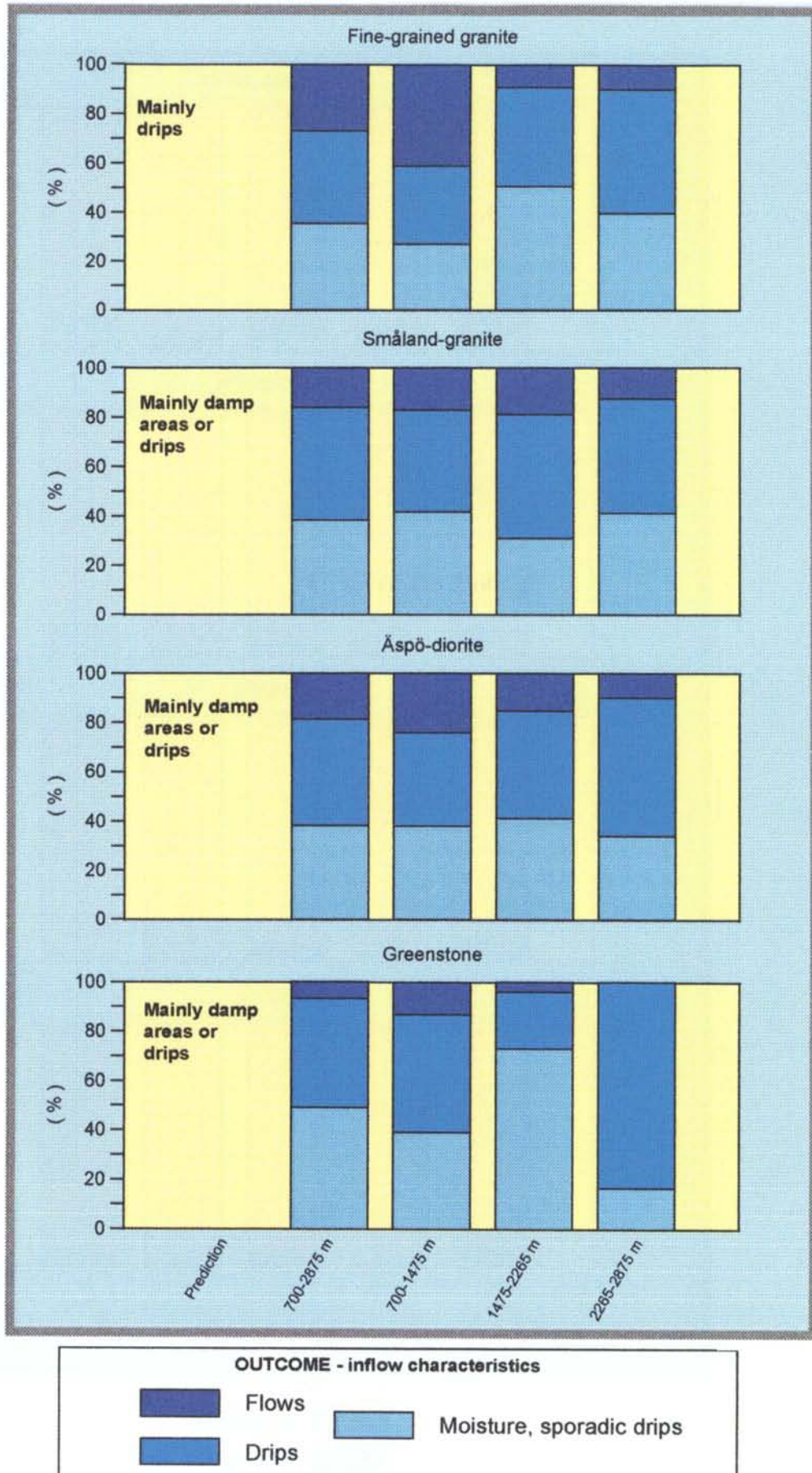


Figure 11-2. The outcome and prediction of inflow characteristics along tunnel section 700 - 2875 m. The prediction was given for the entire tunnel. In the figure above the outcome for tunnel section 700-2875 m should be compared with the prediction. The outcome is also shown for tunnel sections 700-1475 m, 1475-2265 m and 2265-2875 m.

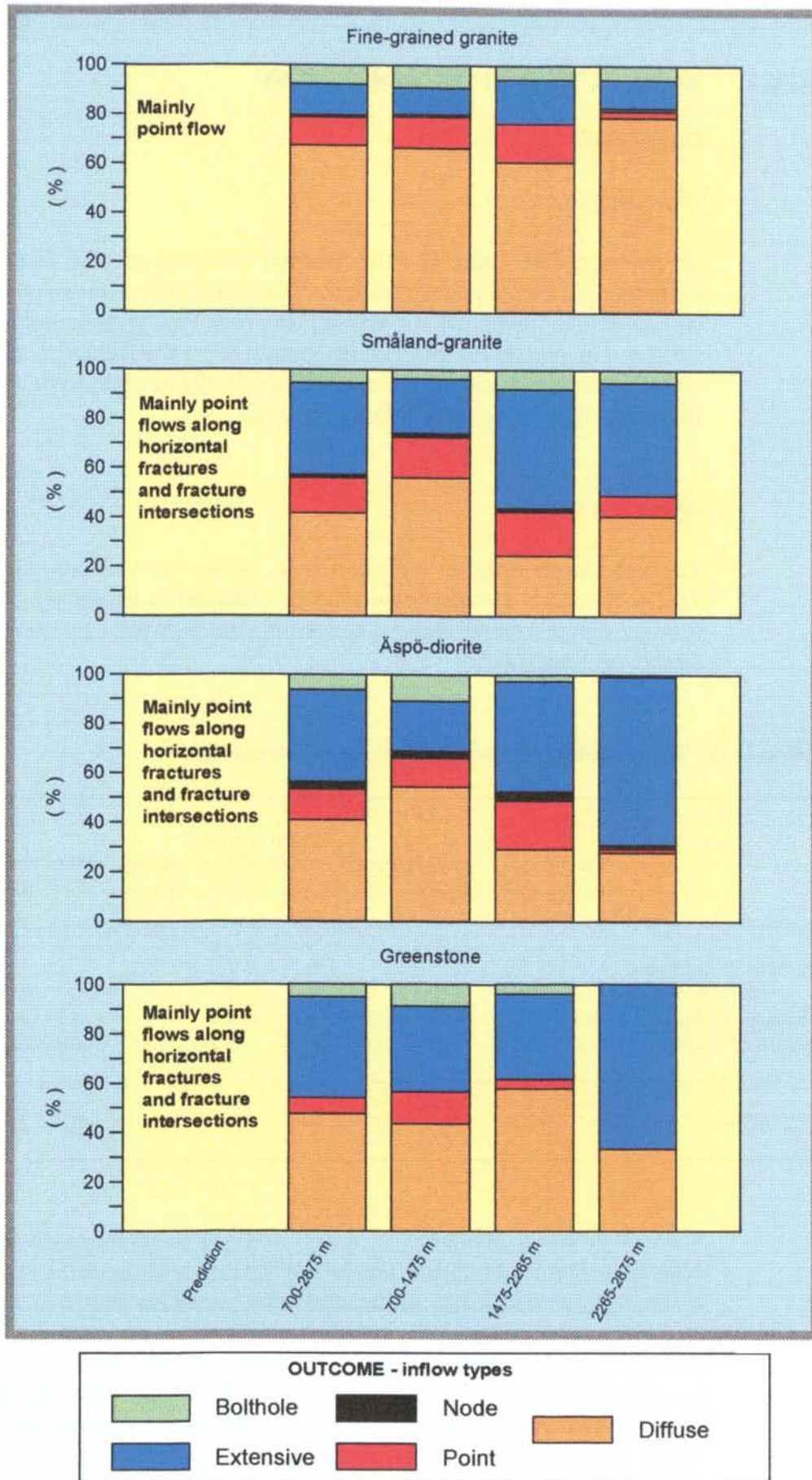


Figure 11-3. The outcome and prediction of inflow types along tunnel section 700 - 2875 m. Type 1, 'Diffuse'. Water leaking from an area that cannot be associated with a fracture. Type 2, 'Point': One distinct leaking spot. Type 3, 'Node': Point leakage at the intersection between two fractures. Type 4, 'Extensive': Inflow spread over a part of the fracture length. Type 5, 'Bolt hole': Leakage from a bolt hole.

11.4 SCRUTINY AND EVALUATION

Discussion

Wet tunnel area

As can be seen in *Figure 11-1* the observed wet area is smaller than predicted, except for Småland granite in tunnel section 2265-2875 m. Fine-grained granite was dryer than predicted but was still the rock type with the largest wetted surface. The reason for fine-grained granite being the wettest is that it is the most fractured rock and there is no tendency for the fractures to be sealed more frequently than in the other lithological units.

Inflow character

The outcome corresponds to predictions as can be seen in *Figure 11-2*. *Figure 11-2* is based on the **number of objects mapped** in the tunnel. The results from the mapped tunnel sections concerning the flow rates are summarized in *Tables 11-1* and *11-2*.

Table 11-1. Total estimated mapped inflow, by character.

	Tunnel section									
	700-1475 m		1475-2265 m		2265-2874.6 m		2874.6-3600 m		700-3600 m	
	(l/min)	(%)	(l/min)	(%)	(l/min)	(%)	(l/min)	(%)	(l/min)	(%)
Character 1 (moisture, sporadic drips)	2.6	0.6	4.1	3.3	0	0	0	0	6.7	0.9
Character 2 (drips)	79.9	17.0	16.1	12.9	8.6	24.9	6.2	5.2	110.8	14.8
Character 3 (flows)	387.0	82.4	104.4	83.8	26.0	75.1	112.1	94.8	629.5	84.3
Total inflow	469.5	100	124.6	100	34.6	100	118.3	100	747.0	100

The total inflow is dominated by 'flows' (84%) although they account for only 22% of the number of objects mapped. If the inflow is divided by the number of objects of each character the mean inflows become as shown in *Table 11-2*.

As can be seen in *Table 11-1* and *11-2* there are differences in relationships between the characters for different tunnel sections. One reason for this is that the mapping procedure has become more consistent, particularly after approximately tunnel section 2000 m. As the time for mapping was limited, all the geological and hydrological documentation has to be very effective. As regards the geohydrological mapping the flow rate was only measured occasionally.

Table 11-2. Estimated average inflow from a single mapped object, by 'character' type.

	Tunnel section				
	700-1475 m (l/min)	1475-2265 m (l/min)	2265-2874.6 m (l/min)	2874.6-3600 m (l/min)	700-3600 m (l/min)
Character 1 (moisture, sporadic drips)	0.01	0.02	0	0	0.011
Character 2 (drips)	0.3	0.08	0.05	0.065	0.146
Character 3 (flows)	2.0	1.5	0.6	1.335	1.648

When a fracture or area was dripping the number of drips per minute was counted. Several tests in the tunnel (by actual measuring of the flow rate) demonstrated that each drop contains 0.25 ml water (experiments with tap-water gave 0.23 - 0.24 ml), and this value was used to estimate the flow rate.

The reason for character 1 having no flow in tunnel section 2874.6 - 3600 m is that 'sporadic drips' was not clearly defined and all drips were mapped as character 2. Discussions late in 1994 resulted in the suggestion that four or less drips per minute could be regarded as 'sporadic drips'.

If the flow rates for character 2 in *Table 11-2* are compared with the measured average volume for a single drop of 0.25 ml, it is found that the mean value of drips per minute becomes very high. The reason is that if there are several spots which are dripping and no dry area or dry part of the fracture between the spots, they are all lumped together into one object. According to the characterization team, it is not uncommon to lump together 3-6 drip spots. The estimation of flow rates from counting drips is considered to be fairly good.

Inflows documented as 'flows' are continuous flows or the number of drips has been too many to be counted. It is not difficult to differentiate between 'drips' and 'flows'. 'Flows' are generally measured if the flow comes from the roof and it has generally only been possible to estimate the flow on the walls.

The estimated flow rates must be considered uncertain when they come from the roof and very uncertain when they come from the walls. The characterization team indicated they may have underestimated the flow rates mapped as 'flows'. The characterization team also say that generally there is only one spot of 'flow' per object.

The reason for the differences in flow rates for character 3 for the different tunnel sections shown in *Table 11-2* is probably due to the fact that a few large inflows certainly influence the mean values.

Inflow type

Inflow type predictions correspond to some extent to the outcome for Småland granite and Äspö diorite (see *Figure 11-3*). *Figure 11-3* is based on the **number of objects mapped** in the tunnel. The 'diffuse' leakage type dominates the outcome for fine-grained granite, which differs from the prediction. The reason is that in many cases it has been difficult to identify which fracture (of many) or part of a fracture is leaking and in such cases the inflow has been mapped as 'diffuse'.

'Bolt holes' were not included in the predictions and 'nodes' are less common than expected. Of the flow rates 'diffuse' and 'bolt holes' dominate and the smallest flow rate was for objects mapped as 'node', (see *Table 11-3*).

Table 11-3. Total estimated mapped inflow, by type. Type 1, 'Diffuse'. Water leaking from an area that cannot be associated with a fracture. Type 2, 'Point': One distinct leaking spot. Type 3, 'Node': Point leakage at the intersection between two fractures. Type 4, 'Extensive': Inflow spread over a part of the fracture length. Type 5, 'Bolt hole': Leakage from a bolt hole.

	Tunnel section									
	700-1475 m		1475-2265 m		2265-2874.6 m		2874.6-3600 m		700-3600 m	
	(l/min)	(%)	(l/min)	(%)	(l/min)	(%)	(l/min)	(%)	(l/min)	(%)
Type 1, (Diffuse)	196.1	41.8	17.2	13.8	7.6	22.0	22.0	18.6	242.9	32.5
Type 2, (Point)	78.7	16.8	46.3	37.2	4.6	13.3	43.7	36.9	173.3	23.2
Type 3, (Node)	11.4	2.4	0.6	0.5	0.5	1.4	8.4	7.1	20.9	2.8
Type 4, (Extensive)	46.5	9.9	15.6	12.5	10.6	30.6	30.2	25.5	102.9	13.8
Type 5, (Bolt hole)	136.8	29.1	44.9	36.0	11.3	32.7	14.0	11.8	207.0	27.7
Total inflow	469.5	100	124.6	100	34.6	100	118.3	100	747.0	100

Conclusions

The quantification and characterization of the leakage into the tunnel when mapping the walls and roof is difficult but it seems to be possible to obtain a rough estimate of the quantity and distribution along the tunnel. However, it is difficult to make quantitative estimates of the water flowing in through the tunnel walls and, frequently, also identifying leaking fractures and locating leaks along fractures.

If the flow into the tunnel is quantified by just mapping flowing features, neglecting dripping features and moisture on the rock surface, this seems to give around 80% of the total flow from the walls and roof. The mapping and quantifying of flowing features only in the tunnel can be done rather quickly and gives approximately the right flow rate through walls and roof.

12 SUBJECT: DISTURBED ZONE - DETAILED SCALE

12.1 SCOPE AND CONCEPTS

Section 8.1 contains an outline of the concepts behind the EDZ (Excavation Disturbed Zone). As mentioned there, the disturbed zone may affect the hydraulic resistance around the tunnel periphery. Grouting was also mentioned as having a large impact on the hydraulic resistance around the tunnel periphery. The hydraulic resistance around the tunnel periphery is mainly of interest for the site scale groundwater flow model, as the total inflow into the tunnel is to a large extent dependent of this resistance, at least because grouting is normally performed in tunnels.

This chapter contains a presentation of the attempts to describe the hydraulic resistance around the tunnel periphery in somewhat greater detail than was used in the site scale groundwater flow model. The purpose of the predictions was to test the ability to predict the general characteristics of the disturbed zone of different rock types.

12.2 METHODOLOGY FOR TESTS OF CONCEPTS AND MODELS

12.2.1 Prediction methodology

Pressure distribution

The average pressure 4 m from the tunnel wall was predicted for the lithological units Småland granite, Äspö diorite, greenstone and fine-grained granite. The head (h_s) around the tunnel was estimated in the predictions as:

$$h_s = \frac{q}{2\pi K} \left(\ln \frac{r_s}{r_o} + SK \right) \quad (12-1)$$

K	=	predicted hydraulic conductivity - median value, 20 m scale	[m/s]
r_o	≈	3, tunnel radius	[m]
r_s	=	7, radius to point for pressure estimate	[m]
SK	=	0 - 10 skin factor	[-]

q	=	3 · 10 ⁻⁷ (average inflow between zones according to numerical model of the Äspö tunnel), /Svensson, 1991, Gustafson, 1991/	[m ² /s]
h _s	=	head at distance r _s from tunnel centre	[m(of water)]

Conductivity changes and axial flow

The predicted hydraulic conductivity perpendicular to the tunnel axis (K_i) in the disturbed zone was predicted on the assumption that the skin factor was 0-10 and the skin zone was 1 m thick, which means that A in *Equation 12-2* becomes 1-0.03, /Gustafson et al, 1991/. As the outcome is for a 7 m thick zone the predicted values have been recalculated with *Equation 12-13*. The recalculated prediction is shown below:

$$\text{prediction: } K_i = K \cdot A = K \cdot (1 - 0.11) \quad (12-2)$$

K_i: hydraulic conductivity perpendicular to the tunnel centre line [m/s]

K: hydraulic conductivity of the undisturbed rock mass [m/s]

As no investigations of the axial flow were made in the tunnel, the predictions made of the axial flow are not outlined here. The predictions are shown in *Gustafson et al /1991/*.

12.2.2 Methodology for determining outcome

Disturbed zone - Pressure distribution

The pressure distribution around the tunnel is estimated from pressures in probe holes. The measured pressures along the tunnel were then assigned to the mapped rock types in order to provide an estimate of the pressure distribution around the tunnel for each rock type. The details concerning the outcome are shown in *Rhén et al /1994a/*.

Representative point for the measured pressure

The pressures around the tunnel were estimated from pressures in the probe holes drilled approximately every fourth round in the left and right walls of the tunnel. The packer was generally installed 5-6 m into the borehole and the borehole depth was generally about 20 m. To estimate the pressure distribution around the tunnel it is necessary to estimate a representative point for the measured pressure (point of application). One way of doing this is to use the flow rate distribution (Q_i) along the borehole to estimate the point of application (L_{e3}), see *Figure 5-1* and *Equations 12-3* and *12-4*.

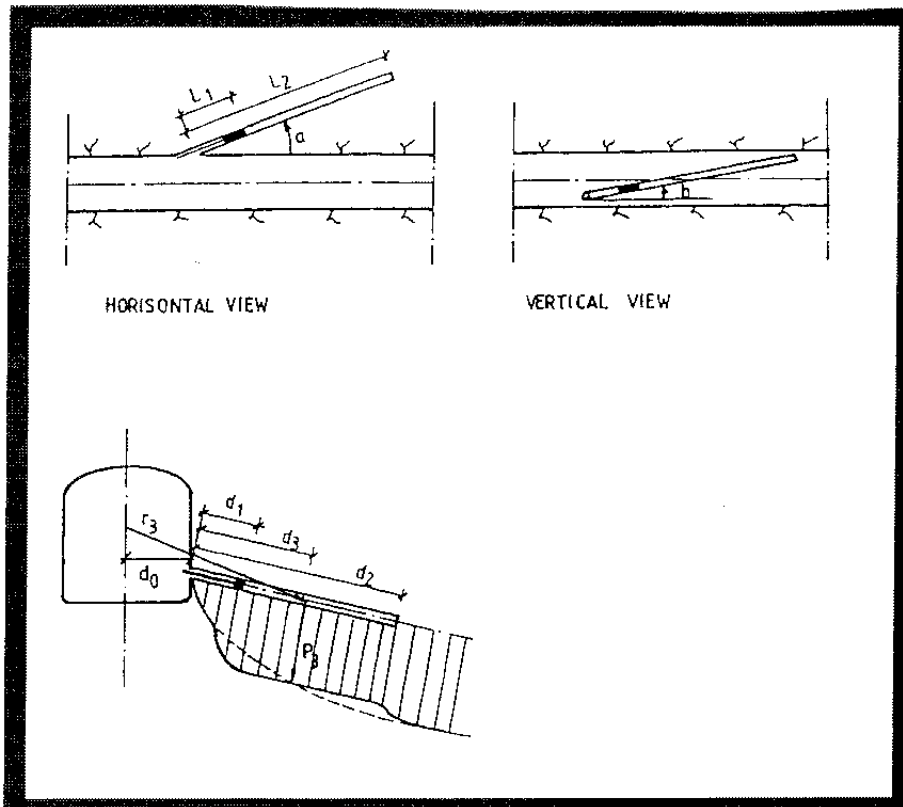


Figure 12-1. Estimation of point of application of the measured pressure (P_3) in a probehole.

$$L_{e3} = \frac{\sum_{i=1}^n (Q_i \cdot L_i)}{\sum_{i=1}^n Q_i} \quad (12-3)$$

where L is the distance along the borehole ($L = 0$ at the tunnel wall).

The distance (r_{e3}) from the tunnel centre line to the point of application (L_{e3}) can be estimated as:

$$r_{e3} = d_o + \sqrt{(L_{e3} \sin a)^2 + (L_{e3} \sin b)^2} \quad (12-4)$$

$d_o \approx 3$ m (the perpendicular distance from the tunnel centre line to the tunnel wall) and a and b are the horizontal and vertical angles between the borehole centre line and the tunnel centre line.

The flow is assumed to be approximately radial and therefore the pressures were plotted as a function of the logarithm of r_{e3} and the pressure distribution was evaluated from a linear approximation between the pressures and $\log(r_{e3})$.

Conductivity changes

Conductivity changes perpendicular to the tunnel axis were estimated for tunnel section 700-2875 m based on the calculated pressure 10 m from the tunnel centre. The hydraulic conductivity of the rock mass (K) was the geometric mean value for the tests along tunnel section 700-2875 m.

Skin factor estimated from a distance draw-down plot

The pressure distribution around the tunnel may be plotted in a distance/draw-down graph. Assuming a homogeneous medium and the fact that the sea level, with $z = 0$, is a positive boundary, the flow into the tunnel can be estimated as:

$$h_0 = \frac{q}{2\pi K} \left(\ln \left(\frac{2z_0}{r_0} \right) + SK \right) \quad (12-5)$$

h_0	=	z_0	[m]
q	=	inflow	[m ³ /(s · m)]
K	=	hydraulic conductivity	[m/s]
r_0	=	tunnel radius	[m]
SK	=	skin factor of the tunnel	[-]

The hydraulic head in a probe hole is:

$$h = \frac{P}{\rho \cdot g} + z \quad (12-6)$$

p	=	pressure in probe hole	[Pa]
ρ	=	1000	[kg/m ³]
g	=	9.81	[m/s ²]
z	=	level of the probe hole $\approx z_0$	[m]

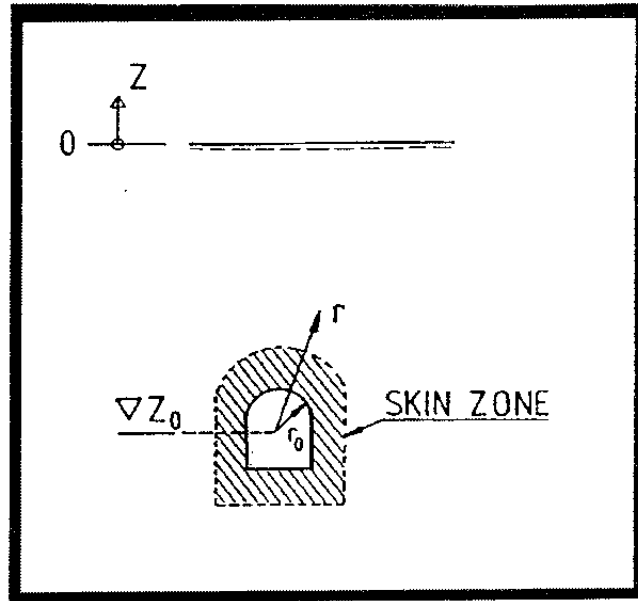


Figure 12-2. Definition of levels in Equation 12-5.

Assuming that the pressure is measured outside the skin zone the hydraulic head equation can be written:

$$h = \frac{q}{2\pi K} \ln \left(\frac{2z_0}{r} \right) \text{ for } r_s < r \ll z_0 \quad (12-7)$$

$$r_s = \text{radius of skin zone} \quad [\text{m}]$$

In a distance/draw-down graph two data points are plotted for each borehole, $h(\text{probe hole } i)$, $r(\text{probe hole } i)$ and $h = 0$, $r = 2z_0(\text{probe hole } i)$. The relative hydraulic head, h/h_0 , was plotted versus the distance r . For tunnel section 2265 - 2875 m h_0 was estimated as $h_0 = z_0 - 30$ m due to the draw-down of the water table.

The effective radius (r_{wf}) of a well with skin factor = SK and radius r_s is:

$$r_{wf} = r_s \cdot e^{-SK} \quad [\text{m}] \quad (12-8)$$

The effective radius is a way of describing the skin effect and r_{wf} can be estimated from the distance/draw-down plots as the radius where the estimated draw-down intersects $h/h_0 = 1$, assuming a draw-down according to Equation (12.7). The skin factor is estimated as:

$$SK = \ln \left(\frac{r_s}{r_{wf}} \right) \quad (12-9)$$

Estimation of the skin factor from flow and hydraulic conductivity measurements

It is possible to estimate the hydraulic conductivity or the transmissivity very approximately if the water inflow and pressure distribution around the tunnel are known. From these values the skin factor, or the local hydraulic resistance around the tunnel, can be estimated.

The transmissivity (T_s) in a hydraulic conductor domain close to the tunnel or hydraulic conductivity (K_s) in the zone closest to the tunnel can be estimated as:

$$T_s = \frac{Q}{2\pi \cdot \Delta p} \ln \left(\frac{r_s}{r_o} \right) \quad [\text{m}^2/\text{s}] \quad (12-10)$$

$$K_s = \frac{q}{2\pi \cdot \Delta p} \ln \left(\frac{r_s}{r_o} \right) \quad [\text{m/s}] \quad (12-11)$$

Q	=	flow rate out of zone	[m ³ /s]
q	=	flow rate/m of tunnel	[m ³ /(s·m)]
r _o	≈	3, tunnel radius	[m]
r _s	=	radial distance to p _s	[m]
Δp	=	p _s pressure difference between tunnel and point r _s	[m (of water)]

The skin factor (SK) can be estimated as:

$$SK = \left(\frac{T}{T_s} - 1 \right) \ln \left(\frac{r_s}{r_o} \right) \quad (12-12)$$

$$SK = \left(\frac{K}{K_s} - 1 \right) \ln \left(\frac{r_s}{r_o} \right) \quad (12-13)$$

The transmissivity (T) and hydraulic conductivity (K) are representative values from the tests in the probe holes, considered to be estimates of undisturbed rock.

12.3 COMPARISON OF PREDICTED AND MEASURED ENTITIES

Disturbed zone - Pressure distribution

The measurements along tunnel sections 700 - 2875 were divided among different rock types. The pressure based on the regression lines (two different times) for all probe holes is shown in *Table 12-1* (for details see *Rhén et al /1994a Appendix 2/*).

Table 12-1. Pressure around the tunnel 4 m from the tunnel wall. Data from tunnel section 700 - 2875 m.

Rock type	Pressure	
	Prediction Range (kPa)	Outcome* Point estimate (kPa)
Småland-granite	20 - 300	500-700
Äspö-diorite	50 - 1000	700-800
Greenstone	50 - 1000	-
Fine-grained granite	2-50	400-800

* Data from *Rhén et al /1994a Appendix 2/* for 'non-reinforced rock'.

Conductivity changes

The outcomes were estimated as below, where K_t is assumed to be the hydraulic conductivity in a zone from the tunnel wall to 7 m outside the tunnel wall:

outcome: $K_t = K \cdot (2 - 0.07)^*$

outcome: $K_t = K \cdot (0.6 - 0.3)^{**}$

* based on the total flow into the tunnel, hydraulic conductivity estimates and all pressure measurements /*Rhén et al /1994a Table 4-1, Appendix 2/*.

** based on pressure measurements in non-reinforced rock, distance/draw-down approach /*Rhén et al /1994a, Table 4-3, Appendix 2/*.

If K_t is assumed to be within a radius of 3-10 m from the tunnel centre line (tunnel radius ≈ 3 m) the skin factor for the tunnel, as defined in *Equation 12-13*, becomes -0.7 to 16.

12.4 SCRUTINY AND EVALUATION

Disturbed zone - Pressure distribution

The point estimates of the pressures in the non-reinforced rock mass were within the predicted range for Äspö diorite, near the range for Småland granite and outside the range for fine-grained granite. It may also be pointed out that the variation in the measured pressures was large and the total range was larger than that predicted.

The pressure range for all probe holes in tunnel section 700 - 2875 m was 100-3000 kPa and the calculated representative point outside the tunnel wall for the measured pressure was 1.5-21 m with a median value of approximately 7 m. When looking at *Table 12-1* it should be remembered that the variability of the pressures is large and some of the measured pressures are high, up to 1000-1500 kPa close to the tunnel wall.

The estimated distance to the appropriate point for the measured pressure may be overestimated in some boreholes because of grouting. Some of the conductive fractures mapped during the first part of the drilling are close to a grouting fan in some cases and the 'risk' of sealing them with grout is probably greater than that of sealing mapped fractures deeper in the borehole.

In spite of the high variability in the measured pressures there is a clear difference in the average pressures in the rock mass that was not reinforced compared with that in the reinforced rock mass, see *Rhén et al /1997/*.

Conductivity changes

The relative change in hydraulic conductivity for the disturbed zone was approximately within the predicted range.

The evaluation based on the draw-down/distance approach indicates skin factors in the range 0.9 to 6.2, if all data along the tunnel are used and only separated into the three mapping classes in the tunnel: 'fracture zones', 'increased fracturing' and 'rock' (= not mapped as 'fracture zones' or 'increased fracturing'), */Rhén et al, 1994a/*. When the 'fracture zones' are reinforced, the skin factor increases from 3.8 to 4.7 on average. The effect of reinforcement is even greater on 'increased fracturing', the skin factor then increases from 0.9 to 6.2. Considering the 'rock' category, reinforcement implies an increase from 2 to 4 on average. The skin factor of the deterministically defined hydraulic conductor domains, which were reinforced, were in the range 2 to 30.

The evaluation based on the evaluated hydraulic conductivities, pressures and flow rates indicates skin factors in the range -0.7 to 15.8, if all data along the tunnel are used and only separated into the three tunnel sections: 700-1475, 1475-2265 and 2265-2875 m. The largest skin factor was for tunnel section 700-1475 m, which was the most conductive tunnel part and where also most

conductor domains, which were reinforced and where the flow measurements are judged to be fairly reliable, were in the range 50 to 120. These values are rather close to the skin factors used in the groundwater flow model /*Wikberg et al, 1991*/.

Conclusions

It is very difficult to estimate the skin factor around a tunnel. The heterogenous nature of the rock mass makes it difficult to establish a pressure profile around the tunnel that is useful for the calculations. Shorter measurement sections at several distances from the tunnel wall would have been preferred, but as the variability of the pressure is large due to the heterogeneity there must also be a large number of measurement sections to obtain a reliable estimate of the pressure distribution.

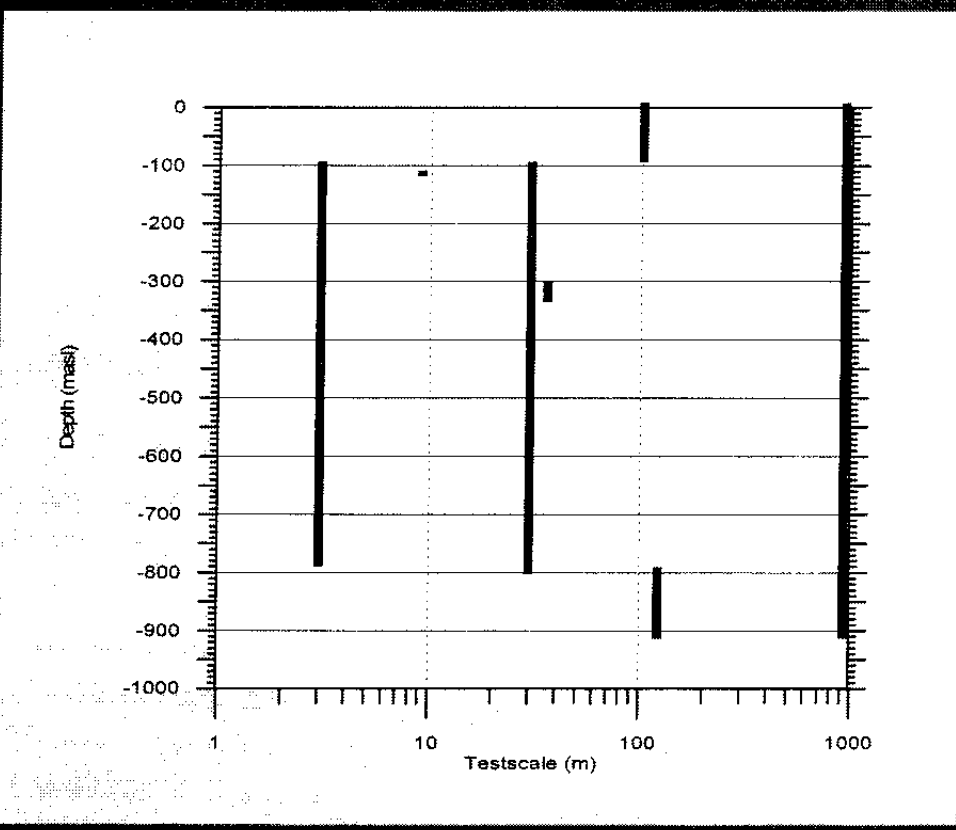
There are also some difficulties, besides the problems with the pressure measurements, with data needed for the calculations of the skin factor. One approach assumes homogenous conditions and a simple boundary condition. They may be neither homogenous conditions nor a simple boundary condition. The other approach assumes that it is possible to estimate a representative value of the hydraulic conductivity (or transmissivity, if it is a hydraulic conductor domain) for the undisturbed rock mass around the tunnel for a specified tunnel section and also that the flow into the tunnel is measured for the same tunnel section.

Despite the difficulties outlined above it seems that for prediction purposes, before any flow rates into the tunnel are known, it is reasonable to choose a skin factor between about 0 and 10 for the rock mass outside the hydraulic conductor domains for a sensitivity study. The skin factor for the hydraulic conductor domains must be calibrated on the basis of an inflow assumption.

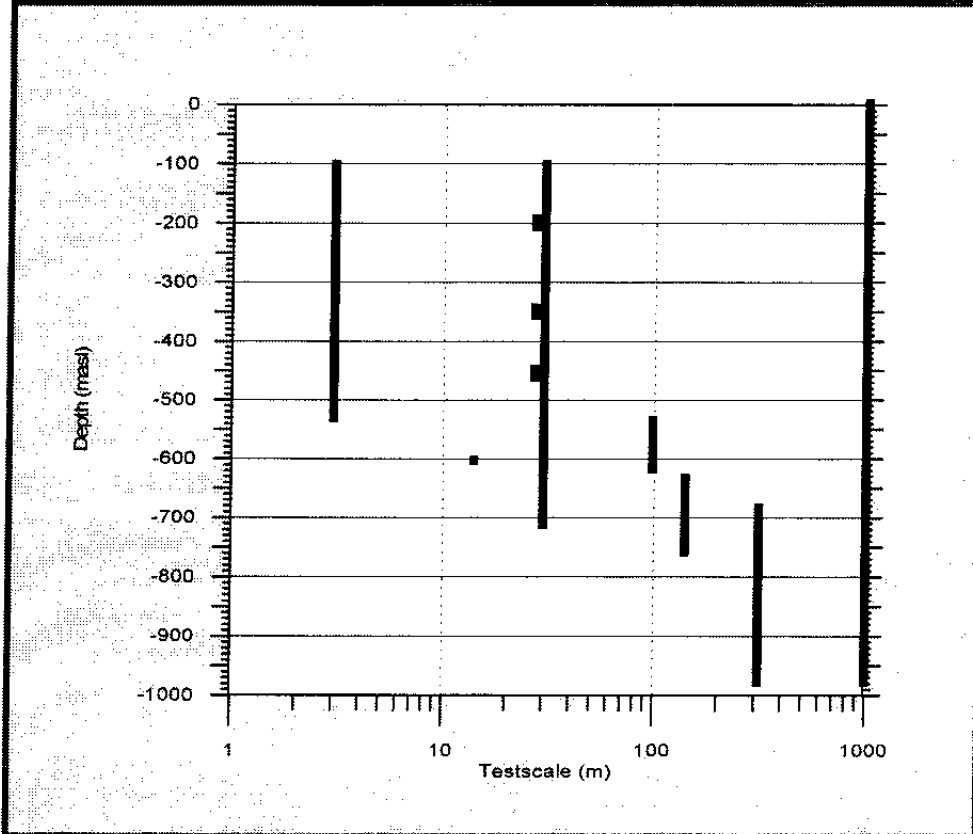
PART 1 - APPENDIX 1

OVERVIEW OF SECTIONS HYDRAULICALLY TESTED IN COREHOLES KAS02-08 AND KLX01.

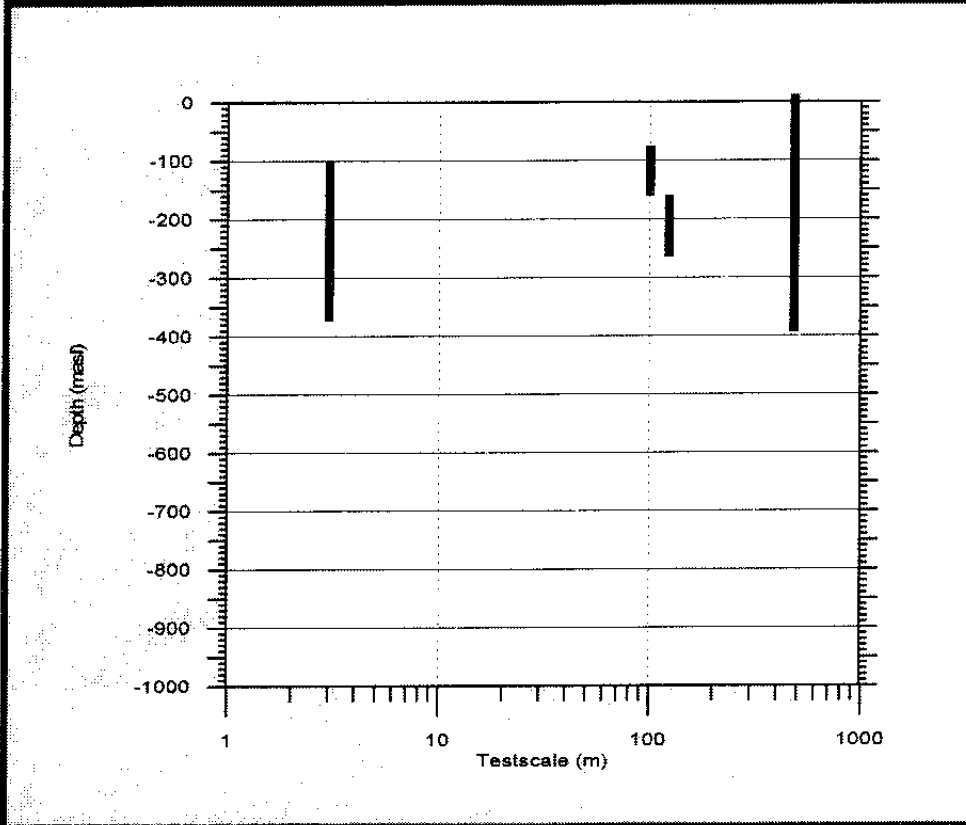
ÄSPÖ HARD ROCK LABORATORY
Test scale in KAS02



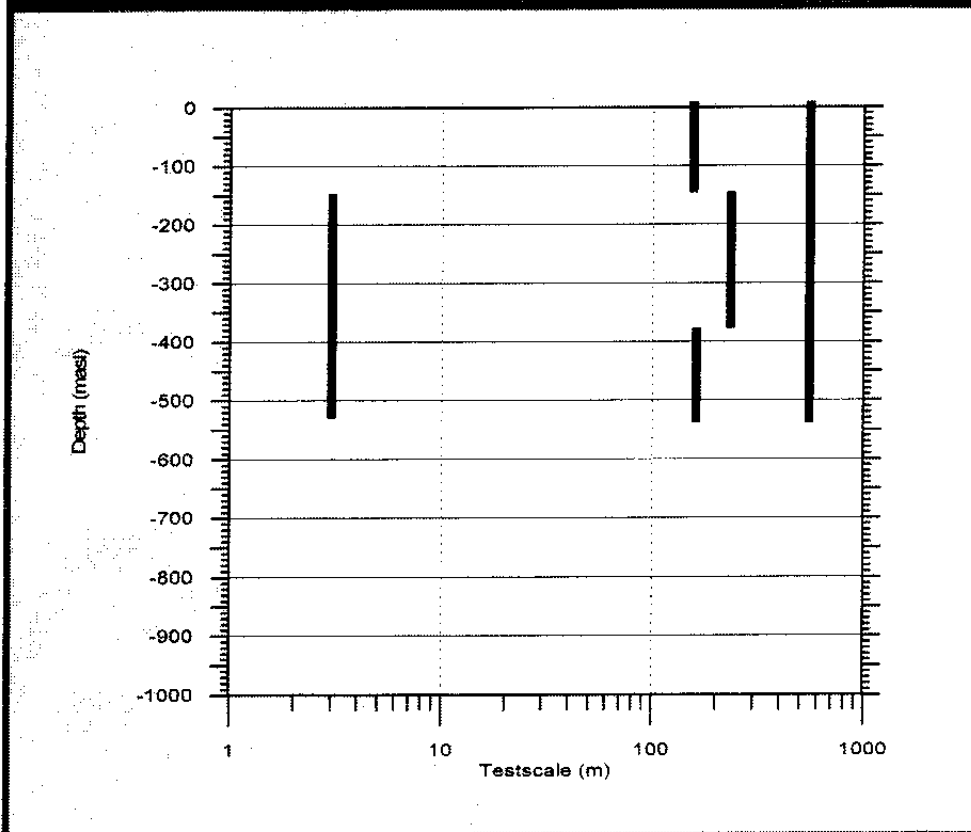
ÄSPÖ HARD ROCK LABORATORY
Test scale in KAS03

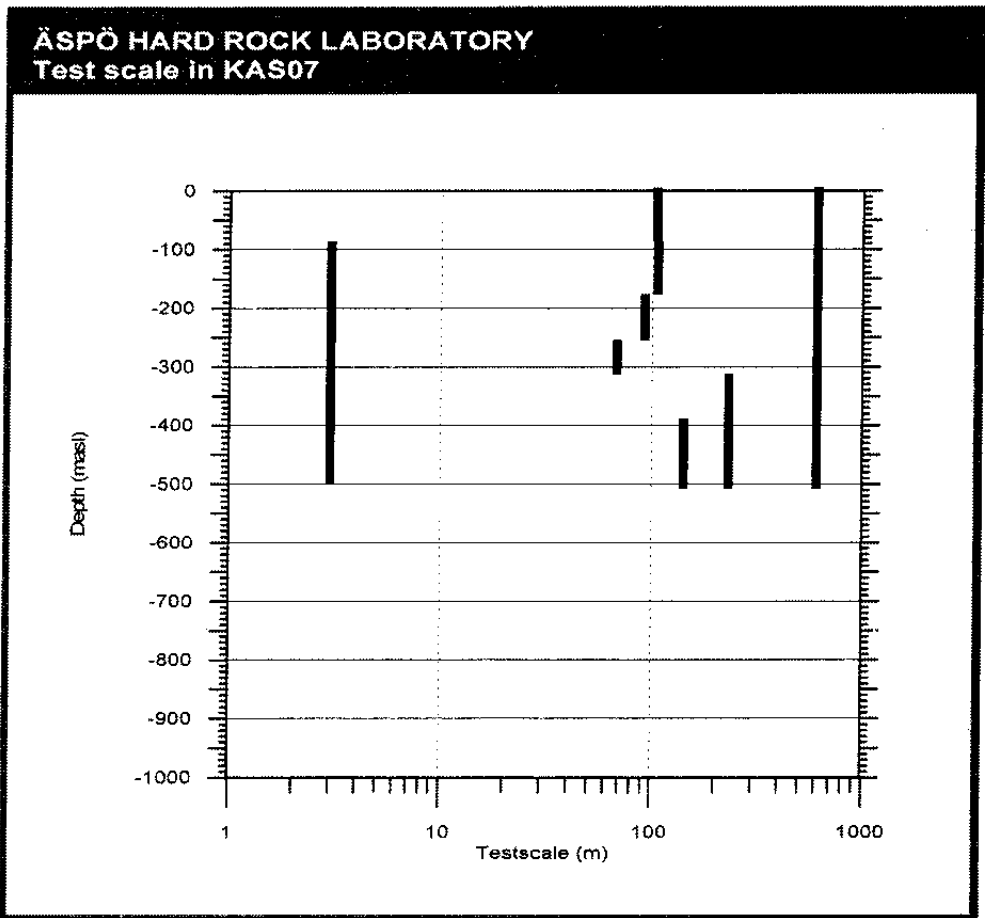
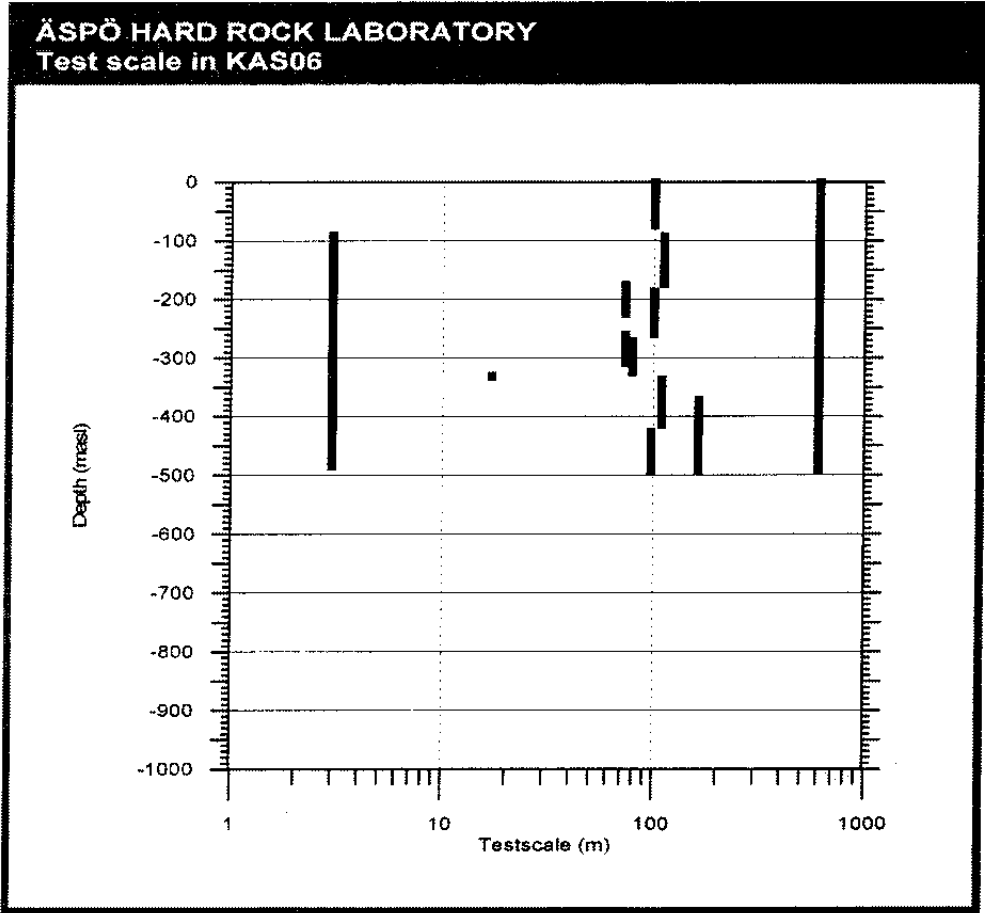


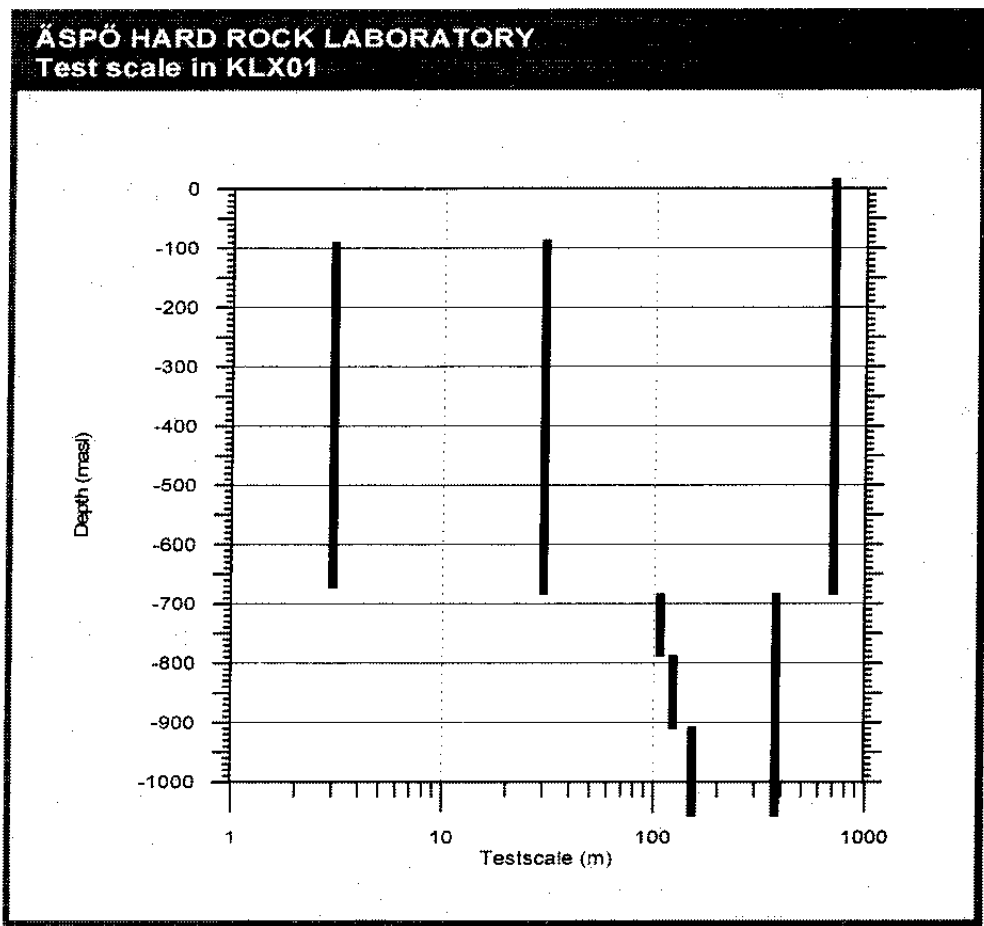
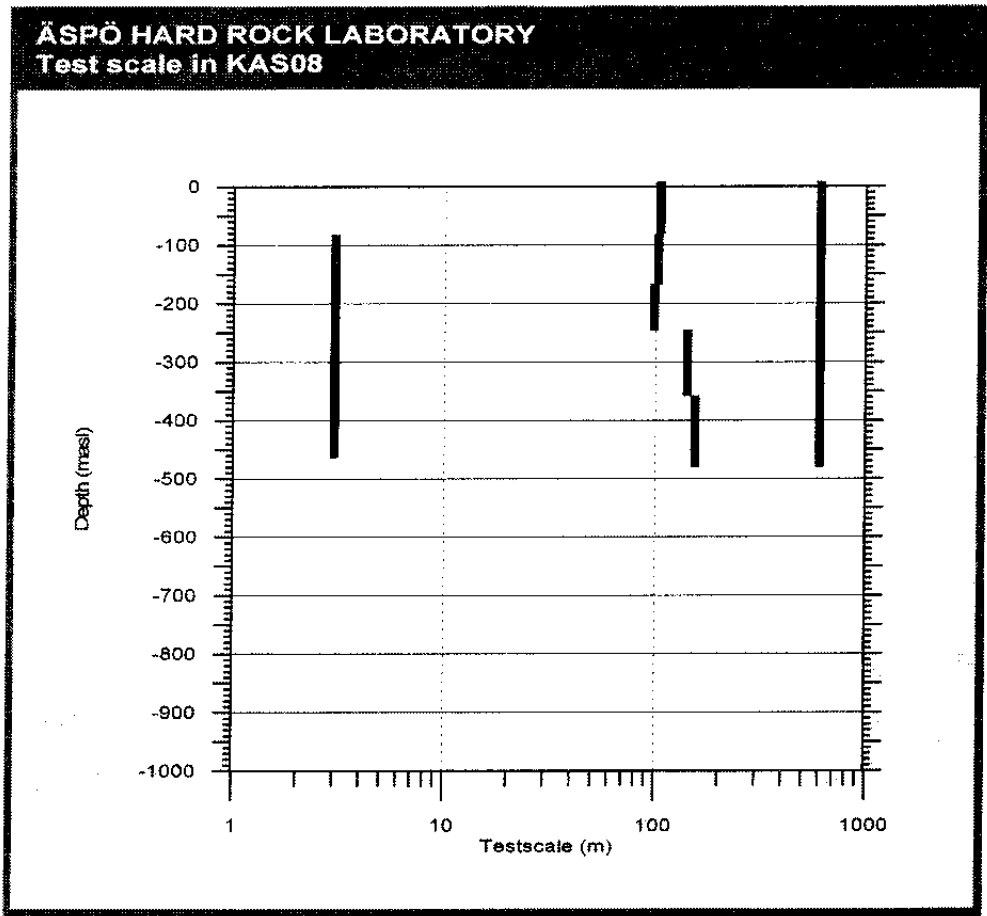
ÄSPÖ HARD ROCK LABORATORY
Test scale in KAS04



ÄSPÖ HARD ROCK LABORATORY
Test scale in KAS05







PART 2

GROUNDWATER CHEMISTRY

1 **SUBJECT: GROUNDWATER CHEMISTRY IN FRACTURE ZONES, SITE SCALE**

1.1 **SCOPE AND CONCEPTS**

The hydro-geochemical properties of the Äspö rock volume were characterized by samples from different points in the rock mass and fracture zones. The identified major fracture zones are commonly also the major water bearing features. The hydraulic properties of the water conducting fractures vary over several orders of magnitude. This in combination with the prevailing hydraulic gradient has a large influence on the chemistry of the groundwater in the different zones.

The evaluation and modelling procedures consist of data collection, single data set evaluation, all data analyses, co-interpretation with geology and hydrogeology and finally the spatial assignment of properties.

The data sets from the individual investigation campaigns are interpreted and modelled in common using both the traditional methods of cross correlation and equilibrium modelling, together with the principal component analyses which is used to classify all the observations. The boundary conditions for the hydro-chemical model are given by the hydrogeological conceptual model and the geometric framework is taken from the geological-structural model.

As a starting point, the groundwater composition is correlated with depth and to the specific fracture zone. The dependence function was evaluated from the data collected during pre-investigations. The predictions were made as described below:

The concentration of a constituent [i] is related to the geometrical position, $f_i(x,y,z)$, of all the major constituents, Na, Ca, Mg, Cl, HCO_3 , SO_4 , see *Figure 1-1*. The extrapolation/interpolation method defines $f_i(x,y,z)$, see *Figure 1-1*.

Predictions of conditions to be observed during the construction phase were made along two different lines. The main line - the one presented here - considers a static situation in which the conditions described in the model of the undisturbed Äspö site are also the conditions to be found in the tunnel phase. The other line is to base the conditions to be found in the tunnel on scoping calculations of what changes the inflow to the tunnel will have on the groundwater composition. This transient prediction is reported in *Part 3, Transport of solutes*.

The spatial assignment was based on a combination of expert judgement and principal component analyses. Later, during the construction phase, several other spatial assignment methods were tested.

An important parameter for describing the hydro-chemical conditions is obviously time. As a basis for the groundwater chemistry predictions it was assumed that the first sample collected at the tunnel front would represent the undisturbed conditions, which would be similar to those that prevailed during pre-investigations. The predicted conditions should therefore be compared with the very first data collected at the tunnel front.

The chemical composition of each predicted sampling point was calculated using Principal Component Analyses (PCA). The PCA value was then adjusted at a few points where it was thought that the flow into the tunnel would have changed the groundwater composition already by the time when the very first sampling was made in the tunnel front. The range of variation of the predicted values is mostly the difference between the PCA value and an estimated value assuming that the conditions were slightly disturbed. In some cases a mean value of the expert judgement and PCA is used and the variation range is put to half the difference.

The pH-values of the water were predicted from the assumed saturation with respect to calcite and the contents of bicarbonate and calcium. The Eh-value was calculated from the pH and the iron content of the water. The iron content was assumed to be the same as the concentrations obtained during pre-investigations (see *Gustafson et al /1991/*).

The range of variation for pH is the difference between the calculated values of calcite saturation and the value calculated from an empirical relation between the potassium concentration and pH (see *Gustafson et al /1991/*).

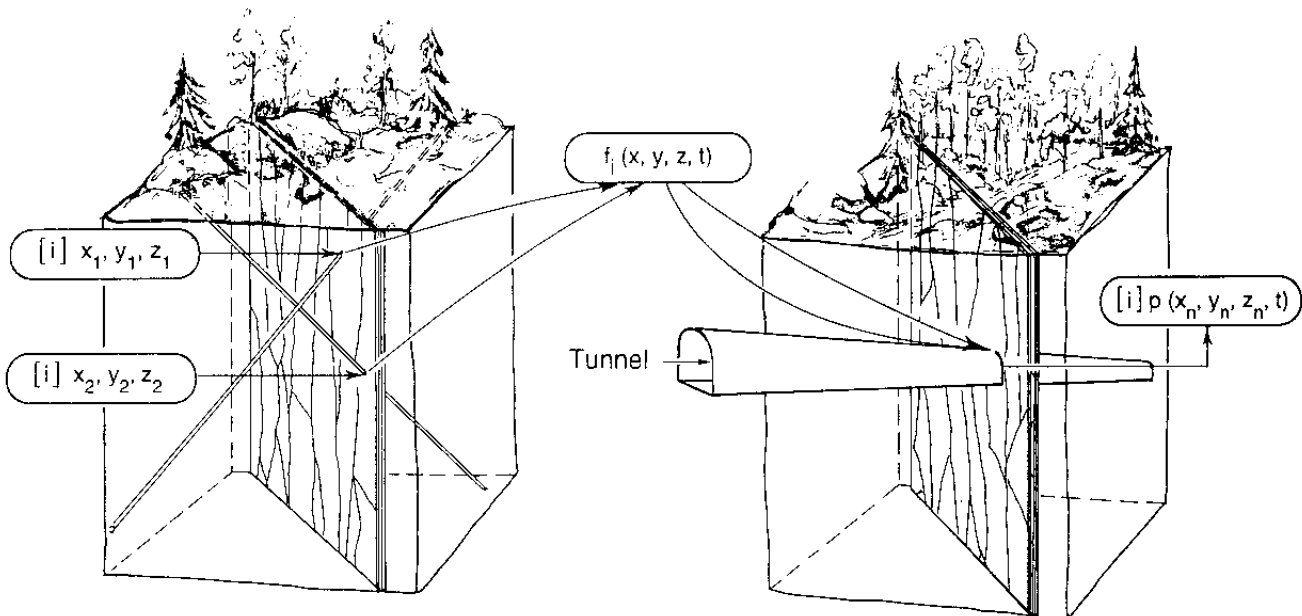


Figure 1-1. A schematic illustration of the way the hydro-chemical predictions were made on the basis of borehole data collected during the course of the pre-investigations.

The evaluation of predictions have been made strictly along the plans initially set up before the construction work started. During the construction phase the methods for evaluating hydrochemical data have been developed considerably. A computer based system for quantitative modelling of mixing and chemical reactions has been developed. The modelling concept mentioned in this report is named M3, **M**ultivariate **M**ixing and **M**ass balance calculations and is described in detail in *Laaksoharju and Wallin /1997/* and in *Rhén et al /1997a and 1997b/*. In *Rhén et al /1997a and 1997b/* the end-members mentioned in this text is also presented in more detail.

1.2 METHODOLOGY FOR TESTS OF CONCEPTS AND MODELS

The assessment of pre-investigation methodology consists of a cycle of activities. These are data collection, evaluation, analyses, co-interpretation, modelling, prediction, validation and assessment of methodology.

1.2.1 Data collection

During pre-investigations groundwater samples were collected at several occasions. Samples were collected during interruption of the drilling, during hydraulic interference pumping tests and during separate groundwater sampling campaigns. The data obtained in the different sampling campaigns were analysed for main constituents, trace elements, isotopes, pH and Eh. The sampling procedures are quite different from each other and so the quality of the data varies. Thus, the usefulness of the data for modelling purposes varies. The analytical programme for groundwater sampling during the pre-investigations and the construction phases are listed in *Table 1-1*.

Sampling in percussion boreholes (3P)

During the drilling of percussion boreholes intersections of water bearing fractures were identified. On this basis a deep section of the borehole was packed off and pumped for one day. Groundwater samples were collected at the beginning and end of the pumping period. The results were used to provide a hydro-chemical description of the uppermost 100 m of the bedrock, regarding the salinity distribution. Redox conditions, groundwater residence time and chemical equilibrium conditions cannot be evaluated on the basis of these data.

Sampling during drilling (SDD)

Generally, air-lift tests were conducted every 100 m of core length during the drilling of the cored boreholes. At the end of the pumping period of a few hours a groundwater sample was collected. The short duration of the pumping and the

fact that the samples in most cases included 10 - 50 % of drilling water, limit the use of the data to give only the salinity of the 'first strike' waters.

Table 1-1. Chemical analyses of samples collected on different occasions at Äspö.

Constituents	3P	SDD	SPT	CCC	Tunnel 1	Tunnel 2
pH	3	-	1	1	0	0
Eh	-	-	-	1	-	4
Sodium	2	3	1	1	-	0
Potassium	2	3	1	1	-	0
Calcium	2	3	1	1	-	0
Magnesium	2	3	1	1	-	0
Chloride	2	3	1	1	0	0
Bicarbonate	2	3	1	1	0	0
Sulphate	2	3	1	1	-	0
Silica	-	3	1	1	-	0
Iron (total)	-	-	1	1	-	0
Iron(II)	-	-	-	1	-	0
Manganese	-	-	1	1	-	0
Strontium	-	-	2	2	-	0
Lithium	-	-	3	3	-	0
Sulphide	-	-	1	1	-	4
Bromide	-	-	3	3	-	4
DOC	-	-	2	2	-	4
Colloids	-	-	-	4	-	-
Uranium	-	-	3	3	-	4
Uranium isotopes	-	-	3	3	-	4
Oxygen-18	3	-	2	2	5	0
Deuterium	3	-	2	2	5	0
Carbon-14	-	-	3	3	-	-
Carbon-13	-	-	-	-	-	4
Strontium-87	-	-	-	-	4	-
Sulphur-34	-	-	3	3	-	4
Dissolved gas	-	-	-	3	-	4

3P	=	sampling of shallow percussion drilled holes, pumping for 12 hours
SDD	=	sampling during drilling of deep, cored holes, pumping for a minimum of 1 hour
SPT	=	sampling during pumping tests, pumping for three days
CCC	=	complete chemical characterization in separate campaigns, pumping for ten days
Tunnel 1	=	sampling at the end of the probe hole drilling in the tunnel
Tunnel 2	=	repeated sampling in the selected probe holes
0	=	analyses are made each time a sample is collected
1	=	analyses are made daily during a pumping campaign lasting for at least three days
2	=	samples are collected for analyses on a few occasions during a pumping period
3	=	samples are collected at the end of a pumping period
4	=	samples are analysed only when some specific questions arise
5	=	stored samples are analysed afterwards if specific needs arise

Sampling during interference pumping tests (SPT)

Pumping tests of packed off borehole sections was also used for groundwater chemical characterization. During the pumping period, 3 days, a mobile field laboratory was connected to the flowing water to provide daily on-line analyses (cf. *Table 1-1*). The interference pumping test provides an opportunity to

characterize the hydro-chemistry of the major water conducting features as well as describing the salinity distribution.

Spinner or flow meter measurements and geophysical logs

During clean-up pumping, water-conducting sections of the borehole were identified through the spinner survey. The results were used to guide the selection of sampling intervals. A combination of different geophysical logs has been evaluated with the same purpose: to find the water conducting sections in the borehole.

Complete Chemical Characterization (CCC)

Suitable properties of borehole sections to be sampled have a hydraulic transmissivity in the range 10^{-5} - 10^{-8} m²/s. The selected sections, based on the spinner survey, were sampled for approximately two weeks with the mobile field laboratory and the downhole measuring devices. The complete chemical characterization is optimized for the needs of the safety assessment. pH and Eh were measured down hole, before any pressure decrease and atmospheric contamination had affected the fragile balance in the hydro-chemistry. Eh and pH sensitive constituents, bicarbonate, iron(II), sulphide and ammonia were analysed on site. Other constituents were sampled and preserved for later analyses at specialized laboratories. A complete list of all analyses and laboratories is given in */Smellie and Laaksoharju, 1992/*.

Figure 1-2 is a schematic chart of the methods and way in which the results are combined to give the final description (model) of the hydro chemistry of Äspö.

1.2.2 Evaluation and prediction

All the data collected in the different sampling campaigns have been evaluated and presented by *Wikberg et al /1991/ and Smellie and Laaksoharju /1992/*. The hydro-chemistry of Äspö, specified for the different water-bearing fracture zones, was used for the prediction of the chemical composition in the tunnel. The concepts and approaches are the ones described in *Section 1.1*. The predictions are reported in */Gustafson et al, 1991/*.

Univariate and multivariate analyses were used to evaluate the hydrochemical data obtained from the samples collected in fracture zones intersected by the deep investigation boreholes, */Smellie and Laaksoharju, 1992/*. Principal Component Analyses (PCA) were used to predict the concentration of the main constituents in the positions where the tunnel was to intersect the fracture zones, i.e. (x,y,z) of the intersection. The intersection point between the tunnel and the fracture zone was estimated from the structural geological model, and the planned layout of the tunnel (see *Stanfors et al, 1997 and Gustafson et al, 1991*).

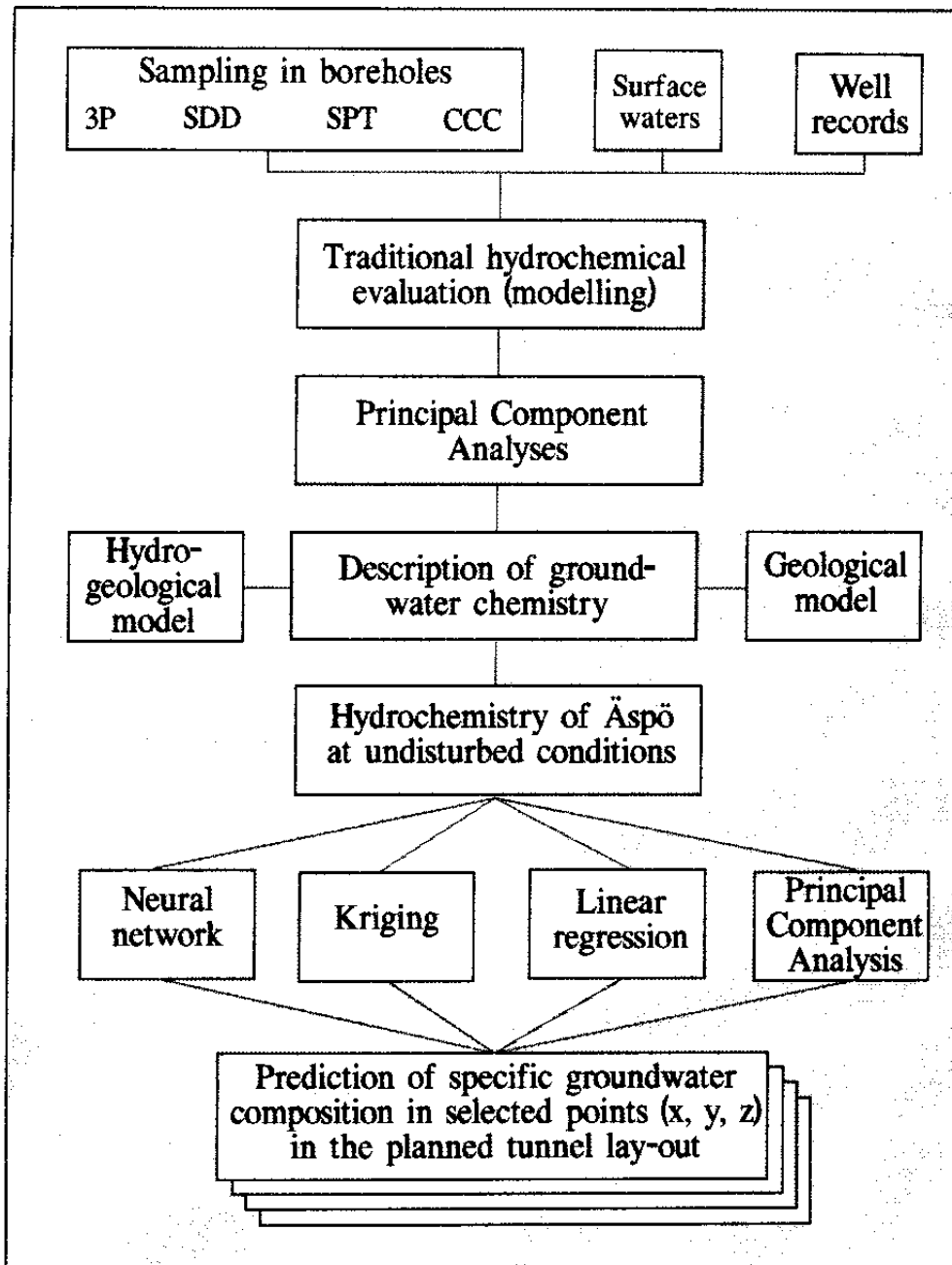


Figure 1-2. A schematic presentation of the methods used for the hydrochemical investigations. '3P', 'SDD', 'SPT', 'CCC' and 'Surface Waters' complemented by well records comprise the sample collection and chemical analysis made by the Äspö HRL project, see Table 1-1.

Initially (before tunnel construction started) the predictions were made by a combination of Principal Component Analysis and expert judgement. The predicted values were fairly easy to calculate, but the variability had to be estimated. At an early stage of the tunnel construction phase, it was evident that there were many disagreements between predictions and observations. It was not clear why there were large discrepancies, because sometimes, e.g. for NE-1, there was an agreement between predictions and observations. However, one

explanation could be that an unsuitable method had been used for the predictions. Therefore, tests of different interpolation methods were made to see which could be used to perform spatial assignment of groundwater chemistry properties. The tested tools were:

- Linear regression analysis
- Principal Component Analysis
- Kriging
- Neural Networks

The multiple *Linear regression* model is based on the least-square method. The linear regression analysis minimizes the distance between the observations and a straight line as a function of the position (x,y,z). The basic requirements of the model is that the observations are independent, normally distributed and have the same variance. In order to give a good correlation all observations need to be linearly depending on the position (x,y,z). The computer program used was *STATISTICA for Windows /1994/* and *STATGRAPHICS PLUS for Windows /1994/*.

Multi-variate (Principal Component) Analysis is a mathematical way of treating the different parameters all together. The values to be predicted could be considered as missing data in a matrix. The principal components are computed directly from the known data values, as a linear function of all the underlying parameters. The principal components are independent and extrapolated to the position (x,y,z). A predicted value for each constituent is obtained from the linear correlation of the principal component versus position. The method used was Fillas in the computer program *PARVUS /Forina et al, 1988/*.

Kriging is an interpolation method based on a spatial correlation function. The basic assumption is that the modelled properties are continuous and that positions physically close to each other also have properties numerically close to each other. Thus an observation physically close to a position to be predicted has a larger weight than an observation which is physically further off from the position to be predicted. The correlation function is obtained from the calibration data and the predictions are more uncertain further off from an observation. All values has an uncertainty, a variance, associated with it. There are different ways of estimating the unknown values and their corresponding variances. The computer program used was *SURFER for Windows /1994/*. Separate calculations are made for each element to be predicted.

Neural networks contain artificial neurones organized in layers and connected to each other in a way simulating the human brain. Each neurone in a layer is connected to all neurones in the previous and the following layers. The connections between the neurones have different strengths. The neurone computes its output signal as a weighted sum of its input signals. Neural networks learn by associations, from examples, by comparison, and by repetition. The neural network is non-linear, highly interconnected and is therefore capable to capture complex relationship between input and output.

Thus, the neural networks possess an ability to treat complicated non-linear problems, generalize, analyse large amounts of data, extrapolate and to optimize data. The software *BRAINMAKER PROFESSIONAL for Windows /1993/* was used to create, train and run neural networks */Hecht-Nielsen, 1991, Hertz et al, 1991 and Lawrence, 1992/* on the chemical data in both the pre-investigation and construction phases.

1.2.3 Methodology for determining the outcome

The groundwater chemical predictions based on the pre-investigation data were compared with the samples collected from probing holes along the tunnel. Samples have been taken from all boreholes with an inflow above 1 l/min. The sampling procedure has been summarized in tunnel section reports, 700-1475 m, 1475-2265 and 2265-2874 m, where the results are also preliminarily evaluated */Wikberg and Gustafsson, 1993, Wikberg et al, 1993 and Wikberg et al, 1994a, and b/*. Appendix 1 contains a listing of the probe holes related to the different fracture zones, the composition of the water and the mixing proportions of different water types.

The sampling points are mainly slightly downwards dipping probe holes 20 m deep at an angle of 20 to 45 degrees out from the tunnel direction. On the basis of the results from the first sampling in all boreholes, a few were selected for renewed sampling. This second sampling campaign was carried out more carefully than the first one. Many more parameters were analysed in these samples (see *Table 1-1*). At the time of sampling the water is on-line filtered through a 0.45 micron membrane and preserved for specific analyses. However, for the comparison with the predictions only the first sample was used. A complete listing of all the sampling and analyses made during the tunnel construction phase was compiled by *Nilsson /1995/*. The samples collected during the course of the probe hole drilling are reported in the different tunnel section reports */Wikberg and Gustafsson, 1993, Wikberg et al, 1993 and Wikberg et al, 1994a and b/*. All data is stored in the SICADA data base.

The sampling procedure in the tunnel provided no possibility of measuring the Eh. This limitation is not considered to cause any serious drawbacks in the evaluation, since the predicted Eh values were based on the predicted pH and the iron concentration. The response of the measured Eh values to the iron system is well established */Grenthe et al, 1992/*. Eh measurements were made in the block scale redox experiment */Banwart et al, 1995/*. The Eh values obtained were in accordance with the ordinary Eh-pH relation, resembling the ferrous-ferric iron system.

At an early stage of the tunnel construction phase it was evident that the observations and predictions disagreed. The reason for the disagreement was not known. The plausible explanations included the idea that the predictions were made using an unsuitable method (PCA). Other prediction methods were therefore tested in order to find out whether or not different prediction tools

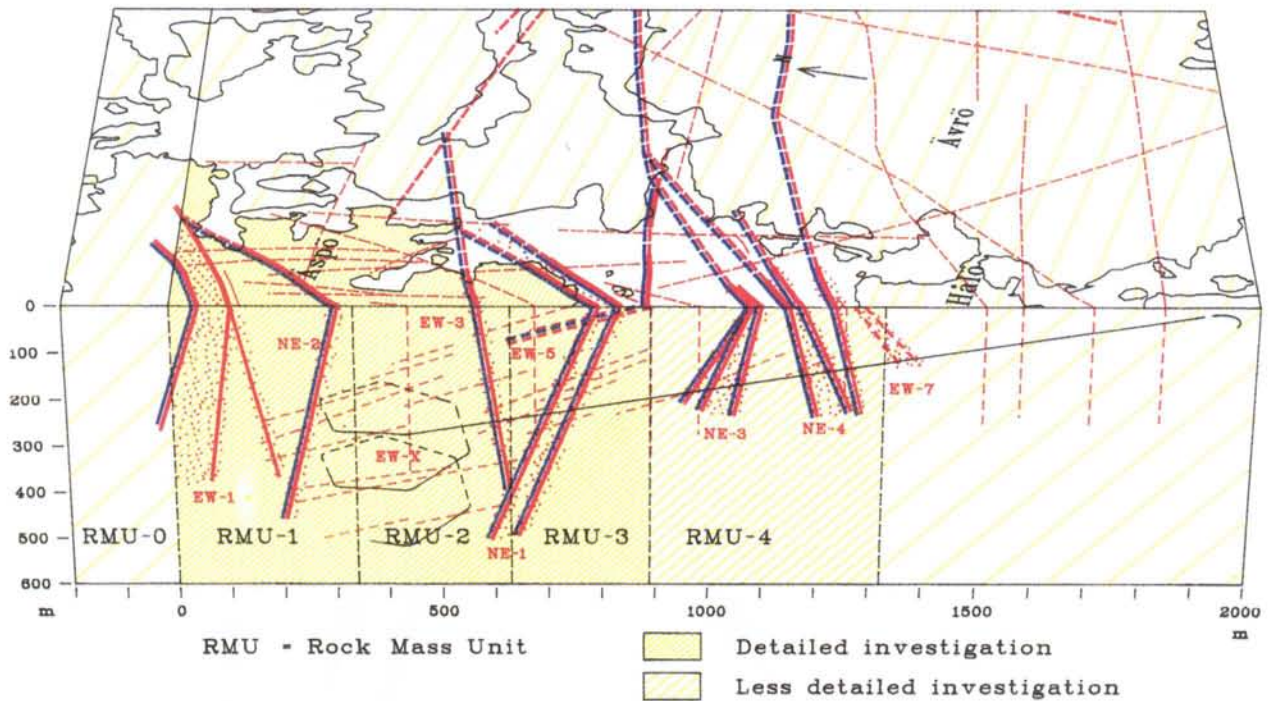


Figure 1-3. A section parallel to the entrance tunnel lay-out, indicating the major fracture zones as interpreted from the pre-investigations.

could explain the observed differences or if the reason for the disagreement should be sought elsewhere, i.e. in the concepts or in the data, see *Section 1.4.2*.

1.3 COMPARISON OF PREDICTED AND MEASURED ENTITIES

A section through the Äspö area is presented in *Figure 1-3* indicating the major fracture zones where hydro-chemical properties were predicted for NE-1, NE-2, NE-3, NE-4, EW-3, EW-5, EW-7 and the minor fracture zone NNW-4 (not indicated on the figure).

NE-1

NE-1 was identified as the hydraulically most conductive feature during the pre-investigation phase. Cored boreholes KAS 09, 10 and 11 were targeted at that fracture zone (see *Figure 1-4*). Two of them were sampled during drilling (SDD) for chemical analyses. As indicated in *Figure 1-4* the groundwater sampled in KAS 09 was outside fracture zone NE-1, since the boreholes did not reach down to the fracture zone. The results of prediction and outcome are shown in *Table 1-2* and graphically in *Figure 1-5*.

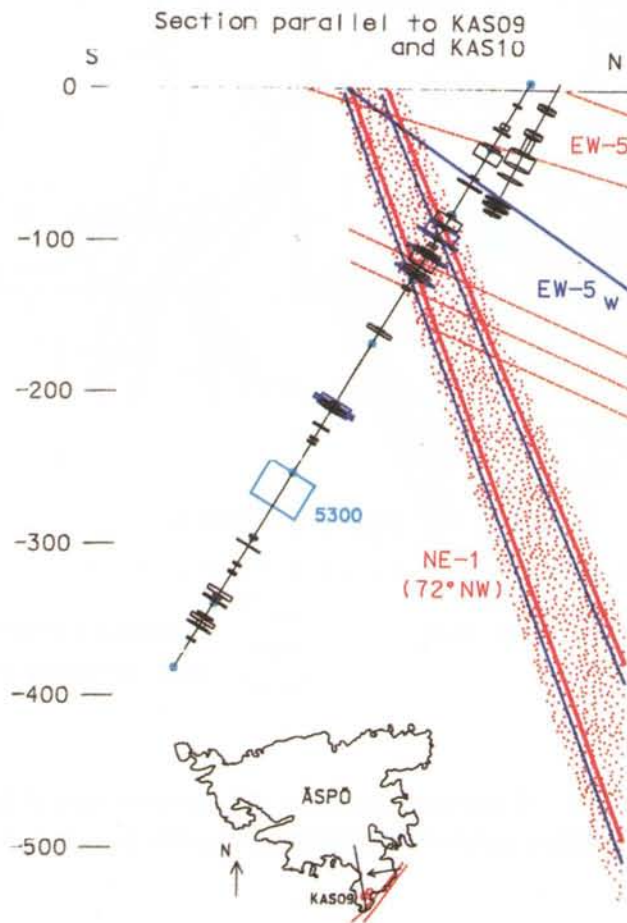


Figure 1-4. Fracture zone NE-1 and the cored holes penetrating it.

Table 1-2. Predicted and observed groundwater chemistry representing the major fracture zone NE-1. The variation covers the range of the observations.

Prediction/ Outcome	Na mg/l	Ca mg/l	Mg mg/l	Cl mg/l	SO ₄ mg/l	HCO ₃ mg/l	pH
Prediction	1900 ±200	1200 ±350	150 ±80	5300 ±400	210 ±50	290 ±100	7.2 ±0.3
Outcome	2000 ±200	1050 ±30	170 ±20	5300 ±300	140 ±50	350 ±160	7.2 ±0.1

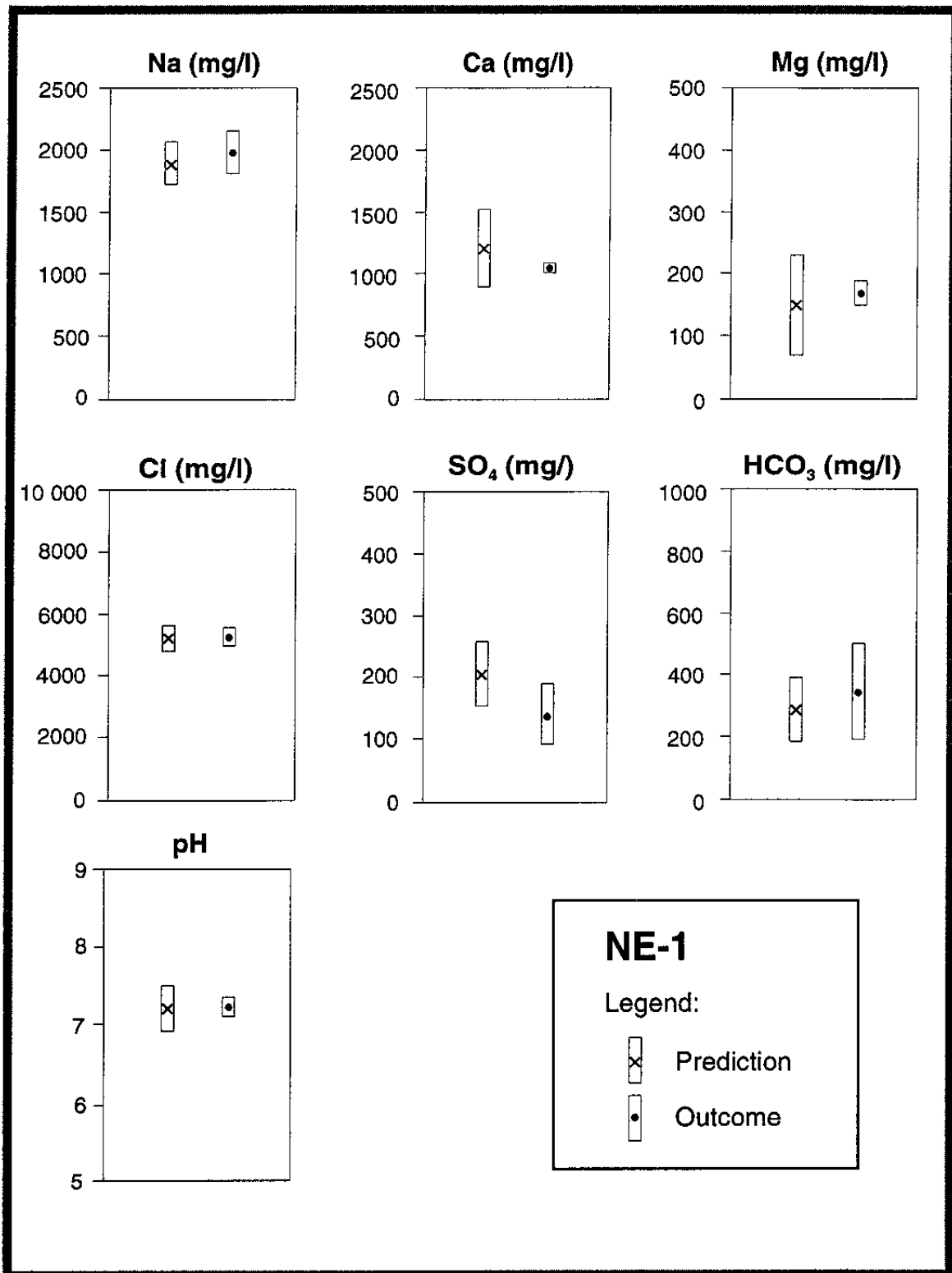


Figure 1-5. Graphical illustration of the predicted and observed concentrations of main constituents in the groundwater in fracture zone NE-1. For the discussion of different prediction methods see Section 1.4.

NE-2

The fracture zone was penetrated by two cored boreholes, KAS 12 and KAS 8, and faintly observed at the surface (see *Figure 1-6*). The water from both these drill holes was sampled in conjunction with drilling. The results of prediction and outcome are presented in *Table 1-3* and graphically in *Figure*

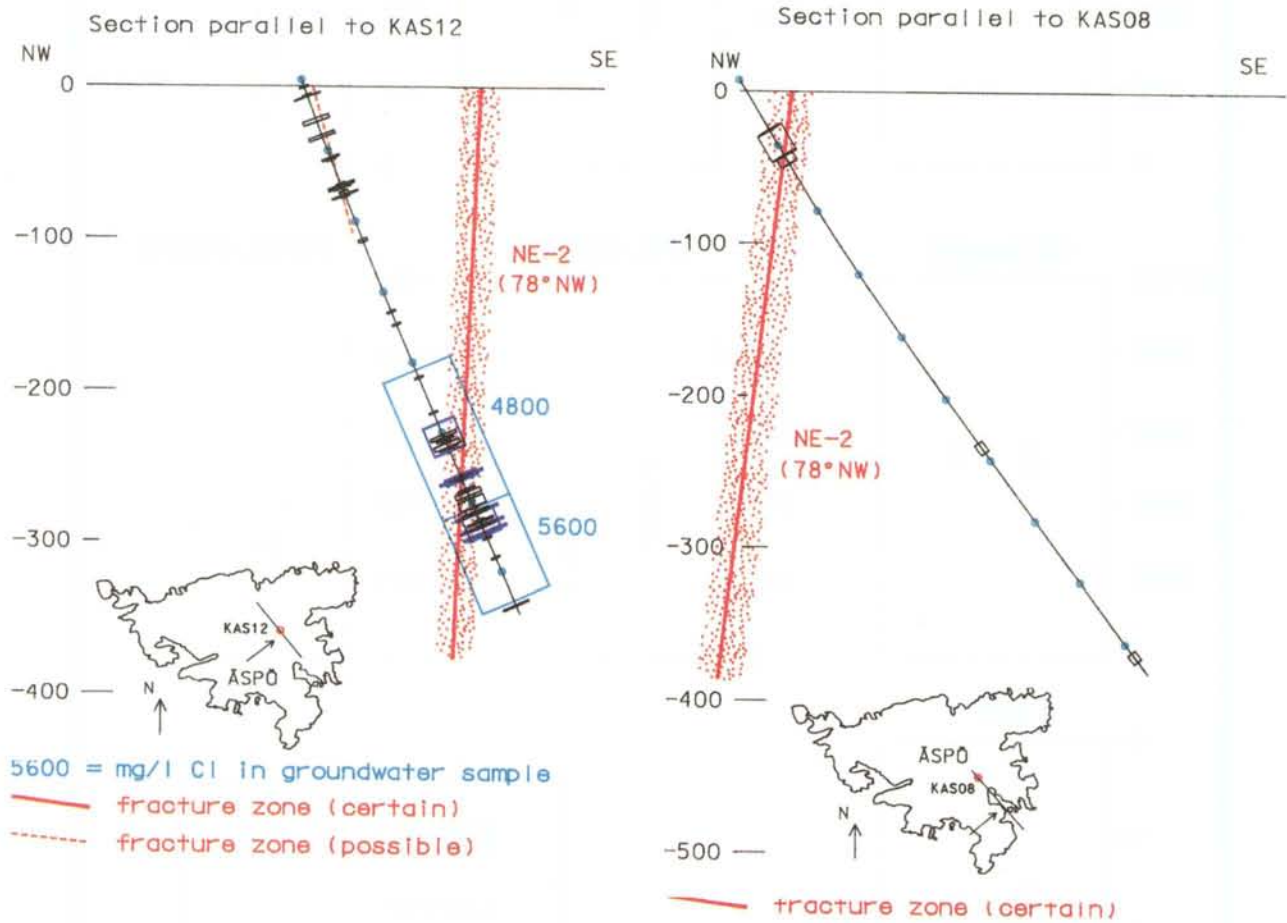


Figure 1-6. Fracture zone NE-2 and the cored holes penetrating it.

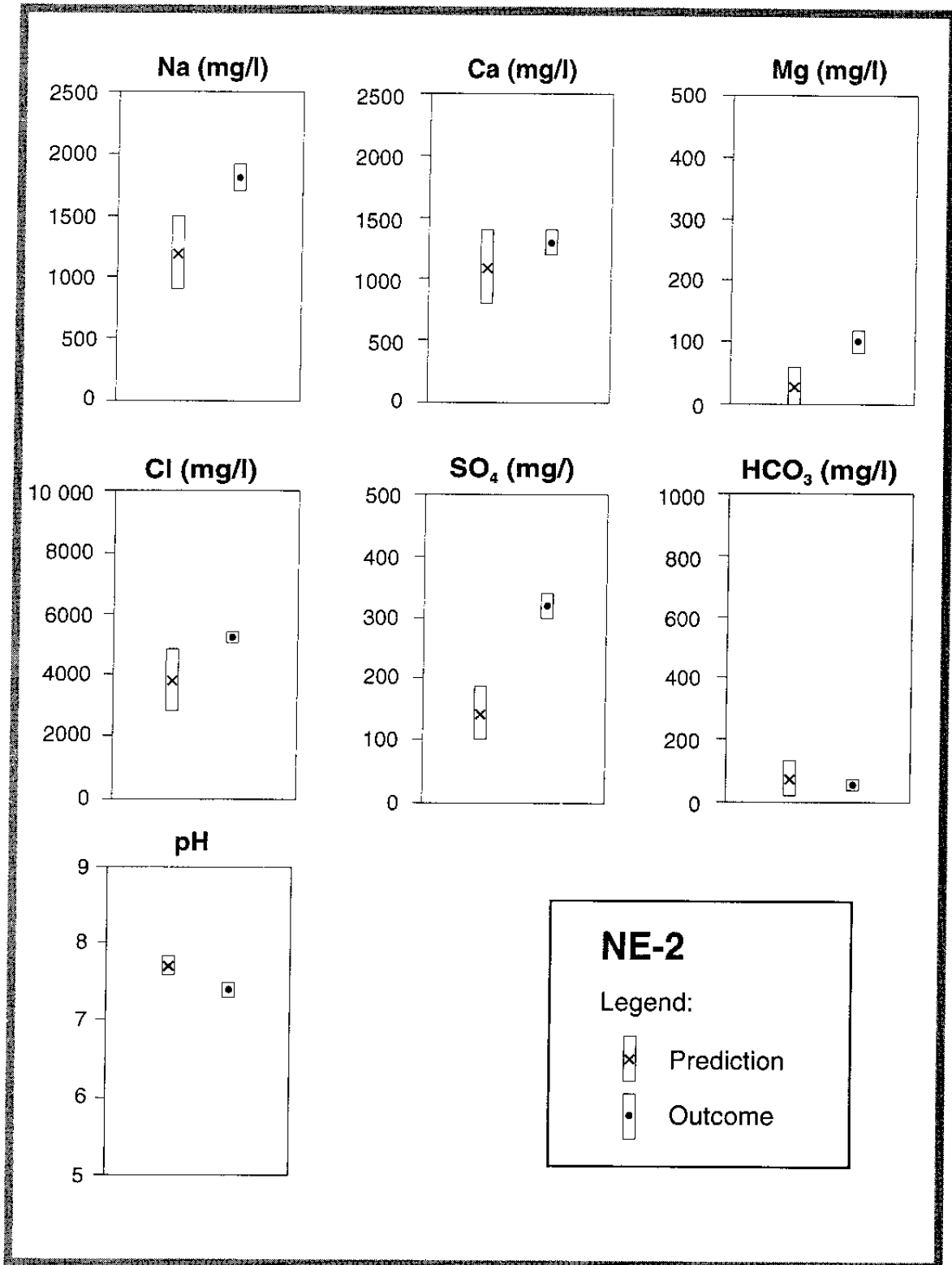


Figure 1-7. Graphical illustration of the predicted and the observed concentrations of main constituents in the groundwater in fracture zone NE-2. For the discussion of different prediction methods see Section 1.4.

Table 1-3. Predicted and observed groundwater chemistry representing major fracture zone NE-2.

Prediction/ Outcome	Na mg/l	Ca mg/l	Mg mg/l	Cl mg/l	SO ₄ mg/l	HCO ₃ mg/l	pH
Prediction	1200 ±300	1100 ±300	30 ±30	3800 ±1000	140 ±40	70 ±50	7.7 ±0.1
Outcome	1800 ±100	1300 ±100	100 ±20	5200 ±100	320 ±20	50 ±10	7.4 ±0.1

NE-3

The fracture zone was penetrated by borehole KBH 02 which was sampled during drilling (see *Figure 1-8*). However, the sampling was made before the borehole had reached the fracture zone so there were no data really representing NE-3. The results of the predictions and the outcome are presented in *Table 1-4* and graphically in *Figure 1-9*.

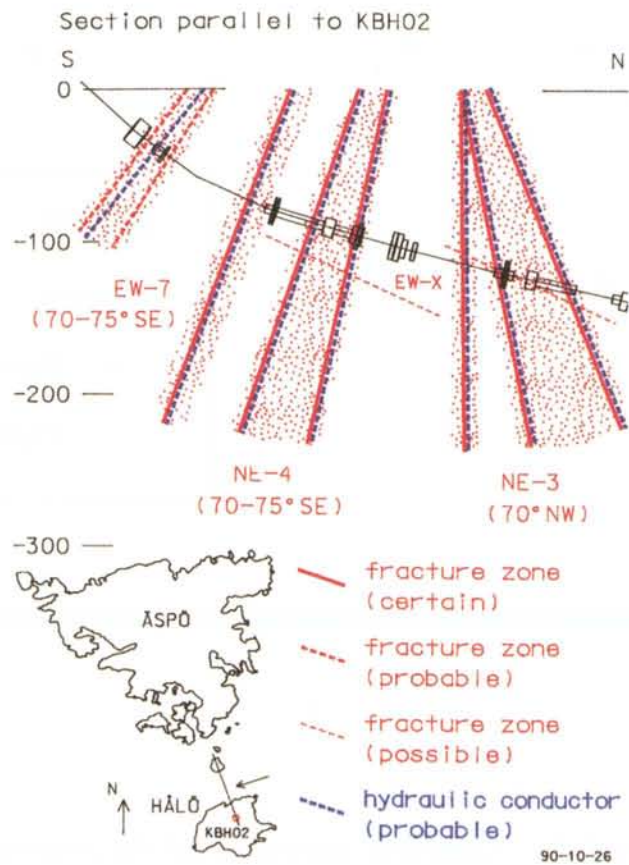


Figure 1-8. Location of fracture zone NE-3.

Table 1-4. Predicted and observed groundwater chemistry representing major fracture zone NE-3.

Prediction/ Outcome	Na mg/l	Ca mg/l	Mg mg/l	Cl mg/l	SO₄ mg/l	HCO₃ mg/l	pH
Prediction	1800 ±100	680 ±250	170 ±15	4500 ±200	170 ±50	280 ±50	7.3 ±0.3
Outcome	2200 ±100	900 ±100	210 ±20	5400 ±100	60 ±10	600 ±100	7.3 ±0.3

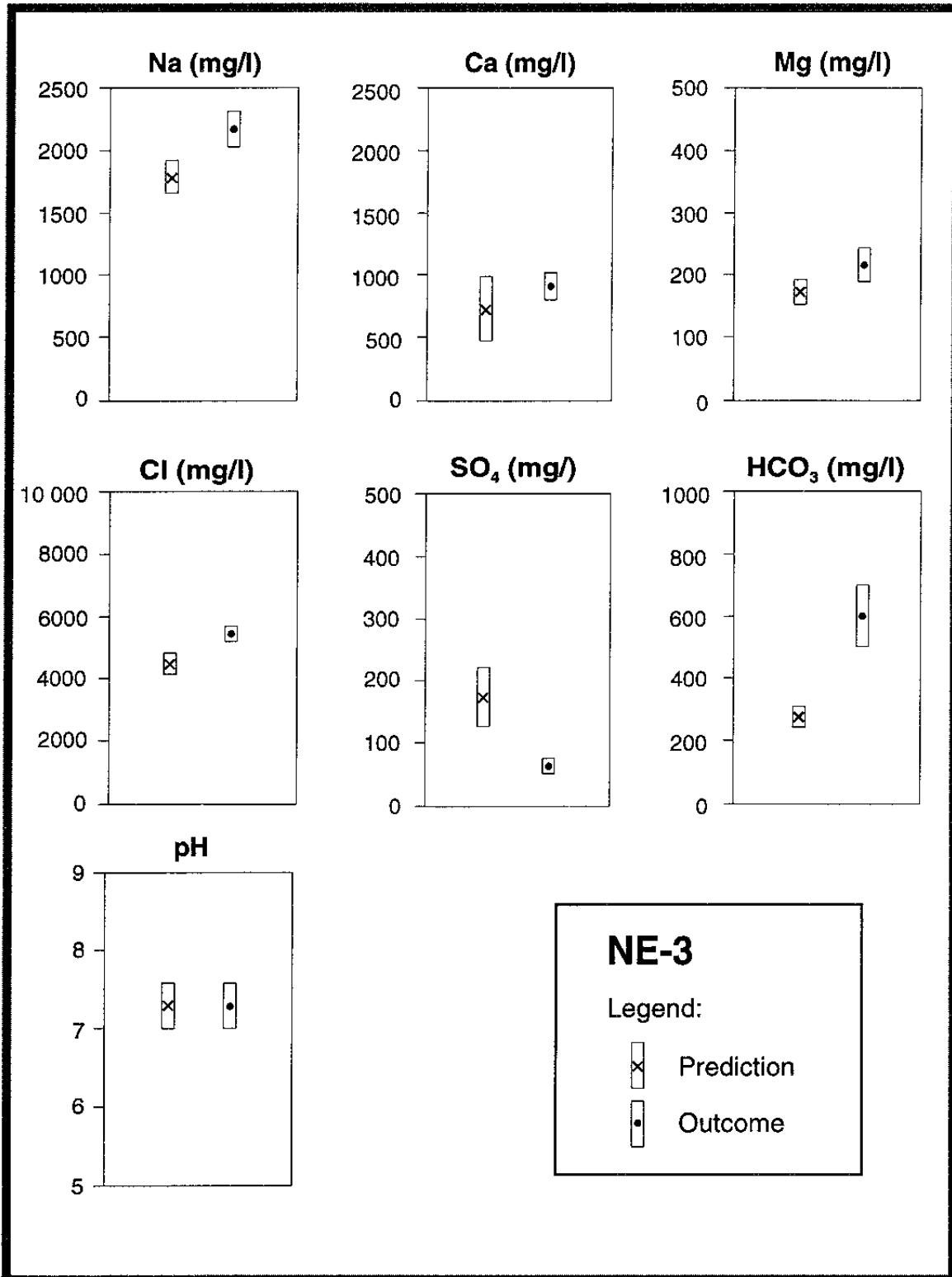


Figure 1-9. Graphical illustration of the predicted and observed concentrations of main constituents in the groundwater in fracture zone NE-3. For the discussion of the different prediction methods see Section 1.4.

NE-4

The fracture zone was located and investigated through borehole KBH02 and sampled during drilling (see *Figure 1-10*). Groundwater samples were collected from the borehole section which penetrated the fracture zone. The results of the predictions and outcome are presented in *Table 1-5* and graphically in *Figure 1-11*.

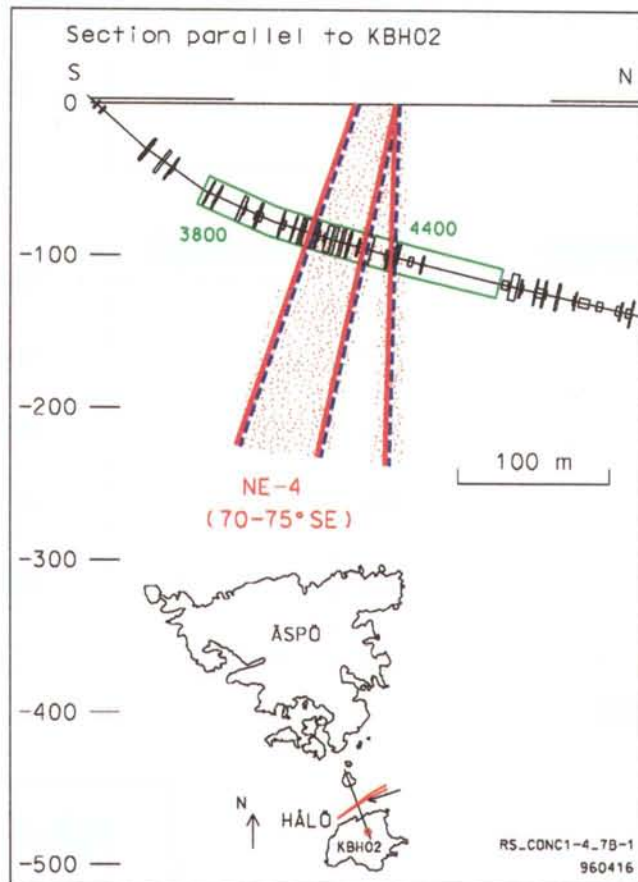


Figure 1-10. Location of fracture zone NE-4.

Table 1-5. Predicted and observed groundwater chemistry representing major fracture zone NE-4.

Prediction/ Outcome	Na mg/l	Ca mg/l	Mg mg/l	Cl mg/l	SO ₄ mg/l	HCO ₃ mg/l	pH
Prediction	1800	680	170	4500	170	280	7.3
	±100	±250	±15	±200	±50	±50	±0.3
Outcome	1800	1300	140	5600	90	180	7.2
	±100	±100	±10	±200	±10	±50	±0.5

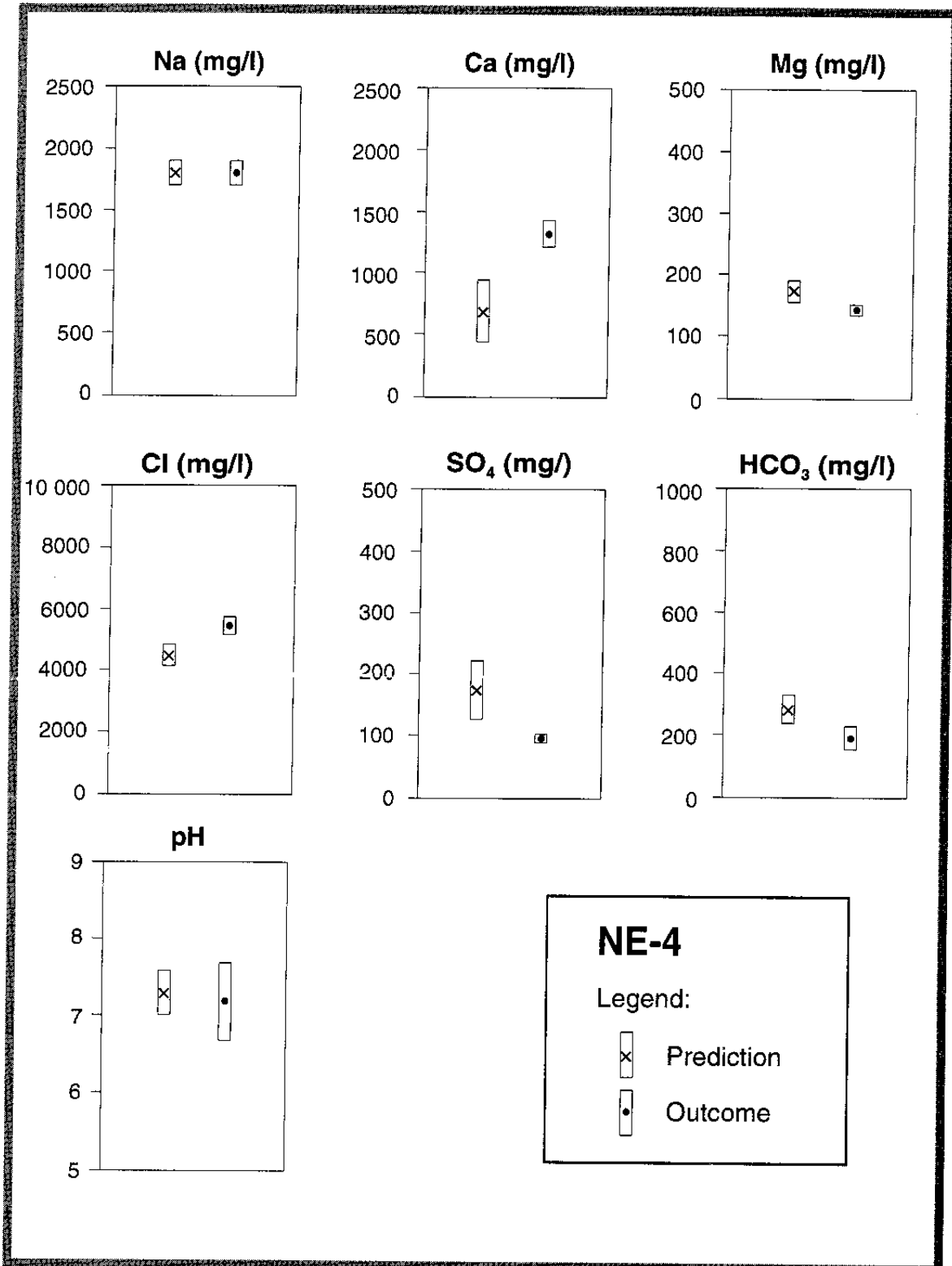


Figure I-11. Graphical illustration of the predicted and observed concentrations of main constituents in the groundwater in fracture zone NE-4. For the discussion of the different prediction methods see Section 1.4.

EW-3

The fracture zone had not been chemically identified during the pre-investigation and was therefore not predicted. The fracture zone was intersected by boreholes KAS06 and KAS07 and sampled during drilling (see Figure 1-12). The observed chemistry is presented in Table 1-6.

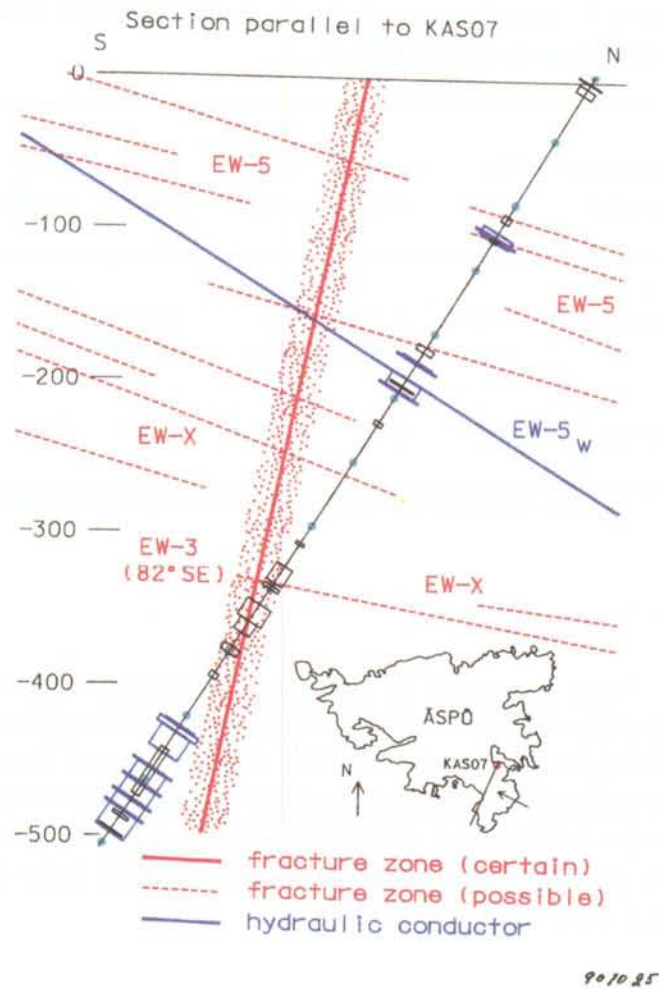


Figure 1-12. Location of fracture zone EW-3.

Table 1-6. Predicted and observed groundwater chemistry representing major fracture zone EW-3.

Prediction/ Outcome	Na mg/l	Ca mg/l	Mg mg/l	Cl mg/l	SO ₄ mg/l	HCO ₃ mg/l	pH
Predictions	No predictions were made for EW-3						
Outcome	1700	1000	120	4600	200	830	7.6

EW-5

Fracture zone EW-5 was indicated as a possible sub-horizontal hydrogeological feature which was difficult to identify geologically. Hydro-chemically there were indications of a separate system as predicted in *Table 1-7*.

Table 1-7. Predicted and observed groundwater chemistry representing possible fracture zone EW-5.

Prediction/ Outcome	Na mg/l	Ca mg/l	Mg mg/l	Cl mg/l	SO ₄ mg/l	HCO ₃ mg/l	pH
Prediction	1300	1200	30	4100	150	70	7.8
	±300	±300	±30	±800	±50	±20	0.2
Outcome*	1600	680	120	3900	290	180	7.5

* The data represents the tunnel position where the EW-5 zone was expected to be found.

EW-7

EW-7 was intersected by borehole KBH02 (see *Figure 1-13*). It was hydro-chemically difficult to separate it from NE-4, during pre-investigations as well as during tunnel construction. The reason for this is that the borehole sections representing EW-7 also represent NE-4. This is due to the existence of the open fractures running N-S which short-circuit the two fracture zones. The results of the predictions and outcome are presented in *Table 1-8* and graphically in *Figure 1-14*.

Table 1-8. Predicted and observed groundwater chemistry representing major fracture zone EW-7.

Prediction/ Outcome	Na mg/l	Ca mg/l	Mg mg/l	Cl mg/l	SO ₄ mg/l	HCO ₃ mg/l	pH
Prediction	1700	410	190	2800	130	250	7.6
	±100	±300	±30	±1400	±50	±10	0.6
Outcome	1800	1100	200	5200	90	300	7.2
	±200	±200	±100	±400	±30	±160	0.2

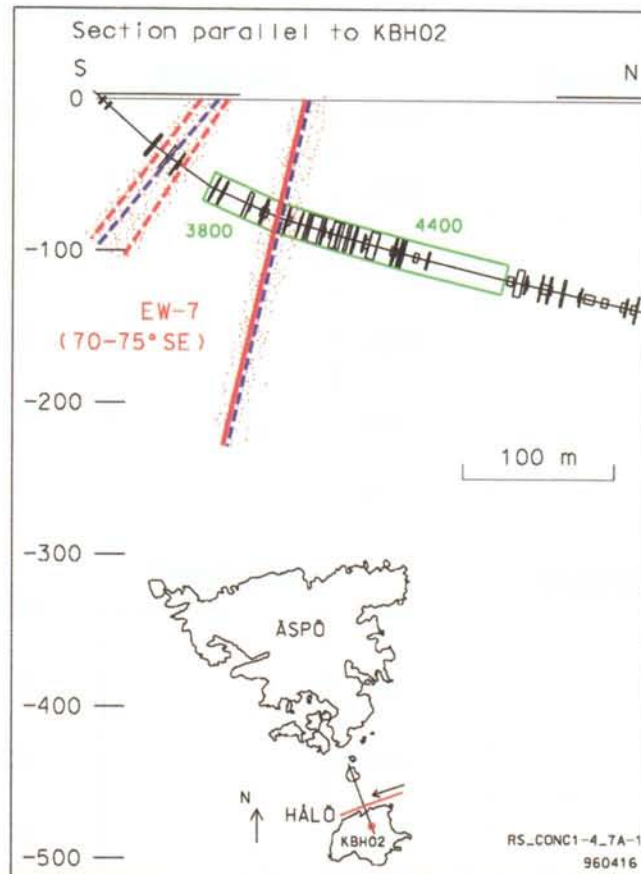


Figure 1-13. Location of fracture zone EW-7.

NNW-4

Minor fracture zones in the NNW-system were predicted mainly on the basis of hydrological observations. These were called NNW-1 to NNW-6. Only some faint geological features could be correlated to the hydraulic observations. In the tunnel mapping, however, it has been clearly found that the NNW-4 zone exists as a separate fracture system. Most of the other 'minor fracture zones' seem to occur rather as 20-50 m wide systems of hydraulically connected fractures trending mainly WNW-NW and approximately N-S rather than real fracture zones. The fracture set trending WNW-NW comprise most water-bearing fractures /Hermansson /1995/ and Mazurek et al /1995/.

Figure 1-15 and Table 1-9 present the prediction and outcome.

The comparisons between prediction and outcome for iron and potassium are presented in Table 1-10. These elements have been separated from the others since their concentrations were predicted purely by expert judgement (see Gustafson et al /1991/ for a discussion).

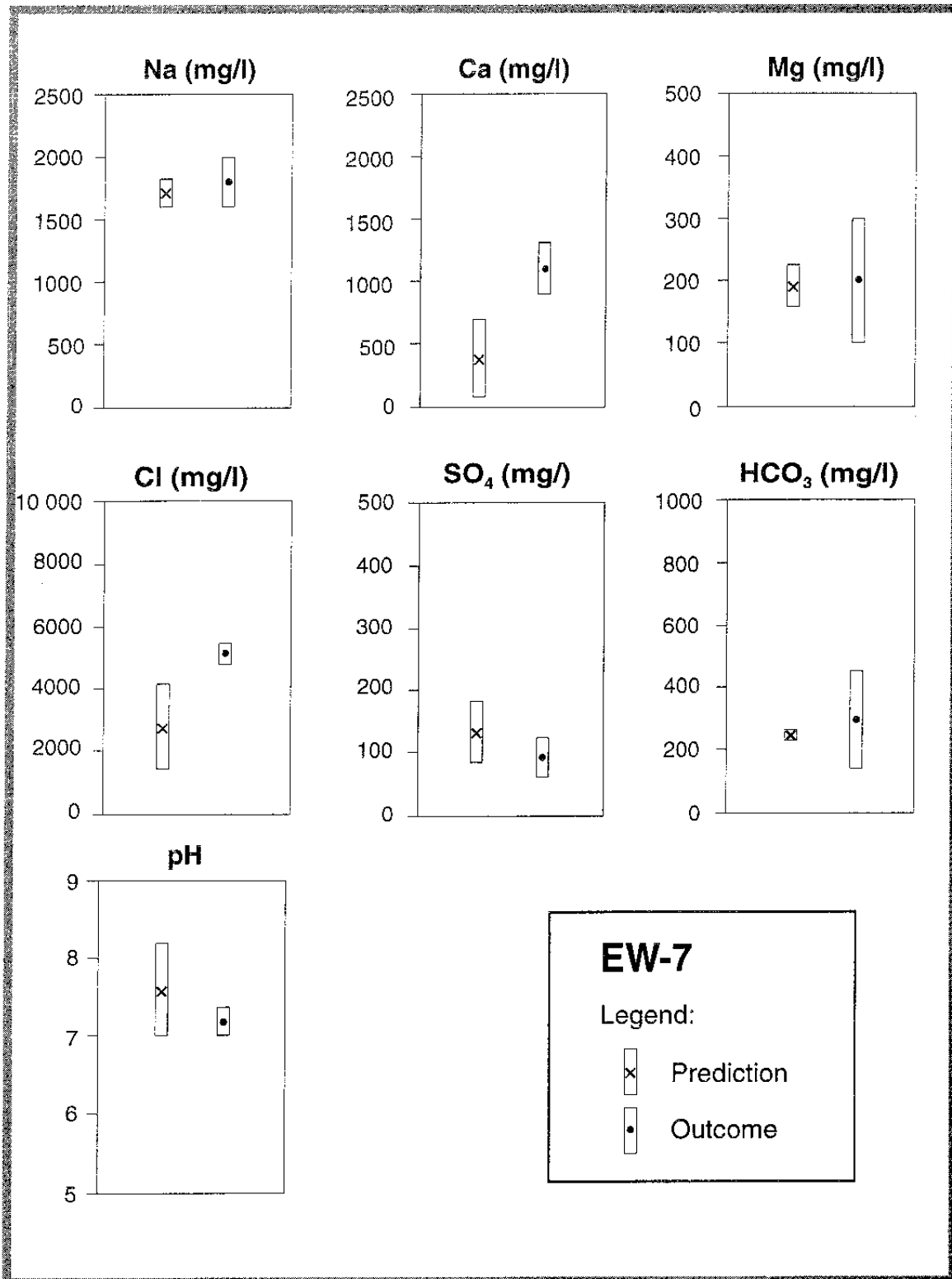


Figure 1-14. Graphical illustration of the predicted and observed concentrations of main constituents in the groundwater in fracture zone EW-7. For the discussion of the results and different prediction methods see Section 1.4.

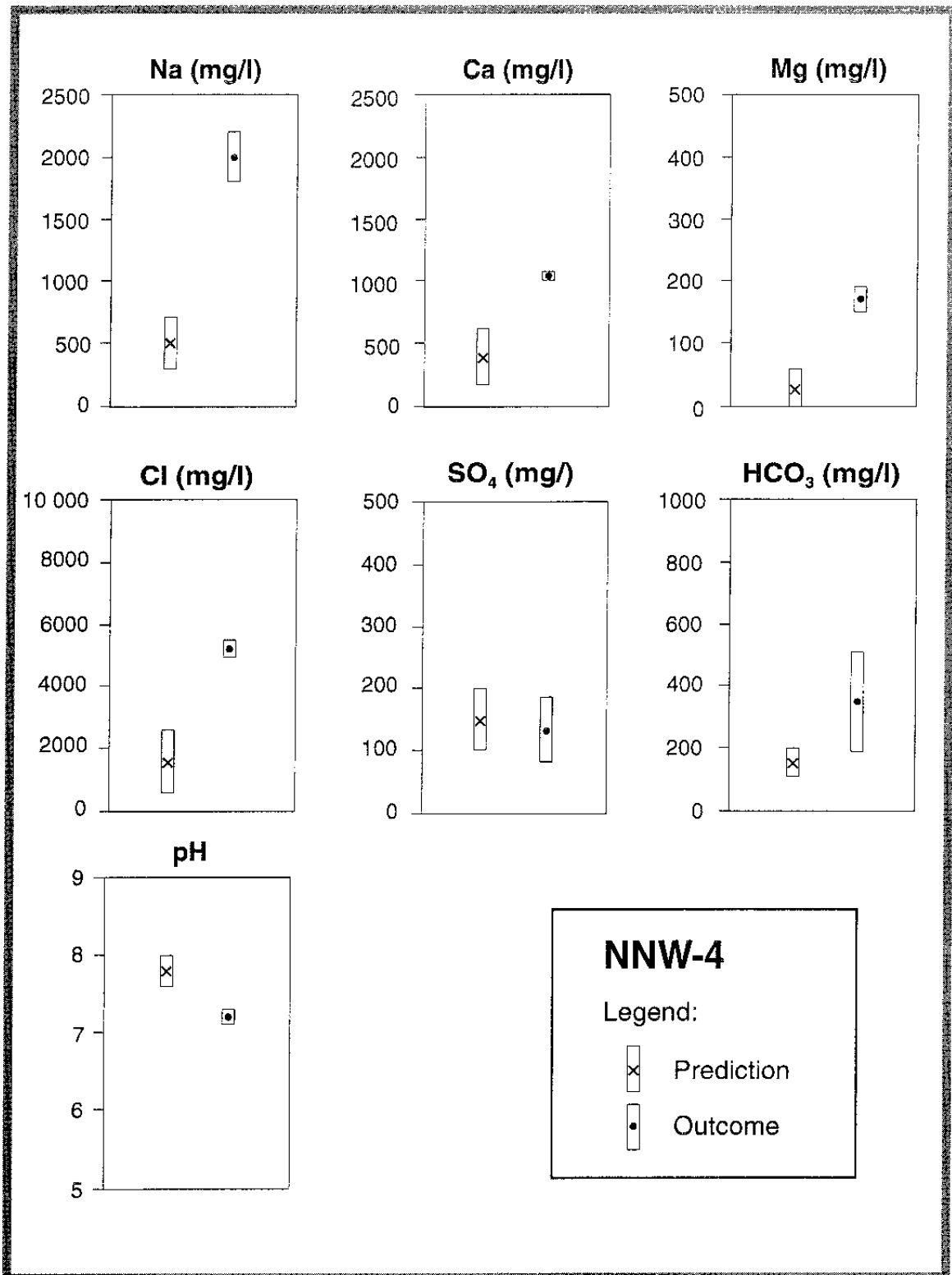


Figure 1-15. Graphical illustration of the predicted and observed concentrations of main constituents in the groundwater in fracture zone NNW-4. For the discussion of prediction methods see Section 1.4.

Table 1-9. Predicted and observed groundwater chemistry representing fracture zone NNW-4.

Prediction/ Outcome	Na mg/l	Ca mg/l	Mg mg/l	Cl mg/l	SO ₄ mg/l	HCO ₃ mg/l	pH
Prediction	500 ±200	400 ±200	30 ±30	1500 ±1000	150 ±50	150 ±50	7.8 ±0.2
Outcome	2000 ±200	1050 ±30	170 ±20	5300 ±300	135 ±50	350 ±160	7.2 ±0.1

Table 1-10. Predictions based on expert judgement and observed concentrations of iron and potassium in the Äspö groundwaters.

ZONES	Fe concentration in mg/l		K concentration in mg/l	
	predicted	observed	predicted	observed
NE-1	0.6 ± 0.6	2.0 ± ---	31 ± 20	9 ± 2
NE-2	0.3 ± 0.3	0.8 ± 0.2	5 ± 5	10 ± 2
NE-3	0.6 ± 0.6	4 ± 1	34 ± 10	25 ± 5
NE-4	0.6 ± 0.6	3 ± 1	35 ± 15	19 ± 10
EW-3	-----	2 ± 1	-----	10 ± 2
EW-5	0.3 ± 0.3	0.2 ± 0.1	5 ± 5	10 ± 10
EW-7	0.6 ± 0.6	0.3 ± 0.2	26 ± 10	23 ± 11
NNW-4	0.3 ± 0.3	-----	5 ± 5	15 ± 5

1.4 SCRUTINY AND EVALUATION

Several aspects of the groundwater chemistry must be assessed. The first one and, in comparison with the predictions, the most important one, is the chemistry of the major water-conducting features where detailed predictions and observations were made at the same location, i.e. sampling of water from major fracture zones identified during pre-investigations and re-sampled during the tunnel construction phase. Other important aspects concern the chemical

and biological processes encountered during the tunnel construction phase and which were not included in the predictions. The tunnel construction, i.e. grouting, also influenced the chemistry. A thorough and detailed examination of chemical conditions observed during the tunnel construction phase has been made by *Laaksoharju and Skårman /1995/*.

1.4.1 Major fracture zones

NE-1

The results listed in *Table 1-2* and shown graphically in *Figure 1-5* indicate that the observed concentrations of sodium, calcium, magnesium, chloride, sulphate, bicarbonate and pH fall within the span of the predictions. The ranges for potassium (*Table 1-10*) also overlap. The iron concentration (*Table 1-10*) differs from the prediction.

The thorough investigation with several boreholes penetrating NE-1 made the predictions more certain for this fracture zone than for the others.

During the course of the tunnel construction there were changes in the chloride concentration from 5300 to 3900 mg/l /*Laaksoharju and Skårman, 1995/*. The variation in the sodium concentration is similar, while there has been a greater variation in the calcium concentration. The bicarbonate concentration shows large variations, from 170 up to 430 and back to 340 mg/l. The reason for these major changes is the extensive microbial sulphate reduction which affects the bicarbonate and the sulphate concentrations in this part of the tunnel /*Laaksoharju, 1995/*. The sulphate concentrations vary between 100 to 260 mg/l. The variation in calcium concentration is probably due to the variation in bicarbonate which affects the calcium content since the groundwater is saturated with respect to the calcite solubility.

NE-2

The chemical character of NE-2 is comparable with the predictions shown in *Table 1-3* and *Figure 1-7*. The main reason for the deviation is considered to be that the fracture zone was intersected at a tunnel position different from that expected, due to a deviation in dip (see *Stanfors et al /1997/*), and the fact that it was narrower at depth than expected. It was also less conductive than expected (see *Part 1*).

The bicarbonate, calcium, potassium and the iron concentrations agree with the predictions. The difference between predicted and observed concentrations is largest for sulphate which is due to higher salinity, sodium and chloride concentrations, than predicted. The pH-value is also outside the predicted range.

Fracture zone NE-2 was intersected by the tunnel at three different positions, whereas it was expected to be observed in only one corner of the tunnel (see *Gustafson et al /1991/*). The intersections of the tunnel at 1600 and 1900 m, which are closest to the predicted position, give a fairly similar groundwater composition. During the course of the tunnel excavation the chloride concentration started at 5100 mg/l and increased to a maximum of 6200 mg/l and then decreased to 5100 mg/l. At tunnel section 2450 m the salinity is higher and the variation is smaller.

The difference between the prediction and outcome for NE-2 has no major impact on the hydro-chemistry of Äspö. From *Figure 1-7* it can be seen that the change in composition with time is larger than the difference between the prediction and outcome (see *Part 3, Transport of solutes*). It might be that the situation already at the tunnel front was largely different from the undisturbed situation or that the variability is large due to the low permeability of the fracture zone.

NE-3

The difference as shown in *Table 1-4 and 1-10* and *Figure 1-9* indicates that the outcomes for calcium, potassium and magnesium were within the predicted ranges. A very large discrepancy exists for bicarbonate and sulphate, and is due to bacterial sulphate reduction (see *Section 1.4.3*). The difference in salinity, sodium and chloride, is small.

During the excavation of the tunnel there was a large variation in the concentration of main constituents. The chloride concentration started at 5600 mg/l and ended at 3600 mg/l. The bicarbonate concentration went from 500 to 531 and to 274 mg/l. The difference in prediction and outcome is probably due to the fact that no good representation of NE-3 existed at the time when the predictions were made. The large variation in time indicates that there might be a large variability in the fracture zone.

NE-4

Sodium, magnesium, potassium, bicarbonate and pH are within the predicted ranges (see *Figures 1-11 Table 1-5, 1-10*). Calcium, chloride, sulphate and iron concentrations are outside the predicted ranges.

During the course of the tunnel excavation there was a decrease in the chloride concentration from 5400 to 3200 mg/l and a change from 170 to 480 to 300 mg/l of bicarbonate. Bacterial sulphate reduction affected the groundwater composition (see *Section 1.4.3*).

EW-3

No predictions were made for this fracture zone. The reason was that there were no indicators for a specific EW-3 groundwater chemistry.

EW-5

In the tunnel only two fracture zones, both less than one metre wide, were found to intersect the tunnel (at 220 m depth between 1744-1850 m tunnel length). Most of the gently dipping fractures occur as fracture swarms rather than zones. Neither the fracture swarms nor the zones are generally water bearing unless they intersect vertical structures.

In the preliminary evaluation of tunnel section 1475-2265 m the water samples collected at tunnel section 1744-1850 m were considered to represent EW-5. It should be noted that the prediction and outcome for EW-5, presented in *Table 1-7*, are as good as for the other fracture zones. This implies that the major influence on the prediction is the depth and the position, i.e. x,y,z, and not the particular fracture zones.

EW-7

The prediction and outcome are in agreement as regards sodium, magnesium, potassium, sulphate, bicarbonate, iron and pH. As for NE-4 the calcium and chloride concentrations are higher than predicted.

There are rather few observations on the chemistry of fracture zone EW-7 since the same sampling points also represent NE-4. These two fracture zones are hydraulically well connected so the groundwater composition is similar.

NNW-system

For NNW-4 the measured concentration of sulphate resembles the predicted value. For all the other constituents there is a large difference. This difference is mainly due to the much higher salinity of the groundwater than predicted. Because of the high connectivity of the NNW-fracture system the water was expected to be derived from the surface. In turn the NNW-4 groundwater seems to be equally mixed from water derived from all possible directions /*Laaksoharju and Skårman 1995*/. The NNW-4 fracture system has the most complex hydro-chemistry of all the fracture zones.

1.4.2 Test of different spatial assignment methods

The initial assumption is that the hydro-chemical, system is static and that the observed composition is dependent on the position in the rock. As already described initially this is not the case, but is a way to handle the groundwater chemistry predictions.

Predictions were presented for all the major fracture zones (see *Section 1.3*). At an early stage of the tunnel construction it was evident that there were sometimes large differences between the predicted and the observed concentrations of different constituents. One obvious reason for the difference would be that the predicted undisturbed conditions were not so undisturbed when the tunnel had been constructed. This was the most important question to resolve, but there were other questions as well. These were related to the prediction method itself, i.e. Could there be different "results" of the predictions simply because the predictive tools were different?

For the comparison between the different prediction methods it is necessary first to find out which is the relevant observations with which to make the comparison and second to estimate the uncertainty of the predicted values. Regarding the relevant output, it is the undisturbed conditions which were predicted and which should be used in any comparison. The relevant output should therefore be the initial value of the outcome. (In *Part 3*, Transport of solutes, it is evident that the initial outcome might also be non-representative of the undisturbed conditions.) As regards the uncertainty, it is dependent on several factors, different for the initial state in relation to the subsequent predictions.

The initial predictions, which were compared with the outcome in *Section 1.4.1*, were made on the basis of Principal Component Analyses (PCA) and an ordinary evaluation of the hydro-chemistry as a function of depth. In most cases the difference between the PCA and the ordinary value was small, whereas in a few cases there were large differences. For small differences the average value was used and the difference was defined as the uncertainty. In a few cases the initial predictions were pure estimates (i.e. for NNW-4).

During the tunnel construction phase other predictions, based purely on mathematical methods, were also compared with the outcome. The results of all the prediction methods are compared with the outcome in *Figures 1-16 to 1-22*.

Most of the groundwater chemistry data measured in the boreholes during the pre-investigations does not follow a normal distribution. Despite this the data is presented by a median value, quartile and interquartile ranges. The same uncertainty values are given to all the different methods. This treatment of the data is justified by the fact that the tunnel data is also expected to have a similar distribution as the borehole data. In *Figures 1-16 to 1-22* the data are given the median value \pm half the interquartile range of the borehole data.

The results for the different fracture zones are:

NE-1

The different prediction methods give an acceptable agreement for sodium, calcium and chloride (see *Figure 1-16*). The difference in predicted sulphate and bicarbonate contents is larger, but it should also be noted that there is a great difference in these concentrations between the initial and some of the later samples. For the NE-1 fracture zone the initial predictions and those made by kriging and neural network are slightly better than PCA and linear regression (see *Table 1-11*).

NE-2

In general, for all constituents, the prediction methods tested later turned out to give a closer agreement to the outcome than the initial prediction (see *Figure 1-17*). The initial prediction assumed an inflow of more shallow non saline water which did not take place, i.e. the expert judgement failed.

NE-3

Some of the later tested prediction methods are closer to the outcome than the initial prediction (see *Figure 1-18*). The reason is probably that the groundwater samples collected during drilling in the pre-investigation phase were not representative of the fracture zone NE-3. The initial predictions rely entirely on samples from the fracture zone whereas the other prediction methods are affected by the entire data set.

NE-4

Predictions and outcomes are presented in *Figure 1-19*. As for NE-3, neural network and kriging gave predicted values closer to the outcome than the initial predictions. The reason is thought to be that the initial predictions rely heavily on the data from the specific fracture zone. As for NE-3, data had been obtained only from sampling during drilling.

EW-3

The predictions made to test the different methods and the outcome are presented in *Figure 1-20*. Except for bicarbonate the outcomes fall within the predicted intervals. No expert judgement was made for EW-3 since there were no specific EW-3 groundwater identified during pre-investigations.

EW-5

No additional predictions were made of the hydro-chemistry of EW-5 since the fracture zone does not exist.

EW-7

The later tested prediction methods are closer to outcome than the expert judgement. In *Figure 1-21* the outcome for all major constituents, sodium, calcium, sulphate, bicarbonate and chloride fall within the predicted range except for the initial predictions.

NNW-system

The predictions made by all the different prediction methods are presented in *Figure 1-22*. For sodium, calcium and chloride, the later predictions gave a better fit to the measured values, while for sulphate the values predicted initially was closer to the outcome than the later predictions.

NE-1

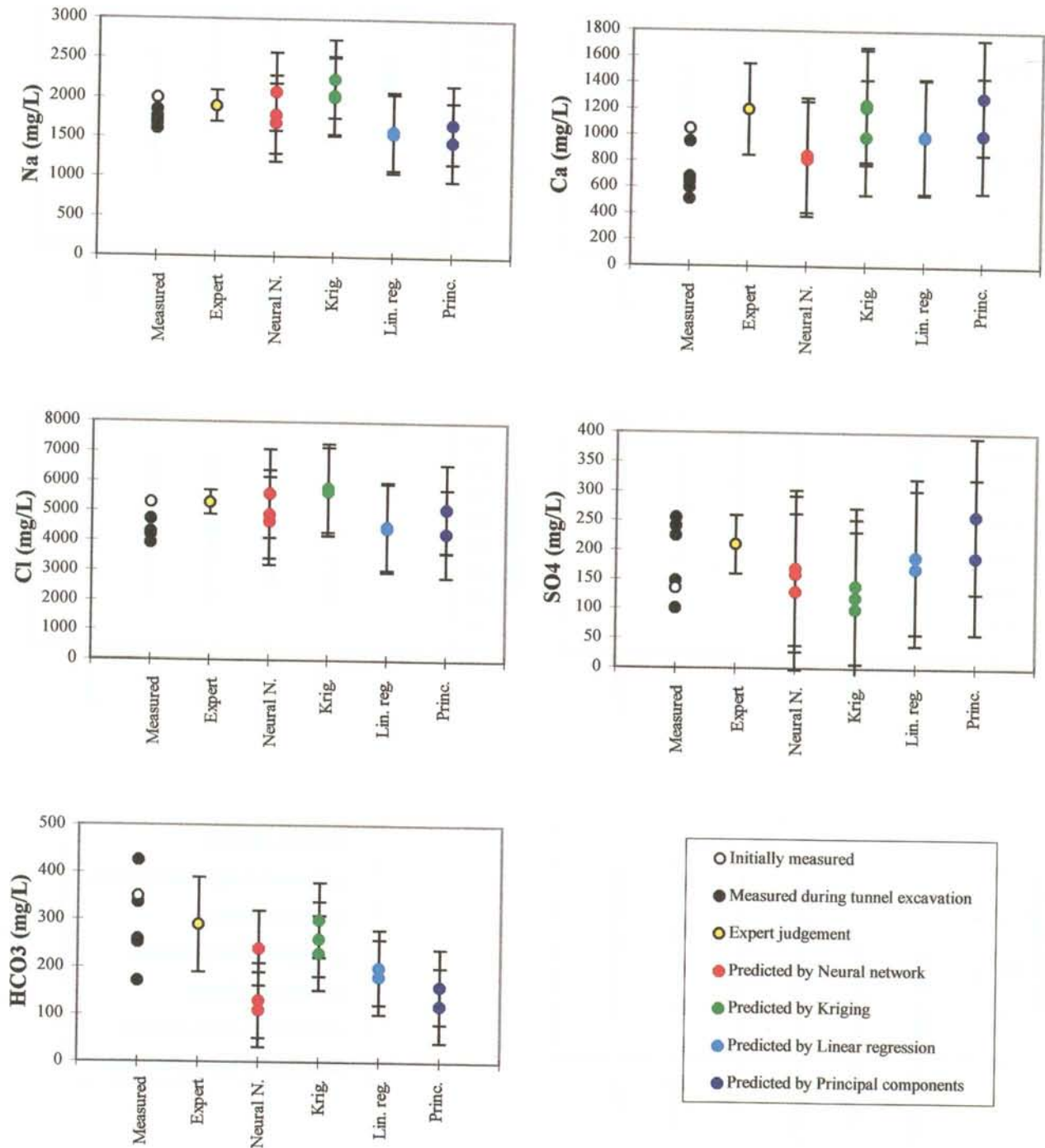


Figure I-16. Graphical illustration of the predicted and observed concentrations of main constituents in the groundwater in fracture zone NE-1.

NE-2

Tunnel length: 1600m

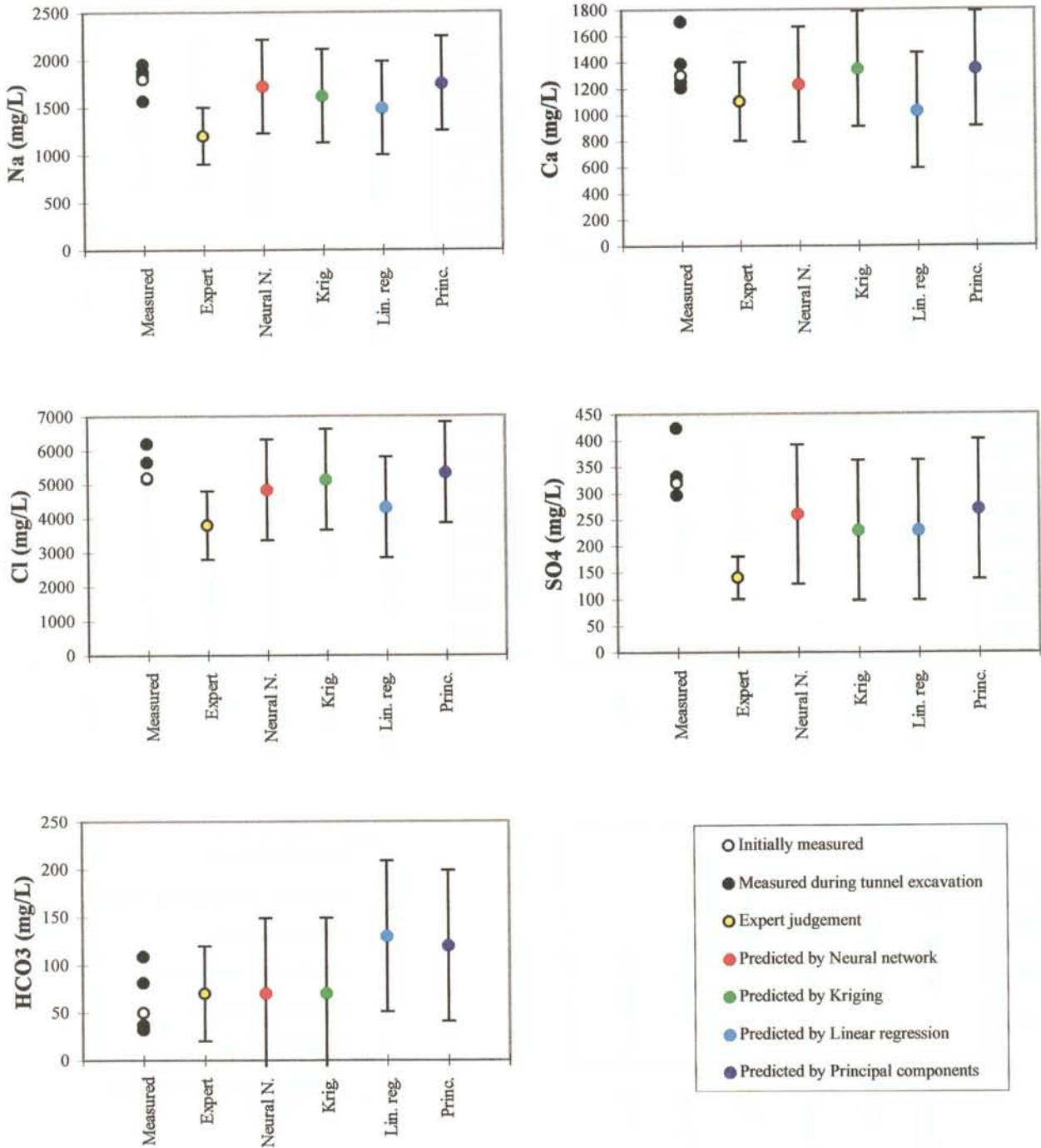


Figure 1-17. Graphical illustration of the predicted and observed concentrations of main constituents in the groundwater in fracture zone NE-2.

NE-3

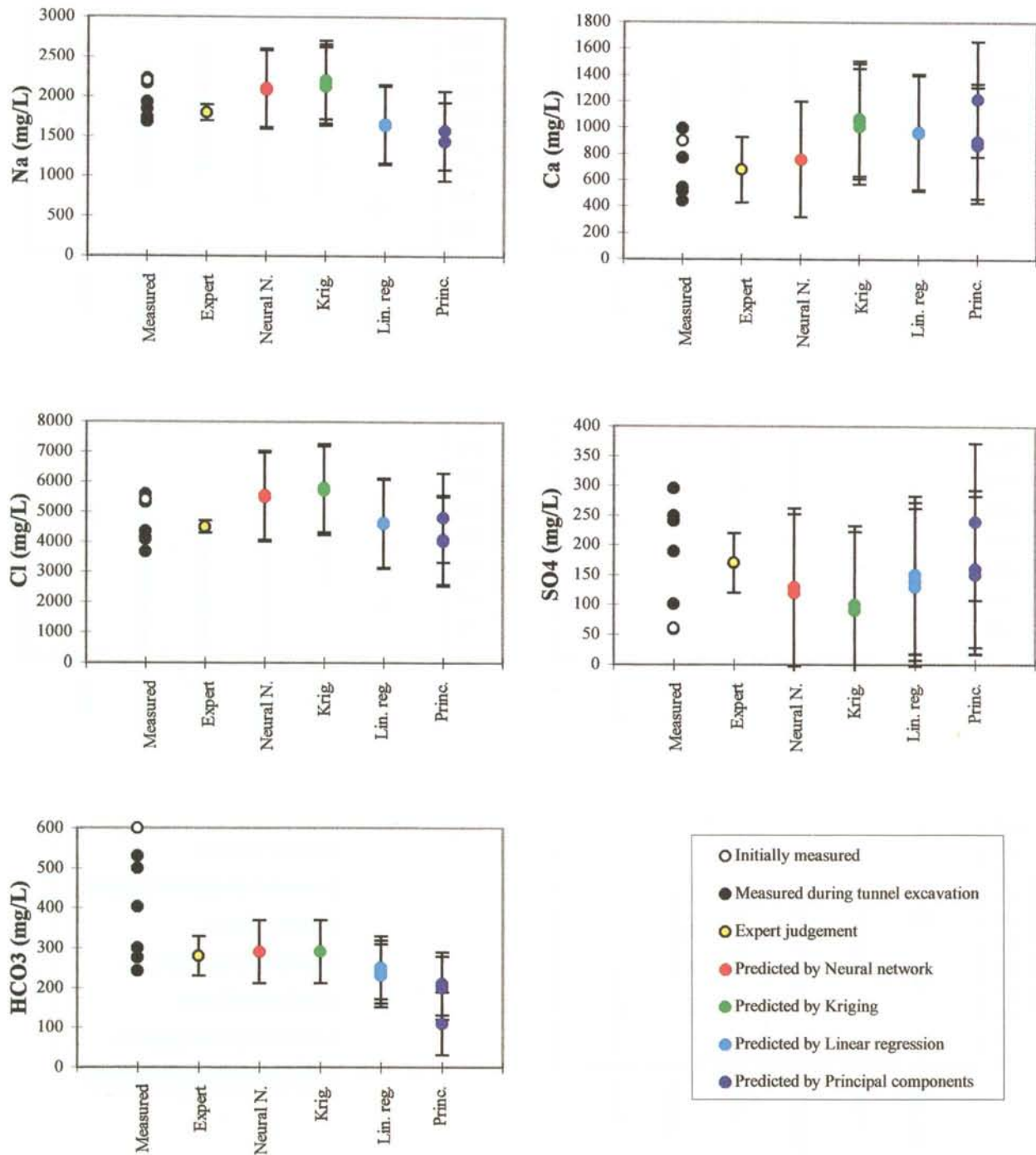


Figure 1-18. Graphical illustration of the predicted and observed concentrations of main constituents in the groundwater in fracture zone NE-3.

NE-4

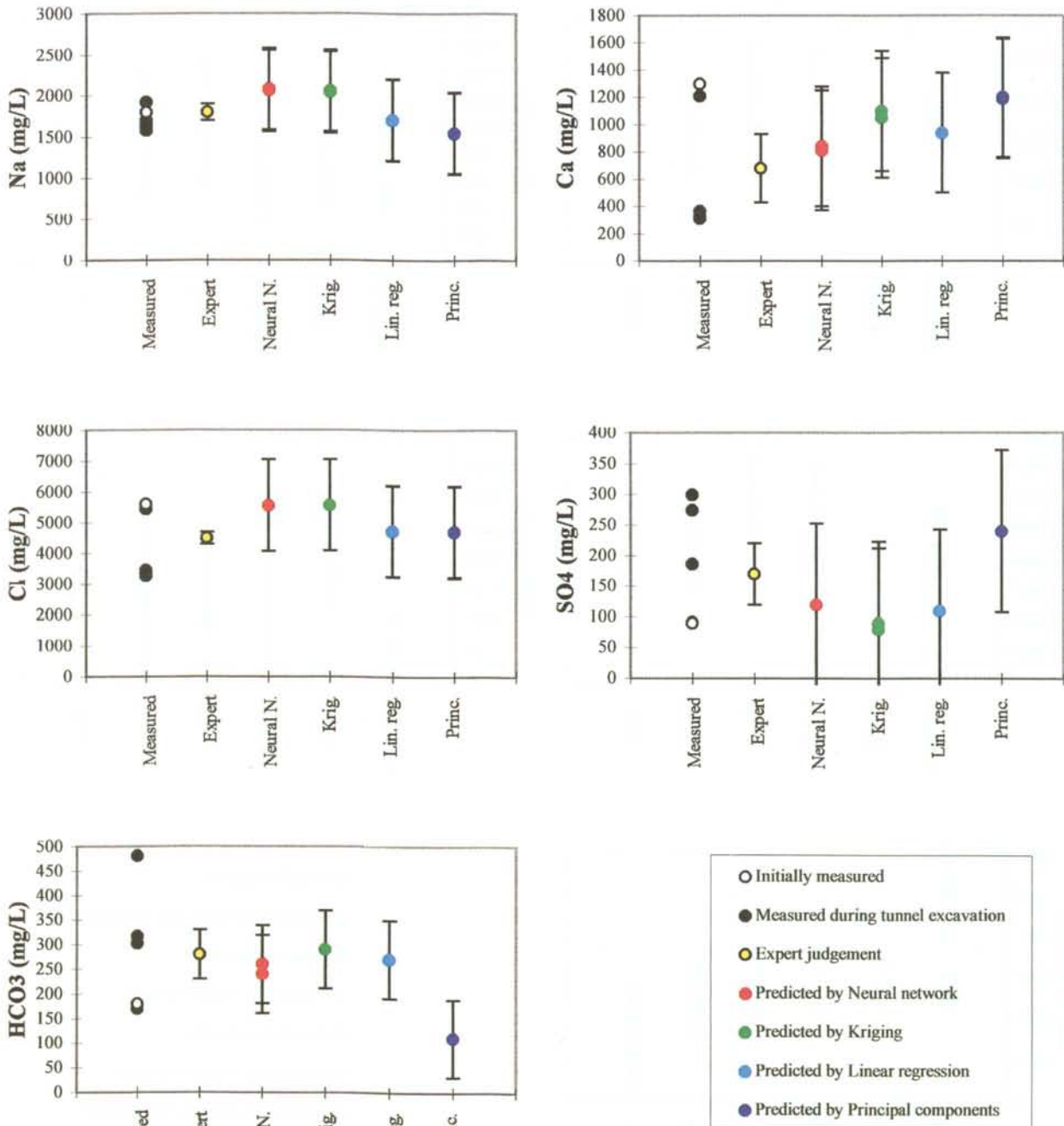


Figure 1-19. Graphical illustration of the predicted and observed concentrations of main constituents in the groundwater in fracture zone NE-4.

EW-3

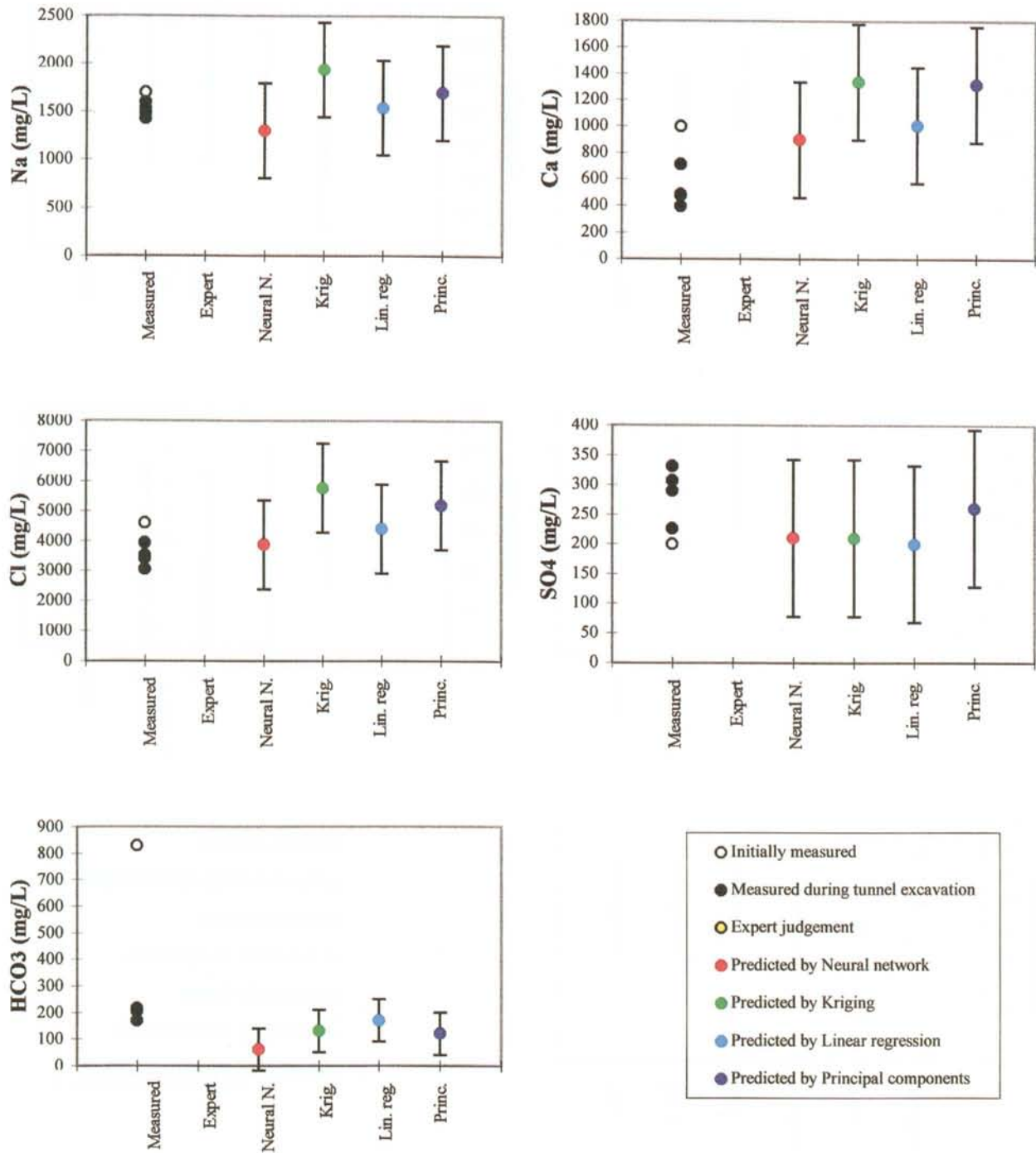


Figure 1-20. Graphical illustration of the predicted and observed concentrations of main constituents in the groundwater in fracture zone EW-3.

EW-7

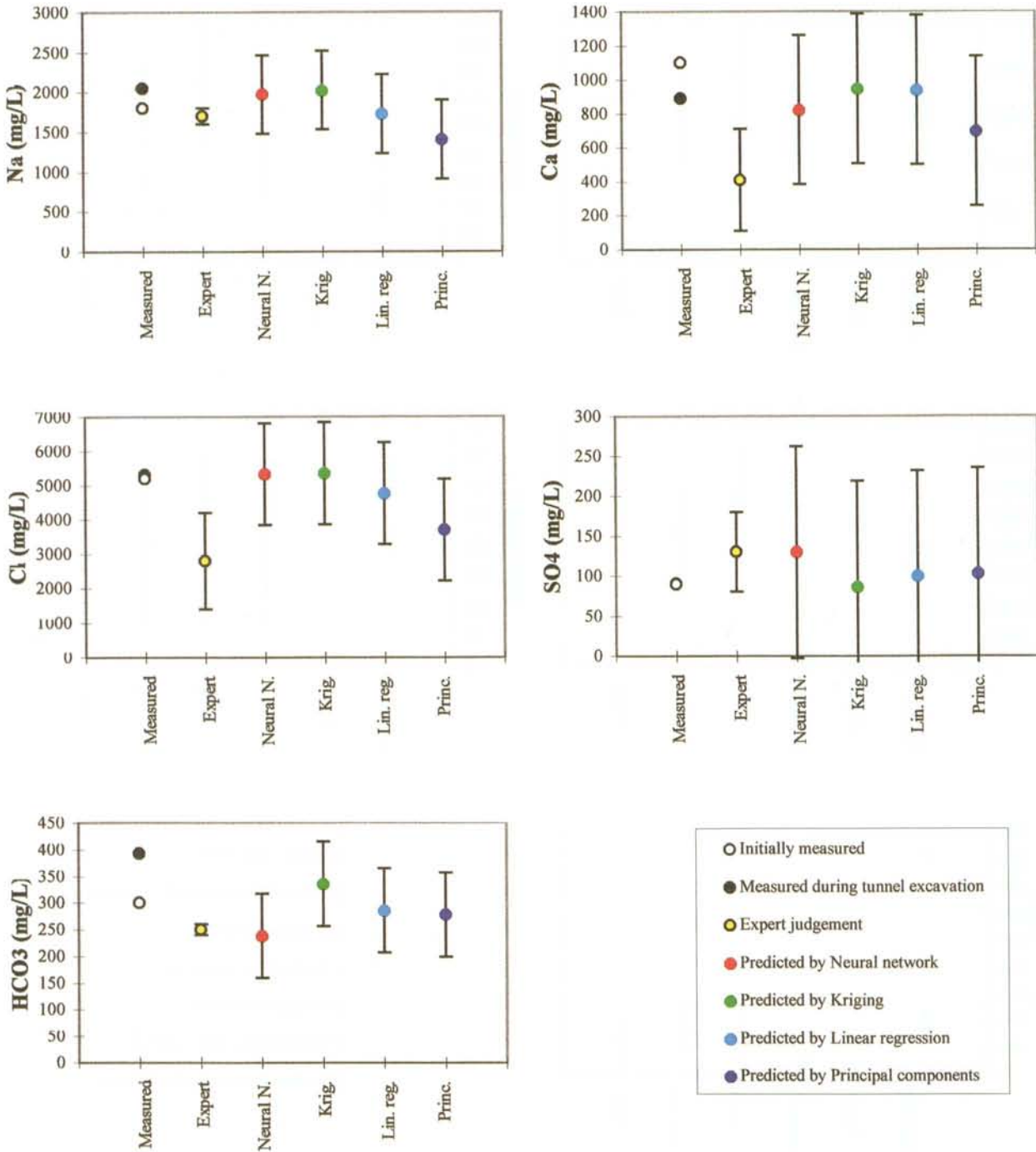


Figure 1-21. Graphical illustration of the predicted and observed concentrations of main constituents in the groundwater in fracture zone EW-7.

NNW-4

Tunnel length: 2020m

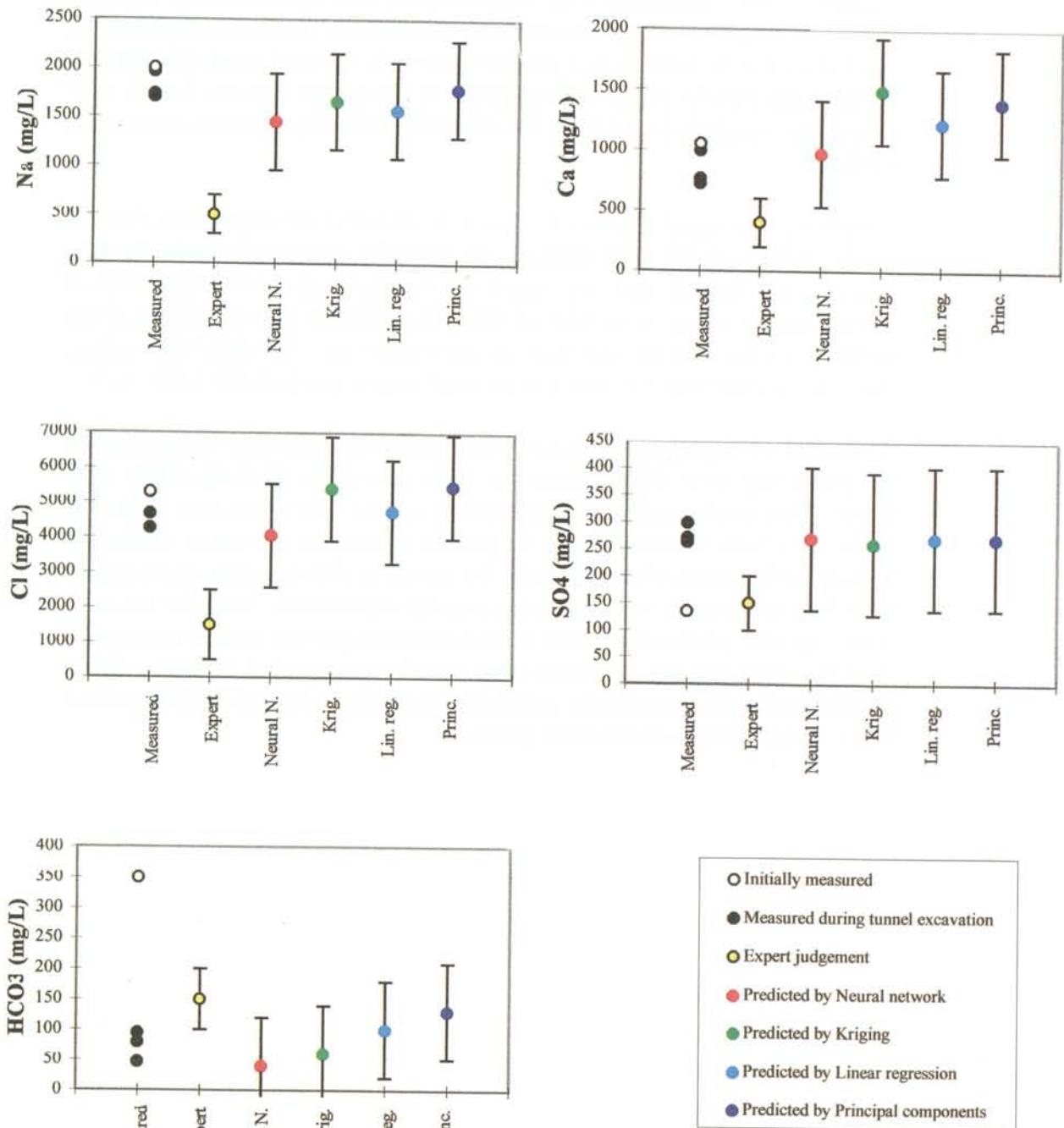


Figure 1-22. Graphical illustration of the predicted and observed concentrations of main constituents in the groundwater in fracture zone NNW-4.

To begin with, the strong and the weak points of each method must be identified. This has been done quite intensively by *Wikberg et al /1994b/*. (The interested reader is encouraged to read the discussion of that report to fully understand the comparison.) All methods are at first adjusted to the borehole data from the pre-investigations (learning, calibration, parameter adjustment), see *Figure 1-23* for location of the data points. In the next stage, the different methods are used for predicting conditions in the tunnel. *Figures 1-24 to 1-33* present the comparison between the different prediction methods, element by element.

Simply by looking at *Figures 1-24 to 1-33* one gets the impression that the results differ and that some methods are generally closer to the outcome than others, even though they are based on the same data sets. One way of comparing the results is to find out for each predicted item which one of the methods is closest to the outcome, second closest, etc. The individual scores, the sum for each fracture zone and the total sum is presented in *Table 1-11*.

In *Table 1-11* kriging has the lowest score and is thus the most suited method for predicting the hydro-chemistry of Äspö among the methods which were tested. This result might be a coincidence and the conclusion that kriging is always the best method cannot be proved simply on this basis. However, looking at the scores of chloride only, the picture is still the same, and it should therefore be possible to draw some general conclusions. Both for the total scores and the scores of chloride neural networks give the second best result. As these methods are non-linear they should be expected to give a better prediction than PCA and linear regression analyses which can only describe a linear trend between observation points.

Table 1-11. Results of scores summing for the different fracture zones. Bold figures indicate the best results.

Fracture zone	Expert judgement	Neural Networks	Kriging	Linear regression	Principal component analyses
NE-1 Sum:	10	11	9	16	22
Na	1	1	1	5	4
Ca	3	4	1	1	5
Cl	1	1	4	5	3
SO ₄	4	1	2	2	5
HCO ₃	1	4	1	3	5
NE-2 Sum	21	12	9	20	10
Na	5	2	3	4	1
Ca	4	2	1	5	2
Cl	5	3	1	4	2
SO ₄	5	2	3	3	1
HCO ₃	2	3	1	4	4
NE-3 Sum	17	7	6	12	17
Na	3	1	1	4	5
Ca	5	3	2	1	4
Cl	5	1	2	4	3
SO ₄	4	2	1	3	5
HCO ₃	--	--	--	--	--
NE-4 Sum	19	13	11	15	14
Na	1	4	2	2	4
Ca	5	4	2	3	1
Cl	5	1	1	3	3
SO ₄	4	3	1	2	5
HCO ₃	4	1	5	3	1
EW-7 Sum	18	18	12	6	18
Na	3	3	1	1	5
Ca	5	4	3	2	1
Cl	5	4	3	1	2
SO ₄	3	3	2	1	5
HCO ₃	2	4	3	1	5
NNW-4 Sum	16	11	11	10	8
Na	5	2	2	4	1
Ca	5	1	4	1	3
Cl	5	3	1	3	2
SO ₄	1	5	4	2	2
HCO ₃	--	--	--	--	--
Sum of all const.	101	72	58	79	89
Sum of chloride	26	13	12	22	15

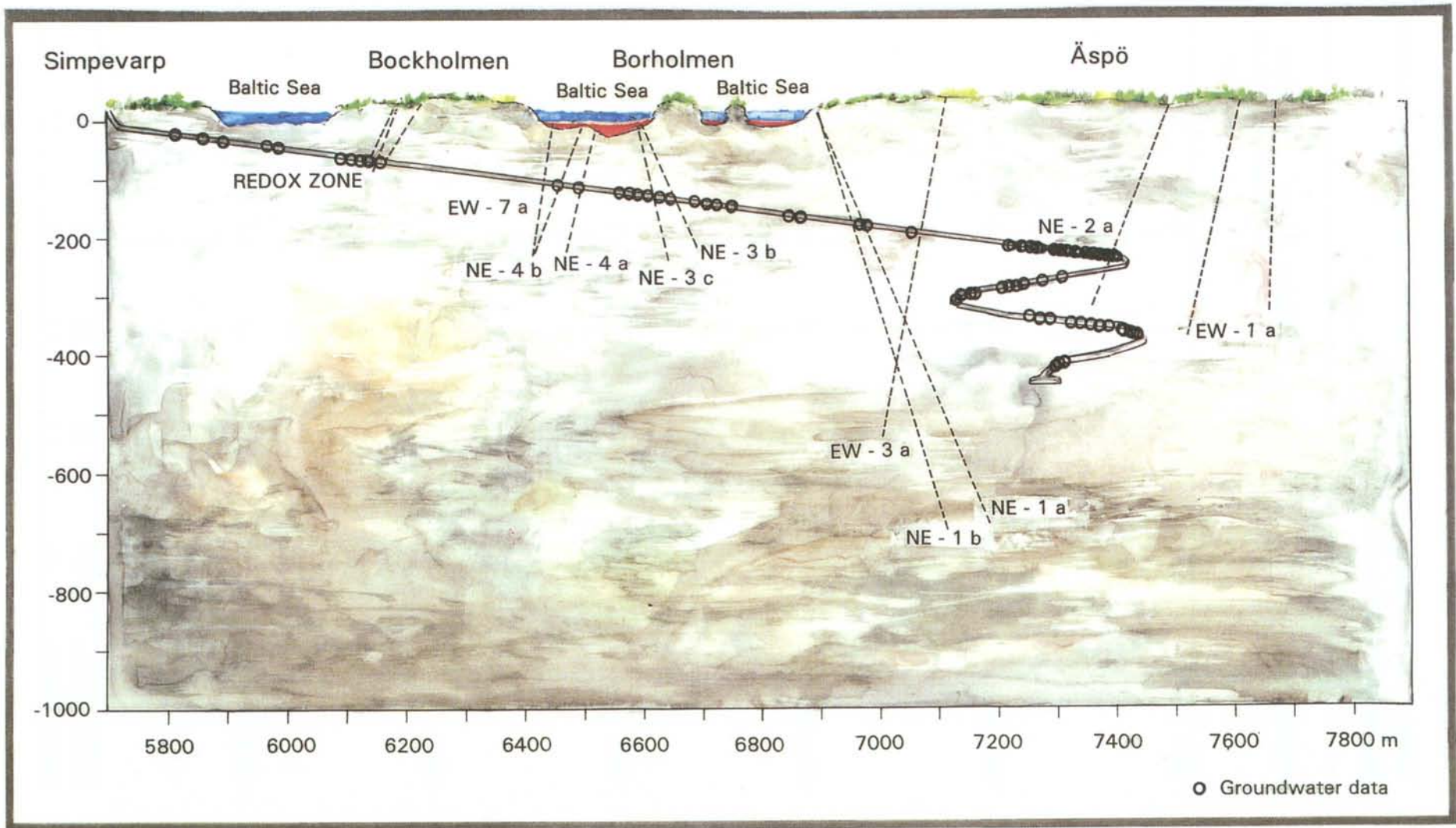


Figure 1-23. A vertical cross section of Äspö presenting the location of data collection in boreholes from the tunnel. For a view of all sampling points see Figures 1-21 and 1-22 in Part 3.

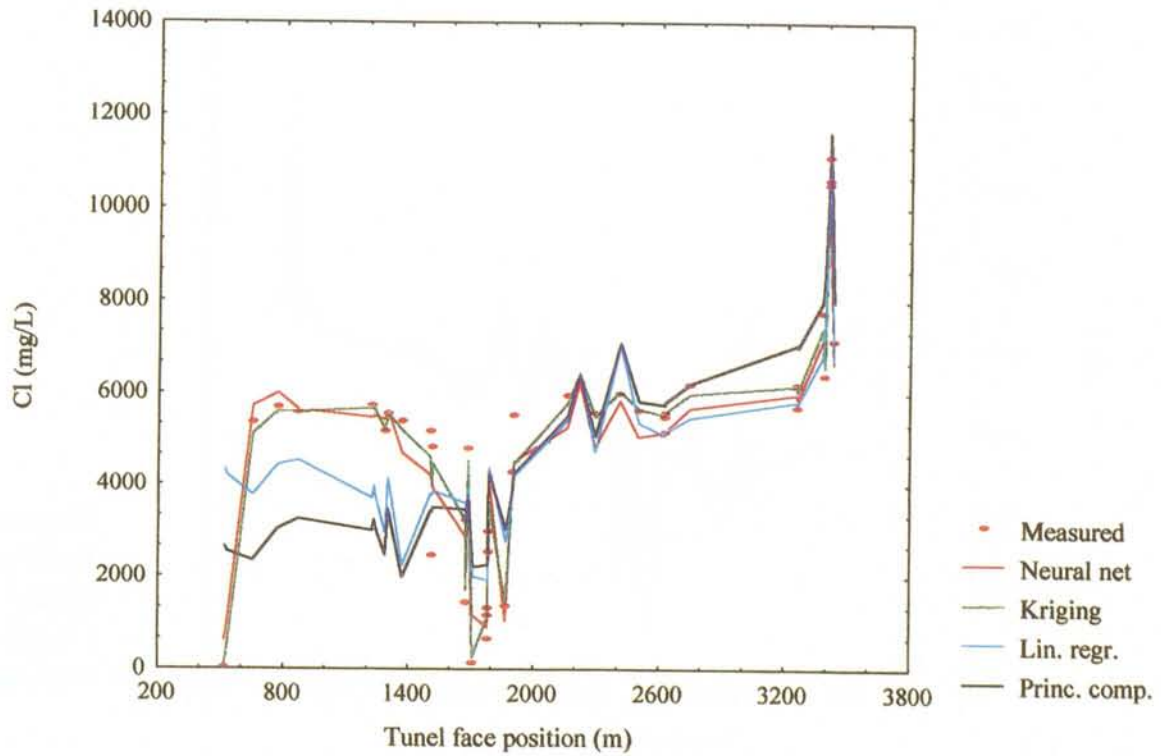


Figure 1-24. Measured chlorine content in boreholes from the pre-investigation phase of the HRL construction and the applied prediction models: neural network, kriging, linear regression and principal components.

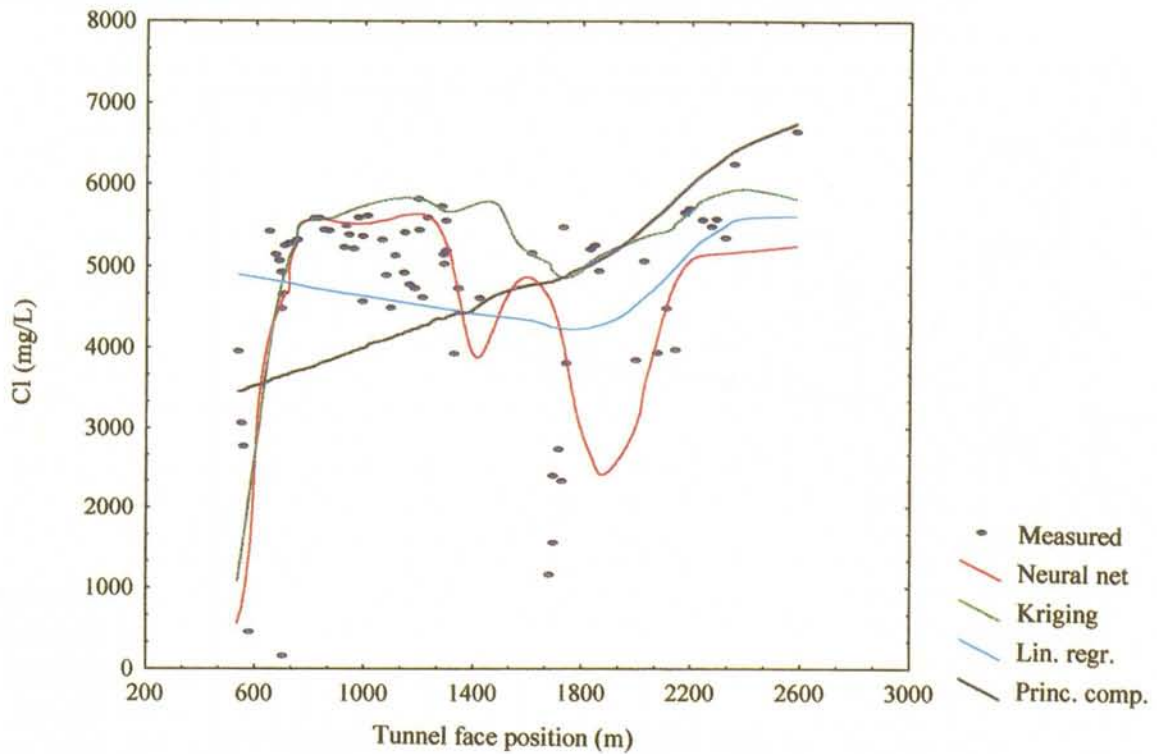


Figure 1-25. The results of the predicted tunnel data for the element chlorine, using neural network, kriging, linear regression and principal components are compared with measured tunnel data.

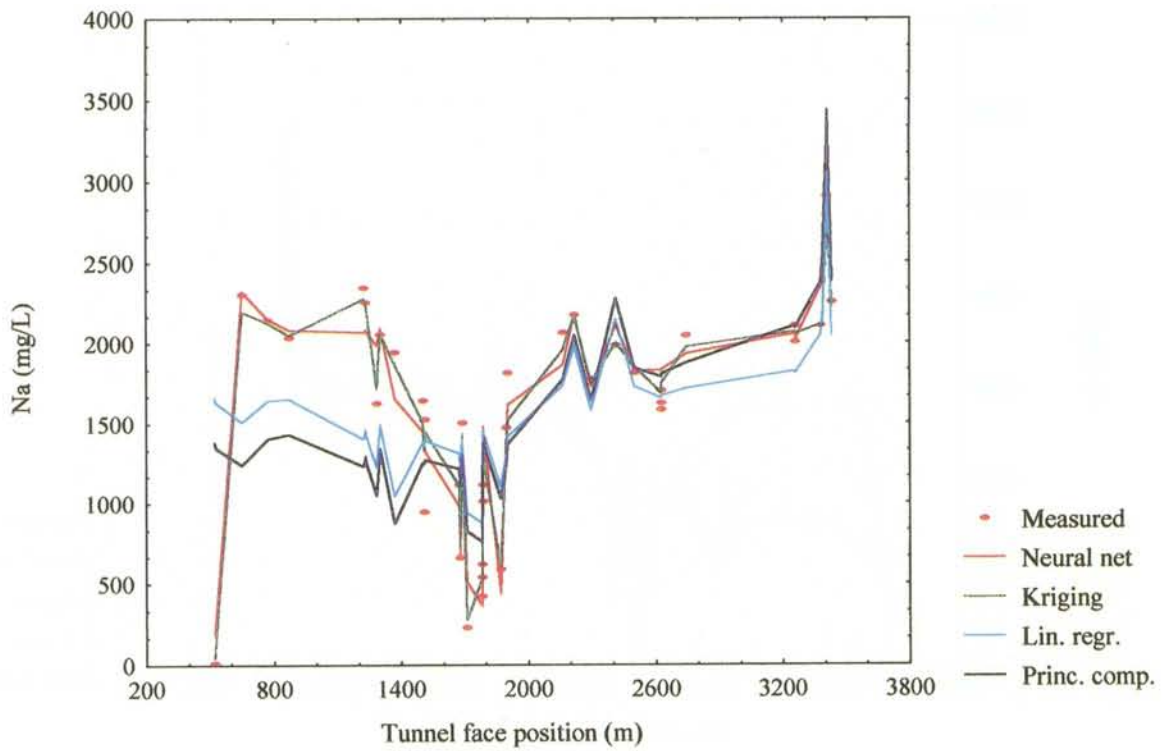


Figure 1-26. Measured sodium content in boreholes from the pre-investigation phase of the HRL construction and the applied prediction models: neural network, kriging, linear regression and principal components.

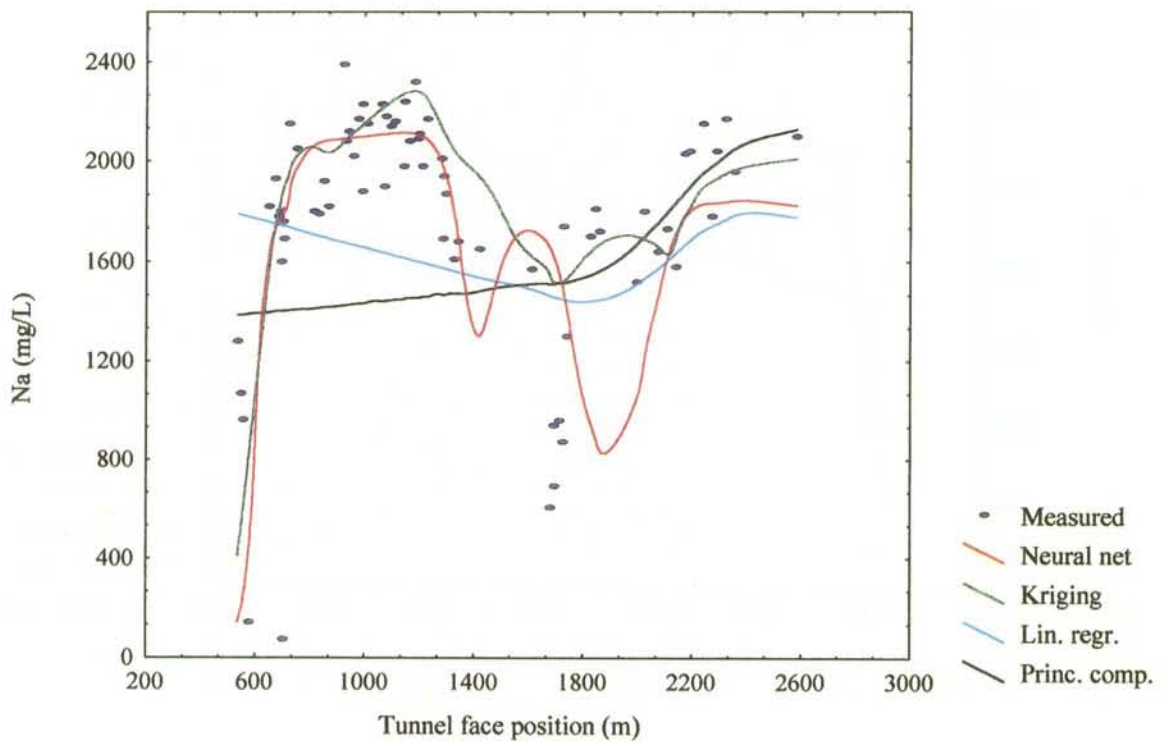


Figure 1-27. The results of the predicted tunnel data for sodium, using neural network, kriging, linear regression and principal components are compared with measured tunnel data.

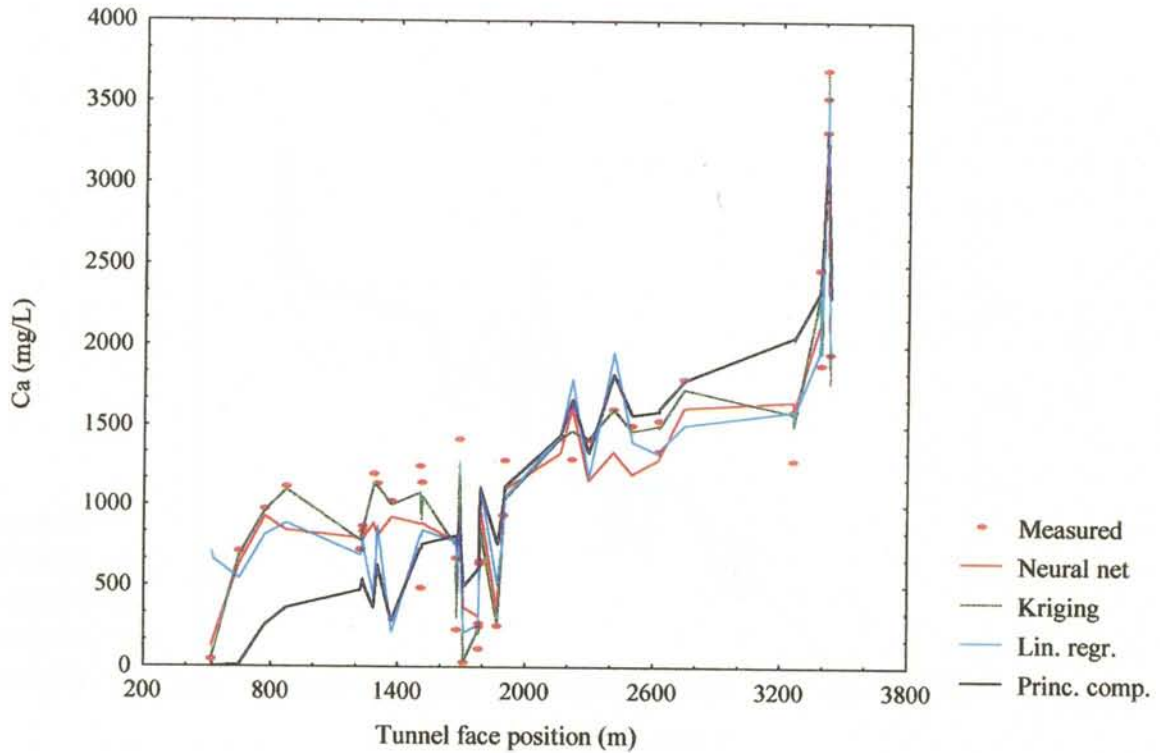


Figure 1-28. Measured calcium content in boreholes from the pre-investigation phase of the HRL construction and the applied prediction models: neural network, kriging, linear regression and principal components.

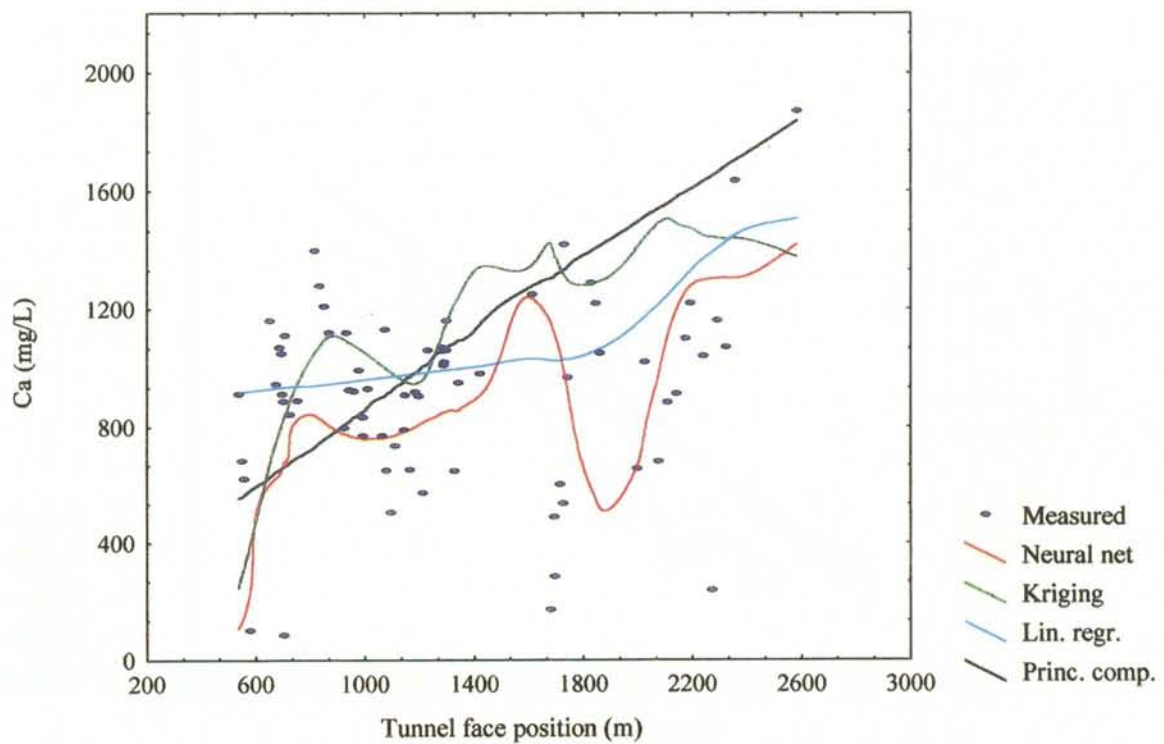


Figure 1-29. The results of the predicted tunnel data for calcium, using neural network, kriging, linear regression and principal components are compared with measured tunnel data.

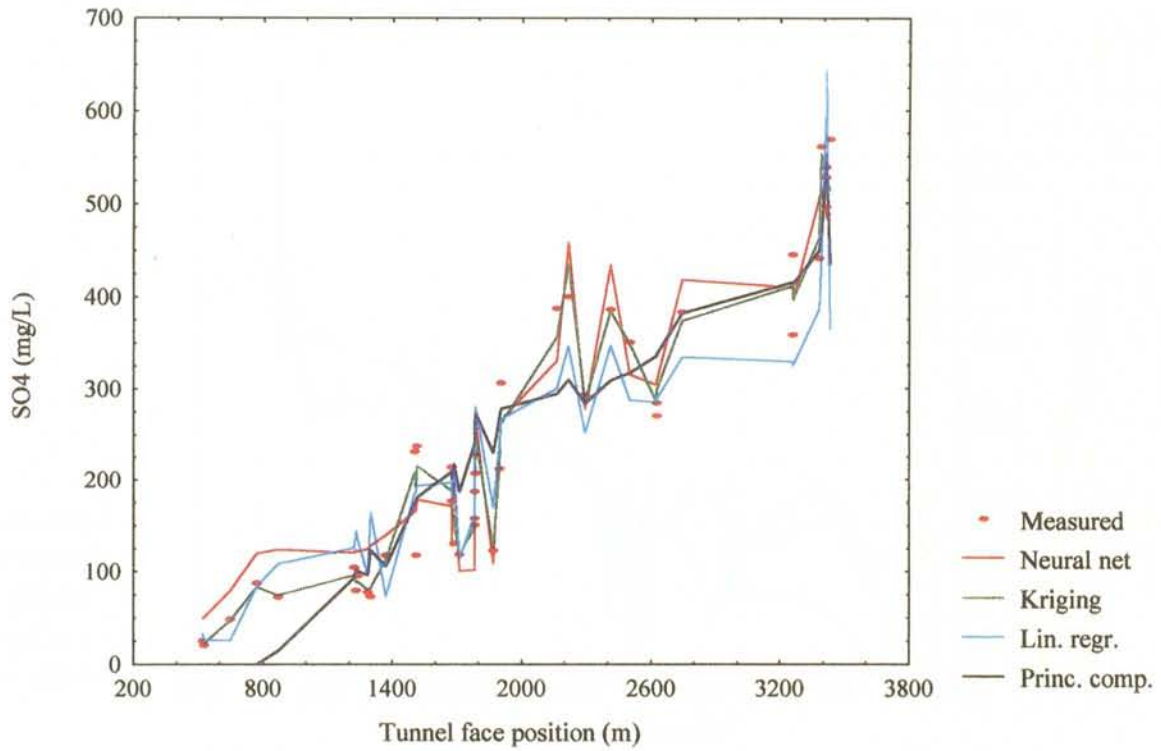


Figure 1-30. Measured sulphate content in boreholes from the pre-investigation phase of the HRL construction and the applied prediction models: neural network, kriging, linear regression and principal components.

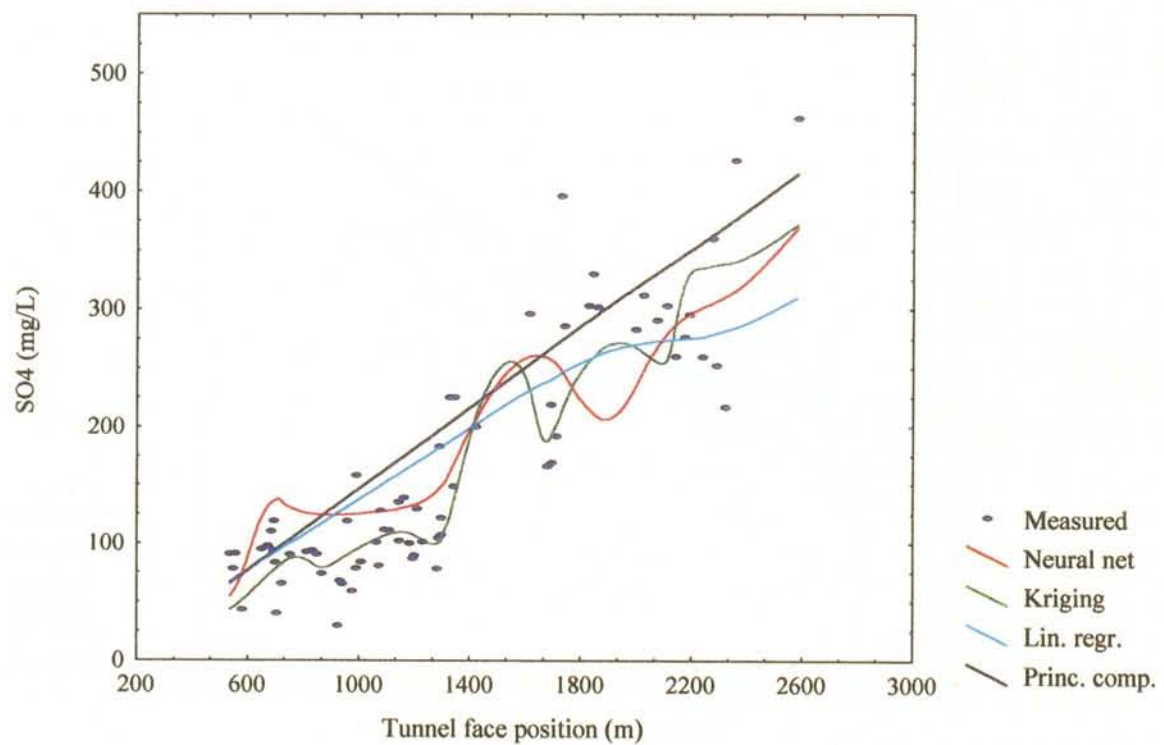


Figure 1-31. The results of the predicted tunnel data for sulphate, using neural network, kriging, linear regression and principal components are compared with measured tunnel data.

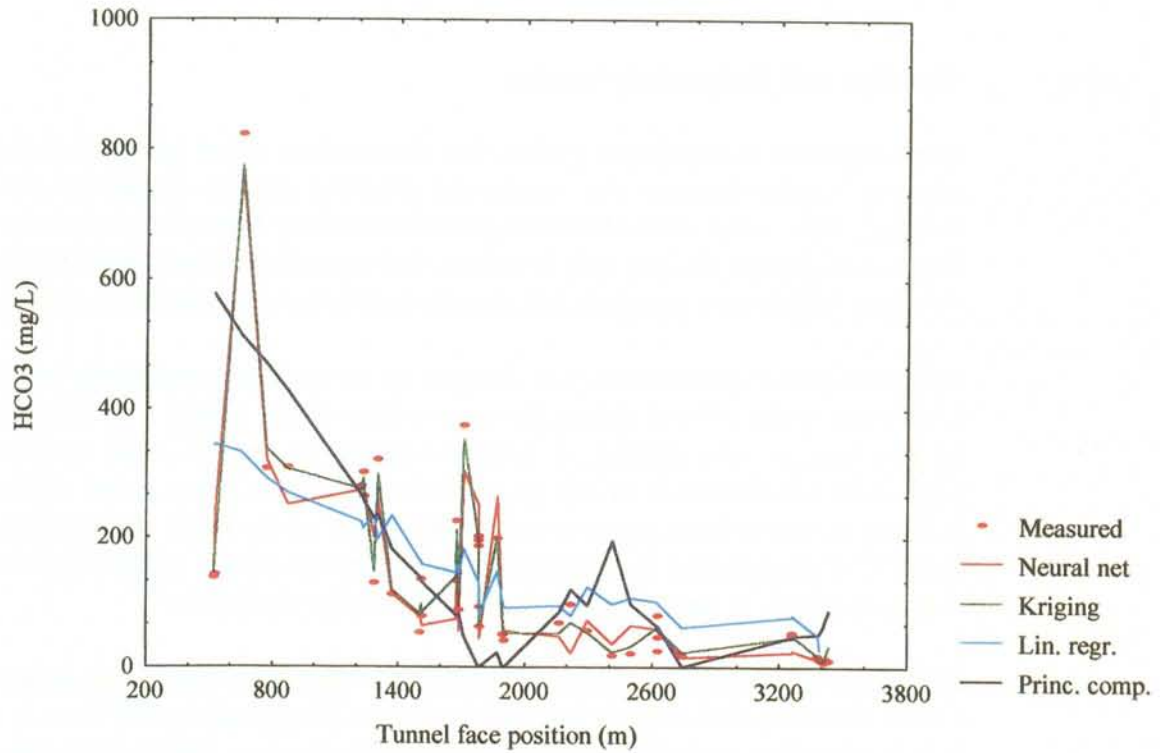


Figure 1-32. Measured HCO_3 content in boreholes from the pre-investigation phase of the HRL construction and the applied prediction models: neural network, kriging, linear regression and principal components.

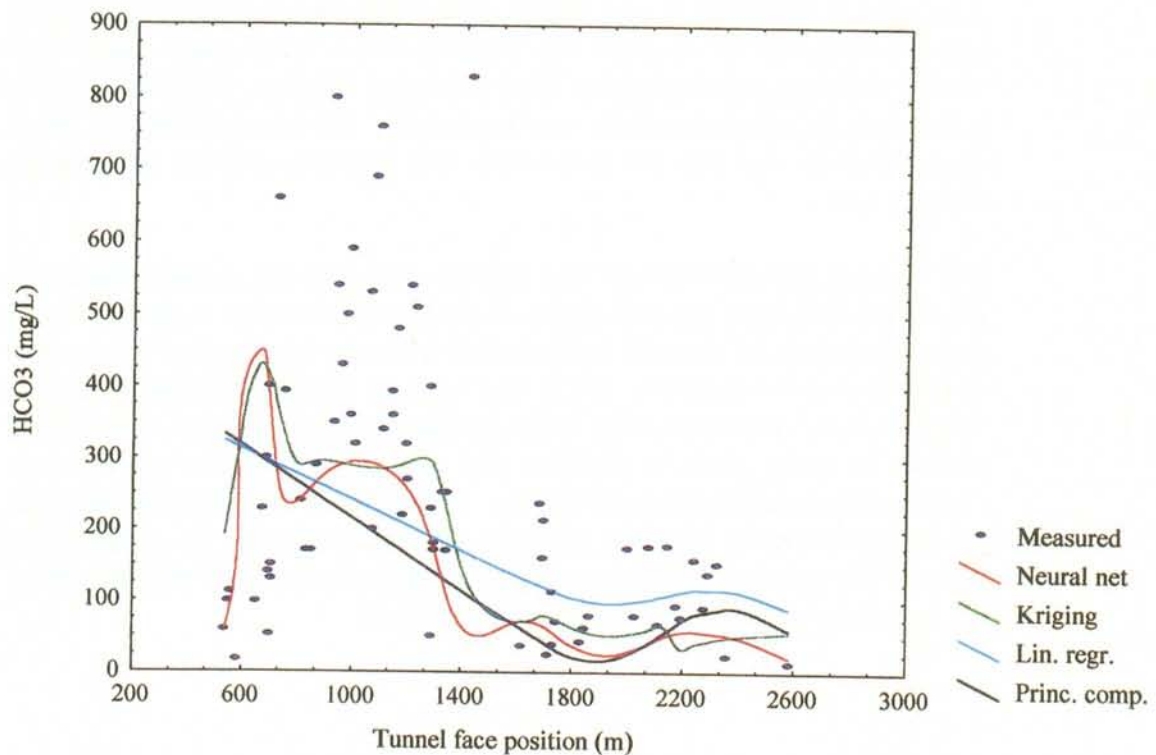


Figure 1-33. The results of the predicted tunnel data for HCO_3 by using neural network, kriging, linear regression and principal components are compared with measured tunnel data.

1.4.3 Chemical and biological processes

It was expected, as mentioned earlier, that the outcome of the hydro-chemical analyses would represent the conditions observed already during the pre-investigations, since most chemical groundwater/rock interactions are slow. This was in general also the case. However, there are other matters affecting the chemistry which were not predicted: tunnel construction and microbial activity.

The groundwater composition was changed by the **grouting materials** which were used to seal off and reduce the water inflow to the tunnel. The effect of the grouting is very distinct, a large increasing in the pH-value and the potassium concentration in the groundwater. However, only a few of the grouting occasions have given an observable effect on the water composition. *Table 1-12* summarizes the tunnel sections which have been grouted and the observed effects in the water composition in nearby boreholes.

The effects of grouting as seen in the time series samples in *Table 1-12* exhibit a short duration. It is only in the very first days after grouting that there is a measurable effect, both in pH and potassium concentration. This means either that the rock has a capacity to quickly readjust to the impact of grouting or that the grout has no influence on the chemistry after consolidation, because the grouted water conductors are no longer active. It could also be explained by the flow of water towards the tunnel which removes the groundwater and dilutes the effects of the grout. Also investigations during the passage of the NE-1 fracture zone gave no observable effects of grouting. Boreholes SA1195A,B SA1210A,B SA1229A,B and 1247B were monitored for two months while approximately 75 m³ of grout was injected over a thirty metre long tunnel section /*Wikberg and Gustafsson, 1993, Rhén and Stanfors, 1993*/. It should be pointed out that these boreholes were located 50 - 100 m away from the actual injection point and that the water flow was probably directed towards the fracture zone.

The high pH potassium plume seen directly after grouting is due to the liquid phase into which the grout is mixed. In the narrow fractures in the rock mass the particulate grout material is filtered off while the liquid phase flows away /*Lagerblad and Trädgårdh, 1995*/. The high pH plume is flushed away and diluted within a few days in the water conductors. Consequently, there are no hazards in using grout to stabilize the rock mass from the groundwater chemical characterization point of view. Grout can be accepted provided that the composition, the amounts, the time and the location of the grouting are known. The grouting of the canister deposition volumes must be assessed by the repository performance and safety assessment.

Table 1-12. Pre-grouted tunnel sections, grouting volume and boreholes where the pH of groundwater samples was above 8 (above 10 in bold). Pre-grouting volumes of less than 5 m³ not have been listed. *indicates that time series samples have been analysed.

Tunnel section metres	Volume of grout m³	Increased pH in borehole
1290 - 1310	60	SA1290
1360 - 1410	60	no indication
1690 - 1740	30	SA1713, SA1726, SA1730*
1865	8	no indication
2010 - 2020	18	YA2013 , SA2013
2080 - 2120	50	KA2048 , SA2090, SA2109
2140 - 2162	40	SA2142 , KA2162
2276	5	no indication
2354	7	no indication
2756	2	SA2756, SA2768, SA2783*
2900-2920	12	SA2897, SA2912 , (SA3045)
3123	12	no indication

Table 1-13. Time series samples from boreholes affected by grouting.

Borehole	sampling date	pH	K (mg/l)	Alkalinity (meqv)
SA1730A	1992-10-29	11.6		5.1
	1993-02-03	7.3	10	0.6
	1993-06-21	7.4	6.1	0.6
	1993-08-24	7.1	8.1	0.6
	1993-09-28	7.2	7.6	0.5
	1994-06-06	7.1	8.2	0.7
	1994-09-07	6.8	9.4	0.5
SA2783A	1994-01-11	8.5		0.2
	1994-02-14	7.7	8.4	0.2
	1994-05-17	6.8	7.8	0.3
	1994-09-07	7.1	9.6	0.3

Biological processes were not in the predictions considered to influence the chemistry. All predictions were based on chemical reactions and the mixing of water with different composition. In the results of the sampling made during tunnel construction phase, it is predominantly the bacterial processes which yielded a groundwater chemistry different from the expected one (see *Section 1.3*). Particularly the occurrence of **extensive microbial sulphate reduction** in the tunnel section from Simpevarp out to Äspö gave a groundwater composition which was different from the predictions. The effects observed in the tunnel spiral at Äspö are much smaller, even though the sulphate reduction also takes place at a few locations in the deep parts of the tunnel.

The microbes themselves do not create new reactions, but they catalyse reactions which would otherwise not take place, e.g. the reduction of sulphate to sulphide and dissolution and reduction of ferric iron minerals. The biological processes turned out to be even more important than the chemical interaction between the groundwater and the minerals. The microbial processes always involve redox reactions. They mostly also produce (or consume) carbon dioxide and thus affect both the calcite and redox systems. Because of the unexpected effects of the biological processes the observed bicarbonate, sulphate and iron concentrations were different from those predicted. This was especially noticeable in the tunnel sections passing below the sea, where the water percolating through the seabed sediments transported large quantities of organic matter into the rock. *Figure 6-14* presents the predicted and observed chemistry of the groundwater from fracture zone NE-3. The low sulphate concentration correlates well with the high bicarbonate concentration as a result of the reduction of sulphate and oxidation of organic matter.

The biological processes were not considered to be of importance at the time of prediction, before the tunnel construction was started. But now we know that the bacterial activity has influenced the chemistry and greatly affected both the redox and calcite systems. It has increased the iron concentration up to 4 mg/l and the bicarbonate content up to 800 mg/l, in the fracture zones NE-3 and EW-3.

The observed biological processes are */Pedersen and Karlsson, 1995/*:

- oxygen consumption by oxidation of organic matter

$$\text{O}_2 + (\text{CH}_2\text{O}) \rightarrow \text{CO}_2 + \text{H}_2\text{O}$$
- reduction of iron(III) minerals through oxidation of organic matter

$$4\text{Fe(III)} + (\text{CH}_2\text{O}) + \text{H}_2\text{O} \rightarrow 4\text{Fe}^{2+} + 4\text{H}^+ + \text{CO}_2$$
- reduction of sulphate by oxidation of organic matter

$$\text{SO}_4^{2-} + 2(\text{CH}_2\text{O}) + \text{H}^+ \rightarrow \text{HS}^- + 2\text{H}_2\text{O} + 2\text{CO}_2$$

These three reactions will continue until one of the components involved in the process has been depleted. In the Äspö case, aerobic respiration continued until all the dissolved oxygen was consumed */Banwart et al, 1995/*.

The sulphate reduction is of importance for the assessment of the copper canister stability. Therefore, a working group was formed to sort out the questions of why, where and to what extent microbial sulphate reduction was occurring. Experts on the disciplines of microbiology, geochemistry, isotope geochemistry, hydro-chemistry and hydro-geology were represented /*Laaksoharju (ed), 1995*).

Additional microbiological data were collected in selected boreholes where the hydro-chemistry indicated an on-going or previously on-going sulphate reduction. The results show that sulphate reducing bacteria are present, sometimes in large quantities and that they can be correlated to the modified groundwater composition with high bicarbonate and low sulphate concentrations. The amounts of bacteria vary from time to time in the sampling points. Generally there are more bacteria more frequently occurring in the boreholes below the sea bed than there are in the tunnel spiral. The conclusion of this is that the sulphate reduction is continuously on-going in the sea-bed sediments and probably also in the bedrock below the sea-bed sediments.

The hydro-geological conditions were evaluated in order to describe the possible transport phenomena related to the sulphate reduction. The questions to be answered were: Can sulphate reduction take place in the bottom sediments and the modified water be transported to the tunnel? Could the groundwater flow conditions in the tunnel either increase or decrease the effect of the biological sulphate reduction?

The answer to the first question is yes, the process can occur in the bottom sediments and the effect in hydro-chemistry be observed in the water inflow in the tunnel. Hydro-geological calculations imply a transport time of approximately 200 days for the seawater passing through the sediments to reach the tunnel in a proportion of 25%. This water might be Baltic Sea water which has recently been modified on its way through the bottom sediments.

The answer to the second question is that the relatively simple groundwater flow conditions around the tunnel would not affect the biological process directly. However, if the sulphate reduction had been an ancient process, then the effects would soon be washed out, which has not been the case. The existence of high bicarbonate and low sulphate concentrations in the probing holes at the very first sampling occasion also strongly imply that the process was ongoing before the tunnel construction started.

Geochemical data were evaluated to find the amount of sulphide which could be calculated to result from the sulphate reduction. The conclusion is that the amount of pyrite normally occurring in the fracture coatings could explain the amount produced. However, there are other processes in the geological time span which have also produced pyrite. The existence of pyrite is not therefore an evidence of sulphate reduction. Small amounts of colloidal sulphur in the groundwater are orders of magnitude lower than the amounts produced.

Isotope data were expected to give a definite answer to where the sulphate reduction takes place, since the bacterial processes always results in an enrichment of the lighter isotopes. Both concerning the carbon-13 and the sulphur-34 isotopes the results generally point towards the existence of the bacterial sulphate reduction. However, there are several processes in the geological evolution which would have given the same isotopic signatures as well. The isotopic data therefore give indications of biological sulphate reduction but no evidence.

Hydro-chemical modelling was performed to define the specific conditions where the process was occurring. The results show that the salinity interval 4000 - 6000 mg/l of chloride is the optimal. This is supported by laboratory experiments as well. Dissolved organic contents above 10 mg/l are also strongly correlated to the high numbers of bacteria.

1.4.4 Conclusions

The predictions made for the deterministic fracture zones were based on a static approach, which was considered to be applicable to the purpose. We considered the situation from the pre-investigations to be valid at least until the time when the tunnel excavation reached the point of sampling. We now have strong reasons to believe that the tunnel construction affected the groundwater situation ahead of the tunnel front. Therefore the characterization of a rock volume must be done from surface boreholes before the excavation starts.

The situation caused by the inflow into the tunnel has been carefully examined by *Laaksoharju and Skårman /1995/*. They find that the groundwater types flowing into the tunnel during the construction phase changed significantly even when the salinity did not change a lot. The reason for this is that there are several end-members involved in the mixing process. There are deep saline, Baltic Sea water and altered marine water which all contain considerable amounts of chloride. Therefore a shift in the proportions of e.g. deep saline and Baltic Sea water is not seen in the salinity, see *Report 2 /Rhén et al, 1997a/*.

The concept of static conditions for predicting the groundwater chemistry during construction phase has several weaknesses. The justification of using the concept is nevertheless that it is the only way we could utilize the data and knowledge of the pre-investigations to assess the usefulness as a tool to test the pre-investigation methodology.

The accuracy of the different mathematical spatial assignment methods is mostly higher than that of the expert judgement. However, this is also dependent on the amount of data. For instance, it is interesting to note that the expert judgement gave a good prediction only for fracture zone NE-1. In all other cases these predictions are further from the outcome than any of the later tested methods. This is most likely related to the fact that NE-1 was hydro-chemically identified through three different boreholes. Thus the expert judgement was quite simple, and gave a good prediction.

1.5 BRIEF ANALYSIS OF ACCURACY AND CONFIDENCE

The confidence levels were set to be 95% unless otherwise stated. For the predictions made before tunnel construction no analyses were made on the variability in the data. The uncertainty put to the data was based on an estimate of the uncertainty in analyses.

A careful evaluation of the variability was made and the different mathematical methods were tested. The number of data points for each position was too small to give a strict statistical distribution. However, the same distribution was used to give the distribution in the predicted values, as the one seen in the pre-investigation data. This approach gave a large span to the predictions, see *Section 1.4.2*.

2 **SUBJECT: QUALITY CHANGES (BLOCK SCALE REDOX EXPERIMENT)**

Redox conditions are important for the safety assessment of a nuclear waste repository /SKB, 1995/. The observed redox potential (Eh) and the redox buffering constituents in the groundwater are extremely sensitive to disturbances caused by sampling and analyses. The redox buffer may in a long term perspective mainly be provided by the fracture filling minerals in contact with the groundwater and by the biological processes /Banwart *et al.*, 1995/.

Great efforts were made to investigate and solve the issue of deep groundwater redox conditions /Grenthe *et al.*, 1992/. The present understanding is that the ferrous and ferric iron minerals generally govern the redox properties. This is also the case for data from the investigations at Äspö. However, occasionally other systems are thought to dominate, e.g. the uranium system /Ahonen *et al.*, 1992/. Regardless of which system controls the Eh it has been clearly demonstrated that the deep groundwaters are reducing.

The redox-sensitive elements, for which analyses are normally made are iron (total and ferrous), manganese, sulphide, uranium and dissolved oxygen. As expected, there are normally no measurable concentrations of dissolved oxygen, but the sensor is needed to register any disturbances in the groundwater pumping and sampling procedure. A zero reading of the dissolved oxygen content indicates that the water is anoxic.

Eh measurements are made using three types of electrode, gold, platinum and glassy carbon. Only the complete chemical characterization (see *Table 1-1*), included the proper Eh measurements in the pre-investigations. The measurements were continued for a period of several days (weeks) until the readings levelled out at roughly the same value for all three electrodes. This is the registered Eh value. During sampling in the tunnel no Eh or dissolved oxygen contents were measured, except for those in the redox experiment /Banwart *et al.*, 1995/.

The enhanced water flow in the upper part of the rock, caused by the inflow to the tunnel, was expected to transport oxygenated water down into the fracture zones and enter the tunnel. This phenomenon was studied in a fracture zone at a depth of 70 m below ground level /Banwart *et al.*, 1995/. The predictions of oxygen breakthrough failed because the effects of biological oxygen consumption were not taken into account. The conclusion is that an enhanced groundwater inflow does not cause oxygenated water to reach any greater depths, as long as the amount of organic matter is larger than the amount of dissolved oxygen. These conditions could of course vary from place to place but as a starting point the situation at Äspö could also be expected at any other place. At the Stripa mine, for example, where the hydrology had been affected by the

drawdown by the mine gallery for several decades, there was no oxygen in the infiltrating groundwater at a depth of 400 metres, /Gnirk P, 1993/. Most evidence suggests that the penetration depth for oxygen is a maximum 100 m for the undisturbed conditions and it is not expected to be significantly deeper under disturbed conditions. The effective oxygen consumption by bacteria strengthens the general opinion that anoxic (oxygen free) conditions could always be expected in the deep groundwater.

The Eh value is coupled to the pH value. An empirical relation is a decrease of 60 mV with an increase of one pH unit. At pH 7 the Eh values are mostly between -100 and -300 mV. Plots of the Eh-pH data from the pre-investigation phase and from a few observations in the tunnel are shown in *Figure 2-1*. At these low Eh-levels uranium exists in a reduced (+IV) form and is extremely insoluble.

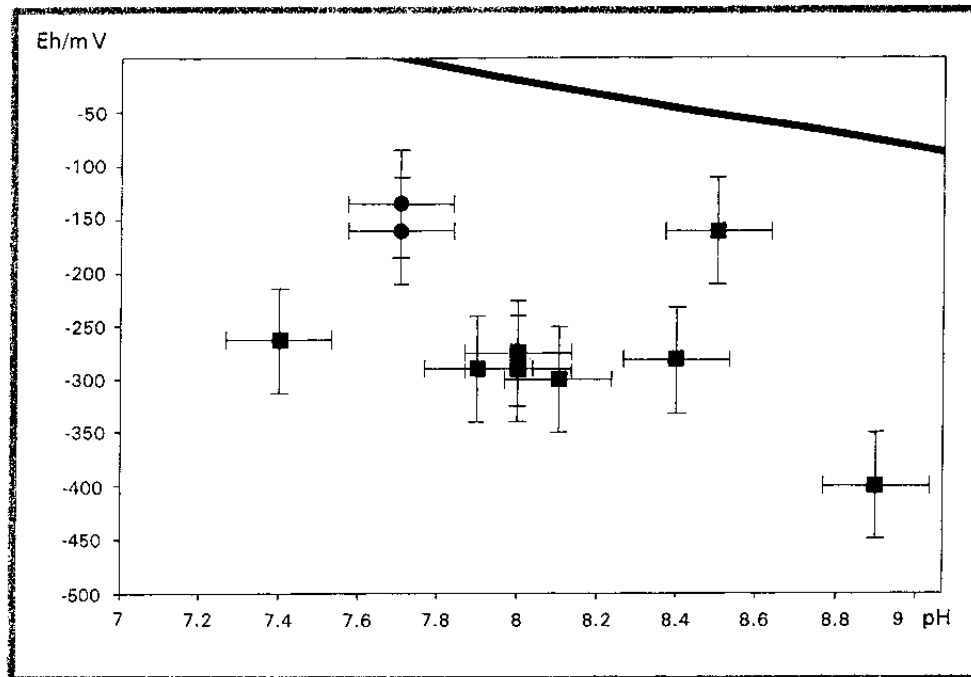


Figure 2-1. Eh versus pH for the data obtained from the pre-investigation phase (squares) and from the construction phase (Circles). The uncertainty in Eh is estimated to be ± 50 mV and the uncertainty in pH is ± 0.1 pH unit. The figure includes the calculated Eh for the equilibrium between UO_2 and dissolved UO_2^{2-} at a concentration of 10 ppb.

A practical approach for nuclear waste disposal safety assessment is therefore to define reducing conditions to be when uranium (plutonium, technetium and neptunium as well) exists in a reduced form, and oxidising conditions when uranium exists in the hexavalent (+VI) state. The usefulness of this approach

is that it resembles well the conditions of the iron system. Under reducing conditions ferrous iron is present in the groundwater in measurable quantities, above ppb levels. In this context it might also be worth mentioning that there is a large difference between reducing and anoxic conditions. Anoxic conditions only mean that there is no measurable amount of dissolved oxygen in the water, whereas reducing means that the Eh value needs to be low enough to have uranium in a reduced form (concentrations at ppb levels). A reducing groundwater is always anoxic.

Oxidizing surface water could be drawn down to a large depth due to the inflow of water to an open repository. At 70 m depth in a minor fracture zone a breakthrough of oxidizing water was predicted to take place in a time span of 1.5 days to 5 years. *(Banwart et al, 1995)*. These calculations were based on a conceptual model for the groundwater flow conditions in the fracture zone and the knowledge of the reaction rates of mineral dissolution. The redox front investigations were organized into a project, the block scale redox experiment (see *Figure 2-2*). A detailed description of the objectives, scope and outcome of the experiment is presented in *Banwart (ed) /1995/*.

The most important result of the experiment was that the dissolved oxygen in the infiltrating surface water was consumed by microbes and not by the reducing minerals of the rock. The population of microbes was rapidly adjusting to the change in flow conditions. The organic matter in the infiltrating water was oxidized by the dissolved oxygen. This reaction is catalysed by bacteria, and is an aerobic respiration. Oxygen consumption, in this manner, will take place anywhere when the content of organic matter is in the order of 10 mg/l or larger. The ultimate conclusion of the results is, however, that the oxidizing water will never reach beyond a certain depth, regardless of how long the repository is kept open.

The results of the experiment were put into the perspective of the performance assessment of a nuclear waste repository. Processes which have been encountered in the redox zone (largely as a result of the enhanced water circulation) are: Dilution, aerobic respiration and iron reduction. Both the aerobic respiration and the iron reduction affect the redox front stability and propagation, whereas the dilution mainly affects the water/rock interaction, i.e. colloid formation and stability and ion exchange reactions.

The aerobic respiration could be considered to be an additional safety barrier which entirely consumes the oxygen in the infiltrating groundwater regardless of flow rate and time. Aerobic respiration will cause:

- Removal of oxygen from groundwater in the soil and upper bedrock thereby protecting the copper canister from exposure to oxidic corrosive water.
- Maintain the reducing conditions under which the long-lived radionuclides are sparingly soluble. This is important in the event of a canister failing.

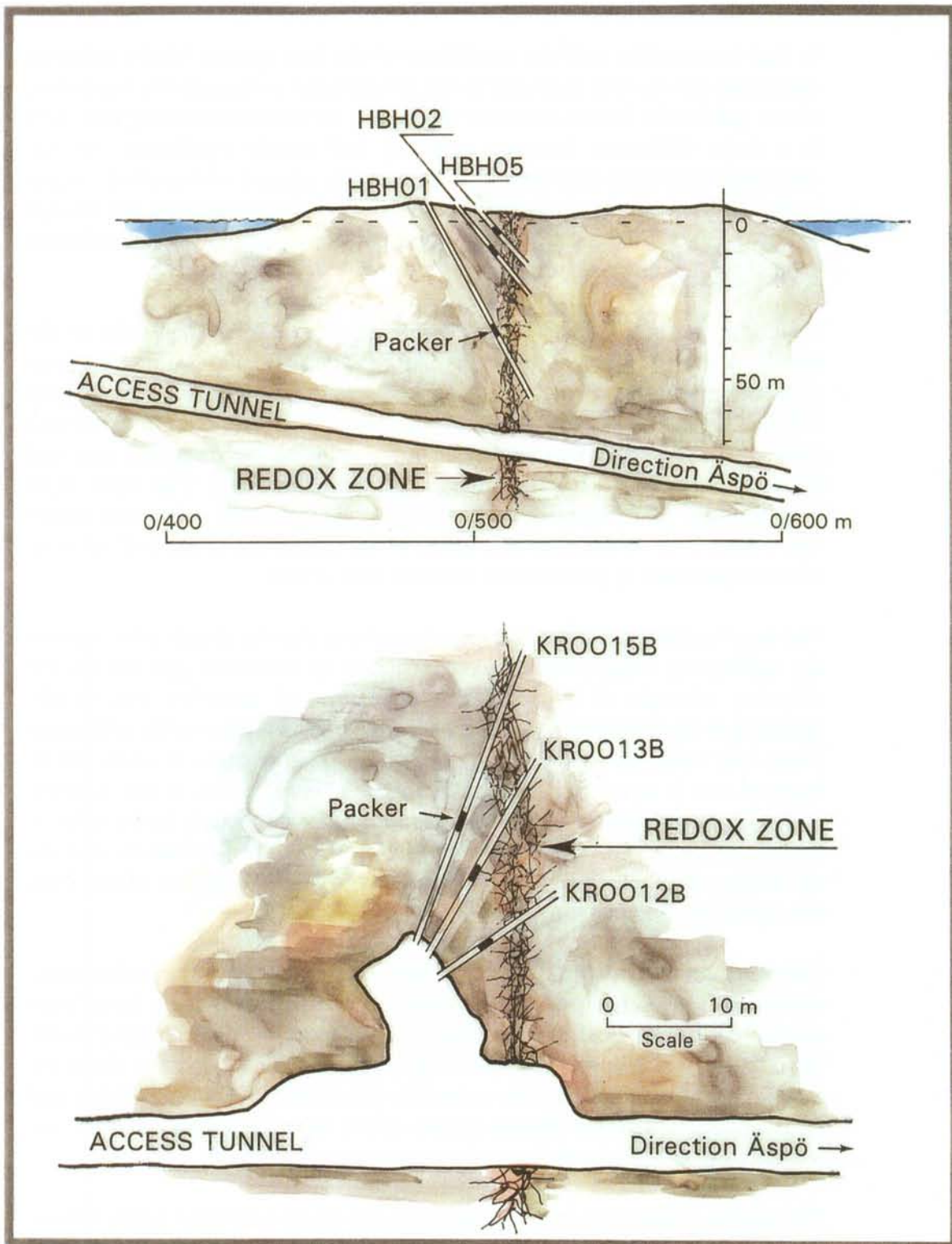


Figure 2-2. A schematic illustration of the block scale redox experiment.

Iron reduction takes place when all dissolved oxygen has been consumed but when there is still organic matter to be oxidized. The bacterial iron reduction is a process similar to aerobic respiration but the iron reduction is an anaerobic respiration. The only difference is that iron instead of oxygen is reduced. The iron reduction results in an increase in the content of dissolved iron and is thus an enhancement of the redox buffer capacity of the groundwater.

A similar outcome to that of the redox experiment on the block scale could be expected at other sites as well. Factors affecting the depth to which the oxidized water could reach are:

- Groundwater recharge rate
- Oxygen diffusion rate
- Relative amounts of reactive reductants
- Oxygen consumption rate for each reductant
- Spatial distribution of flow-paths and reductants

The fact that the soil cover is very thin on top of the redox zone implies that the scavenging effect is probably much larger at sites with a thicker soil cover.

To maintain the anoxic conditions at shallow depths favourable conditions are:

- An organic-rich soil layer
- No preferential flow paths
- Ongoing biomass production
- Rapid decomposition of complex biomass
- Abundant ferrous and sulphide minerals
- Vertical transport of organic matter

3 **SUBJECT: REDOX CONDITIONS AND WEATHERING, DETAILED SCALE**

No specific investigations were focused on the issues of weathering and redox properties on a detailed scale. However, the Äspö diorite was generally expected to give both a higher content of iron in the groundwater and to cause a larger degree of iron coatings on the tunnel walls. None of these predictions were evaluated because the fluctuations in iron concentration are mostly due to bacterial activity (see *Section 1.4.2* and *Chapter 2*).

A pilot study has been conducted to sample and analyse the water of rock of low conductivity. The samples were taken from boreholes KA1639A and KA1750A as illustrated in *Figure 3-1*. In addition to the water samples core samples were also prepared and analysed. The entire pilot study is presented by *Wikström and Björklund /1994/*. The hydro-chemical data from the study is also reported by *Nilsson /1995/*.

The objectives of the study were to:

- Develop and test equipment and methods for sampling water from rock of low conductivity without introducing (trace element) contamination of the sample.
- Find a suitable analytical method or combination of methods for analysing trace elements in very saline waters (chlorine content 4000-7000 mg/l).
- Compare the reproducibility of analyses performed at different laboratories.
- Investigate the geochemical interaction between the water and rock, especially as regards trace elements.
- Find out the hydro-chemical differences between the water in rock of low conductivity and high conductivity

The development and testing of equipment and methods for sampling extremely slowly water flowing was successful. Minor changes in the sampling procedure have been suggested.

Only one of the tested analytical methods turned out to be practically (and economically) feasible for the trace element analyses. The high salinity caused serious problems for most of the methods. The successful technique was ICP-MS with a modified nebulizer. AAS and INAA methods failed.

The results of analyses gave no clear indications of differences regarding rock type and hydraulic conductivity. *Table 3-1* summarizes the relevant data.

Table 3-1. The composition of groundwater in the Äspö rock mass of low conductivity and high conductivity in both Äspö diorite and greenstone. Concentrations are mostly given in mg/l. Constituents with * are given in µg/l. A represents the chloride range 6200-6600 mg/l and B 3900-4300 mg/l.

Constituent	Äspö diorite		Greenstone	
	High cond.	Low cond.	High cond.	Low cond.
flow (ml/min):	600	30	11	2.5
Na(A)	2030	1990		2080
Na(B)	1720		1610	1640
Ca(A)	1700	1680		1720
Ca(B)	620		650	750
Mg(A)	77	72		68
Mg(B)	142		128	43
HCO ₃ (A)	40	34		24
HCO ₃ (B)	260		252	17
Cl(A)	6400	6200		6600
Cl(B)	4100		3920	4200
Br(A)	34	38		45
Br(B)	18		16	26
SO ₄ (A)	435	444		450
SO ₄ (B)	243		225	125
Sr(A)	26	27		30
Sr(B)	10		9	14
Fe(A)	0.44	0.32		0.05
Fe(B)	2.4		2.3	0.05
Mo(A)*	50	71		79
Mo(B)*	10		7	17
U(A)*	0.6	0.07		0.53
U(B)*	2		3	0.06
La(A)*	0.7	0.56		0.76
La(B)*	0.3		0.45	0.26

4 CONCLUSIONS

The project of validation consisted of two main parts. One was the demonstration of the investigation techniques and their ability to give accurate and relevant data for the construction and safety assessments of a final repository. The second one was to assimilate the new knowledge to which the investigations and evaluations have contributed. Conclusions and recommendations are therefore based on both the new results and the new experience. The conclusions are that the pre-investigations are relevant to the purpose of understanding the site for a repository, while recommendations are merely to improve the investigation techniques as a result of the experience gained. A critical issue is to judge how closely these recommendations are to the specific conditions of Äspö and to what extent they can be adapted at other possible sites.

Hydro-chemical investigations

There are different needs for hydro-chemical data. These can be grouped into three categories:

- Reliable data on safety related parameters such as pH, Eh, redox and pH buffers, (like bicarbonate, iron and sulphide and radionuclide analogous) are needed as input to the safety assessment calculations.
- Chemical processes which determine the present day situation but also the evolution of the hydro-chemistry in the future. Major and minor constituents and end members for different water types are essential in order to understand present day conditions and useful for the prediction of future conditions.
- For assessment of the groundwater residence time, there is a need to analyse for stable and radiogenic isotopes as well as for conservative constituents, which reflect the past conditions.

The listed sets of data are in some cases extremely sensitive to disturbance while others are fairly robust. Based on the experience obtained from the SKB's early study site investigations in 1982-1984, the Finnsjön project and the Äspö project, 1986-1995, a well defined classification can be made:

- i Major constituents, sodium, potassium, calcium, magnesium, bicarbonate, chloride, sulphate and silica are unaffected by disturbances from drilling or contamination from other investigation methods, as long as the proportion of drilling or testing water can be analysed.
- ii Trace elements and stable oxygen-18 and deuterium isotopes are reliable even with a proportion of up to 5 % of the drill flushing water.

- iii pH-sensitive trace elements, tritium and carbon-14 data are reliable only when the contamination by drilling water or meteoric water entering through the borehole is less than 0.1%.
- iv Eh and redox-sensitive elements are reliable when the readings have stabilized and the Eh value can be interpreted. Normally several days of continuous pumping is needed with measurements in on-line flow through cells.

With the techniques used at Äspö, *Level iv* can only be reached using the procedures of the complete chemical characterization, CCC. An improvement in the procedures and technique of sampling during interference pumping tests could perhaps result in *Level iv* data.

Level iii is reached by the CCC and the pumping tests, SPT. A modification of the pumping technique, which has now been made, makes it possible to achieve reliable pH readings as well.

Sampling during drilling and sampling with the 3P equipment provided data of *Level i*. A more carefully planned drilling and sampling procedure should give data of *Level ii*. A more comprehensive development of downhole samplers could perhaps result in data of *Level iii*. This possibility is now being tested.

Evaluation and prediction methods

The improvement of the evaluation and prediction methods achieved using standardized mathematical/statistical tools has two major advantages. The first one is that with the computer-based programs it is much easier to assess and control the quality of the evaluation and the prediction procedures compared with the use of 'expert judgement' methods. The second advantage is that the mathematical/statistical methods are reproducible and not entirely dependent on the person who does the modelling. A general way of adapting the modelling tools is to start by expert methods, to 'look at the data and try to understand it', followed by a thorough multivariate Principal Component Analyses. After the PCA one should identify the end members involved in the groundwater and calculate the proportion of the end members in all the collected samples. A good description of the conditions of the site facilitates the prediction of the future evolution of the groundwater system.

Computer based prediction tools have been tested and found to give varying results. As a first attempt PCA was used both for the evaluation of the investigation data as well as for prediction purposes. Still the PCA method is the best evaluation tool while for prediction purposes kriging and neural networks have turned out to be superior to the PCA and linear regression analyses.

There are simple ways of checking the predictive ability of a model. The simplest is to compare the prediction and the outcome to see if they agree. In

practice this was the intention when the predictions of construction phase groundwater chemistry were made on the basis of the pre-investigation models. Some general comments on this approach are:

- The initial predictions were based on a combination of expert judgements and principal component analyses. However, the range was only estimated by expert judgements. It seems now that the estimated ranges were too narrow, because the estimate did not include the natural variability, only the uncertainty in the data.
- When the different mathematical methods were tested, the range of variation was calculated on the basis of the variation in input data. The same variation was expected for the observations. The result is that most of the observations fall within the predicted ranges for all constituents except sulphate and bicarbonate. In some cases the range of variations is so wide that it could be questioned whether the prediction is meaningful or not. Sulphate and bicarbonate predictions failed in positions where sulphate reducing bacteria have been active.

The approach to consider the hydrochemistry as a static system reflecting the conditions of the pre-investigations are of course dubious. However, by selecting a suitable predictive tool, kriging or neural networks, the observations all fall within the predicted ranges. It is therefore possible to predict a repository rock volume on the basis of pre-investigation data. Observations must then be made in a way to be comparable to predictions, e.g. through longer probing holes in the tunnel front.

The approach of predicting the groundwater composition to be observed during construction might not be worthwhile for a real repository anyway. The reason is that too many conditions which will affect the outcome cannot be foreseen. Also the need for predictions is not urgent, since the chemical conditions during construction are expected to be different from the conditions prevailing after closure of the repository. These conditions are important and probably more close to the initial undisturbed conditions provided the disturbances disappear quickly. Therefore, it is important to obtain a good description of the chemical conditions during the pre-investigations when the groundwater system has not been mixed up by drawdown into excavated tunnels. A carefully planned and performed site investigation programme can fulfill such criteria.

Quantitative predictions of groundwater composition are sometimes useful for planning construction work. The salinity of the groundwater has a severe impact on the corrosion of steel structures in the tunnel. Such predictions could however, be made as quantitative estimates of the salinity, for instance.

If hydrochemical predictions were to be made at Äspö, or when they are made elsewhere, they would be based on the concept of mixing and include the mixing proportions of the identified and selected end-members and reference waters. These predictions would have two different purposes. One to assess the

waters. These predictions would have two different purposes. One to assess the long term performance issues and the second to assess the groundwater flow model with the mixing caused by the tunnel drawdown.

PART 2 - APPENDIX 1
GROUNDWATER CHEMISTRY IN
FRACTURE ZONES

GROUNDWATER CHEMISTRY IN FRACTURE ZONES

The chemical composition of the groundwater, the saturation index of calcite and carbon dioxide, indication of sulphate reduction, in the different fracture zones (EW-3a, NE-4a,4b, NE-1a,1b, NE2a-1, NE2a-2, NE2a-3, NE-3b,3c, NNW-4H₂O-1, NNW-4H₂O-2, NNW-4H₂O-3) and in the Redox zone over time are listed. In fracture zones with no groundwater sampling boreholes, the boreholes ± 100 m from the actual fracture zone were set to represent that fracture zone. If two borehole observations fall inside the range the observation closest to the fracture zone was selected. When the results are interpolated in space (± 100 days) the accuracy decreases.

Fracture zone	Representing day (0=90-10-14)	ID code	Penetrating zone	Tunnel length (m)	Date	Inflow rate (m ³ /s*10E ⁻³)	SNO	Na (mg/L)	K (mg/L)	Ca (mg/L)	Mg (mg/L)	HCO ₃ (mg/L)	Cl (mg/L)	SO ₄ (mg/L)
Redox zone	150	KR0012B	x	513	91-05-07			352.0	2.0	143.0	15.4	198	695.0	70.0
Redox zone	550	KR0012B	x	513	92-04-22		1940	604.0	4.9	268.0	37.7	245	1330.0	134.4
Redox zone	750	KR0012B	x	513	92-10-28		2026	497.0	5.0	186.0	27.9	292	970.0	176.0
Redox zone	950	KR0012B	x	513	93-05-16		2094	424.0	4.3	136.0	25.1	315	710.0	142.2
Redox zone	1150	KR0012B	x	513	93-11-08		2193	387.0	4.3	118.0	20.4	324	619.0	134.7
Redox zone	1350	KR0012B	x	513	94-08-10		2270	346.6	3.4	100.1	17.4	325	590.0	125.8
NE-4a,4b	350	SA0850B	x	850	91-08-20	0.1-1.2		1920.0	18.0	1210.0	141.0	170	5440.0	90.6
NE-4a,4b	750	SA0813B	x	813	92-12-02	0.1-1.2	2049	1700.0	21.0	364.0	123.0	481	3450.0	186.0
NE-4a,4b	1150	SA0813B	x	813	93-09-29	0.1-1.2	2190	1640.0	19.1	310.0	124.0	317	3350.0	274.5
NE-4a,4b	1350	SA0813B	x	813	94-06-07	0.1-1.2	2253	1578.0	11.9	322.1	121.1	302	3272.3	299.6
NE-3b,3c	350	SA0976B	x	976	91-10-15	3.9		2170.0	20.6	993.0	203.0	500	5590.0	58.8
NE-3b,3c	550	SA1062B		1062	92-04-23	3.9		2230.0	23.5	770.0	220.0	531	5320.0	100.8
NE-3b,3c	750	SA1062B		1062	92-12-02	3.9	2050	1930.0	34.0	545.0	177.0	403	4350.0	189.0
NE-3b,3c	950	SA0958B	x	958	93-06-23	3.9	2121	1829.2	22.4	595.2	137.2	371	4087.9	243.0
NE-3b,3c	1150	SA0958B	x	958	93-09-28	3.9	2181	1810.0	19.6	657.0	144.0	296	4260.0	239.4
NE-3b,3c	1350	SA0958B	x	958	94-06-07	3.9	2254	1634.1	21.4	477.8	125.1	274	3641.0	295.2
NE-1a,1b	550	SA1342B		1342	92-06-16	5.0		1680.0	11.0	950.0	152.0	170	4730.0	148.5
NE-1a,1b	750	HA1327B	x	1327	92-10-15	5.0	2023	1610.0	9.4	648.0	128.0	252	3920.0	225.0
NE-1a,1b	950	SA1229A		1229	93-06-23	5.0	2120	1847.9	24.5	598.5	156.1	426	4210.9	101.0
NE-1a,1b	1150	HA1327B	x	1327	93-12-15	5.0	2208	1760.0	13.7	684.0	157.0	259	4310.0	255.3
NE-1a,1b	1350	SA1229A		1229	94-06-07	5.0	2256	1735.4	26.1	512.1	151.7	336	3928.2	241.5
EW-3a	750	SA1420A	x	1420	92-10-15	0.8	2024	1540.0	10.2	715.0	123.0	170	3930.0	226.2
EW-3a	950	SA1420A	x	1420	93-06-22	0.8	2116	1484.2	9.7	487.9	124.5	215	3419.9	307.0
EW-3a	1150	SA1420A	x	1420	93-09-29	0.8	2183	1600.0	13.7	480.0	139.0	214	3530.0	331.8
EW-3a	1350	SA1420A	x	1420	94-06-07	0.8	2257	1426.5	15.7	395.8	116.8	206	3052.5	290.3
NE-2a-1	750	SA1614B		1614	92-11-19	0.003	2035	1570.0	8.3	1250.0	80.2	37	5160.0	296.4
NE-2a-1	950	SA1614B		1614	93-06-22	0.003	2117	1953.7	5.2	1710.4	65.9	32	6207.3	424.0
NE-2a-1	1150	SA1614B		1614	93-09-28	0.003	2184	1880.0	6.7	1390.0	90.8	81	5650.0	332.4
NE-2a-1	1350	SA1614B		1614	94-06-06	0.003	2249	1831.3	7.4	1207.0	98.3	109	5176.1	322.0
NE-2a-2	750	SA1828B	x	1828	92-11-19	0.003		1700.0	8.5	1290.0	92.2	43	5200.0	303.0
NE-2a-2	950	SA1828B	x	1828	93-06-21	0.003	2115	1909.2	8.0	1392.4	113.9	48	5849.7	362.9
NE-2a-2	1150	SA1828B	x	1828	93-09-28	0.003	2187	1930.0	10.0	1450.0	108.0	48	6010.0	362.7
NE-2a-2	1350	SA1828B	x	1828	94-06-06	0.003	2252	1861.5	11.7	1063.9	138.8	111	5123.0	259.9
NE-2a-3	1150	SA2583A		2583	94-03-07	0.003	2223	2099.0	8.3	1870.0	56.9	13	6647.0	462.0
NE-2a-3	1350	SA2583A		2583	94-05-18	0.003	2240	2170.0	8.5	1859.6	73.9	44	6895.6	442.6
NNW-4H ₂ O-1	950	SA2074A		2074	93-06-17	0.06-0.12	2113	1959.4	8.6	992.6	172.0	47	5282.5	299.0
NNW-4H ₂ O-1	1150	SA2074A		2074	93-09-28	0.06-0.12	2173	1730.0	11.0	764.0	144.0	79	4670.0	263.1
NNW-4H ₂ O-1	1350	SA2074A		2074	94-06-07	0.06-0.12	2258	1701.7	10.2	723.2	141.5	94	4275.6	270.9
NNW-4H ₂ O-2	950	SA2109B	x	2109	93-02-15	0.06-0.12		1730.0	17.0	884.0	107.0	67	4480.0	303.0
NNW-4H ₂ O-2	1150	SA2142A		2142	93-12-02	0.06-0.12	2202	1720.0	25.0	581.0	128.0	127	3880.0	367.8
NNW-4H ₂ O-2	1350	SA2175B		2175	94-05-30	0.06-0.12	2244	1959.5	15.3	1037.1	161.6	127	5442.0	261.6
NNW-4H ₂ O-3	1350	KA3191F		3191	94-06-04	0.06-0.12	2248	2225.3	8.6	2093.1	64.3	29	7409.7	445.2

Fracture zone	Representing day (0=90-10-14)	ID code	¹ H (TU)	² H (SMOW)	¹⁸ O (SMOW)	Fe(tot) (mg/L)	Fe ²⁺ (mg/L)	DOC (mg/L)	pH (units)	Calcite (log IAP/KT)	Log pCO ₂ (bar)	Indicator of sulphat reduction
Redox zone	150	KR0012B	34.0	-82.1	-11.4	0.200	0.200		7.8	0.49	-2.62	
Redox zone	550	KR0012B	25.0	-77.3	-10.2	0.287	0.291	12.0	7.7	0.66	-2.46	
Redox zone	750	KR0012B	17.0	-79.9	-9.9	0.218	0.216	14.0	7.7	0.60	-2.37	
Redox zone	950	KR0012B	17.0	-72.0	-9.9	0.186		18.0	7.5	0.32	-2.14	
Redox zone	1150	KR0012B	34.0	-69.6	-9.6	0.179		11.3	7.4	0.18	-2.03	
Redox zone	1350	KR0012B	31.3	-68.1	-9.8	0.189			7.3	0.02	-1.93	
NE-4a,4b	350	SA0850B	6.8	-67.2	-8.3				7.7	0.93	-2.70	
NE-4a,4b	750	SA0813B	6.8	-59.8	-7.5	6.330	6.330	8.3	7.3	0.53	-1.82	Bacteria
NE-4a,4b	1150	SA0813B	14.0	-50.4	-7.3				7.1	0.07	-1.82	
NE-4a,4b	1350	SA0813B	28.7	-53.7	-7.2				7.0	-0.05	-1.75	
NE-3b,3c	350	SA0976B	14.0	-60.4	-7.4				7.2	0.79	-1.75	GW
NE-3b,3c	550	SA1062B	8.0	-58.0	-7.7			11.0	7.3	0.83	-1.81	GW
NE-3b,3c	750	SA1062B	9.3	-57.6	-7.3	2.160	2.160	9.1	7.3	0.59	-1.91	Bacteria
NE-3b,3c	950	SA0958B	8.4	-56.0	-7.5	3.334	3.323		7.0	0.27	-1.68	
NE-3b,3c	1150	SA0958B	14.0	-57.5	-7.4				7.5	0.75	-2.24	
NE-3b,3c	1350	SA0958B	28.7	-55.6	-7.2				7.0	0.06	-1.80	
NE-1a,1b	550	SA1342B	5.9	-61.9	-8.7				7.3	0.44	-2.30	
NE-1a,1b	750	HA1327B	17.0	-65.3	-7.4	2.160	2.150		7.4	0.58	-2.21	Bacteria
NE-1a,1b	950	SA1229A	16.0	-60.0	-7.3	2.891		21.0	7.0	0.33	-1.62	GW
NE-1a,1b	1150	HA1327B	18.0	-50.6	-7.5	2.640	2.430	4.8	6.9	0.05	-1.76	
NE-1a,1b	1350	SA1229A	22.0	-52.8	-7.0				7.0	0.17	-1.72	
EW-3a	750	SA1420A	17.0	-72.0	-8.7	1.110	1.110		7.6	0.66	-2.57	
EW-3a	950	SA1420A	31.0	-59.0	-7.5	1.941	1.920		7.3	0.30	-2.18	
EW-3a	1150	SA1420A	22.0	-52.5	-7.0				7.3	0.29	-2.18	
EW-3a	1350	SA1420A	33.8	-57.0	-7.5				7.2	0.10	-2.10	
NE-2a-1	750	SA1614B	8.0	-103.1	-13.1			1.0	7.4	-0.01	-3.06	
NE-2a-1	950	SA1614B	4.2	-85.5	-11.5	0.309	0.298	1.0	7.6	0.22	-3.34	
NE-2a-1	1150	SA1614B	4.2	-77.6	-10.4			1.0	7.4	0.35	-2.73	
NE-2a-1	1350	SA1614B	8.4	-71.9	-9.7				7.2	0.22	-2.41	
NE-2a-2	750	SA1828B	4.2	-84.4	-10.8				7.4	0.06	-3.00	
NE-2a-2	950	SA1828B	4.2	-75.9	-10.3	0.865	0.848	1.0	7.4	0.12	-2.96	
NE-2a-2	1150	SA1828B	4.2	-71.4	-10.3			1.0	7.3	0.03	-2.87	
NE-2a-2	1350	SA1828B	8.4	-67.8	-8.9				7.2	0.18	-2.40	
NE-2a-3	1150	SA2583A	4.2	-85.9	-10.7	0.242	0.236	0.4	7.5	-0.25	-3.64	
NE-2a-3	1350	SA2583A	5.9	-83.5	-11.1	0.373			7.9	0.67	-3.51	
NNW-4H ₂ O-1	950	SA2074A	5.9	-65.2	-8.5	0.755	0.734	1.0	7.0	-0.45	-2.60	
NNW-4H ₂ O-1	1150	SA2074A	7.0	-60.0	-8.4			1.0	7.1	-0.20	-2.45	
NNW-4H ₂ O-1	1350	SA2074A	10.1	-63.3	-8.5				7.3	0.08	-2.55	
NNW-4H ₂ O-2	950	SA2109B	5.9	-64.5	-8.2				8.1	0.82	-3.49	
NNW-4H ₂ O-2	1150	SA2142A	21.0	-56.2	-7.2	0.881		3.4	7.4	0.23	-2.50	
NNW-4H ₂ O-2	1350	SA2175B	8.4	-62.0	-8.2	0.882			7.8	0.84	-2.92	
NNW-4H ₂ O-3	1350	KA3191F	8.4	-81.6	-11.2				7.3	-0.08	-3.11	

Fracture zone	Representing day (0=90-10-14)	ID code	Dominating ions	Cation:Anion	Glacial	Deep Saline	Baltic Sea	Modified Baltic	Shallow
					Influx	Influx	Influx	Influx	Influx
Redox zone	150	KR0012B	Cl-Na-HCO ₃ -Ca-SO ₄ -K	Na-Ca-K:Cl-HCO ₃ -SO ₄	20%	1%	2%	4%	73%
Redox zone	550	KR0012B	Cl-Na-Ca-HCO ₃ -SO ₄ -K	Na-Ca-K:Cl-HCO ₃ -SO ₄	17%	2%	7%	10%	64%
Redox zone	750	KR0012B	Cl-Na-HCO ₃ -Ca-SO ₄ -K	Na-Ca-K:Cl-HCO ₃ -SO ₄	18%	2%	6%	10%	63%
Redox zone	950	KR0012B	Cl-Na-Ca-HCO ₃ -SO ₄ -K	Na-Ca-K:Cl-HCO ₃ -SO ₄	9%	3%	5%	8%	75%
Redox zone	1150	KR0012B	Cl-Na-HCO ₃ -SO ₄ -Ca-K	Na-Ca-K:Cl-HCO ₃ -SO ₄	1%	0%	7%	10%	81%
Redox zone	1350	KR0012B	Cl-Na-HCO ₃ -SO ₄ -Ca-K	Na-Ca-K:Cl-HCO ₃ -SO ₄	1%	0%	7%	9%	82%
NE-4a,4b	350	SA0850B	Cl-Na-Ca-HCO ₃ -SO ₄ -K	Na-Ca-K:Cl-HCO ₃ -SO ₄	17%	11%	21%	23%	29%
NE-4a,4b	750	SA0813B	Cl-Na-HCO ₃ -Ca-SO ₄ -K	Na-Ca-K:Cl-HCO ₃ -SO ₄	9%	2%	24%	42%	23%
NE-4a,4b	1150	SA0813B	Cl-Na-HCO ₃ -Ca-SO ₄ -K	Na-Ca-K:Cl-HCO ₃ -SO ₄	9%	3%	29%	40%	20%
NE-4a,4b	1350	SA0813B	Cl-Na-Ca-HCO ₃ -SO ₄ -K	Na-Ca-K:Cl-HCO ₃ -SO ₄	7%	1%	23%	46%	23%
NE-3b,3c	350	SA0976B	Cl-Na-Ca-HCO ₃ -SO ₄ -K	Na-Ca-K:Cl-HCO ₃ -SO ₄	6%	3%	34%	42%	15%
NE-3b,3c	550	SA1062B	Cl-Na-Ca-HCO ₃ -SO ₄ -K	Na-Ca-K:Cl-HCO ₃ -SO ₄	6%	3%	37%	40%	13%
NE-3b,3c	750	SA1062B	Cl-Na-Ca-HCO ₃ -SO ₄ -K	Na-Ca-K:Cl-HCO ₃ -SO ₄	8%	4%	37%	38%	14%
NE-3b,3c	950	SA0958B	Cl-Na-Ca-HCO ₃ -SO ₄ -K	Na-Ca-K:Cl-HCO ₃ -SO ₄	11%	4%	32%	34%	18%
NE-3b,3c	1150	SA0958B	Cl-Na-Ca-HCO ₃ -SO ₄ -K	Na-Ca-K:Cl-HCO ₃ -SO ₄	12%	4%	32%	33%	18%
NE-3b,3c	1350	SA0958B	Cl-Na-Ca-SO ₄ -HCO ₃ -K	Na-Ca-K:Cl-SO ₄ -HCO ₃	8%	2%	27%	42%	20%
NE-1a,1b	550	SA1342B	Cl-Na-Ca-HCO ₃ -SO ₄ -K	Na-Ca-K:Cl-HCO ₃ -SO ₄	17%	10%	21%	23%	30%
NE-1a,1b	750	HA1327B	Cl-Na-Ca-HCO ₃ -SO ₄ -K	Na-Ca-K:Cl-HCO ₃ -SO ₄	15%	4%	24%	31%	25%
NE-1a,1b	950	SA1229A	Cl-Na-Ca-HCO ₃ -SO ₄ -K	Na-Ca-K:Cl-HCO ₃ -SO ₄	7%	2%	27%	44%	20%
NE-1a,1b	1150	HA1327B	Cl-Na-Ca-HCO ₃ -SO ₄ -K	Na-Ca-K:Cl-HCO ₃ -SO ₄	11%	4%	33%	35%	17%
NE-1a,1b	1350	SA1229A	Cl-Na-Ca-HCO ₃ -SO ₄ -K	Na-Ca-K:Cl-HCO ₃ -SO ₄	6%	2%	32%	44%	16%
EW-3a	750	SA1420A	Cl-Na-Ca-SO ₄ -HCO ₃ -K	Na-Ca-K:Cl-SO ₄ -HCO ₃	23%	6%	23%	20%	29%
EW-3a	950	SA1420A	Cl-Na-Ca-SO ₄ -HCO ₃ -K	Na-Ca-K:Cl-SO ₄ -HCO ₃	11%	3%	23%	39%	25%
EW-3a	1150	SA1420A	Cl-Na-Ca-SO ₄ -HCO ₃ -K	Na-Ca-K:Cl-SO ₄ -HCO ₃	10%	3%	30%	37%	19%
EW-3a	1350	SA1420A	Cl-Na-Ca-SO ₄ -HCO ₃ -K	Na-Ca-K:Cl-SO ₄ -HCO ₃	9%	2%	22%	43%	25%
NE-2a-1	750	SA1614B	Cl-Na-Ca-SO ₄ -HCO ₃ -K	Na-Ca-K:Cl-SO ₄ -HCO ₃	65%	12%	6%	6%	10%
NE-2a-1	950	SA1614B	Cl-Na-Ca-SO ₄ -HCO ₃ -K	Na-Ca-K:Cl-SO ₄ -HCO ₃	51%	17%	9%	9%	15%
NE-2a-1	1150	SA1614B	Cl-Na-Ca-SO ₄ -HCO ₃ -K	Na-Ca-K:Cl-SO ₄ -HCO ₃	38%	14%	13%	13%	21%
NE-2a-1	1350	SA1614B	Cl-Na-Ca-SO ₄ -HCO ₃ -K	Na-Ca-K:Cl-SO ₄ -HCO ₃	30%	13%	15%	16%	26%
NE-2a-2	750	SA1828B	Cl-Na-Ca-SO ₄ -HCO ₃ -K	Na-Ca-K:Cl-SO ₄ -HCO ₃	45%	13%	11%	12%	19%
NE-2a-2	950	SA1828B	Cl-Na-Ca-SO ₄ -HCO ₃ -K	Na-Ca-K:Cl-SO ₄ -HCO ₃	36%	16%	13%	14%	22%
NE-2a-2	1150	SA1828B	Cl-Na-Ca-SO ₄ -HCO ₃ -K	Na-Ca-K:Cl-SO ₄ -HCO ₃	33%	16%	14%	14%	23%
NE-2a-2	1350	SA1828B	Cl-Na-Ca-SO ₄ -HCO ₃ -K	Na-Ca-K:Cl-SO ₄ -HCO ₃	19%	13%	17%	19%	32%
NE-2a-3	1150	SA2583A	Cl-Na-Ca-SO ₄ -HCO ₃ -K	Na-Ca-K:Cl-SO ₄ -HCO ₃	47%	18%	9%	10%	15%
NE-2a-3	1350	SA2583A	Cl-Na-Ca-SO ₄ -HCO ₃ -K	Na-Ca-K:Cl-SO ₄ -HCO ₃	45%	18%	10%	10%	16%
NNW-4H ₂ O-1	950	SA2074A	Cl-Na-Ca-SO ₄ -HCO ₃ -K	Na-Ca-K:Cl-SO ₄ -HCO ₃	17%	15%	18%	20%	30%
NNW-4H ₂ O-1	1150	SA2074A	Cl-Na-Ca-SO ₄ -HCO ₃ -K	Na-Ca-K:Cl-SO ₄ -HCO ₃	17%	12%	20%	22%	29%
NNW-4H ₂ O-1	1350	SA2074A	Cl-Na-Ca-SO ₄ -HCO ₃ -K	Na-Ca-K:Cl-SO ₄ -HCO ₃	18%	11%	20%	22%	30%
NNW-4H ₂ O-2	950	SA2109B	Cl-Na-Ca-SO ₄ -HCO ₃ -K	Na-Ca-K:Cl-SO ₄ -HCO ₃	18%	13%	18%	20%	31%
NNW-4H ₂ O-2	1150	SA2142A	Cl-Na-Ca-SO ₄ -HCO ₃ -K	Na-Ca-K:Cl-SO ₄ -HCO ₃	14%	6%	37%	27%	16%
NNW-4H ₂ O-2	1350	SA2175B	Cl-Na-Ca-SO ₄ -HCO ₃ -K	Na-Ca-K:Cl-SO ₄ -HCO ₃	15%	12%	22%	25%	26%
NNW-4H ₂ O-3	1350	KA3191F	Cl-Na-Ca-SO ₄ -HCO ₃ -K	Na-Ca-K:Cl-SO ₄ -HCO ₃	45%	19%	10%	10%	16%

PART 3

TRANSPORT OF SOLUTES

1 SUBJECT: SALINITY- SITE SCALE

1.1 SCOPE AND CONCEPTS

Flow rates distribution in the rock mass during natural conditions and during the construction of the tunnel is dependent of the salinity distribution in the rock mass. Calculation of the groundwater flow and salinity distribution is therefore made simultaneously. The model comprises therefore of the same geometrical concepts as for groundwater flow:

- Hydraulic conductor domains
- Hydraulic rock mass domains.

Hydraulic conductor domains are large two-dimensional features with hydraulic properties different from the surrounding rock. Generally they are defined geologically as major discontinuities but in some cases they may mainly be defined by interpretation of results from interference testing.

Hydraulic rock mass domains are geometrically defined volumes in space with properties different from surrounding domains (rock mass and conductor). They may either be defined by lithological domains or purely by interpretation of results from hydraulic tests.

Material properties for the steady-state groundwater flow model are transmissivity (hydraulic conductor domains) and hydraulic conductivity (hydraulic rock mass domains). The material properties of importance for the transport of salinity are kinematic porosity and hydrodynamic dispersion (molecular diffusion + mechanical dispersion).

Predictions were made with the numerical code PHOENICS /Spalding , 1981/ to test the ability to make a prediction of the salinity of the flow into the tunnel and the salinity in borehole sections.

1.2 METHODOLOGY FOR TESTS OF CONCEPTS AND MODELS

1.2.1 Prediction methodology

A groundwater flow model made with the numerical code PHOENICS was used to make the predictions. A linear relationship between the salinity and fluid density was used and this variable fluid density was included in the pressure term in the equation of motion /Rhen et al, 1997/. Dispersivity was set to a constant value equal to 2 m /Svensson, 1991a/. The calculations was performed as a stationary simulation for a number of tunnel face positions. See Chapter 3 in Part 1 for an overview of other parts of the model.

The predictions were made for cored boreholes that were equipped with packed off sections and for defined parts of the tunnel (called “legs” in the prediction). A summary of the calibrated model was presented in *Wikberg et al /1991/*. The detailed predictions of the transformed flow rates were presented in *Rhén et al /1991/*.

The predictions shown here has not been complimented with the results from the simulation with the measured flow rates into the tunnel as was done for the pressures, *see Chapter 4, Part 1*. According to *Chapter 3, Part 1* the predicted flow into the tunnel was about 15 % larger than the outcome for tunnel section 700-2875 m, but the measured flow into tunnel section 1460-2875 m was approximately $10 \cdot 10^{-3} \text{ m}^3/\text{s}$ compared to the predicted $20 \cdot 10^{-3} \text{ m}^3/\text{s}$.

1.2.2 Methodology for determining outcome

Boreholes

Water samples were taken for chemical characterization in corehole sections equipped for sampling by pumping (generally two sections per corehole where also dilution measurements were made) before starting excavation of the tunnel and were repeated for some of the borehole sections as the excavation proceeded. The results are reported in *Nilsson /1995/*. The results from the boreholes are considered to be reliable.

The electric conductivity of the water in each measurement section in the coreholes were measured after the packers were installed and generally a few times thereafter. Each section was generally pumped by airlift so long that at least twice the volume in the measurement section and in the pipes up to surface were discharged. Thereafter the electrical conductivity of the outflowing water was measured. These measurements are considered less reliable than the water sampling mentioned above, particularly when a borehole section had a low hydraulic conductivity.

Resistivity of the borehole fluid was measured by geophysical logging during the pre-investigations. These data have not been used for the comparison.

The flowchart for how the salinity distribution was estimated from measurements is illustrated in *Figure 1-1*.

Inflow to tunnel

At the end of the construction phase water samples were also taken at the weirs and generally Cl content, pH and electrical conductivity were measured. These results are reported in *Rhén (ed) /1995b/*. The calculation of the salinity was based on the mean measured electrical conductivity for a period in 1995. Positions of the weirs and ‘legs’ are shown in *Part 1, Chapter 3, Figures 3-1 and 3-2*. The results from weirs are considered to be reliable.

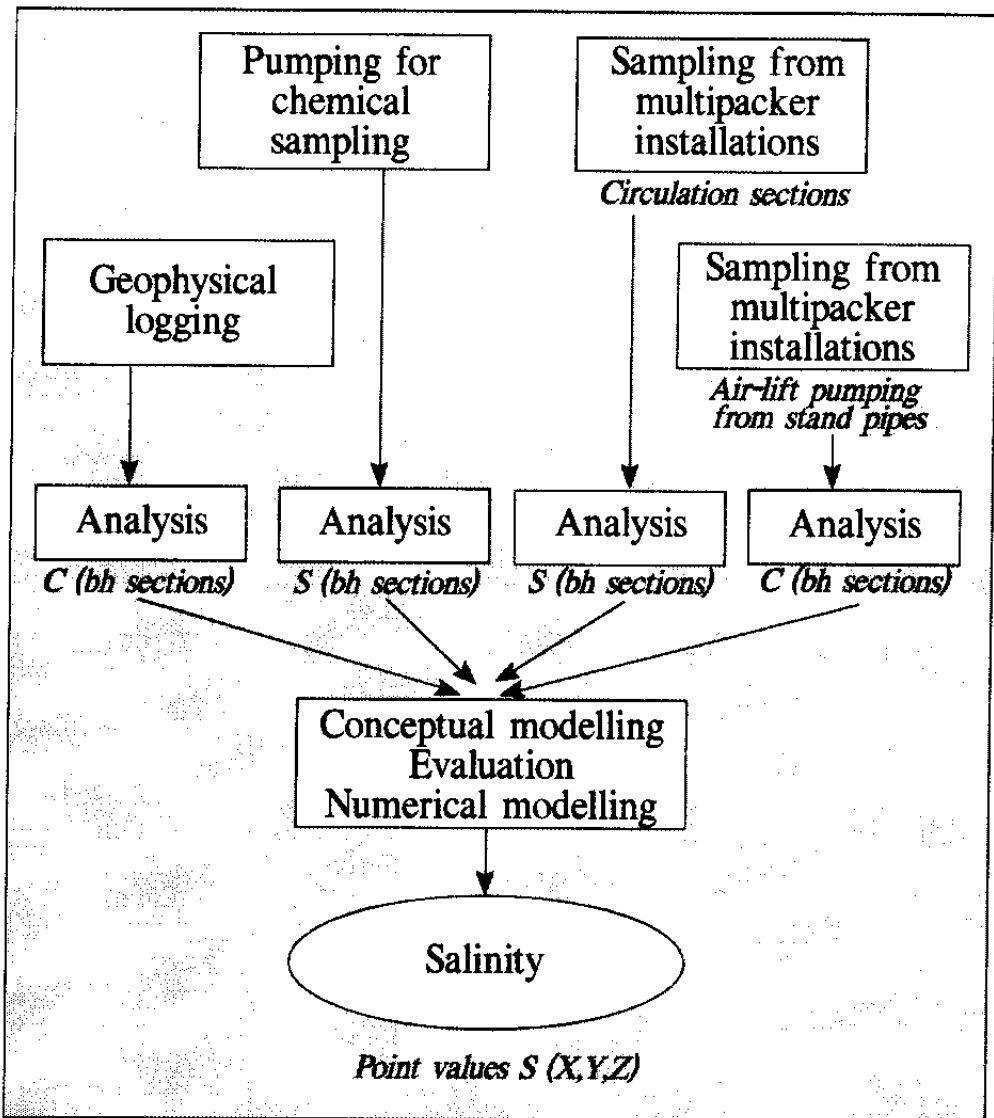


Figure 1-1. Salinity-flow chart. (C = electrical conductivity, S = salinity, xyz = coordinates).

1.3 COMPARISON OF PREDICTED AND MEASURED ENTITIES

1.3.1 Salinity of the water flowing into the tunnel

Prediction and outcome of the salinity of the water flowing into the tunnel is shown in *Figure 1-2*. The measurements were mainly performed during February to April 1995. The measurements in the three last sections in the tunnel were from November and December 1995 */Rhén(ed) 1995b/*. As the

measurements were performed after the excavation was finalized, it was judged that the most relevant comparison with the predictions should be the final tunnel face position according to the predictions. Therefore the predictions shown are for final tunnel face position (3854 m) according to *Gustafson et al/1991/*.

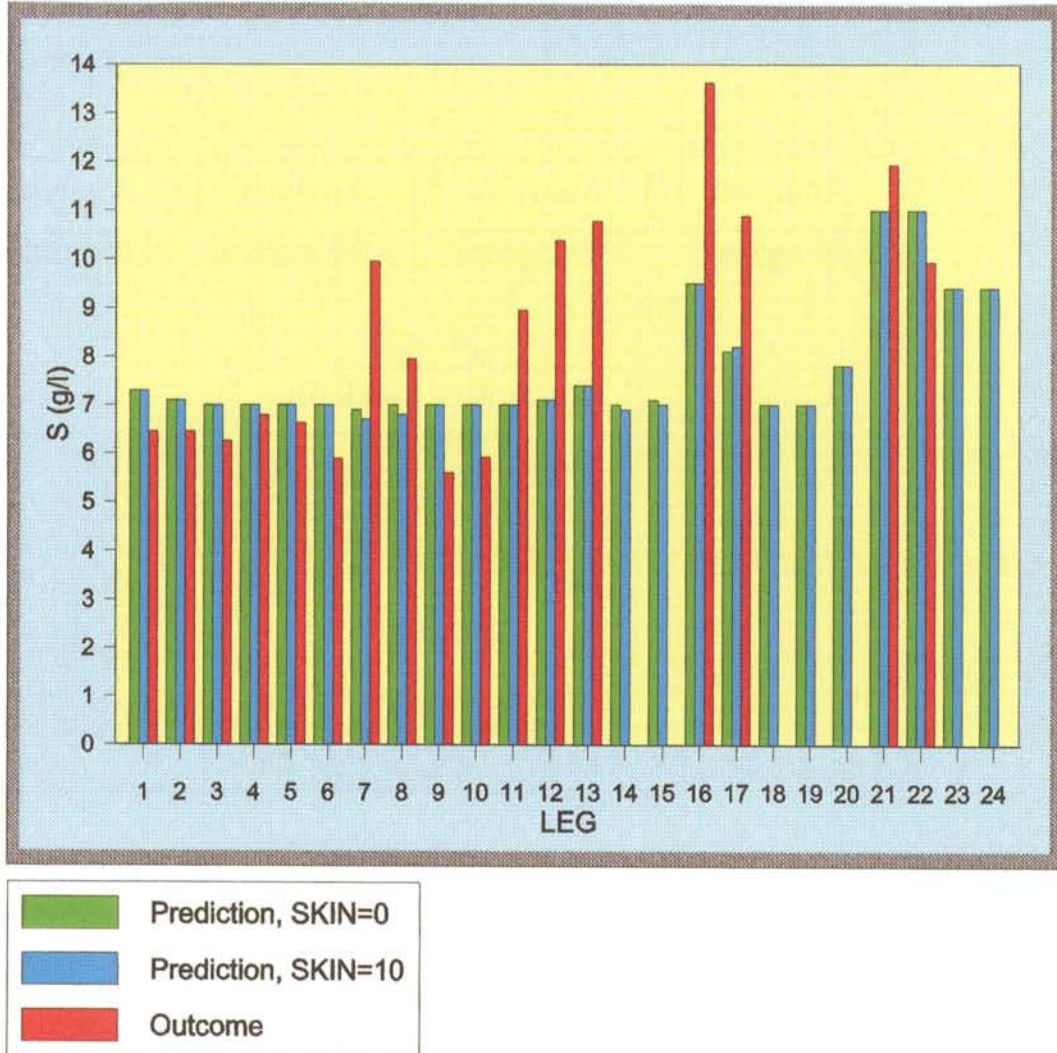


Figure I- 2. Salinity of the water flowing into the tunnel. Predictions for final tunnel face position (3854 m) according to *Gustafson et al/1991/*. Outcome measured during 1995 /*Rhén (ed) 1995b/*. No measurements of the water from the shafts down to -333 m (= Leg 14 and 15) has been made. The measured value for leg 17 is based on tunnel section 2840-2994 m, which is somewhat east of the position of the tunnels in the prediction. Leg 22 is the shaft between -333 and -450 m. Leg 21 is judged to be at approximately the position where the TBM tunnel is today. Leg 21 is therefore compared with results from tunnel section 3179-3411 m. Legs 18, 19, 20, 23, and 24 cannot be compared to any measurements.

1.3.2 Salinity in borehole sections

Predictions and outcomes of the salinity in borehole sections, where at least one water sample for chemical analysis is available, shown in *Figures 1- 3 to 1- 16*. As can be seen in the figures the borehole sections are generally in the depth interval 200-500 m below sea level. Only two sections are deeper.

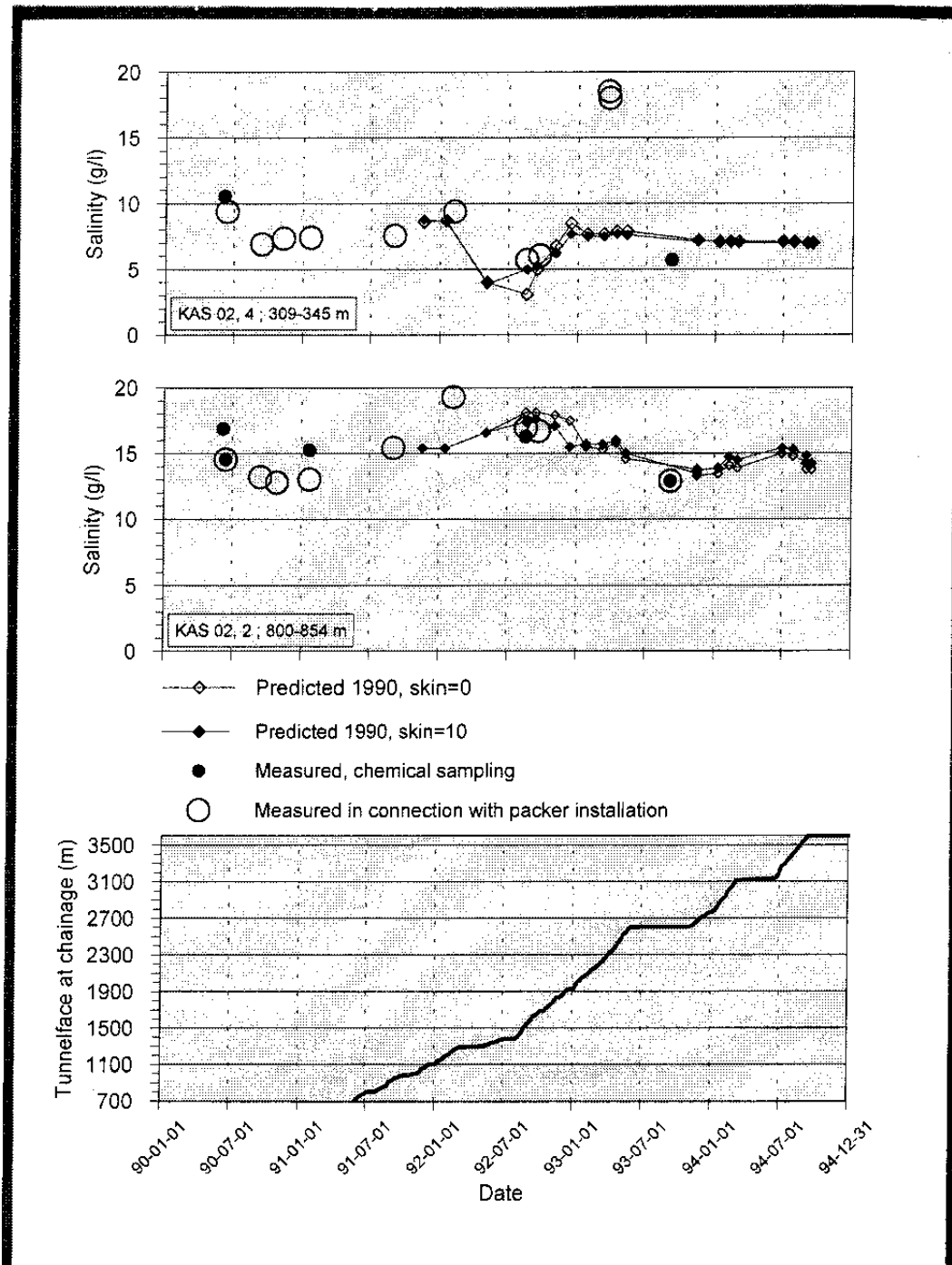


Figure 1-3. Salinity in borehole sections.

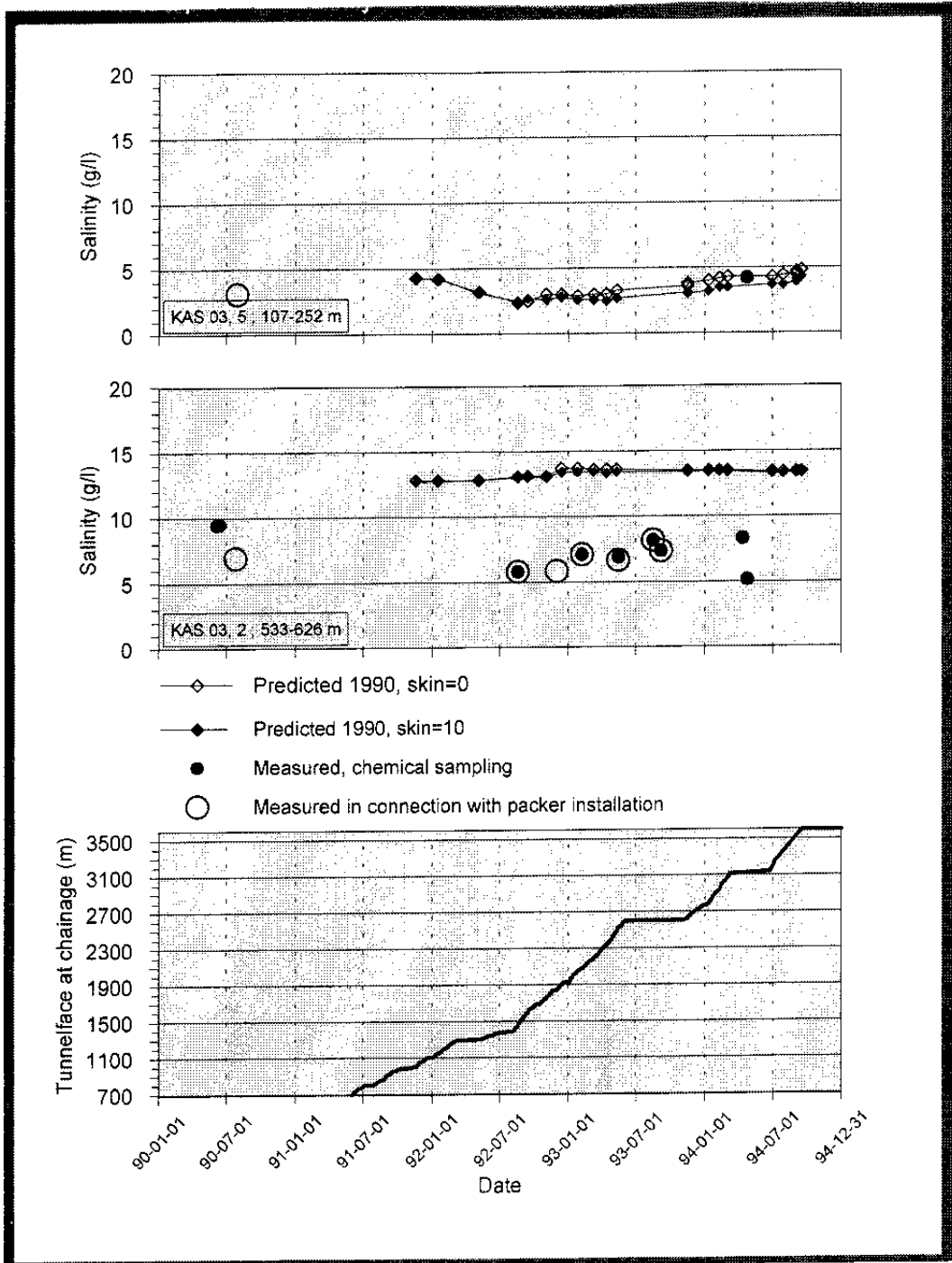


Figure 1-4. Salinity in borehole sections.

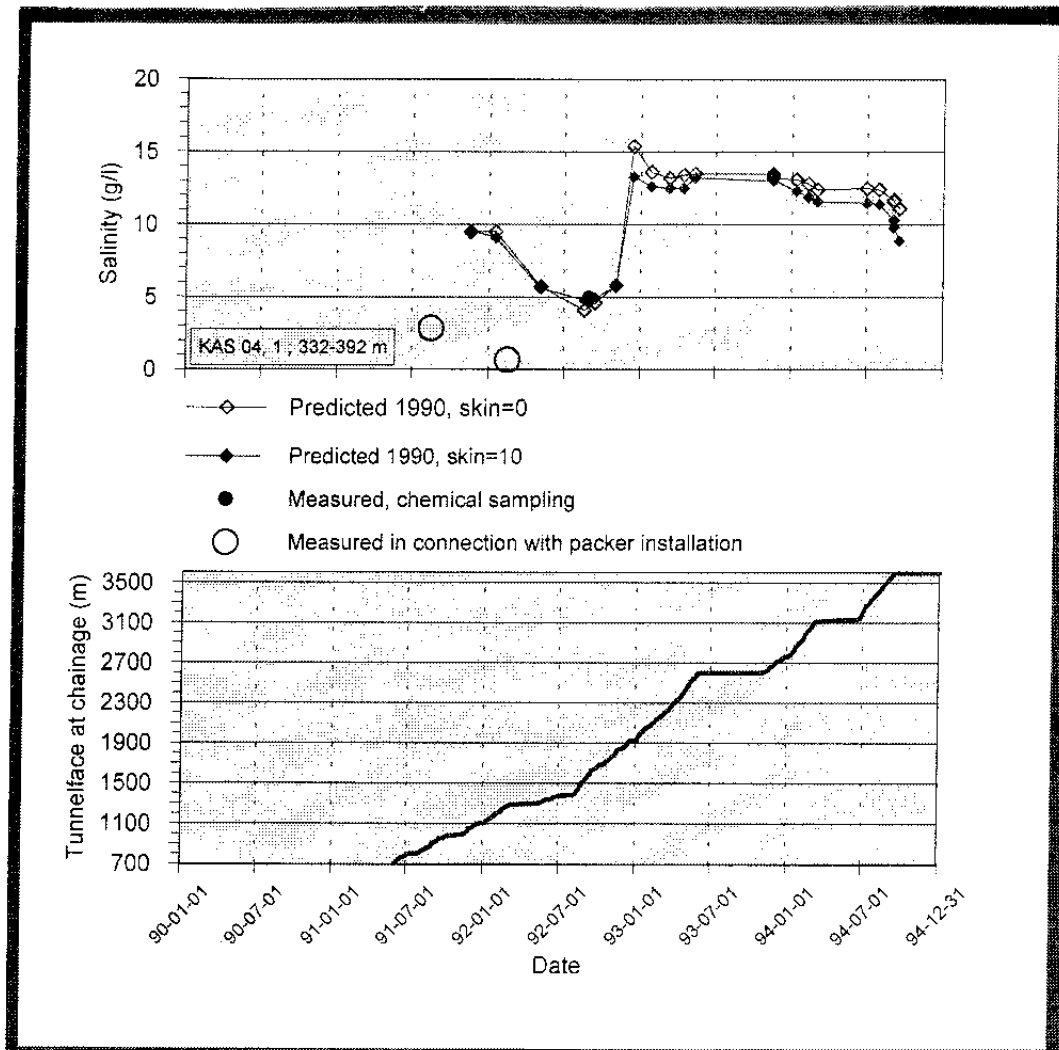


Figure 1- 5. Salinity in borehole sections.

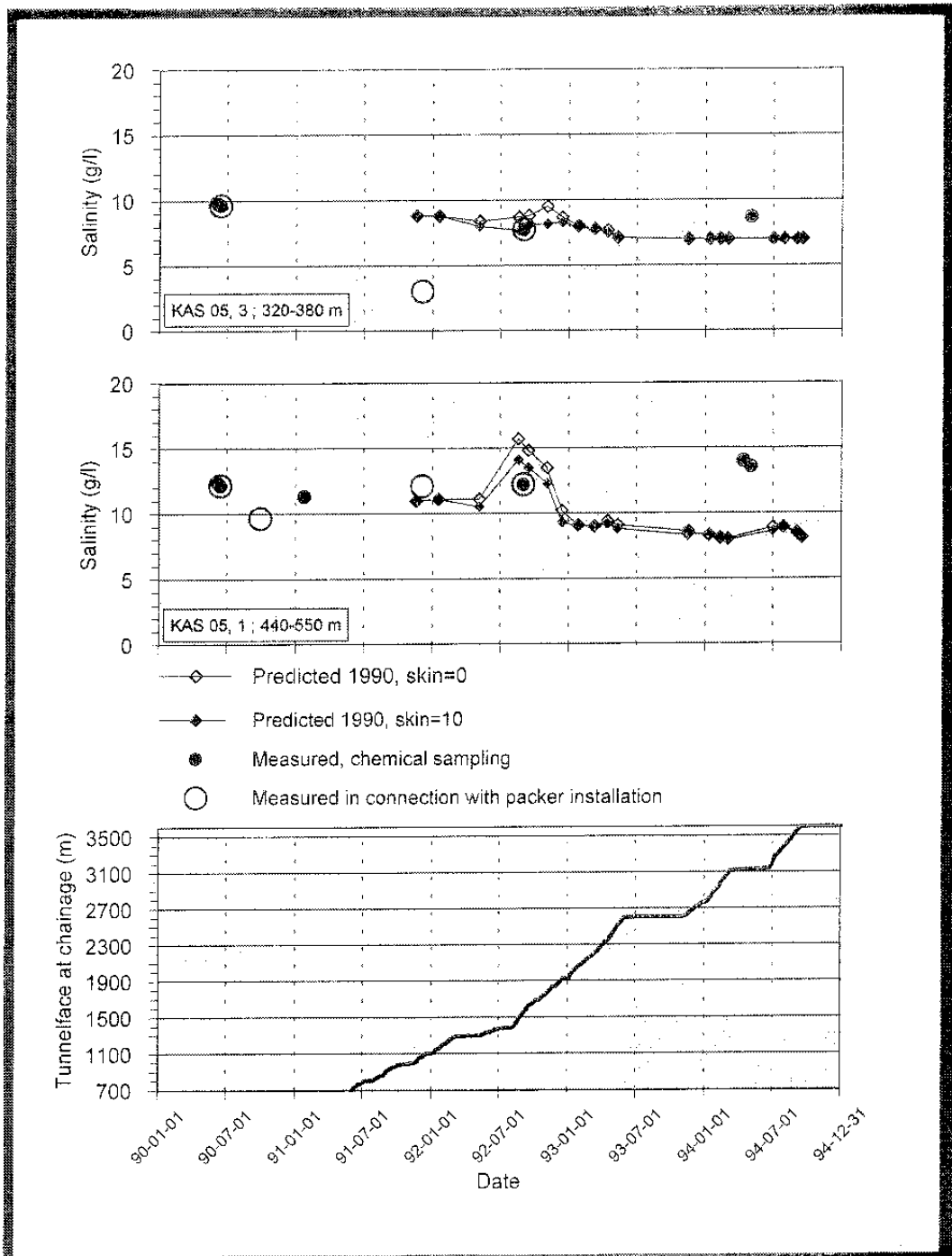


Figure 1- 6. Salinity in borehole sections.

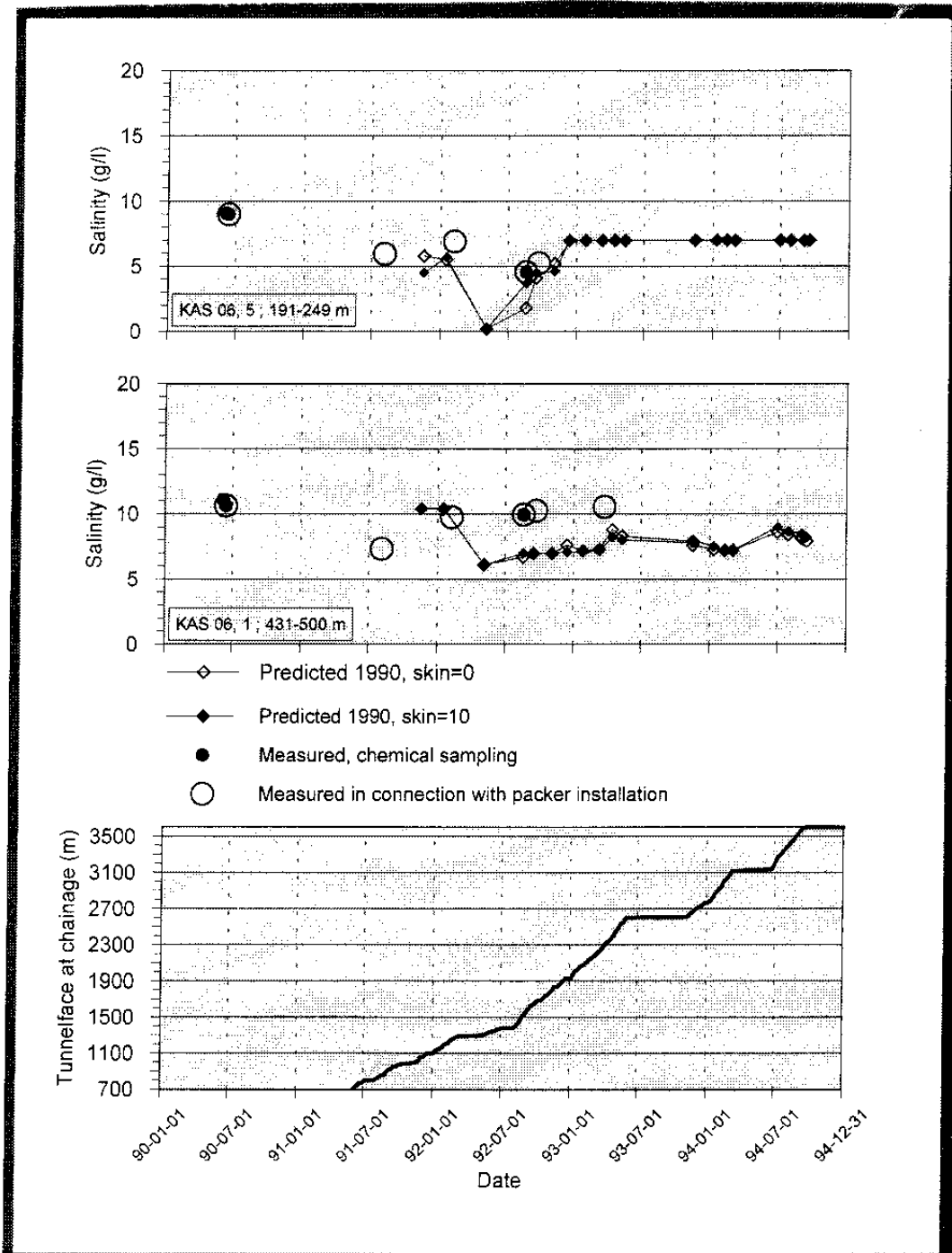


Figure 1-7. Salinity in borehole sections.

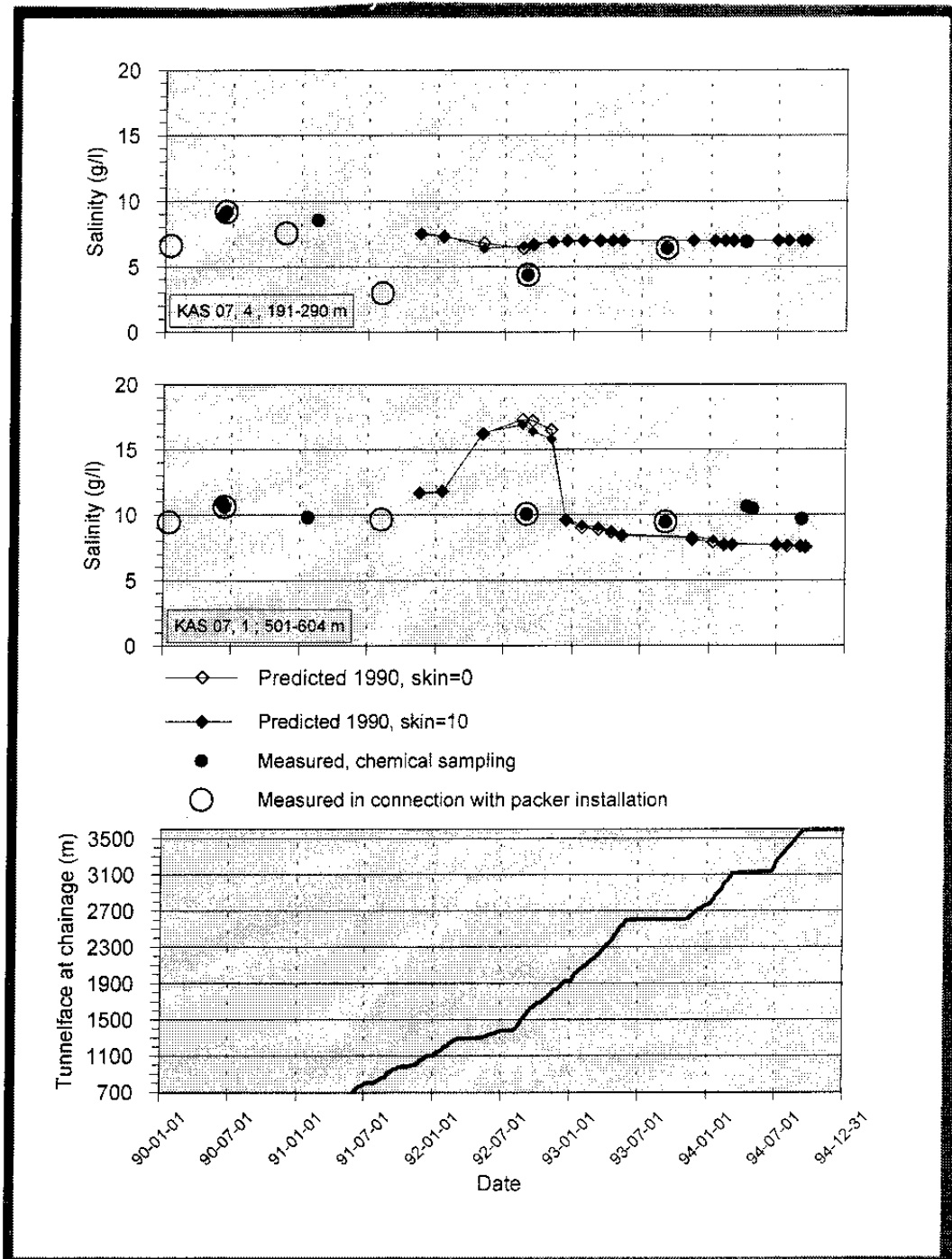


Figure I- 8. Salinity in borehole sections.

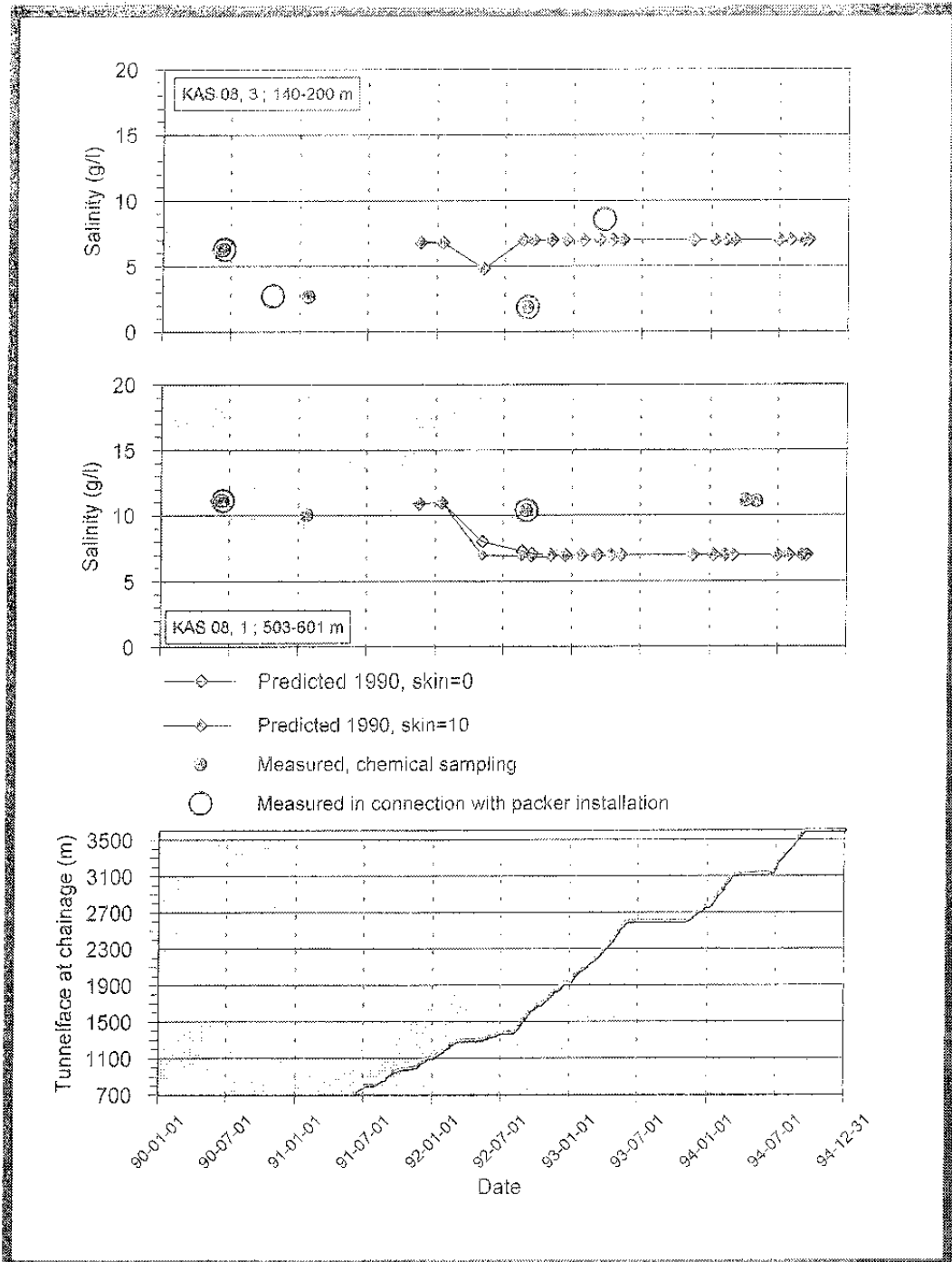


Figure 1-9. Salinity in borehole sections.

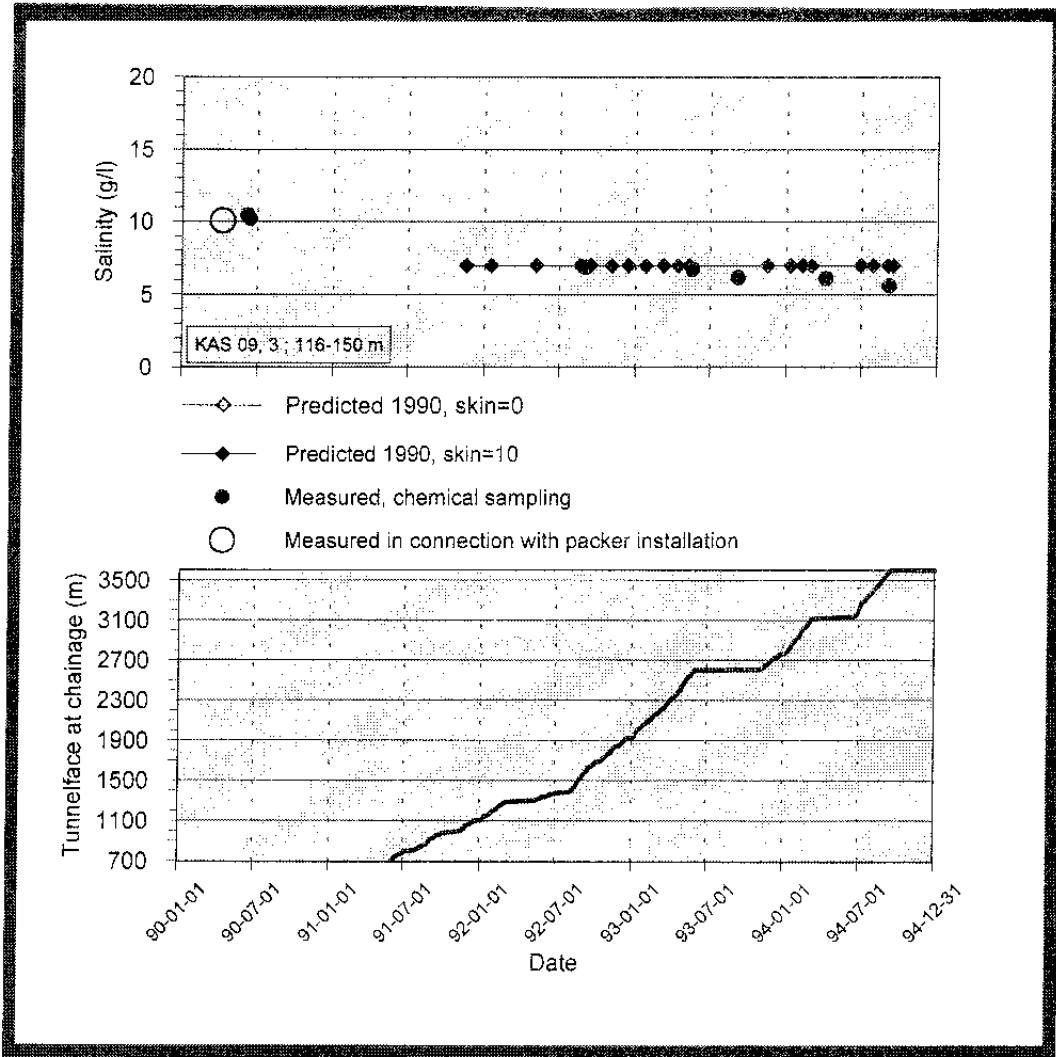


Figure 1- 10. Salinity in borehole sections.

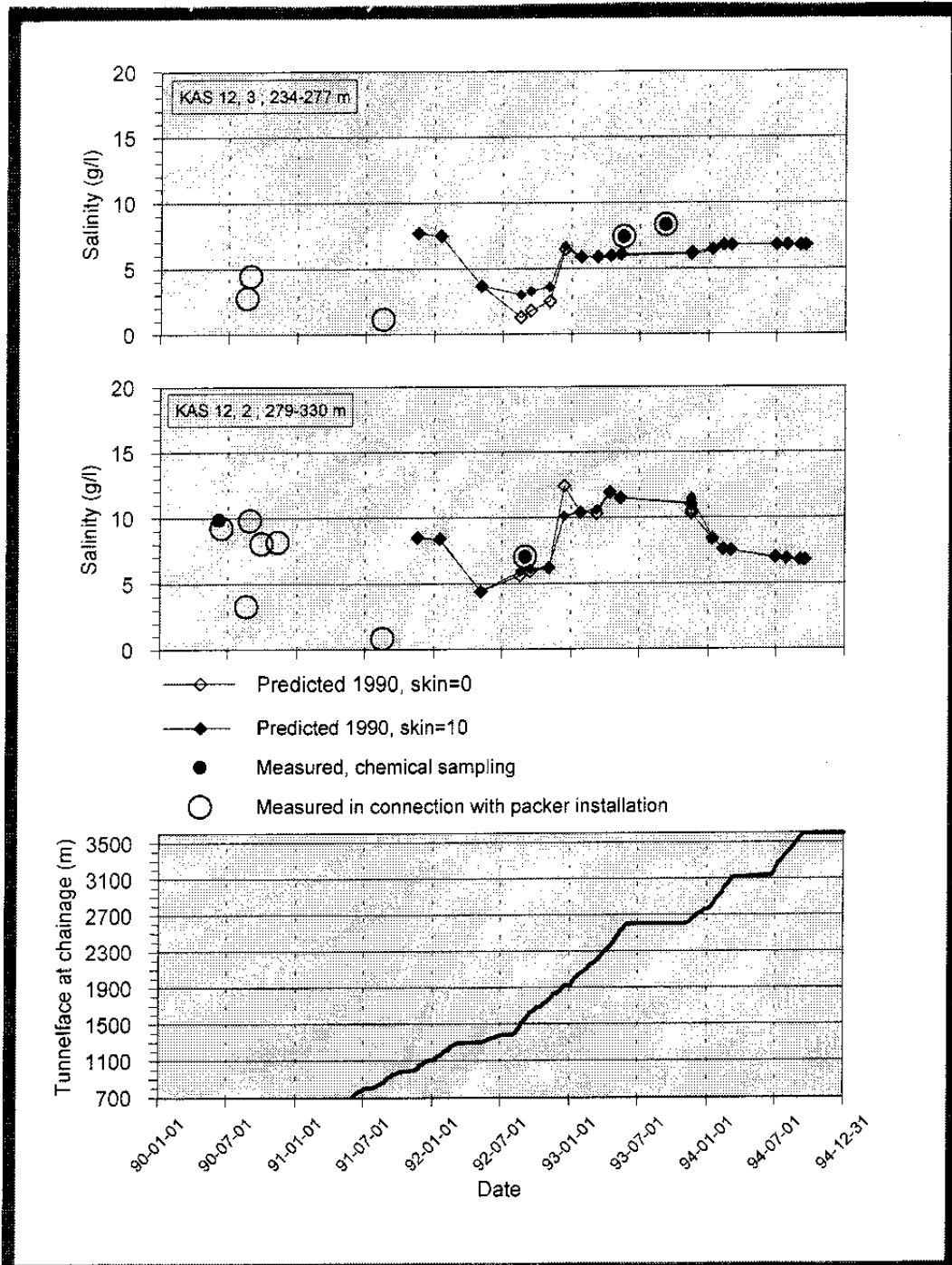


Figure I- 11. Salinity in borehole sections.

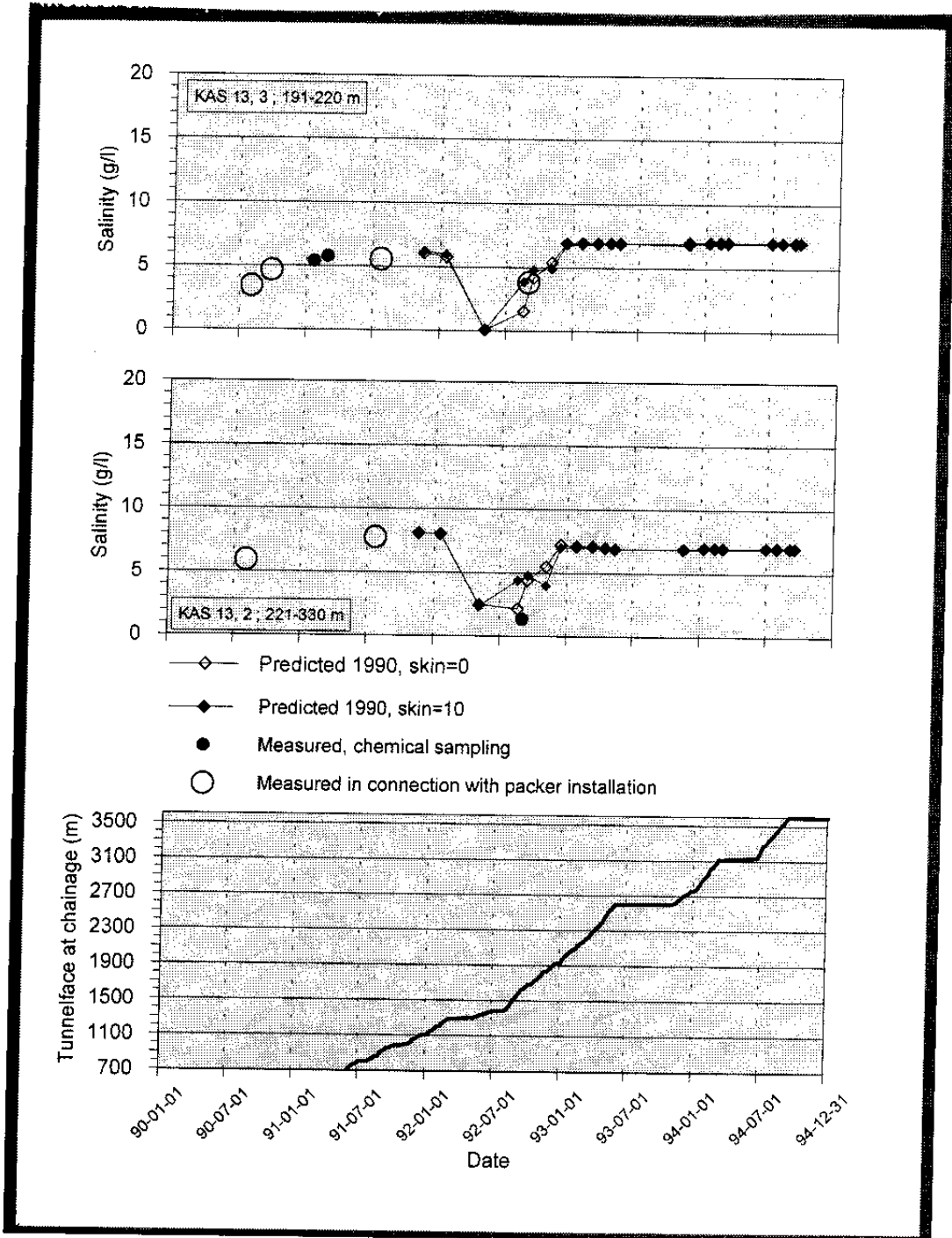


Figure I-12. Salinity in borehole sections.

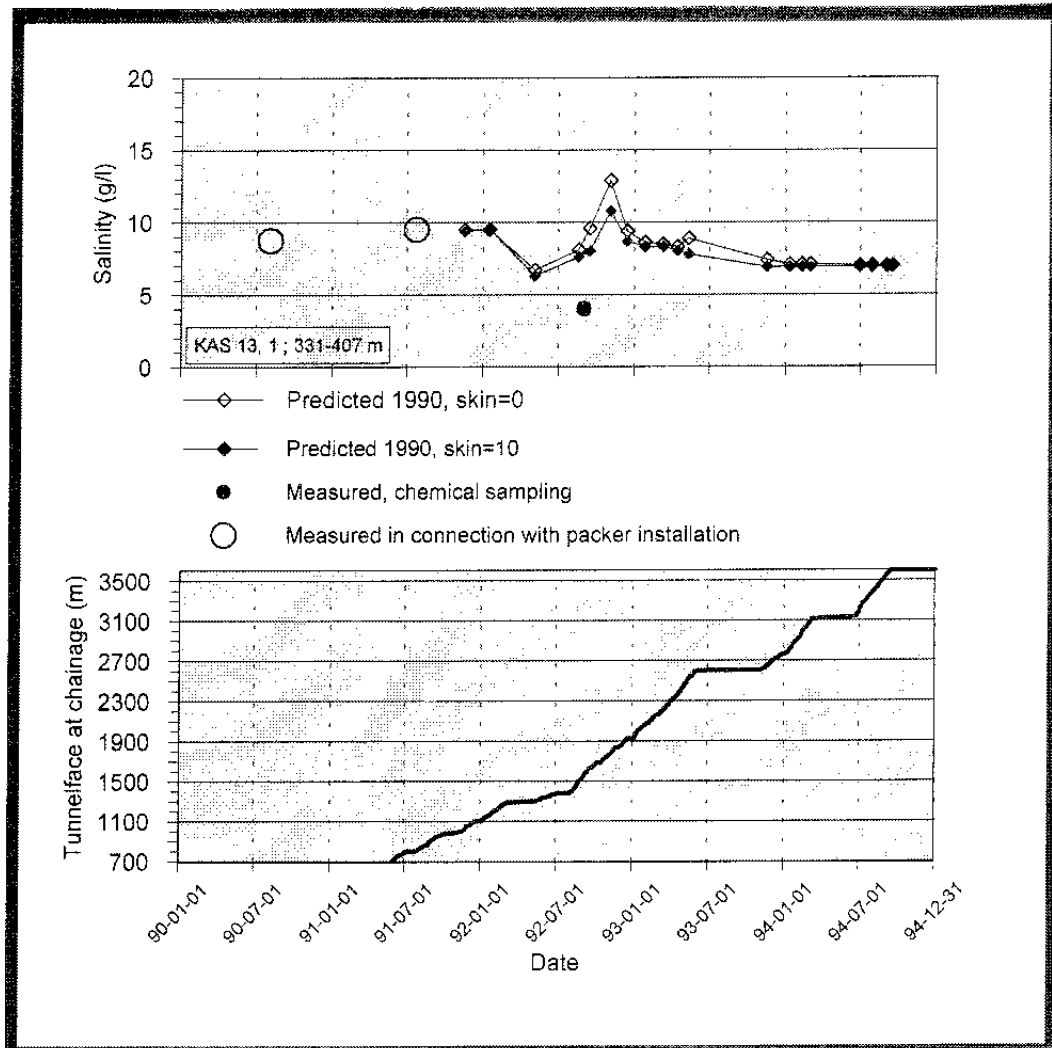


Figure 1-13. Salinity in borehole sections.

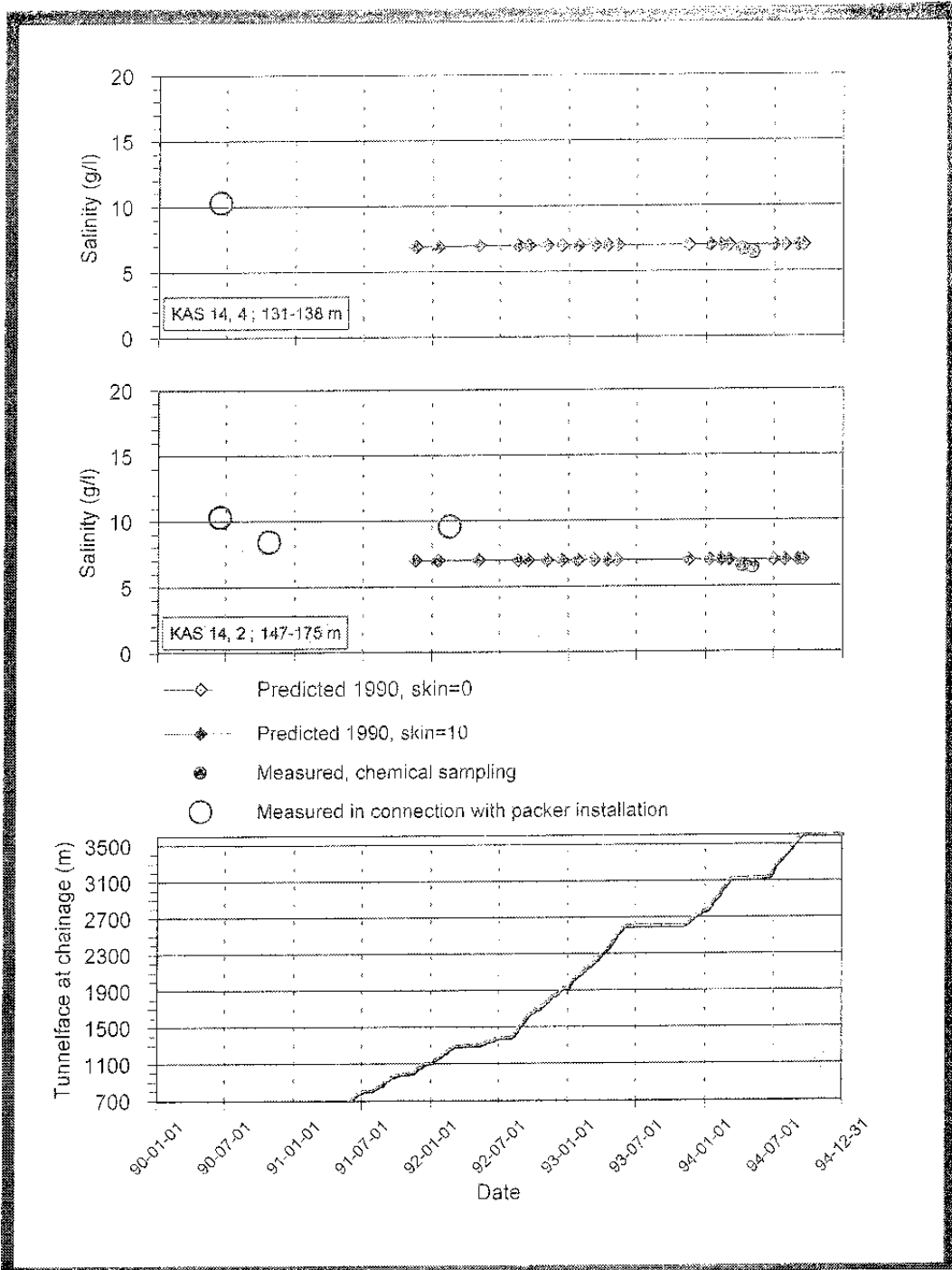


Figure I-14. Salinity in borehole sections.

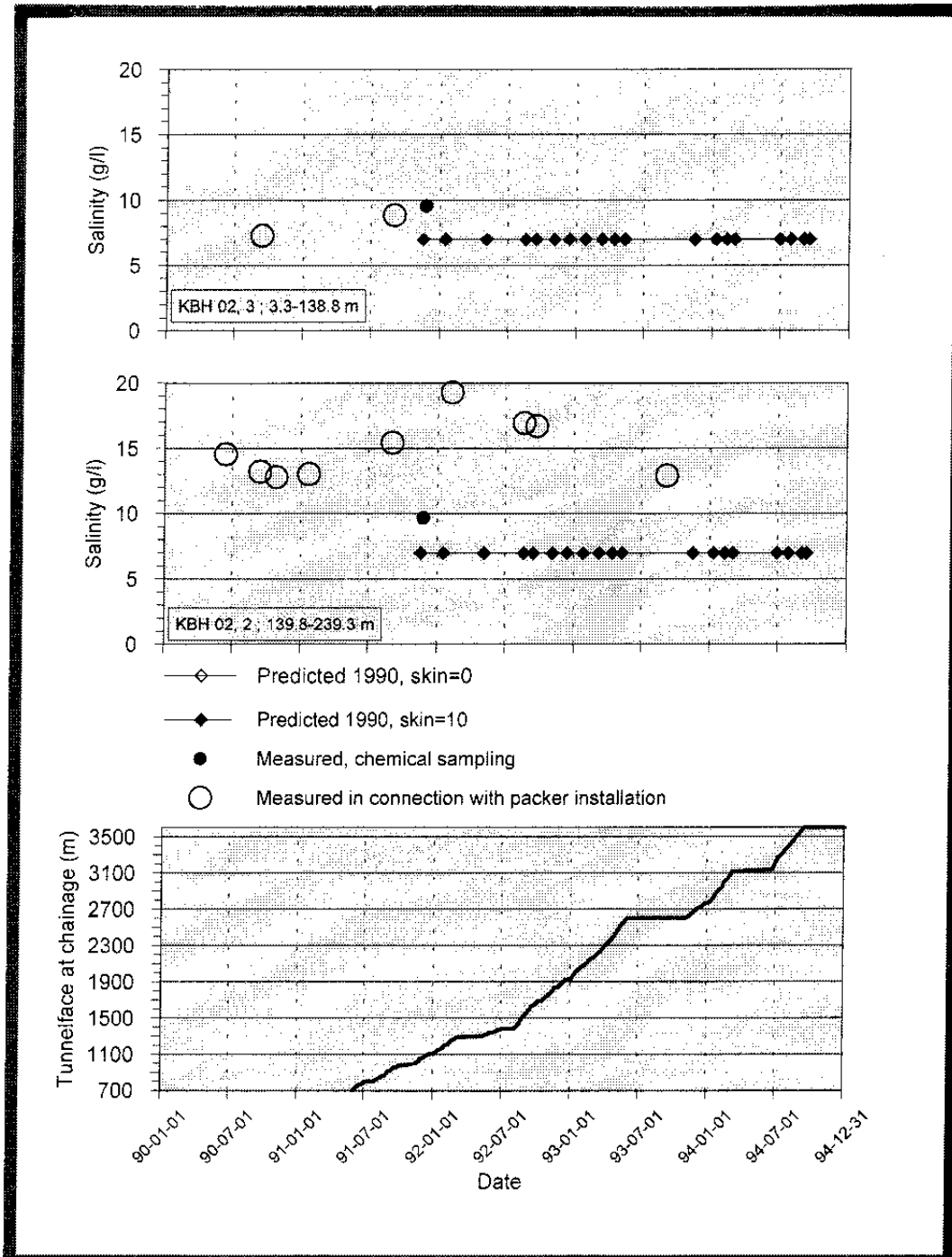


Figure 1-15. Salinity in borehole sections.

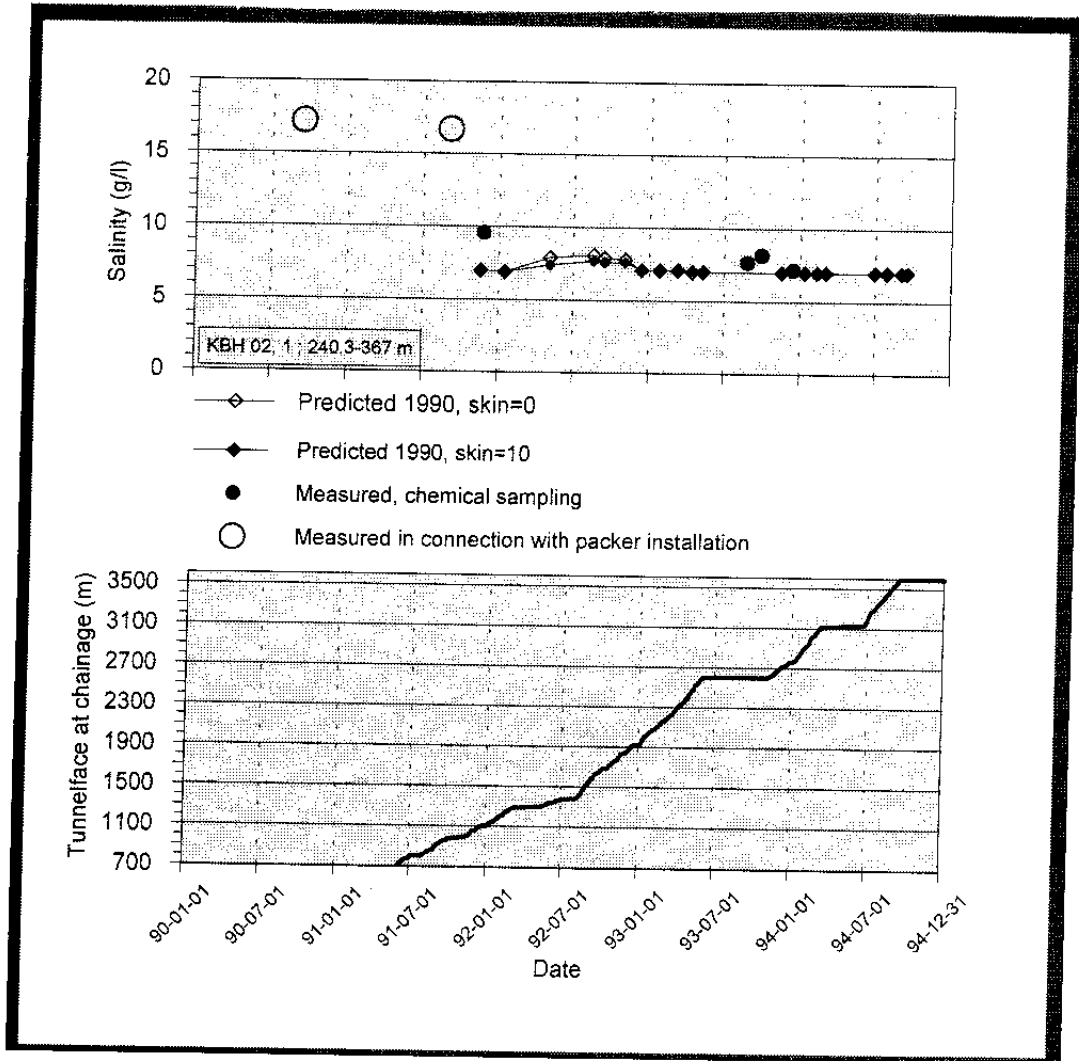


Figure 1-16. Salinity in borehole sections.

1.3.3 Salinity field

The predicted salinity distribution in space for natural conditions (undisturbed by the tunnel) and for a few tunnel-face positions during construction were presented in *Gustafson et al /1991/* and *Wikberg et al /1991/*. Details of the prediction was presented in *Rhén et al /1991/*. The predicted salinity distributions for natural conditions and for the final tunnel-face position after construction are shown in *Figures 1-17* and *1-19*. The simulations presented in *Svensson /1991a/* and *Wikberg et al /1991/* were replotted and are therefore not exactly as the figures presented previously. Due to the interpolation of the simulated results, the salinity field has become less irregular in *Figures 1-17* and *1-19* compared to the initial plots. *Figures 1-17* and *1-19* are based on interpolation of the original data from the simulations. Interpolation was made with a program called *Voxel Analyst* and with an interpolation algorithm called the *Metric method*. It uses the powers of the inverse distance as weight. The salinity distributions for natural conditions and for the final tunnel-face position after construction based on measurements was also estimated by interpolation in three dimensions using *Voxel Analyst*. The interpolation algorithm used for the measured data is a distance-based method, called the *Multiquadric method*. The modelled values at the points for the input data exactly match the original input values, except for some minor truncation errors, and the interpolation function also approximately preserves the gradient inherent in the input data.

The data used are measured values from the Baltic Sea, the properties of the meteoric water (on land), samples from the boreholes made during the pre-investigations (29 borehole sections). Samples were also taken from boreholes made during the construction (19 sections in boreholes from the surface and 18 sections in boreholes from the tunnel). The samples representing the tunnel construction are from the end or after the tunnel construction. Most of the observations are above 600 m depth and also focused below Äspö island, central part of the figures. The observation points for the measured values in boreholes are shown in *Figures 1-21* and *1-22*. Due to this the interpolated values should be considered uncertain below 600 m depth and near the vertical boundaries. The assumed boundary conditions for the total salinity of the box for interpolation were:

Land:	0 mg/l
Baltic Sea:	6008 mg/l
Side top corners of the box, $z = 0$ m:	6008 mg/l
Side bottom corners of the box, $z = 850$ m:	18870 mg/l (the values in the bottom borehole section in KAS02 (depth 850 m))

The results based on the interpolation are shown in *Figures 1-18* and *1-20* for the same vertical sections as the ones for the prediction in *Figures 1-17* and *1-19*.

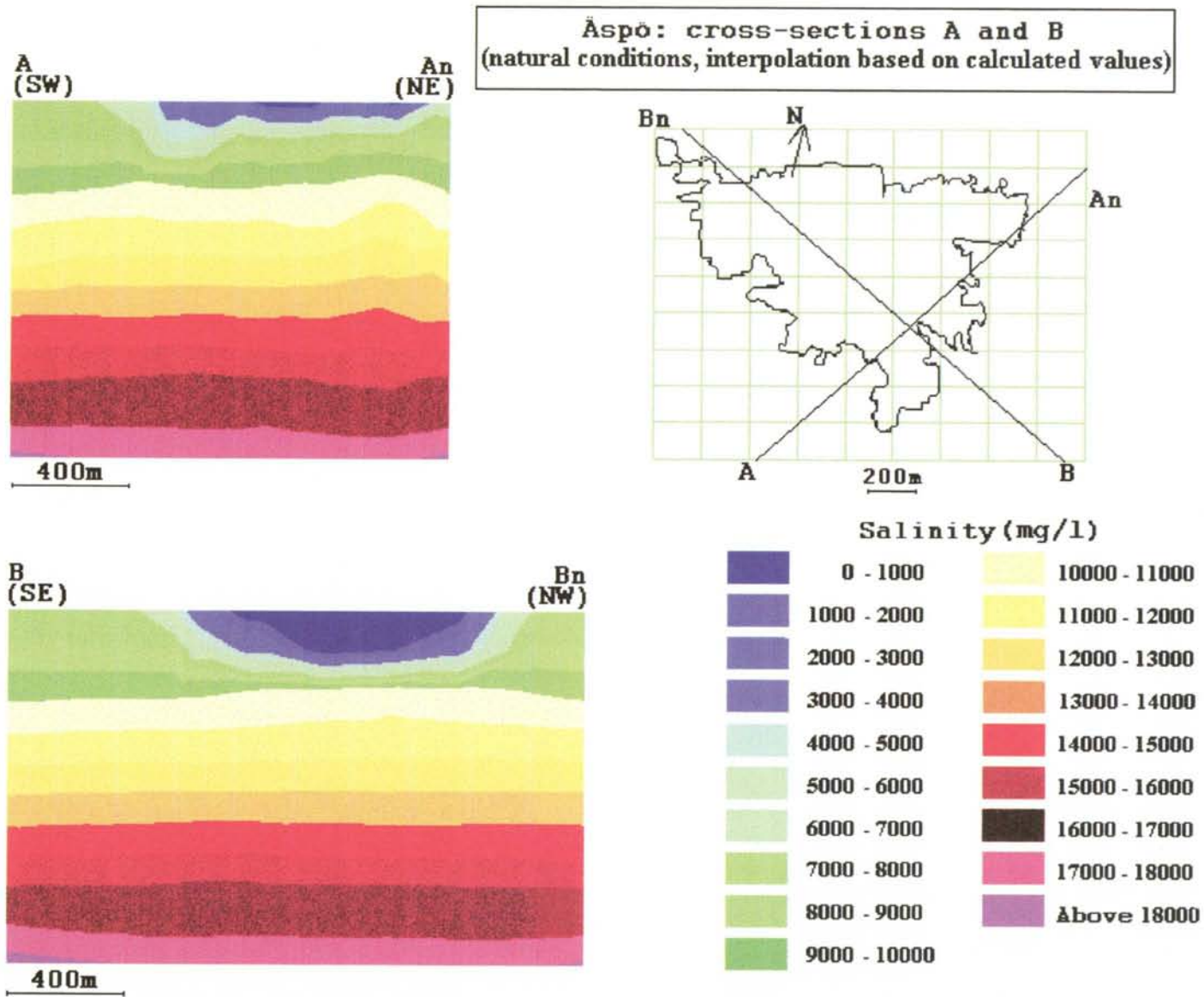


Figure 1-17. Natural conditions - Numerical groundwater flow simulations. The salinity distribution is shown for two vertical sections, section A (above) and B (below). Salinity is given in mg/l. The maximum depth of the vertical sections is 1250 m, which correspond to the bottom in the numerical model. (Simulations presented in Svensson, /1991a/ and Wikberg et al, /1991/ have been replotted and are therefore not exactly as the figures presented in these reports).

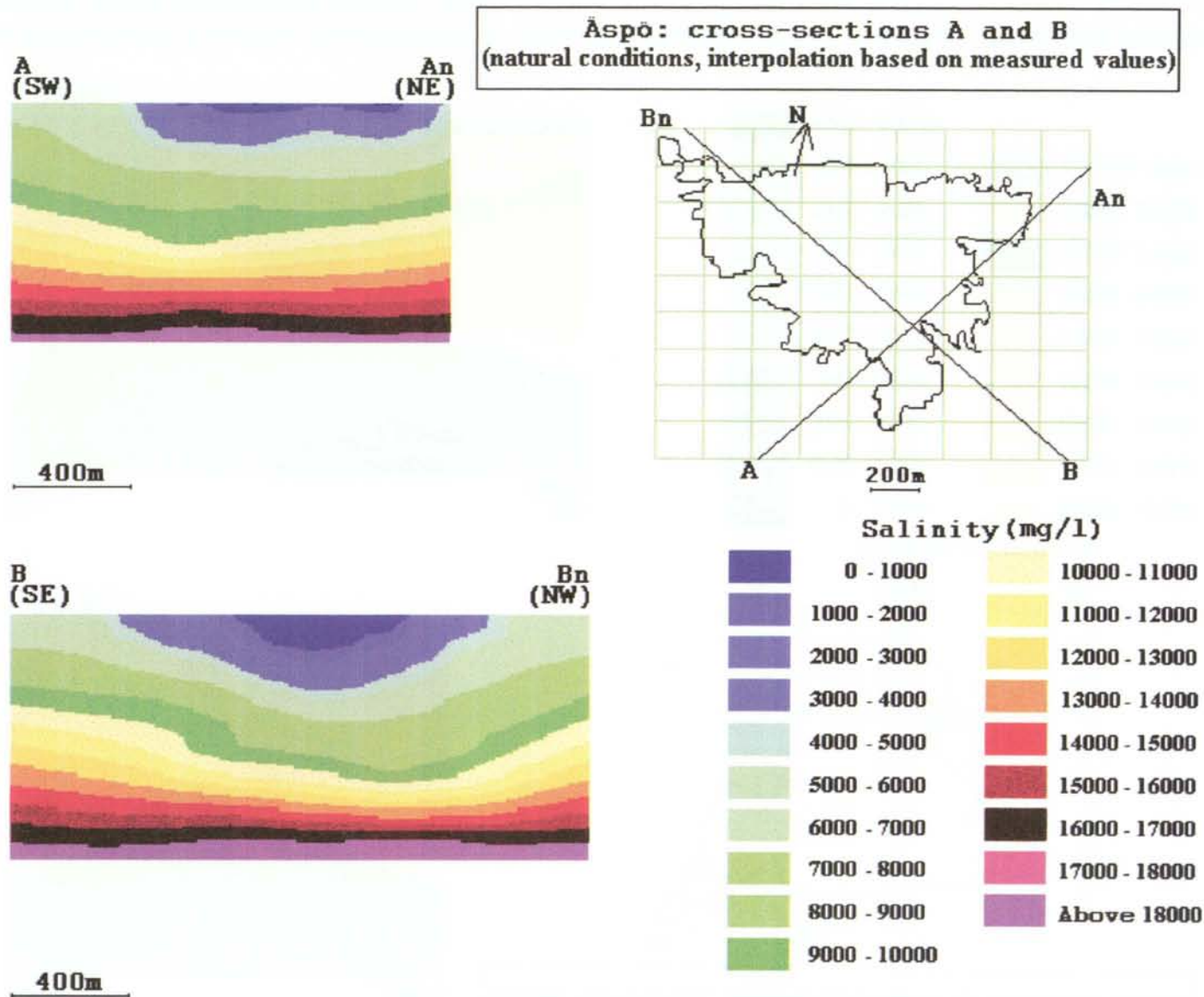


Figure 1-18. Natural conditions - Interpolation based on the measured values. The observation points for the measured values in boreholes are shown in Figures 6-10 and 6-11. The salinity distribution is shown for two vertical sections, section A and B (below). Salinity is given in mg/l. The maximum depth of the vertical sections is 850 m, which corresponds to the deepest measurement point.

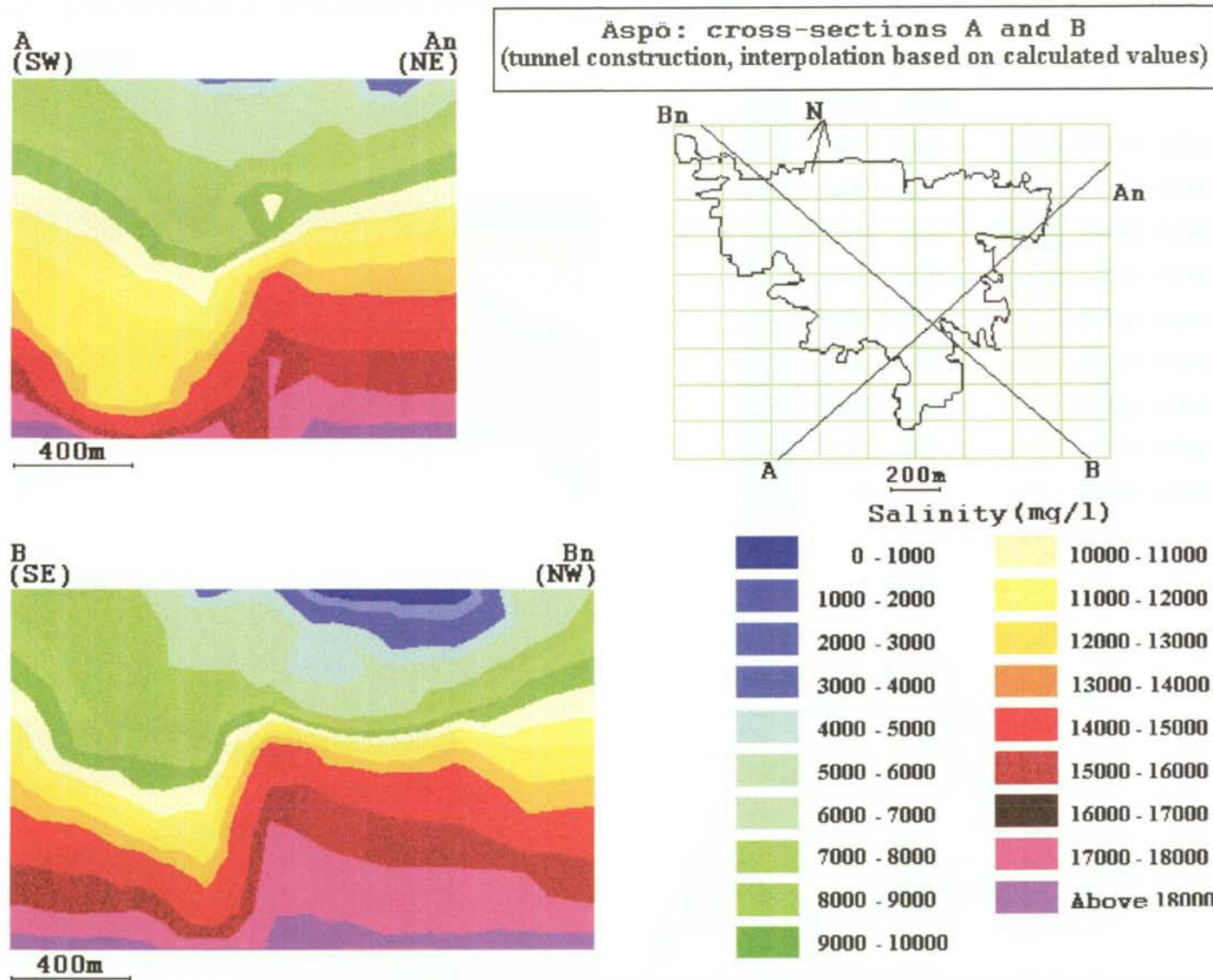
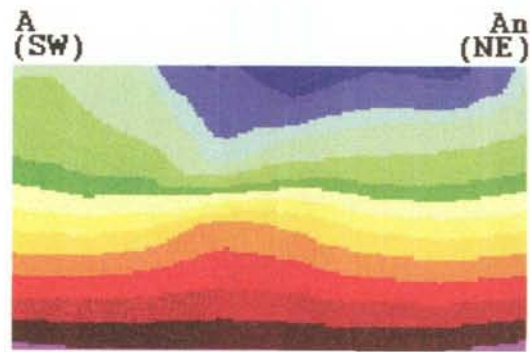
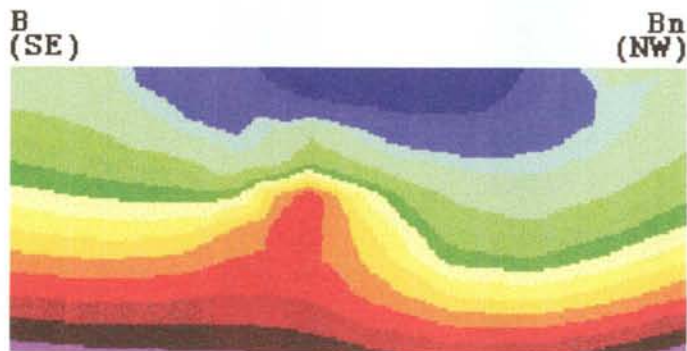


Figure 1-19. The final tunnel-face position after construction - Numerical groundwater flow simulations. The salinity distribution is shown for two vertical sections, section A (above) and B (below). Salinity is given in mg/l. The maximum depth of the vertical sections is 1250 m, which correspond to the bottom in the numerical model. (Simulations presented in Svensson, /1991a/ and Wikberg et al, /1991/ have been replotted and are therefore not exactly as the figures presented in these reports).

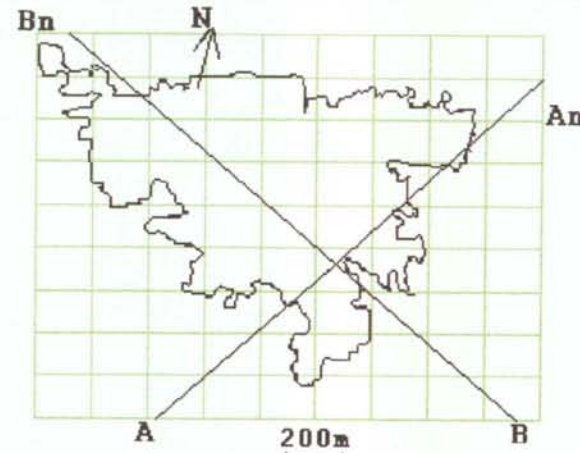


400m



400m

Äspö: cross-sections A and B
(tunnel construction, interpolation based on measured values)



Salinity (mg/l)

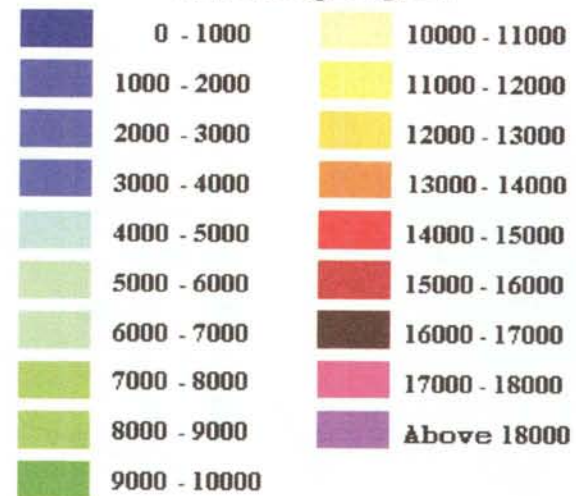


Figure 1-20. The final tunnel-face position after construction - Interpolation based on the measured values. The observation points for the measured values in boreholes are shown in Figures 6-10 and 6-11. The salinity distribution is shown for two vertical sections, section A and B (below). Salinity is given in mg/l. The maximum depth of the vertical sections is 850 m, which corresponds to the deepest measurement point.

Aspo: Preinvestigation Phase

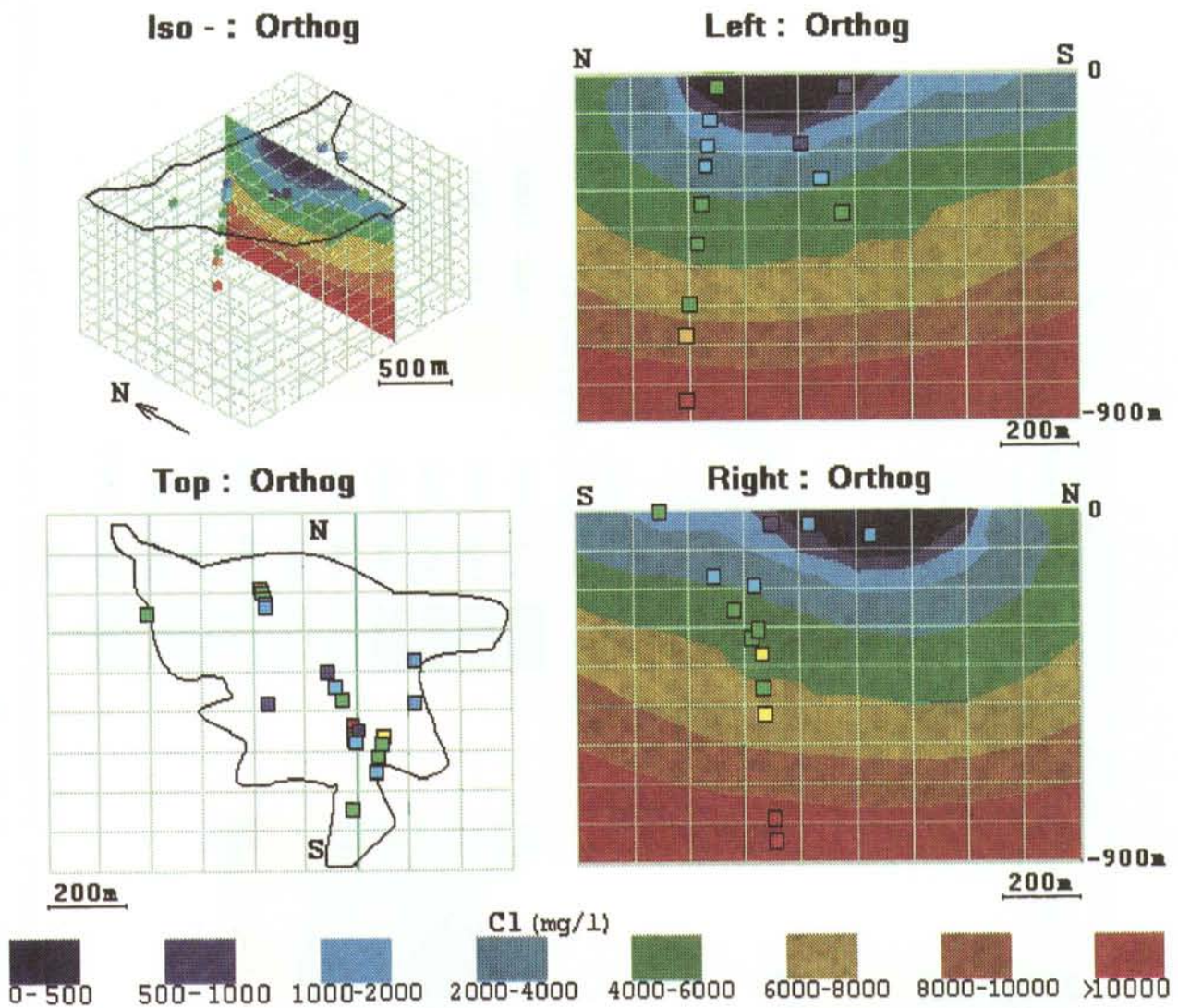


Figure 1-21. The salinity distribution presented as the chloride concentration under the undisturbed conditions prior to excavation. The sampling locations are marked in the figure. (Total salinity = 1.7 times the chloride concentration).

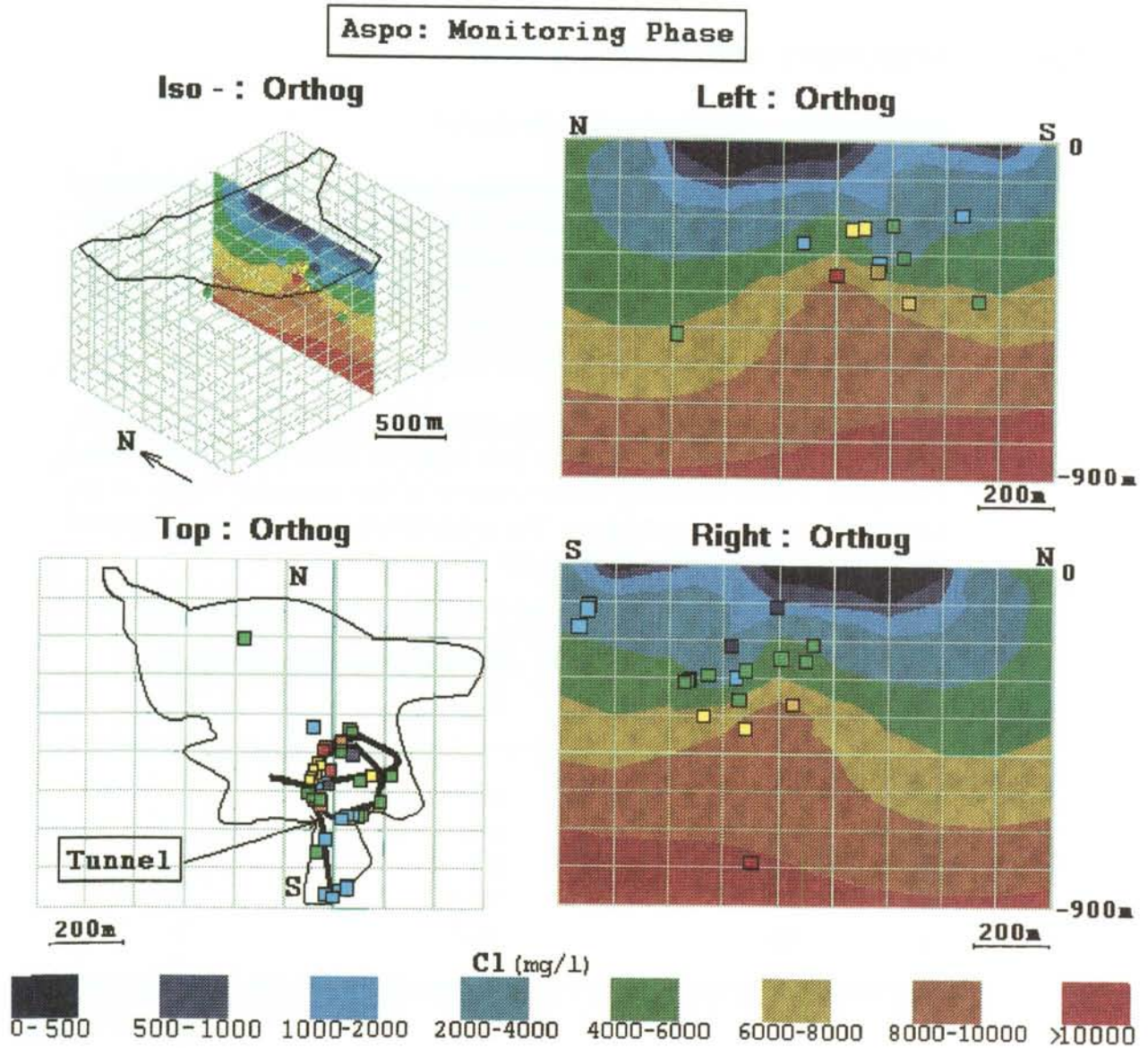


Figure 1-22. The salinity distribution presented as the chloride concentration under the disturbed conditions after construction. The sampling locations are marked in the figure. (Total salinity = 1.7 times the chloride concentration).

1.4 SCRUTINY AND EVALUATION

Salinity of the water flowing into the tunnel

The salinity was not measured for the inflow to the two uppermost sections of the shaft (leg 14 and 15). The position of the tunnel according to the predictions is approximately the same as the actual tunnel position after excavation up to leg 17. Leg 22 (shaft $-z = 333-444$ m) in the predictions is also approximately in the position for the constructed shaft. Leg 21 is considered to be relevant for comparison of the results from the first part of the TBM tunnel.

At the vertical boundaries hydrostatic pressure distribution, based on 0.7 ‰ salinity at sea level and 1.8 ‰ at the depth of 1290 m, was prescribed /Svensson, 1991a/ based on approximation of the measured values of the salinity during natural conditions. The depth below sea level for the legs and the salinity at the model boundaries are about:

Leg	Depth below sea level (m)	Salinity at model boundaries (g/l)
1	100	7.9
6	200	8.7
10-11	300	9.6
17	400	10.4
21	450	10.8

Legs 7 and 8 are at the western and northwestern part of the tunnel spiral ("high" salinity measured), legs 9 and 10 are at the northeastern and eastern part ("low" salinity measured, see *Figure 1-2*), legs 11-13 are at the southern and western part ("high" salinity measured) and legs 16-17 are at the northern part of the tunnel spiral ("high" salinity measured).

According to the predictions increased levels (compared to other legs) of the salinity were expected in leg 16, 17, 21- 24. This agrees rather well with the outcome. However, the measured increase of the salinity towards depth is larger than predicted. Leg 9 and 10, with the somewhat low salinity, are the eastern part of the first spiral.

One problem with the evaluation is the difference between the predicted and measured flow rates into the tunnel. The measured flow (December 1995) into tunnel section 700-1460 m (leg 1-5) was larger than predicted (about $17 \cdot 10^{-3}$ m³/s compared to $14 \cdot 10^{-3}$ m³/s) and less than predicted for tunnel section 1460 m to the end of the tunnel (about $12 \cdot 10^{-3}$ m³/s compared to $25 \cdot 10^{-3}$ m³/s) /Rhén *et al*, 1997/. As was mentioned in *Section 1.2.1* the predicted flow into the tunnel with the tunnel face at 2875 m was about 15 ‰ larger than the outcome

for tunnel section 700-2875 m, but the measured flow into tunnel section 1460-2875 m was approximately $10 \cdot 10^{-3} \text{ m}^3/\text{s}$ compared to the predicted $20 \cdot 10^{-3} \text{ m}^3/\text{s}$. Using the measured flow rates in the simulations probably change the calculated values of the salinity to some extent.

Salinity in borehole sections

The predicted values are in several cases relatively stable during the construction. The measured values are relatively few but in some of the boreholes one can see that also the measured values are relatively stable during the construction. Some of the predictions indicate decreasing salinity and a few increasing salinity values during the construction. In most cases these agree approximately with the measured values (chemical analysed samples). The largest differences are for KAS03 (borehole section 533-626 m), KAS05 (borehole section 440-550 m, last part of the construction phase), KAS08 and KAS13 (borehole section 331-407 m). The trend for the salinity change is reproduced well in some cases, for example KAS02, or at least in the right direction (KAS05-borehole section 320-380 m).

The salinity measurements in borehole sections based on the electric conductivity of the water from individual measurement sections deviates largely sometimes and agree rather well sometimes with the salinity according to the chemical sampling. The large deviations from the values from the chemical sampling are strange as the sections are rather hydraulically conductive, but the probable reason is that there has been insufficient pumping before sampling.

Salinity field

Natural conditions

Changes in salinities were modelled based on the pre-construction *Model 90* and assessing the impact of excavation response on the flow field. Under undisturbed conditions the maximum depth of the fresh water bubble was predicted to be some 200 m (*Figure 1-17*) and the measurements indicate a maximum depth of about 250 m (*Figure 1-18*). Observations in boreholes from the surface show that water with a salinity of 17000 mg/l under undisturbed, natural, conditions was found at a depth of about 700-800 m. Salinity of 8000-10000 mg/l under undisturbed, natural, conditions was found at a depth of 400-500 m.

After excavation of the tunnel

Upconing of the saline water was predicted. Water with a salinity of 1.4 ‰ (14000 mg/l) was predicted to reach a maximum level below sea level of about 500-600 m from about 800-900 m at natural conditions. Upconing is also clearly present in the section based on the interpolated data. The interpolation indicates that water with a salinity of 1.4 ‰ (14000 mg/l) has reached a

maximum level below sea level of about 400 m from about 700 m at natural conditions. If one studies the individual values used for the interpolation one sees that the changes of the salinity in the surface-borehole sections are relatively small but there are several tunnel boreholes with high salinity. After excavation of the tunnel, water in a few boreholes drilled from the tunnel at a depth of about 360 m showed a salinity of about 17000 mg/l. The with interpolation calculated up-coning is dependent of these last boreholes.

Conclusions

Generally, the salinity of the water flowing into tunnel sections and in the boreholes did not change very much during the construction of the tunnel. The salinity of the water flowing into the tunnel changed more than that of the water to boreholes drilled from the surface. In some boreholes along the tunnel the salinity increased considerably compared with the values measured at about the same level before construction in boreholes from the surface. This was also in line with the predictions based on the numerical model. Measured and predicted values indicate up-coning of the saline water in the same range.

Although the predicted flow rates for the tunnel spiral were about twice the measured ones, the predicted salinity distribution was about the same as the measured! However, the predicted drawdown was in the same range as that measured (see *Rhén et al /1997a/*), and the drawdown seems to control the distribution of the salinity. The salinity distribution is more dependent on the pressure field than on the hydraulic conductivity field and is thus easier to predict than, for example, the water flux in the rock.

The *Model 90* was a stationary simulation but due to the different stages of prevailing hydrological conditions since the last glaciation the boundary conditions are changing and may play a role for the present situation at Äspö. There remains uncertainties of how the shore displacement, and also the development of the Baltic sea since the last glaciation, influence the distribution of salinity at present.

It can here be added that a theoretical study was made by *Claesson /1992/* in order to show how the salinity in the water affects the groundwater flow under different conditions.

2 **SUBJECT: NATURAL TRACERS, FLOW PATHS AND ARRIVAL TIME- SITE SCALE**

2.1 **SCOPE AND CONCEPTS**

Flow paths and transport times during natural conditions and during the construction of the tunnel is dependent of the hydraulic properties of the rock mass, boundary conditions and salinity distribution in the rock mass. Calculation of the groundwater flow and salinity distribution is made simultaneous in a groundwater flow simulation. The concepts comprises of the same geometrical concepts as for groundwater flow:

- Hydraulic conductor domains
- Hydraulic rock mass domains.

See *Section 1.1* for more details concerning the groundwater flow simulations and the properties for the domains. In the text below hydraulic conductor domains are also mentioned with the geological term “ fracture zone”.

Predictions and re-calculations of the flow paths were made with the numerical code PHOENICS /Spalding , 1981/.

Groundwater chemical composition and transport of solutes

The groundwater chemistry was predicted and observed according to the presentations given in *Part 2* of this report. The basis for those predictions was that the situation observed during pre-investigations would be unchanged until the tunnel draw-down had changed the flow and mixing conditions. This was not expected to happen before the tunnel face had reached the specific positions of the predictions (x,y,z).

The water inflow to the tunnel causes both mixing and transport in the hydraulically active fracture system and thus a change in the groundwater chemical composition in parts of the rock mass. In order to handle these predictions the flow, the flow paths and the flow porosity were estimated. Qualitatively the assumptions made were tested by comparing the predicted and the measured flow and chemistry in the packed off borehole intervals. Another way of assessment was to compare the time for and magnitude of the changes in groundwater composition and mixing proportions to the predicted flow directions.

Hydraulic connectivity

Up to 1995 only a few attempts have been made at the Äspö HRL to estimate transport properties in the rock mass. *Rhén et al /1997/* contains a brief presentation of these results together with some data from other sites compiled in *Andersson /1995/* in order to give possible values or ranges for some of the transport parameters. The transport parameters, flow porosity for example, are not discussed in this report, except for some minor comments in the final section, as they were not predicted. Only hydraulic connectivity is discussed as it has been used to check the model of the hydraulic conductor domains. These tests are described below briefly.

At the Äspö HRL a Long-Term-Pumping test (called LPT2) was performed on the southern part of Äspö in 1990 */Rhén et al 1992/*. During this test tracers were injected into a number of boreholes with the main purpose of testing the connectivity of the hydraulic conductor domains. The dilution in the injection sections was monitored and the arrival of the tracers was monitored in the pumped borehole.

During the construction of the tunnel a simple tracer test was performed in hydraulic conductor NE-1 */Rhén and Stanfors 1993, Stanfors et al 1992/*. The purpose was to obtain some indications of the kinematic porosity before the tunnel penetrated the hydraulic conductor NE-1.

Extensive investigations were performed in a conductive structure intersecting the tunnel at approximately tunnel section 500 m, at about 70 m depth below Hålö */Gustafsson et al, 1994; Banwart et al 1995/*. As a part of these investigations, hydro tests and a tracer test were performed in the conductive structure.

A project called Tracer Understanding Experiment (TRUE) was started in 1995 and the first tracer test was performed in late 1995 */Winberg (ed), 1996/*. The tests were performed in a rock of fairly low conductivity.

The evaluations of the hydraulic properties in the reports above were based on analytical methods assuming radial or linear flow.

2.2 METHODOLOGY FOR TESTS OF CONCEPTS AND MODELS

2.2.1 Prediction methodology

Groundwater chemical composition and transport of solutes

Predictions of groundwater chemical composition and transport of solutes were made in site scale (100 - 1000 m) prior to the excavation of Äspö HRL. Predictions were based on data from borehole investigations during the pre-investigation program. In some major conductive zones and five selected borehole sections the chemical composition and transport of solutes were

predicted for undisturbed conditions before start of excavation of the HRL tunnel and for successive intervals as the tunnel approached its final length /*Rhén (ed), 1991, Gustafson et al, 1991/*.

The groundwater chemical composition of fracture zones NE-1, NE-2 and the NNW conductor domains at their intersection with the tunnel was predicted. Only one of the borehole sections selected for prediction of groundwater flow and transport of solutes straddled any of the fracture zones selected for this study. Borehole KAS02, section 309-345 m straddle fracture zone NE-2. The rest of the points for predictions for fracture zones were localized along the tunnel.

The procedure of predictions made in 1990 is illustrated in *Figure 2-1*. The predictions were based on the knowledge gained during the pre-investigation program about natural chemical conditions before start of tunnel excavation, i.e. groundwater samples in borehole sections. The chemical data were then related to the structural model of the Äspö island, including fracture zone geometry, interconnections, hydraulic conductivity, porosity and measurements of natural flow rates, hydraulic heads and estimated flow directions.

To predict the change in chemical composition and transport of solutes at successive intervals during the proceeding of the tunnel construction, effects of the tunnel were added to the natural undisturbed conditions. These effects were; tunnel breaches through fracture zones causing leakage into the tunnel, increased groundwater flow rate, changed flow directions and mixing. Also other water types than the original waters found in the fracture zones were added, as they were judged being potential contributors to the waters drained by the tunnel. The water types added were; Baltic seawater, shallow groundwater and precipitation. Thus, for prediction of the disturbed conditions four chemical end-members were considered 1. Rainwater, 2. Shallow groundwater, 3. Baltic seawater and 4. Fracture zone groundwater. The latter, Fracture zone groundwater, is specific to every fracture zone and varies depending on which fracture zone is considered and also to depth in the zone. The predictive calculations were mainly made utilizing simple analytical expressions, but also principal component analyses were used.

CHEMICAL END MEMBERS	FRACTURE ZONES	TUNNEL	TUNNEL EFFECTS
Fracture zone groundwaters (zone and depth/position unique values)	Geometry	Geometry	Leakage into tunnel (influence area)
Shallow groundwater	Porosity	Fracture zone intersections	Mixing
Baltic seawater	Hydraulic conductivity		Changed flow direction
Precipitation (rainwater)	Interconnections		Increased flow rate (velocity)
	Flow direction (gradients)		
	Flow rate (velocity)		

Figure 2-1 Principle of predictions made and items considered /Ittner and Gustafsson, 1995/.

Hydraulic connectivity

As was mentioned in *Section 2.1* a number of tracer tests have been made. In all but one test the purpose was to test the connectivity within one single hydraulic conductor domain and to roughly estimate the transport properties. In the LPT 2 test the purpose was to test the connectivity within several hydraulic conductor domains */Figure 2-2/*. The base in the prediction was of course the geometrical model of hydraulic conductor domains. Before the performance of the LPT2 pumping tests simulation of the pumping test was performed. Flow paths were calculated using the particle-tracking technique assuming an effective porosity */Svensson, 1991b/*.

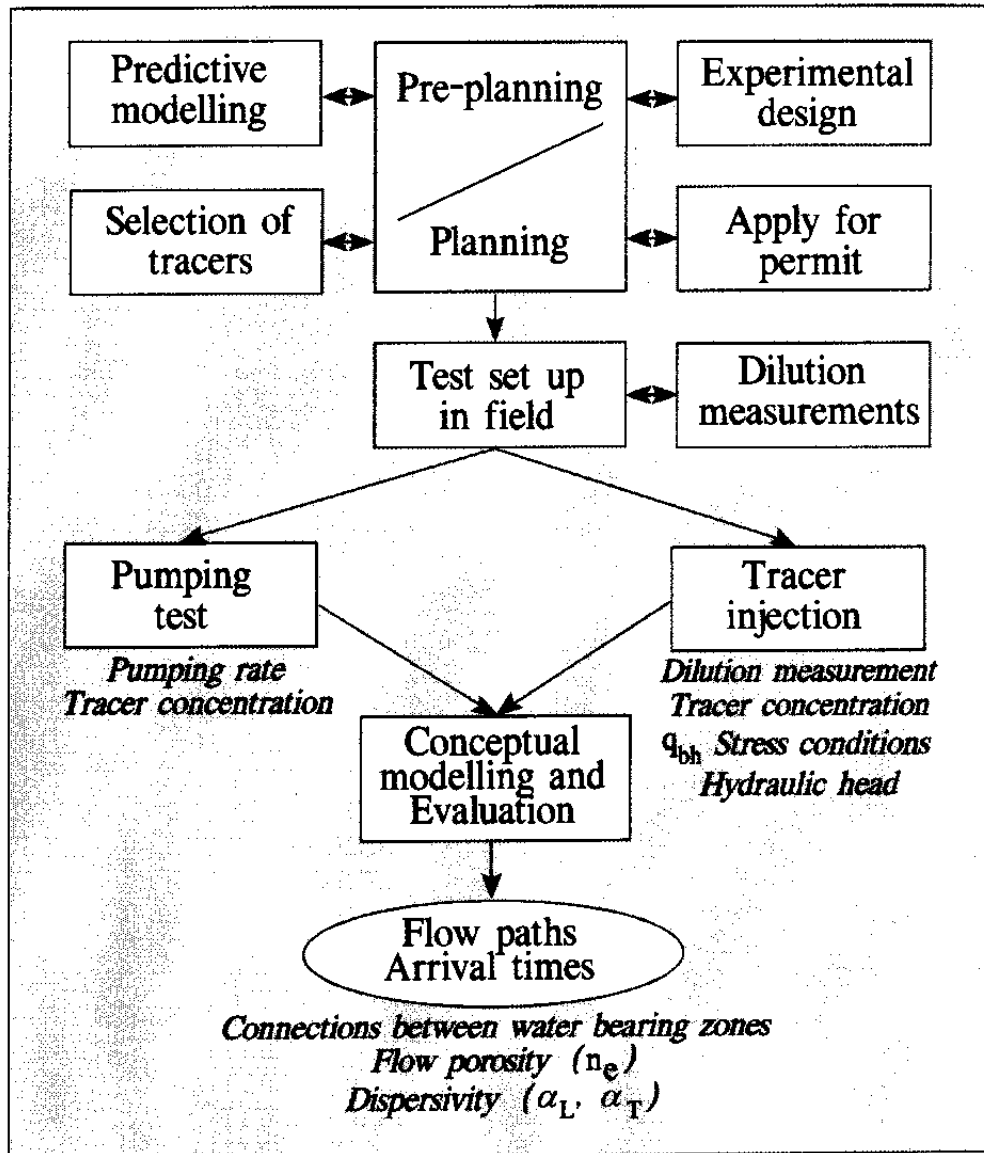


Figure 2-2. Flow paths and arrival times - flow chart.

2.2.2 Methodology for determining outcome

Groundwater chemical composition and transport of solutes

Water sampling

Water samples were taken and analysed during the entire construction period from sections in boreholes from the surface and from the tunnel. The chemical sampling program is outlined in more detail in *Part 2*.

PHOENICS simulations

The model of the Äspö site was made after the pre-investigation phase /Wikberg et al 1991/. After the construction of the Äspö HRL the model was revised /Stanfors et al 1994b and Rhén 1997/.

As shown in Part 1, a groundwater flow model was made 1990, called *Model 90*. The computer code used was PHOENICS /Spalding, 1981/. The groundwater flow below Äspö island was re-calculated during the construction phase based on *Model 90* and the revised model of the hydraulic conductor domains. Measured flow into the tunnel was used in the simulations /Svensson 1994a,b, 1995/.

Based on the model presented in Svensson /1995/, new images of flow, pressure and salinity were made for the major fracture zones NE-1, NE-2 and NNW-4 at three different positions of the tunnel face during the construction. The tunnel face positions 0 m, 1475 m and 2874 m were presented. From these images, flow were transferred to figures representing the major fracture zones indicating the groundwater flow and flow directions in relation to intersecting fracture zones and tunnel breach positions as well as the position of boreholes used for chemical sampling /Ittner and Gustafsson, 1995/. The fracture zones, or hydraulic conductor domains, that were studied are shown in *Figure 2-3*.

Multivariate mixing calculations

Multivariate mixing calculations of groundwater at Äspö /Laaksoharju 1990/ have been used to support the groundwater flow model and to study how the different groundwater types will mix during the construction of the Äspö HRL. The origin of groundwater may be the rock, shallow or deep parts, as well as from the Baltic sea and it will be reflected by different chemical compositions. The main aim with the multivariate mixing calculations in this evaluation was to differentiate between groundwater types (end-members) of different origin and to investigate how they mix in the major fracture zones during the construction of the tunnel. The data used for the mixing calculations are chemical compositions analysed in groundwater sampled from various packed-off borehole sections during the periods of pre-investigation and construction.

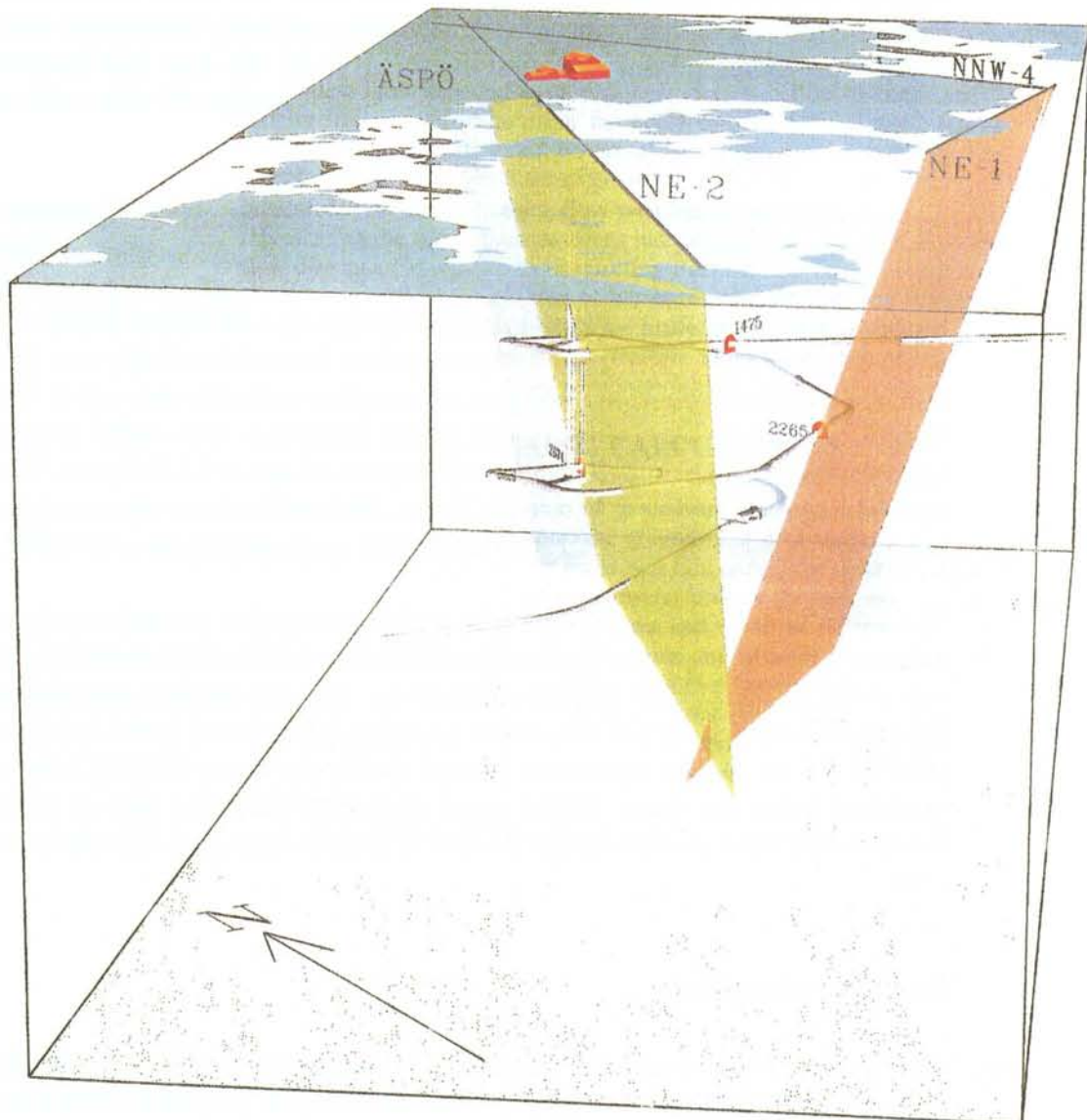


Figure 2-3. The studied fracture zones in relation to the tunnel and prediction points /Ittner and Gustafsson, 1995/.

The mixing calculations are made in two ways, with *five* or *three* end-members. The lack of environmental isotope analysis data, which is required for a five end-member mixing calculation, have made it necessary to present a three end-member mixing calculation to obtain more information for the evaluation of changes during the construction phase. The three end-member mixing calculation is less exact due to that the distinction between old and young water cannot be made. The selected end-members are only valid to the mixing calculation chosen e.g. the end-member "Baltic", used in both types of mixing calculations, is not the same or transferable from the three end-member diagram to the five end-member diagram or vice versa. The major components chloride, calcium, sodium, magnesium, potassium, sulphate, bicarbonate were used in the three end-member calculations and for the five end-member calculation the natural isotopes deuterium, tritium, oxygen-18 were used as well.

The selected end-members in the *five end-member* manner represent extreme waters found in the Äspö area. The end-member **shallow** represents a modern surface water found in the borehole HBH02 7.5 m. **Baltic sea** represents modern Baltic sea water (sampling point SEA01) and **Modified Baltic** sea water represents an water type that is older than the modern Baltic sea. It is found in the tunnel below the Baltic sea and sulphate reduction may occur. The **Glacial meltwater** represents an old glacial meltwater. The stable isotope values indicate cold climate recharge and a carbon-14 age of 31 365 years. This type of water is found in KAS03 129-134 m. **Old saline** water represents the brine type of water found in KLX02 1631-1681 m /Laaksoharju et al 1995/.

The selected new end-members in the *three end-member* manner represent extreme waters found in the Äspö area and the new selected end-members are only valid to the present mixing calculations. The end-member **non-saline** represents a modern or old non-saline (surface) water found in the borehole HBH02 7.5 m. **Baltic** represents modern Baltic sea water (SEA01) and a modified Baltic sea water. **Saline** water represents the saline type of water found in SA2703A (sampling date 94-05-17) /Laaksoharju and Skårman pers com/.

Hydraulic connectivity

Tracer tests were to test the connectivity within one or several hydraulic conductor domains and to roughly estimate the transport properties within the hydraulic conductor domains. One or several borehole sections were used for tracer injection and sampling was made in the pumped borehole or, in the tunnel, flowing boreholes. The main purpose with the LPT 2 test was to test the connectivity within several hydraulic conductor domains. See the reports mentioned in *Section 2.1* for details concerning the reported tests.

2.3 COMPARISON BETWEEN PREDICTION AND MEASURED ENTITY

2.3.1 Introduction

Groundwater chemical composition and transport of solutes

The predictions are summarized in *Table 2-1*. The outcome and discussion of the results are presented in the *Sections 2.3.2 -2.3.4* and is , with some minor modifications, based on *Ittner and Gustafsson /1995/*.

Table 2-1. Prediction of groundwater chemical composition at the location of the HRL tunnel intersection with fracture zones NE-1, NE-2 and NNW at successive intervals (Tunnel Face Position, TFP) during the tunnel excavation. Compiled from */Gustafson et al /1991/*.

Conductive zones	TFP m	Na mg/l	K mg/l	Ca mg/l	Mg mg/l	Cl mg/l	HCO ₃ mg/l	SO ₄ mg/l	Fe ^{tot} mg/l	pH mV	Eh
NE-1	700-1475	1900 ±200	31 ±20	1200 ±350	150 ±80	5300 ±400	290 ±100	210 ±50	0.67.2 ±0.6	-230 ±0.3	±25
NE-1	3064-3854	2000 ±500	8 ±5	2000 ±800	80 ±20	7000 ±2000	14 ±5	320 ±80	0.3 ±0.3	8.0 ±0.5	-340 ±25
NE-2	1475-2265	1200 ±300	5 ±5	1100 ±300	30 ±30	3800 ±1000	70 ±50	140 ±40	0.3 ±0.3	7.7 ±0.1	-290 ±25
NNW	1475-2265	500 ±200	5 ±5	400 ±200	30 ±300	1500 ±1000	150 ±50	150 ±50	0.3 ±0.3	7.8 ±0.2	-300 ±25
NNW	2265-3064	800 ±300	7 ±5	800 ±300	40 ±30	2500 ±1000	170 ±70	120 ±80	0.3 ±0.3	7.7 ±0.3	-290 ±25
NNW	3064-3854	1000 ±500	8 ±5	1000 ±500	50 ±20	3500 ±1000	120 ±20	160 ±80	0.3 ±0.3	7.6 ±0.2	-290 ±25

An example on how the distribution between different end members changes as the construction of the tunnel proceeds is shown in *Ittner and Gustafsson /1995/*. In the tunnel sections 1680-1750, 2600-2783 m, i.e. the western part of the tunnel spiral, the content of water with Baltic origin is low and saline water increases, see *Figure 2-4*. As for the tunnel section 2175-2322 m, i.e. the southern part of the tunnel spiral, water of Baltic origin is present. Here the saline water is slowly diminishing as the tunnel construction proceeds. The end-member changes as the tunnel construction proceeds / *Rhén et al, 1997/*. (In the text below TFP is used. TFP = Tunnel Front Position, or the actual length of the tunnel during the construction).

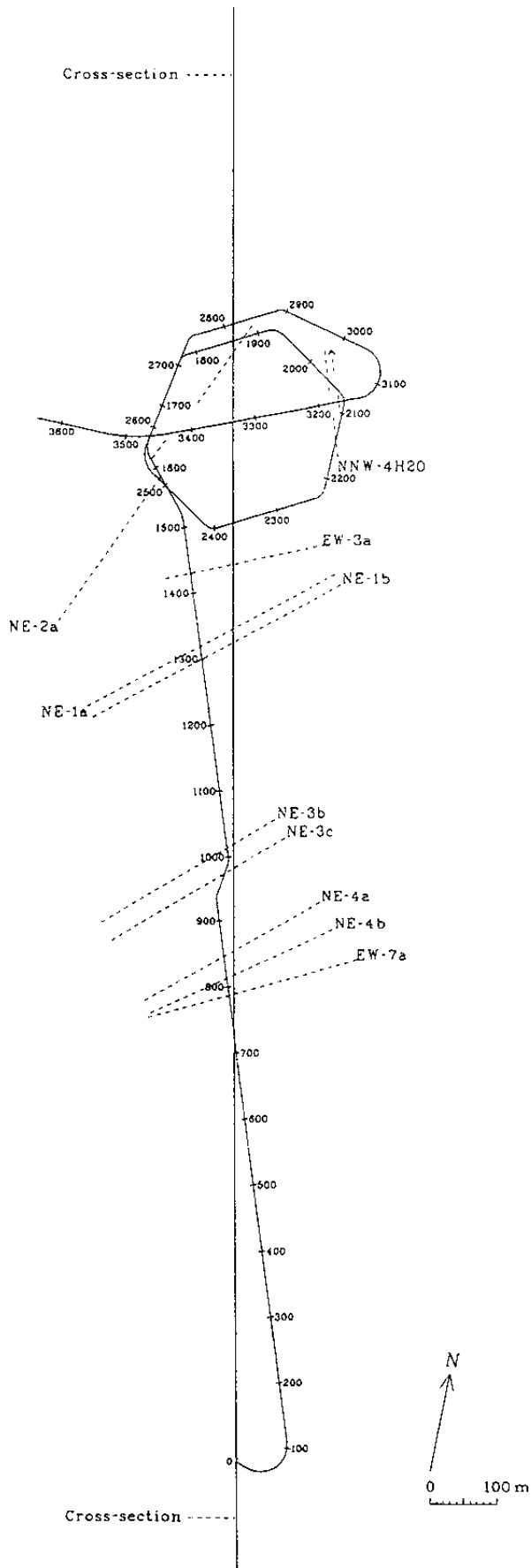


Figure 2-4. The studied fracture zones in relation to intersections in the tunnel /Ittner and Gustafsson, 1995/.

Hydraulic connectivity

In Section 2.3.5 the results from the tests that aimed to test the hydraulic connectivity are briefly outlined.

2.3.2 Results: Fracture zone NE-1

Natural conditions, TFP = 0 m

The *multivariate mixing calculations* show that the lower part (-500 masl) of NE-1 have a large proportion, about 50-60%, of deep water (old saline, glacial or saline water) from the crystalline rock. This indicates low circulation and low flow velocity of the groundwater during natural gradient conditions. For the upper part (-70 to -100 masl) of NE-1 during natural gradient conditions, it was not possible to calculate the mixing but the data indicate the presence of a Baltic water to a large extent (60 to 80 %).

The major characteristics of NE-1, during natural conditions, can be summarized as that the upper part of the zone contains a large part of Baltic water whereas the lower part contains a deep saline water. The chloride concentrations are about the same, 5000 to 6000 mg/l.

The *numerical flow and transport model* used to present images of flow, pressure and salinity in NE-1 show that flow and salinity under natural conditions are dependent on depth below ground surface and intersecting fracture zone. The pressure is however only dependent on depth below ground surface.

The main outline of NE-1, during natural conditions, can be summarized as that the upper part (0-400 m) of the zone has mainly a sub-horizontal flow and that the water below -400 masl is stagnant.

The groundwater flow direction in NE-1 during natural conditions is upwards in the vertical zones NNW-3/NNW-7 and the horizontal component towards NNW-3.

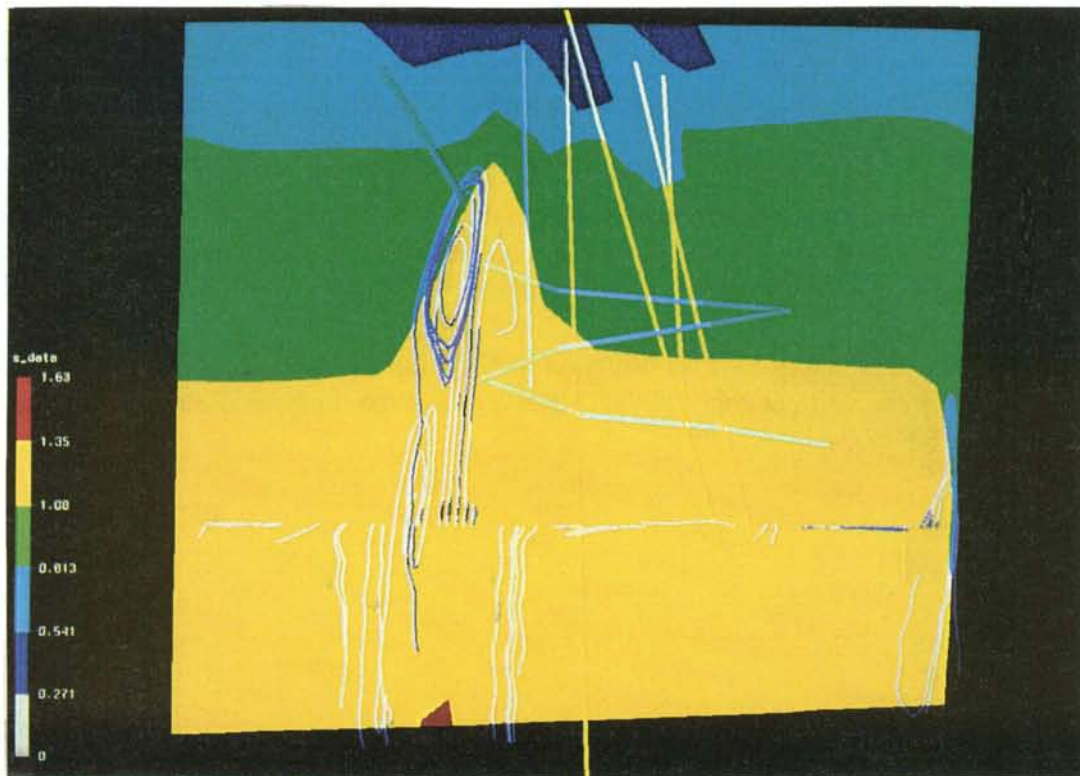
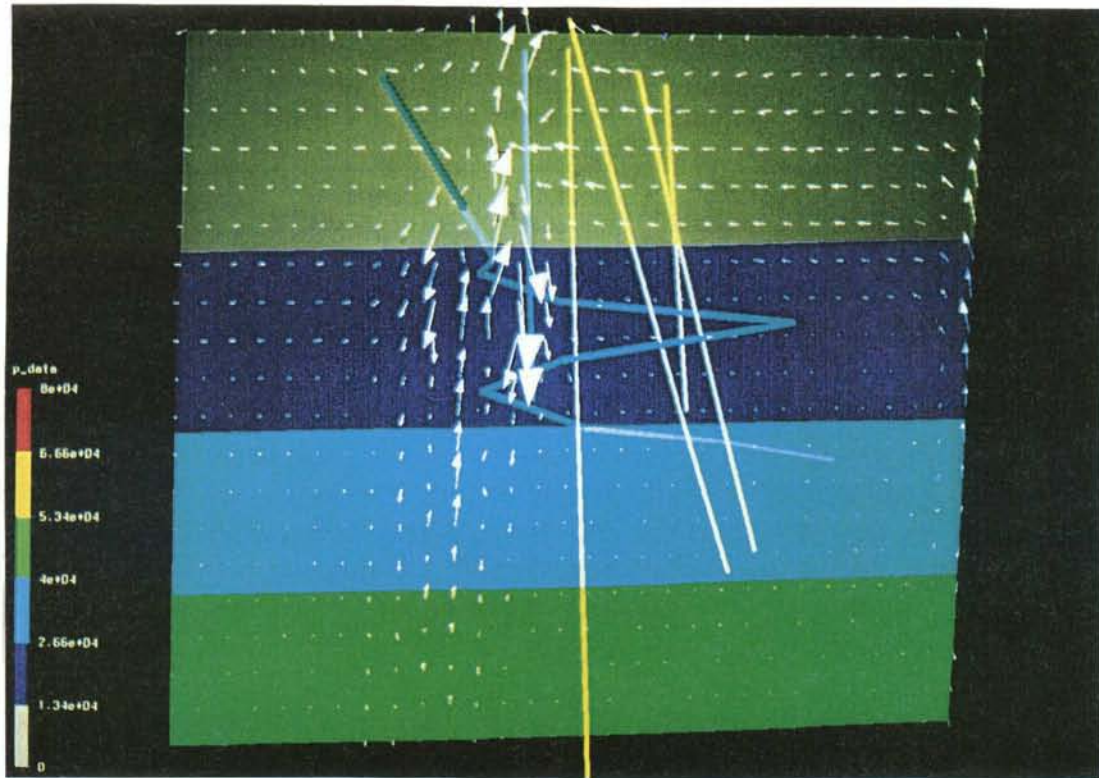


*Figure 2-5. Natural conditions - Numerical groundwater flow simulations. Hydraulic conductor domain NE-1, view from south.
 Top: Flow and pressure, with the hydrostatic component $\rho_0 \cdot g$ subtracted ($\rho_0 = 1000 \text{ kg/m}^3$).
 Bottom: Salinity and some stream lines.*

Construction phase, TFP = 1475 m

The tunnel breaches NE-1 at TFP 1306 m, -180 masl, and a large inflow to the tunnel starts, about 2000 l/min. The drawdown caused by the tunnel creates new flow directions and enhanced groundwater flow in NE-1 and adjacent fracture zones. This new situation affects not only the near field around the tunnel but also the conditions far away. The flow directions and flow rates changes quite far away from the tunnel. This new flow situation causes mixing of different types of groundwater. Saline groundwater in the lower part will mix with surface water and with Baltic sea water.

At TFP 1475 m the fracture zone EW-3 as well as NE-1 have been passed. The two fracture zones are connected to each other. The nearest groundwater sampling to TFP 1475 m are made at TFP 1525 m and is assumed to be valid for TFP 1475 m.

The *multivariate mixing calculations* show that in the lower part of NE-1 (-500 masl) the chloride content is fairly constant but that the deep saline water increases in KAS08-1 and the Baltic water decreases. In KAS07-1 the proportions seems to be fairly constant. In the upper part (-70 to -100 masl) of NE-1 Baltic water mixes with surface water.

Construction phase, TFP = 2874 m

The northern part of the tunnel in turn II, TFP 2874 m, is reached in January 25 1994. The mixing of water in the studied borehole sections, situated in NE-1, follows the trends from earlier prediction points in the tunnel.

The *numerical flow and transport model* used to present images of flow, pressure and salinity in NE-1 show that they are clearly affected of the tunnel drainage at TFP 2874 m as well as at 1475 m. The tunnel drastically changes the conditions in NE-1 except for the deeper (500 m) parts where slowly deep water is on its way up to the tunnel intersection at TFP 1475 m. This upward transport of deep saline water is at TFP 2874 m calculated to cease and the area of NE-1 affected of Baltic water increases downwards. This in-mixing of Baltic water to deeper levels in NE-1 might be the result of interconnections between the tunnel-spiral and the NE-1 fracture zone.

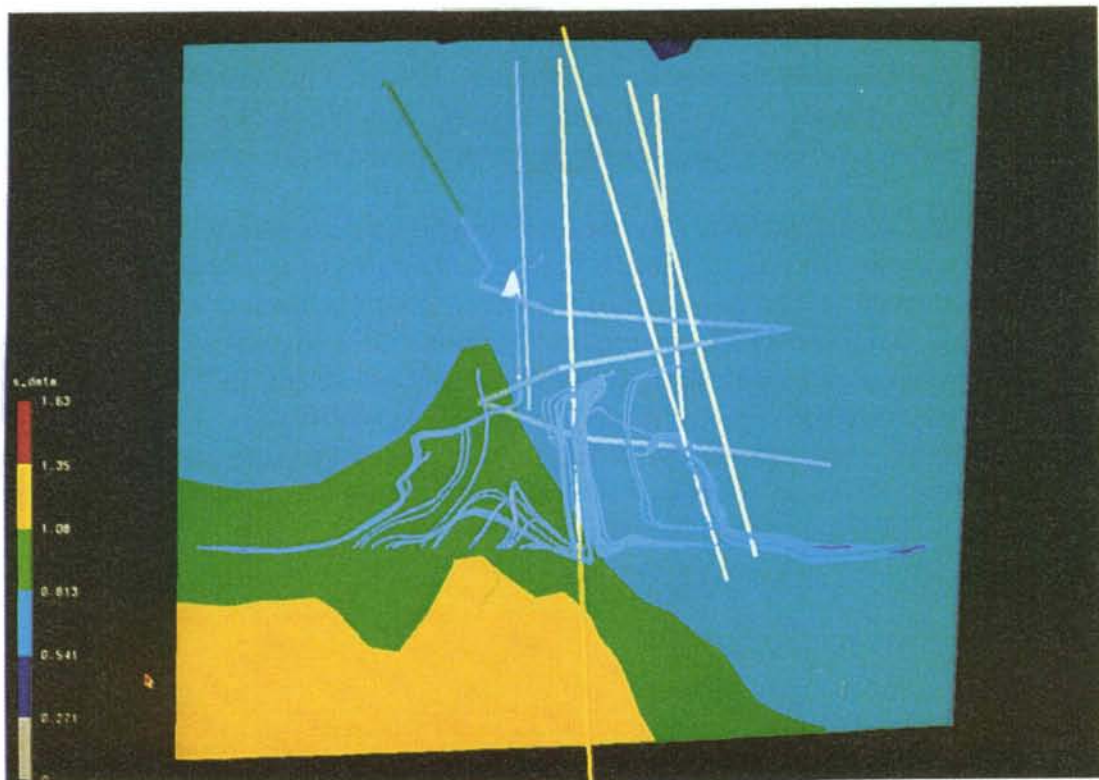
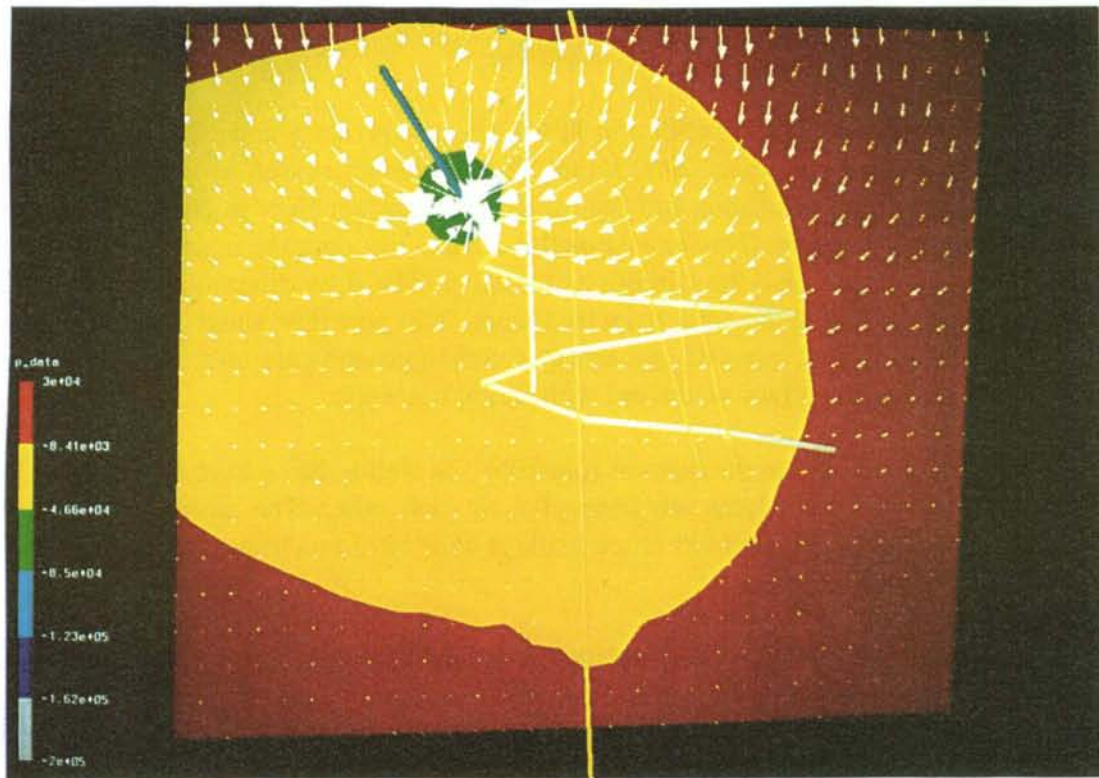


Figure 2-6. Construction phase, TFP = 2874 m - Numerical groundwater flow simulations. Hydraulic conductor domain NE-1, view from south.
 Top: Flow and pressure, with the hydrostatic component $\rho_0 g$ subtracted ($\rho_0 = 1000 \text{ kg/m}^3$).
 Bottom: Salinity and some stream lines.

2.3.3 Results: Fracture zone NE-2

Natural conditions, TFP = 0 m

The *multivariate mixing calculations* show that the lower part of NE-2 (represented by KAS05-1 at -400 masl) have a large proportion, about 70%, of deep water (old saline, glacial water). This indicates slow circulation and low flow velocity of the groundwater at -400 masl during natural conditions. The intermediate part (-200 masl) of NE-2 indicates the presence of modified Baltic water to about 20% and a non-saline (surface, glacial) to about 60%. KAS08-3, although situated in NNW-2 50-100 m away, shows about the same. The water in KAS13-3 is probably to a large proportion a mix of shallow and modified Baltic water and to a minor proportion glacial meltwater. KAS02-4 and KAS05-1 have a large proportion of old water and KAS05-1 has almost no Baltic water.

The *numerical flow and transport model* used to present images of flow, pressure and salinity in NE-2 show that flow and salinity distributions are dependent on depth below ground surface and intersecting fracture zones, but also of the local groundwater level. One can see relatively superficial flow paths from local recharge and discharge areas. The character of fracture zone NE-2 at natural conditions is a near-surface water circulation in the uppermost 300 metres. Active zones in the upper 300 m are, from SW to NE, NNW-5, NNW-7, NNW-1, NNW-2 and NNW-4 and at a depth of 500 to 800 m NE-1. NNW-5,7,1 and 2 supplies the target area with sufficient water containing low chloride and high bi-carbonate concentrations. The flow direction is from north towards the south through or via NE-2 to NE-1. The intersection NE-2/NNW-4, upper 300 m, water originating from NE and EW-1 is transported in NE-2 and further south in NNW-4 and then upward to the sea (not to NE-1) whereas below 300 m there is a downward directed water flow (to NE-1?).

Construction phase, TFP = 1475 m

The *numerical flow and transport model* used to present images of flow, pressure and salinity, show that NE-2 is clearly affected by tunnel drainage at TFP 1475 m. The groundwater flow direction is clearly affected by the tunnel intersecting NE-1. The groundwater flow is directed mainly via the NNW fracture zones towards NE-1. As NE-2 is 'almost about parallel' to NE-1 the flow of the groundwater is 'passing through' the rock mass separating NE-1 and NE-2. This flow is primarily made via NNW-5, NNW-7, NNW-4, EW-5 and also directly to NE-1 (NE-1 70°NW) at a depth of 500-600 metres. Due to the large drainage in the NE-1 passage and good hydraulic contact in NNW structures, the groundwater flow in NE-2 is mainly directed towards NNW-5 and then flows in NNW-5 to the south. The groundwater composition in the uppermost 500 m gets a larger proportion of non-saline water except for KAS05-1 where instead the old saline water increases in proportion.

The *multivariate mixing calculations* show that the lower part (-400 masl), has a chloride content fairly constant but that the deep water (old saline, glacial or saline water) in KAS02-4 diminishes. The in-mixing in KAS02-4 and KAS05-1 are primarily of glacial type but the proportion of glacial water in KAS05-1 is smaller. KAS13-3 show in-mixing of both surface and glacial water.

Construction phase, TFP = 2265 m

When the tunnel intersects NE-2 for the first time, at TFP 1600 m, the groundwater chemical composition in NE-2 is not the original as it has been influenced by earlier drainage into the tunnel, e.g. the intersection of NE-1.

The *numerical flow and transport model* used to present images of flow, pressure and salinity, were not used for calculations at the prediction point TFP 2265 m

The *multivariate mixing calculations* show that water at 250 m depth in SA1828B seems to be a mixture of primarily modified Baltic and glacial meltwater with a smaller proportion of deep saline water in-mixed.

Construction phase, TFP = 2874 m

The flow in NE-2 have again changed character. The *numerical flow and transport model* indicates one large drainage point around the intersection with the tunnel at TFP 1600 m and the vertical shaft, and a small at the tunnel intersection at TFP 2874 m. The groundwater flow is directed upward from the deeper parts which may support the *multivariate mixing calculations* in KAS05-1 and the very high chloride concentration in KAS02-4 (12200 mg/l, 1993-03-21, TFP=2226 m) which indicate an increase of deep saline water. The composition in SA1828B changes and the amount of modified Baltic increases and the amount of deep water decreases. The two types of water, modified Baltic and glacial meltwater are the main end members.

Fracture zone NE-2. Summary

The fracture zone NE-2 is verified on ground and down to a depth of about -350 mbsl. Whether the fracture zone is extending deeper or not is not yet verified. The fracture zone may be of very low transmissivity in deeper parts. The groundwater flow during natural conditions in NE-2 in the upper 300 m can be seen as a flow mainly from north towards south through or via NE-2 to NE-1. Flow in NE-2 is also directed to SW into the sea. Below 300 m depth below surface is under natural conditions flow directed down in NNW-4/NE-2 intersection and upward in the intersection NNW-5/NE-2 up to EW-5/NE-2 at about -200 masl.

2.3.4 Results: Fracture zone NNW-4

Natural conditions, TFP = 0 m

The character of fracture zone NNW-4 at natural conditions is a near-surface water circulation in the uppermost 250 metres. The direction is from land and south to the sea. Fracture zones intersecting NNW-4 involved in transport of groundwater are NE-2 and NE-1. NE-2 is clearly active in transporting groundwater downward at least to a depth of 800-900 m below ground surface. NE-1 has only a very weak indication of participation.

Construction phase, TFP = 1475 m

The *numerical flow and transport model* used to present images of flow, pressure and salinity in NNW-4 show that they are clearly affected by the tunnel drainage at TFP 1475 m. The groundwater flow direction is clearly affected by the tunnel intersecting NE-1. The groundwater flow that earlier (TFP=0 m) was dominant e.g. flow from the northern (from land) to the southern (to sea) and the down-ward directed flow in the NE-2 intersection, is now more or less stagnant. Instead the earlier, just weakly indicated, flow at the intersection with NE-1 (NNW-2, EW-5) has become very dominant. The upper 400 metres in NNW-4 will, already when the tunnel intersects NE-1 at TFP 1306 m, be influenced by surface water from both land and from the Baltic sea.

The *multivariate mixing calculations* in KAS08-1 show a clear change in composition when passing NE-1. According to the simulations this could be explained as the water in the KAS08-1 section primarily is supported by water from deeper levels.

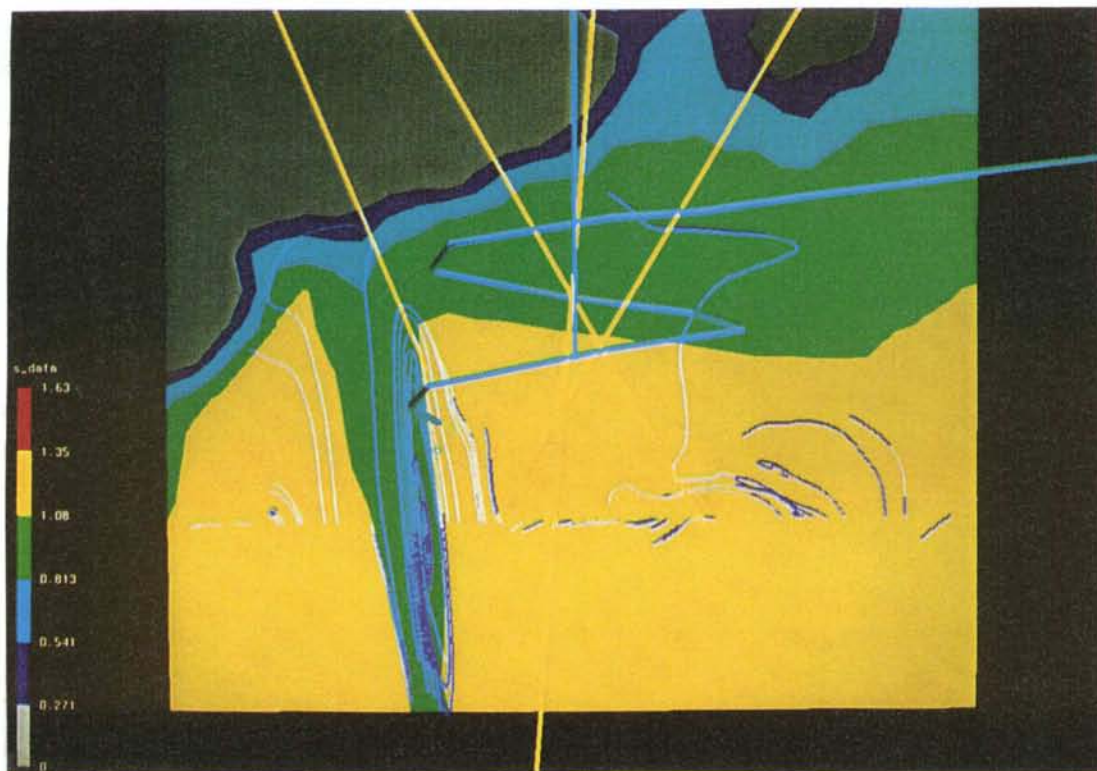
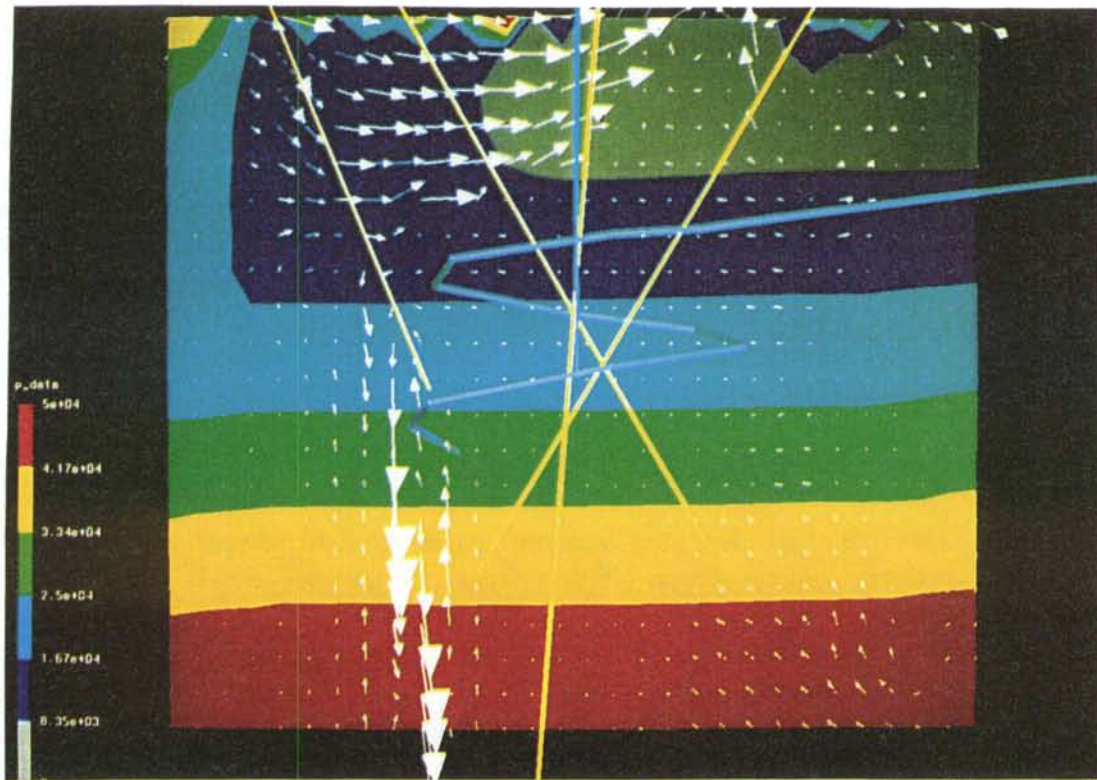


Figure 2-7. Natural conditions - Numerical groundwater flow simulations. Hydraulic conductor domain NNW-4, view from west.
 Top: Flow and pressure, with the hydrostatic component $\rho_0 \cdot g$ subtracted ($\rho_0 = 1000 \text{ kg/m}^3$).
 Bottom: Salinity and some stream lines.

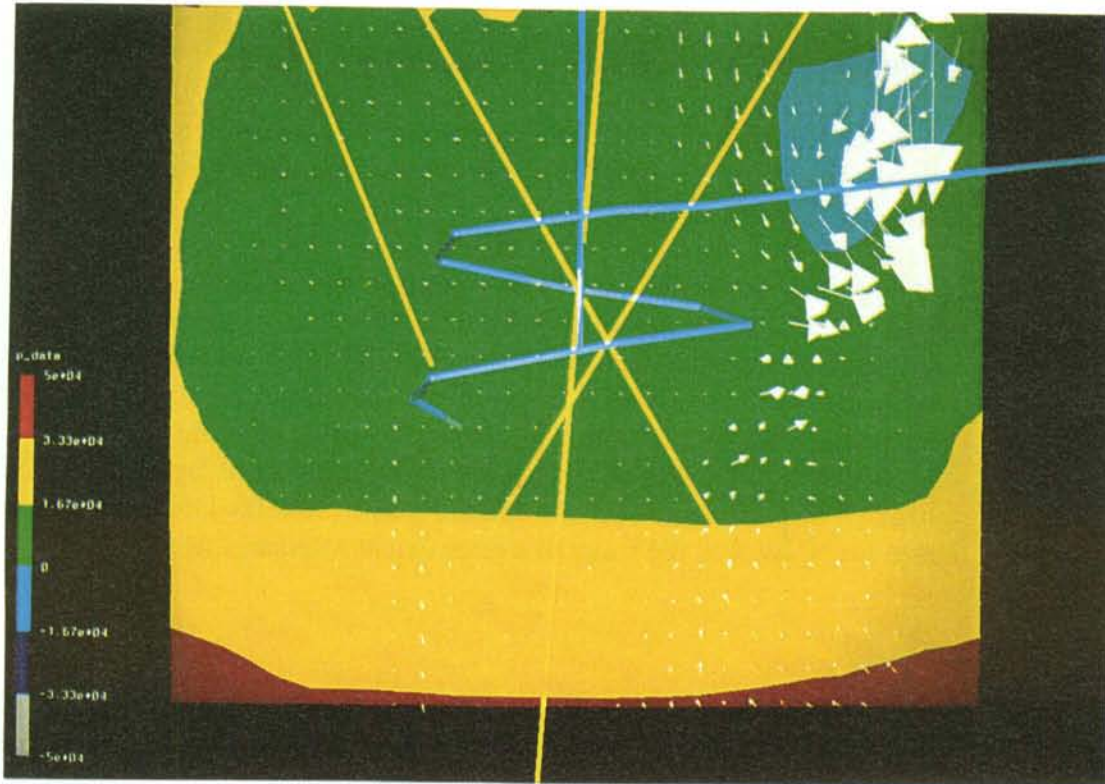


Figure 2-8. Construction phase, TFP = 1475 m - Numerical groundwater flow simulations. Hydraulic conductor domain NNW-4, view from west.
 Top: Flow and pressure, with the hydrostatic component $\rho_0 g$ subtracted ($\rho_0 = 1000 \text{ kg/m}^3$).
 Bottom: Salinity and some stream lines.

Construction phase, TFP = 2265 and 2874 m

With the tunnel face at TFP 2265 m, the tunnel had intersected NNW-4 twice at 2020 m and at 2120-2123 m. The intersections are verified in the tunnel /*Rhén and Stanfors, 1995*/.

At TFP 2874 m the flow in NNW-4 have changed character. The *numerical flow and transport model* indicates one large drainage point around the intersection with the tunnel at TFP 2021 m to 2121 m and just as at TFP 1475 m the intersection with NE-1 is significant. The groundwater flow is directed downward from both the ground surface (only Baltic sea) and from NE-1. The water that is drained to the tunnel is to a large extent of Baltic and of NE-1 origin. The *multivariate mixing calculations* in KAS08-1 could probably be used for NNW-4 as the water to a large extent originates from NE-1.

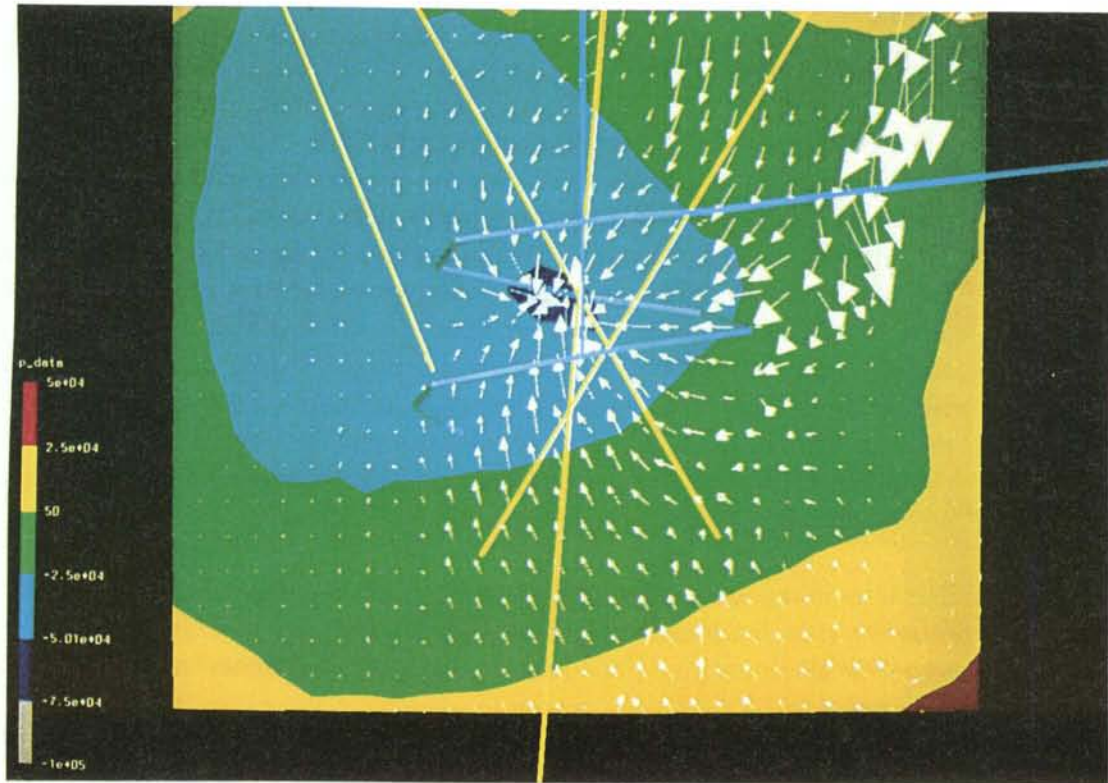


Figure 2-9. Construction phase, TFP = 2874 m - Numerical groundwater flow simulations. Hydraulic conductor domain NNW-4, view from west. Top: Flow and pressure, with the hydrostatic component $\rho_0 g$ subtracted ($\rho_0 = 1000 \text{ kg/m}^3$). Bottom: Salinity and some stream lines.

2.3.5 Hydraulic connectivity

The LPT2 test confirmed the hydraulic conductor domain NNW-2 /*Rhén et al 1992*/. It was shown that there was a good connectivity between the injection point and the pumped borehole, both boreholes assumed to intersect NNW-2. The injected tracer that was intended to show the connectivity within hydraulic conductor domain EW-5 never showed up. It was interpreted that EW-5 was possibly highly fractured with a high porosity but low hydraulic conductivity and that the test duration was not long enough to show the break-through. NNW-2 was confirmed by hydraulic tests in the tunnel, see *Part I*. EW-5 could not be confirmed in the tunnel, only subhorizontal fracture sets and a few minor subhorizontal fracture zones were found. The present model does not include any feature corresponding to EW-5.

The tests in the hydraulic conductor domains NE-1 /*Rhén and Stanfors 1993, Stanfors et al 1992*/ and the Redox zone /*Gustafsson et al, 1994; Banwart et al 1995*/ also confirmed connectivity between the points in the interpreted domains.

2.4 SCRUTINY AND EVALUATION

Groundwater chemical composition and transport of solutes

The combined effect of few predictions (with only a few points in tunnel- and surface boreholes with complete time series of chemical, head and flow data) together with changed tunnel lay-out, revised fracture zones and changed chemical end-members, makes evaluation of prediction reliability cumbersome. However, the overall conclusion is that the predictions made during the pre-investigation as a whole are in accordance with the outcome, although the tunnel breach of zone NE-1 changed the transport of solutes and chemical composition in zones NE-2 and NNW-4 to a larger extent than what was predicted. Also the surface type of waters penetrated the fracture zones to a smaller extent than expected from the predictions.

Concerning the groundwater flow simulations the predicted transmissivities used in the *Model 90* were approximately as the new estimates of the transmissivities made 1995 except for NE-2 and EW-5 /*Rhén et al, 1997*/. The predicted transmissivity for NE-2 was $4 \cdot 10^{-6}$ m²/s but in the new model the median value is $0.4 \cdot 10^{-6}$ m²/s. The variability of the transmissivity within NE-2, for the points interpreted to be representative for NE-2, is however large. In the new model EW-5 is excluded. These changes will to some extent change the flow pattern in the rock volume where the tunnel spiral is situated, but probably to a minor extent as the transmissivities of these two domains in the predictions were fairly low.

A method for calculating the proportions of different water types with the numerical groundwater flow model was tried. The calculated flow field is used for back-tracking of marked fluid elements, released around the tunnel or near

a borehole section. Back-tracking means that all flow vector components are used with reversed sign. If it assumed that stationary conditions prevail it is possible to calculate the paths for the water passing the borehole section or entering the tunnel. It is also possible calculate the composition of the water passing the borehole section or entering the tunnel by assuming that the particles represents the water composition at the boundaries, see *Figure 2-10*. It is then also assumed that no chemical reactions will take place along the flow path.

It is also possible to visualize the region in the rock mass where the most of the particles are at a certain time before entering the tunnel or passing a borehole section, see *Figure 2-11* and *2-12*. The figures show simulation of the LPT2 pumping and tracer test. The assumed flow porosity was $2 \cdot 10^{-4}$. The figures show an iso-surface for the particle concentration. It can of course be argued that the flow conditions are transient and will affect the composition by time of the water flowing into the tunnel. However, it seems to be a simple and fast (as it is stationary flow field) method to get some idea of the flow paths and the possible origin of the water. As a next step one would of course like to do transient simulations and releasing particles at relevant points, or evenly distributed throughout the rock mass. However, it is important to release a very large number of particles in order to calculate the proportions by time. The computer simulations may thus become "heavy".

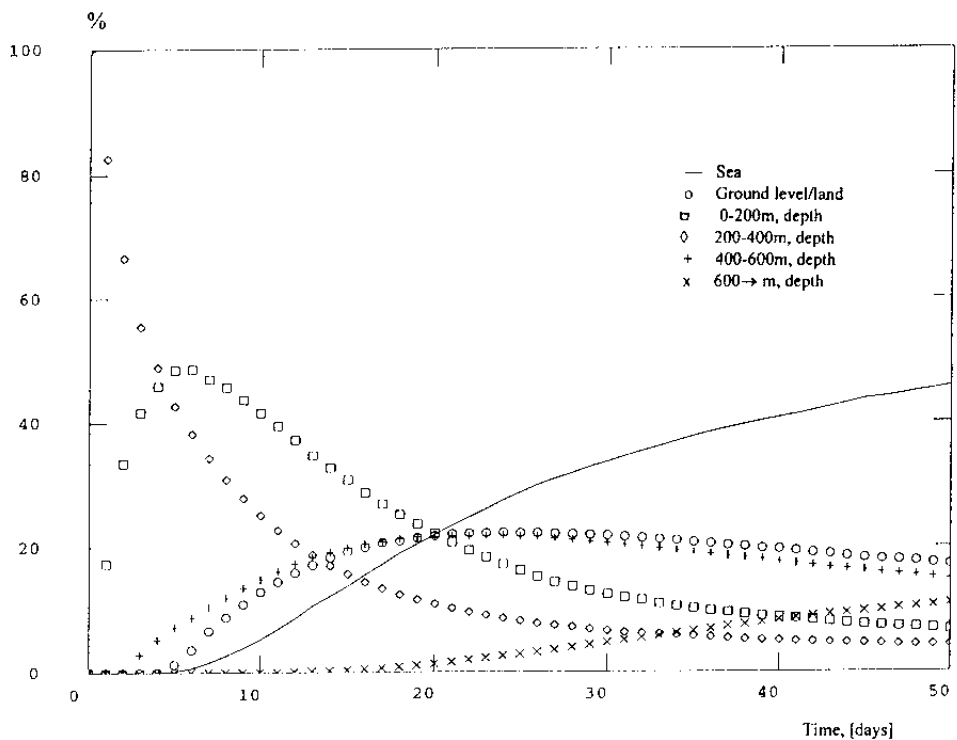
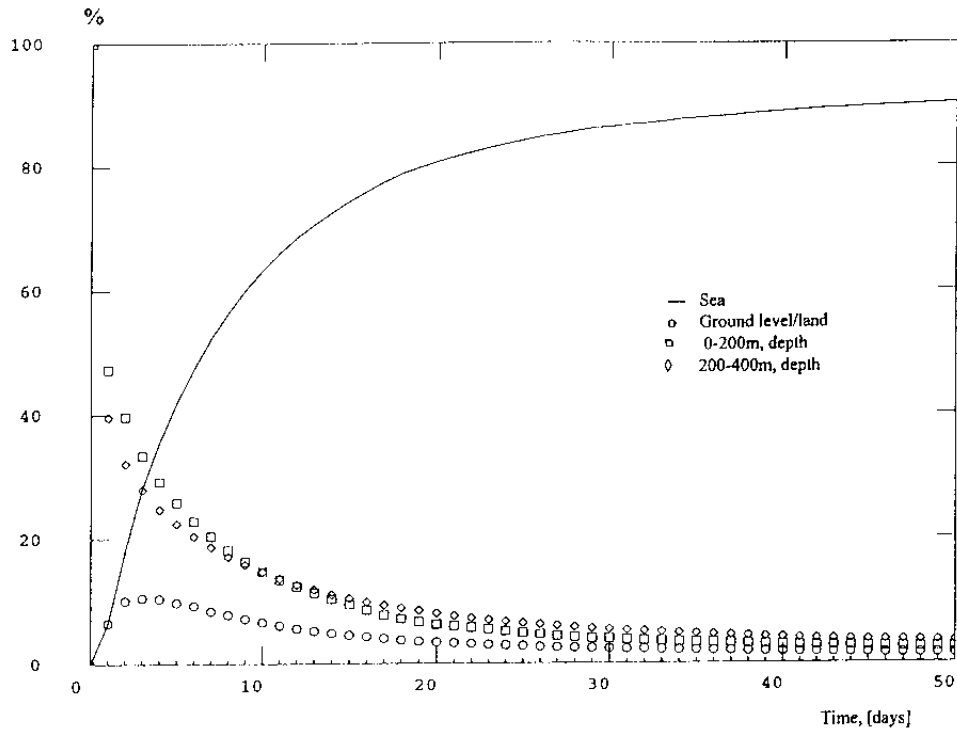
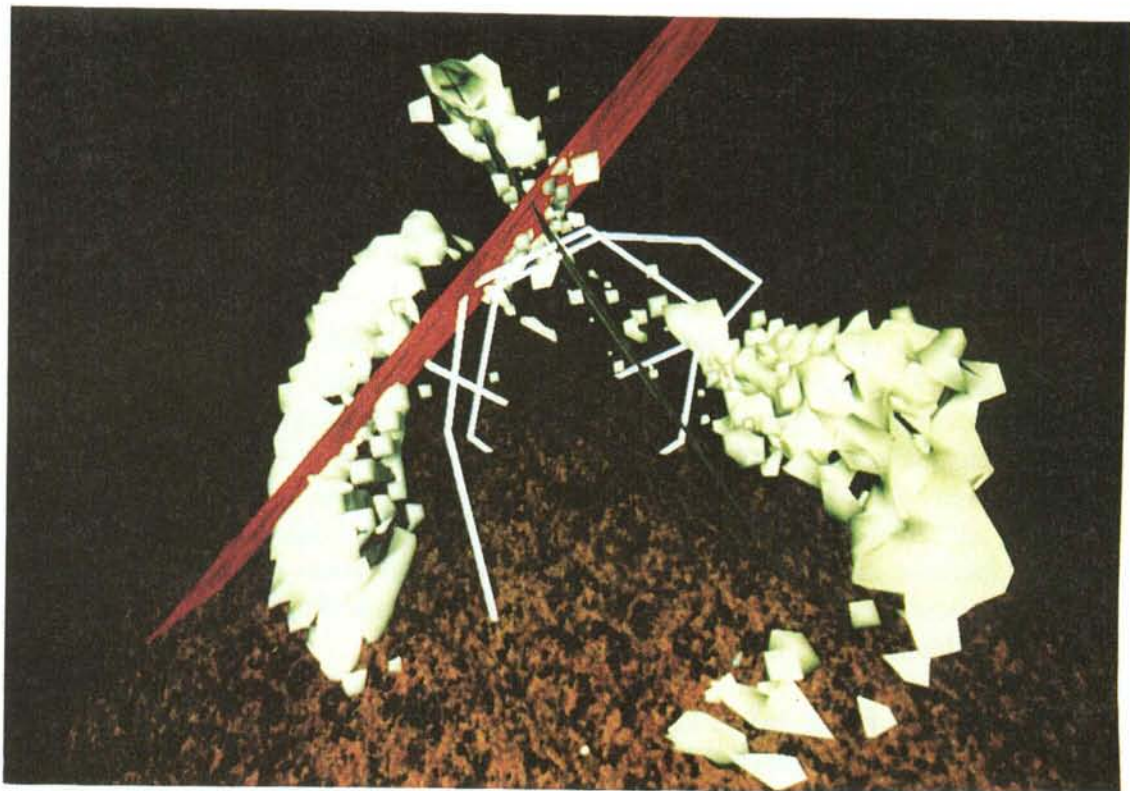
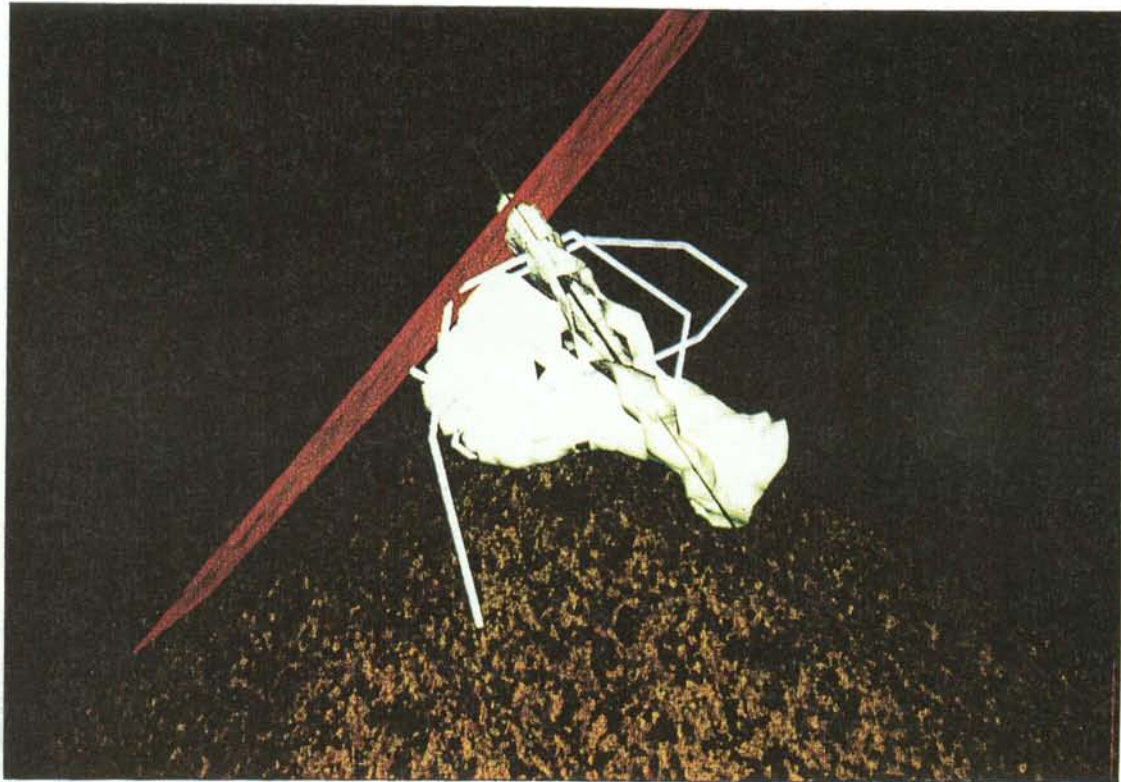


Figure 2-10. Construction phase - Numerical groundwater flow simulations. Origin of water flowing into the tunnel where the tunnel intersect a hydraulic conductor domain. The total flow into the tunnel = 100%.
 Top: Hydraulic conductor domain NE-1.
 Bottom: Hydraulic conductor domain NNW-4.



*Figure 2-11. Pumping test LPT2 - Numerical groundwater flow simulations. Influenced regions of water flowing toward the pumped borehole KAS06.
Top: 10 days of pumping
Bottom: 100 days of pumping.*

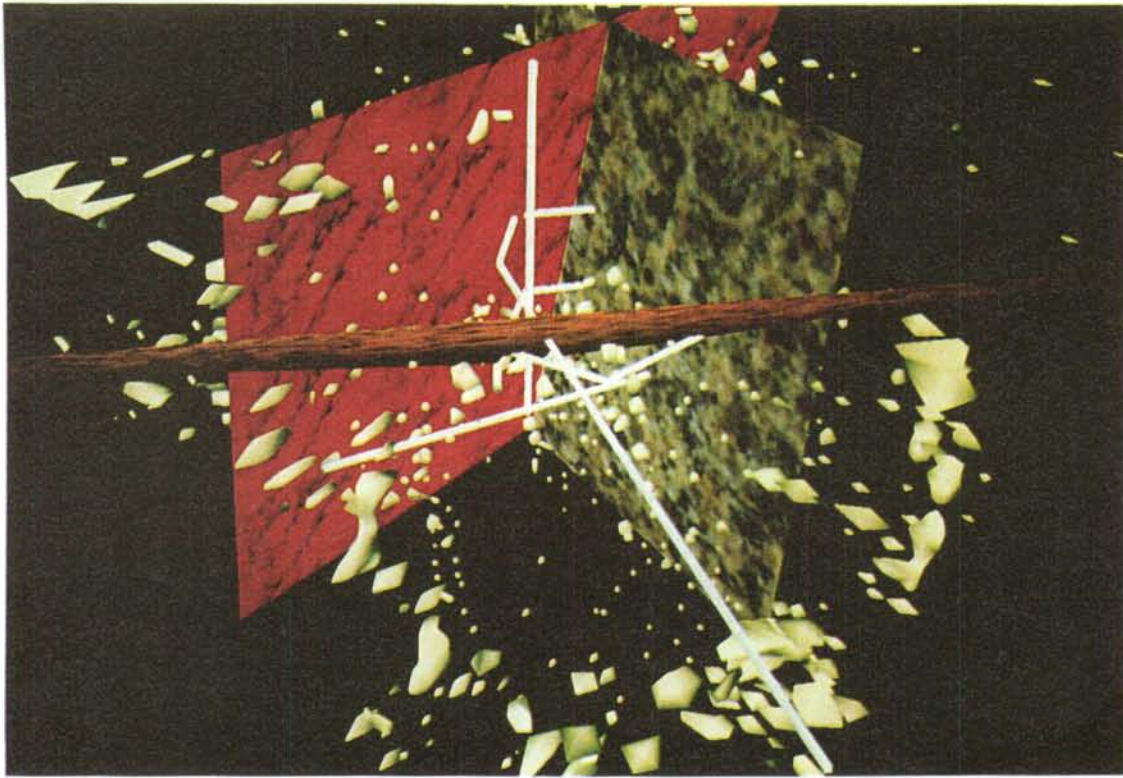


Figure 2-12. Pumping test LPT2 - Numerical groundwater flow simulations. Influenced regions of water flowing toward the pumped borehole KAS06. 1000 days of pumping

The sets of chemical end-members have also changed from the prediction stage in 1991 to the evaluation in 1995. The dominant change is that the groundwater in the fracture zones have been split up from one, location and depth specific end-member "Fracture zone groundwater" (see *Figure 2-1*) to three end-members "Modified Baltic seawater, Glacial meltwater, Old saline groundwater". Secondly the precipitation water has been excluded as an end-member because the groundwater recharge to the fracture zones was never so fast that precipitation type of waters were recharged into the fracture zones in the influence area of the tunnel.

Because of the difference in the dilution rates mentioned above, a systematic scrutiny of the separate measurement points was judged not to be meaningful. However, a more important question now is how the enhanced knowledge of groundwater evolution would have changed the way the predictions were made. The present hydrochemistry model includes the definition of five water types ('reference waters') which in varying proportions describe all observations. In *Table 2-2* the proportions of the different reference waters are listed for the different time steps (=days from start of tunnel construction). The data in the table is difficult to assimilate since there are many components. A simplifica-

tion is to sum modified and Baltic sea water. In such a case one could summarize:

NE-4 is dominated by sea water, which increased from 44 to 69 per cent during construction while shallow water decreased from 29 to 23 per cent. (Depth below sea level at the tunnel intersection: ~ 110 m.)

NE-3 is dominated by seawater, which decreased from 76 to 69 per cent during tunnel construction. (Depth below sea level at tunnel intersection: ~ 140 m.)

NE-1 is dominated by seawater, which increased from 44 to 76 per cent while the shallow water decreased from 30 to 16 per cent. (Depth below sea level at tunnel intersection: ~ 180 m.)

EW-3 is dominated by seawater, which changed from an initial 43 to a stable 65 per cent with a decrease of shallow and glacial water. (Depth below sea level at tunnel intersection: ~ 200 m.)

NE-2 is dominated by glacial water at all three intersections with the tunnel. The proportion of glacial water decreased from 65 to 30 per cent, 45 to 19 per cent and 47 to 45 per cent respectively during construction of the tunnel. (Depth below sea level at tunnel intersections: ~ 220-350 m.)

NNW-4 is dominated by shallow water in the proportion of some 30 per cent (Depth below sea level at tunnel intersections: ~ 250-400 m.)

The general picture of the proportion and the distribution of the 'reference waters' along the tunnel show that there is a general agreement between the observations and predictions.

Table 2-2. Proportions of different groundwater types for the different fracture zones during tunnel excavation at Äspö HRL.

Fracture zone	Representing day (0=90-10-14)	ID code	Glacial Influx	Deep Saline Influx	Baltic Sea Influx	Shallow Influx
Redox zone	150	KR0012B	20%	1%	6%	73%
Redox zone	550	KR0012B	17%	2%	17%	64%
Redox zone	750	KR0012B	18%	2%	16%	63%
Redox zone	950	KR0012B	9%	3%	13%	75%
Redox zone	1150	KR0012B	1%	0%	17%	81%
Redox zone	1350	KR0012B	1%	0%	16%	82%
NE-4a,4b	350	SA0850B	17%	11%	44%	29%
NE-4a,4b	750	SA0813B	9%	2%	66%	23%
NE-4a,4b	1150	SA0813B	9%	3%	68%	20%
NE-4a,4b	1350	SA0813B	7%	1%	69%	23%
NE-3b,3c	350	SA0976B	6%	3%	76%	15%
NE-3b,3c	550	SA1062B	6%	3%	77%	13%
NE-3b,3c	750	SA1062B	8%	4%	75%	14%
NE-3b,3c	950	SA0958B	11%	4%	67%	18%
NE-3b,3c	1150	SA0958B	12%	4%	66%	18%
NE-3b,3c	1350	SA0958B	8%	2%	70%	20%
NE-1a,1b	550	SA1342B	17%	10%	43%	30%
NE-1a,1b	750	HA1327B	15%	4%	56%	25%
NE-1a,1b	950	SA1229A	7%	2%	71%	20%
NE-1a,1b	1150	HA1327B	11%	4%	68%	17%
NE-1a,1b	1350	SA1229A	6%	2%	76%	16%
EW-3a	750	SA1420A	23%	6%	43%	29%
EW-3a	950	SA1420A	11%	3%	61%	25%
EW-3a	1150	SA1420A	10%	3%	68%	19%
EW-3a	1350	SA1420A	9%	2%	64%	25%
NE-2a-1	750	SA1614B	66%	12%	12%	10%
NE-2a-1	950	SA1614B	50%	17%	18%	15%
NE-2a-1	1150	SA1614B	39%	14%	26%	21%
NE-2a-1	1350	SA1614B	30%	13%	31%	26%
NE-2a-2	750	SA1828B	45%	13%	23%	19%
NE-2a-2	950	SA1828B	35%	16%	27%	22%
NE-2a-2	1150	SA1828B	33%	16%	28%	23%
NE-2a-2	1350	SA1828B	19%	13%	36%	32%
NE-2a-3	1150	SA2583A	46%	18%	21%	15%
NE-2a-3	1350	SA2583A	45%	18%	20%	16%
NNW-4H ₂ O-1	950	SA2074A	17%	15%	38%	30%
NNW-4H ₂ O-1	1150	SA2074A	17%	12%	42%	29%
NNW-4H ₂ O-1	1350	SA2074A	18%	11%	41%	30%
NNW-4H ₂ O-2	950	SA2109B	18%	13%	38%	31%
NNW-4H ₂ O-2	1150	SA2142A	14%	6%	64%	16%
NNW-4H ₂ O-2	1350	SA2175B	15%	12%	47%	26%
NNW-4H ₂ O-3	1350	KA3191F	45%	19%	20%	16%

Hydraulic connectivity

The tracer tests in NE-1 and Redox zone were rather successful for defining hydraulic connectivity but also to approximately estimate the flow porosity. The test scale (distance between injection sections in boreholes and inflow to boreholes or tunnel) was up to about 100 m and the hydraulic conductor domains were fairly well defined geologically.

The LPT2 test was performed in a large test scale, several 100 m, and several hydraulic conductor domains were tested. As a connectivity test it was useful but the evaluation of the transport properties were more difficult. A number of modelling groups used the data from the LPT2 test and simulated the transport, but found it difficult to find a “unique” solution concerning the transport parameters. The modelling work is summarized in *Gustafson and Ström /1995/* and reported in detail in *Rhén et al /1992/, Hautojärvi /1994/, Taivassalo et al /1994/, Billaux et al /1994/, Noyer and Fillion /1994/, Barthelemy et al /1994/, Holton and Milický /1996/, Gylling et al /1994/, Kobayashi et al /1994/, Igarashi et al /1994/ and Uchida et al /1994/.*

The tracer tests were useful for testing the hydraulic connectivity between borehole sections assumed to be in a hydraulic conductor domain. Hydraulic interference tests give rather good opportunities to indicate hydraulic communication within a defined hydraulic conductor domain, if the transmissivity is high compared with the transmissivities of the possible hydraulic conductor domains intersecting the tested domain fairly close to the pumped borehole. However, it is pressure responses that are measured at observation points in an interference test and not flow rates. It is possible that a packed off borehole section intersects close to a boundary of a very transmissive fracture. In such a case the interference test indicates good hydraulic communication with the pumped borehole but still the water in the fracture may be more or less stagnant. Thus, in some cases there may be problems when performing a tracer test, but if the rock is highly fractured in the borehole section where tracer is to be injected the risk of problems is probably minimal. Dilution test is a useful method for finding out if a borehole section is in good contact in terms of groundwater flow.

Conclusion

Flow path and arrival times could be more exactly described with the end-member and reference water mixing concept than with the method used in this work. The multivariate groundwater mixing and mass balance modelling concept was developed during the tunnel construction period. See *Laaksoharju and Wallin /1997/* for a detailed description. The modelling concept is also presented in *Report 5* of this series */Rhén et al, 1997/*. The multivariate groundwater mixing and mass balance modelling concept seems to be one of the tools that can be useful for the interpretation of the flow paths and transport times. Another tool is of course a groundwater flow model for calculations of flow paths in the rock mass that can be compared to the multivariate groundwater mixing and mass balance modelling. However, there is still much work to

do to improve the integration between the groundwater flow, groundwater chemical and transport of solutes models.

Tracer tests are useful for checking the connectivity within and between hydraulic conductor domains. At a relatively small scale, about 50-100 m it seems possible to get rough estimates of the flow porosity and dispersivity within a hydraulic conductor domain. At larger scale it is difficult to evaluate the transport properties but the tests can be useful for defining hydraulic connectivity. The tests at larger scale may also demand a fairly long test time, involve a large number of observation points for pressure measurements and points for tracer injection. Because of this the large scale tests also become quite expensive to perform.

In the next phase of the Äspö HRL a continued efforts will be made on finding useful concepts and parameters for calculations of transport of solutes.

PART 4

REFERENCES

REFERENCES

REFERENCES - CHAPTER 1

Gustafson G, Liedholm M, Rhén I, Stanfors R, Wikberg P, 1991. Äspö Hard Rock Laboratory. Predictions prior to excavation and the process of their validation, SKB TR 91-23, Stockholm.

R&D-Programme 86, 1986, Parts I-III. Handling and final disposal of nuclear waste. Programme for research, development and other measures, SKB, Stockholm.

R&D-Programme 89, 1989, Parts I-II. Handling and final disposal of nuclear waste. Programme for research, development and other measures, SKB, Stockholm.

R&D-Programme 95, 1995, Parts I-II. Treatment and final disposal of nuclear waste. Programme for encapsulation, deep geological disposal and research, development and demonstration, SKB, Stockholm.

REFERENCES - PART 1

Ahlbom K, Andersson J-E, Nordqvist R, Ljunggren C, Tirén S, Voss C, 1991a. Gideå study site, Scope of activities and main results, SKB TR 91-51.

Ahlbom K, Andersson J-E, Nordqvist R, Ljunggren C, Tirén S, Voss C, 1991b. Fjällveden study site. Scope of activities and main results, SKB TR 91-52.

Ahlbom K, Andersson J-E, Andersson P, Ittner T, Ljunggren C, Tirén S, 1992a. Klipperås study site. Scope of activities and main results, SKB TR 92-22.

Ahlbom K, Andersson J-E, Andersson P, Ittner T, Ljunggren C, Tirén S, 1992b. Kamlunge study site. Scope of activities and main results, SKB TR 92-15.

Ahlbom K, Olsson O, Sehlstedt S, 1995. Temperature conditions in the SKB study sites, SKB TR 95-16.

Almén K-E, Zellman O, 1991, Äspö Hard Rock Laboratory. Field investigation methodology and instruments used in the pre-investigation phase 1986-1990, SKB TR 91-21.

Almén K, Johansson B, 1992. The Hydro Monitoring System (HMS) of the Äspö Hard Rock Laboratory. SKB PR 25-92-09.

Almén K-E, Olsson P, Rhén I, Stanfors R, Wikberg P, 1994, Äspö Hard Rock Laboratory. Feasibility and usefulness of site investigation methods. Experience from the pre-investigation phase. SKB TR 94-24.

Andersson P, Ittner T, Gustafsson E, 1992. Groundwater flow measurements in selected sections at Äspö before tunnel passage of fracture zone NE-1. SKB PR 25-92-05.

Axelsson C, Jonsson E-K, Geier J, Dershowitz W, 1990. Discrete fracture modelling. SKB PR 25-89-21.

Cooper H H and Jacob C E, 1946, A generalized graphical method for evaluating formation constants and summarizing well field history. Am. Geophys. Union Trans. Vol. 27, pp 526-534.

Christiansson R, Stenberg L, 1991, Manual for field work in the tunnel. Documentation of the geological, hydrogeological and groundwater chemistry conditions in the access tunnel, SKB PR 25-91-10.

Drost W, Klotz D, Koch A, Moser H, Neumaier F, Rauert W, 1968. Point dilution methods of investigating groundwater flow by means of radioisotopes. Water Resources Research, Vol. 4, No. 1, pp 125-146.

Earlougher R C, 1977, Advances in well test analysis. Monograph volume 5 of the Henry L Doherty series, SPE, New York.

Ericsson L-O, 1987. Fracture mapping on outcrops. SKB PR 25-87-05.

- Ericsson L O, 1988.** Fracture mapping study on Äspö island. Findings of directional data. SKB PR 25-88-10.
- Forsmark T, 1992.** Hydraulic tests at Äspö in KAS16. PR 25-92-15.
- Forsmark T, Stenberg L. 1993.** Supplementary investigations of fracture zones in the tunnel. Hydrogeology. Measurements performed during construction of section 1475-2265 m. Compilation of Technical Notes. SKB PR 25-94-06.
- Gustafson G, Liedholm M, Rhén I, Stanfors R, Wikberg P, 1991.** Äspö Hard Rock Laboratory. Predictions prior to excavation and the process of their validation. SKB TR 91-23.
- Gustafson G, Ström A, 1995.** The Äspö Task Force on Modelling of Groundwater Flow and Transport of Solutes. Evaluation report on Task No 1, the LPT2 large scale field experiments. SKB. SKB ICR 95-05.
- Halevy E, Moser H, Zellhofer O, Zuber A, 1967.** Borehole dilution techniques: A critical review. Proceedings of the symposium on isotopes in hydrology in Vienna, 14-18 November 1966. International Atomic Energy Agency
- Hermanson J, 1995.** Structural geology of water-bearing fractures. SKB PR 25-95-23.
- Ittner T, Gustafsson E, Andersson P, Eriksson C-O, 1991.** Groundwater flow measurements at Äspö with the dilution method. SKB PR 25-91-18.
- Ittner T, 1992.** Groundwater flow measurements (TP2) in selected sections at Äspö after tunnel passage of fracture zone NE-1. SKB PR 25-92-17.
- Ittner Thomas, 1994.** Äspö Hard Rock Laboratory. Groundwater Flow Measurements during Tunnel Construction Phase. Dilution measurements (TP4) at tunnel length 3168 m. SKB PR 25-94-26.
- Ittner T, Gustafsson E, 1995.** Groundwater chemical composition and transport of solutes. Evaluation of the fracture zones NE-1, NE-2 and NNW-4 during pre-investigation and tunnel construction. SKB PR HRL-96-03.
- Kuylenstierna H-O, Svensson U, 1994.** On the numerical generation of fracture aperture distributions. SKB PR 25-94-18.
- Kickmaier W, 1993.** Definition and characterisation of the N-S fracture system - tunnel sections 1/600 m to 2/400 m. Relationships to grouted sections - some remarks. SKB ICR 95-02.
- Landberg J, 1982.** Hydrogeological consequences of excavating gravel-pits below the water-table in glaciofluvial deposits. Doctoral Thesis. Department of Geology, Chalmers University of Technology and University of Gothenburg. Publ. A 39. Göteborg.
- La Pointe P R, 1994.** Evaluation of stationary and non-stationary geostatistical models for inferring hydraulic conductivity values at Äspö. SKB TR 94-22.
- La Point P R, Wallman P, Follin S, 1995.** Estimation of effective block conductivities based on discrete network analysis using data from the Äspö site. SKB TR 95-15.
- Liedholm M (ed), 1991 a,** Conceptual Modelling of Äspö. Technical Notes 1-17. General geological, hydrogeological and hydrochemical information, SKB PR 25-90-16 a.
- Liedholm M (ed), 1991 b,** Conceptual Modelling of Äspö. Technical Notes 18-31. General geological, hydrogeological and hydrochemical information, SKB PR 25-90-16 b.
- Niemi A, 1995.** Modelling of Äspö hydraulic conductivity data at different scales by means of 3-dimensional Monte Carlo simulations. SKB ICR 95-08.
- Nilsson L, 1989.** Hydraulic tests at Äspö and Laxemar. Evaluation. SKB PR 25-88-14.
- Nilsson L. 1990.** Hydraulic tests at Äspö KAS05 - KAS08. HAS 13 -HAS 17. Evaluation. SKB PR 25-89-20.
- Nyberg G. 1991.** Ground water level program, 1987-89. SKB PR 25-90-18.

- Nyberg G, Jönsson S, Ekman L. 1992a.** Groundwater level program, Report for 1990. SKB PR 25-91-19.
- Nyberg G, Jönsson S, Ekman L. 1992b.** Äspö Hard Rock Laboratory. Groundwater level program. Report for 1991. SKB PR 25-92-16.
- Nyberg G, Jönsson S, Ekman L. 1993.** Äspö Hard Rock Laboratory. Groundwater level program. Report for 1992. SKB PR 25-93-09.
- Nyberg G, Jönsson S, Ekman L, 1994.** Äspö Hard Rock Laboratory. Groundwater level program. Report for 1993. SKB PR 25-94-23.
- Nyberg G, Jönsson S, Ekman L, 1995.** Groundwater level program. Report for 1994. SKB PR 25-95-08.
- Nyberg G, Jönsson S, Ekman L, 1996.** Äspö Hard Rock Laboratory. Hydro monitoring program. Report for 1995. SKB PR HRL-96-17.
- Moye D G, 1967,** Diamond drilling for foundation exploration, Civ. Eng. Trans. 7th Inst. Eng. Australia, pp 95-100.
- Olsson O, Stanfors R, Ramqvist G, Rhén I. 1994.** Localization of experimental sites and layout of turn 2. Results of investigations. SKB PR 25-94-14
- Olsson O, Emsley S, Bauer C, Falls S, Stenberg L, 1996.** Zedex, a study of the zone of excavation disturbance for blasted and bored tunnels. SKB ICR 96-03.
- Rhén I. 1988.** Transient interference tests on Äspö 1988. Evaluation. SKB PR 25-88-13.
- Rhén I. 1990a.** Transient interference tests on Äspö 1989 in KAS06, HAS13 and KAS07. Evaluation. SKB PR 25-90-09.
- Rhén I, 1990b.** Information for numerical modelling 1990. General information. SKB PR 25-90-17 A.
- Rhén I, Gustafson G, 1990.** DDP evaluation of hydrogeological data, Report U(G) 1990/59, Vattenfall, Vällingby.
- Rhén I (ed), Gustafson G, Gustafsson E, Svensson U, Wikberg P. 1991a.** Prediction prior to excavation of the Äspö Hard Rock Laboratory. Supplement. SKB PR 25-91-02.
- Rhén I, Forsmark T, Nilsson L. 1991b.** Hydraulic test on Äspö, Bockholmen and Laxemar 1990 in KAS09, KAS11-14, HAS18-20, KBH01-02 and KLX01. Evaluation. SKB PR 25-91-01.
- Rhén I, Svensson U, Andersson J-E, Andersson P, Eriksson C-O, Gustafsson E, Ittner T, Nordqvist R, 1992.** Äspö Hard Rock Laboratory. Evaluation of the combined long term pumping and tracer test (LPT2) in borehole KAS06. SKB TR 92-32.
- Rhén I, Stanfors R. 1993.** Evaluation of Investigation in Fracture Zones NE-1, EW-7 and NE-3. SKB PR 25-92-18.
- Rhén I, Danielsson P, Forsmark T, Gustafson G, Liedholm M. 1993a.** Geo-hydrological evaluation of the data from section 700-1475 m. SKB PR 25-93-06.
- Rhén I, Forsmark T, Danielsson P. 1993b.** Piezometric levels. Evaluation of the data from section 700-1475 m. SKB PR 25-93-08.
- Rhén I, Danielsson P, Forsmark T, Gustafson G, Liedholm M. 1993c.** Geo-hydrological evaluation of the data from section 1475 - 2265 m. SKB PR 25-93-11.
- Rhén I, Forsmark T, Danielsson P. 1993d.** Piezometric levels. Evaluation of the data from section 1475 - 2265 m. SKB PR 25-93-13.
- Rhén I, Danielsson P, Forsmark T, Gustafson G, Liedholm M. 1994a.** Geo-hydrological evaluation of the data from section 2265-2874 m. SKB PR 25-94-20.
- Rhén I, Forsmark T, Danielsson P. 1994b.** Piezometric levels. Evaluation of the data from section 2265-2874 m. SKB PR 25-94-22.
- Rhén I, Stanfors R, 1995.** Supplementary investigations of fracture zones in Äspö tunnel. SKB PR 25-95-20.

- Rhén I, Stanfors R, Wikberg P, Forsmark T, 1995a.** Comparative study between the cored test borehole KA3191F and the first 200 m extension of the TBM tunnel. SKB PR 25-95-09.
- Rhén I (ed), 1995b.** Documentation of tunnel and shaft data, tunnel section 2874 - 3600 m, hoist and ventilation shafts 0- 450 m. SKB PR 25-95-28.
- Rhén I (ed), Gustafson G, Stanfors R, Wikberg P, 1997.** Äspö HRL - Geoscientific evaluation 1997/5. Models based on site characterization 1986-1995. SKB TR 97-06.
- Rosén L, Gustafson G, 1995.** Suitable nearfield design. Stage 2. Provisional positioning index (PPI) predictions with respect to lithology, hydraulic conductivity and rock designation index along the TBM-tunnel. SKB PR 25-95-19.
- Spalding D B, 1981.** A general-purpose computer program for multi-dimensional one and two phase flow. Math and Comp in Simulations, XIII, pp 267-276.
- Sundberg J, 1991.** Thermal properties of the rocks on Äspö island. Thermal conductivity, heat capacity, geothermal gradient and heat flow. SKB PR 25-91-09.
- Svensson U, 1991.** Groundwater flow at Äspö and changes due to the excavation of the laboratory. SKB PR 25-91-03.
- Svensson U, 1992.** Refinements of the numerical model of the Äspö Hard Rock Laboratory. SKB PR 25-92-13.
- Svensson U, 1994.** Calculation of pressure, flow and salinity fields using measured inflow to the tunnel. SKB PR 25-94-27.
- Svensson U, 1995b.** Calculation of pressure, flow and salinity fields, with tunnel front at 2874 metres. SKB PR 25-95-25.
- Stanfors R et al 1992.** Passage through water-bearing fracture zones. Compilation of technical notes. SKB PR 25-92-18 A. Investigation during passage of fracture zone EW-7 and NE-3. SKB PR 25-92-18 B Passage through fracture zone NE-1 Geology and geophysics. SKB PR 25-92-18 C Passage through fracture zone NE-1. Hydrogeology and groundwater chemistry. SKB PR 25-92-18 D Construction and grouting.
- Stanfors R, Liedholm M, Munier R, Olsson P, 1993a.** Geological-Structural evaluation of the data from tunnel section 700-1475 m. SKB PR 25-93-05.
- Stanfors R, Liedholm M, Munier R, Olsson P, Stille H. 1993b.** Geological-structural and rock mechanical evaluation of data from tunnel section 1475 - 2265 m. SKB PR 25-93-10.
- Stanfors R, Liedholm M, Munier R, Olsson P, Stille H, 1994.** Geological-structural and rock mechanical evaluation of data from tunnel section 2265-2874 m. SKB PR 25-94-19.
- Stanfors R, Erlström M, Markström I, 1997a.** Äspö HRL - Geoscientific evaluation 1997/1. Overview of site characterization 1986-1995, SKB TR 97-02.
- Stanfors R, Olsson P, Stille H, 1997b.** Äspö HRL - Geoscientific evaluation 1997/3. Results from pre-investigations and detailed site characterization. Comparison of prediction and observations. Geology and Mechanical stability. SKB TR 97-04.
- Wikberg P (ed), Gustafson G, Rhén I, Stanfors R. 1991.** Äspö Hard Rock Laboratory. Evaluation and conceptual modeling based on the pre-investigations. SKB TR 91-22.
- Winberg A, 1989.** PROJECT -90. Analysis of the spatial variability of hydraulic conductivity data in the SKB data base GEOTAB, SKI TR 89:12.

Öhberg A, Saksä P, Ahokas H, Routsalainen P, Snellman M, 1994. Summary report of the experiences from TVO's site investigations, SKB TR 94-17.

REFERENCES - PART 2

Ahonen L, Ervanne H, Ruskeenieni T, Jaakkola T and Blomqvist R, 1992. Uranium Mineral - Groundwater Equilibration at the Palmottu Natural Analogue Study Site, Finland. Scientific Basis for Nuclear Waste Management XVI, 294, 1992.

Banwart S (ed.), 1995. The Äspö redox investigations in block scale. Project summary and implications for repository performance assessment. SKB TR 95-26.

Banwart S, Laaksoharju M, Skärman C, Gustafsson E, Pitkänen P, Snellman M, Landström O, Aggeryd I, Mathiasson L, Sundblad B, Tullborg E-L, Wallin B, Pettersson C, Pedersen K, Arlinger J, Jahromi N, Ekendahl s, Hallbeck L, Degueldre C, Malmström M, 1995. The Redox experiment in block scale. Final reporting of results from the Three Year Project. SKB PR 25-95-06.

BRAINMAKER PROFESSIONAL for Windows, 1993. Simulated biological intelligence by California Scientific Software. Nevada City, California, USA.

Forina M, Leardi R, Armanino C and Lanteri S, 1988. PARVUS. Elsevier Science Publisher B.V., Amsterdam.

Fortner B, 1992. The Data Handbook. Spyglass, Inc. Champaign, Illinois, USA.

Gnirk P, 1993. OECD/NEA International Stripa project, Overview volume II, Natural Barriers, p. 182, SKB, Stockholm, ISBN 91-971906-3-2.

Grenthe I, Stumm W, Laaksoharju M, Nilsson A-C and Wikberg P, 1992. Redox potentials and redox reactions in deep groundwater systems. Chemical Geology, 98, 131.

Gustafson G, Liedholm M, Rhén I, Stanfors R and Wikberg P, 1991. Äspö Hard Rock Laboratory. Predictions prior to excavation and the process of their validation. SKB Technical Report TR 91-23, Stockholm.

Hecht-Nielsen R, 1991. Neurocomputing. Addison-Wesley Publishing Company, Reading, Massachusetts.

Henley S, 1981. Nonparametric geostatics. Elsevier Applied Science Publishers Ltd, Essex, England.

Hermansson J, 1995. Structural geology of water-bearing fractures. PR 25-95-23.

Hertz J, Krogh A and Palmer R G, 1991. Introduction to the theory of neural computation. Addison-Wesley Publishing Company, Reading, Massachusetts.

Laaksoharju M (ed.), 1995. Sulphate reduction in the Äspö HRL tunnel. SKB TR 95-25.

Laaksoharju M, Skärman C, 1995. Groundwater sampling and chemical characterization of the Äspö HRL tunnel in Sweden. PR 25-95-29.

Laaksoharju and Wallin, 1997. Evolution of the groundwater chemistry at the Äspö Hard Rock Laboratory. Proceedings of the second Äspö International Geochemistry Workshop, June 6-7, 1995. SKB ICR 97-04.

Lagerblad B, Trägårdh J, 1995. Conceptual model for concrete long time degradation in a deep nuclear waste repository. SKB TR 95-21.

Lawrence J, 1992. Introduction to neural networks and expert systems. California Scientific Software, Nevada City.

Mazurek M, Bossart P, Eliasson T, 1995. Classification and characterization of water-conducting features at Äspö: Results of Phase I Investigations. PR 25-95-03.

Nilsson A-C, 1995. Compilation of groundwater chemistry data from Äspö 1990-1994. PR 25-95-02.

- Pedersen K, Karlsson F, 1995.** Investigations of subterranean microorganisms. Their importance for performance assessment of radioactive waste disposal. SKB TR 95-10.
- Rhén I, Stanfors R, 1993.** Evaluation of Investigation in Fracture Zones NE-1, EW-7 and NE-3. SKB PR 25-92-18.
- Rhén I (ed), Bäckblom (ed), Gustafson G, Stanfors R, Wikberg P, 1997a.** Äspö HRL - Geoscientific evaluation 1997/2. Results from pre-investigations and detailed site characterization. Summary report. SKB TR 97-03.
- Rhén I (ed), Gustafson G, Stanfors R, Wikberg P, 1997b.** Äspö HRL - Geoscientific evaluation 1997/5. Models based on site characterization 1986-1995. SKB TR 97-06.
- Smellie J, Laaksoharju M, 1992.** The Äspö Hard Rock Laboratory. Final evaluation of the hydro-geochemical pre-investigations in relation to existing geologic and hydraulic conditions. SKB TR 92-31.
- Stanfors R, Olsson P, Stille H, 1997.** Äspö HRL - Geoscientific evaluation 1997/3. Results from pre-investigations and detailed site characterization. Comparison of predictions and observations. Geology and Mechanical stability. SKB TR 97-04.
- STATGRAPHICS PLUS for Windows, 1994.** Statistical graphics system by Manugistics, Inc. Rockville, Maryland, USA.
- SKB, 1995.** RD&D Programme 95. Treatment and final disposal of nuclear waste.
- STATISTICA for Windows, 1994.** Complete Statistical System by StatSoft, Inc. Tulsa, USA.
- SURFER for Windows, 1994.** Contouring and 3D Surface Mapping by Golden Software, Inc. Golden, Colorado, USA.
- Wikberg P (ed), Gustafson G, Rhén I and Stanfors R, 1991.** Äspö Hard Rock Laboratory. Evaluation and conceptual modelling based on the pre-investigations 1986-1990. SKB Technical Report TR 91-22.
- Wikberg P and Gustafsson E, 1993.** Groundwater chemistry and transport of solutes. Evaluation of the data from section 700 - 1475 m. SKB Progress Report 25-93-07.
- Wikberg P, Skårman C, Laaksoharju M, Ittner T, 1993.** Groundwater chemistry and transport of solutes. Evaluation of the data from tunnel section 1475-2265 m. PR 25-93-12.
- Wikberg P, Skårman C, Laaksoharju M and Ittner T, 1994a.** Groundwater chemistry and transport of solutes. Evaluation of the data from tunnel section 1475-2265 m. SKB Progress Report PR 25-93-12, Stockholm.
- Wikberg P, Skårman C, Laaksoharju M and Ittner T, 1994b.** Groundwater chemistry and transport of solutes. Evaluation of the data from tunnel section 2265-2874 m. PR 25-94-21.
- Wikström L, Björklund A, 1994.** Trace elements in waters of low-conductivity rocks in the Äspö Hard Rock Laboratory.

REFERENCES - PART 3

Andersson P, 1995. Compilation of tracer tests in fractured rock. SKB PR 25-95-05.

Banwart S (ed), Laaksoharju M, Skårman C, Gustafsson E, Pitkänen P, Snellman M, Landström O, Aggeryd I, Mathiasson L, Sundblad B, Tullborg E-L, Wallin B, Pettersson C, Pedersen K, Arlinger J, Jahromi N, Ekendahl S, Hallbeck L, Degueldre C, Malmström M, 1995. The Redox experiment in block scale. Final reporting of results from the Three Year Project. SKB PR 25-95-06.

Barthelemy Y, Schwartz J, Sebtí K, 1994. Hydrodynamic modelling of the original steady state and LPT2 experiments. MARTHE and SESAME codes. SKB ICR 94-16.

- Billaux D, Guérin F, Wendling J, 1994.** Hydrodynamic modelling of the Äspö HRL. Discrete fracture model. SKB ICR 94-14.
- Claesson J, 1992.** Bouyancy flow in fractured rock with a salt gradient in the groundwater - An initial study. SKB TR 92-05.
- Gustafson G, Liedholm M, Rhén I, Stanfors R, Wikberg P, 1991.** Äspö Hard Rock Laboratory. Predictions prior to excavation and the process of their validation. SKB TR 91-23.
- Gustafsson E, Andersson-Ludvigson J E, Gentzschlein B, Hautojärvi A, Koskinen L, Löfman J, 1994.** Hydraulic modelling and tracer tests on the Redox experiment in the Äspö Hard Rock Laboratory tunnel. SKB PR 25-94-37.
- Gustafson G, Ström A, 1995.** The Äspö Task Force on Modelling of Groundwater Flow and Transport of Solutes. Evaluation report on Task No 1, the LPT2 large scale field experiments. SKB ICR 95-05.
- Gylling B, Moreno L, Neretnieks I, Birgersson L, 1994.** Analysis of LPT2 using the Channel Network model. SKB ICR 94-05.
- Hautojärvi A, 1994.** Data analysis and modelling of the LPT2 Pumping and Tracer Transport Test at Äspö. Tracer experiment. SKB ICR 94-11.
- Holton D, Milický M, 1996.** Simulating the LPT2 and tunnel drawdown experiment at Äspö using a coupled continuum-fracture network approach. SKB ICR xxx (in prep).
- Ittner T, Gustafsson E, 1995.** Groundwater chemical composition and transport of solutes. Evaluation of the fracture zones NE-1, NE-2 and NNW-4 during pre-investigation and tunnel construction. SKB PR HRL-96-03.
- Igarashi T, Tanaka Y, Kawanishi M, 1994.** Application of three-dimensional smeared fracture model to the groundwater flow and the solute migration of LPT-2 experiment. SKB ICR 94-08.
- Kobayashi A, Yamashita R, Chijimatsu M, Nishiyama H, Ohnishi Y, 1994.** Analyses of LPT2 in the Äspö HRL with continuous anisotropic heterogeneous model. SKB ICR 94-07.
- Laaksoharju M, 1990.** Measured and predicted groundwater chemistry at Äspö. SKB PR 25-90-13.
- Laaksoharju M, Smellie J, Nilsson A-C, Skårman C, 1995.** Groundwater sampling and chemical characterisation of the Laxemar deep borehole KLX02. SKB TR 95-05.
- Laaksoharju and Wallin, 1997 (in prep.).** Evolution of the groundwater chemistry at the Äspö Hard Rock Laboratory. Proceedings of the second Äspö International Geochemistry Workshop, June 6-7, 1995. SKB ICR 97-04.
- Noyer M L, Fillion E, 1994.** Hydrodynamic modelling of the Äspö Hard Rock Laboratory. ROCKFLOW code. SKB. ICR 94-15.
- Nilsson A-C, 1995.** Compilation of groundwater chemistry data from Äspö 1990-1994. SKB PR 25-95-02.
- Rhén I (ed), Gustafson G, Gustafsson E, Svensson U, Wikberg P. 1991.** Prediction prior to excavation of the Äspö Hard Rock Laboratory. Supplement. SKB PR 25-91-02.
- Rhén I, Svensson U, Andersson J-E, Andersson P, Eriksson C-O, Gustafsson E, Ittner T, Nordqvist R, 1992.** Äspö Hard Rock Laboratory. Evaluation of the combined longterm pumping and tracer test (LPT2) in borehole KAS06. SKB TR 92-32.
- Rhén I, Stanfors R, 1993.** Evaluation of Investigation in Fracture Zones NE-1, EW-7 and NE-3. SKB PR 25-92-18.
- Rhén I, Stanfors R, 1995.** Supplementary investigations of fracture zones in Äspö tunnel. SKB PR 25-95-20.
- Rhén I (ed), 1995b.** Documentation of tunnel and shaft data, tunnel section 2874 - 3600 m, hoist and ventilation shafts 0- 450 m. SKB PR 25-95-28.

Rhén I (ed), Gustafson G, Stanfors R, Wikberg P, 1997. Äspö HRL - Geoscientific evaluation 1997/5. Models based on site characterization 1986-1995. SKB TR 97-06.

Spalding D B, 1981. A general-purpose computer program for multi-dimensional one and two phase flow. Math and Comp in Simulations, XIII, pp 267-276.

Stanfors R et al, 1992. PASSAGE THROUGH WATER-BEARING FRACTURE ZONES. Compilation of technical notes. SKB PR 25-92-18 C. Passage through fracture zone NE-1. Hydrogeology and groundwater chemistry.

Stanfors R, Liedholm M, Munier R, Olsson P, Stille H, 1994b. Geological-structural and rock mechanical evaluation of data from tunnel section 2265-2874 m. SKB PR 25-94-19.

Svensson U, 1991a. Groundwater flow at Äspö and changes due to the excavation of the laboratory. SKB PR 25-91-03.

Svensson U, 1991b. Predictions of flow trajectories for the LPT2 pump test. SKB PR 25-91-17.

Svensson U, 1994a. Flow, pressure and salinity distributions around planned experimental sites at the Äspö Hard Rock Laboratory. SKB PR 25-94-11.

Svensson U, 1994b. Calculation of pressure, flow and salinity fields using measured inflow to the tunnel. SKB PR 25-94-27.

Svensson U, 1995. Modelling the unsaturated zone at Äspö under natural conditions and with the tunnelfront at 2874 metres. SKB PR 25-95-24.

Taivassalo V, Koskinen L, Laitinen M, Löfman J, Mészáros F, 1994. Modelling the LPT2 Pumping and Tracer Test at Äspö. Pumping test. SKB ICR 94-12.

Uchida M, Doe T, Dershowitz W, Thomas A, Wallmann P, Sawada A, 1994. Discrete-fracture modelling of the Äspö LPT-2, large-scale pumping and tracer test. SKB ICR 94-09.

Wikberg P (ed), Gustafson G, Rhén I, Stanfors R. 1991. Äspö Hard Rock Laboratory. Evaluation and conceptual modelling based on the pre-investigations. SKB TR 91-22.

Winberg A (ed), 1996. Descriptive Structural-hydraulic Models on Block and Detailed Scales of the TRUE-1 Site. SKB ICR 96-04.

This report is based on the following text files:

004pa0ir.wpd:	Summary, Introduktion
004pa1ir.wpd:	Part 1
004pa1ap.wpd:	Part 1 Appendix
004pa2pw.wpd:	Part 2
004pa3ir.wpd:	Part 3
004pa4re.wpd:	Part 4

List of SKB reports

Annual Reports

1977-78

TR 121

KBS Technical Reports 1 – 120

Summaries

Stockholm, May 1979

1979

TR 79-28

The KBS Annual Report 1979

KBS Technical Reports 79-01 – 79-27

Summaries

Stockholm, March 1980

1980

TR 80-26

The KBS Annual Report 1980

KBS Technical Reports 80-01 – 80-25

Summaries

Stockholm, March 1981

1981

TR 81-17

The KBS Annual Report 1981

KBS Technical Reports 81-01 – 81-16

Summaries

Stockholm, April 1982

1982

TR 82-28

The KBS Annual Report 1982

KBS Technical Reports 82-01 – 82-27

Summaries

Stockholm, July 1983

1983

TR 83-77

The KBS Annual Report 1983

KBS Technical Reports 83-01 – 83-76

Summaries

Stockholm, June 1984

1984

TR 85-01

Annual Research and Development Report 1984

Including Summaries of Technical Reports Issued during 1984. (Technical Reports 84-01 – 84-19)

Stockholm, June 1985

1985

TR 85-20

Annual Research and Development Report 1985

Including Summaries of Technical Reports Issued during 1985. (Technical Reports 85-01 – 85-19)

Stockholm, May 1986

1986

TR 86-31

SKB Annual Report 1986

Including Summaries of Technical Reports Issued during 1986

Stockholm, May 1987

1987

TR 87-33

SKB Annual Report 1987

Including Summaries of Technical Reports Issued during 1987

Stockholm, May 1988

1988

TR 88-32

SKB Annual Report 1988

Including Summaries of Technical Reports Issued during 1988

Stockholm, May 1989

1989

TR 89-40

SKB Annual Report 1989

Including Summaries of Technical Reports Issued during 1989

Stockholm, May 1990

1990

TR 90-46

SKB Annual Report 1990

Including Summaries of Technical Reports Issued during 1990

Stockholm, May 1991

1991

TR 91-64

SKB Annual Report 1991

Including Summaries of Technical Reports Issued during 1991

Stockholm, April 1992

1992

TR 92-46

SKB Annual Report 1992

Including Summaries of Technical Reports Issued during 1992

Stockholm, May 1993

1993

TR 93-34

SKB Annual Report 1993

Including Summaries of Technical Reports Issued during 1993

Stockholm, May 1994

1994

TR 94-33

SKB Annual Report 1994

Including Summaries of Technical Reports Issued during 1994

Stockholm, May 1995

1995

TR 95-37

SKB Annual Report 1995

Including Summaries of Technical Reports Issued during 1995

Stockholm, May 1996

1996

TR 96-25

SKB Annual Report 1996

Including Summaries of Technical Reports Issued during 1996

Stockholm, May 1997

List of SKB Technical Reports 1997

TR 97-01

Retention mechanisms and the flow wetted surface – implications for safety analysis

Mark Elert

Kemakta Konsult AB

February 1997

TR 97-02

Äspö HRL – Geoscientific evaluation 1997/1. Overview of site characterization 1986–1995

Roy Stanfors¹, Mikael Erlström²,

Ingemar Markström³

¹ RS Consulting, Lund

² SGU, Lund

³ Sydkraft Konsult, Malmö

March 1997

TR 97-03

Äspö HRL – Geoscientific evaluation 1997/2. Results from pre-investigations and detailed site characterization. Summary report

Ingvar Rhén (ed.)¹, Göran Bäckblom (ed.)², Gunnar Gustafson³, Roy Stanfors⁴, Peter Wikberg²

¹ VBB Viak, Göteborg

² SKB, Stockholm

³ VBB Viak/CTH, Göteborg

⁴ RS Consulting, Lund

May 1997

TR 97-04

Äspö HRL – Geoscientific evaluation 1997/3. Results from pre-investigations and detailed site characterization. Comparison of predictions and observations. Geology and mechanical stability

Roy Stanfors¹, Pär Olsson², Håkan Stille³

¹ RS Consulting, Lund

² Skanska, Stockholm

³ KTH, Stockholm

May 1997